

ANL-06/53

ARGONNE NATIONAL LABORATORY
9700 S. Cass Avenue
Argonne, Illinois 60439-4801

**PHYSICS DIVISION ANNUAL REPORT
2005**

Donald F. Geesaman
Director

December 2006

Preceding Annual Reports

ANL-03/23 2002

ANL-04/22 2003

ANL-05/61 2004

Edited by Jeannie Glover

FOREWORD

This report highlights the research performed in 2005 in the Physics Division of Argonne National Laboratory. The Division's programs include operation of ATLAS as a national user facility, nuclear structure and reaction research, nuclear theory, medium energy nuclear research and accelerator research and development. The mission of Nuclear Physics is to understand the origin, evolution and structure of baryonic matter in the universe – the matter that makes up stars, planets and human life itself. The Division's research focuses on innovative new ways to address this mission and 2005 was a year of great progress.

One of the most exciting developments is the initiation of the Californium Rare Ion Breeder Upgrade, CARIBU. By combining a Cf-252 fission source, the gas catcher technology developed for rare isotope beams, a high-resolution isobar separator, and charge breeding ECR technology, CARIBU will make hundreds of new neutron-rich isotope beams available for research. The cover illustration shows the anticipated intensities of low-energy beams that become available for low-energy experiments and for injection into ATLAS for reacceleration. CARIBU will be completed in early 2009 and provide us with considerable experience in many of the technologies developed for a future high intensity exotic beam facility.

Notable results in research at ATLAS include a measurement of the isomeric states in ^{252}No that helps pin down the single particle structure expected for superheavy elements, and a new low-background measurement of ^{16}N beta-decay to determine the $^{12}\text{C}(\alpha,\gamma)^{16}\text{O}$ reaction rate that is so important in astrophysical environments. Precise mass measurements shed new light on the unitarity of the quark weak-mixing matrix in the search for physics beyond the standard model. ATLAS operated for 4686 hours of research in FY2005 while achieving 95% efficiency of beam delivery for experiments.

In Medium-Energy Physics, radium isotopes were trapped in an atom trap for the first time, a major milestone in an innovative search for the violation of time-reversal symmetry. New results from HERMES establish that strange quarks carry little of the spin of the proton and precise results have been obtained at JLAB on the changes in quark distributions in light nuclei.

New theoretical results reveal that the nature of the surfaces of strange quark stars. Green's function Monte Carlo techniques have been extended to scattering problems and show great promise for the accurate calculation, from first principles, of important astrophysical reactions. Flame propagation in type 1A supernova has been simulated, a numerical process that requires considering length scales that vary by factors of eight to twelve orders of magnitude.

Argonne continues to lead in the development and exploitation of the new technical concepts that will truly make an advanced exotic beam facility, in the words of NSAC, "the world-leading facility for research in nuclear structure and nuclear astrophysics." Our science and our technology continue to point the way to this major advance. It is a tremendously exciting time in science for these new capabilities hold the keys to unlocking important secrets of nature.

The great progress that has been made in meeting the exciting intellectual challenges of modern nuclear physics reflects the talents and dedication of the Physics Division staff and the visitors, guests and students who bring so much to the research.

A handwritten signature in black ink, appearing to read 'D. Geesaman', with a long horizontal flourish extending to the right.

Donald F. Geesaman, Director, Physics Division

TABLE OF CONTENTS

Page

I.	LOW-ENERGY NUCLEAR PHYSICS RESEARCH	1
A.	REACTIONS OF ASTROPHYSICAL IMPORTANCE	5
a.1.	A New Measurement of the E1 Component of the Low-Energy $^{12}\text{C}(\alpha,\gamma)^{16}\text{O}$ Cross Section	5
a.2.	The Spin of the 2.643 MeV State in ^{20}Na , Studied Through the $^{19}\text{Ne}(^3\text{He},d)^{20}\text{Na}$ Reaction	7
a.3.	In-Beam Spectroscopy of the rp-Process Nucleus ^{26}Si	7
B.	WEAK INTERACTIONS	11
b.1.	Q Value of the Superaligned Decays of ^{14}O , ^{42}Sc , ^{26m}Al , ^{34}Cl , and the Unitarity of the CKM Matrix	11
b.2.	Properties of Nuclei Relevant to $(0\nu 2\beta)$ Decay	13
b.3.	Progress at the Beta-Decay Paul Trap	14
b.4.	β -Decay of $^{69,70,71}\text{Kr}$	15
C.	SPECTROSCOPY OF VERY HEAVY ELEMENTS	17
c.1.	Properties of the Lightest Nobelium Isotopes.....	17
c.2.	$K = 8^-$ Isomers and $K = 2^-$ Octupole Bands in ^{252}No and $N = 150$ Isotones	19
c.3.	Two-Quasiparticle States in ^{254}No and the Stability of Superheavy Nuclei	20
c.4.	Limiting Angular Momentum in ^{254}No and ^{220}Th	23
c.5.	Structure of the Odd-A, Shell-Stabilized Nucleus ^{253}No	23
c.6.	Calculations of 2-Quasiparticle Energies in Heavy Shell-Stabilized Nuclei.....	24
c.7.	Octupole Correlations in the Lightest Even-Even Pu Isotopes.....	25
c.8.	Strength of Octupole Correlations in the Actinides: Contrasting Behavior in the Isotones ^{237}U and ^{239}Pu	28
c.9.	Measurement of the ^{240}Pu Half-Life	28
c.10.	Energy Levels of the $N = 153$ Neutron Nucleus ^{251}Cf	28
D.	STRUCTURE OF NUCLEI FAR FROM STABILITY	31
d.1.	Neutron-Rich Nuclides	31
d.1.1.	Is the Nuclear Spin-Orbit Interaction Changing with Neutron Excess?.....	31
d.1.2.	Structure in Neutron-Rich ^{52}Ca and ^{52}Sc and the $N = 32$ Shell Gap	31
d.1.3.	Yrast Structure of Neutron-Rich ^{53}Ti	33
d.1.4.	Structure of the Even-Even Neutron-Rich $^{56,58,60}\text{Cr}$ Isotopes	33

d.1.5.	Changes in $\nu g_{9/2}$ Shape Polarization Across the Odd Neutron-Rich Cr Isotopes	34
d.1.6.	Stabilization of Nuclear Isovector Valence-Shell Excitations.....	36
d.1.7.	Investigation of the Nuclear Structure of Heavy Fission Fragments Using the CPT Mass Spectrometer	37
d.1.8.	Study of $N = 50$ Nuclei Near ^{78}Ni Using Deep Inelastic Reactions	38
d.1.9.	Structure of Neutron-Rich Zn Isotopes.....	39
d.1.10.	Deep Inelastic Reactions with CHICO: The Case of $^{48}\text{Ca} + ^{208}\text{Pb}$	41
d.2.	Proton-Rich Nuclides.....	43
d.2.1.	Shape Coexistence in ^{71}Br and the β -Decay of ^{71}Kr	43
d.2.2.	Neutron-Proton P-Correlations and Odd-Odd Nuclei: A Search for Excited States in ^{78}Y	44
d.2.3.	New $T = 1$ and $T = 0$ States in ^{74}Rb and the np Pairing Gap	45
d.2.4.	Mapping the Periphery of Deformation in the $A \sim 80$ Region: A Study of ^{83}Nb	46
d.2.5.	A Search for Isomers in ^{86}Tc	47
d.2.6.	Observation of the ^{105}Te α Decay.....	48
d.2.7.	Level Structure of ^{181}Tl	50
E.	OTHER NUCLEAR STRUCTURE RESEARCH	53
e.1.	Rotational Damping, Ridges and the Quasicontinuum of γ Rays in ^{152}Dy	53
e.2.	Narrow Spreading Widths of Excited Bands in a Superdeformed Well	55
F.	THE PHOBOS EXPERIMENT AT RHIC	59
f.1.	The Phobos Experiment at RHIC	59
f.2.	Consequences of Energy Conservation in Relativistic Heavy-Ion Collisions.....	66
G.	REACTION MECHANISM STUDIES	69
g.1.	Neutron Spectroscopic Factors in ^9Li from $d(^8\text{Li},p)^9\text{Li}$	69
g.2.	Search for Excited States in ^7He with the (d,p) Reaction	70
g.3.	First Evidence in Fusion Hindrance for a Small $ Q $ -Value System.....	72
g.4.	Fusion-Fission of $^{16}\text{O} + ^{197}\text{Au}$ at Sub-Barrier Energies	74
g.5.	Systematics of Heavy-Ion Fusion Hindrance at Extreme Sub-Barrier Energies	76
H.	DEVELOPMENT OF NEW EXPERIMENTAL EQUIPMENT	81
h.1.	Proposal for a Radioactive Beam Upgrade to ATLAS: the CARIBU Project	81
h.2.	A High Resolution Isobar Separator for the CARIBU Project	83
h.3.	Beam Intensity Expectations for a 200 MeV/u 400 kW Radioactive Beam Driver Accelerator	85
h.4.	HELIOS – a Solenoidal Spectrometer for Inverse Reactions.....	87
h.5.	Commissioning of the APT Isobar Separator	88
h.6.	Gammasphere Operations	90

h.7.	α -Calibration of the Twin-Ionization Chambers	91
h.8.	Nuclear Target Development	91
h.9.	Completion of the SCARLET Data Acquisition System.....	93
h.10.	Evaluation of a Planar Germanium Detector with Amorphous Contacts	93
h.11.	Silicon Array Upgrade to MUSIC Detector.....	94
I.	HIGH-PRECISION AND HIGH-SENSITIVITY EXPERIMENTS	97
i.1.	A Bragg Scattering Method to Search for the Neutron Electric Dipole Moment	97
J.	ATLAS USER PROGRAM	99
a.	Experiments Involving Outside Users	100
b.	Outside Users of ATLAS During the Period October 1, 2004 - September 30, 2005	104
II.	OPERATION AND DEVELOPMENT OF ATLAS	107
A.	OPERATION OF THE ACCELERATOR	109
a.1.	Operations Summary	109
B.	DEVELOPMENTS RELATED TO ATLAS	111
b.1.	Status of the ECR Ion Sources.....	111
b.1.1.	Hexapole and Plasma Chamber Redesign Update.....	111
b.1.2.	Production of Ti-50 Using an Induction Oven	111
b.1.3.	Three-Frequency Heating on ECR1.....	112
b.2.	New RF Amplifiers for ATLAS Superconducting Resonators	113
b.3.	ATLAS Control System.....	114
b.4.	ATLAS Cryogenic System	116
b.4.1.	Gas Cell Solenoid Helium Recovery Project.....	116
b.4.2.	Cryogenic Alarm System Project.....	116
b.5.	A 50-kV RF Chopper for In-Flight RIB Beams	117
III.	ACCELERATOR PHYSICS AND EXOTIC BEAM TECHNOLOGY	119
A.	SUPERCONDUCTING RF	121
a.1.	Spoke Cavity Development for RIA.....	121

a.2.	Joint ANL/FNAL Superconducting Cavity Surface Processing Facility (SCSPF)	122
a.3.	Cavities and Prototype Cryomodule for RIA and the ATLAS Upgrade	123
B.	BEAM DYNAMICS AND INJECTORS	125
b.1.	Injector System for High-Intensity Heavy-Ion Driver.....	125
b.2.	Design, Construction and Test of a One-Segment Prototype of the RIA Driver RFQ	126
b.3.	Study of Voltage Breakdown Limits in the 12 MHz RFQ	129
b.4.	Automatic Longitudinal Tuning of a Multiple-Charge-State Heavy-Ion Beam	131
b.5.	Benchmarking the New Beam Dynamics Code TRACK.....	133
b.6.	Proton Beam Dynamics in the RIA Driver Linac and Redesign of the Front-End	135
b.7.	Parallel Beam Dynamic Simulation in Radio Frequency Quadrupole with Space Charge Effect.....	137
b.8.	Beam Dynamics of the 8-GeV H-Minus Linac	139
b.9.	Optimization of Steering Elements in the RIA Driver Linac.....	141
b.10.	Reliability and Availability Studies in the RIA Driver Linac	144
C.	RARE ISOTOPE PRODUCTION AND SEPARATION	146
c.1.	Development of Windowless Liquid Lithium Stripper for RIA	146
c.2.	Fragment Separator Design and Simulations.....	148
c.3.	Development of Uranium Carbide Material for High Power ISOL Applications	149
c.4.	Conductance Measurement of Permeable Samples	152
c.5.	Testing of the Full-Scale RIA Gas Catcher Prototype at High Energy at GSI.....	156
c.6.	Preparation for the High Intensity RIA Gas Catcher Test at ATLAS	160
IV.	MEDIUM-ENERGY NUCLEAR PHYSICS RESEARCH	165
A.	HADRON PROPERTIES	169
a.1.	The Charged Pion Form Factor.....	169
a.2.	Precision Measurements the Proton Electromagnetic Form Factors and Two-Photon Exchange Effects	170
a.3.	Parity Violating Electron-Proton Scattering and the Strangeness Content of the Nucleon	171
a.4.	$N \rightarrow \Delta$ Transition Form Factors	172
a.5.	Separated and Unseparated Structure Functions in the Nucleon Resonance Region	172
a.6.	Search for Additional Pentaquark States at JLab.....	173

B.	HADRONS IN THE NUCLEAR MEDIUM	175
b.1.	Measurement of the EMC Effect in Very Light Nuclei.....	175
b.2.	Search for the Onset of Color Transparency: JLab E02-110 Experiment	176
b.3.	Search for Color Transparency in Pion Electroproduction.....	178
b.4.	Measurement of High Momentum Nucleons in Nuclei and Short Range Correlations.....	179
b.5.	Proton Polarization Angular Distribution in Deuteron Photo Disintegration.....	181
b.6.	Measurements of the Nuclear Dependence of $R = \sigma_L/\sigma_T$ at Low Q^2	182
C.	QUARK STRUCTURE OF MATTER	185
c.1.	Studies of Nucleon Spin Structure and Related Measurements of Deep- Inelastic Scattering at HERA	185
c.1.1.	Polarization of the Strange Quark Sea in the Proton from Semi-Inclusive Deep-Inelastic Scattering on the Deuteron	186
c.1.2.	Collins and Sivers Asymmetries for Charged Kaons with a Transversely Polarized Target	188
c.1.3.	Transverse Single-Spin Asymmetries in Leptoproduction of Charged Pion Pairs.....	190
c.1.4.	A Model-Dependent Constraint on $J_u + J_d$ from Deeply-Virtual Compton Scattering at HERMES	191
c.1.5.	Double-Hadron Leptoproduction in the Nuclear Medium.....	192
c.1.6.	HERMES Dual Radiator RICH – Performance and Impact.....	193
c.2.	Measurement of the Absolute Drell-Yan Cross Section on Hydrogen and Deuterium	195
c.3.	Measurement of the Drell-Yan Angular Distributions	195
c.4.	Drell-Yan Measurements with 120 GeV Protons, FNAL E906	196
D.	FUNDAMENTAL SYMMETRIES IN NUCLEI	199
d.1.	Laser Trapping of ^{226}Ra Atoms and Progress Towards an EDM Measurement.....	199
d.2.	Measurement of $\sin^2 \theta_W$ Through Parity Violation in Deep Inelastic Scattering (PV DIS) on Deuterium	201
E.	ATOMIC TRAP TRACE ANALYSIS	203
e.1.	Measuring the Nuclear Charge Radius of ^8He	203
e.2.	ATTA-3: The Next-Generation Instrument for ^{81}Kr -Dating	204

V.	THEORETICAL PHYSICS	205
A.	NUCLEAR DYNAMICS WITH SUBNUCLEONIC DEGREES OF FREEDOM	207
a.1.	Possible Evidence for “Dark Radiation” from Big Bang Nucleosynthesis Data	208
a.2.	Space-Time Variation of Strong Interactions and Fine Structure Constant	209
a.3.	Coulomb Problem for Vector Bosons.....	210
a.4.	Pair Production and Optical Lasers.....	211
a.5.	The Strange Star Surface: A Crust with Nuggets	211
a.6.	Bremsstrahlung Neutrinos from Electron-Electron Scattering in a Relativistic Degenerate Electron Plasma	212
a.7.	Direct Urca Neutrino Rate in Color Superconducting Quark Matter	213
a.8.	Quark Deconfinement in Neutron Star Cores: The Effects of Spin-Down	214
a.9.	Pseudoscalar Meson Radial Excitations	215
a.10.	Electromagnetic Properties of Ground and Excited State Pseudoscalar Mesons	216
a.11.	Nucleon Electromagnetic Form Factors	217
a.12.	Sigma Terms of Light-Quark Hadrons	218
a.13.	Nucleon Weak and Strong Form Factors.....	219
a.14.	Hadron Masses from Schwinger Functions	221
a.15.	Dynamical Coupled-Channel Model of Meson Production Reactions in the Nucleon Resonance Region	221
a.16.	Effects of Nucleon Resonances on Hyperon Production Reactions	223
a.17.	Effects of Nucleon Resonances on ω Production Reactions	225
a.18.	Electroweak Meson Production on Nuclei	227
a.19.	Pentaquark $\Theta^+(1540)$ Production in $\gamma N \rightarrow K\bar{K}N$ Reactions.....	228
B.	NUCLEAR FORCES AND NUCLEAR SYSTEMS	231
b.1.	Quantum Monte Carlo Calculations of Light Nuclei Energies.....	232
b.2.	Scattering Methods for Quantum Monte Carlo Calculations	233
b.3.	Spectroscopic Factors and Cluster Form Factors of Light Nuclei.....	234
b.4.	Calculations of RMS Radii of Helium Isotopes	235
b.5.	Pair Counting, Pion-Exchange Forces, and the Structure of Light Nuclei	235
C.	NUCLEAR ASTROPHYSICS	237
c.1.	Moments Methods for Response Functions with Momentum Transfer Dependence.....	238
c.2.	Sedimentation and Type I X-Ray Bursts at Low Accretion Rates	239
c.3.	Capturing the Fire: Flame Energetics and Neutronization for Type Ia Supernova Simulations	240

D.	NUCLEAR STRUCTURE AND HEAVY-ION REACTIONS	243
d.1.	Sensitivity to Multi-Phonon Excitations in Heavy-Ion Fusion Reactions	244
d.2.	Hindrance of Heavy-Ion Fusion Due to Nuclear Incompressibility	246
d.3.	Signature of Shallow Quasi-Molecular Potentials in Sub-Barrier Fusion	247
d.4.	Reconciling Coulomb Dissociation and Radiative Capture Measurements	248
d.5.	Dipole Response and Charge Radius of Two-Neutron Halo Nuclei	250
d.6.	Mean Field and Many Body Wave Functions	251
d.7.	Variational Approach to Configuration Interaction	252
d.8.	Neutron-Proton Pairing	254
d.9.	Energy Levels of the Heavy Elements	255
E.	ATOMIC THEORY AND FUNDAMENTAL QUANTUM MECHANICS	257
e.1.	Interactions of Photons with Matter.....	257
e.2.	Interactions of Charged Particles with Matter	258
e.3.	Representation of Real and Complex Numbers in Quantum Theory	258
F.	OTHER ACTIVITIES	261
f.1.	New Theoretical Tools for Nucleon Resonance Analysis	261
f.2.	18 th Annual Midwest Theory Get-Together.....	261
VI.	OTHER EDUCATIONAL AND COMMUNITY OUTREACH ACTIVITIES	263
a.	Minority Program.....	263
b.	Recruitment Efforts at the 2006 Joint Annual Conference of the National Society of Black Physicists and the National Society of Hispanic Physicists	264
	Staff Members	265
	Publications	277
	Low-Energy Nuclear Physics Research.....	277
	Operation and Development of ATLAS.....	291
	Accelerator Physics and Exotic Beam Technology	291
	Medium-Energy Nuclear Physics Research.....	297
	Theoretical Physics	301

I. LOW-ENERGY NUCLEAR PHYSICS RESEARCH

OVERVIEW

The structure, stability, reactions and decays of nuclei are studied in this research. This information is crucial for understanding the evolution of the universe, the workings of stars and the abundances of the elements that form the world around us. The forefront area of research is investigating the properties of nuclei which lie very far from stability, which are critical in understanding nucleosynthesis, and provide stringent tests of our understanding of nuclear structure. Exploiting nuclear beta decay to investigate weak interaction is another forefront activity. Most of our research is based at the Argonne Tandem-Linac Accelerator (ATLAS), a national heavy-ion user facility. During this year programs were also mounted at the Relativistic Heavy Ion Collider (RHIC), at Michigan State University, at Yale University, and at other forefront facilities. The major thrusts of the program are: a) studying the reactions that are important in the cataclysmic events in the cosmos which lead to the synthesis of the chemical elements, b) deepening and generalizing our understanding of nuclear structure to allow a reliable description of all bound nuclear systems, and c) testing the limits of the Standard Model, the fundamental theory that currently best represents our understanding of the laws and fundamental symmetries of nature.

Many approaches are used to investigate reactions of astrophysical importance, including the production and acceleration of short-lived nuclei in order to measure key reaction rates, the measurement of ions in traps, and the use of Gammasphere to investigate the properties of states in the “Gamow window”. Gammasphere operating on two beamlines offers world-unique opportunities for gamma-spectroscopy and a wide range of experiments are being carried out on very heavy, neutron-rich and neutron-poor nuclei. The key thrust of spectroscopic studies is to investigate the modification of residual interactions in nuclei that lie far from stability. In addition, there are complimentary efforts in the use of Accelerator Mass Spectrometry (AMS) for environmental research and in the investigation of nuclear matter at relativistic energies. The ATLAS-based research exploits the unique capabilities of the accelerator, both in the stable beam program, and in production of accelerated beams of short-lived isotopes. The experiments employ state-of-the-art research equipment, including the national gamma ray facility, Gammasphere, the Fragment Mass Analyzer (FMA), a large solid angle silicon array, “Ludwig”, and the Advanced Penning Trap switchyard that includes open- and mass-measuring traps. Several new detector initiatives

are being pursued including a new superconducting spectrometer for light ion reactions HELIOS, refining the “in-flight” radioactive beam facility and its detector systems, improving the Advanced Penning Trap (APT) and building a new high-efficiency FMA focal plane array, AEIDA. Effort continues in developing the next generation gamma ray detectors in the GRETINA project, and in completing data analysis for the PHOBOS experiment at Brookhaven.

Some key areas of effort are:

- Making high-precision measurements of nuclear masses with the Canadian Penning Trap (CPT), particularly the masses of $N = Z$ nuclei which are of astrophysical interest and are important for testing Conserved Vector Current (CVC) theory, and measuring the masses of neutron fission fragments that lie close to the anticipated r-process path. We are working to improve the efficiency for production, separation, cooling, transportation, and trap loading of ions to increase sensitivity. The open geometry Paul trap for weak interaction studies, and the “Advanced Penning Trap” high resolution mass-selection switchyard are being commissioned.
- Studying the properties of very heavy nuclei ($Z > 100$) through “in-beam”, “isomer”, and “decay” spectroscopy. The measurements reveal information on the single particle sequence, shell gaps, pairing strength, and fission barriers of very heavy systems. These properties govern the mass limits of nuclear existence.
- Developing and utilizing beams of short-lived nuclei, ${}^6\text{He}$, ${}^8\text{Li}$, ${}^8\text{B}$, ${}^{11}\text{C}$, ${}^{14}\text{O}$, ${}^{16}\text{N}$, ${}^{17,18}\text{F}$, ${}^{20,21}\text{Na}$, ${}^{25}\text{Al}$, ${}^{37}\text{K}$, ${}^{44}\text{Ti}$, ${}^{56}\text{Ni}$, and others, in order to improve the understanding of reactions of astrophysical importance. Emphasis is focused on “in-flight” production of short-lived ion-species using kinematically inverse reactions on light gaseous targets. Considerable scope still remains for further improving the intensity and quality of these beams in the future, and the beamline is being continually upgraded.
- Designing and constructing new equipment needed for radioactive beam physics. In particular developing a high resolution efficient spectrometer for inverse-direct-reaction studies. A superconducting solenoid design, HELIOS, is being pursued. We are also working on position-sensitive germanium detectors, for “tracking” gamma rays in order to allow the imaging of the source of radiation. The ANL focus is on developing planar germanium wafer technologies, in parallel with involvement in the GRETINA project to construct a 1π germanium tracking detector. These new technologies are essential for fully exploiting radioactive beams in the future.
- Studying the structure of neutron-rich nuclei in order to understand the modification of shell gaps and the apparent changes in spin-orbit splitting. Studying transfer reactions on spherical tin isotopes, the decay and Coulomb excitation of exotic nuclei produced in fragmentation, and the most neutron rich nuclei that can be reached by multi-nucleon transfer and heavy-ion fusion.

- Study the shapes, stability and decay modes of nuclei along the proton dripline in order to improve understanding of partially bound nuclei and study proton tunneling through deformed barriers, in order to increase the spectroscopic information obtained through proton radioactive decay rates. The techniques for proton-radioactivity now allow the study of excited states in nuclei beyond the dripline using the recoil-decay tagging technique to trigger Gammasphere. This approach is being continually refined and is key to accessing very heavy nuclei and approaching ^{100}Sn .
- R&D studies for future radioactive beam accelerators continues and we participate in all efforts to refine the designs for the accelerators, target stations, post accelerator, and experimental equipment. Intense effort is being directed to development of the “gas catcher” technology for cooling primary beams, and in making reliable estimates of accelerator yields.



A. REACTIONS OF ASTROPHYSICAL IMPORTANCE

Research into nuclear reactions that are relevant to astrophysical processes is at the core of our science program, and encompass both neutron rich and neutron deficient nuclei. A wide variety of techniques are currently used, exploiting almost all of our equipment, including experiments with radioactive beams, studies with Gammasphere, measurements with the Canadian Penning Trap (CPT), and the use of Accelerator Mass Spectrometry (AMS) for trace element analysis.

a.1. A New Measurement of the E1 Component of the Low-Energy $^{12}\text{C}(\alpha,\gamma)^{16}\text{O}$ Cross Section (X. D. Tang, K. E. Rehm, I Ahmad, J. Greene, A. Hecht, D. Henderson, R. V. F. Janssens, C. L. Jiang, D. Kahl, F. Moore, R. C. Pardo, N. Patel, G. Savard, J. P. Schiffer, S. Sinha, B. Shumard, M. Notani,* M. Paul,† A. Champagne,‡ C. Brune,§ L. Jisonna,¶ R. E. Segel,¶ and A. Wuosmaa||)

The elements carbon and oxygen are crucial to all living organisms. Their main isotopes, ^{12}C and ^{16}O , are produced by helium burning in red giant stars, with their ratio determined by the competition between the triple α process ($\alpha + \alpha + \alpha \rightarrow ^{12}\text{C}$) and the $^{12}\text{C}(\alpha,\gamma)^{16}\text{O}$ reaction. This ratio also has an effect on the future evolution of the star during its carbon, neon and oxygen burning phases. While the cross section of the triple α process is experimentally quite well determined, our knowledge of the $^{12}\text{C}(\alpha,\gamma)^{16}\text{O}$ reaction under typical red giant conditions ($E_\alpha \sim 300$ keV) is still inadequate and is considered as the most serious uncertainty in nucleosynthesis.

During the last three years we have been working on a new detector system consisting of two pairs of twin-ionization chambers which are used for a measurement

of the beta-delayed alpha decay of ^{16}N . A schematic of the setup is shown in Fig. I-1. A ^{16}N beam ($E \sim 60$ MeV) produced by the in-flight technique via the $d(^{15}\text{N}, ^{16}\text{N})p$ reaction is slowed down in the gas-filled attenuation cell and stopped in a thin carbon foil mounted on a rotating wheel. After an irradiation time of about two half-lives (~ 15 sec) the foil is rotated by 120° and placed between one of the two pairs of ionization chambers for the coincident detection of ^{12}C - α pairs. During the counting period, which lasts 15 sec, a second foil is being irradiated for a subsequent measurement in the other pair of detectors. Some of the advantages of ionization chambers over Si detectors, which have been used in previous measurements, are the absence of dead layers and the very low sensitivity to beta particles.

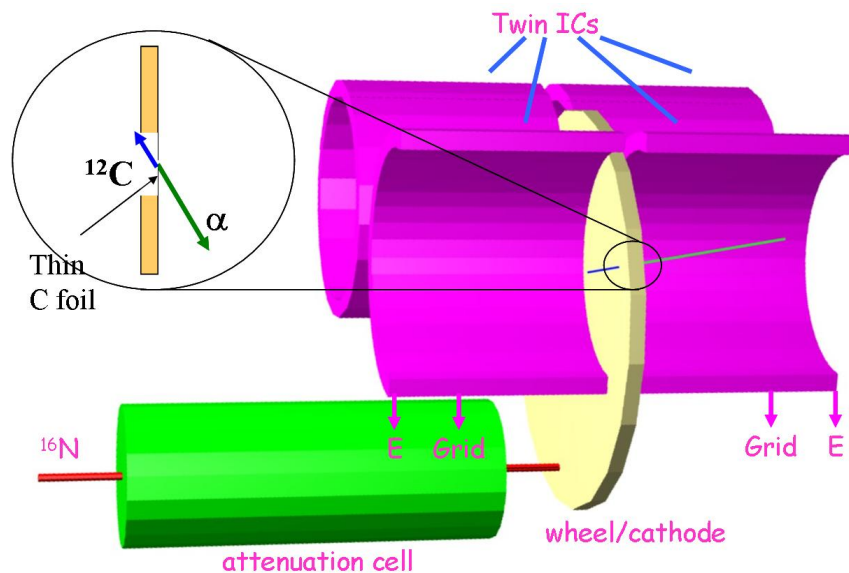


Fig. I-1. Schematic of the experimental setup used for measuring the β -delayed α decay of ^{16}N .

In a first experiment performed last year, about 2×10^5 ^{12}C - α pairs were accumulated. Very clean and background-free α spectra extending down to energies below 500 keV had been obtained (see Annual Report 2004). A comparison among the α spectra from earlier experiments^{1,2} indicates a somewhat shallower slope in the low-energy part of the spectrum obtained in Ref. 2, when compared to the results from Ref. 1. In this energy region our spectrum is in better agreement with the results from Ref. 2.

In this first experiment the pressure in the ionization chamber ($P = 150$ Torr) was chosen to optimize the

detection of low-energy alpha particles. As a consequence, particles above an energy of 1.9 MeV were not completely stopped. In a second set of runs, performed in FY2005, we have increased the pressure in the ionization chambers to 190 Torr in order to obtain a spectrum where α particles with energies up to 2.4 MeV were stopped. The spectrum measured in this experiment is shown by the solid points in Fig. I-2 compared to the result from the previous year (solid line). While on the high energy part of the spectrum the expected change is observed, the data agree on the low energy side within their statistical accuracies.

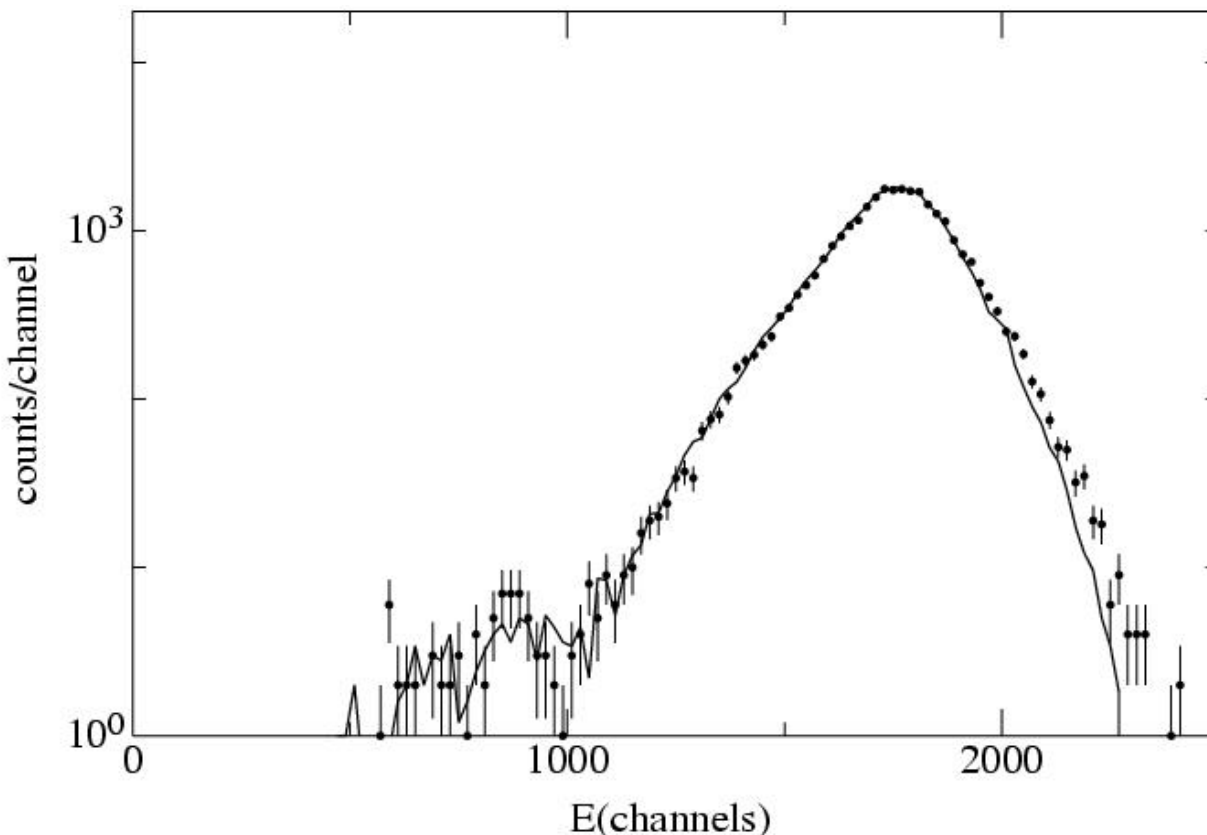


Fig. I-2. β delayed α -spectra from the decay of ^{16}N measured with the twin-ionization chamber at two different pressures: $p = 190$ Torr (solid points) and $p = 150$ Torr (solid line). The differences at the highest energies are caused by incomplete stopping of the α particles.

With this new experiment the number of ^{12}C - α coincidences was doubled (to about 4×10^5). A preliminary analysis of the data from one set of detectors ($\sim 2.2 \times 10^5$ events), using the R-matrix formalism, resulted in a S-factor $S(E1) = 73 \pm 17$ keV. The uncertainty does not include systematic errors and will be reduced, once the full data set is analyzed. The systematic errors in previous experiments were dominated by uncertainties in the energy calibration

and in the value of the relative branching ratio between the two 1^- states populated in the beta decay of ^{16}N . To improve the energy calibration extensive tests of the twin-ionization chambers have been performed (see section h.7.). To improve the contribution to the error budget resulting from the relative branching ratio, a new measurement of the beta decay of ^{16}N will be performed at Gammasphere in the near future.

*Joint Institute for Nuclear Astrophysics, †Hebrew University, Jerusalem, Israel, ‡University of North Carolina, §Ohio University, ¶Northwestern University, ||Western Michigan University.

¹R. Azuma *et al.*, Phys. Rev. C **50**, 1194 (1994).

²Z. Zhao *et al.*, Phys. Rev. Lett. **70**, 726 (1993).

a.2. The Spin of the 2.643 MeV State in ²⁰Na Studied Through the ¹⁹Ne(³He,d)²⁰Na Reaction (K. E. Rehm, J. Greene, D. Henderson, R. V. F. Janssens, C. L. Jiang, R. C. Pardo, N. Patel, J. P. Schiffer, B. Shumard, X. D. Tang, L. Jisonna,* R. E. Segel,* M. Notani,† M. Paul,‡ N. Goodman,§ J. Lightall,§ S. Marley,§ A. Wuosmaa,§ and J. Fernandez-Niello¶)

The temperature-density conditions in a nova are such that neither the ¹⁵O(α,γ)¹⁹Ne nor ¹⁸Ne(α,p)²¹Na route can lead to an appreciable breakout from the hot CNO cycle into the rp-process. In an X-ray burst, however, higher density-temperature values are achieved, resulting in a considerable breakout from the hot CNO cycle into the rp-process, first proceeding through ¹⁵O(α,γ)¹⁹Ne and, at higher temperatures, through ¹⁸Ne(α,p)²¹Na. The ¹⁵O(α,γ)¹⁹Ne reaction is then followed by the proton capture reaction ¹⁹Ne(p, γ)²⁰Na, whose rate is still unknown. This uncertainty originates from the two possible spin-parity assignments (1^+ or 3^+) that have been proposed for the 2.643 MeV state through which the capture proceeds.

We have performed an experiment to determine the spin of this state through a measurement of the angular distribution of the 2.643 MeV state populated in the one-proton transfer reaction ¹⁹Ne(³He,d)²⁰Na. The groundstate spin of ¹⁹Ne is $1/2^+$. Therefore, a 1^+ state in ²⁰Na will be populated mainly via an $l = 0$ transition, while a 3^+ state requires $l = 2$. For $l = 0$ there is a minimum and maximum in the angular distribution between $\theta_{cm} \sim 30^\circ$ - 60° , while for $l = 2$ we expect a continuous fall off in this region.

The ¹⁹Ne beam was produced via the ¹⁹F(p,n)¹⁹Ne reaction by bombarding a hydrogen-filled gas cell ($p = 1.4$ bar and cooled to liquid nitrogen temperatures) with a ¹⁹F beam from the ATLAS accelerator. Because of the strong kinematic shift of the inverse (³He,d) reaction, the beam spot of the secondary beam had to be reduced with a collimator to a diameter of 2 mm. With a 60 pA primary ¹⁹F beam a secondary beam intensity of 4×10^5 ¹⁹Ne/sec was obtained under these conditions.

For the reaction target a 1.5 mm long gas cell filled with 700 mbar of ³He and cooled to 90 K was used. To reduce the small angle straggling of the outgoing low-energy particles, the exit foil of the gas cell (normally 1.3 mg/cm² of Ti) was replaced with a 1.3 mg/cm² thick Kapton foil. The outgoing particles (d and ²⁰Na) were detected in coincidence in an array consisting of three annular position sensitive Si detectors and a Bragg-type ionization chamber at forward angles.

The data from this experiment are presently being analyzed.

*Northwestern University, †Joint Institute for Nuclear Astrophysics, ‡Hebrew University, Jerusalem, Israel, §Western Michigan University, ¶TANDAR, Buenos Aires, Argentina.

a.3. In-Beam Spectroscopy of the rp-Process Nucleus ²⁶Si (D. Seweryniak, M. P. Carpenter, R. V. F. Janssens, T. Lauritsen, C. J. Lister, S. Sinha, P. J. Woods,* T. Davinson,* D. G. Jenkins,† C. Ruiz,‡ J. Shergur,§ and A. Woehr¶)

Quantitative understanding the abundance of the recently observed cosmogenic γ emitter ²⁶Al requires a determination of the ²⁵Al(p, γ)²⁶Si reaction rate. The ²⁵Al(p, γ)²⁶Si reaction is dominated by a handful of states situated just above the proton threshold in ²⁶Si.

In order to determine the properties of these resonances and other subthreshold states in ²⁶Si an in-beam γ -ray experiment was performed. The ¹²C(¹⁶O,2n)²⁶Si reaction was used to populate states above the threshold in ²⁶Si. Their γ decay was detected using the

Gammasphere array. The Argonne Fragment Mass Analyzer (FMA) was used to select $A = 26$ reaction products. Their atomic number was deduced by measuring ΔE - E in the ionization chamber placed behind

the FMA focal plane. Figure I-3 contains a clean ^{26}Si γ -ray spectrum. A preliminary ^{26}Si level scheme is shown in Fig. I-4. The energies, spins and parities shown in Figs. I-3 and I-4 are tentative.

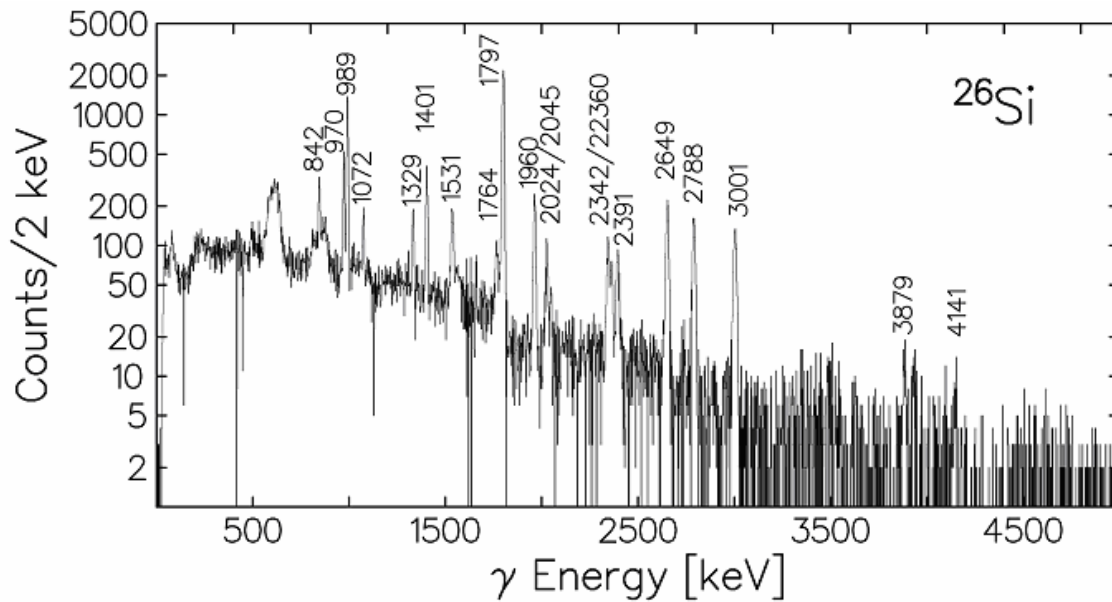


Fig. I-3. The ^{26}Si γ -ray spectrum selected in the FMA.

The data allowed a more precise determination of the level energies and provided evidence for spin assignments complementary to earlier transfer studies. Among others, a triplet of states at 4798, 4810 and 4831 keV was observed and spins 4^+ , 2^+ and 0^+ , respectively, were assigned to these states. This triplet was not resolved in previous studies due to an inferior energy resolution. The proton capture on ^{25}Al is dominated by 3 states above the threshold at 5670 keV,

5912 keV, and 5946 keV, respectively. Only the first and the last state are expected to have a significant γ -ray branch. The 3879 keV transition, which can be seen in Fig. I-3, was observed in coincidence with the 1797 keV transition and was interpreted as corresponding to the decay of the 5670 keV resonance. The impact of the new ^{26}Si level scheme on the structure of ^{26}Si and on the astrophysical $^{25}\text{Al}(p,\gamma)^{26}\text{Si}$ reaction rate will be presented in the forthcoming paper.

*University of Edinburgh, United Kingdom, †University of York, United Kingdom, ‡Simon Fraser University, Burnaby, British Columbia, §University of Maryland, ¶University of Notre Dame.

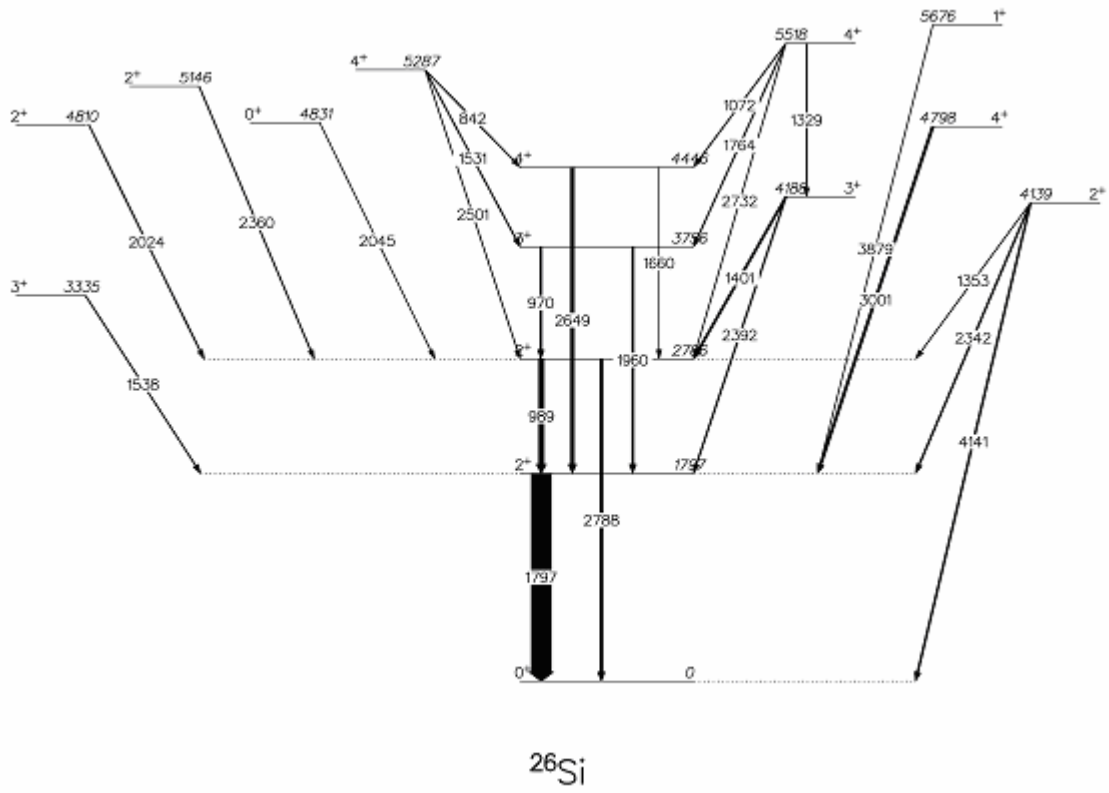


Fig. I-4. A preliminary ^{26}Si level scheme.

B. WEAK INTERACTIONS

Studies of β -decay have always played an important role in nuclear science, as a major tool for elucidating the properties of the weak interaction, as a laboratory for seeking physics beyond the standard model, and as a tool for investigating nuclear structure. The opportunities in this domain at ATLAS have been growing, and will continue into the CARIBU era. When the APT switchyard or the FMA are combined with the gamma and electron spectroscopic arrays, considerable progress should be possible in many facets of β -decay, particularly in studying the decays of very neutron-rich isotopes. These nuclides and their decays are important in determining the r-process path and rate, and some have significance in determining decay heat and delayed neutrons when burning minor actinides in advanced fuel cycles.

b.1. Q Value of the Superallowed Decays of ^{14}O , ^{42}Sc , $^{26\text{m}}\text{Al}$, ^{34}Cl , and the Unitarity of the CKM Matrix (G. Savard,* S. Caldwell,* J. A. Clark,† J. Fallis,† A. A. Hecht,‡ D. Lascar,§ A. Levand, N. D. Scielzo, H. Sharma,† K. S. Sharma,† I. Tanihata, A. C. C. Villari,¶ Y. Wang,† F. Buchinger,|| J. E. Crawford,|| S. Gulick,|| J. C. Hardy,** J. K. P. Lee,|| and R. Segel††)

Superallowed $0^+ \rightarrow 0^+$ decays test the CVC hypothesis, provide the most precise value for the weak vector coupling constant and hence V_{ud} , and play a critical role in the test of the unitarity of the top row of the CKM matrix. The data on the superallowed Fermi decays used to obtain the most precise value of V_{ud} involves Q-value, lifetime and branching ratio measurements and comes from over 100 different experiments. They contribute less than 20% of the total uncertainty on V_{ud} , the remainder coming from the small theoretical corrections that must be applied to the data. In particular, the corrections for nuclear structure effects, though not the largest contributors, have a significant impact on the uncertainty. One test of the latter corrections is to examine how precisely they convert the scatter in experimental ft values to the CVC-predicted constancy of the ft values. Improved precision for individual transitions sharpen that test. This was demonstrated last year at the CPT with a first high precision Penning trap measurement on one of the 9 most precisely known cases, ^{46}V , that yielded a large shift in that value compared to tabulated values and resulted in a first statistically significant shift of the corrected ft value from the mean value used to determine V_{ud} . To see if this is an isolated case or a

first sign of a general trend, it is necessary to apply the high precision available with ion trap measurements to others emitters. This was done this year with precision Q-value measurements performed on the superallowed emitters ^{14}O , ^{42}Sc , $^{26\text{m}}\text{Al}$ and ^{34}Cl .

The mass measurements were performed at the Canadian Penning Trap (CPT) mass spectrometer located online at the ATLAS accelerator. The ^{14}O and ^{14}N isotopes were produced with a 112 MeV beam of ^{14}N impinging on a cryogenic hydrogen gas target. The measurement cycle alternated measurements on ^{14}O , ^{14}N and CH_2 so that the presence of possible systematic effects could be tested with the last two ion species whose masses are known to exquisite precision. The relative masses of the ^{14}N ions and the CH_2 molecular ions were in agreement with known values to -0.04 ± 0.09 keV, indicating that the system is free from systematic errors at least the 6×10^{-9} level. A similar accuracy has been obtained on the ^{14}O isotope measured simultaneously. This is the highest precision Penning trap mass measurement on a short-lived isotopes ever performed anywhere and the CPT seems capable of going further. This new result is compared to other measurements in Fig. I-5.

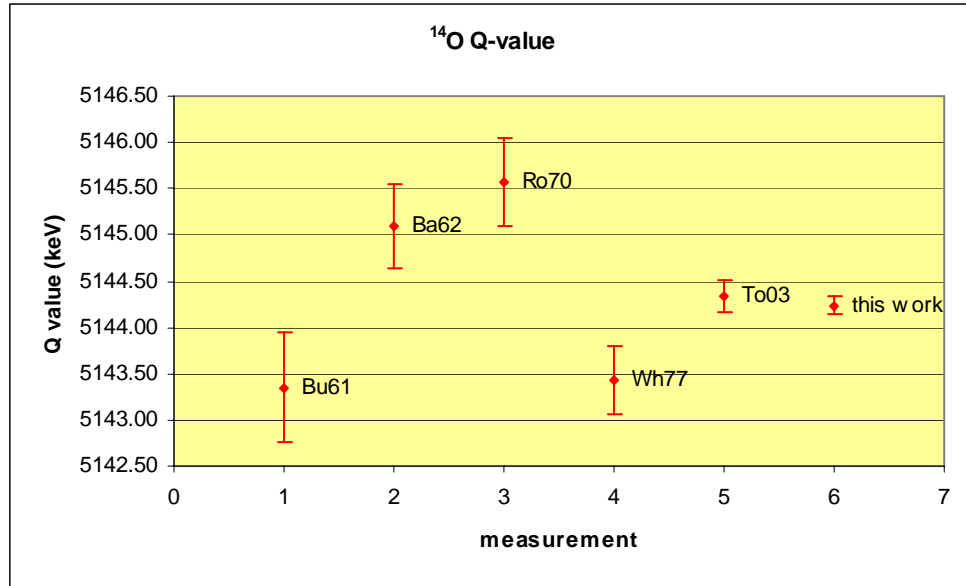


Fig. I-5. Q -value obtained for the superallowed decay of ^{14}O in this work compared to previous high precision results. Bu61,¹ Ba62,² Ro70,³ Wh77,⁴ and To03.⁵

The ^{26}Al isotopes were produced with a ^{16}O beam at 60 MeV impinging on a 1 mg/cm^2 rotating target of natural carbon. The reaction produces mostly the higher-spin long-lived groundstate of ^{26}Al rather than the 0^+ isomer ^{26m}Al , but since the excitation energy of this state is known to 13 eV accuracy we could perform the measurement on the groundstate and just add the excitation energy to get the superallowed decay Q value without loss in accuracy. The mass of the stable daughter nucleus ^{26}Mg is known extremely accurately from work at the SMILETRAP facility. We measured the mass of ^{26}Al to 0.17 keV accuracy and combining our result with the other quantities mentioned above yields the superallowed Q value to an accuracy of 0.175 keV. Similarly, the ^{42}Sc and ^{42}Ca isotopes were produced using a ^{32}S beam on a 1 mg/cm^2 natural carbon target. Again the low-lying long-lived higher spin isomer ^{42m}Sc is produced more abundantly than the 0^+ groundstate and its mass (in the doubly charged state) was measured to high accuracy together with those of ^{42}Ca (also doubly charged) and the singly

charged ions ^{21}Ne , ^{20}Ne and H_3^{18}O . The three calibration masses were found to agree to better than 1×10^{-8} and the Q value to the beta decay of ^{42m}Sc was measured to an accuracy of 0.22 keV. The excitation energy of the isomer is known to 0.06 keV accuracy and the corresponding superallowed decay Q value is obtained to 0.23 keV accuracy. Finally, the ^{34m}Cl long-lived isomer and ^{34}S isotopes were produced with a ^{24}Mg beam on the same carbon targets. They were measured together with the calibrating molecule $^{13}\text{CH}_5\text{O}$. The Q value of the superallowed decay is obtained from these measurements, together with the excitation energy of ^{34m}Cl which is known to 0.03 keV, to an accuracy of 0.24 keV.

These results reduce the experimental uncertainty on all these decays and significantly raise the ft value for two of them. The resulting ft value plot is shown in Fig. I-6. A paper presenting the resulting changes in the quality of the CVC test and the value of V_{ud} is in preparation.

*Argonne National Laboratory and The University of Chicago, †Argonne National Laboratory and University of Manitoba, Winnipeg, Manitoba, ‡Argonne National Laboratory and University of Maryland, §Argonne National Laboratory and Northwestern University, ¶Argonne National Laboratory and GANIL, Caen, France, ||McGill University, Montreal, Quebec, **Texas A&M University, ††Northwestern University.

¹J. W. Butler and R. O. Bondelid, Phys. Rev. **121**, 1770 (1961).

²R. K. Barden *et al.*, Phys. Rev. **127**, 583 (1962).

³M. L. Roush *et al.*, Nucl. Phys. **A147**, 235 (1970).

⁴R. E. White and H. Naylor, Nucl. Phys. **A276**, 333 (1977).

⁵N. R. Tolich *et al.*, Phys. Rev. C **67**, 035503 (2003).

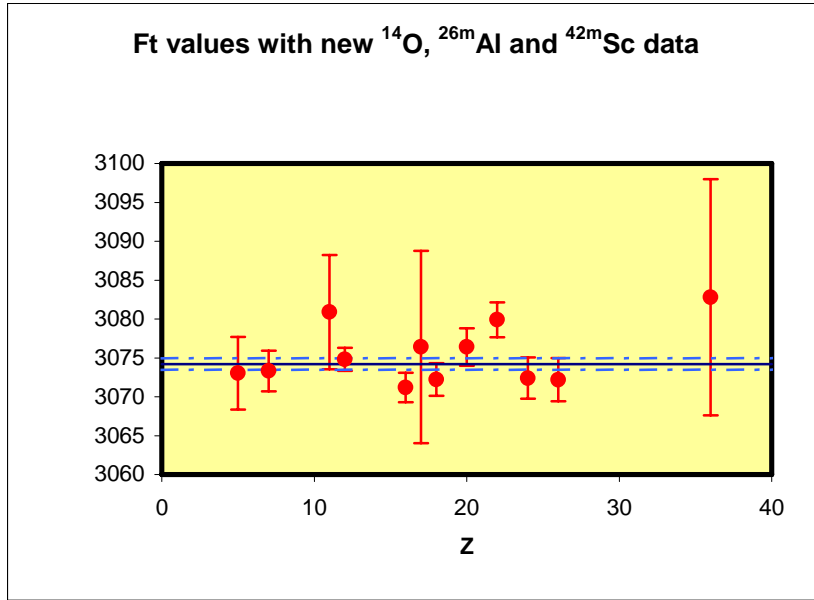


Fig. I-6. Ft -values for the most accurately known superallowed Fermi emitters with the inclusion of our new results for ^{14}O , ^{26m}Al and ^{42m}Sc .

b.2. Properties of Nuclei Relevant to $(0\nu 2\beta)$ Decay (J. P. Schiffer, S. Gros, C. L. Jiang, K. E. Rehm, X. Tang, J. Clark,* C. Deibel,* S. J. Freeman,† A. Heinz,* B. Kay,† K. Lesko,‡ P. D. Parker,* J. Qian,* A. Villari,§ V. Werner,* and C. Wrede*)

If neutrinoless double beta decay were to be observed, the very fact of the neutrino being its own antiparticle will be of great fundamental importance. In addition, the rate for this process would be the only direct measure of the neutrino mass, *if* the nuclear matrix element for this process is known. Unfortunately, at present, theoretical estimates of this matrix element vary by more than an order of magnitude for the case that is perhaps the most practical: $^{76}\text{Ge} \rightarrow ^{76}\text{Se} + 2\beta$. While this matrix element cannot be measured directly, other experiments can be related to aspects of the wavefunctions that are relevant. A program has been undertaken to carry out such measurements, that may help quantify the experimental knowledge of the relevant nuclei, and thereby provide bench marks for theoretical calculations. These measurements are of two types – the study of the occupancy of valence orbits and the measurement of pair-correlations in the nuclei relevant to ^{76}Ge decay.

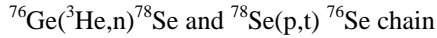
a) *Occupancy of Valence Orbits.* Since the process connects the 0^+ groundstates of ^{76}Ge to ^{76}Se , the occupation of the neutron and proton orbitals in these nuclei, and especially the differences in these

occupations are relevant to the process. Some data is available on this from past measurements, but the uncertainties are large and the results inconsistent. For the neutron occupations, since the orbits between $N = 28$ and 50 are almost filled with 44 neutrons, the best reaction is the neutron adding (d,p) reaction, and measurements were carried out at the Yale ESTU tandem with 15-MeV deuterons. These data are being analyzed. Special attention was paid to the relative cross sections. With 32 protons, the proton removal reaction is likely to be the most sensitive. The attempt to make a similar set of measurements of the $(d,^3\text{He})$ reaction at Yale were not successful and other options are being investigated.

b) *Pair correlations.* The 0^+ groundstates of even nuclei are characterized by strong pair correlations. To investigate the similarity in this respect between ^{76}Ge and ^{76}Se more quantitatively one would like to measure the

$^{76}\text{Ge}(p,t)^{74}\text{Ge}$ and $^{74}\text{Ge}(^3\text{He},n)^{76}\text{Se}$ reactions,

and also the



at or near 0° , where these reactions peak. The concentration of strengths in the lowest 0^+ states and the comparison of the magnitudes of the cross sections is

related to the similarity of the pair correlations in the two nuclei for neutrons and protons. Measurements of the (p,t) reactions cross sections have been made at 3 degrees at Yale, and possibilities for the (${}^3\text{He},n$) reactions are being investigated (e.g. at Notre Dame, in collaboration with J. Kolata, A. Aprahamian, H. Amro *et al.*).

*Yale University, †University of Manchester, United Kingdom, ‡Lawrence Berkeley National Laboratory, §GANIL, Caen, France.

b.3. Progress at the Beta-Decay Paul Trap (N. D. Scielzo, G. Savard, A. Levand, I. Tanihata, B. J. Zabransky, S. Caldwell,* J. A. Clark,† J. Fallis,† A. A. Hecht,§ D. Lascar,¶ H. Sharma,† K. S. Sharma,† A. Villari,** Y. Wang,† S. Gulick,‡ and R. Segel||)

The Beta-decay Paul Trap (BPT) is a radiofrequency quadrupole trap that has been specially designed to allow four sets of silicon and HPGe detectors to be brought close to the trapped ions. Radioactive ions held in this trap are a nearly ideal source of activity for measurements of β -decay angular correlations. The neutrino momentum can be inferred from the low-energy recoil of the daughter nucleus, which emerges from the trap volume without scattering. We are now prepared to make a measurement of the β - v correlation in the decay of ${}^{14}\text{O}$. The superallowed Fermi decay to the 0^+ excited state in ${}^{14}\text{N}$ is sensitive to scalar contributions to the weak interaction. Although recent experimental efforts using laser-trapped ${}^{38}\text{mK}$ have placed the tightest limits on scalar interactions by measuring the time-of-flight of the recoil ions in a drift electric field,¹ contributions as large as 6% of the dominant vector term are still not excluded. We will measure the β - v correlation using a different technique that will be subject to an entirely different set of systematic effects. We will infer the recoil momentum by measuring the Doppler shift of the 2.313 MeV γ -rays emitted from the 0^+ state detected in coincidence with the β particle.

We demonstrated that a sufficient amount of ${}^{14}\text{O}$ created in a $p({}^{14}\text{N},{}^{14}\text{O})n$ reactions could be brought nearly to rest as singly charged ions by the gas catcher and bunched in the radiofrequency (RF) ion cooler for subsequent transport to the BPT. The efficiency of this process is limited by the performance of the gas catcher for these low masses. Increasing the RF frequency applied to the cone from 1.6 to 3.5 MHz has increased the efficiency for extraction of light ions such as ${}^{14}\text{O}^{1+}$ by an order of magnitude. Using a 250 enA ${}^{14}\text{N}^{7+}$ beam, 500 ${}^{14}\text{O}^{1+}$ ions/sec were transported to the low-

energy beamline which is sufficient for achieving a $\sim 1\%$ statistical uncertainty for preliminary measurements of the β - v correlation coefficient. Further improvements in efficiency are expected with planned upgrades to the gas catcher, such as cooling the device to improve the purity of the helium buffer gas which is currently limited by outgassing.

We have tested the performance of the BPT offline using both stable ions such as ${}^{84}\text{Kr}^{1+}$ and fission fragments from a 300 μCi ${}^{252}\text{Cf}$ source placed directly in front of the gas catcher. Using ${}^{84}\text{Kr}^{1+}$, we have optimized the potentials for capture and storage of ions in the trap. The transfer of cooled ions from the Advanced Penning Trap to the BPT with nearly 100% efficiency was achieved. Cooling the BPT trap structure with LN_2 eliminates most impurities from the He buffer gas (only $\sim 1 \times 10^{-8}$ torr of H_2 remains) and allows us to achieve confinement times in the trap of longer than 50 seconds. With a He buffer gas pressure of roughly 10^{-5} torr, the trapped ions are cooled in 100 ms to energies of less than 0.3 eV. Ion cloud properties such as temperature, population, and fraction of impurities in the trap can be monitored by measuring the time-of-flight to a microchannel plate detector after deliberate ejection from the trap. The performance of the silicon and HPGe detectors, electronics, and data acquisition has been tested offline under a variety of operating conditions by detecting β - γ coincidences from the decay of trapped ${}^{146}\text{La}^{2+}$ ions which has a strong γ -ray transition at 258 keV. In 2006, the BPT will be loaded with ${}^{14}\text{O}$ ions and preliminary measurements of the β - v correlation will be made to determine the appropriate measures needed to minimize or eliminate any systematic effects that are discovered.

*Argonne National Laboratory and The University of Chicago, †Argonne National Laboratory and University of Manitoba, Winnipeg, Manitoba, ‡McGill University, Montreal, Quebec, §Argonne National Laboratory and University of Maryland, ¶Argonne National Laboratory and Northwestern University, ||Northwestern University
 **Argonne National Laboratory and GANIL, Caen, France.

¹A. Gorelov *et al.*, Phys. Rev. Lett. **94**, 142501 (2005).

b.4. β -Decay of ^{69,70,71}Kr (C. J. Lister, S. M. Fischer, D. Seweryniak, G. Savard, S. Gros, B. Blank,* G. Canchiel,* J. Giovinazzo,* I. Matea,* G. de France,† F. de Oliveira Santos,† J. C. Thomas,† S. Grevy,† J.-C. Dalouzy,† I. Stefan,† R. Wadsworth,‡ D Jenkins,‡ M. Bentley,‡ N. Singh Bondili,‡ P. Davies,‡ and J. A. Clark§)

The β -decay of neutron-deficient krypton isotopes can provide insights into distortion of Mirror Symmetry, can reveal information on the “waiting points” in rp-nucleosynthesis, and can clarify the influence of “deuteron-like” T = 0 np-pair correlations. However, to produce enough of these activities to allow spectroscopic measurement, and to make the environment free from other radio isotopes is very difficult. ^{69,70,71}Kr all have short lifetimes ($T_{1/2} = 32, 52, 101$ ms) so there is little time for production and separation.

A unique opportunity for decay spectroscopy of neutron-deficient krypton is offered using the SSSI production target at GANIL, followed by separation of the interesting fragments with the LISE spectrometer and velocity filter. The unique feature at GANIL is the high degree of purity of the final implanted residues which reduce the flux of interfering gamma-rays and

electrons. The short interval between implant and β -decay is ideal for this type of study. A primary beam of ~ 5 eμA of ⁷⁸Kr is fragmented on a nickel target. The light krypton isotopes are separated and implanted into a stack of silicon detectors, surrounded by an array of gamma-ray counters. Identified-implant-decay correlations can then be performed.

A collaboration has been formed and a proposal written and accepted for an experiment in 2006. Several physics questions can be addressed in one experiment. The decay of ⁶⁹Kr should reveal the ⁶⁹Br mass, which is important for rp-nucleosynthesis. The decay of ⁷⁰Kr provides information about np-pairing with T = 0 and T = 1, by identifying low-lying $J^\pi = 0^+$ and 1^+ . Finally, the decay of ⁷¹Kr reveals information on charge symmetry breaking and on the quenching of Gamow-Teller strength.

*Centre d'Etudes Nucleaires de Bordeaux-Gradignan, France, †GANIL, Caen, France, ‡University of York, Heslington, United Kingdom, §Yale University.

C. SPECTROSCOPY OF VERY HEAVY ELEMENTS

Detailed “in-beam” and isomer spectroscopy of very heavy nuclei ($Z > 100$), pioneered at ATLAS, is redefining our understanding of the stability of heavy nuclei. We have continued to inelastically excite actinide targets with very heavy beams above the Coulomb barrier. We have continued to use fusion reactions to study the entry regions, groundstate α -decays, and isomers in odd-A and even nuclei. This forefront research on very heavy nuclei continues to be a domain where the ATLAS beams and the Fragment Mass Analyzer (FMA) allow us to make unique contributions. Investment in rotating targets and new focal-plane detectors has been important in making this research competitive with gas-filled separators.

c.1. Properties of the Lightest Nobelium Isotopes (D. Peterson, B. B. Back, R. V. F. Janssens, T. L. Khoo, C. J. Lister, D. Seweryniak, M. P. Carpenter, C. Davids, C. L. Jiang, T. Lauritsen, S. Zhu, A. Hecht,* X. Wang,† F. G. Kondev,‡ P. Chowdhury,§ S. K. Tandel,§ S. Tandel,§ A. Heinz,¶ J. Qian,¶ and R. Winkler¶)

Recent experiments in the synthesis of superheavy elements utilizing beams of ^{48}Ca are both exciting and puzzling at the same time. To study some systematics in the $Z > 100$ region, two separate studies^{1,2} of neutron-deficient nobelium isotopes via the $^{204}\text{Pb}(^{48}\text{Ca},\text{xn})$ reaction were undertaken by groups working in Dubna. Both experiments only observed spontaneous fission (SF) decay, but measured three different lifetimes (60[1], 36[2], and 6[2] μs). Belozеров *et al.*² attributed the 36 μs lifetime to ^{249}No , but the possibility of it being an isomeric decay in ^{250}No could not be excluded. Those experiments also suffered from limited statistics, and the 3n channel necessary to produce ^{249}No is expected to be very small at the energies of Ref. 2. The present experiment was designed to reconcile these apparent discrepancies utilizing the Fragment Mass Analyzer (FMA) at Argonne National Laboratory. The experimental details were provided in a previous annual report.³ The results are presented here.

A total of 158 implant-fission correlations were observed, consisting of two different activities. The FMA unambiguously identified both activities as originating from the same compound nucleus, ^{250}No . The decays are presented in Fig. I-7, where the implant-decay correlation time is plotted against the mass number provided by the FMA in the left panel. The right panels of Fig. I-7 show the projection onto the mass axis for different time windows—either long or short correlations. The mass distributions have essentially the same width and centroid regardless of correlation time. This indicates the same origin for all decays. Performing a two-component fit to the decay

curve yields half-lives of $t_{1/2} = 3.7^{+1.1}_{-0.8}$ μs and $t_{1/2} = 43^{+22}_{-15}$ μs for the activities. We also obtained production cross sections of 12^{+18}_{-4} nb and 5^{+3}_{-2} nb for the short and long components, respectively. The shorter lifetime has been assigned to the groundstate of ^{250}No and the longer lifetime was assigned to an isomeric state based on the cross section ratios and the prediction of a 2-quasineutron isomer around 1050 keV from multi-quasiparticle blocking calculations. Furthermore, from those calculations and analogy to the $N = 148$ isotope, ^{244}Cm , the isomeric state is predicted to be a $K^\pi = 6^+$ configuration.

The sensitivity of the experiment was insufficient to determine whether the fission activity associated with the isomeric state is due to direct fission from that state or whether the isomer γ -decays through a K-forbidden transition to the groundstate first, which then proceeds to fission. Thus, the SF partial half-life from the isomer is $t_{1/2}^{\text{iso}} \geq 43$ μs which further implies that there is an extremely large SF hindrance factor associated with this 2-quasiparticle state of the order of 10^6 assuming a 1 MeV excitation and the average increase in penetrability through the barrier due to that excitation. The fact that the groundstate SF lifetime of ^{250}No is 10^6 times shorter than that of ^{252}No indicates a drastic change of the fission barrier height or width for the nobelium isotopes away from the $N = 152$ deformed subshell closure.

This experiment also searched for an α -decay branch from ^{250}No . No definitive decays were observed. One decay with an energy of 7.5 MeV was correlated to an implant 19.4 μs prior. Though this time correlation is

interesting, the expected energy for α -decay from ^{250}No is in excess of 9 MeV. The background rates in the experiment were such that the chance of this correlation being random is $<10^{-8}$. No other No nuclei have α -decay energies this low. If it is real, the anomalously low energy could be due to partial energy loss from the α particle escaping the detector. In any case, the observation of a single decay would place limits on the α branch at 1.8% for the groundstate and 4.4% for the isomer.

The results of this experiment require an update to the latest compilations of data sheets which improperly assign the longer (43 μs) activity to the isotope ^{249}No rather than the isomer $^{250\text{m}}\text{No}$. As in the studies of Refs. 1 and 2, this experiment also found no evidence for the 250 μs SF activity originally assigned to ^{250}No in 1975.⁴

*University of Maryland, †University of Notre Dame, ‡Nuclear Engineering Division, Argonne National Laboratory, §University of Massachusetts-Lowell, ¶Yale University.

¹Yu. Ts. Oganessian *et al.*, Phys. Rev. C **64**, 054606 (2001).

²A. V. Belozherov *et al.*, Eur. Phys. J. A **16**, 447-456 (2003).

³D. Peterson *et al.*, section c.4. of the 2004 annual report (2005).

⁴G. M. Ter-Akopyan *et al.*, Nucl. Phys. **A255**, 509 (1975).

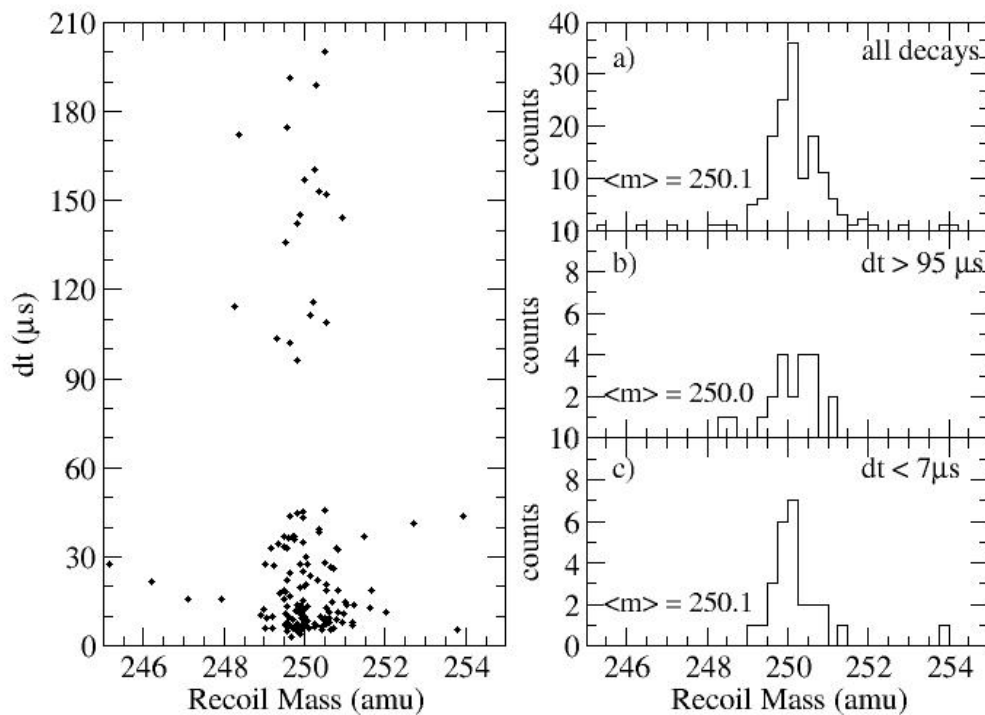


Fig. I-7. Characteristics of the spontaneous fission decays observed in the present experiment. The left panel plots the implant-decay time correlation, dt , versus the mass number of the implanting residue determined from the focal plane of the FMA. The right panels illustrate the projection onto the mass axis for all decays (a), purely long decays (b), and primarily short decays (c). The centroid of each mass distribution is also listed.

c.2. $K = 8^-$ Isomers and $K = 2^-$ Octupole Bands in ^{252}No and $N = 150$ Isotones

(A. Robinson, T. L. Khoo, D. Seweryniak, S. Gros, D. Peterson, I. Ahmad, B. B. Back, M. P. Carpenter, C. N. Davids, J. Greene, A. Hecht, R. V. F. Janssens, F. G. Kondev, T. Lauritsen, C. J. Lister, E. F. Moore, S. Zhu, S. K. Tandel,* P. Chowdhury,* U. Tandel,* A. Heinz,† X. Wang,‡ P. A. Butler,§ R. Herzberg,§ G. Jones,§ S. Eeckhaudt,¶ P. T. Greenlees,¶ R. Julin,¶ M. Leino,¶ J. Uusitalo,¶ P. Reiter,|| and G. Mukherjee**)

In shell-stabilized, heavy nuclei around ^{254}No , many of the orbitals around the Fermi level have large projections of their spin along the symmetry axis so that high- K isomers should be common. The isomers, which can be studied in a quiet environment far from the target, provide opportunities to investigate the excited configurations of nuclei populated with sub-microbarn cross sections, not only of the isomers, but also of lower-lying rotational bands fed in the isomeric decays. The occurrence of K isomers reveal the violation of K -selection rules, indicating that K is a good quantum number and that the nucleus has prolate shape with axial symmetry. The energies of 2-quasiparticle states provide incisive tests of theories. An example is the $K = 8^-$ isomer at 1296 keV in ^{254}No (see section c.3.), which decays to a $K = 3^+$ band. The energies of the $K = 3^+$, 8^- states, which are built on proton configurations, reveal that Woods-Saxon proton single-particle energies are accurate for Z up to at least 102. In ^{252}No , 2-quasiparticle energies calculated with the Woods-Saxon potential also suggest a $K = 8^-$ isomer, but built instead on neutron states, at a lower energy of 1.01 MeV. Hence, detection of this predicted isomer constitutes a test of the Woods-Saxon single-particle energies.

The $^{206}\text{Pb}(^{48}\text{Ca},2n)$ reaction was used to populate states in ^{252}No . The nuclides were transported and uniquely identified by the Fragment Mass Analyzer (FMA). The nuclides implanted into individual $1 \times 1 \text{ mm}^2$ pixels of a double-sided Si strip detector. Time and spatial correlations then identified the decay of an isomer, i.e. in each pixel, a delayed coincidence between the

implant and an electron signal, with sum energy 100-500 keV. Gamma rays from the isomer were detected in prompt coincidence with the delayed electron signal. In this manner, an isomer was discovered in ^{252}No , with a half-life of 114 ms. Preliminary analysis suggests that the isomer has quantum numbers $I, K^\pi = 8, 8^-$, and that it decays via multiple pathways into a $K^\pi = 2^-$ octupole vibrational band.

The preliminary energy of the isomer, ~ 1.25 MeV, is close the predicted energy of a neutron $K = 8^- \{[934]9/2, [624]7/2\}$ state, but nearer to the measured energy for the proton $K = 8^-$ configuration in ^{254}No . At the moment, the configuration in ^{252}No is not clear, but the neutron configuration is favored since the decay pattern is analogous to that of the $N = 150$ isotones, ^{246}Cm and ^{250}Fm .^{1,2} Comparisons with theoretical 2-quasiparticle $K = 8^-$ energies are currently being conducted, so that the $K = 8^-$ energies in the $N = 150$ isotones can be used as tests of theory.

In like fashion, the $K = 2^-$ octupole vibrational energy of the $N = 150$ isotones will serve as another test. For $Z = 96-102$, the $K = 2^-$ energies are 842, 592, 880 and 931 keV. Qualitatively, the exceptionally low energy in ^{248}Cf is understood in terms of a favorable confluence of low energies for both neutron and proton $K = 2^-$ configurations, which is predicted with the Woods-Saxon potential. In the other nuclei, the proton configuration moves to higher energy. It will be an interesting challenge for self-consistent theories to reproduce this trend.

*University of Massachusetts-Lowell, †Yale University, ‡University of Notre Dame, §University of Liverpool, United Kingdom, ¶University of Jyväskylä, Finland, ||Universität zu Köln, Germany, **Variable Energy Cyclotron Center, Kolkata, India.

¹I. Ahmad, in Proc., Frontiers in Nuclear Physics, Dubna, p. 31 (1995).

²P. T. Greenlees *et al.*, private communication (2006).

c.3. Two-Quasiparticle States in ^{254}No and the Stability of Superheavy Nuclei

(T. L. Khoo, D. Seweryniak, I. Ahmad, B. Back, R. Blinstrup, M. P. Carpenter, J. Chapman, C. N. Davids, R. V. F. Janssens, F. G. Kondev, T. Lauritsen, C. J. Lister, E. F. Moore, D. Peterson, S. F. Zhu, S. K. Tandel,* G. Mukherjee,*[†] P. A. Butler,[‡] P. Chowdhury,* P. T. Greenlees,[§] A. A. Hecht,[†][¶] A. Heinz,^{||} R.-D. Herzberg,[‡] P. Ikin,[‡] G. D. Jones,[‡] P. Reiter,** U. S. Tandel,* and X. F. Wang[†],^{††})

Two-quasiparticle (qp) states in shell-stabilized nuclei probe the levels that govern the stability of superheavy nuclei, test 2-qp energies from theory and, thereby, check their predictions of magic gaps. We have identified in ^{254}No ($Z = 102$) 2- and 4-qp isomers, with quantum numbers $K^\pi = 8^-$ and (14^+) , and a low-energy 2-qp $K^\pi = 3^+$ state (Figs. I-8 and I-9). It is significant that a constituent of the $K^\pi = 3^+$ configuration is the $[521]1/2$ orbit, from the spherical $f_{5/2}$ shell, which lies above a $Z = 114$ gap that appears with Woods-Saxon (WS) single-particle energies. The use of WS single-particle energies reproduces the experimental proton 2-qp energies in ^{254}No (Fig. I-10). The WS potential also systematically reproduces the 1-qp energies in odd-A heavy nuclei.² These results indicate that WS energies are valid for Z up to 102 and suggest that a proton gap would occur at $Z = 114$ -- if the WS potential continues to describe the proton energy levels of nuclei with $Z > 102$. In contrast, there are shortcomings in the 2-qp energies from self-consistent mean-field theories (Fig. I-10). Therefore, their

predictions of magic gaps at $Z = 120$ and 126 should be viewed with reservations. The parameters of the interactions used in self-consistent mean-field SHFB and RMF models have been adjusted to fit bulk properties of closed-shell nuclei. Thus, the success of their single-particle energies⁵ is impressive, but definitely do require improvements, e.g. a lowering of the proton $i_{13/2}$ orbit,⁴ to reproduce *all* measured 1- and 2-qp energies. To preserve the virtue of self-consistency when extrapolating to the heaviest nuclei, there is a need for a new interaction designed for this purpose.⁵

In summary, spectroscopic measurements of 2-qp states in ^{254}No provide the first experimental information on the proton magic shell gap for superheavy nuclei by discriminating among the theories that make predictions on the gap. A preliminary report of this work has been given⁶ and has been published in Physical Review Letters.⁷

*University of Massachusetts-Lowell, [†]Argonne National Laboratory, [‡]University of Liverpool, United Kingdom, [§]University of Jyväskylä, Finland, [¶]University of Maryland, ^{||}Yale University, ^{**}Universität zu Köln, Germany, ^{††}University of Notre Dame.

¹S. Ćwiok *et al.*, *Comp. Phys. Comm.* **46**, 379 (1987).

²R. Chasman *et al.*, *Rev. Mod. Phys.* **49**, 833 (1978); A. Parkhomenko and A. Sobiczewski, *Acta Phys. Pol.* **B35**, 2447 (2004), *ibid.* **B36**, 3115 (2005).

³P.-H. Heenen, private communication (2006).

⁴M. Bender *et al.*, *Nucl. Phys.* **A723**, 354 (2003).

⁵A. V. Afanasjev *et al.*, *Phys. Rev. C* **67**, 024309 (2003).

⁶G. Mukherjee *et al.*, *AIP Conf. Proc.* **764**, 243 (2005), D. Seweryniak and T. L. Khoo editors.

⁷S. K. Tandel *et al.*, *Phys. Rev. Lett.* **97**, 082502/1-4 (2006).

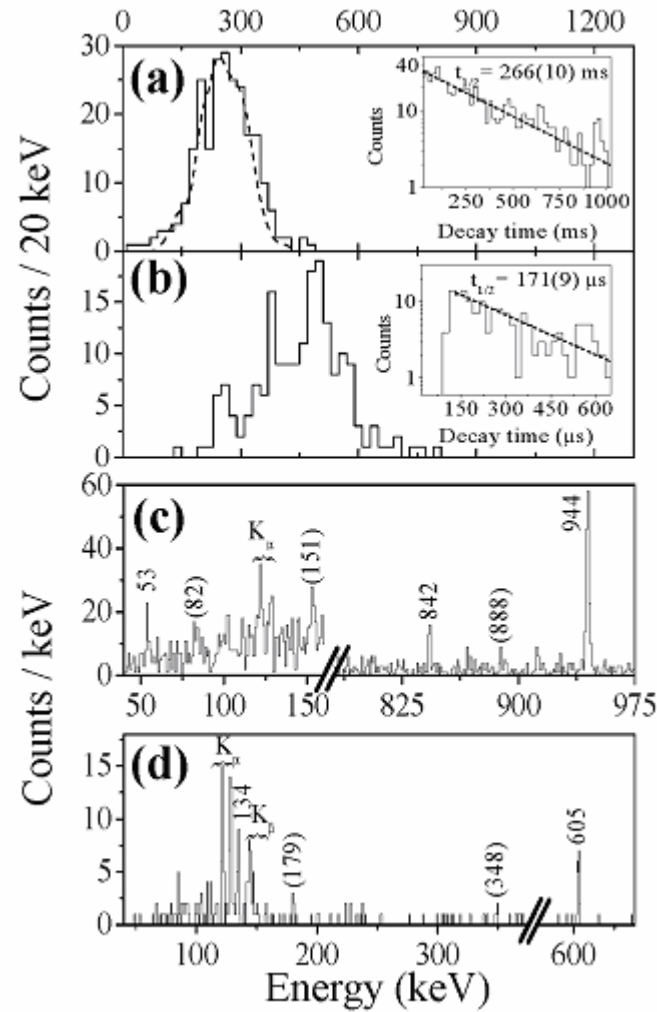


Fig. I-8. (a) Electron-sum energy spectrum from the decay of the 266-ms isomer. The attenuation at low energy is due to electronic thresholds; the calculated spectrum (dashed line) includes this effect. (b) Same as (a) for the 171- μ s isomer. Insets in (a,b) show decay time distributions, with the results of least-squares fits given as dashed curves. Electronic dead time negates the first ~ 80 μ s of data. (c, d) Gamma-ray spectra from the long- and short-lived isomers, respectively.

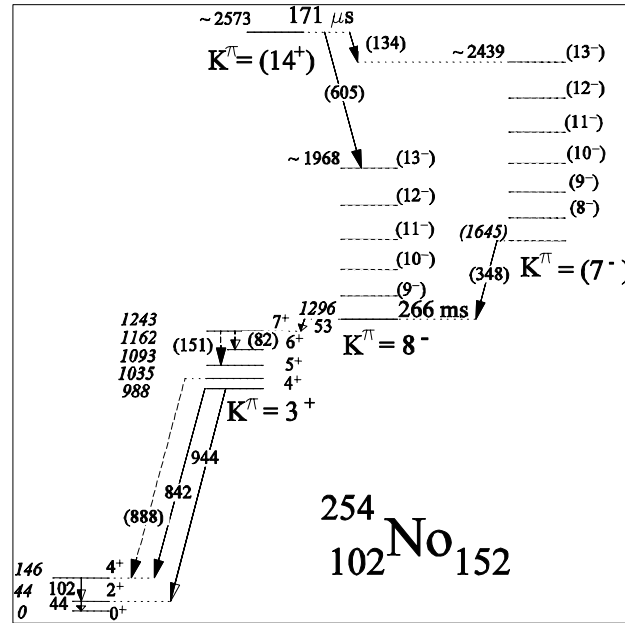


Fig. I-9. Decay schemes proposed for the 2- and 4-qp isomers. Although transitions are not detected from every level of the $K^\pi = 3^+$ band, the levels are firmly established via a model that accounts for all observed level spacings. The scheme above the 266 ms isomer is based on our model of the decay; γ rays within the $K^\pi = 8^-$ and $K = 7^-$ bands were not detected.

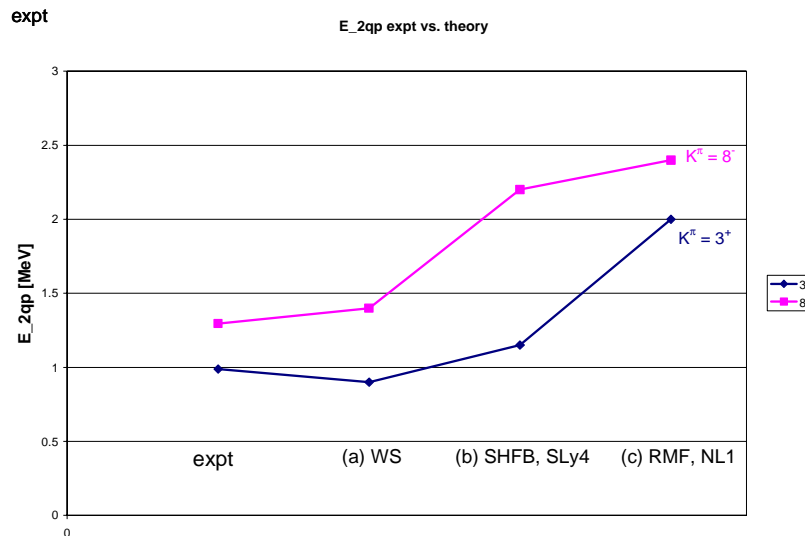


Fig. I-10. Comparison of 2-qp energies from experiment (expt) and theory (a-c). The 2-qp states are built on the proton configurations $K^\pi = 3^+ \{[514]7/2, [521]1/2\}$ and $K^\pi = 8^- \{[514]7/2, [624]9/2\}$. (a) From Woods-Saxon single-particle energies (“universal” parameters)¹ and a Lipkin-Nogami treatment for pairing. We assume -100 keV for the residual interaction in the spin-singlet configurations; the strengths of the neutron and proton pairing force ($G_n = 17.2/A$, $G_p = 24/A$) are chosen so that the calculated groundstate pair gaps for nuclei near ^{254}No are close to Δ ,⁵ the 5-point groundstate mass difference, which provides a good approximation of the pair gap. Our results, together with systematic examinations of 1-qp energies by Ref. 2, indicate that WS energies are valid for Z up to ~ 102 . (b) Skyrme Hartree-Fock Bogolyubov theory with the SLy4 interaction.^{3,4} (c) Relativistic mean-field theory with the NL1 interaction (based on qp energies given in Fig. 5 of Ref. 5).

c.4. Limiting Angular Momentum in ^{254}No and ^{220}Th (T. L. Khoo, M. Asai, D. Seweryniak, I. Ahmad, M. P. Carpenter, C. N. Davids, S. Freeman, J. Greene, N. Hammond, R. V. F. Janssens, F. G. Kondev, T. Lauritsen, C. J. Lister, P. A. Butler,[‡] P. Chowdhury,[†] J. A. Cizewski,[§] R. Gramer,[†] R. D. Herzberg,[‡] A. Heinz,[¶] P. Ikin,[‡] M. Johnson,[§] G. D. Jones,[‡] G. Mukherjee,^{*} E. Ngijoi-Yogo,[†] and P. Reiter^{||})

Our investigations¹ of the shell-stabilized nobelium nuclei have shown that they survive up to high angular momentum and that the fission barrier is >5 MeV for spins larger than $10 \hbar$. In other words, shell-stabilized nuclei are quite robust at high spin. Stimulated by these experiments, several self-consistent mean-field theory calculations have found that the fission barrier that the barrier remains sizeable at high spin. The HFB predictions of Egido and Robledo² suggest that ^{254}No should survive up to spin 30 - 35 \hbar .

To determine how much angular momentum a ^{254}No nucleus can sustain against fission, we have conducted an experiment with Gammasphere operated in coincidence with the FMA. This combination provides a capability, which is unique in the world for reactions

with μb cross sections, namely the ability to detect γ rays with both high resolution and with 4π calorimetric capability. The maximum input angular momentum was increased from ~ 22 to $\sim 33 \hbar$ by increasing the beam energy from 219 to 223 MeV. Although ^{254}No is loosely bound, it is quite stable against rotation; its fission barrier remains large enough at high angular momentum for it to survive to a spin 33 \hbar . This is strikingly demonstrated by the fact that the maximum angular momentum that we have observed in ^{220}Th is substantially lower, only 20 \hbar , even though thorium has 12 protons less than nobelium. The reason is that the fission barrier in thorium is due mainly to the liquid drop term, whereas in nobelium the principal contribution is from the shell-correction energy.

*Argonne National Laboratory and University of Massachusetts-Lowell, [†]University of Massachusetts-Lowell, [‡]University of Liverpool, United Kingdom, [§]Rutgers University, [¶]Yale University, ^{||}Universität zu Köln, Germany.

¹P. Reiter *et al.*, Phys. Rev. Lett. **84**, 3542 (2000).

²L. Egido and L. Robledo, Phys. Rev. Lett. **85**, 1198 (2000).

c.5. Structure of the Odd-A, Shell-Stabilized Nucleus ^{253}No (T. L. Khoo, I. Ahmad, A. Heinz, T. Lauritsen, C. J. Lister, D. Seweryniak, M. P. Carpenter, C. N. Davids, J. P. Greene, F. Kondev, R. V. F. Janssens, A. A. Sonzogni, I. Wiedenhöver, P. Reiter,^{*} A. Afanasjev,[†] P. A. Butler,[‡] A. J. Chewter,[‡] J. A. Cizewski,[§] P. T. Greenlees,[¶] K. Helariuta,[¶] R.-D. Herzberg,[‡] G. Jones,[‡] R. Julin,[¶] H. Kankaanpää,[¶] H. Kettunen,[¶] W. Korten,[§] P. Kuusiniemi,[¶] M. Leino,[¶] S. Siem,^{||} and J. Uusitalo[¶])

The heaviest nuclei are stabilized by a shell-correction energy, which lowers the groundstate, thereby creating a barrier against fission. The shell-correction energy originates from the clustering of single-particle orbitals. Hence, the single-particle eigenstates form the basis of the shell stabilization. The most direct data on the orbital energies come from odd-A nuclei, providing our motivation to investigate the odd-N nucleus ^{253}No . The single-particle energies also provide a direct test of nuclear models that predict the properties of superheavy nuclei. Thus, by testing model predictions¹ against data on the heaviest nuclei that are accessible for spectroscopy, one may judge their reliability for predicting the properties of superheavy elements, e.g. the next spherical shell closures beyond ^{208}Pb .

The production cross section of $^{207}\text{Pb}(^{48}\text{Ca},2n)^{253}\text{No}$ reaction was measured as $\sim 0.5 \mu\text{b}$ at Jyväskylä. In a subsequent experiment at Argonne, the γ rays were detected with Gammasphere, in coincidence with ^{253}No residues detected in the FMA. The γ -ray spectrum for ^{253}No has many weak lines, but is dominated by the K X-rays. Heavy odd-A nuclei, such as ^{253}No , represent the limits of in-beam γ spectroscopy due to overwhelming conversion electron competition in M1 transitions. Of the expected low-lying configurations in ^{253}No , only the $7/2^+[624]$ orbital is expected to have sufficiently small M1 branching ratios to permit detection of intraband E2 γ rays. However, due to the low γ -ray cross sections of 25-50 nb, it was necessary to develop new methods based on (a) quantitative comparisons of results from experiment and from

model predictions; (b) enhancement of transitions with high γ multiplicity; and (c) finding evidence for a rotational band in a sparse $\gamma\gamma$ matrix.

The kinematic and dynamic moments of inertia, $J^{(1)}$ and $J^{(2)}$, of the $7/2^+[624]$ band in ^{253}No are rather well reproduced³ by the self-consistent cranked relativistic Hartree Bogoliubov (CRHB) theory. The moments of inertia in an odd-even nucleus is sensitively dependent on (and hence characteristic on) the occupied orbital. In contrast, the theoretical description¹ of the $J^{(2)}$ moments of inertia of the even-even nuclei $^{252,254}\text{No}$ is not as good. That is due to a less-than-perfect description of the quasiparticle energies.

A bandhead energy of 355 keV was deduced from the data for the $7/2^+[624]$ configuration. This energy

compares with theoretical predictions of 240, 400 and 1200 keV, which are given by, respectively, a Nilsson model based on the Wood-Saxon potential and by self-consistent mean-field theories using the Skyrme Hartree-Fock or CRHB methods.¹⁻² Of course, a systematic test of theory should encompass a set of quasiparticle states, and has recently been performed for self-consistent mean-field theories.¹⁻² For example, Ref. 1 points out that the relativistic mean-field method is able to describe many single-particle energies, but that several (including the $7/2+[624]$ orbital) that originate from specific spherical orbitals deviate by more than 1 MeV from experimental energies.

This work has been published in Phys. Rev. Lett.³

*Universität zu Köln, Germany, †University of Notre Dame, ‡University of Liverpool, United Kingdom, §Rutgers University, ¶University of Jyväskylä, Finland, ||University of Oslo, Norway.

¹A. Afanasjev *et al.*, Phys. Rev. C **67**, 024309 (2003).

²M. Bender *et al.*, Nucl. Phys. A**723**, 354 (2003).

³P. Reiter *et al.*, Phys. Rev. Lett. **95**, 032501 (2005).

c.6. Calculations of 2-Quasiparticle Energies in Heavy Shell-Stabilized Nuclei

(T. L. Khoo and F. G. Kondev*)

Two-quasiparticle (qp) states in shell-stabilized nuclei probe the levels that govern the stability of superheavy nuclei, test 2-qp energies from theory and, thereby, check their predictions of magic gaps. Spurred by our observations of 2-qp states in ^{254}No (see section c.3.), we have calculated the energies for a number of 2-qp states in the heaviest nuclei. The calculations are based on single-particle energies from the “universal” parameterization of the Woods-Saxon potential and the Lipkin-Nogami prescription for pairing. The strengths of the pairing interaction were taken as $G_p = 24/A$ and $G_n = 17.8/A$ for protons and neutrons. With these strengths, the values of the calculated pair gaps are in fair agreement with experimental values (where known) of $\Delta^{(5)}$, the 5-point mass differences. Ref. 1 has shown that $\Delta^{(5)}$ provides a close approximation of the pair gap, which is given by $\Delta + \lambda_2$ in the Lipkin-Nogami formalism. The calculated energies for neutron and proton configurations are given in columns 6 and 7 in Table I-1; where no values are given, calculations have not yet been performed.

It is seen that the calculation reproduce measured energies within 0.3 MeV, indicating that (a) the Woods-Saxon energies are accurate and (b) that the pairing strength has been satisfactorily chosen. For ^{254}No , calculations with the self-consistent Skyrme Hartree-Fock Bogolyubov theory with the SLy4 force reproduce the $K^\pi = 3^+$ energy, but the calculated 8^- energy is too high by ~ 1 MeV. Estimated energies for the relativistic mean-field theory with the NL1 force show discrepancies of >1 MeV for both states. These results demonstrate that (i) 2-qp energies provide discriminating tests of theory; (ii) the single-particle energies from self-consistent mean-field theories require improvements; (iii) the predicted proton gaps at $Z = 120$ and 126 given by self-consistent theories should be treated with caution; and (iv) that a gap of ~ 2.2 MeV would occur at $Z = 114$, if the Woods-Saxon potential continues to provide accurate energies for $Z > 102$.

*Nuclear Engineering Division, Argonne National Laboratory.

¹T. Duguet *et al.*, Phys. Rev. C **65**, 014311 (2002).

Table I-1. 2-qp energies from experiment and from calculations with a Woods-Saxon potential.

Nucleus	K^π	configuration	E(exp)	$E_{2n}(\text{calc})$	$E_{2p}(\text{calc})$
^{244}Cm	6^+	nn[622]5/2 [624]7/2	1.042	1.06	
^{246}Cm	8^-	nn[734]9/2 [624]7/2	1.180	1.01	
^{250}Fm	8^-	nn[734]9/2 [624]7/2	1.196		
^{256}Fm	7^-	pp[514]7/2 [633]7/2	1.426		
^{250}No	6^+	nn[622]5/2 [624]7/2		0.96	
^{252}No	8^-	nn[734]9/2 [624]7/2	1.284	1.01	
	8^-	pp[514]7/2 [624]9/2			1.42
^{254}No	3^+	pp[514]7/2 [521]1/2	0.988		0.90
	8^-	pp[514]7/2 [624]9/2	1.296		1.40
	5^-	pp[624]9/2 [521]1/2			1.23
	7^-	pp[514]7/2 [633]7/2	(1.645)		1.50
	4^-	nn[734]9/2 [620]1/2		1.36	
	6^-	nn[734]9/2 [622]3/2		1.47	
	8^-	nn[734]9/2 [624]7/2		2.04	
	8^-	nn[734]9/2 [613]7/2			
	4^+	nn[624]7/2 [620]1/2		1.68	
	3^+	nn[613]7/2 [620]1/2			

c.7. Octupole Correlations in the Lightest Even-Even Pu Isotopes (R. V. F. Janssens, S. Zhu, M. P. Carpenter, I. Ahmad, J. P. Greene, T. L. Khoo, T. Lauritsen, C. J. Lister, D. Seweryniak, X. Wang,* S. Freeman,† F. G. Kondev,‡ I. Wiedenhöver,§ A. Bernstein,§ P. Wilson,§ E. Diffenderfer,§ C. Teal,§ A. Larabee,¶ B. Meredith,¶ and U. Garg*)

Octupole correlations have attracted much attention over the years, and the actinide nuclei remain an interesting source of information because they offer the possibility to investigate the interplay between collective rotation and octupole degrees of freedom. In previous work by I. Wiedenhöver, *et al.*,¹ it was suggested that, in the lightest Pu isotopes, strong octupole correlations lead to the absence (239, 240) or delay in frequency (238) of the strong proton alignment observed in the heavier (241, 242, 243, 244) Pu isotopes.

The present work is centered on investigating the octupole correlations in even-even (238, 240, 242) Pu nuclei by (1) extending the yrast band (GSB) and excited bands to the highest spins and identifying every possible connecting transition between bands; (2) extracting the relevant properties of the bands such as alignments, routhians, branching ratios etc.; (3) searching for new band structures.

A series of 3 experiments has been carried out with Gammasphere at ATLAS. The so-called "unsafe"

Coulomb excitation technique (beam energy is about 15% above Coulomb barrier) was used in order to enhance the feeding of the highest spin states. Billions of events with fold 3 or higher were collected. In the subsequent data analysis, the raw data was converted into both the traditional RADWARE format (Cube and Hypercube) and the latest BLUE database format.

In ^{240}Pu , which possibly evolves from an octupole vibrator at low spin to an octupole rotor at high spin,¹ in agreement with theoretical suggestions by Jolos and von Brentano,^{2,3} we extended both the GSB and octupole band, and found $(I + 1)^+ \rightarrow I^-$ E1 linking transitions at high spins, which can be viewed as the solid evidence for an octupole rotor. Moreover, the investigation in the branching ratios, between the inter- and in-band transitions, also supports the conclusion of a stable octupole deformation present at high spin. Simultaneously, we found 1 new positive and 1 new negative band. Their interpretation is under discussion.

In ^{242}Pu , we observed the GSB and 5 excited bands (1 of positive and 4 of negative parity) (see Fig. I-11).

One of the most notable differences between ^{242}Pu and ^{240}Pu is that in ^{242}Pu all excited bands decay to the GSB. The so-called “Backbending” occurs at $\hbar\omega \sim 0.25$ MeV, and no pattern of interleaved states with alternating spin and parity is observed.

The analysis of the ^{238}Pu data is on-going. In the meantime more detailed calculations are also being carried out.

*University of Notre Dame, †University of Manchester, United Kingdom, ‡Nuclear Engineering Division, Argonne National Laboratory, §Florida State University, ¶Greenville College.

¹I. Wiedenhöver *et al.*, Phys. Rev. Lett. **83**, 2143 (1999).

²R. V. Jolos and P. von Brentano, Phys. Rev. C **49**, R2301 (1994).

³R. V. Jolos and P. von Brentano, Nucl. Phys. **A587**, 377 (1995).

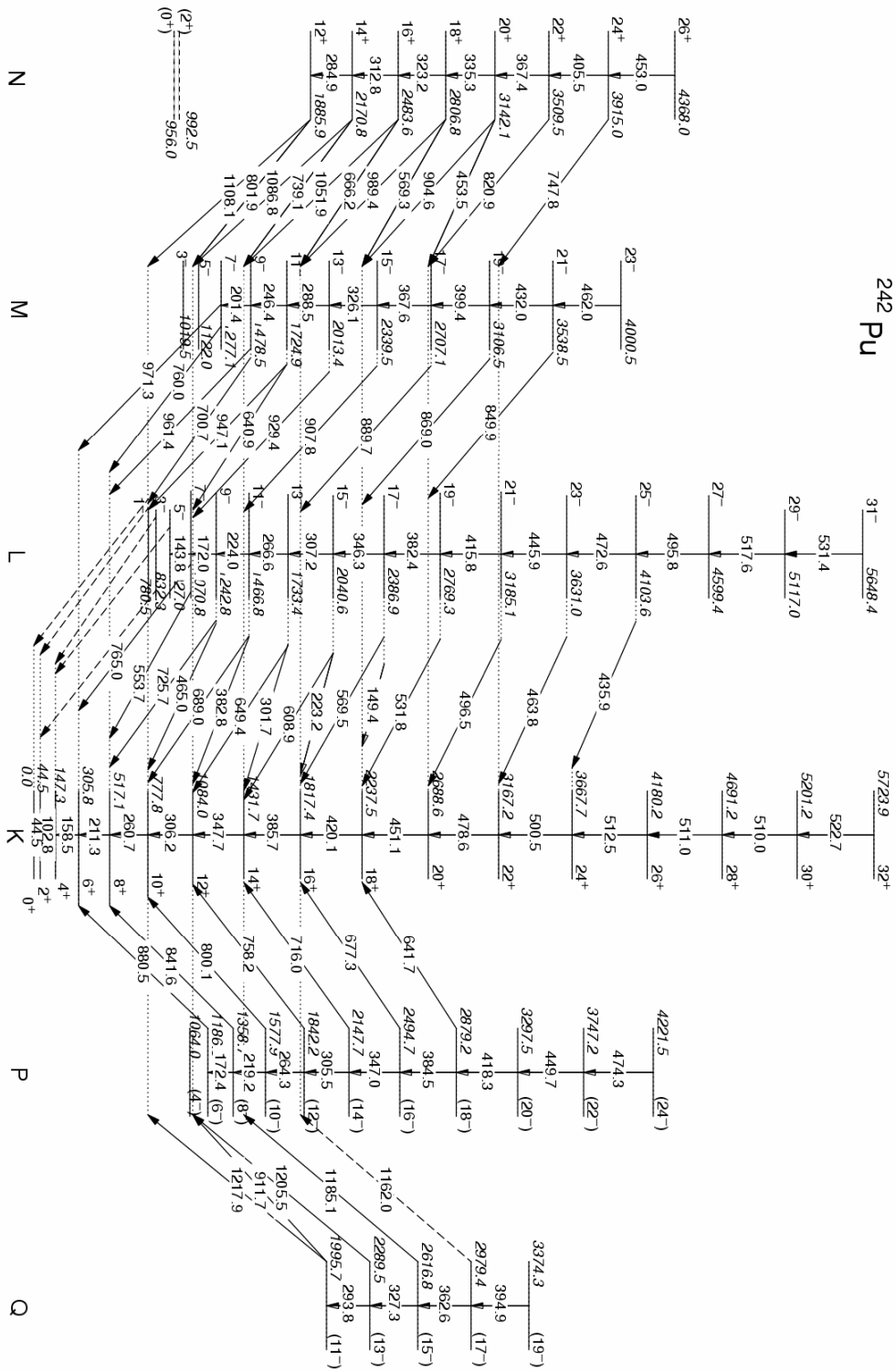


Fig. I-11. Proposed level scheme for ^{242}Pu .

- c.8. Strength of Octupole Correlations in the Actinides: Contrasting Behavior in the Isotones ^{237}U and ^{239}Pu** (S. Zhu, R. V. F. Janssens, M. P. Carpenter, I. Ahmad, N. J. Hammond, T. L. Khoo, F. G. Kondev, T. Lauritsen, C. J. Lister, E. F. Moore, D. Seweryniak, G. J. Lane*,[†] I. Wiedenhöver,[‡] A. P. Byrne,* P. Chowdhury,[§] D. Cline,[¶] A. N. Deacon,[|] G. D. Dracoulis*, S. J. Freeman,[|] G. D. Jones,** A. O. Macchiavelli,[†] J. F. Smith,[|] and C. Y. Wu[¶])

The high spin states in the odd-neutron isotones ^{239}Pu and ^{237}U have been studied. Striking differences were found in the high-spin properties of rotational bands built on the $1/2^+[631]$ groundstates in these two nuclei.

These differences mirror those observed in the even-even Pu and U immediate neighbors and appear to be related to the strength of octupole correlations. The results of this study were published.¹

*Australian National University, Canberra, Australia, [†]Lawrence Berkeley National Laboratory, [‡]Florida State University, [§]University of Massachusetts-Lowell, [¶]University of Rochester, [|]University of Manchester, United Kingdom, **University of Liverpool, United Kingdom.

¹S. Zhu *et al.*, Phys. Lett. **B618**, 51 (2005).

- c.9. Measurement of the ^{240}Pu Half-Life** (I. Ahmad, F. G. Kondev, J. P. Greene, M. A. Kellett,* and A. L. Nichols*)

Precise half-life values of actinide nuclei, in particular Pu isotopes, are needed for the conversion of measured activity to mass. For this reason we have measured the half-life of ^{240}Pu by a method quite different from previous techniques. The half-life of ^{240}Pu was determined by measuring its growth in a ^{244}Cm source. A thin source of ^{244}Cm was prepared by an electromagnetic isotope separator for this measurement in the 1970s, and the daughter nuclide ^{240}Pu was allowed to grow for 32.7 years. The alpha spectrum of

the ^{244}Cm source was measured with silicon detectors and the ratio of the ^{240}Pu and ^{244}Cm activities was determined. From this ratio and the previously known half-life of ^{244}Cm (18.11 ± 0.03 yr), the half-life of ^{240}Pu was determined to be $T_{1/2} = 6545 \pm 19$ yr. This is in excellent agreement with the value of 6564 ± 11 yr recommended by the U.S. Half-Life Evaluation Committee.¹ The results of this study have been accepted for publication in Nucl. Instrum. and Methods.

*International Atomic Energy Agency, Vienna, Austria.

¹W. W. Strohm, Int. J. Appl. Radiat. Isot. **35**, 155 (1984).

- c.10. Energy Levels of the N = 153 Neutron Nucleus ^{251}Cf** (I. Ahmad, J. P. Greene, E. F. Moore, F. G. Kondev, R. R. Chasman, C. E. Porter,* and L. K. Felker*)

Single-particle level energies in the heaviest nuclei are needed both for the understanding of the levels observed in superheavy nuclei and to test theoretical models which predict their stability. The heaviest odd-neutron nuclide available in milliCurie quantity is the 20.07-h ^{255}Fm which decays by alpha particle emission to ^{251}Cf . We obtained 5 separate milliCurie samples of ^{255}Fm from the High Flux Isotope Reactor (HFIR), Oak Ridge and measured their gamma singles spectra with a high-resolution 2-cm 2×10 -mm germanium LEPS detector and with a 25% Ge spectrometer. The high sensitivity of the measurement allowed us to identify gamma rays with intensities as low as $1.0 \times 10^{-6}\%$ per

^{255}Fm alpha decay. Mass-separated sources of ^{251}Es were prepared and their gamma and electron spectra were measured with high-resolution semiconductor detectors. These measurements provided the multipolarities of transitions in ^{251}Cf . The present measurements confirmed the previous assignments of single-particle states in ^{251}Cf . A partial level scheme of ^{251}Cf is displayed in Fig. I-12. The levels identified include: $1/2^+[620]$, 0.0 keV; $7/2^+[613]$, 106.30 keV; $3/2^+[622]$, 177.59 keV; $11/2^- [725]$, 370.47 keV; $9/2^- [734]$, 433.91 keV; $5/2^+[622]$, 543.98 keV; $1/2^- [750]$, 632.0 keV; $9/2^+[615]$, 683 keV and $9/2^+[604]$, 974.0 keV. A vibrational band was

identified in previous studies at 981.4 keV and given an assignment of $\{7/2+[613]\times 2^-\}3/2^-$. Three new vibrational bands are identified in the present work at 942.5, 1086.5, and 1250.0 keV with tentative assignments of $\{7/2+[613]\times 1^-\}5/2^-$, $\{7/2+[613]\times 1^-\}9/2^-$, and $\{7/2+[613]\times 0^+\}7/2^+$, respectively. A

level was identified at 1185.5 keV with spin of $5/2$ or $7/2$ but it was not given any configuration assignment. Another level was identified at 1077.5 keV and given a spin of $9/2$. Again, no configuration could be assigned to this level. The results of this study were published.

*Oak Ridge National Laboratory.

¹I. Ahmad *et al.*, Phys. Rev. **72**, 054308 (2005).

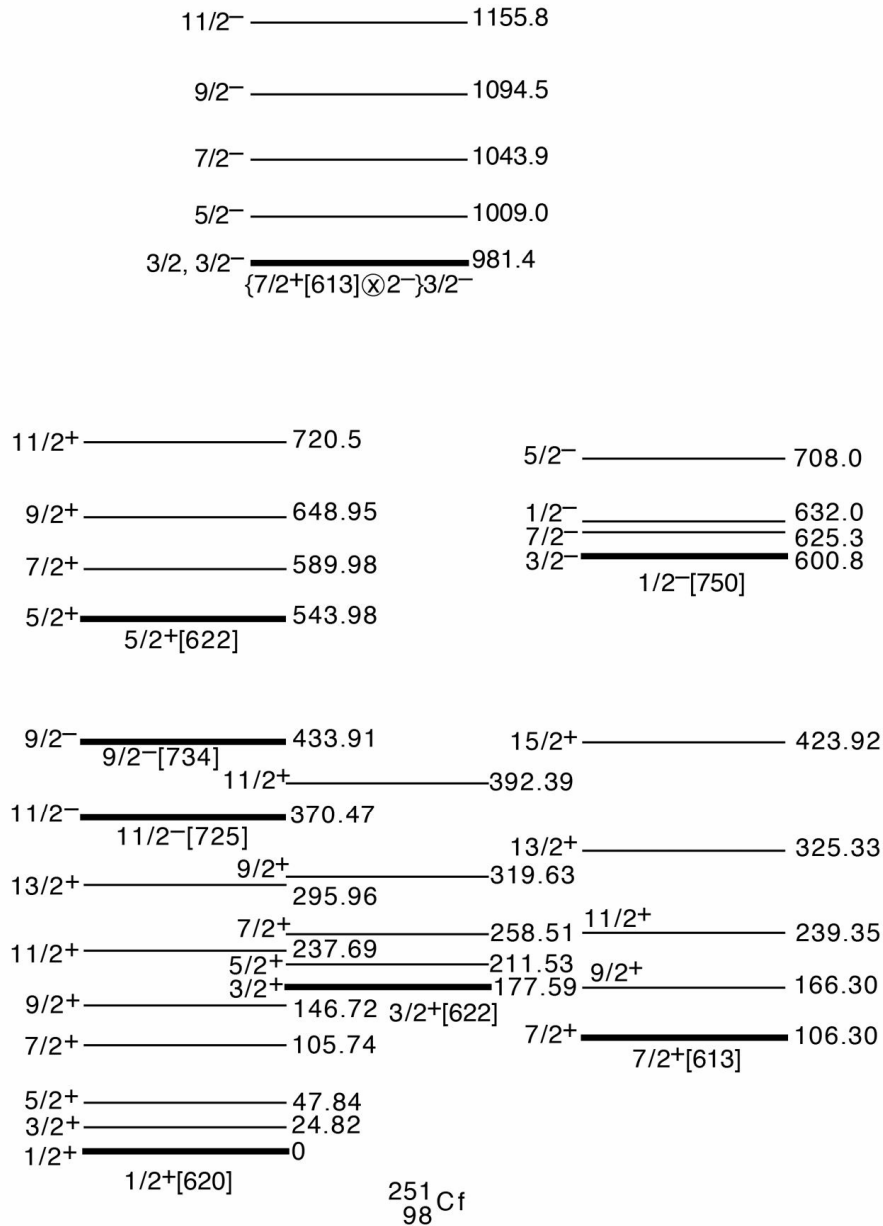


Fig. I-12. A partial level scheme of ^{251}Cf . Level energy is shown on the right in keV and spin-parity is shown on the left.

D. STRUCTURE OF NUCLEI FAR FROM STABILITY

A core issue in nuclear structure research concerns the evolution of nuclear behavior as one moves away from stability by varying the neutron-to-proton ratio. Traditional shell gaps are shown to disappear and new gaps arise. The exact origins of these phenomena still have to be fully understood, though modification of the spin-orbit effect, the influence of the tensor force, and other residual interactions all appear important. We continue to probe nuclei along the proton dripline from light masses to heavy. Considerable progress is being made in the approach to ^{100}Sn . In addition, our efforts to reach neutron-rich nuclei have grown, through fragmentation experiments, traditional fusion of very neutron-rich species, and using multi-nucleon transfer.

d.1. Neutron-Rich Nuclides

d.1.1. Is the Nuclear Spin-Orbit Interaction Changing with Neutron Excess?

(J. P. Schiffer, C. L. Jiang, K. E. Rehm, C. Deibel,* S. J. Freeman,† B. Kay,† P. D. Parker,* and C. Wrede*)

The single-particle character of nuclei underlies much of our understanding of nuclear structure. The states formed by a proton outside the closed shell of 50 protons, the $g_{7/2}$ - $h_{11/2}$ separation in particular, was studied with the (α,t) reaction on all the stable, even Sn isotopes two years ago to demonstrate that the spin-orbit splitting for the proton states was changing with neutron excess.¹ A closely related experiment, to

obtain quantitative information on neutron single-particle states outside $N = 82$ with the $(\alpha,^3\text{He})$ reaction, and the $i_{13/2}$ - $h_{9/2}$ separation in particular, has been delayed because of ion source problems. These measurements are scheduled for June 2006. Targets are likely to be more difficult to prepare because of the chemically active nature of $N = 82$ isotopes (e.g. Ba and Ce).

*Yale University, †University of Manchester, United Kingdom.

¹J. P. Schiffer *et al.*, Phys. Rev. Lett. **92**, 162501 (2004).

d.1.2. Structure in Neutron-Rich ^{52}Ca and ^{52}Sc and the $N = 32$ Shell Gap

(R. V. F. Janssens, M. P. Carpenter, S. Zhu, A. Gade,* D. Bazin,* B. A. Brown,* C. M. Campbell,* J. M. Cook,* D.-C. Dinca,* T. Glasmacher,* P. G. Hansen,* P. F. Mantica,* W. F. Mueller,* J. R. Terry,* A. N. Deacon,† S. J. Freeman,† B. P. Kay,† J. A. Tostevin,‡ R. Broda,§ and B. Fornal§)

Recent observations in exotic, neutron-rich nuclei have demonstrated that the sequence and energy spacing of single-particle orbits is not as immutable as once thought: some of the familiar magic numbers disappear and new shell gaps develop. Over the last few years, our collaboration has initiated a program to investigate the properties of neutron-rich nuclei above doubly-magic ^{48}Ca and evidence has been found for a sub-shell closure at $N = 32$ in Ti and Cr nuclei.¹ This issue has now been investigated further by exploring the structure of the $N = 32$ nucleus ^{52}Ca . The two-proton knockout reaction $^9\text{Be}(^{54}\text{Ti},^{52}\text{Ca} + \gamma)$ was studied at the NSCL using 72 MeV/nucleon fragments produced with a 130 MeV/nucleon primary beam.

The main observations of the experiment are summarized in Fig. I-13. Besides the strong feeding of the ^{52}Ca groundstate (with a cross section of 0.21(3) mb), the only other sizeable cross section (0.11 mb) proceeds to a 3^- level at 3.9 MeV and there is no measurable direct yield to the first excited 2^+ state at 2.6 MeV. Qualitatively, the observations can be understood in the following way: (1) the strong feeding of the groundstate is a direct result of the semi-magic nature of the ^{54}Ti projectile, with a closed $N = 32$ neutron shell and two $f_{7/2}$ protons outside the $Z = 20$ core, (2) since the first excited 2^+ state is understood as a neutron particle-hole excitation across the $N = 32$ shell gap, involving the $p_{3/2}$ and $p_{1/2}$ orbitals, such an

excitation is not expected to be populated appreciably in the reaction of a ^{54}Ti projectile with two $f_{7/2}$ valence protons and no valence neutrons, (3) the same reasoning leads to the complementary conclusion that the sizable cross section to the 3^- state is a direct indication of a proton excitation.

This first principle reasoning has been substantiated by detailed calculations using eikonal theory and shell model wave functions. In particular, the comparison between computed and measured cross sections results in a ratio between the measured and calculated strength of ~ 0.6 , i.e., a reduction similar that that seen in one-particle knock-out reactions.

The present work has demonstrated that two-proton knockout reactions represent a powerful tool in the arsenal of experimental techniques aimed at the study of neutron-rich nuclei. The specific $^9\text{Be}(^{54}\text{Ti}, ^{52}\text{Ca} + \gamma)$ reaction investigated here was instrumental in

identifying a proton cross-shell excitation in an exotic nucleus with large neutron excess. In addition, the data provided strong confirmation of the $N = 32$ sub-shell closure in ^{54}Ti . A paper reporting these results has been submitted for publication.²

As a by-product of this experiment, the odd-odd fp -shell nucleus ^{52}Sc was also investigated using in-beam γ -ray spectroscopy following secondary fragmentation of a ^{55}V and ^{57}Cr cocktail beam. Aside from the known γ -ray transition at 674(5) keV, a new decay at $E_\gamma = 212(3)$ keV was observed. It is attributed to the depopulation of a low-lying excited level. This new state can be understood within the framework of shell-model calculations with the GXPF1, GXPF1A, and KB3G effective interactions. These calculations are found to be fairly robust for the low-lying level scheme of ^{52}Sc , irrespective of the choice of the effective interaction. A paper reporting these results has been published.³

*Michigan State University, †University of Manchester, United Kingdom, ‡Niewodniczanski Institute of Nuclear Physics, Krakow, Poland, §University of Surrey, United Kingdom, ¶Polish Academy of Sciences, Krakow, Poland.

¹D.-C. Dinca *et al.*, Phys. Rev. C **71**, 041302(R) (2005).

²A. Gade, R. V. F. Janssens *et al.*, to be published.

³A. Gade, R. V. F. Janssens *et al.*, Phys. Rev. C **73**, 037309 (2006).

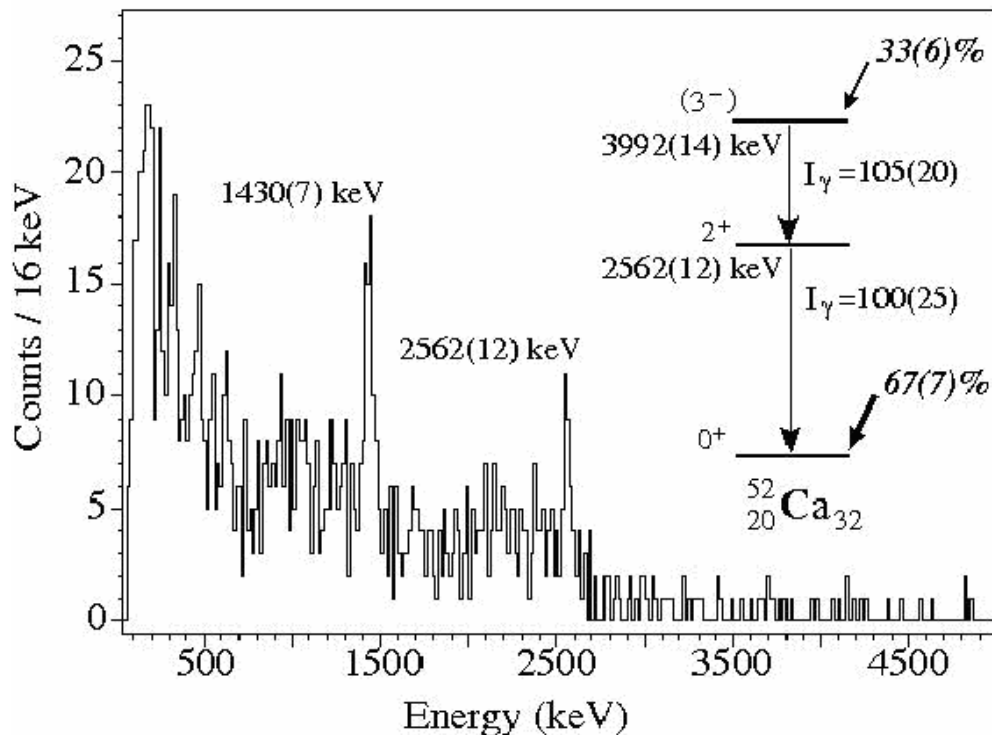


Fig. I-13. γ -ray spectrum in coincidence with the ^{52}Ca knock-out residues. The two γ -ray transitions establish the cascade shown in the inset. The arrows indicated the feeding profile by the reaction ($\sigma(3^-) = 0.11(3)$ mb and $\sigma(0^+) = 0.21(3)$ mb).

d.1.3. Yrast Structure of Neutron-Rich ^{53}Ti (S. Zhu, R. V. F. Janssens, M. P. Carpenter, S. J. Freeman, N. Hammond, T. Lauritsen, C. J. Lister, E. F. Moore, D. Seweryniak, B. Fornal,* R. Broda,* W. Krolas,* T. Pawlat,* J. Wrzesinski,* S. N. Liddick,† P. F. Mantica,† and B. E. Tomlin†)

Gamma rays from neutron-rich Ti nuclei in the vicinity of $N = 32$ have been studied at Gammasphere using deep-inelastic reactions induced by ^{48}Ca beams on thick ^{208}Pb and ^{238}U targets. The ^{53}Ti yrast cascade was identified for the first time and the location in energy of states with spin up to $I = 21/2$ was determined. The excitations of ^{53}Ti provide new tests of effective interactions for full pf -shell calculations. Comparisons

between theory and experiment for the highest spin states in ^{53}Ti favor the recently proposed GXPF1A interaction which accounts for the appearance of a neutron subshell closure at $N = 32$ in Ti isotopes as well as for the lack of a similar subshell closure at $N = 34$, as predicted by earlier calculations with another interaction. A paper describing these results has recently been published.¹

*Polish Academy of Sciences, Krakow, Poland, †Michigan State University.

¹B. Fornal *et al.*, Phys. Rev. C **72**, 044315 (2005).

d.1.4. Structure of the Even-Even Neutron-Rich $^{56,58,60}\text{Cr}$ Isotopes (S. Zhu, R. V. F. Janssens, M. P. Carpenter, T. Lauritsen, C. J. Lister, D. Seweryniak, A. N. Deacon,* S. J. Freeman,* J. F. Smith,* B. J. Varley,* R. Calderin,† S. L. Tabor,† R. Broda,‡ and B. Fornal‡)

As stated in the previous contribution, the existence of the $N = 32$ sub-shell above doubly-magic ^{48}Ca has been firmly established in a series of recent experiments.^{1,2} With the proton $f_{7/2}$ shell half-filled, Cr isotopes are among the nuclei best suited for studying the possible role of collectivity in the region, and the results on odd, neutron-rich Cr isotopes above $N = 32$ indicate an increasing involvement of the shape-driving $g_{9/2}$ orbital in the low-lying structure of these nuclei.³ Experimental information on the excited states in the even-even, neutron-rich Cr nuclei provides further tests of the suitability of the fp shell-model space for the description of their level structure and of the possible shape-driving influence of the $vg_{9/2}$ orbital.

The yrast states of the neutron-rich Cr isotopes were populated via two deep inelastic reactions of ^{48}Ca on 50 mg/cm² ^{208}Pb and ^{238}U targets at beam energies ~20% above the Coulomb barrier. Another approach used here for producing neutron-rich Cr isotopes involved fusion of ^{48}Ca projectiles with ^{14}C radioactive targets (thickness 100 $\mu\text{g}/\text{cm}^2$, ~90% enrichment). The beam energy was selected as 130 MeV to optimize two-proton evaporation producing ^{60}Cr . Reaction products were dispersed according to their charge-to-mass (A/q) ratio with the Fragment Mass Analyzer (FMA). An ion chamber behind the focal plane was used to provide Z

resolution and separate ^{60}Cr residues from other isotopes with stronger yields.

The deduced level schemes of $^{56,58,60}\text{Cr}$ represent significant extensions over previous knowledge. Specifically, despite a low-spin structure reflecting the $N = 32$ sub-shell closure in ^{56}Cr , evidence was found at higher energy for a negative-parity sequence associated with prolate, collective rotation. This band exhibits striking similarities with those seen in the odd neighbors $^{55,57}\text{Cr}$. The data collected for ^{58}Cr demonstrate unambiguously that the level scheme proposed recently by Marginean *et al.*⁴ from a PRISMA + CLARA experiment is in error, raising considerable doubt about an interpretation in terms of an $E(5)$ dynamical symmetry proposed in the latter work. In addition, the lowest observed negative-parity state in ^{58}Cr is ~1.1 MeV lower than that in ^{56}Cr , a trend similar to that exhibited by the $9/2^+$ ($vg_{9/2}$) bandheads in the odd Cr neighbors. Furthermore, the properties of the sequence built on this negative-parity state differ significantly from those seen in ^{56}Cr , consistent with the spherical or slightly oblate shape proposed for ^{59}Cr by Freeman *et al.*⁵ The yrast sequence observed for the first time in ^{60}Cr is also consistent with an interpretation in terms of an oblate deformation.

*University of Manchester, United Kingdom, †Florida State University, ‡Polish Academy of Sciences, Krakow, Poland.

¹R. V. F. Janssens *et al.*, Phys. Lett. **B546**, 55 (2002).

²D. C. Dinca *et al.*, Phys. Rev. C **71**, 041302(R) (2005) and references therein.

³A. N. Deacon *et al.*, Phys. Lett. **B622**, 151 (2005).

⁴N. Marginean *et al.*, Phys. Lett. **B633**, 696 (2006).

⁵S. J. Freeman *et al.*, Phys. Rev. C **60**, 064301 (2004).

d.1.5. Changes in $\nu g_{9/2}$ Shape Polarization Across the Odd Neutron-Rich Cr Isotopes

(R. V. F. Janssens, M. P. Carpenter, N. J. Hammond, T. Lauritsen, C. J. Lister, D. Seweryniak, S. Zhu, A. N. Deacon,* S. J. Freeman,* J. F. Smith,* B. J. Varley,* F. R. Xu,† R. Calderin,‡ S. L. Tabor,‡ and P. Chowdhury§)

The existence of the $N = 32$ sub-shell above doubly-magic ^{48}Ca has been firmly established in a series of recent experiments.^{1,2} Shell model calculations with the GXPF1A effective interaction are able to account for this gap as resulting from a weakening of the $\pi f_{7/2} - \nu f_{5/2}$ proton-neutron monopole interaction as protons are removed from the $f_{7/2}$ orbital (filled at $Z = 28$), combined with a significant $\nu 2p_{1/2} - \nu 2p_{3/2}$ spin-orbit splitting.³ With the proton $f_{7/2}$ shell half-filled, Cr isotopes are among the nuclei best suited for studying the possible role of collectivity in the region.

With Gammasphere and the FMA, excited states in ^{57}Cr have been populated to high spin in the $^{14}\text{C}(^{48}\text{Ca}, \alpha n)$ reaction with a beam energy of 130 MeV delivered by ATLAS. A regular sequence of stretched quadrupole transitions has been established above the yrast $9/2^+$

level (see Fig. I-14). This sequence is interpreted as a rotational band associated with prolate deformation induced by the excitation of the odd neutron into the $1/2^+[440]$ orbital. Total Routhian surface calculations, which follow this configuration to high spin, reproduce the observed features of the band. They are also able to account for a similar, but less well developed structure in ^{55}Cr . In contrast, the isomeric yrast $9/2^+$ state in ^{59}Cr that was studied earlier by our collaboration appears to be a band-head state dominated by the $9/2^+[404]$ configuration, which is favored at oblate deformations. Such a marked difference presents a significant challenge for theoretical descriptions, but is consistent with features exhibited by the low-lying negative-parity states in ^{59}Cr .⁴ A paper presenting our results has recently been published.⁵

*University of Manchester, United Kingdom, †Peking University, China, ‡Florida State University, §University of Massachusetts-Lowell.

¹R. V. F. Janssens *et al.*, Phys. Lett. **B546**, 55 (2002).

²D. C. Dinca *et al.*, Phys. Rev. C **71**, 041302(R) (2005) and references therein.

³M. Honma *et al.*, Phys. Rev. C **65**, 061301 (2002).

⁴S. J. Freeman *et al.*, Phys. Rev. C **60**, 064301 (2004).

⁵A. N. Deacon *et al.*, Phys. Lett. **B622**, 151 (2005).

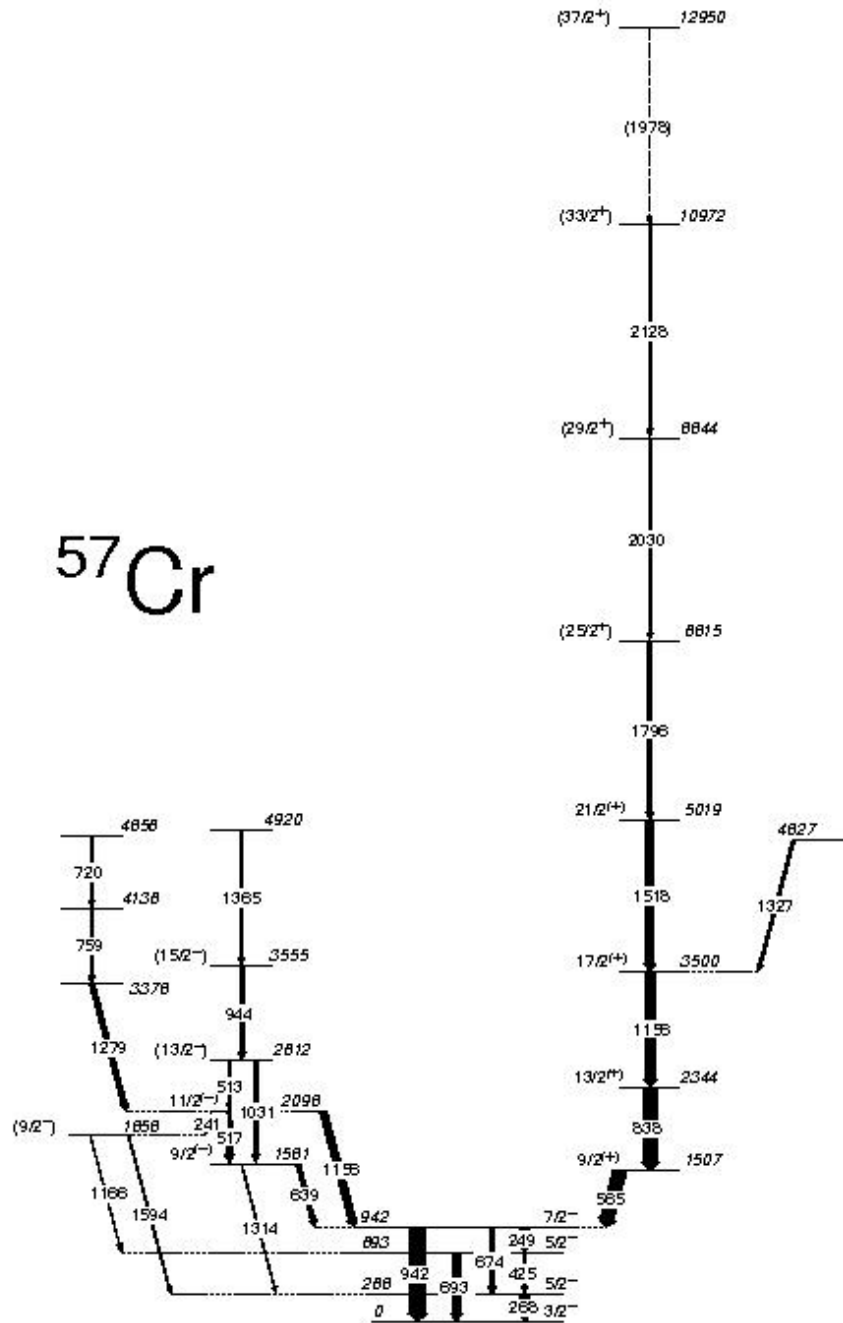


Fig. I-14. The level scheme of ^{57}Cr deduced in the present experiment.

d.1.6. Stabilization of Nuclear Isovector Valence-Shell Excitations (C. J. Lister, R. V. F. Janssens, M. P. Carpenter, S. Zhu, G. Rainovski,*† N. Pietralla,*‡ T. Ahn,* and C. J. Barton III§)

Atomic nuclei are examples of mesoscopic two-fluid quantum systems. The physics of these systems is determined by three main properties: the many-body aspect, the quantum nature, and the two-fluid character. Nuclear phenomena that reflect these three properties are collectivity, shell structure, and the isospin degree of freedom. Of particular importance for studying the mutual balance of these aspects are those excitations that are related to the collective two-fluid character of nuclei and to their shell structure. Quadrupole-collective isovector valence-shell excitations, so-called mixed-symmetry states (MSSs),¹ are the best studied examples of this class of phenomena.

The fundamental MSS in collective two-fluid quantum systems with quadrupole residual interactions, such as heavy nuclei, is the one-quadrupole phonon $2^+_{1,ms}$ state.¹ Because of its role as a building block of isovector excitations in nuclei, and in quadrupole-collective two-fluid quantum systems in general, it is important to study its properties and the mechanisms that determine those. However, information on MSSs is scarce due to experimental challenges.

It was the purpose of this work to demonstrate that the observation of γ rays from inverse kinematics Coulomb excitation can identify and probe the $2^+_{1,ms}$ state of any vibrational nucleus that can be made available as an ion beam by studying the nucleus ^{138}Ce which has a natural

abundance of 0.25%. The technique is generic and equally applicable to radioactive beams that can be produced with sufficient intensity ($\sim 10^6$ ions/s for detailed spectroscopy, $\sim 10^3$ ions/s for identification).

Excited states in ^{138}Ce were studied via the $^{12}\text{C}(^{138}\text{Ce}, ^{138}\text{Ce}^*)$ Coulomb excitation reaction at 480 MeV. Relative cross sections were determined from the γ -ray yields observed with Gammasphere (see Fig. I-15). The $E2$ and $M1$ strength distributions between the lowest six 2^+ states up to 2.7 MeV enabled the identification of the 2^+_{4} state in ^{138}Ce as the dominant fragment of the one-phonon $2^+_{1,ms}$ mixed symmetry state. Mixing between this level and a nearby isoscalar state was observed and found to be more than 4 times larger than in the neighboring isotope ^{136}Ba . Indeed, in contrast to the isotope ^{136}Ba , the $2^+_{1,ms}$ state is strongly mixed with another 2^+ level located nearby and the mixing element between the two states was evaluated to be of the order of 14 keV. The observed mixing in ^{138}Ce can be attributed to the lack of shell stabilization at the proton $g_{7/2}$ subshell closure. In other words, the evolution of the MSSs from ^{136}Ba to ^{138}Ce shows for the first time that the strength concentration of isovector excitations in the valence shell reflects the mutual balance between the isospin degree of freedom and the shell structure. A paper describing these results has recently been published.²

*SUNY at Stony Brook, †University of Sofia, Bulgaria, ‡Universitat zu Koln, Germany, §University of York, United Kingdom.

¹F. Iachello, Phys. Rev. Lett. **53**, 1427 (1984).

²G. Rainovski *et al.*, Phys. Rev. Lett. **96**, 122501 (2006).

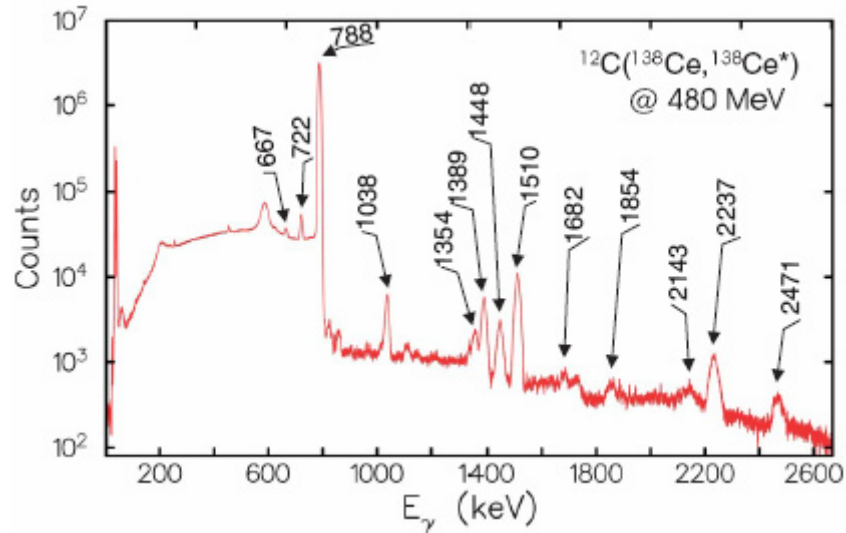


Fig. I-15. Background-subtracted, Doppler-corrected γ -ray spectrum in ^{138}Ce observed with Gammasphere after Coulomb excitation on a carbon target.

d.1.7. Investigation of the Nuclear Structure of Heavy Fission Fragments Using the CPT Mass Spectrometer (H. Sharma,* G. Savard,† S. Caldwell,† J. A. Clark,* J. Fallis,* A. A. Hecht,§ D. Lascar,¶ A. Levand, N. D. Scielzo, K. S. Sharma,* I. Tanihata, A. C. C. Villari,**, Y. Wang,* F. Buchinger,‡ J. E. Crawford,‡ S. Gulick,‡ J. K. P. Lee,‡ and R. Segel||)

Mass measurements of the $^{141-147}\text{Ba}$, $^{143-148}\text{La}$, $^{145-151}\text{Ce}$, $^{148-153}\text{Pr}$ nuclei have been carried out to a few tens of keV/c^2 precision at the CPT mass spectrometer. The energetic fission fragments from a $300\ \mu\text{Ci}$ ^{252}Cf source were cooled and bunched using a combination of gas catcher and gas-filled RFQ-cooler devices and then sent to an isobar separator for the removal of the undesired contaminating ions. The selected ions were further cooled in a gas filled linear trap before being injected into the CPT precision Penning trap where measurements with a 1000 ms excitation time were carried out.

The neutron separation energies have been determined from these measurements with a significant improvement in accuracy. The two neutron separation energies (S_{2n}) values for the Ba and La isotopes agree well with the S_{2n} values from recent compiled data in the Atomic Mass Evaluation of 2003 (AME 2003), except for the ^{147}Ba and ^{148}La nuclei. For both the ^{147}Ba and ^{148}La nuclei, the S_{2n} values are about 400 keV less than the S_{2n} values known or extrapolated in AME2003 (Fig. I-16 A, B). The new S_{2n} values for the Pr and Ce nuclei are essentially consistent with the S_{2n} values

from AME2003 (Fig. I-16 C, D).

Any change in shell structure is expected to show up as a sudden deviation in the smooth behavior of the S_{2n} plotted as a function of neutron number. The transitional nuclei with $Z > 50$ are known to have quadrupole deformation at $N \sim 92$. The present S_{2n} values for Ce nuclei show a change in the smooth behavior of the S_{2n} at $N = 92$. There is however no sign of a similar change for Pr nuclei. In the case of the Ba and La nuclei, the S_{2n} values are only determined up to $N = 91$ and additional data on more neutron-rich isotopes is required. More generally, the most neutron-rich isotope measured here for the Ba, La and Ce chains are less bound than expected and data on more neutron rich isotopes could confirm this trend that would have important consequences for nuclear structure in this region and the location of the r-process path.

With the newly installed high-resolution isobar separator, the mass measurements for the more weakly produced fission fragments (in particular the Ba and La nuclei beyond $N = 91$) are now possible and will be performed in the coming year.

*Argonne National Laboratory and University of Manitoba, Winnipeg, Manitoba, †Argonne National Laboratory and The University of Chicago, ‡McGill University, Montreal, Quebec, §Argonne National Laboratory and University of Maryland, ¶Argonne National Laboratory and Northwestern University, ||Northwestern University, **Argonne National Laboratory and GANIL, Caen, France.

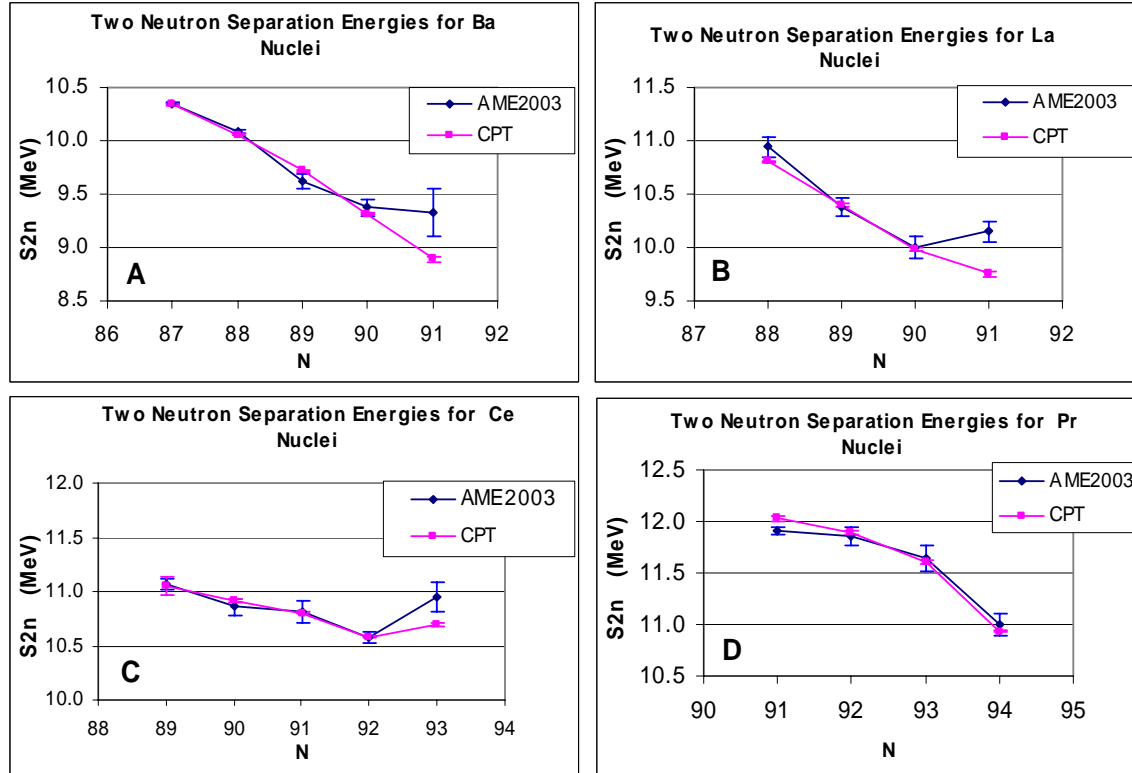


Fig. I-16. (A, B, C, D) show the two neutron separation energies for Ba, La, Ce and Pr nuclei.

d.1.8. Study of $N = 50$ Nuclei Near ^{78}Ni Using Deep Inelastic Reactions (M. P. Carpenter, F. G. Kondev, R. V. F. Janssens, N. Hoteling, T. L. Khoo, T. Lauritsen, C. J. Lister, D. Seweryniak, X. Wang, S. Zhu, R. Broda,* B. Fornal,* A. Galindo-Uribarri,† A. Ibanez,‡ E. Padilla-Rodal,†,§ and J. P. Ureggo-Blanco§)

The study of doubly and semi magic nuclei have historically proven to be important in establishing for example the parameter strengths for the shell model. Until recently, these parameters were set by nuclei lying near the line of beta-stability, however, with the utilization of first and second generation radioactive beam facilities, studies of exotic neutron rich nuclei at and near closed shells have begun. What has motivated many of these measurements from a nuclear structure standpoint is the fact that rearrangements of single-particle energies are observed in neutron rich systems. Such changes in the single-particle energies have been attributed to the attractive strength of the spin-isospin

part of the effective nuclear interaction. As a result, one has observed the disappearance of certain magic numbers and the emergence of new closed shells.

Gammasphere is not located at a traditional radioactive beam facility; however, one can still access neutron rich nuclei using techniques that do not require the acceleration of radioactive ions. For example, by studying the γ rays emitted after spontaneous fission of ^{248}Cm , important new information on excited states has been obtained for nuclei near ^{132}Sn . We have also studied neutron rich nuclei using so-called deep inelastic reactions. In these studies, ^{208}Pb or ^{238}U

targets are bombarded by a neutron rich stable beam at energies $\sim 25\%$ above the Coulomb barrier. By swapping protons and neutrons with the target, neutron-rich nuclei relative to the beam are produced, and their de-excitation by γ rays is studied with Gammasphere.

Our collaboration has been actively studying neutron rich nuclei in the Ca-Ti region. A number of our studies have been performed at MSU utilizing fragmentation to produce the neutron rich nuclides of interest. Our Gammasphere measurements have utilized a ^{48}Ca beam bombarding Pb and U targets. These studies have allowed us, for example, to identify excited states in $^{54,56}\text{Ti}$ in order to test shell-model calculations which have suggested that both isotopes should be semi-magic.^{1,2} The ATLAS studies have proven to be quite complimentary to the MSU experiments.

With the success of the Gammasphere experiments utilizing a ^{48}Ca beam to explore the yrast sequences in the neutron rich Ti isotopes, we have extended our measurements into the region around $N = 50$ and $Z = 28$ (^{78}Ni). Neutron rich nuclides in this region are of particular interest due to their role in the r-process,

and in particular, their contribution to the peak in the solar elemental abundance near $A = 80$. While much is known with regards to the $N = 50$ isotones starting at ^{86}Kr and proceeding up towards ^{100}Sn , very little is known about the isotones approaching and including ^{78}Ni . In the Gammasphere measurement, data were collected using an ^{82}Se beam incident on both thick ^{208}Pb and ^{238}U targets. As a result, all products produced in these reactions are stopped in the target. Data were taken at two different beam energies 525 and 630 MeV. In addition, the time between beam pulses was 400 ns allowing for the identification of isomers with lifetimes as long as several μsec .

One of the main purposes of this measurement was to identify the yrast structures for both ^{84}Se and ^{82}Ge to spins up to $\sim 12 \hbar$. In addition, we hoped to develop detailed level structures for ^{81}Se , ^{83}Se , ^{83}As , ^{81}Ge , and possibly ^{83}Ge . Two separate databases have been created from the data taken at 630 MeV that correspond to the ^{208}Pb and ^{238}U targets respectively. While the analysis is ongoing, current results include a more extensive level scheme for ^{84}Se up to $I = 12 \hbar$ and excited states in ^{82}Ge have been identified up to $I = 6 \hbar$.

*Niewodniczanski Institute of Nuclear Physics, Cracow, Poland, †Oak Ridge National Laboratory, ‡Instituto de Fisica, UNAM, Mexico, §University of Tennessee.

¹R. V. F. Janssens *et al.*, Phys. Lett. **B546**, 55 (2002).

²B. Fornal *et al.*, Phys. Rev. C **70**, 064304 (2004).

d.1.9. Structure of Neutron-Rich Zn Isotopes (A. A. Hecht,* N. Hoteling,* M. P. Carpenter, R. V. F. Janssens, T. Lauritsen, D. Seweryniak, X. Wang, S. Zhu, W. B. Walters,† B. Fornal,‡ R. Broda,‡ W. Krolas,‡ J. Wrzesinski,‡ A. Woehr,§ J. Stone,† and N. J. Stone¶)

The neutron rich region near doubly magic ^{78}Ni is significant for both nuclear structure and nuclear astrophysics: as experimental input for models on shell structure far from stability and as the seed region for the beginning of the rapid neutron capture process of nucleosynthesis. This region is not easily accessible, most of the data on excited states is from beta decay studies¹ and can follow the trends and orbital contributions only up through the first few levels. Expanding this knowledge to high spin states, deep inelastic scattering (DIS) experiments were performed at the ATLAS accelerator center at Argonne National Laboratory. Pulsed beams of ^{82}Se and of ^{64}Ni impinged on a target of ^{238}U and the gamma rays emitted from the DIS products were observed using the Gammasphere detector array.

Focusing on Zn, excited states in the even-even nuclei $^{66-78}\text{Zn}$ were observed using $\gamma\text{-}\gamma\text{-}\gamma$ coincidence matrices. Several new levels were found for $^{66-74}\text{Zn}$, and many previously known levels were confirmed. Levels were tentatively identified up to 12^+ in ^{66}Zn , 14^+ in ^{68}Zn , 12^+ in ^{70}Zn , 12^+ in ^{72}Zn , and 10^+ in ^{74}Zn . Using the angular sensitivity of Gammasphere, angular correlations were performed to extract the spin of several of the new states, and fix the spins of levels that were previously tentatively assigned.

The variation in energy of the positive parity yrast levels as a function of neutron number for the even Zn isotopes is plotted in Fig. I-17. Many interesting properties emerge in these systematics, such as the trend in 8^+ energies. For these heavy Zn isotopes, the

neutron Fermi level ranges from the low $f_{5/2}$ subshell, through the $p_{1/2}$, and up to the higher lying positive parity $g_{9/2}$. With 30 protons, the proton Fermi level is in the middle of the $p_{3/2}$ subshell. From ^{64}Zn to heavier isotopes, as the neutron Fermi surface nears the $g_{9/2}$ orbitals and the 8^+ level can be composed of a $v(g_{9/2})^2$

two quasiparticle configuration, the 8^+ levels begin to drop relative to the 0^+ energy. The levels continue a smooth downward trend until an abrupt drop from ^{74}Zn to ^{78}Zn .

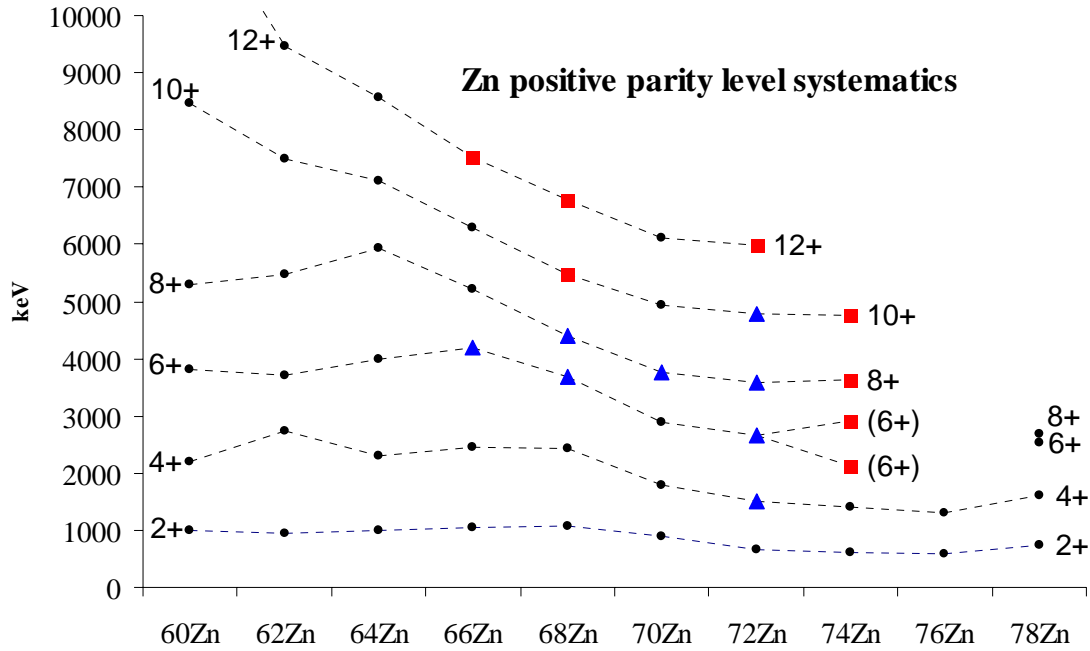


Fig. I-17. Even parity yrast level energies for Zn isotopes as a function of neutron number.¹⁻⁵ Red squares represent new levels found in this work. Blue triangles represent levels with previously unsure level spins and parities which were fixed in this work. Ordering of $8^+ \rightarrow 6^+$ and $6^+ \rightarrow 4^+$ quadrupole transitions in ^{74}Zn to be determined.

It is interesting to note these systematics in relation to Grodzins' rule. Calculated $B(E2)$ values derived from the relation $B(E2:0^+ \rightarrow 2^+) [e^2 b^2] = 2.57 Z^2 A^{-2/3} E(2_1^+)^{-1} [\text{keV}^{-1}]$ (following Eq. 12 in Ref. 6) are plotted alongside experimental $B(E2:0^+ \rightarrow 2^+)$ values in Fig. I-18. While the 2^+ level energies remain relatively unperturbed by the change in neutron number, Grodzins' rule breaks down for heavier Zn. The experimental $B(E2)$ values are surprisingly low for the heavier isotopes $^{76,78}\text{Zn}$.

Moving towards the closed shell at $N = 50$, the expected trend would be towards sphericity - especially with the nearly magic $Z = 30$ - with an increase in the $E(2^+)$ and lowering of collectivity demonstrated by decreasing $B(E2)$ values. Instead, while the $E(2^+)$ values remain fairly constant, the $B(E2)$ values decrease rapidly. The drop in $B(E2)$ and a breakdown in Grodzins' rule for extreme cases of N/Z has been observed in other regions,⁶ and may be indicative of a drop in the p-n and n-n pairing interactions.⁸

As for the level energy systematics, both the $E(2^+)$ and $E(8^+)$ values are anomalously low with increasing neutron number towards the closed N shell, and indeed $E(8^+)$ plummets. This too is consistent with the breakdown of pairing. A breakdown in the pairing interaction decreases the difference between the 0^+ groundstate and the levels produced by breaking pairs, keeping the relative energy of the 2^+ level low and reducing the 8^+ level energy dramatically. Note that while the 2^+ level may be a mixture of several orbital configurations, above ^{64}Zn the neutron Fermi surface is in the $g_{9/2}$ subshell and the lowest 8^+ level is fairly pure $v(g_{9/2})^2$. The 8^+ level energy, being independent of configuration mixing, serves as a clean indicator of the pairing interaction. While the $B(E2)$ value for ^{74}Zn was known previously, the $E(8^+)$ value was not. From our work we see that the descent to the $E(8^+)$ value in ^{78}Zn is remarkable in its abruptness, and shows the suddenness of the weakening of the pairing interaction with an increased N/Z ratio. Further analysis is ongoing.

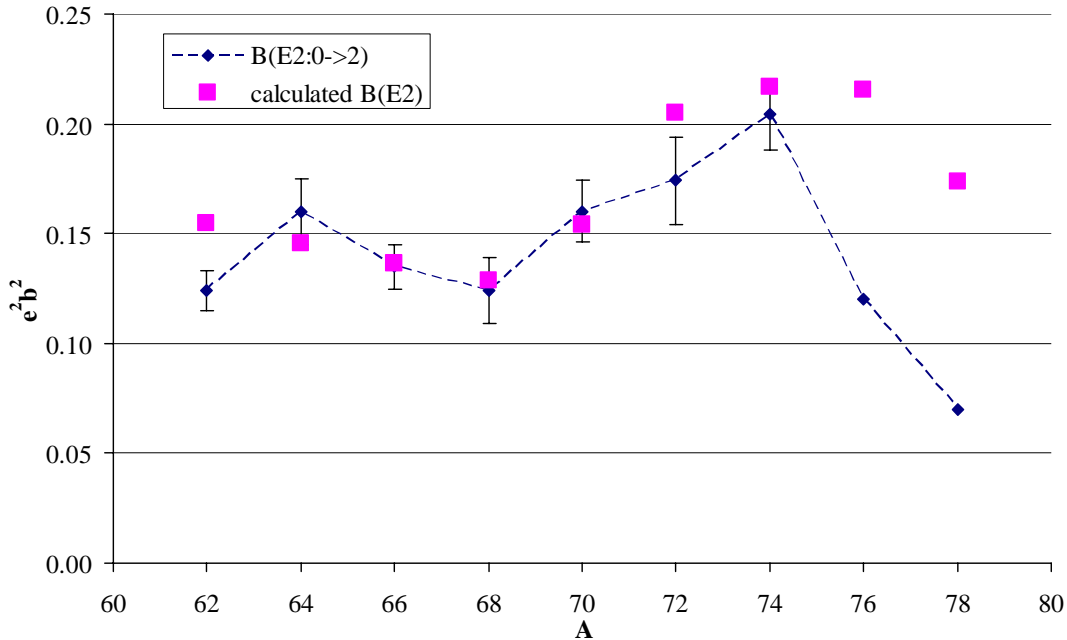


Fig. I-18. Experimental [2, 3, 6, 7] and calculated $B(E2)$ values in Zn. Experimental errors not known by the authors for $^{76,78}\text{Zn}$. Calculations use the Grodzins' relation following (Ref. 6). See text for details.

*University of Maryland and Argonne National Laboratory, †University of Maryland, ‡Niewodniczanski Institute of Nuclear Physics, Krakow, Poland, §University of Notre Dame, ¶University of Tennessee.

¹J. Van Roosbroeck *et al.*, Phys. Rev. C **71**, 054307 (2005); <http://www.nndc.bnl.gov>.

²S. Leenhardt *et al.*, Eur. Phys. J. A **14**, 1 (2002).

³O. Perru *et al.*, Phys. Rev. Lett. **96**, 232501 (2006).

⁴J. M. Daugas *et al.*, Phys. Lett. **B476**, 213 (2000).

⁵A. N. Wilson *et al.*, Eur. Phys. J. A **9**, 183 (2000).

⁶S. Raman, C. W. Nestor, Jr., and P. Tikkanen, At. Data Nucl. Data Tables **78**, 1 (2001).

⁷M. Huyse, private communication; P. Van Duppen, Conf. Proc., Radioactive Nuclear Beams (RNB7), to be published.

⁸W. Walters, Conf. Proc., Radioactive Nuclear Beams (RNB7), to be published.

d.1.10. Deep Inelastic Reactions with CHICO: The Case of $^{48}\text{Ca} + ^{208}\text{Pb}$ (S. Zhu, R. V. F. Janssens, M. P. Carpenter, T. Lauritsen, C. J. Lister, D. Seweryniak, A. Hecht,* X. Wang,† J. A. Becker,‡ D. Cline,§ A. B. Hayes,§ A. Gade,¶ R. Macri,‡ and C.Y. Wu‡)

Over the last few years, our collaboration has initiated a program to investigate the properties of neutron rich nuclei above doubly-magic ^{48}Ca . At the onset, the primary motivation for these studies was the expectation that substantial modifications can occur to the intrinsic shell structure of nuclei with a sizable neutron excess.^{1,2} Deep inelastic reactions on thick targets with ^{48}Ca beams are one of the experimental approaches we have utilized. In the experiments, the γ rays were detected by Gammasphere.³ The success of

this approach has been demonstrated in a number of publications on the onset of a new shell gap at $N = 32$ in the neutron-rich Ti and Cr isotopes.^{2,4} Our experimental results have also led to a number of shell-model calculations with the most modern interactions.

However, due to Doppler broadening effects, the method used thus far was not sensitive to fast transitions emitted before the nuclei are fully stopped. The transitions from higher spins, or from collective

states, which are lost in thick target data, can be detected with proper Doppler correction if a thin target is used and the direction of the emitting nucleus is determined. These transitions are important for testing further theoretical calculations, and search for signatures of collectivity.

The experiment was performed with a 255 MeV ^{48}Ca beam bombarding on a 1 mg/cm^2 ^{208}Pb target at ATLAS. The heavy-ion counter CHICO⁵ was used to detect the target-like and projectile-like products at the same time. The γ rays, emitted in flight by both reaction products, were detected by Gammasphere. Event-by-event Doppler correction was applied based on the velocity vectors of the reaction partners determined from the intrinsic position and time information of CHICO, and the direction of the emitted γ rays given by the position of the Ge detectors in Gammasphere. CHICO was calibrated with events

corresponding to Rutherford scattering. The energy losses of the reaction products in the target vary with scattering angle for the target-like and projectile-like products. Therefore, an iterative method was applied to determine the masses of the binary products. Energy losses were also subtracted for the determination of their velocities. With an average velocity of about 10% of the speed of light, the FWHM of γ rays from projectile-like fragments was about 1.5% after Doppler correction. New transitions, which were totally absent in the thick target experiment, have been observed. The level scheme of ^{49}Sc , for example, was extended to higher energy. In Fig. I-19, the effects after Doppler correction with CHICO are illustrated by comparing the peaks in thick target (left) and thin target (right) experiments. ^{50}Ca and ^{50}Ti are among the other nuclei where fast transitions were observed for the first time. The analysis is still in progress.

*Argonne National Laboratory and University of Maryland, †Argonne National Laboratory and University of Notre Dame, ‡Lawrence Livermore National Laboratory, §University of Rochester, ¶Michigan State University.

¹B. A. Brown, *Prog. in Part. and Nucl. Phys.* **47**, 517 (2001).

²R. V. F. Janssens *et al.*, *Phys. Lett.* **B546**, 55 (2002).

³I. Y. Lee, *Nucl. Phys.* **A520**, 641c (1990).

⁴D. C. Dinca *et al.*, *Phys. Rev. C* **71**, 041302(R) (2005) and references therein.

⁵M. W. Simon *et al.*, *Nucl. Instrum. Methods* **A452**, 205 (2000).

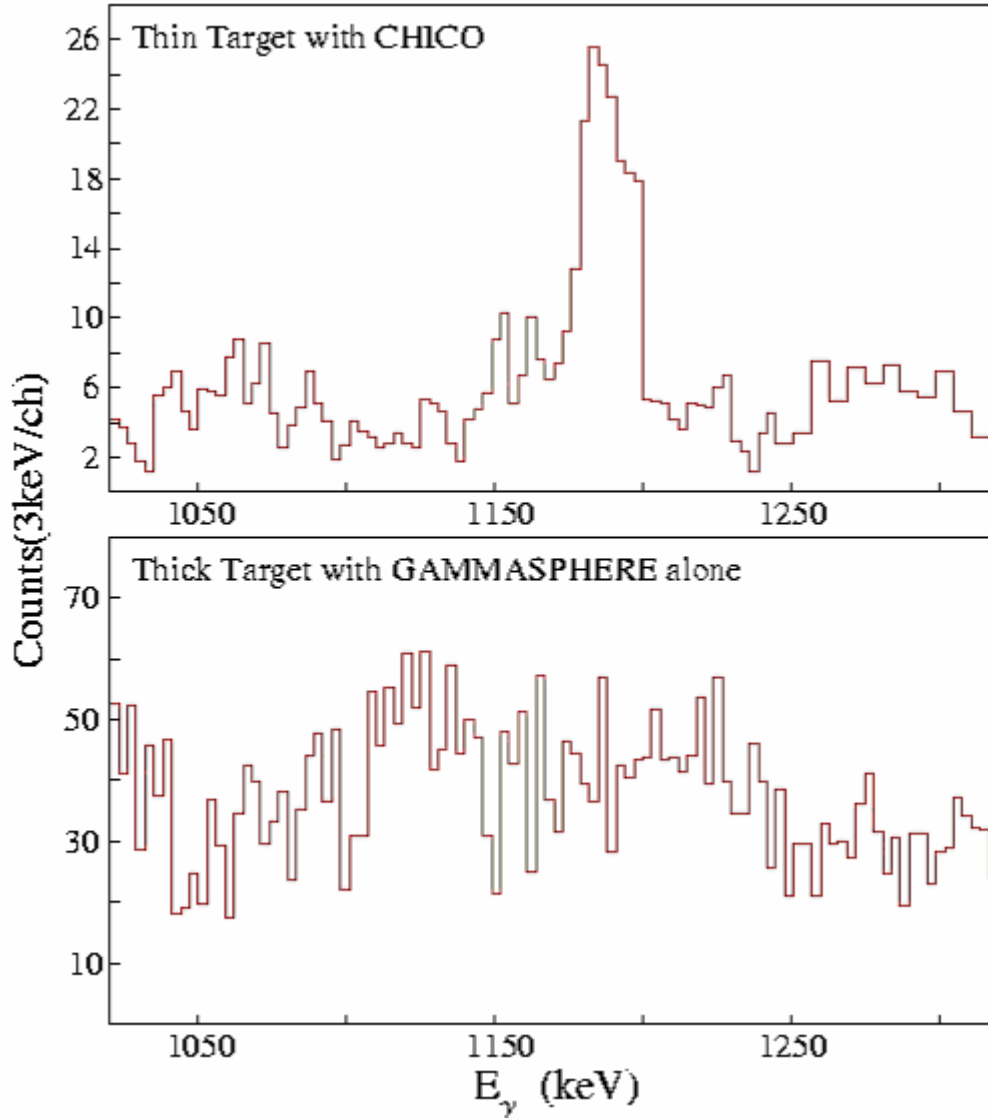


Fig. I-19. The effects of Doppler corrections with CHICO. The peaks in both figures were from spectra double gated by stopped transitions in both experiments.

d.2. Proton-Rich Nuclides

d.2.1. Shape Coexistence in ^{71}Br and the β -Decay of ^{71}Kr (C. J. Lister, S. M. Fischer, D. Seweryniak, G. Savard, S. Gros, B. Blank,* G. Canchiel,* J. Giovinazzo,* I. Matea,* G. de France,† F. de Oliveira Santos,† J. C. Thomas,† S. Grevy,† J.-C. Dalouzy,† I. Stefan,† R. Wadsworth,‡ D Jenkins,‡ M. Bentley,‡ N. Singh Bondili,‡ P. Davies,‡ and J. A. Clark§)

The breakdown of mirror symmetry due to Coulomb distortion and other charge-symmetry breaking effects provides a test of our knowledge of nuclear structure physics. Beyond that, it is important to understand as

the degree of breakdown sensitively influences the precise study of β -decays to confirm the unitarity of the CKM matrix, and seek physics beyond the standard model. Further, the wavefunction distortion affects

rp-nucleosynthesis reaction rates that are often estimated assuming perfect mirror symmetry.

The mass $A = 71$ pair ^{71}Br and ^{71}Kr have turned out to be very sensitive to mirror distortion. In a perfectly symmetrical world, the groundstate of $T_z = -1/2$ ^{71}Kr would have the same spin and parity as its $T_z = +1/2$ partner ^{71}Br , and the dominant decay mode would be a groundstate-to-groundstate Fermi transition. In fact, Gamow-Teller decays and mixing of wavefunctions due to the Coulomb energy, lead to decay branches to excited states. Usually they are small, a few percent of the flux and are used to measure the distortion. However, in ^{71}Kr the decay was reported to be $>15\%$, a level that is sufficiently large that it was suggested that ^{71}Kr may have a different spin to ^{71}Br . This would represent an unprecedented breakdown.

The key to understanding this puzzle lies in careful, detailed spectroscopy. We have reinvestigated ^{71}Br and considerably modified the decay scheme.¹ The new scheme lifts some β -decay puzzles, and clearly points to the fact that ^{71}Kr and ^{71}Br indeed have the same spin. However, our measurements, taken with the β -decay study² indicate the excited flux is even bigger than was thought. The decay can only be explained if there is shape co-existence in the groundstate of these nuclei and that the ^{71}Kr groundstate has quite different mixing to ^{71}Br .

This research has been published.¹ It has also led to a PAC-approved experiments to investigate ^{71}Kr “in-beam”, both using Gammasphere at Argonne and using Juroball at Jyväskylä. It has led to the initiation of a new β -decay collaboration to work at GANIL in France, to study this and even more neutron deficient $^{69,70}\text{Kr}$ isotopes.

*Centre d’Etudes Nucleaires de Bordeaux-Gradignan, France, †GANIL, Caen, France, ‡University of York, Heslington, United Kingdom, §Yale University.

¹S. M. Fischer *et al.*, Phys. Rev. C **72**, 024321 (2005).

²M. Oinonen *et al.*, Phys. Rev. C **56**, 745 (1997).

d.2.2. Neutron-Proton Correlations and Odd-Odd Nuclei: A Search for Excited States in ^{78}Y (S. M. Fischer,* C. J. Lister, R. Wadsworth,† C. Baktash,‡ and S. Paul‡)

Excited states in odd-odd $N = Z$ nuclei reveal the relative strength of np-pairing fields. If $T = 0$ deuteron pairing were on an equal footing to $T = 1$ correlations, the nuclei would have a degenerate pair of levels with $J = 1$, $T = 0$ and $J = 0$, $T = 1$ close to the groundstate. In fact, in ^{66}As , ^{70}Br , and ^{74}Rb the lowest $T = 0$ state appears near 1 MeV. However, these nuclei have complicated spectra due to shape-coexistence. ^{78}Y has always been thought to be the ideal laboratory for this kind of correlation physics, as it has large, stable prolate deformation.

Two efforts to investigate ^{78}Y have been made during the last year. In the first, an old Gammasphere/microball/neutron study of the $^{40}\text{Ca}(^{40}\text{Ca},\text{pn})^{78}\text{Y}$

reaction at 120 MeV has been revived and the data reanalyzed. Secondly, the superallowed β -decay of the ^{78}Y groundstate has been used to tag- ^{78}Y nuclei using the GREAT spectrometer at the RITU focal plane, in Jyväskylä, and prompt gammas were sought using Jurosphere.

The Recoil-Beta-Tagging experiment was a success and excited states in ^{78}Y were identified for the first time.¹ However, even with this knowledge, the reanalysis of the Gammasphere data was disappointing; the level of contamination from ^{12}C and ^{16}O in the target was too great to allow sufficiently good channel selection. This research is continuing.

*Argonne National Laboratory and DePaul University, †University of York, Heslington, United Kingdom, ‡Oak Ridge National Laboratory.

¹R. Wadsworth, private communication (2006).

d.2.3. New $T = 1$ and $T = 0$ States in ^{74}Rb and the np Pairing Gap (S. M. Fischer,*
C. J. Lister, P. Chowdhury, N. J. Hammond, R. V. F. Janssens, T. L. Khoo,
F. G. Kondev, T. Lauritsen, E. F. Moore, D. Seweryniak, S. Sinha, D. P. Balamuth,†
P. A. Hausladen,‡ D. G. Sarantites,‡ W. Reviol,‡ S. D. Paul,§ and C. Baktash§)

Odd-Odd, $N = Z$ nuclei are interesting laboratories for studying many nuclear structure effects, including neutron-proton correlations and the breakdown in analog symmetry. Charge symmetry breaking in nuclei is usually small but is important for extracting reliable Fermi matrix elements from superallowed beta-decays and testing CVC theory, a topic of current interest. We have used the $^{40}\text{Ca}(^{36}\text{Ar},\text{pn})^{74}\text{Rb}$ and $^{40}\text{Ca}(^{40}\text{Ca},\alpha\text{pn})^{74}\text{Rb}$ reactions at 108 MeV and 123, 160 MeV, respectively, to populate ^{74}Rb and determine the analog distortion through comparison of $T = 1$ states in ^{74}Rb with their corresponding ^{74}Kr levels. We have traced the analogs of the ^{74}Kr groundstate band in ^{74}Rb to spin $J = 8$ and determined

the Coulomb Energy Differences (CEDs). They are small, positive and increase smoothly with spin. New information was found on the $T = 0$ states which delineate the deformed band structure and clarify the de-excitation from high spin.¹ A new $T = 0$ band was found, together with several other candidate bandheads, revealing the distinct “np pairing gap” originally suggested by Rudolph *et al.*² between the highly correlated $T = 1$ groundstate and other excited configurations. The new bands are shown in Fig. I-20. Despite a careful search, no evidence was found for gamma decay to or from a low-lying $J^\pi = 0^+$ state in ^{74}Rb . A paper reviewing data from several experiments has been accepted for publication in 2006.

*Argonne National Laboratory and DePaul University, †University of Pennsylvania, ‡Washington University, §Oak Ridge National Laboratory.

¹C. D. O’Leary *et al.*, Phys. Rev. C **67**, 021301(R) (2003).

²D. Rudolph *et al.*, Phys. Rev. Lett. **76**, 376 (1996).

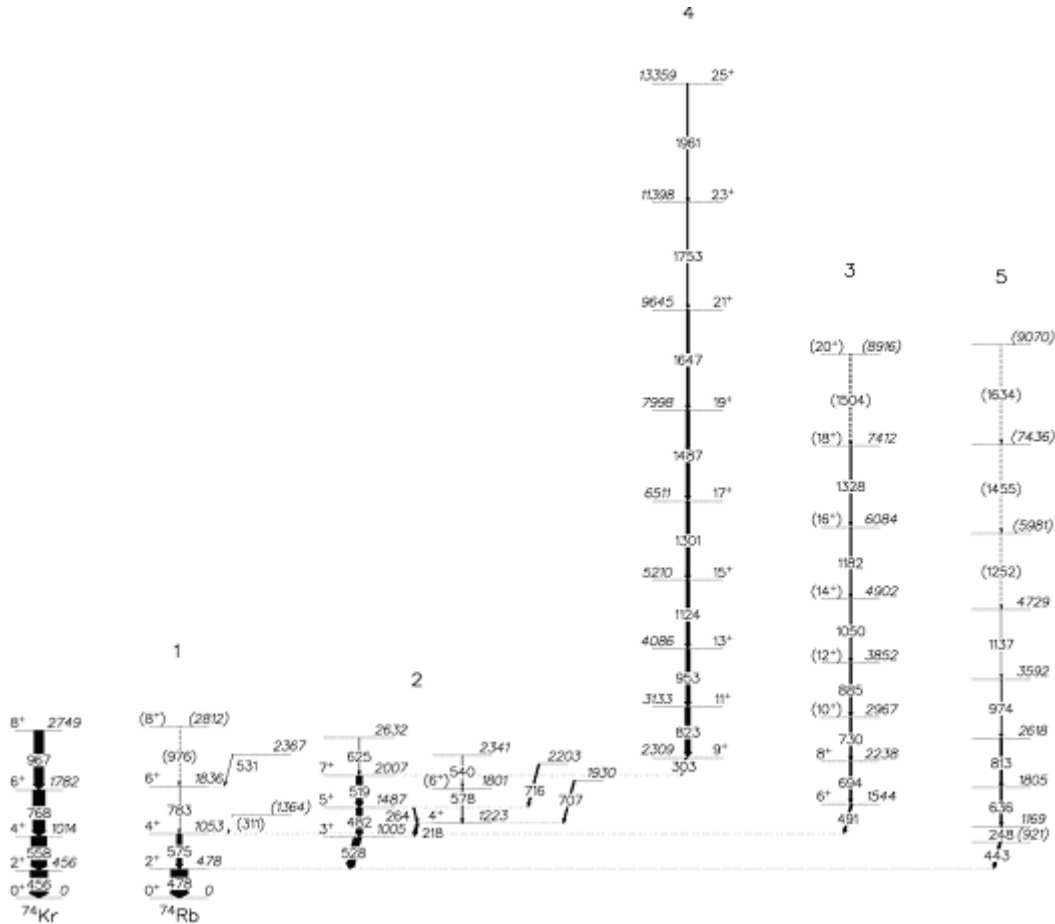


Fig. I-20. The new ⁷⁴Rb decay scheme derived from this work and previous studies.^{1,2}

d.2.4. Mapping the Periphery of Deformation in the A ~ 80 Region: A Study of ⁸³Nb
 (S. M. Fischer,* C. J. Lister, M. P. Carpenter, N. Hammond, R. V. F. Janssens,
 T. Lauritsen, S. Zhu, Y. Sun,† and D. P. Balamuth‡)

⁸³Nb has been studied in order to quantify the upper extent of large prolate deformation in the N~Z~40 region and ascertain its magnitude. The decay scheme has been considerably extended by studying gamma decay following the ⁵⁸Ni(²⁸Si,p2n) reaction at 204 and 215 MeV and using Gammasphere. Both signature partners of two clear rotational bands have been observed. A Projected Shell Model (PSM) analysis has been made which provides good reproduction of all the

features found for both bands. The inferred deformation is similar for the positive and negative bands, close to $\beta_2 = 0.4$, and appears nearly axially symmetric. ^{82,83}Nb may be the heaviest nuclei in the A ~ 80 region with such large deformation. The conditions appear right for the occurrence of K-Isomers.

A paper has been written and will be submitted in 2006.¹

*Argonne National Laboratory and DePaul University, †University of Notre Dame, ‡University of Pennsylvania.

¹S. M. Fischer *et al.*, to be submitted to Phys. Rev. C (2006).

d.2.5. A Search for Isomers in ^{86}Tc (C. J. Lister, S. Gros, D. J. Henderson, D. Seweryniak, B. R. Shumard, S. Zhu, A. B. Garnsworthy,* P. H. Regan,* B. B. Blank,† I. J. Cullen,* G. A. Jones,* Z. Liu,* N. J. Thompson,* and S. J. Williams*)

“In-flight” separation of ions in a spectrometer like the Argonne Fragment Mass Analyzer (FMA) allows sensitive searches to be made for interesting short-lived nuclear isomers in the 1-1000 μ -sec range. This time regime is long enough to allow physical “in-flight” separation from the point of production (~ 1 μ sec through the 8.2 m of the FMA) but is too short for separation by traditional ISOL methods, or even gas-catcher cooling (which takes 10-100 m-sec). The regime has the advantage that the time between arrival of the ion at a counting station and its subsequent decay is short enough that “random” or “chance” coincidences can be strongly suppressed, as can β -decay from nearer stability which usually has lifetimes in the approximate seconds regime.

In middle-mass nuclei, fusion-evaporation reactions of stable heavy ions can lead to the production of interesting isomers near the proton dripline. The shortcoming of “in-flight” separation with the FMA at near barrier energies is that the device selects by A/q, so whole chains of isobars can be produced and are all efficiently transported to the focal plane. As an example, an attempt to study microsecond isomers in the N = Z nucleus ^{86}Tc via the $^{58}\text{Ni}(^{32}\text{S},p3n)^{86}\text{Tc}$ reaction was swamped by radioactive ^{86}Mo , ^{86}Nb and ^{86}Zr all of which were produced at the same time. The isomers of interest were produced on the ~ 1 μ b level, while the more stable nuclei were produced with cross sections at the 50 mb level. To achieve the required suppression of the near-stability nuclei by a factor 104 two techniques were attempted: stopping in fast-flowing gas, and implant-gamma timing.

Isomer searches do not require any reaction detection at the target position, so intense beams can be used. In the current study, a rotating target wheel allowed 100's pA of ^{32}S to impinge on the target allowing copious production of mass A = 86 activity. Careful selection of A = 86 ions at the focal pane was achieved using mechanical slits. A channel plate detector imaged the

arrival of nuclei at rates up to 5×10^4 pps, mostly A = 86 residues but with a small scattered beam component. The ions then passed through a pressure window and were stopped in a tube of fast-flowing gas which could be varied from 10-1000 torr, and which carried the long-lived β -decays away on a timescale of ~ 1 s. However, states decaying on the microsecond scale could be efficiently counted. The tube was surrounded by 2 “clover” gamma detectors and a LEPS planar counter to detect gamma rays with an efficiency $>15\%$ for low-energy transitions. The gas pressure could be varied to stop the activity at the most efficient position.

A short commissioning run was made. It was found that using a natural chromium target was ideal, as it strongly produced well known isomers in ^{80}Rb which could be used for optimization and efficiency determinations. In practice, the clover counter could be used for tuning the gas pressure: if radioactivity was stopped in the right place then all four “leaves” count at the same rate. The pressure window was apparently thicker than estimated, so in practice a quite low gas pressure was optimal, on the ~ 10 s torr level. The need for shielding, to block the detectors from activity built up on the slits and downstream pumping system was evident. However, even with the most intense beams attempted (~ 100 pA) the total focal plane array never counted at more than 2000 gamma/s. Thus, the opportunity for using much more intense beams seems possible. Several electronic arrangements were considered, but using traditional analog time-to-amplitude converters had the least dead time.

The final test run to produce ^{86}Tc was inconclusive as the integrated beam-on-target was insufficient, and the collection time was short due to optimizing the setup. However, as a proof of principle, the experiment was successful. Another study will be made in the next cycle when Gammasphere is not located at the FMA target position and very intense beams can be used.

*University of Surrey, Guildford, United Kingdom, †Centre d'Etudes Nucléaire de Bordeaux-Gradignan, France.

d.2.6. Observation of the ^{105}Te α Decay (D. Seweryniak, C. N. Davids, S. Gros, T. L. Khoo, D. Peterson, A. Robinson, S. Zhu, K. Starosta*, A. A. Hecht,† N. Hoteling,† G. Lotay,‡ K. Vaman,* W. B. Walters,† and P. J. Woods‡)

The island of α activity north-east of ^{100}Sn offers a unique opportunity to search for “superaligned” α decay in $N \sim Z$ nuclei where protons and neutrons fill the same orbitals. The ^{105}Te nucleus has only one neutron more than ^{104}Te , which can be considered as an α particle coupled to the ^{100}Sn core.

A ^{58}Ni beam from the ATLAS impinged on a ^{50}Cr target to produce ^{105}Te nuclei following the evaporation of 3 neutrons. Three beam energies, namely 224, 214, and 204 MeV, were used during the experiment to optimize the ^{105}Te yield. Reaction products recoiling from the target were separated from the beam and dispersed according to their mass over charge state ratio in the Argonne Fragment Mass Analyzer. Mass slits were used to select only $A = 105$ residues with charge states $Q = 25^+$ and $Q = 26^+$ ($A = 106/Q = 25^+$ and $A = 106/Q = 26^+$ residues were partially allowed as well). After passing through a position sensitive Parallel Grid Avalanche Counter at the focal plane of the FMA, the recoils were implanted into a Double-Sided Si Strip detector (DSSD). The $32 \times 32 \text{ mm}^2$, 60 μm -thick DSSD was divided into 80 horizontal front strips and 80 vertical back strips, forming 6400 pixels. Subsequent α decays took place in the same pixel as the implantation. In the analysis, the implants were correlated with their subsequent α decays using spatial and temporal relations.

Due to the expected short half-life of ^{105}Te , special care was taken to optimize the detection of fast α -decay events. First, delay-line amplifiers, which recovered within 0.6 μs after the implantation signal, were used to detect α decays. Second, only implant events followed by decay events within 8 μs triggered the data acquisition system. This reduced the dead time drastically and allowed running with high rates in the DSSD.

Figure I-21 shows the α spectra collected during the experiment. A line containing 7 counts around 4 MeV is visible in the $A = 106$ spectrum. The properties of these 7 events are consistent with the known ^{106}Te α decay. The $A = 105$ spectrum contains a group of 13 counts just above 4.5 MeV. These events were interpreted as the α decay from ^{105}Te - all other known $A = 105$ nuclei produced in this reaction do not exhibit such a decay. Their time distribution is given in the

inset. The observed yield for the ^{105}Te events corresponds to a cross section ~ 10 nb, if an FMA efficiency of 5% is assumed together with a factor of 4 loss due to the short half-life.

To avoid systematic errors associated with implant-decay pile-up, the ^{105}Te energy was determined relative to the ^{106}Te events. A value of 4128(9) keV from Ref. 1 was adopted for $E_\alpha(^{106}\text{Te})$. The ^{105}Te half-life was obtained from the decay times of the ^{105}Te events using the maximum likelihood method. As a result, an energy of $E_\alpha = 4720(50)$ keV, corresponding to $Q_\alpha = 4900(50)$ keV, and a half-life of $T_{1/2} = 0.7(-0.17+0.25)$ μs were extracted. This is the shortest half-life ever observed using the implantation-decay correlation technique.

A reduced width of $\delta^2 = 230(-140+100)$ keV was obtained for ^{105}Te , after taking into account the errors associated with the energy and half-life. The reduced width, relative to the 70 keV reduced width in ^{212}Po , was calculated to be $W_\alpha = 3.3(-1.7+2.1)$. This should be compared to $W_\alpha = 4.6(-1.3+0.7)$,² $W_\alpha = 1.46(0.64)$, and $W_\alpha = 2.57(0.24)$ for ^{106}Te , ^{107}Te , and ^{108}Te , respectively. The ^{105}Te and ^{106}Te widths appear to increase modestly compared to these of ^{107}Te and ^{108}Te , supporting the idea of an increasing α -particle formation probability toward the $N = Z$ line, although the errors are rather large.

The Q_α -value for ^{105}Te obtained in this work is larger by about 600 keV than the corresponding value for ^{106}Te . It compares very well with a prediction of $Q_\alpha(^{105}\text{Te}) = 4.69$ MeV from the Liran-Zeldes semi-empirical formula,³ which is known to give good results far from the line of stability. A much larger value, $Q_\alpha(^{105}\text{Te}) = 6.31$ MeV, was calculated using the FRDM model.⁴ The Q_α -values increase by about 300 keV between ^{109}Te and ^{108}Te , and between ^{107}Te and ^{106}Te . Thus, the extrapolation from ^{105}Te to ^{104}Te suggests a Q_α -value of about 5.2 MeV for the latter nucleus, which in turn implies a half-life of the order of 50 ns. The observed ^{105}Te yield makes the search for a 1% α decay branch to the neutron $g_{7/2}$ excited state in ^{101}Sn possible.

The results of this experiment were already published in Ref. 5.

*National Superconducting Cyclotron Laboratory, †University of Maryland, ‡University of Edinburgh, United Kingdom.

¹R. D. Page *et al.*, Phys. Rev. C **49**, 3312 (1994).

²Z. Janas *et al.*, Eur. Phys. J. A **23**, 197 (2005).

³S. Liran and N. Zeldes, At. Data Nucl. Data Tables **17**, 431 (1976).

⁴P. Moller, J. R. Nix, and K.-L. Kratz, At. Data Nucl. Data Tables **66**, 131 (1997).

⁵D. Seweryniak *et al.*, Phys. Rev. C **73**, 061301(R) (2006).

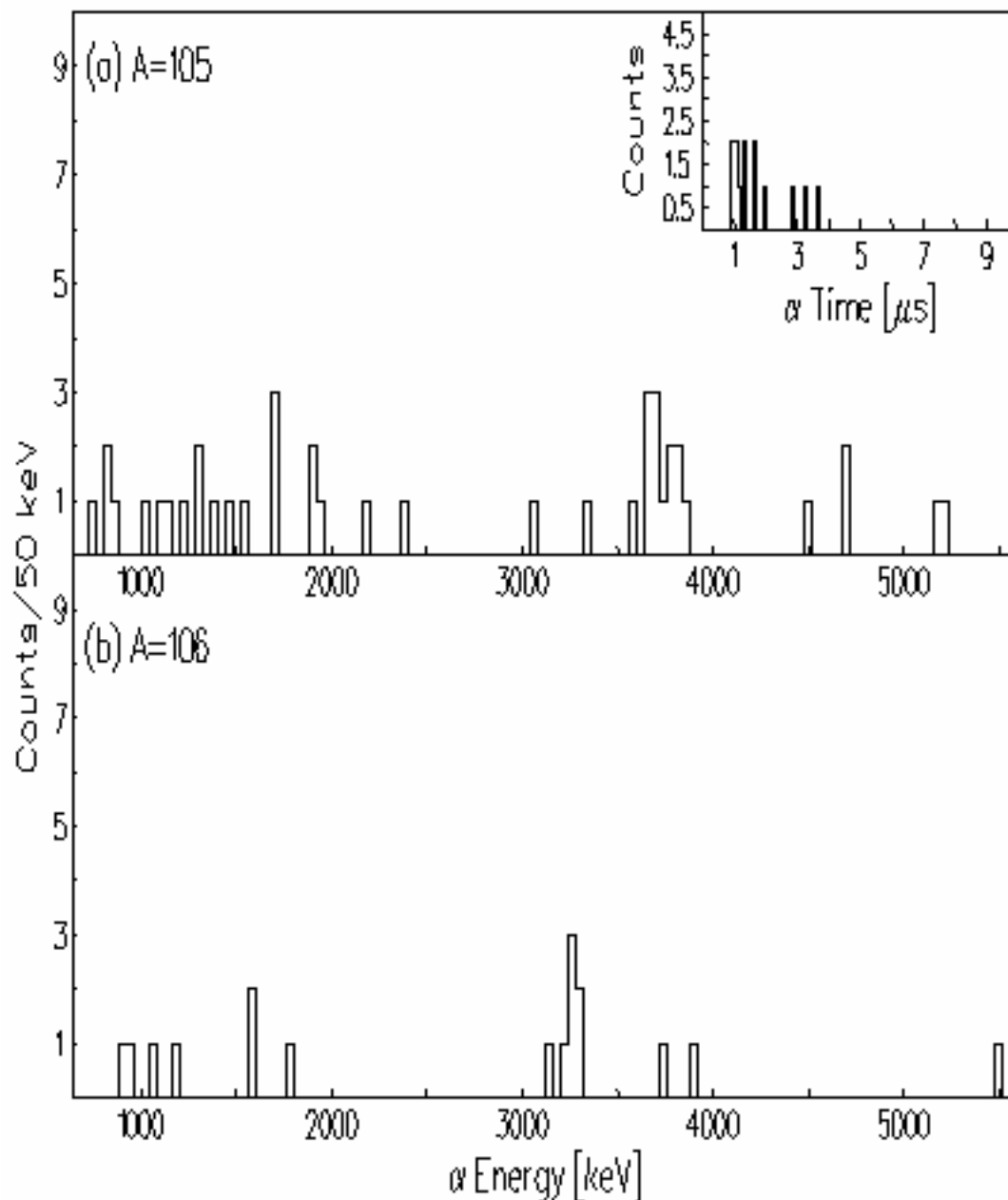


Fig. I-21. Alpha spectrum for (a) $A = 105$ and (b) $A = 106$ residues. The inset in the top panel contains the decay time spectrum for the 13 events corresponding to the full energy ^{105}Te α decay. Only decays with decay times longer than $0.6 \mu\text{s}$ and shorter than $8 \mu\text{s}$ were detected.

d.2.7. Level Structure of ^{181}Tl (M. P. Carpenter, F. G. Kondev, R. V. F. Janssens, I. Ahmad, C. N. Davids, N. Hammond, T. L. Khoo, T. Lauritsen, C. J. Lister, G. Mukherjee, D. Seweryniak, S. Sinha, D. J. Jenkins,* P. Raddon,* R. Wadsworth,* S. F. Freeman,† S. M. Fischer,‡ G. Jones,§ A. J. Larabee,¶ and A. Liechty¶)

With the return of Gammasphere to ATLAS, we have continued our program to look at proton rich nuclei in the vicinity of the $Z = 82$ closed proton shell. One of our most recent experiments utilized the $^{90}\text{Zr} + ^{92}\text{Mo}$ reaction to produce ^{181}Tl and ^{181}Pb via the $1p$ and $1n$ channel, respectively. For this measurement, Gammasphere was coupled with the FMA to characterize both the ground and excited states in these two nuclei. At the focal plane of the FMA, the PGAC measured the mass, the DSSD detected the energies of both the implants and the α particles emitted during the decay of the implanted ions. In addition, four Ge detectors surrounded the DSSD in order to measure γ rays in coincidence with detected particles.

The mid-shell Tl isotopes mimic the mid-shell Pb isotopes in that structures built on spherical, oblate and prolate shapes have been established in $^{183,185,187}\text{Tl}$.¹⁻³ A comparison of the excitation energy of single-particle states associated with the different shapes shows that the excitation energy of the $13/2^+$ prolate state continues to decrease as one approaches mid-shell ($N = 102$) while the oblate structure built on the $h_{9/2}$ orbital minimizes in excitation energy at $N = 108$ and rises in energy with decreasing neutron number. In all of these isotopes the groundstate remains spherical. It is an open question whether this same trend continues beyond mid-shell.

In the analysis of our Gammasphere experiment, we have followed the de-excitation of the $i_{13/2}$ prolate band

in ^{181}Tl down to the 1.4 msec isomer built on the $9/2^-$ oblate state. Based on our RDT measurements, most of the decay of this isomer precedes via γ emission to the groundstate while a small α decaying branch directly feeds an excited $9/2^-$ state in the daughter nucleus, ^{177}Au . For our Gammasphere measurement, we were not sensitive to the γ decay of the isomer to the spherical groundstate. However, in a recent measurement with the FMA and two clover detectors placed at its focal plane, we were able to measure the γ decay of this isomer and thus establish its excitation energy at 834 keV.

The complete level scheme of our results is given in Fig. I-22. While the $9/2^-$ isomer and $11/2^-$ spherical states are only 20 keV apart, the excitation of the $11/2^-$ state and $13/2^+$ rotational band which decays into the $11/2^-$ state are established by a weak 257-keV M2 transition linking the $13/2^+$ state with the $9/2^-$ isomer. With the excitation energy of these states known, we have established that both the $h_{9/2}$ oblate structure and the $i_{13/2}$ prolate band rise in excitation energy when compared to the same states in ^{183}Tl . In the case of the prolate structures, this is the same trend observed for the prolate bands in the even-even Pb and Hg isotopes. Finally, a rotational band is observed to feed the groundstate directly. We have tentatively assigned $1/2^+$ to the bandhead of this structure and $1/2[440]$ as its Nilsson configuration. This is the same configuration that has been suggested for the proton emitting state in ^{185}Bi . A manuscript of these results is in preparation.

*University of York, United Kingdom, †University of Manchester, United Kingdom, ‡DePaul University,

§University of Liverpool, United Kingdom, ¶Greenville College.

¹W. Reviol *et al.*, Phys. Rev. C **61**, 044310 (2000).

²M. Muikku *et al.*, Phys. Rev. C **64**, 044308 (2002).

³G. J. Lane *et al.*, Nucl. Phys. **A586**, 316 (1995).

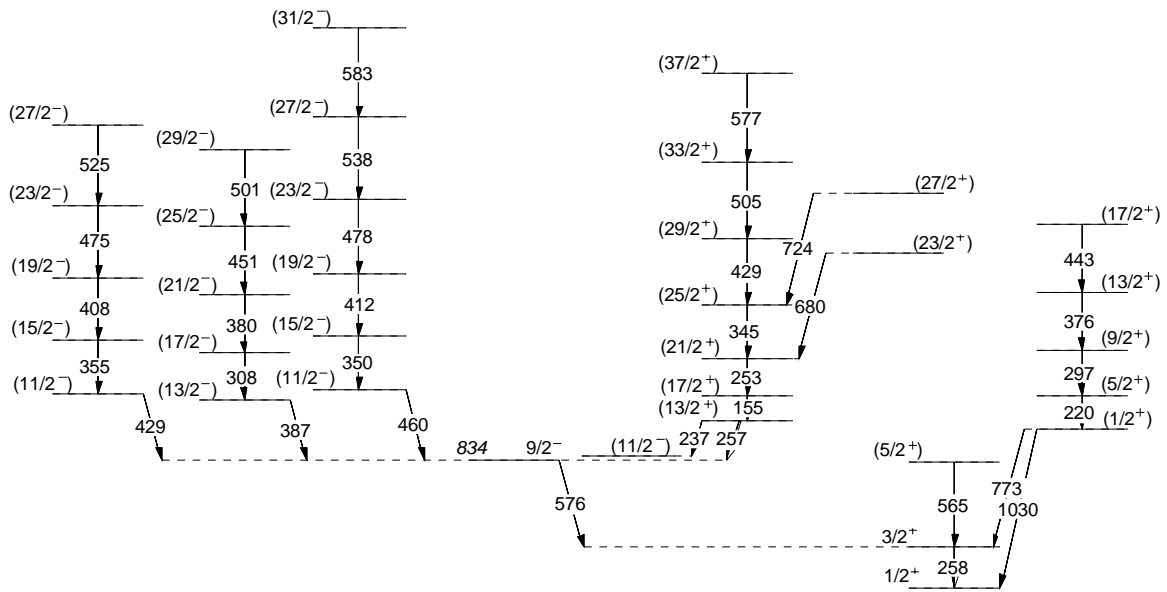


Fig. I-22. Partial level scheme for ^{181}Tl deduced from this work.

E. OTHER NUCLEAR STRUCTURE RESEARCH

Gammasphere at ATLAS allows a full program of gamma-ray spectroscopy to be explored. “Two-beamline” operation has allowed both the FMA and Gammasphere projects to be productive. A wide variety of programs continue at Gammasphere, including studying hot nuclei and studying nuclei at the very highest angular momenta.

e.1. Rotational Damping, Ridges and the Quasicontinuum of γ Rays in ^{152}Dy

(T. Lauritsen, I. Ahmad, M. P. Carpenter, A. M. Heinz, R. V. F. Janssens, D. G. Jenkins, T. L. Khoo, F. G. Kondev, C. J. Lister, D. Seweryniak, P. Fallon,* A. O. Macchiavelli,* D. Ward,* R. M. Clark,* M. Cromaz,* G. Lane,* B. Herskind,† T. Døssing,† A. Lopez-Martens,‡ A. Korichi,‡ and S. Siem‡)

Significant progress has been made in the final analysis of the ^{152}Dy data in an effort to extract the rotational damping at finite temperature in this nucleus. A preliminary level scheme has been developed which helped settle where the normal yrast line is located at high spins. More realistic level densities in the superdeformed well were applied as well. The final results have been written up in a detailed Phys. Rev. C article that will be submitted for publication shortly. This article will present the results of the analysis - as well as document, the procedures and techniques that were used to analyze the 1D and 2D quasi continuum gamma ray spectra.

The 1D and 2D quasi continuum gamma-ray spectra that were measured, along with Monte Carlo simulations reproducing these spectra, are shown in Fig. I-23. Panels A and C show the 1D quasi continuum and panels B and D the ridges that comes

from gamma-gamma correlations at finite temperature. From these ridges one can extract the rotational damping.

The Monte Carlo calculations now also use more realistic (renormalized) functions of the rotational damping parameters Γ_{rot} , Γ_{μ} , and the fraction of narrow to wide component, I_{nar} , taken from theoretical models. The values of the rotational damping parameters that were used to reproduce the experimental spectra are given in Table I-2, including the renormalizations factors.

A proposal was made, and accepted by the ATLAS PAC, to expand the extraction of the ridges of gamma-gamma ridges using other beam energies in the $^{48}\text{Ca} + ^{108}\text{Pd}$ reaction in order to probe the rotational damping at different spins and heat energies in ^{152}Dy .

*Lawrence Berkeley National Laboratory, †Niels Bohr Institute, Copenhagen, Denmark, ‡C.S.N.S.M., IN2P3-CNRS, Orsay, France.

Table I-2. In order to reproduce the ND and SD QC spectra and ridges in the MC calculation, it was necessary to multiply the theoretical rotational damping widths and narrow fractions with the factors shown in this table. Also shown are the resulting mean values of the distributions of Γ_{μ} , Γ_{rot} and I_{nar} .

Quantity	ND factor	ND mean value	SD factor	SD mean value
Γ_{μ}	0.14	21 keV	0.05	6 keV
Γ_{rot}	0.41	156 keV	3.2	214 keV
I_{nar}	28	14%	3.2	42%

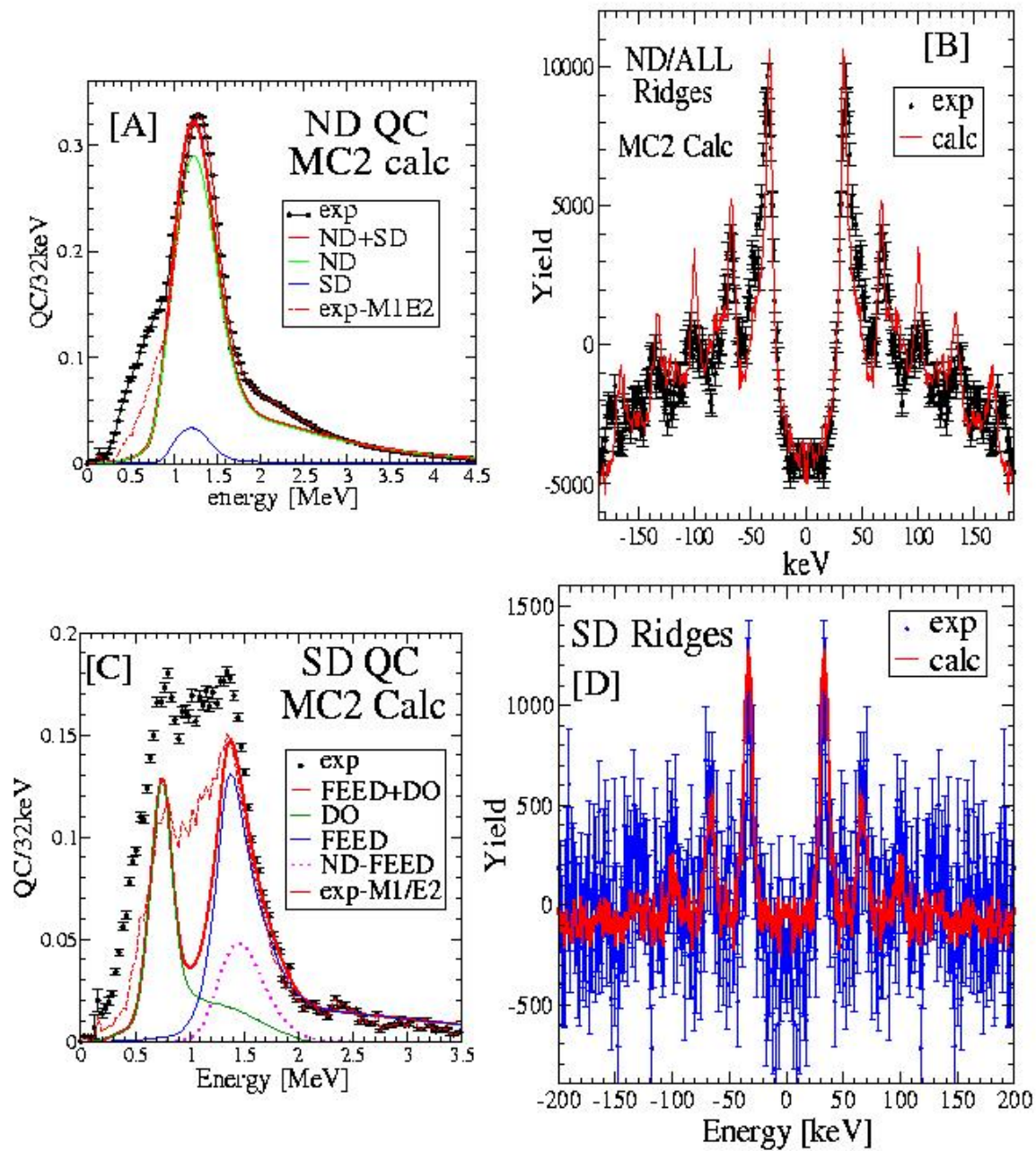


Fig. I-23. [A] ([C]). The QC spectra of gamma rays and [B] ([D]) gamma-gamma ridges when pairwise coincidence gates are set on combinations of clean ND (SD band 1) lines in ^{152}Dy . The lines show the results of MC calculations, which reproduce the spectra.

e.2. Narrow Spreading Widths of Excited Bands in a Superdeformed Well (T. L. Khoo, T. Lauritsen, A. Lopez-Martens,* T. Døssing,† B. Herskind,† M. Matsuo,‡ and K. Yoshida§)

Superdeformed nuclei are produced in fusion reactions at high angular momentum and excitation energy. The hot compound nucleus cools by evaporating neutrons, then by emitting γ rays. As the temperature decreases, a small fraction (typically $\sim 1\%$) of the cascades are trapped in the SD minimum. Rotation of the resulting elongated nucleus gives rise first to unresolved collective electric quadrupole (E2) transitions and then to an impressively long series of 20-25 discrete, nearly equi-spaced E2 transitions, which reveal one of nature's best rotors. This process represents a transition from a chaotic system, where symmetries and quantum numbers (apart from spin and parity) are broken, to a cold, ordered system. The resolved SD bands can be assigned the quantum numbers of states in a rotating mean field. Given the robustness of collective rotation exhibited by SD bands, it is interesting to explore if the change from chaos to order evolves through an ergodic¹ regime. This represents a situation where the wavefunctions are complicated, representative of a chaotic system, yet collective rotation and flow is preserved, e.g., with Porter-Thomas fluctuations in the strengths of all transitions except the collective E2 rays.¹ This work addresses the transition from chaos to order by investigating the structure of excited states in the SD well, which itself is an excited minimum (false vacuum).

We have examined the correlations of quasicontinuum E2 transitions, as revealed in an E_{γ_1} - E_{γ_2} matrix, which was obtained by gating on pairs of transitions in the yrast SD band of ^{194}Hg . We find exceptionally narrow ridges, which reveal rotational bands connecting unique states with spins differing by 2 \hbar , even though the wavefunctions of the eigenstates are complicated, containing many mean-field configurations. Figure I-24 shows a portion of the matrix in the region of transition energy 650-900 keV. Clear rotational correlations show up in the form of 2-3 ridges running parallel to the diagonal in the interval 650 to 900 keV. Transitions contributing to the ridges can be sampled by cutting slices of the matrix and projecting along the E_{γ_1} - E_{γ_2} coordinate, as indicated on Fig. I-24a, with the result displayed on Fig. I-24c and I-24d. The absolute intensity present in the ridges is given in Fig. I-25a together with the intensity of the one-dimensional E2 bump and of the yrast SD band intensity. Three other properties of the first ridge are shown in Fig. I-25. First, the energy separation between the first ridge and

the diagonal is shown together with that of consecutive transitions in the yrast SD band of ^{194}Hg (Fig. I-25b). Second, its width is displayed (Fig. I-25c). Finally, the number of bands (Fig. I-25d) which contribute to the ridge structure could be extracted from a fluctuation analysis.

The experimental observations imply many new and exciting features. The narrow ridges mean that the energy difference between any two consecutive transitions remains almost constant. The narrow width (Fig. I-25c) is a striking feature when one realizes that of the order of 100-150 bands contribute to the ridge. The ridge separation is a measure of the dynamical moment of inertia, $J^{(2)}$. Figure I-25b indicates, extraordinarily, that the moment of inertia from the ridge separation is practically identical to that of the yrast SD band. This is intimately related to the phenomenon of identical SD bands or, more accurately, identical dynamical moments of inertia $J^{(2)}$ in the mass 190 region. Figure I-24b shows how the coincidences between transitions in 20 discrete SD bands from the mass 190 region form narrow ridge-like patterns. The overall E_{γ_1} - E_{γ_2} coincidence matrix resembles that for excited quasicontinuum states in ^{194}Hg , including even giving the same $J^{(2)}$ value. Hence, the nearly identical $J^{(2)}$ values for discrete SD bands observed in the $A = 190$ region recurs even for excited SD states in ^{194}Hg . From the ridge intensities displayed in Fig. I-25, we can deduce that practically all the unresolved E2 strength is concentrated in the SD ridges and that there is little or no branching out from any band to another. The small width of the ridge and the large number of excited bands found in ^{194}Hg are quite different from all other cases for which rotational energy correlations have been studied. Both for the rotational states in ^{168}Yb and ^{163}Er , which have normal (smaller) deformation, as well as for the SD bands of ^{143}Eu , the fraction of E2 transitions carrying rotational energy correlations is much smaller, typically less than 10%, with the remaining transitions out of each state being fragmented over many weak transitions covering a quite wide energy interval, the rotational damping width (typically around 200 keV). In the feeding of SD bands in ^{152}Dy , the narrow fraction is somewhat larger ($\sim 30\%$) – (section e.1.), Lauritsen *et al.* In the present case of ^{194}Hg , the narrow SD ridge nearly exhausts the entire E2 strength, accounting for 80-100% of the E2 transitions in the 1-dimensional spectrum. Also, the

number of paths contributing to the ridge, that is the effective number of rotational bands carrying rotational energy correlations, is much larger in ^{194}Hg than in these other nuclei, by a factor of about 3 to 5.

Theory² indicates that the excited bands have many (2-10) components in their wavefunctions. With so many components, one could not assign any particular structure or any specific quantum numbers to them other than the energy, angular momentum and parity. In that sense, the bands approach an ergodic situation. The condition for ergodic bands¹ is that the rotational damping width Γ_{rot} is smaller than the average level spacing D . The present calculations show that the condition $\Gamma_{\text{rot}} < D$ is not met in the spin domain of the observed ridges (20 to 46 hbar). However, if one

considers instead D_2 , the average distance between states which interact via the residual two-body interaction, the condition $\Gamma_{\text{rot}} < D_2$ is met in the onset region of mixing. Also, the damping width is reduced relative to the full value $\Gamma_{\text{rot}} \sim 4\Delta\omega$, implied by the dispersion $\Delta\omega$ among the unmixed bands. This last effect is called motional narrowing, which is achieved when $2\Delta\omega < \Gamma_{\mu}$, where Γ_{μ} is the compound damping width arising from the mixing of mean-field configurations. For the SD bands in ^{194}Hg , all mixed bands are predicted to carry motional narrowing. This is a peculiar situation and has never been observed before.

This work is being prepared for submission to Phys. Rev. Lett.

*C.S.N.S.M., Orsay, France, †The Niels Bohr Institute, Copenhagen, Denmark, ‡Niigata University, Japan, §Nara University, Japan.

¹B. R. Mottelson, Nucl. Phys. **A557**, 717c (1993).

²K. Yoshida and M. Matsuo, Nucl. Phys. **A636**, 169 (1998).

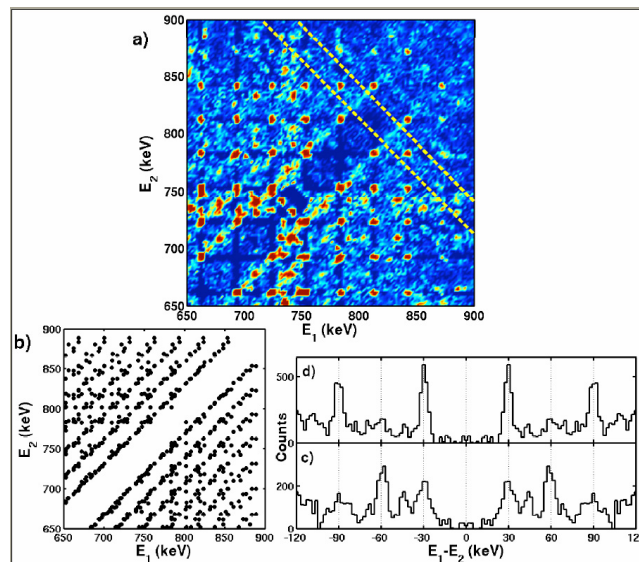


Fig. I-24. a) Experimental double SD-gated $E_{\gamma 1}$ - $E_{\gamma 2}$ coincidence matrix in ^{194}Hg . The yrast SD band shows up as a regular grid pattern of points. The first and second ridges are clearly visible from 650 to 850 keV. b) Schematic $E_{\gamma 1}$ - $E_{\gamma 2}$ coincidence matrix between transitions in 20 SD bands of even-even, odd-odd and odd-even mass 190 nuclei. c) and d) Projections perpendicular to the diagonal of the matrix shown in panel a). The diagonal is set at 0 keV and the projections, which are centered at 812 (c) and 798 keV (d), cover 20 of the ~ 30 keV interval between SD peaks. The projection region of panel c), illustrated by the dashed lines in a), has been selected to exclude the contribution of the intense SD yrast band from the first, but not the second, ridge. In panel d), the projection instead excludes this contribution from the second, but not the first ridge.

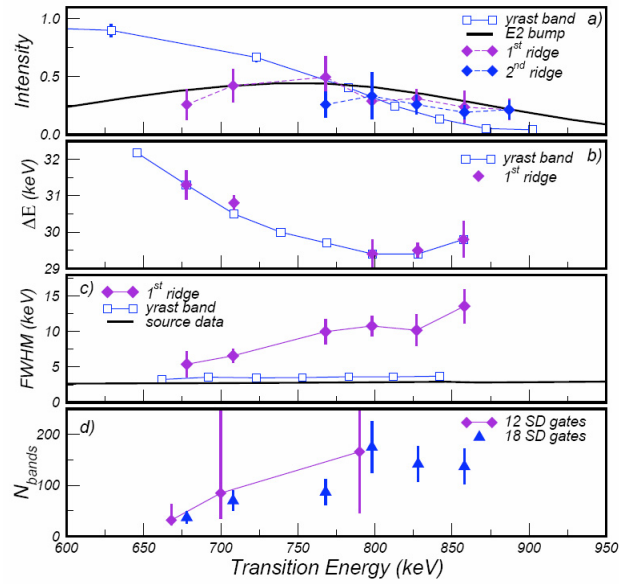


Fig. I-25. a) Intensity, in units of multiplicity/30 keV, present in the first and second ridges, the 1-dimensional quasicontinuum E2 peak and the SD yrast transitions. b) Inverse dynamical moment of inertia for the yrast SD band in ^{194}Hg and for the first ridge as a function of average transition energy. c) Widths (FWHM) of the first ridge, SD lines and calibration peaks. d) Number of bands contributing to the first ridge.

F. THE PHOBOS EXPERIMENT AT RHIC

2005 was the last year that Phobos acquired data at RHIC. Because the Phobos collaboration finished its goal of providing an experimental overview of the bulk properties of heavy-ion collisions at RHIC energies for several systems including proton-proton, d + Au, Cu + Cu and Au + Au, further data taking was curtailed and the Phobos detector was dismantled at the end of September 2005. The collaboration still has a wealth of data that is presently being analyzed and prepared for publication. It is expected that this activity will continue for another couple of years. The 2005 RHIC run provided collisions for the experiments for about 23 weeks. Phobos acquired data for Cu + Cu collisions at $\sqrt{s_{NN}} = 22.4, 62.4, \text{ and } 200 \text{ GeV}$, as well as p + p collisions at $\sqrt{s_{NN}} = 200 \text{ and } 410 \text{ GeV}$. Some analysis of data from these runs have already been completed and the results accepted for publication.

In the following, several new results obtained by the Phobos collaboration will be discussed.

f.1. The Phobos Experiment at RHIC (B. B. Back for the Phobos Collaboration*)

Charged-Particle Multiplicities in 62.4 GeV Au + Au Collisions

The multiplicity of charged particles emitted in 62.4 GeV Au + Au collisions has been measured as a function of pseudo-rapidity, η , and collision centrality.¹ The multiplicity of central collisions follow the energy dependence seen in previous Au + Au collisions measured at 19.6, 56, 130, and 200 GeV.² In particular, the new data is in excellent agreement with the early data point at 56 GeV,³ which combined with the new data indicate a small, but possibly significant, deviation from the logarithmic behavior observed over two orders of magnitude in collision energy. The 62.4 GeV measurement also substantiates the earlier observation

of extended longitudinal scaling and a factorization of the centrality and energy dependence of the charged particle multiplicity at mid-rapidity, which was seen previously at 19.6, 130, and 200 GeV. The total number of charged particles, obtained by integration over the full pseudo-rapidity distribution, is seen to scale linearly with the number of participant nucleon pairs, $N_{part}/2$. Also this observation is in accordance with the trend observed at the other energies. The pseudo-rapidity distributions for 62.4 GeV Au + Au collisions are shown in Fig. I-26 for six different centrality bins.

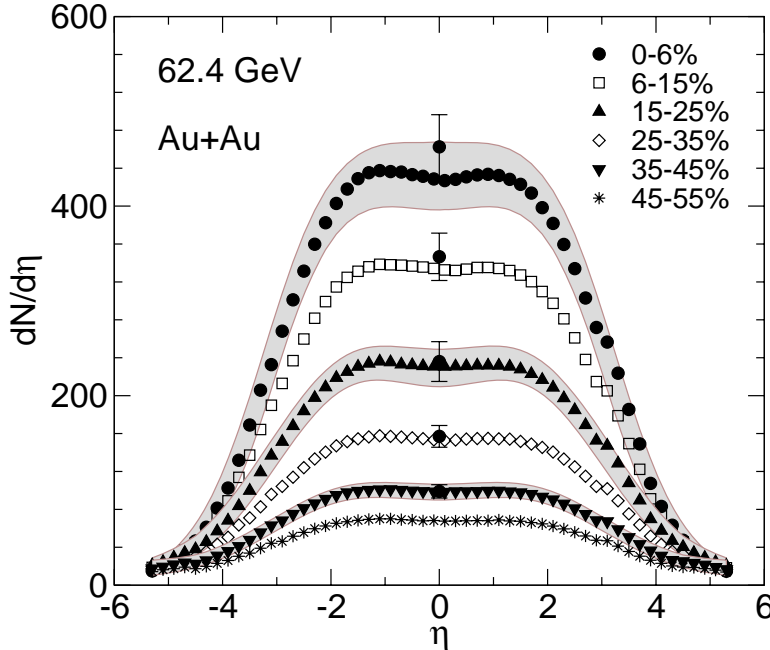


Fig. I-26. Pseudo-rapidity distribution of charged particles emitted in Au + Au collisions at $\sqrt{s_{NN}} = 62.4$ GeV for six centrality bins expressed as a fraction of the total inelastic cross section, the 0-6% bin being the most central.

Grey bands indicate the systematic uncertainties (90% C.L.). Data obtained from “tracklet” counting (hit combinations in two consecutive Si detectors) shown as single data points at $\eta = 0$ are seen to agree well with data from the pseudo-rapidity region covered by a single Si detector layer which represent an average of “hit-counting” and “energy deposition” methods of obtaining the charged particle multiplicity.

Directed Flow in Au + Au Collisions

Recently it has been possible to extract the directed flow component over a wide range of pseudo-rapidity in Au + Au collisions at energies of 19.6, 62.4, 130 and 200 GeV.⁴ This quantity, denoted v_1 , represents the first Fourier component of the azimuthal distribution of charged particles, i.e.

$$\frac{dN}{d(\phi - \psi_R)} = \frac{1}{2\pi} \left\{ 1 + \sum_{n=1}^{\infty} 2v_n \cos[n(\phi - \psi_R)] \right\},$$

where $\phi - \psi_R$ is the azimuthal angle relative to the reaction plane and n is the order of the Fourier component. The second Fourier component, v_2 , is normally referred as the elliptical flow. Because of the symmetry of the entrance channel in Au + Au collisions the v_1 component must equal zero at mid-rapidity ($v_1(0) = 0$) and it must be forward-backward anti-symmetric ($v_1(\eta) = -v_1(-\eta)$). In addition, since no reaction plane can be identified in truly central collisions one should expect $v_1(\eta) = 0$ for all values of η . Although it is not an explicit requirement in the analysis, the fact that the final data do exhibit these

symmetries, see Fig. I-27, speaks to the validity of the data analysis.

The data analysis was carried out using two different methods. In the symmetric sub-event method (solid points in Fig. I-27), the reaction-plane angle, ψ_R , determined from particles emitted in one pseudo-rapidity interval was used to determine the azimuthal angle, ϕ , distribution of particles emitted in another pseudo-rapidity region. The results are corrected for the resolution of the reaction plane determination. In the mixed harmonic event-plane analysis the reaction plane angle is obtained from the elliptical flow signal, and the directed flow signal seen out-of-plane is subtracted from the one measured in-plane. Assuming that the out-of-plane signal arises from non-flow correlations, the remaining in-plane signal should therefore represent the true directed flow signal.

Fig. I-27 shows that these two analyses are in good agreement for mid-central collisions at all four collision energies. It is therefore concluded that these symmetric sub-event method provides a reliable measure of the directed flow component.

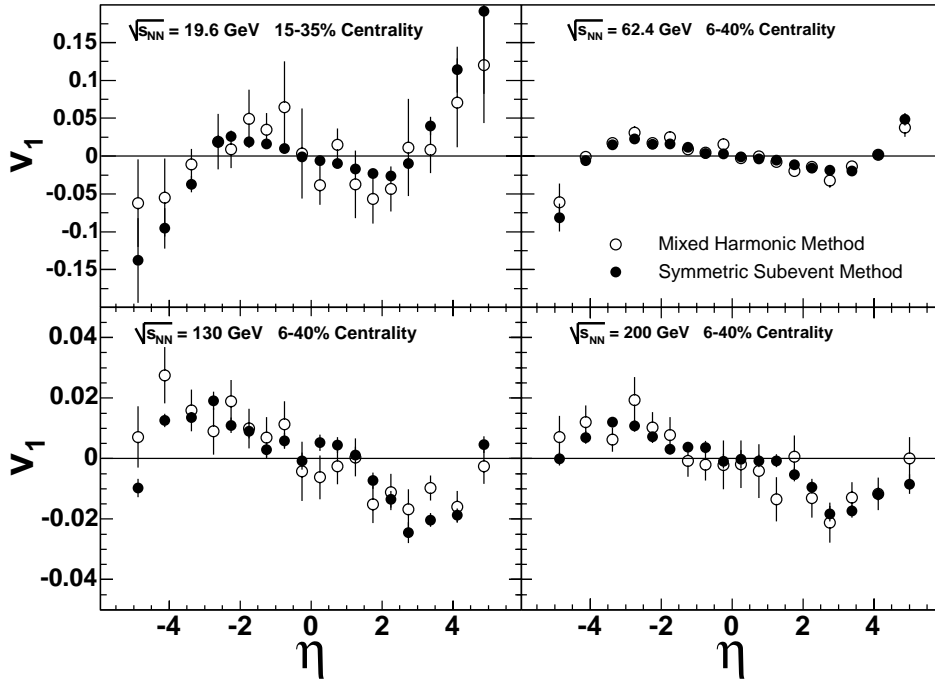


Fig. I-27. The measured directed flow signal, v_1 , is shown as a function of η for Au + Au collisions at 19.6, 62.4, 130, and 200 GeV. Results of the mixed-harmonic event-plane method are shown as open circles whereas the solid circles represent the standard symmetric η sub-event method. The centrality ranges were selected to optimize the quality of the mixed harmonic reaction determination. Only statistical errors are shown.

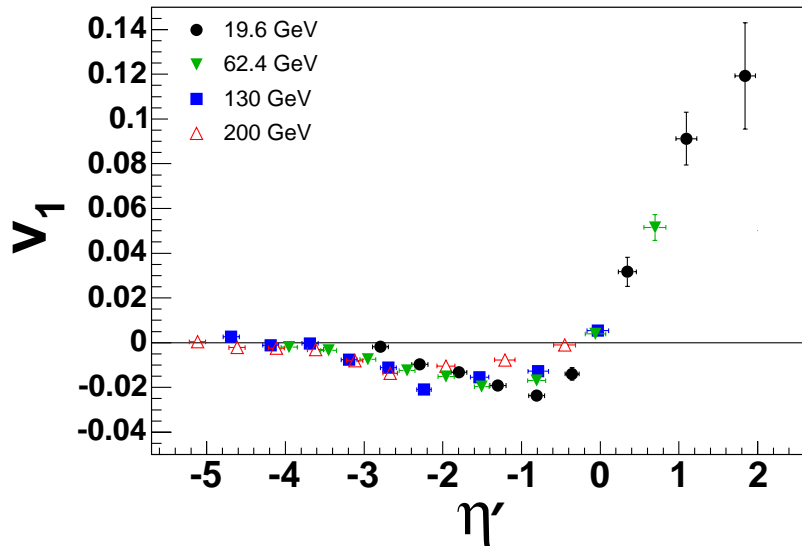


Fig. I-28. The directed flow signal, v_1 , averaged over the centrality range 0-40% is shown as a function of the parameter $\eta' = |\eta - y_{\text{beam}}|$ for four collision energies. Error bars represent statistical errors only.

As illustrated in Fig. I-28, we find that the directed flow component exhibit the same extended longitudinal scaling feature that has been observed for the elliptical

flow component as well as for the overall charged particle multiplicity.²

Transverse Momentum Spectra in Au + Au And Cu + Cu Collisions

The study of transverse momentum spectra in Au + Au collisions at RHIC led to the discovery of suppression of the high- p_T part of the spectrum, which has been taken as one of the early indications that a strongly interacting Quark Gluon Plasma was created in these collisions. This interpretation holds that the high- p_T particles belong to jets that stem from hard parton collisions. The fact that such high- p_T particles are produced less frequently in central Au + Au as compared to pp collisions at the same energy therefore signal an extremely high energy loss of high- p_T partons as they propagate through the hot fire ball formed in such collisions. Theoretical calculations indicate that only a deconfined phase of quarks and gluons can provide such a high energy loss which indicates that this phase is indeed present in the collision. Subsequent control measurements of $d + Au$ collisions verified that the high- p_T suppression is not an

entrance channel effect – another possible explanation of the phenomenon.

In view of the importance of the high- p_T suppression result, it is mandatory to study its dependence on the size and extend of the plasma through which the high momentum partons must travel. In the Au + Au system this was done by varying the centrality and the effect was observed to diminish and eventually disappear as the overlap area between the two incoming ions was reduced while going from central to peripheral collisions.⁵ This method, however, strongly modifies the geometry of the overlap zone, and it is therefore of interest to study the effect for a smaller system. This was done during the Cu + Cu runs in 2005. Transverse momentum spectra have thus been measured for Cu + Cu collisions at collision energies of 62.4 and 200 GeV as shown in Fig. I-29.

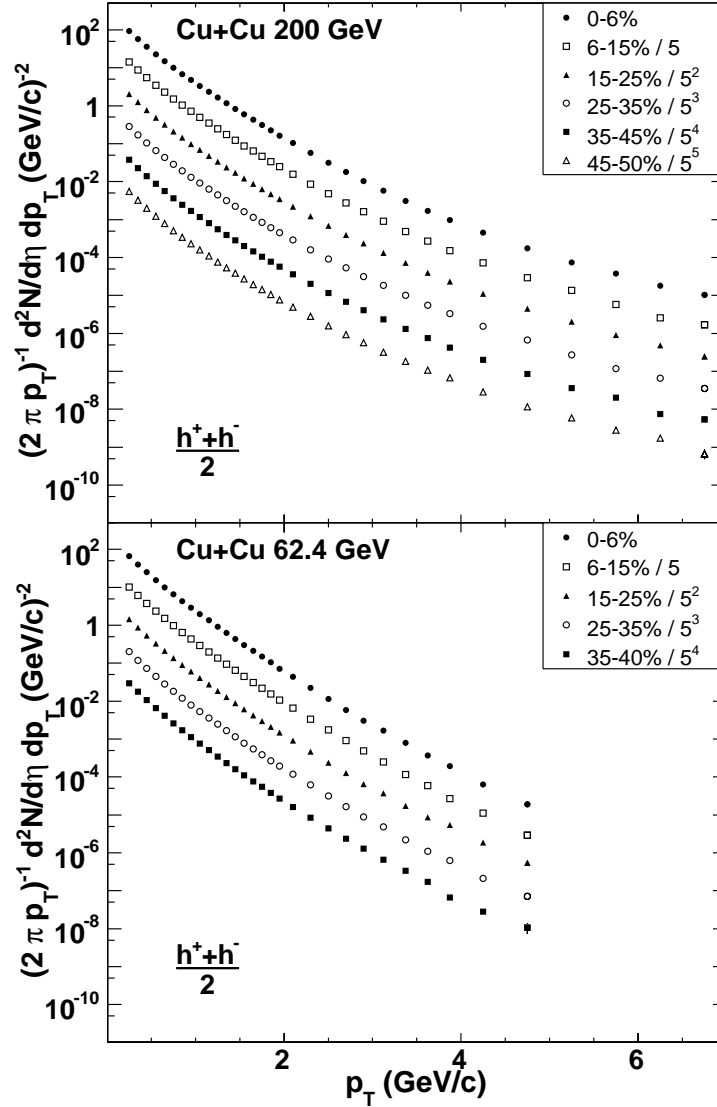


Fig. I-29. The invariant yield of charged hadrons within $0.3 < \eta < 1.4$ for Cu + Cu collisions is shown as a function of transverse momentum, p_T , in the top panel for 200 GeV, and the bottom panel for 62.4 GeV. For clarity, consecutive centrality bins are reduced by a factor of five. Statistical and systematic errors are smaller than the symbol size.

At 200 GeV the transverse momentum spectra were measured up to 4.75 GeV/c whereas the spectra were extended up to 6.75 GeV/c at 200 GeV.

In order to compare the particle emission in heavy-ion collisions to those in pp collisions it is customary to study the ratio

$$R_{AA}(p_T) = \frac{\sigma_{pp}^{inel}}{\langle N_{coll} \rangle} \frac{d^2 N_{AA} / dp_T d\eta}{d^2 \sigma_{pp} / dp_T d\eta},$$

where σ_{pp}^{inel} is the pp inelastic cross section, $\langle N_{coll} \rangle$ is the average number of nucleon-nucleon collisions obtained from Glauber model simulations, and $d^2 N_{AA} / dp_T d\eta$ and $d^2 N_{pp} / dp_T d\eta$ are the double differential cross sections for charged hadron production in heavy-ion and pp collisions, respectively. A value of $R_{AA} = 1$ is obtained if the particle production in heavy-ion collisions scales directly with the average number of binary nucleon-nucleon collisions occurring within the collision between two heavy ions.

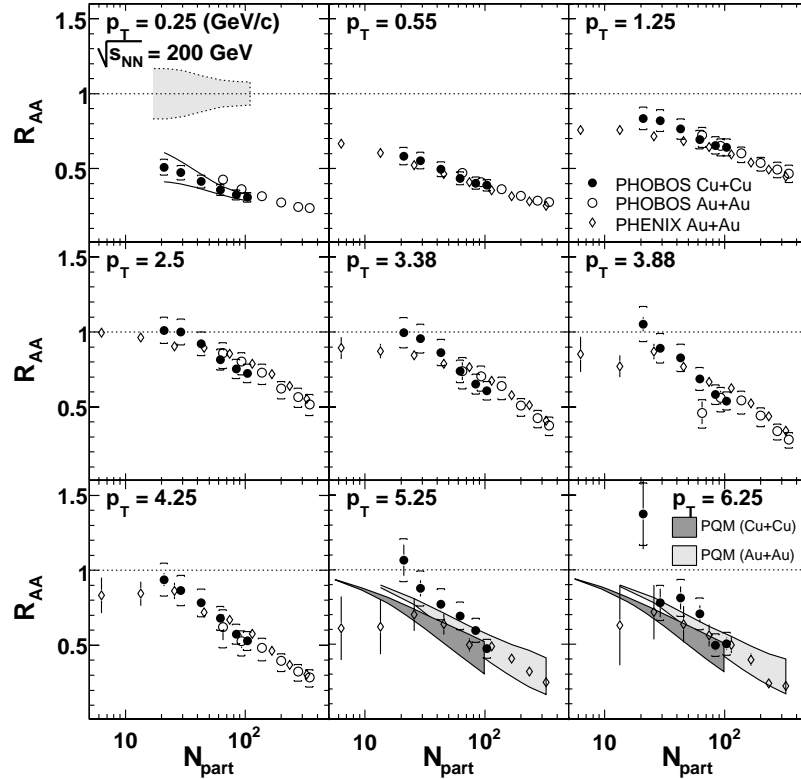


Fig. I-30. The nuclear modification factor, R_{AA} , for Au + Au (solid symbols) and Cu + Cu (open symbols) collisions at 200 GeV is shown as a function of centrality (N_{part}) for different bin of transverse momentum, p_T . The grey band in the top-left panel represents the relative uncertainty in $\langle N_{coll} \rangle$ and the solid lines show the corresponding effect on the measured value of R_{AA} . The bands shown at $p_T = 5.25$ and 6.25 GeV/c represent predictions of the parton quenching mode.⁶

In Fig. I-30 we observe that for $p_T > 3$ GeV/c the R_{AA} ratio decreases from a $R_{AA} = 1$ for peripheral collisions to $R_{AA} \sim 0.2 - 0.3$ for the most central collisions. For all p_T bins we see good agreement between the Au + Au^{5,7} and Cu + Cu data in the overlap region with the same number of participants, N_{part} , which is consistent with the fact that the spectral shape for Cu + Cu and Au + Au collisions are identical for the same size of the overlap volume. The present Phobos data are also

compared with Au + Au data from PHENIX (open diamonds) showing good agreement up to $p_T \sim 3$ GeV/c but deviating somewhat above this value. The shaded bands for the two highest p_T bins represent predictions by the Parton Quenching Model⁶ which gives a good representation of the experimental trend, but exhibits a larger dependence on the mass of the colliding ions than seen experimentally.

Forward-Backward Multiplicity Correlations in Au + Au Collisions

The study of correlations between particles emitted in relativistic heavy-ion collisions is an important tool for assessing the underlying mechanisms for particle production. Several measures of such correlations have been suggested and used.^{8,9} One of these⁹ relies on a differentiation between positive and negatively charged

particles and is consequently not appropriate for application to Phobos data. On the other hand, the large angular acceptance for non-identified charged particles facilitates a different type of analysis based on comparing the particle multiplicity in symmetric forward-backward bins in pseudo-rapidity.

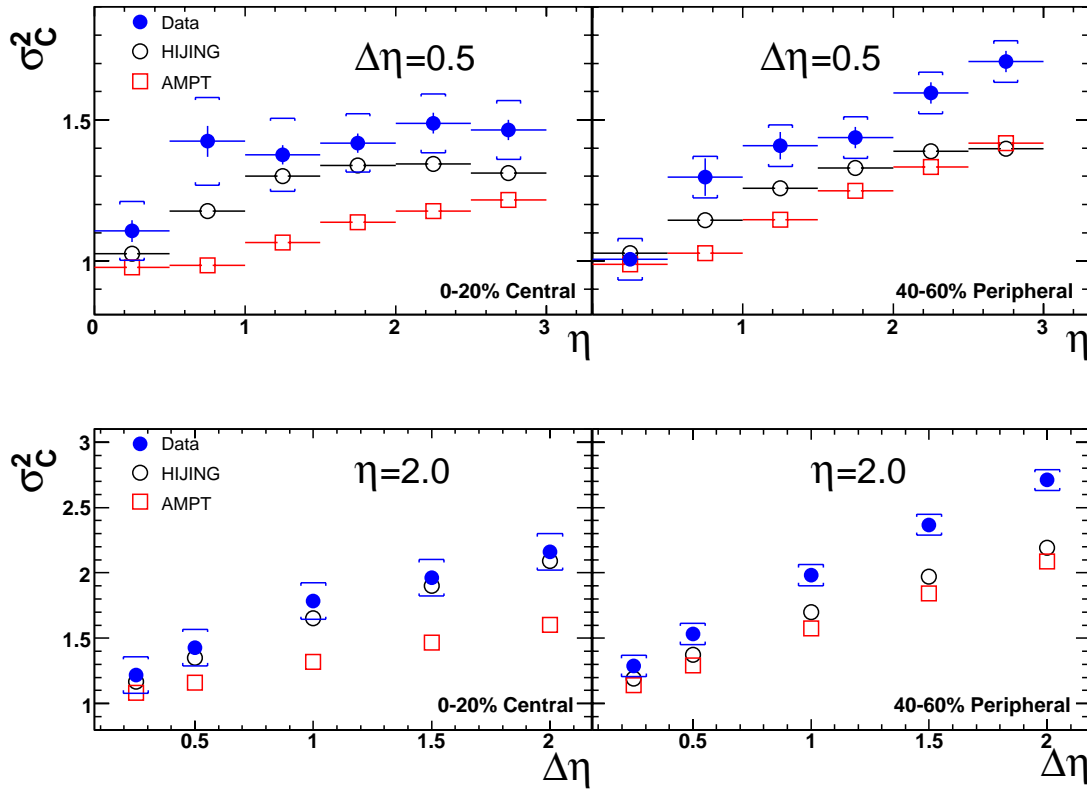


Fig. I-31. Upper panels: The correlation measure σ_c^2 for a fixed $\Delta\eta = 0.5$ pseudo-rapidity bin width is shown as a function of η for central (0-20%) and peripheral (40-80%) 200 GeV Au + Au collisions, respectively. The data (solid blue) are compared to predictions of the HIJING¹⁰ and AMPT¹¹ models shown as open circles and squares, respectively. Lower panels: Same as above but shown as a function of the width $\Delta\eta$ of the pseudo-rapidity interval around $\eta = 2.0$.

In the present analysis, based on the 200 GeV Au + Au data from Phobos, the correlation between particles emitted in a pseudo-rapidity bin of width $\Delta\eta$ centered at η with those emitted at $-\eta$ in a bin of the same width is probed. Denoting the number of charged particles emitted in the forward and backward bin, N_F and N_B , respectively one can construct the event-wise observable

$$C = \frac{N_F - N_B}{N_F + N_B},$$

which measures the forward-backward asymmetry in particle emission. Because of the entrance channel symmetry in Au + Au collisions the distribution of this quantity will be centered at zero, but its variance, σ_c^2 will contain information on the contribution of cluster emission (e.g. resonance decays) to the observed particle emission. The data have been corrected for contributions from detector granularity and efficiency as well as secondary particles emission. The results are

compared with predictions of the HIJING¹⁰ and AMPT¹¹ models in the upper panels of Fig. I-31, where σ_c^2 is shown for particles falling with a pseudo-rapidity window of width $\Delta\eta = 0.5$ centered at η as a function of η for 0-20% central (left panel) and 40 - 60% peripheral (right panel) Au + Au collisions at 200 GeV. The data (solid circles) are seen to exceed the predictions of both theoretical models indicating a stronger contribution of clusters than predicted theoretically. However, the comparison shown in the lower panels of Fig. I-31, where σ_c^2 is shown for a pseudo-rapidity windows of varying width, $\Delta\eta$, centered at $\eta = 2.0$, indicates that the cluster size is predicted approximately correctly by the HIJING models whereas both models fail to reproduce the data for peripheral events. These results indicate that the theoretical understanding of the details of particle emission in heavy-ion collisions is inadequate.

*Brookhaven National Laboratory, Institute of Nuclear Physics, Krakow, Poland, Massachusetts Institute of Technology, National Central University, Taoyuan, Taiwan, University of Rochester, University of Illinois at Chicago, and University of Maryland.

¹B. B. Back *et al.*, (Phobos), nucl-ex/0509034, submitted to Phys. Rev. C.

²B. B. Back *et al.*, (Phobos), Phys. Rev. Lett. **91**, 052303 (2003).

³B. B. Back *et al.*, (Phobos), Phys. Rev. Lett. **85**, 3100 (2000).

⁴B. B. Back *et al.*, (Phobos), nucl-ex/0511045, submitted to Phys. Rev. Lett.

⁵B. B. Back *et al.*, (Phobos), Phys. Lett. **B578**, 297 (2004).

⁶A. Dainese, C. Loizides, and G. Paic, Eur. Phys. J. C **38**, 461 (2005).

⁷K. Adcox *et al.*, Phys. Lett. **B561**, 82 (2003).

⁸J. Adams *et al.*, (STAR), Phys. Lett. **B634** (2006) 347.

⁹J. Adams *et al.*, (STAR), Phys. Rev. Lett. **90**, 172301 (2003).

¹⁰M. Gyulassy and X. N. Wang, Comp. Phys. Comm. **83**, 307 (1994).

¹¹Z. W. Lin *et al.*, Phys. Rev. C **72**, 064901 (2005).

f.2. Consequences of Energy Conservation in Relativistic Heavy-Ion Collisions (B. B. Back)

Experimentally, a complete characterization of particle production and emission in relativistic heavy-ion collisions is in general not feasible. It has recently been shown, however, that the availability of essentially complete measurements of the charged-particle multiplicity in pseudo-rapidity space allows for a reliable estimate of the average transverse momentum and energy of emitted particles by imposing energy conservation in the process.¹ Based on the requirement that a fraction, f_{ch} , of the energy carried by the N_{part} collision participants appear as charged particles in the exit channel, it is possible to place severe constraints on the mean transverse momentum of charged particles as a function of pseudo-rapidity. The exit channel energy is thus:

$$E_{ch}^{out} = \int_{-\infty}^{\infty} \frac{dE}{d\eta} d\eta,$$

where

$$\frac{dE}{d\eta} = \frac{dN}{d\eta} \int_0^{\infty} \sqrt{\langle m \rangle^2 + p_T^2} \cosh^2 \eta \frac{dN}{dp_T} dp_T.$$

Here $dN/d\eta$ is the pseudo-rapidity distribution of charged particles, which is measured by PHOBOS,² $\langle m \rangle$ is the average mass of charged particles and $dN/d\eta$ is their transverse momentum distribution. The latter has been measured at mid-rapidity and found to follow a power law spectrum.³ Figure I-32b demonstrates the validity of using an average mass instead of separately integrating over the transverse momentum distribution for particles of different mass, *e.g.* pions, kaons and protons/anti-protons. The effect of the particle mass is significant only near mid-rapidity as shown in Fig. I-32a.

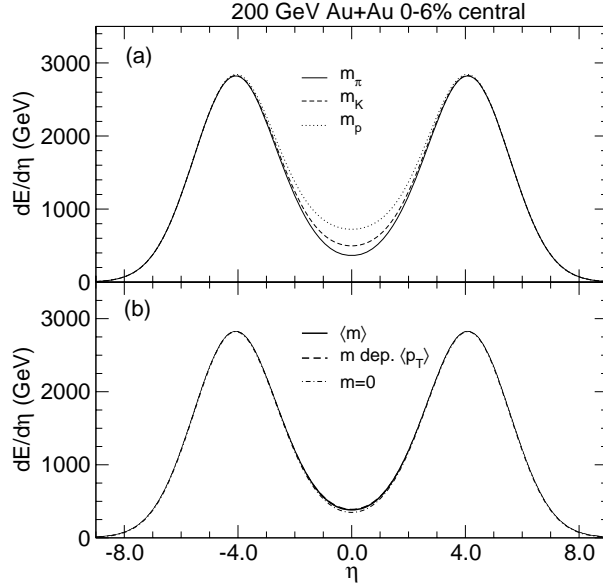


Fig. I-32. Panel a): Only in the mid-rapidity region does the particle mass affect the energy; for $|\eta| > 3$ the particle mass is irrelevant. Panel b): Comparison of $dE/d\eta$ calculated using a actual particle masses and the corresponding values of $\langle p_T \rangle_i$ (dashed curve) with one that uses an average particle mass (solid curve). A calculation with $m = 0$ (dash-dotted curve) gives slightly smaller values near $\eta = 0$ only.

A simple accounting of the energy balance shows that the mean p_T must fall off away from mid-rapidity. Based on p_T spectra measured by BRAHMS⁴ over a limited (pseudo)-rapidity range it is believed that a Gaussian dependence of $\langle p_T \rangle$ as a function of η , for which the maximum value at $\eta = 0$ is realistic. The energy balance in the collision can therefore be established by varying the width of the Gaussian function.

The results of this analysis are shown in Fig. I-33 for $Au + Au$ collisions at 130 GeV (left figure) and 200 GeV (right figure) for six centrality bins. The grey error bands include contributions from the errors on experimental input parameters.

Given the mean transverse momentum as a function of η , it is possible to estimate the energy density, ε_0 , for particles emitted in different regions of pseudo-rapidity.

This estimate is based on the prescription of Bjorken,⁵ namely

$$\varepsilon_0 = \frac{\langle m_T \rangle}{\tau_0 A} \frac{dN}{dy},$$

where $\langle m_T \rangle$ is the average transverse mass, τ_0 is the assumed equilibration time, A is the overlap area between the two nuclei, and dN/dy is the particle density per unit rapidity, y . The results are shown as $\varepsilon_0 \tau_0$ in Fig. I-34 for 200 GeV $Au + Au$ collisions at two centralities. For an assumed relaxation time of $\tau_0 = 1$ fm/c one finds that the energy density peaks rather sharply at $\eta = 0$ and falls off quickly away from this region. It is clear, however, that the energy density exceed that of about 0.7-1.0 GeV/fm³ corresponding to the transition from a hadronic to a quark-gluon phase of matter predicted on the basis of lattice QCD models⁶ for a wide range of pseudo-rapidities around $\eta = 0$.

¹B. B. Back, Phys. Rev. C **72**, 064906 (2005).

²B. B. Back *et al.*, (PHOBOS), Phys. Rev. Lett. **91**, 052303 (2003).

³C. Adler *et al.*, (STAR), Phys. Rev. Lett. **87**, 112303 (2001); *ibid* **89**, 202301 (2002); nucl/ex/0311017.

⁴I. G. Bearden *et al.*, (BRAHMS), Phys. Rev. Lett. **93**, 102301 (2004); *ibid* **94**, 162301 (2005).

⁵J. D. Bjorken, Phys. Rev. D **27**, 140 (1983).

⁶F. Karsch, J. Phys. G **30**, S887 (2004).

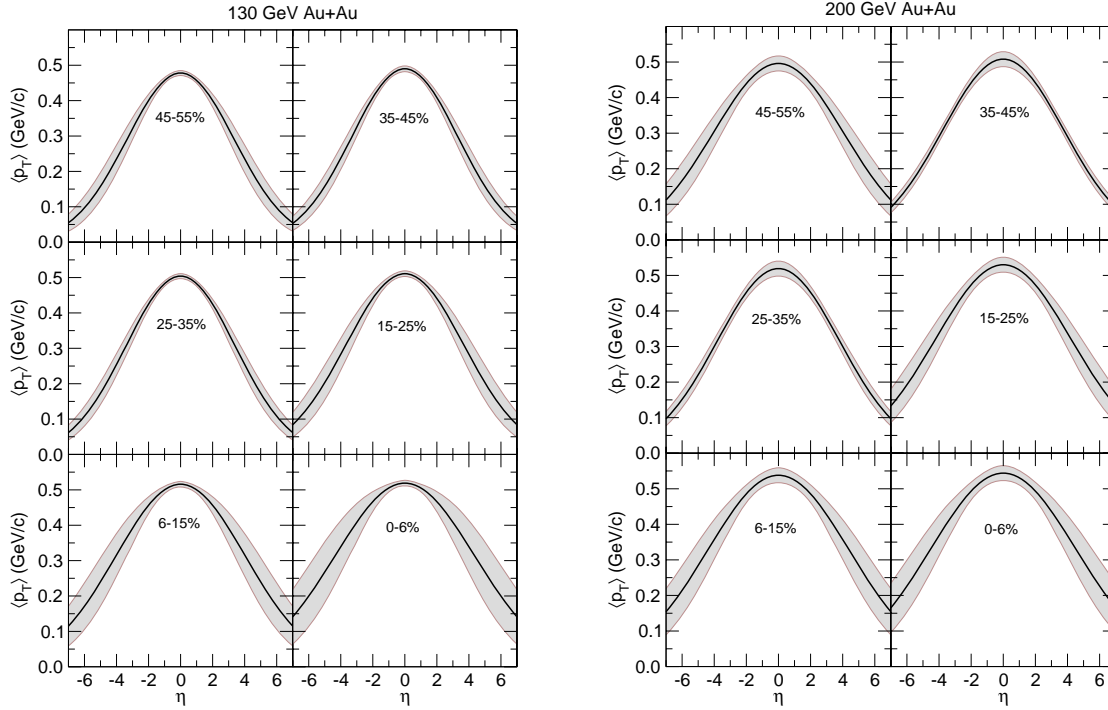


Fig. I-33. Left panel: Mean transverse momentum is shown as a function of pseudo-rapidity for six different centrality bins in Au + Au collisions at 130 GeV. Solid curves are Gaussian pseudo-rapidity dependence. Right panel: Same, but for 200 GeV collision energy.

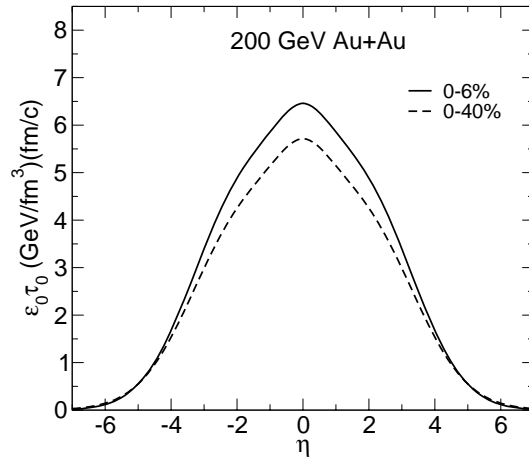


Fig. I-34. Energy density, ϵ_0 times the equilibration time, τ_0 calculated for 200 GeV Au + Au collisions at 0-6% (solid curve) and 0-40% (dashed curve) centrality is shown as a function of pseudo-rapidity. A Gaussian $\langle p_T \rangle$ dependence on η was used which satisfies energy conservation.

G. REACTION MECHANISM STUDIES

Direct Reactions have played a pivotal role in understanding nuclear wavefunctions, the residual interactions between nucleons, and in investigating collective correlation of particles in nuclei. Historically, the light ion transfers like the (d,p) reaction, were used on stable targets to investigate the structure of states. However, using radioactive beams, reactions in inverse kinematics, and sophisticated detector arrays, the possibility of performing direct reactions on unstable nuclei has emerged. This seems to be a technique with great potential for the future, both at ANL using “in-flight” production of radioactive beams with CARIBU, and at other radioactive beam facilities. To this end, a new spectrometer HELIOS, is being developed.

g.1. Neutron Spectroscopic Factors in ${}^9\text{Li}$ from $d({}^8\text{Li},p){}^9\text{Li}$ (K. E. Rehm, J. P. Greene, D. J. Henderson, R. V. F. Janssens, C. L. Jiang, E. F. Moore, R. C. Pardo, D. Peterson, S. C. Pieper, G. Savard, J. P. Schiffer, S. Sinha, X. Tang, R. B. Wiringa, A. H. Wuosmaa,* L. Jisonna,† M. Paul,‡ and R. E. Segel†)

We have studied the $d({}^8\text{Li},p){}^9\text{Li}$ reaction using a radioactive ${}^8\text{Li}$ beam to determine neutron spectroscopic factors in the nucleus ${}^9\text{Li}$. In the p shell, (d,p) reactions have been used extensively to determine single-neutron spectroscopic factors.¹ Modern computational methods for calculating the structure of few-body nuclear systems have had considerable success in reproducing the binding energies, spins, parities, and other properties of many nuclei with $A \leq 10$.² These calculations may also be critically tested by experimental data on spectroscopic factors, in particular for nuclei away from stability.

One example is the nucleus ${}^9\text{Li}$. Here only 5 levels are known, with only the groundstate assigned a firm spin-parity value of $3/2$.³ To extend the available data for this nucleus, we have studied the inverse-kinematic reaction $d({}^8\text{Li},p){}^9\text{Li}$ using a radioactive ${}^8\text{Li}$ beam produced at the in-flight facility at the ATLAS accelerator at Argonne National Laboratory. Backward emitted protons were detected using an array of segmented annular silicon detectors, and the coincident ${}^7,8,9\text{Li}$ ions were detected and identified using an array of silicon EAE telescopes at very forward angles. Figure I-35 shows a representative Q-value spectrum.

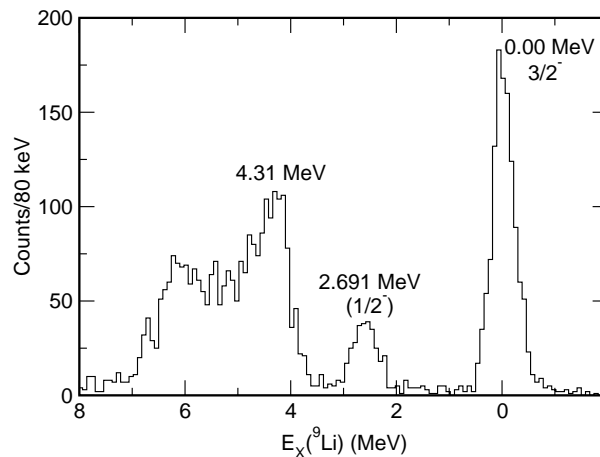


Fig. I-35. Q-value spectrum for the $d({}^8\text{Li},p){}^9\text{Li}$ reaction.

Measured proton angular distributions for the first three levels in ${}^9\text{Li}$ are shown in Fig. I-36. All fall off with a form characteristic of an angular-momentum transfer

$\Delta L = 1$. Also shown in Fig. I-36 are curves that represent the results of *absolute* predictions for the angular distributions of these states from the code

PTOLEMY, with neutron spectroscopic factors obtained from the QMC calculations described in Ref. 2 and using two different forms of the optical potentials as given by Ref. 1. The curves are already in reasonable agreement with the data. In order to estimate the “experimental” spectroscopic factor, we adjust the normalization of the curves shown in Fig. I-36.

These measurements demonstrate that neutron stripping via the (d,p) reaction performed in inverse kinematics can provide data of sufficient quality to quantitatively measure spectroscopic factors, and such data can provide new tests for modern *ab-initio* calculations of nuclear structure.

*Western Michigan University, †Northwestern University, ‡Hebrew University, Jerusalem, Israel.

¹J. P. Schiffer *et al.*, Phys. Rev. **164**, 1274 (1967).

²S. C. Pieper and R. B. Wiringa, Ann. Rev. Nucl. Part. Sci. **91**, 53 (2001) and S. C. Pieper, K. Varga, and R. B. Wiringa, Phys. Rev. C **66**, 044310 (2002).

³P. G. Young and R. H. Stokes, Phys. Rev. C **4**, 1597 (1971) and F. Ajzenberg-Selove *et al.*, Phys. Rev. C **17**, 1283 (1978).

⁴A. H. Wuosmaa *et al.*, Phys. Rev. Lett. **94**, 082502 (2005).

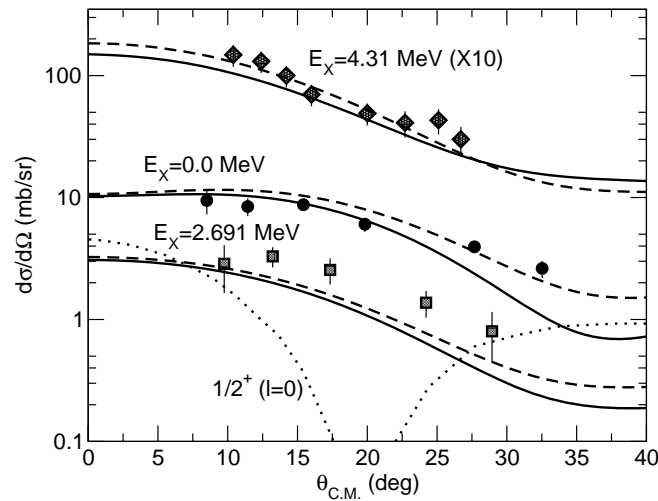


Fig. I-36. Proton Angular distributions for states at $E_x = 0.0, 2.691$ and 4.31 MeV. The curves represent absolute predictions using neutron spectroscopic factors from QMC methods.

g.2. Search for Excited States in ${}^7\text{He}$ with the (d,p) Reaction (K. E. Rehm, J. P. Greene, D. J. Henderson, R. V. F. Janssens, C. L. Jiang, E. F. Moore, R. C. Pardo, D. Peterson, S. C. Pieper, G. Savard, J. P. Schiffer, S. Sinha, X. Tang, R. B. Wiringa, A. H. Wuosmaa,* L. Jisonna,† M. Paul,‡ and R. E. Segel†)

We have studied the $d({}^6\text{He},p){}^7\text{He}$ reaction using a ${}^6\text{He}$ beam to study the properties of the exotic, neutron-rich nucleus ${}^7\text{He}$. The nucleus ${}^7\text{He}$, which possesses no particle-bound states, is one of the simplest nuclei for which there remains considerable debate about its structure. The structure of ${}^7\text{He}$ is particularly interesting in light of the current interest in systems containing many loosely bound neutrons. In addition to the well established groundstate,¹ several experimental efforts have been made to understand the properties of

possible excited states of this system.²⁻⁴ In one of these⁴ it has been suggested that there may exist a low-lying level that possesses significant overlap with ${}^6\text{He}_{\text{g.s.}} + n$, and should thus be populated strongly in the $d({}^6\text{He},p){}^7\text{He}$ reaction.

To examine the properties of possible low-lying excited states in this nucleus, we have studied the inverse-kinematic reaction $d({}^6\text{He},p){}^7\text{He}$ using a radioactive ${}^6\text{He}$ beam produced at the in-flight facility at the ATLAS

accelerator at Argonne National Laboratory. Backward emitted protons were detected using an array of segmented annular silicon detectors, and coincident ${}^4,{}^6\text{He}$ ions were detected and identified using an array of silicon EAE telescopes at very forward angles. Figure I-37 shows a representative Q-value spectrum. The groundstate is strongly populated, and we also observe a broad distribution of counts at higher excitation energy. The limit in excitation energy

imposed by the proton-detector energy threshold is $E_x \sim 5$ MeV. To reproduce the spectrum we simulate the response of the detector to states with lineshapes characteristic of the groundstate, a featureless continuum and a broad resonance with varying excitation energy and width. The data are best reproduced by including a resonance centered at an excitation energy of 2.6 MeV and width 2.0 MeV.

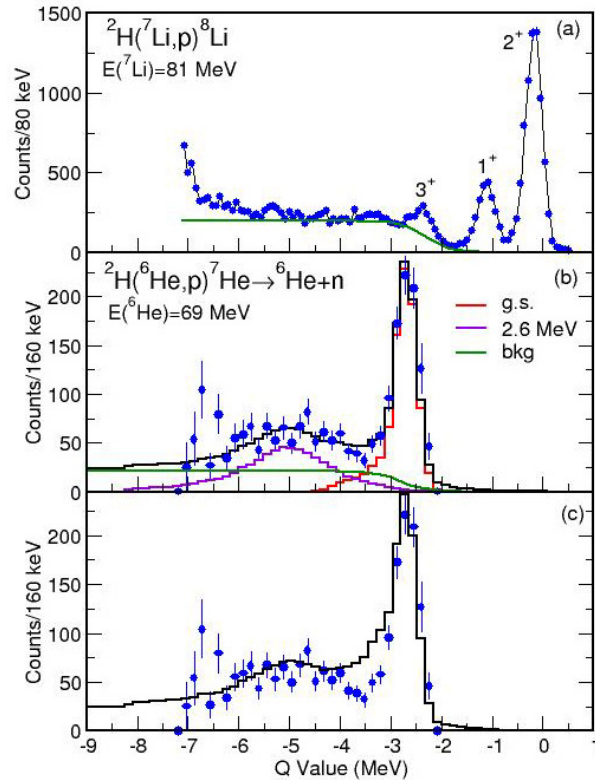


Fig. I-37. Q-value spectra for (a) $d({}^7\text{Li},\text{p}){}^8\text{Li}$ calibration reaction (b) $d({}^6\text{He},\text{p}){}^7\text{He}$ with fits (c) $d({}^6\text{He},\text{p}){}^7\text{He}$ including state at low excitation energy from Ref. 4.

The angular distributions for the groundstate and possible excited state appear in Fig. I-38. Also shown in Fig. I-38 are curves corresponding to predictions for the angular distribution obtained using the code PTOLEMY with spectroscopic factors calculated using the QMC method.⁵ The shape of the groundstate angular distribution is in good agreement with the calculation and a comparison to the magnitude suggests

a groundstate neutron spectroscopic factor of 0.37. We can confirm also the tentative spin assignment of $J^\pi = 3/2^-$ for the groundstate in the literature.¹ For the excited region, when a featureless continuum is taken into account, the angular distribution is only in fair agreement with the data, suggesting that there may be additional processes at work in this region of excitation energy.⁶

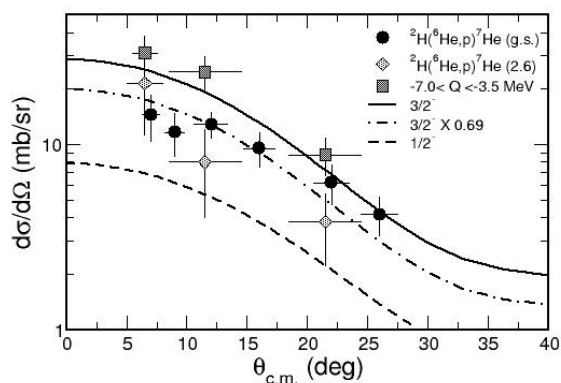


Fig. I-38. Proton angular distributions for the ground and excited states of ${}^7\text{He}$ from the $d({}^6\text{He},p){}^7\text{He}$ reaction.

*Western Michigan University, †Northwestern University, ‡Hebrew University, Jerusalem, Israel.

¹R. H. Stokes and P. G. Young, *Phys. Rev.* **178**, 2024 (1969).

²A. A. Koshennikov *et al.*, *Phys. Rev. Lett.* **82**, 3581 (1999).

³H. G. Bohlen *et al.*, *Phys. Rev. C* **64**, 024312 (2001).

⁴M. Meister *et al.*, *Phys. Rev. Lett.* **88**, 102501 (2002).

⁵S. C. Pieper and R. B. Wiringa, *Ann. Rev. Nucl. Part. Sci.* **91**, 53 (2001) and S. C. Pieper, K. Varga, and R. B. Wiringa, *Phys. Rev. C* **66**, 044310 (2002).

⁶A. H. Wuosmaa *et al.*, *Phys. Rev. C* **72**, 061301(R) (2005).

g.3. First Evidence in Fusion Hindrance for a Small $|Q|$ -Value System (C. L. Jiang, B. B. Back, H. Esbensen, R. V. F. Janssens, S. Mişicu, K. E. Rehm, C. N. Davids, J. Greene, D. J. Henderson, L. Jisonna, C. J. Lister, M. Notani, R. Pardo, D. Peterson, D. Seweryniak, B. Shumard, X. D. Tang, I. Tanihata, X. Wang, S. Zhu, P. Collon,* S. Kurtz,* and M. Paul†)

In our measurements of the fusion hindrance phenomenon,¹⁻⁵ one experiment was for a system with nearly zero fusion Q -value, that is collision ${}^{28}\text{Si} + {}^{64}\text{Ni}$, $Q = -1.78$ MeV. The preliminary experimental result has been presented in the last Annual Report.⁶

The experimental cross sections, covering more than 7 orders of magnitude, are presented in Fig. I-39, as an excitation function in the center-of-mass system. Comparisons with the previous data⁸ are provided as well.

Detailed coupled-channels calculations have been carried out in order to account for the data. As in previous studies,¹⁻⁵ the conventional coupled-channels calculations (with a Woods-Saxon potential) reproduce the data well for all cross sections above ~ 0.1 mb, but over predict the measurements at extreme sub-barrier energies (dot-dashed curve in Fig. I-39). A new mechanism was proposed to explain fusion hindrance at

extreme sub-barrier energies by considering explicitly the incompressibility of the overlapping reaction partners and estimating the ion-ion potential in a double folding mode.⁷ The inclusion of this compressional energy results in a shallower potential and thicker barriers, that is ultimately responsible for the fast fall-off of the excitation function at the lowest beam energies. The same approach was adopted to analyze the present experiment. The calculation results with this shallow potential are given by the solid curve in Fig. I-39. The agreement between the model and the data is satisfactory and of the same order as in the ${}^{64}\text{Ni} + {}^{64}\text{Ni}$ case.

The logarithmic derivatives $L(E)$ and the S factor have also been derived using the expressions given in Ref. 2. These two quantities are shown in Figs. I-40a and I-40b, respectively. In Fig. I-40a the star symbols are obtained from a least squares fit to three neighboring entries for the cross sections. The heavy solid line in

the figure is the so-called constant S factor expression, $L_{cs}(E) = \frac{\pi\hbar^2}{E}$, derived in Ref. 2, while the dotted line corresponds to a linear fit to the low-energy part of $L(E)$. The crossing point of these two lines determines the location of the maximum in the S factor curve, which occurs at $E_s = 45.6$ MeV and $L_s = 2.78$ MeV⁻¹. Obviously, there is a significant, but broad maximum in the S factor curve as a function of energy (see Fig. I-40b). Again, this behavior cannot be reproduced by the calculations based on the Woods-Saxon potential (dot-dashed curves). On the other hand, the new

potential by using the recipe of Ref. 7 (solid curves) follows the patterns exhibited by the data.

The extracted values for the parameters L_s and E_s in the reaction $^{28}\text{Si} + ^{64}\text{Ni}$ are described well by the empirical expressions given in Ref. 9.

In summary, this work is in accordance with the systematics of subbarrier fusion hindrance⁹ and has been submitted to Phys. Lett. B for publication.

*University of Notre Dame, †Hebrew University, Jerusalem, Israel.

¹C. L. Jiang *et al.*, Phys. Rev. Lett. **89**, 052701 (2002).

²C. L. Jiang, H. Esbensen, B. Back, R. V. F. Janssens, and K. E. Rehm, Phys. Rev. C **69**, 014604 (2004).

³C. L. Jiang *et al.*, Phys. Rev. Lett. **93**, 012701 (2004).

⁴C. L. Jiang *et al.*, Phys. Rev. C **71**, 044613 (2005).

⁵For reaction $^{58}\text{Ni} + ^{89}\text{Y}$, C. L. Jiang *et al.*, ANL Phys. Div. Annual Report ANL-05/61, p. 81.

⁶C. L. Jiang *et al.*, ANL Phys. Div. Annual Report ANL-05/61, p. 88.

⁷Ş. Mişicu and H. Esbensen, Phys. Rev. Lett. **96**, 112701 (2006).

⁸A. M. Stefanini *et al.*, Nucl. Phys. **456**, 509 (1986); Phys. Rev. C **30**, 2088 (1984).

⁹C. L. Jiang, B. Back, H. Esbensen, R. V. F. Janssens, and K. E. Rehm, Phys. Rev. C **73**, 014613 (2006).

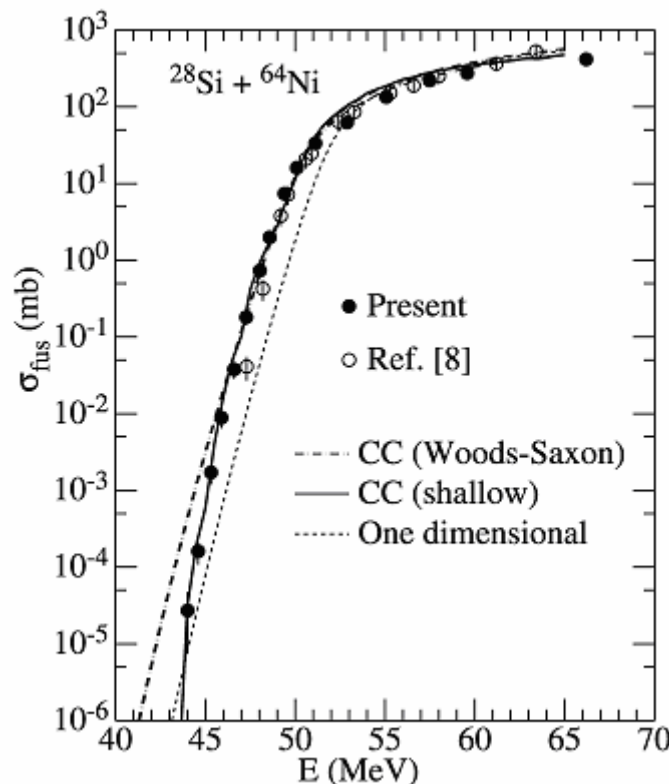


Fig. I-39. Excitation function for the fusion of $^{28}\text{Si} + ^{64}\text{Ni}$. The solid circles are the present results, while the open ones are taken from Ref. 8. The dot-dashed and solid curves are the results of coupled-channels calculations with a usual Woods-Saxon potential and a shallow potential incorporating the effects of nuclear incompressibility, respectively (see text for details). The dotted curve is the result of a one-dimensional, no-coupling calculation.

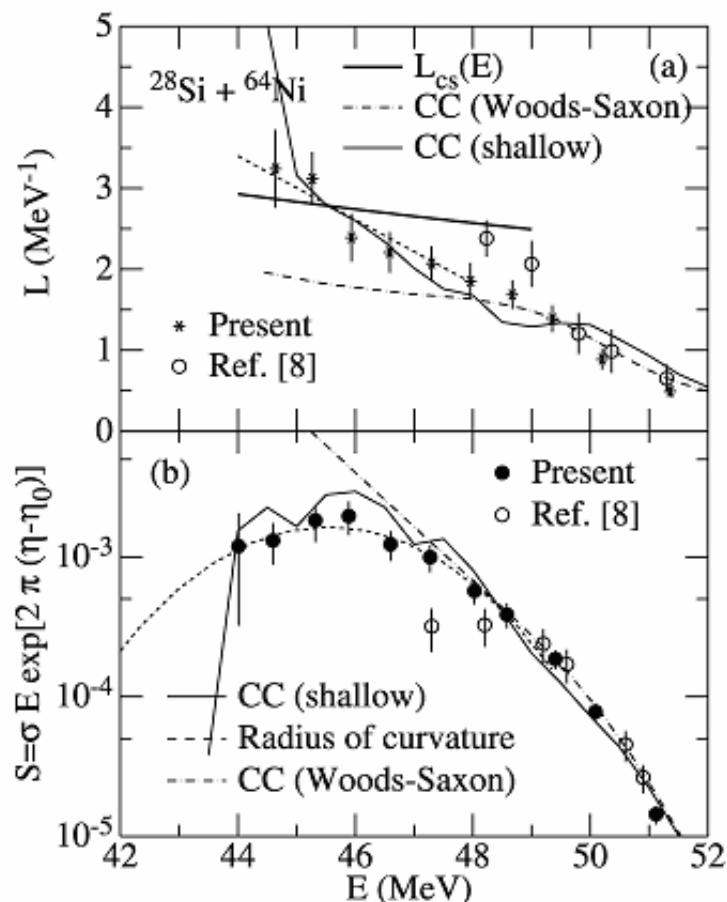


Fig. I-40. (a) The logarithmic derivative $L(E) = d(\ln\sigma E)/dE$, plotted as a function of the center-of-mass energy E for the fusion of $^{28}\text{Si} + ^{64}\text{Ni}$. The stars are obtained from least squares fits to three data points. (b) The S factor $S(E) = \sigma E \exp(2\pi\eta)$, plotted as a function of the center-of-mass energy E . The solid circles are the experimental results. The $L(E)$ and $S(E)$ values obtained from the data of Ref. 8 are shown as open circles. The heavy solid line corresponds to a constant S factor. See text for details.

g.4. Fusion-Fission of $^{16}\text{O} + ^{197}\text{Au}$ at Sub-Barrier Energies (B. B. Back, C. L. Jiang, R. V. F. Janssens, D. J. Henderson, B. R. Shumard, C. J. Lister, D. Peterson, K. E. Rehm, X. Tang, S. Zhu, I. Tanihata,* and X. Wang†)

Fusion hindrance at far sub-barrier energies has recently been discovered¹ by studying medium-heavy systems such as $\text{Ni} + \text{Ni}$ to $\text{Zr} + \text{Zr}$. This discovery has engendered much additional experimental and theoretical work in order to achieve an understanding of

this phenomenon. Most of the experimental evidence comes from medium-heavy systems decaying by particle emission.¹ In order to study heavier systems, it is therefore also necessary to measure the fraction of the decay that goes into fission fragments.

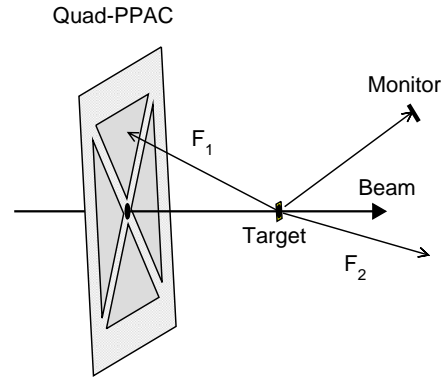


Fig. I-41. Schematic illustration of the experimental setup using a quad PPAC detector at backward angles as well as a monitor Si detector located at 60° .

In the present experiment we have therefore measured the fission cross section of $^{16}\text{O} + ^{197}\text{Au}$ down to unprecedented far sub-barrier energies using the detector arrangement illustrated in Fig. I-41. Here a large position sensitive PPAC is placed at backward angles whereby the ratio of elastically scattered ^{16}O ions to fission fragments is minimized. A Si monitor detector, located at 60° , was used to normalize to the elastic Rutherford cross section. The PPAC, consisting of four independent quadrants, is x-y position sensitive and it provides a ΔE signal of sufficient quality to discriminate between elastically scattered ^{16}O ions and fission fragments. Additional separation was achieved from the time-of-flight signal derived from the detector timing and the time structure of the ATLAS beam.

The resulting preliminary fission cross section is shown as solid circles in Fig. I-42, and compared to previous measurements at above barrier energies.² The two measurements exhibit very good agreement within the overlapping energy range except for the lowest data point of Ref. 2 (in parenthesis) which clearly deviates from the present data. Evaporation residue measurements³ are shown as open triangles. When added to the present data we obtain the total fusion cross section (open squares) which agrees very well

with a simple model estimate based on the modified proximity potential.⁴

Fig. I-42b shows the fission cross section in terms of the astrophysical S -factor, which is defined as $S = \sigma_{fis} E_{cm} \exp(2\pi\eta)$, where η is the Sommerfeld parameter. A maximum in the S -factor representation indicates the onset of sub-barrier hindrance.¹ From the present data it is not obvious whether there is a maximum in the S -factor, but it is also not excluded as shown by the two curves that are obtained from fits to the logarithmic derivative of the cross section excluding the lowest data points. These fits, represented by solid and dashed curves in Fig. I-42b, give an S -factor maximum at E_s . From the systematics¹ of a large number of systems with sub-barrier hindrance, one expects that the hindrance should set in, and the maximum of the S -factor occur, at the energy indicated by the arrow labeled E_s^{ref} , *i.e.* substantially lower in energy than probed in the present work. Judging from the present experience it may be very difficult to measure the fission cross section at this cross section level. However, as it appears that a large fraction of the total fusion cross section goes into the evaporation channel, a measurement of this exit channel may indeed reveal the sub-barrier hindrance in this system.

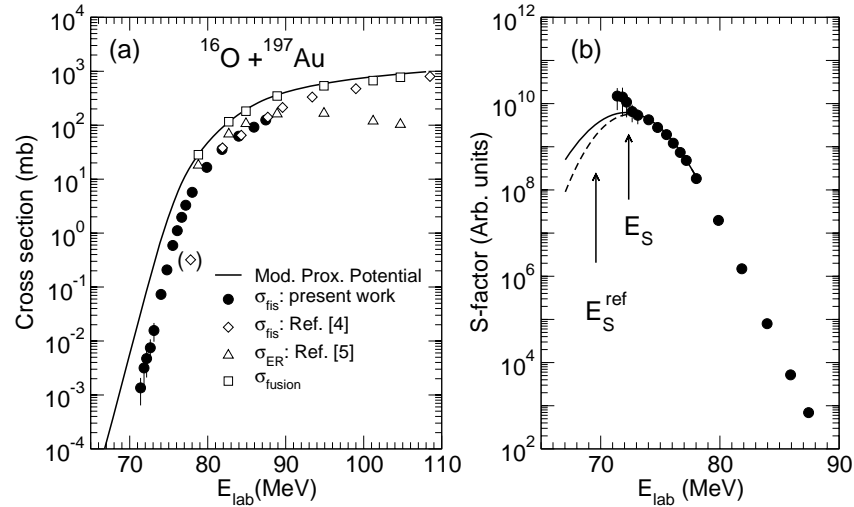


Fig. I-42. Panel a: Preliminary fission cross sections (solid circles) are compared to those of Sikkeland *et al.*² (open diamonds). Also evaporation residue *et al.*,³ (open triangles) and total fusion cross sections (open squares) are shown, the latter compared to predictions using a modified proximity potential.⁴ Panel b: S -factor representation of the present fission cross section. See text for further details.

*Present address: TRIUMF, Vancouver, Canada, †Joint with University of Notre Dame.

¹C. L. Jiang *et al.*, Phys. Rev. Lett. **89**, 052701 (2002); Phys. Rev. C **69**, 014604 (2004); Phys. Rev. Lett. **93**, 012701 (2004); Phys. Rev. C **71**, 044613 (2005).

²T. Sikkeland, Phys. Rev. B **669**, 135 (1964).

³K.-T. Brinkmann *et al.*, Phys. Rev. C **50**, 309 (1994).

⁴J. Blocki, J. Randrup, W. J. Swiatecki, and C. F. Tsang, Ann. Phys. **105**, 477 (1977); B. B. Back *et al.*, Phys. Rev. C **32**, 195 (1985); J. Toke *et al.*, Nucl. Phys. **A440**, 327 (1985).

g.5. Systematics of Heavy-Ion Fusion Hindrance at Extreme Sub-Barrier Energies (C. L. Jiang, B. B. Back, H. Esbensen, R. V. F. Janssens, and K. E. Rehm)

Recently, a new phenomenon of hindrance in heavy-ion fusion reactions (a steep fall off of the fusion cross section) has been found in medium-heavy systems, which cannot be described by the conventional coupled channels calculations by using a Woods-Saxon potential.¹⁻⁴ This hindrance occurs at extreme sub-barrier energies whereas the fusion cross section at near barrier energies agrees fairly well with the conventional coupled-channels calculations. We have studied the dependence of the hindrance on the mass, and by extension also on the Q -value of the fusing systems over a wide range of projectile-target combinations. In general, the Q -value becomes less negative with

decreasing mass, and even positive for the lightest systems.

The systematics of the logarithmic derivative $L(E) = d(\ln(\sigma E))/dE$ of fusion excitation functions is illustrated in Fig. I-43 for a number of systems ranging from $^{10}\text{B} + ^{10}\text{B}$ to $^{90}\text{Zr} + ^{92}\text{Zr}$ (Q -values ranging from 31 to -154 MeV). The logarithmic derivatives are represented by open circles for five-point derivatives, whereas the stars were obtained by a fit to three consecutive data points. We observe that $L(E)$ for all systems increases with decreasing energy. The dashed curves represent the logarithmic slopes $L_{cs}(E)$ for constant S -factor.

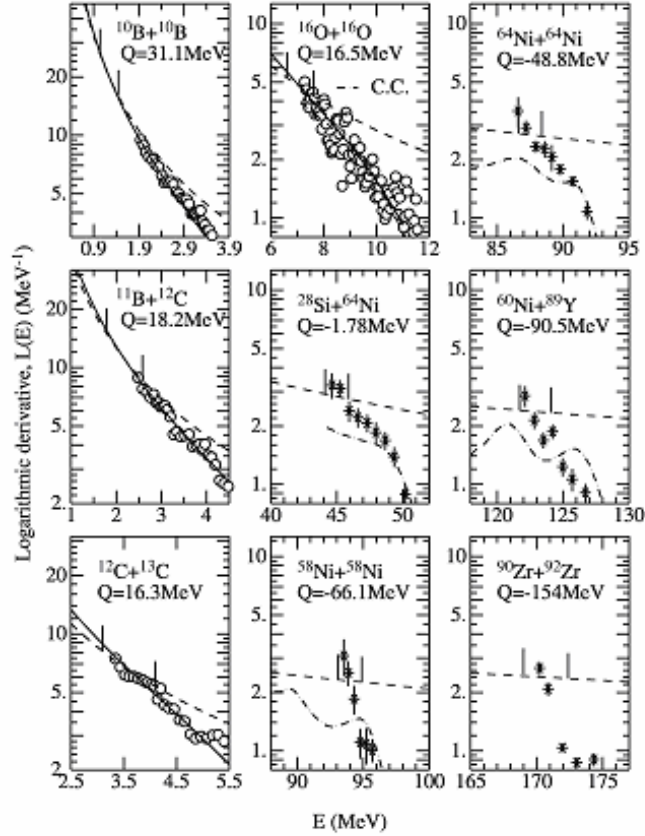


Fig. I-43. Logarithmic derivative representations for a range of systems. The dashed curves correspond to a constant S -factor, whereas the dot-dashed curves display results of coupled-channels calculations, and the solid curves represent a fit to the data using the function $A_0 + B_0/E^{3/2}$. The data are taken from Refs.: $^{10}\text{B} + ^{10}\text{B}$, $^{11}\text{B} + ^{12}\text{C}$, $^{12}\text{C} + ^{13}\text{C}$, $^{12}\text{C} + ^{16}\text{O}$, $^{16}\text{O} + ^{16}\text{O}$, $^{28}\text{Si} + ^{64}\text{Ni}$, $^{64}\text{Ni} + ^{64}\text{Ni}$, $^{60}\text{Ni} + ^{89}\text{Y}$,¹ and $^{90}\text{Zr} + ^{92}\text{Zr}$.⁹

Studying the full range of systems, we observe that the crossing point, L_s and E_s , for lighter systems, which have increasingly positive Q -values, indeed occurs at larger values of $L(E)$. For the lightest systems, the logarithmic derivatives of the data intersect the constant S -factor curve at a small angle and it is, therefore, difficult to accurately estimate E_s . Consequently, we have used fits to the data with the expression $A_0 + B_0/E^{3/2}$ (solid curves), A_0 and B_0 being adjustable parameters, to obtain a less subjective estimate of E_s . Relatively large error bars are, however, assigned to the resulting E_s values for the lightest systems. We also observe that the value of the logarithmic slope, $L(E)$, obtained by the conventional coupled-channels calculations for heavy systems (dot-dashed curves in Fig. I-43) saturates at a value of $\sim 1.5 - 2.0 \text{ MeV}^{-1}$, much lower than measured. It has been shown that coupled-channels calculations using reasonable Woods Saxon potentials are unable to reproduce the extreme sub-barrier hindrance behavior.²

The systematics of sub-barrier hindrance is illustrated in Fig. I-44. Here, the derived values of E_s and $L_s = L(E_s)$ are plotted as a function of the parameter $Z_1 Z_2 \sqrt{\mu}$ in (panel a) and (panel b), respectively. Aside from local deviations of L_s from the value of 2.33 MeV^{-1} in medium-heavy systems (of the order of $\sim 10\%$, arising from nuclear structure effects) L_s clearly starts deviating from this value in lighter systems. The corresponding E_s values also fall below the E_s^{ref} expression (solid curve). A purely empirical expression

$$L_s^{\text{emp}} = 2.33 + 500/(Z_1 Z_2 \sqrt{\mu}) \text{ (MeV}^{-1}\text{)} \quad (1)$$

(dashed curve in Fig. I-44b) is seen to provide a good approximation to the experimental data, and it reproduces the asymptotic value of 2.33 MeV^{-1} observed earlier for heavy systems with $Z_1 Z_2 \sqrt{\mu} > 2500$. The corresponding curve for E_s^{emp} obtained from Eq. 1, namely

$$E_s^{emp} = (0.495Z_1Z_2 \sqrt{\mu} / L_s^{emp})^{2/3} \text{ (MeV)}, \quad (2)$$

is seen also to reproduce the experimental values in Fig. I-44a.

These two equations thus represent the overall systematics for the onset of sub-barrier fusion hindrance. This systematics appears to be correlated with the parameter $Z_1 Z_2 \sqrt{\mu}$ in the simple fashion expressed in Eqs. 1 and 2, but it should be kept in mind that both the Q -value and the fusion (interaction) barrier vary smoothly, although not quite monotonically, with this parameter. Hence, it is not possible to ascertain whether the observed physical effect of fusion hindrance is associated with either, or with both of these quantities.

Figure I-44c presents the ratio of the logarithmic slopes, $R = (dL/dE)_{exp} / (dL/dE_{cs})$, for the data $L(E)$ relative to the constant S -factor curve at $E = E_s$. For $Z_1Z_2\sqrt{\mu} > 2000$, this ratio is substantially larger than unity which means that there is a sharp intersection point between the two curves and, consequently, a well defined, narrow maximum in the S -factor curve. For

$Z_1Z_2\sqrt{\mu}$ values below about 200, the slope ratio approaches unity which results in a less well defined intercept point. For the lightest systems, it appears that the logarithmic slope of the data approaches the value for a constant S -factor and the sub-barrier hindrance may well disappear.

In conclusion, fusion hindrance appears to be a general phenomenon at sub-barrier energies. Simple empirical formulae are given for both the energy and the logarithmic slope of the cross section at which the onset of fusion hindrance occurs. These point to an entrance channel effect as the source of this phenomenon. We have also noted that the possible occurrence of fusion hindrance in the lightest nuclei is of great astrophysical interest.

After the publishing of this study,¹⁰ a new mechanism was proposed,¹¹ which appears to explain the fusion hindrance (a S factor maximum) quite well for the reaction $^{64}\text{Ni} + ^{64}\text{Ni}$. This model might be useful for understanding the hindrance phenomenon for all mass systems discussed in this paper.

¹C. L. Jiang *et al.*, Phys. Rev. Lett. **89**, 052701 (2002).

²C. L. Jiang, H. Esbensen, B. B. Back, R. V. F. Janssens, and K. E. Rehm, Phys. Rev. C **69**, 014604 (2004).

³C. L. Jiang *et al.*, Phys. Rev. Lett. **93**, 012701 (2004).

⁴C. L. Jiang *et al.*, Phys. Rev. C **71**, 044613 (2005).

⁵M. Berkerman *et al.*, Phys. Rev. C **23**, 1581 (1982).

⁶M. D. High and B. Cujec, Nucl. Phys. **A259**, 513 (1976).

⁷R. G. Stokstad *et al.*, Phys. Rev. Lett. **37**, 888 (1976).

⁸C. L. Jiang *et al.*, section I.g.3. *ibid.*

⁹J. G. Keller *et al.*, Nucl. Phys. **A452**, 173 (1986); Phys. Lett. **B254**, 25 (1991).

¹⁰C. L. Jiang *et al.*, Phys. Rev. C **73**, 014613 (2006).

¹¹Ş. Mişicu and H. Esbensen, Phys. Rev. Lett. **96**, 112701 (2006).

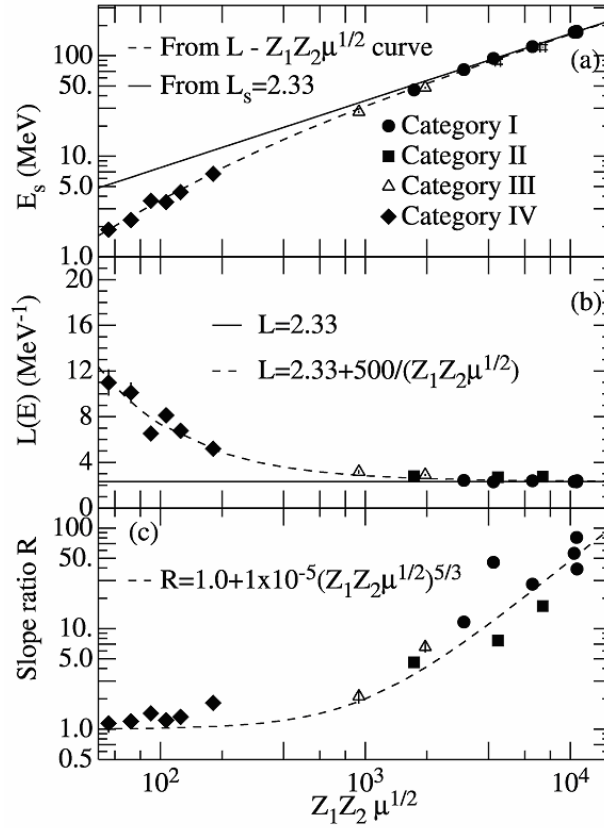


Fig. 1-44. Experimentally determined values are shown as a function of $Z_1 Z_2 \sqrt{\mu}$ for E_s (panel a), L_s (panel b) and logarithmic slope ratio, $R = (dL/dE)_{exp} / (dL/dE)_{cs}$ at E_s (panel c). Solid lines in panels a and b correspond to $L_s = 2.33 \text{ MeV}^{-1}$, whereas dashed curves represent the empirical trends of the data. Open symbols represent values obtained with the extrapolation method.

H. DEVELOPMENT OF NEW EXPERIMENTAL EQUIPMENT

New techniques and new approaches drive the field of nuclear physics forward. It is encouraging that the current year has been very rich in equipment developments. In almost all our experimental areas new projects are emerging that offer unparalleled opportunities for the future.

h.1. Proposal for a Radioactive Beam Upgrade to ATLAS: the CARIBU Project (G. Savard, R. C. Pardo, S. Baker, E. F. Moore, and the Physics Division Heavy Ion Group)

The research program at the ATLAS heavy-ion superconducting linac contributes to the fields of nuclear structure, nuclear astrophysics, fundamental interactions and applications. The present capabilities of the machine make it well suited to these endeavors, particularly for studies on the proton-rich side of the valley of stability. The research directions in these fields are however evolving and emerging questions in nuclear structure and astrophysics now require beams of heavy neutron-rich isotopes to be answered. Particularly important questions have to do with the r-process responsible for the formation of about half of the heavy elements and the expected changes in nuclear structure for very neutron rich isotopes. For the r-process, the quantities of interest to determine the r-process path are the mass, lifetime and beta-delayed neutron emission probability of isotopes in this region. In addition, information on neutron capture cross section and fissionability for the heaviest isotopes at the end of the path would be enlightening. From the nuclear structure point of view, the evolution when going to more neutron rich isotopes of the basic signatures such as the single particle structure, pairing interaction and collective properties, would indicate if and how nuclear structure is modified in these systems. The required information is best obtained with stopped beams of neutron-rich isotopes for the groundstate properties listed above and Coulomb barrier energy beams of these same isotopes for the nuclear structure studies. Such beams are partly available for example at CERN/ISOLDE for stopped beams and HRIBF for reaccelerated beams. These facilities are however limited in the isotopes available by the release of ISOL type targets that is only fast and efficient for part of the isotope chart and by the too low energy of their post-accelerated beams. It is found that what is required is a more universal extraction technique that will make available beams of all species in this region, coupled to a post-accelerator with energy range extending to in excess of 10 MeV/u for some of the transfer studies.

This is an ambitious goal that to fully fulfill will require a RIA-like facility. It is however possible to make important steps in this direction with less powerful smaller size facilities. This is the goal we aimed at with the writing of a proposal for a neutron-rich isotope radioactive beam upgrade to ATLAS: the CARIBU project.

The proposal for the CARIBU project is available on the Argonne Physics Division web site at <http://www.phy.anl.gov/atlas/caribu.html>. It was written following a critical survey of the nuclear information that is needed to start addressing the questions highlighted above and of the most suitable techniques to gather this information. This pointed to the need for the broad access to isotopes in the mid-mass neutron-rich region at energies ranging from ion source energy to up to about 12 MeV/u. The ATLAS facility with its current energy upgrade can provide stable beams at these energies. The access to the broad range of radioactive ions however requires a new approach for the production and extraction of these ions. This is made possible by an extension of the work performed at the CPT spectrometer at ATLAS where the mass of a number of short-lived neutron-rich isotopes produced by fission from a ^{252}Cf source has been measured using the gas catcher technology developed here to stop these recoils and transform them into a low-energy radioactive beam. This technology has been extended to larger gas catchers for the proposed RIA facility (see section III.c.5.). A gas catcher of size similar to the RIA gas catcher prototype built at Argonne could thermalize and extract as beam about 20% of all fission products from a thin 1 Ci californium source. The resulting low energy beam intensity would peak at over 10^7 ions/s and is given in Fig. I-45. The yield is essentially determined by the fission production since there are little additional chemical or half-life limitations present in this approach.

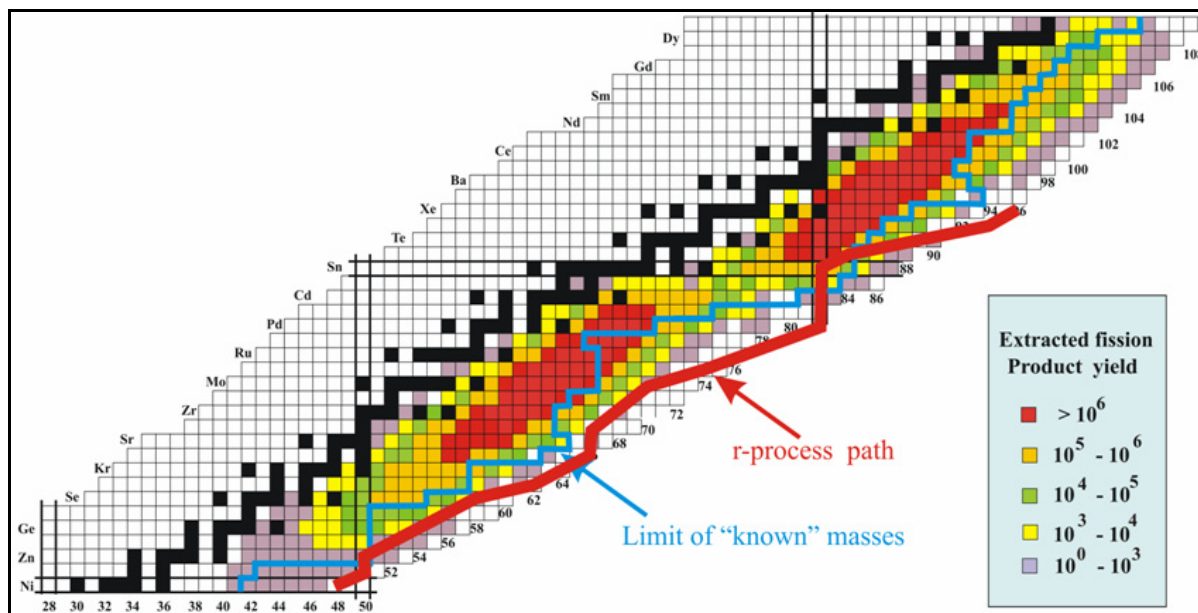


Fig. I-45. Distribution of fission products from the spontaneous fission of ^{252}Cf . The color code gives the extracted low-energy ion beam intensity (s^{-1}) for a 1 Curie source.

These beams will be made available as singly or doubly charged ions (depending on the species) and can be purified in a compact isobar separator since they have excellent beam properties. Post-accelerating these beams with ATLAS requires increasing the charge state of these ions to obtain a charge-to-mass ratio suitable for acceleration through ATLAS. This can be done by modifying one of the existing ECR source, ECR-1, into a charge breeder where the ions are injected and their charge state increased before injection into ATLAS in a fashion similar to that used in normal operation with stable beams. The complete scheme is shown in Fig. I-46. A building addition located north from the ECR-1 platform will host the high-voltage platform on which the californium source, gas catcher, shielding and mass separator will be located. Out of this platform will come a mass separated neutron-rich radioactive ion beam that can be sent either to a low-energy experimental area located in the same building or to the ECR-1 ion source platform in the existing building. The ECR-1 source, modified as a charge breeder, will accept the incoming ions, capture them in its ECR

plasma where the charge state will be increased, and then deliver them to the ATLAS linac for acceleration following the path used normally for stable ions. Acceleration through ATLAS will be tuned using a mixture of guide beam and low intensity diagnostics and the beam delivered to any of the existing experimental areas.

The radioactive beam intensities predicted for this upgrade are listed in the proposal. They are complementary in energy and isotope access to existing and other near-future planned facilities. The intensities will be sufficient to perform groundbreaking experiments that will help answering the questions highlighted above and establish the landscape for future larger scale facilities.

The proposal was reviewed favorably during the year and construction of the CARIBU upgrade will start in January 2006. Low-energy neutron-rich radioactive beams are expected to be available in 2008 while delivery of reaccelerated beams is expected in 2009.

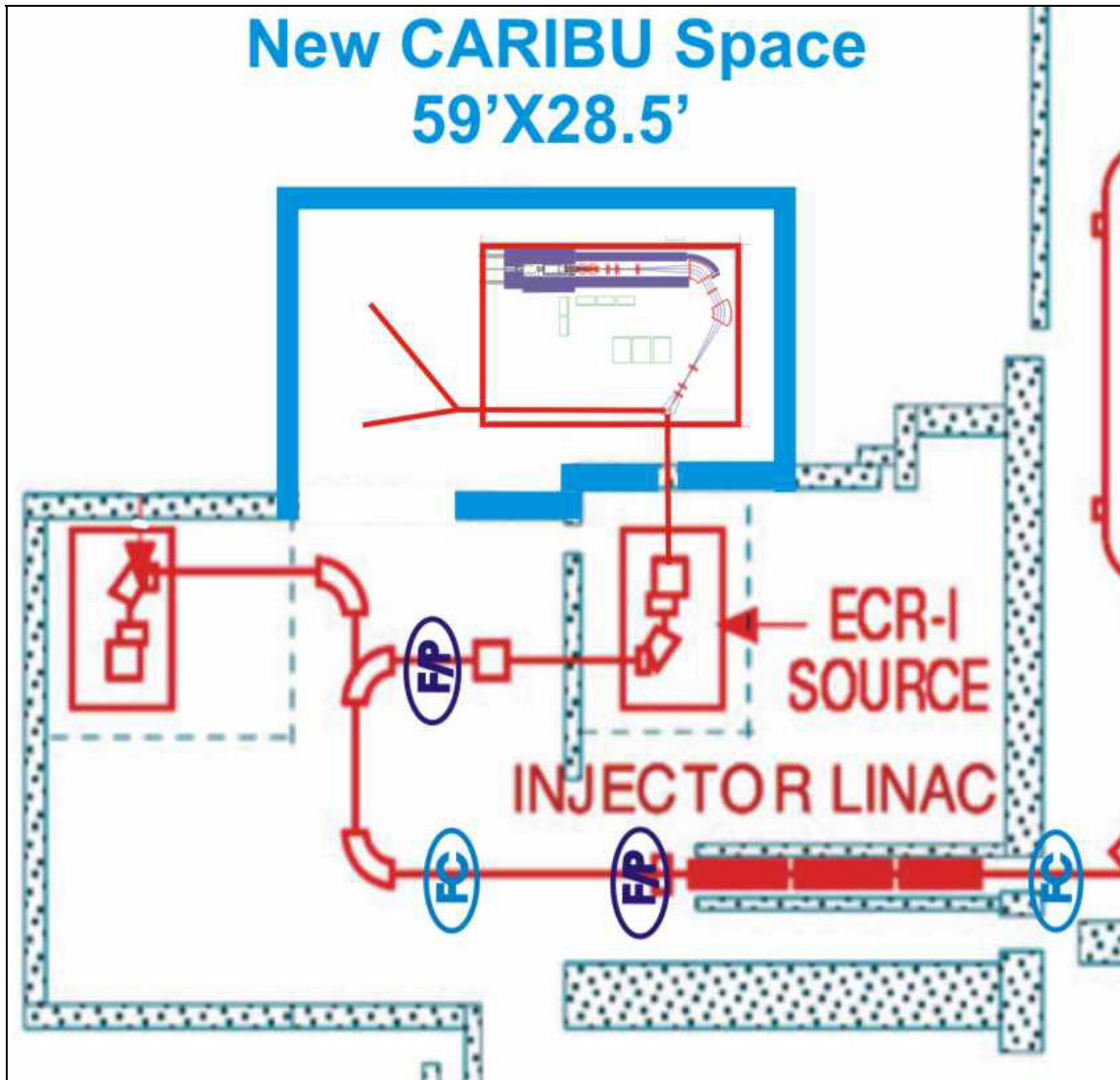


Fig. I-46. Schematic overview of the proposed ^{252}Cf fission fragment beam facility in the new building addition. The existing ECR-1 ion source will be modified for charge breeding and then injecting these beams into the ATLAS linac. Location of planned weak-beam diagnostics is shown by ellipses labeled “FC” and “FP” for Faraday cup only and profile monitor with Faraday cup.

h.2. A High Resolution Isobar Separator for the CARIBU Project (C. N. Davids and D. Peterson)

A design study has been initiated on a high-resolution isobar separator for the CARIBU project. The goals are: high transmission (>95%), high mass resolution (>20,000:1), and compact size. The CARIBU project will take fission fragments from spontaneously-fissioning ^{252}Cf , thermalize them into the 1^+ ionic state in a gas catcher, cool the ions, accelerate them to an

energy of 50 keV, and pass them to the isobar separator. After separation, the isobar of interest will either be studied directly, or be sent to an ECR source serving as a charge breeder, where the charge state will be increased to a level suitable for injection into the ATLAS accelerator. In ATLAS the ions will be accelerated and used for experiments.

The isobar separator will operate with only magnetic dispersive elements. This is possible because the energy spread of the 50 keV beam is less than 1 eV, or 1 part in 50,000. Because of the low energy, all focusing elements will be electrostatic. This simplifies tuning of the device, since the focusing is thus independent of the ion mass, and only depends on energy per unit charge. The compact size is necessary because the whole device will be mounted on a high-voltage platform.

Figure I-47 shows the layout of the resulting separator. It consists of the symmetric combination of quadrupole

doublet matching sections, quadrupoles which defocus in the dispersive plane, and 60° bending magnets. Correction of higher order aberrations is accomplished using 2 electrostatic sextupoles and an electrostatic multipole. The ion optic design was studied for 3rd order and below using the code GICOSY, and for higher order (up to 6th order) using COSY INFINITY. Figure I-48 shows a calculated mass spectrum in the dispersive plane (X-direction) and non-dispersive plane (Y-direction) for 3 isobars differing in mass by 1 part in 20,000. Maximum input angles are ±6 mr, and the initial beam spot is 1 mm in diameter.

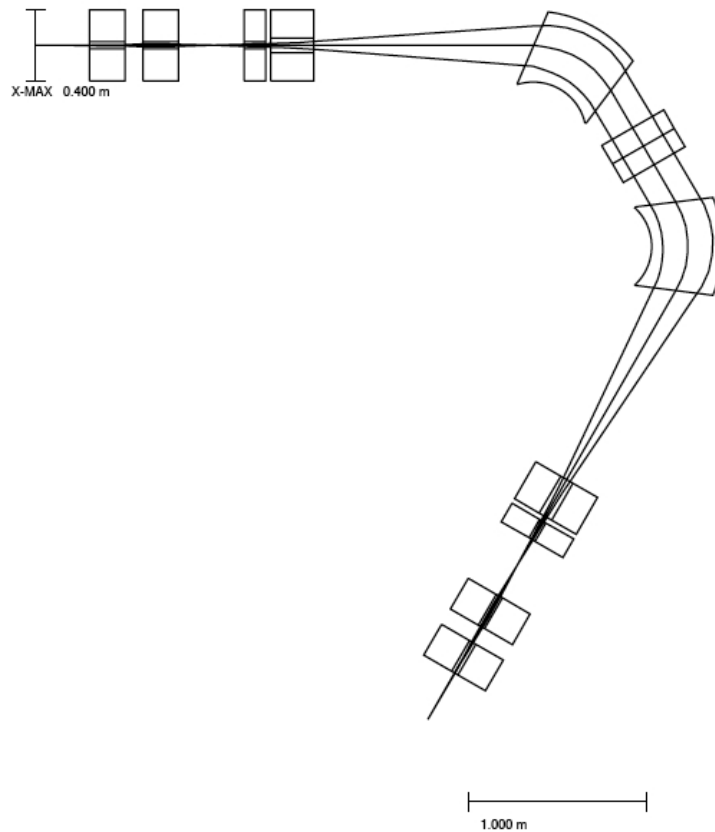


Fig. I-47. Schematic layout of high-resolution Isobar Separator for CARIBU.

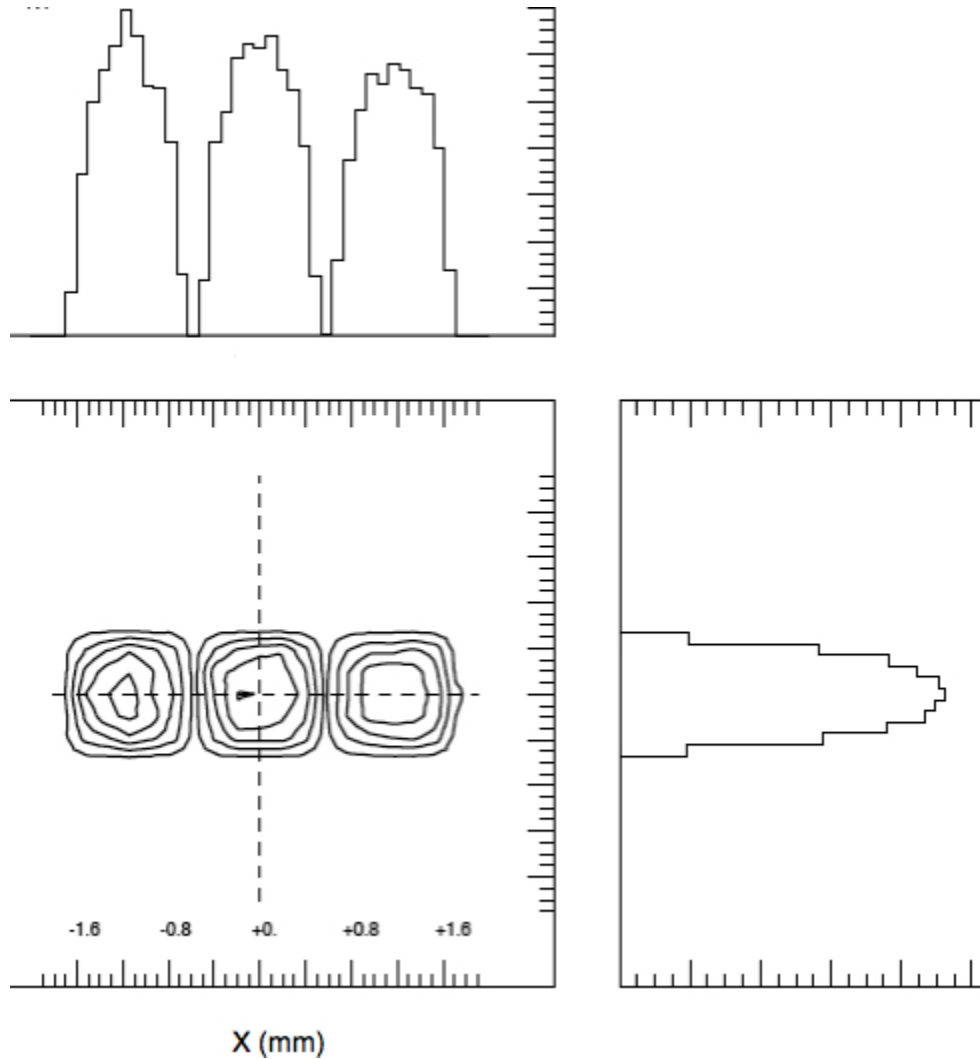


Fig. I-48. Calculated mass spectrum for 3 masses differing by 1 part in 20,000. X- and Y-dimensions are the same scale, and are shown in mm.

h.3. Beam Intensity Expectations for a 200 MeV/u 400 kW Radioactive Beam Driver Accelerator (B. B. Back and C. L. Jiang)

Recently, there has been growing interest in exploring options for a somewhat scaled down version of the Rare Ion Accelerator (RIA), the aim of which is to preserve its core scientific capabilities, but at a reduced cost.¹ We have, therefore, performed estimates of the intensities of re-accelerated beams that can be delivered by a driver linac consisting of 221 superconducting resonators as opposed to 302 resonators for the full RIA

facility. This modification reduces the maximum beam energy for ^{238}U from 400 MeV/u to about 200 MeV/u. A similar reduction entails for lighter ions as well. However, the recent improvements in ECR source technology² allows for increased primary beam intensities such that the total beam power remains unchanged at 400 kW as projected for the full RIA facility.³

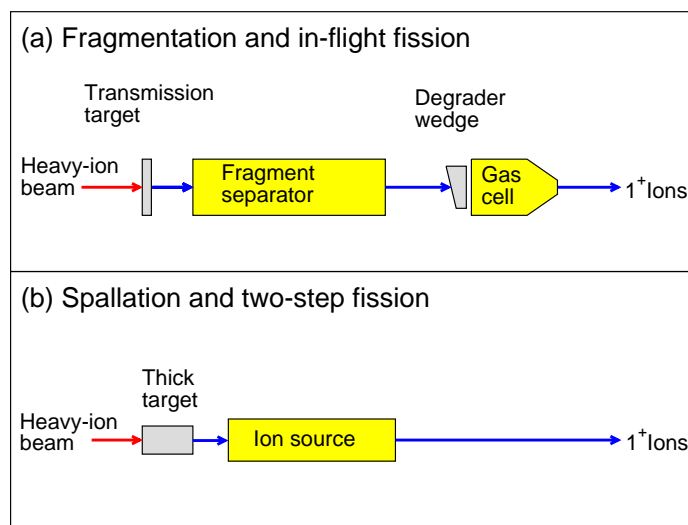


Fig. I-49. Concepts for production of radioactive 1^+ -ions using in-flight methods (fragmentation and in-flight fission) and diffusion/effusion from thick targets (spallation and two-step fission).

The methods for secondary beam production remain the same, namely: Projectile fragmentation and in-flight fission, the products of which are stopped and reduced to the 1^+ charge state in a gas cell irrespective of chemical properties, and spallation and two-step fission, which rely on effusion/diffusion from a thick target where the radioactive species are produced. See Ref. 3 for further details. These are shown schematically in Fig. I-49.

The resulting yields of secondary ions in the 1^+ charge state available for re-acceleration are presented as a color-coded contour map in Fig. I-50. Only the yield for the optimum production method is shown for each isotope. Losses arising from charge state fraction, transmission through the mass separator, wedge, and gas cell, as well as decay losses during the 20 ms residence period in the gas cell have been taken into account for the fragmentation and in-flight fission

production methods. Yields for light-ion spallation production on thick target were derived from experimental data from Isolde at CERN⁴ and a recent prescription for correcting for decays occurring before the ions are extracted from the target.⁵ The latter is especially important for extrapolations to shorter-lived neutron-rich nuclei. For most isotopes we find that the yield for the 200 MeV/u machine is almost equal to that predicted for the 400 MeV/u 400 kW RIA driver accelerator. Thus it is found that the increased beam intensity largely balances the reduction in beam energy relative to the full RIA driver accelerator, although especially the in-flight fission method suffers from the reduced forward focusing that results from the lower beam energy.

In conclusion, we find that a rare ion facility based on a 200 MeV/u 400 kW driver linac represents an attractive and cost effective alternative to the full RIA project.

¹B. B. Back and C. L. Jiang, ANL Internal Report ANL-06/55.

²D. Leitner and C. M. Lyneis, in Proceedings of the 2005 Particle Accelerator Conference, Knoxville, TN, May 16-20, 2005, p. 179.

³C. L. Jiang *et al.*, Nucl. Instrum. Methods **A492**, 57 (2002).

⁴SC Isolde Production Yields, <http://www94.web.cern.ch/ISOLDE/>.

⁵S. Lukic *et al.*, nucl-ex/0601031.

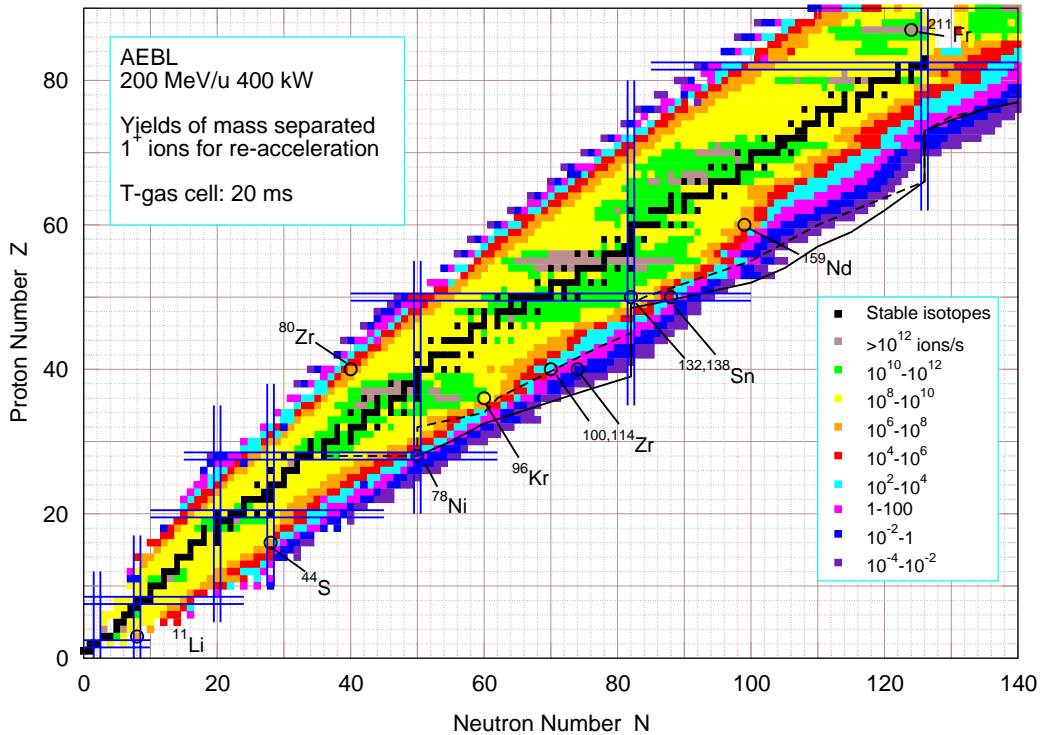


Fig. I-50. Yields for production of radioactive I^+ -ions in a 200 MeV/u 400 kW machine.

h.4. HELIOS – a Solenoidal Spectrometer for Inverse Reactions (B. B. Back, C. J. Lister, R. Pardo, K. E. Rehm, J. P. Schiffer, S. J. Freeman,* and A. H. Wuosmaa†)

The effort to design and build a spectrometer based on a large superconducting solenoid, HELIOS (HELICAL Orbit Spectrometer), is continuing. This design offers substantial advantages over conventional spectrometers by providing automatic particle identification and a very large solid angle for detecting light low-energy particles emitted in inverse kinematics those with low momentum transfer, where the DWBA approximation works best) while preserving the energy dispersion corresponding to the center-of-mass system. These characteristics will be particularly beneficial for the

study of single particle transfer, pick-up or inelastic scattering reactions on light targets (H, He) with heavy radioactive beams produced either at the ATLAS in-flight facility or at the future CARIBU radioactive ion injector. The device will be based on a large superconducting solenoid magnet of the type used in modern Magnetic Resonance Imaging (MRI) scanners. General characteristics and capabilities of the instrument are described in.¹ A schematic drawing of the spectrometer is shown in Fig. I-51.

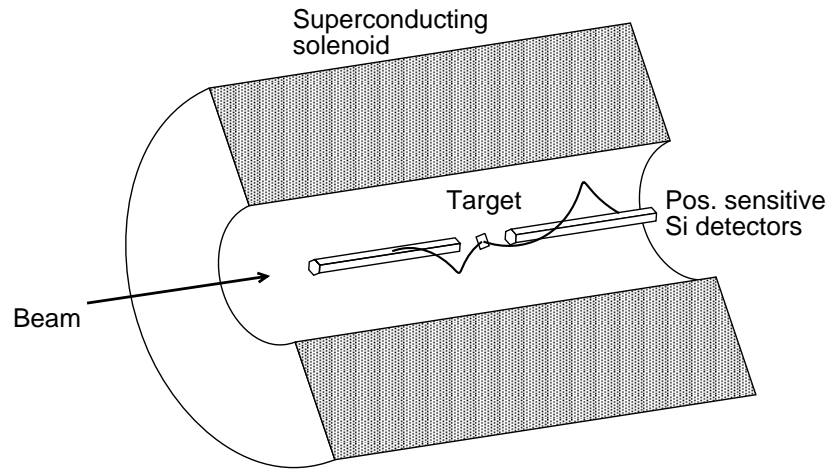


Fig. I-51. Cut-away schematics of the superconducting solenoid spectrometer. Two helical particle trajectories are indicated by thick solid curves. Particles are detected in position-sensitive Si detectors surrounding the beamline.

The principle of the spectrometer is to bring in the beam along the axis of the large superconducting solenoid magnet to strike a target near its center.² Reaction products emitted from the target follow helical trajectories in the uniform longitudinal field inside the solenoid and, if their transverse momenta are not too large, will return to the beam axis. By placing a hollow array of position-sensitive Si detectors around the beam axis, the particle trajectories will be intercepted and one will thus achieve a solid angle for detection that approaches 4π . From the measured quantities, namely ΔT - the time-of-flight obtained using the pulsed structure of the ATLAS beam, z - the distance from target to the intercept with the detector, and E_{lab} - the energy deposited in the Si detector, the quantities m/q , the mass-to-charge ratio of the particle, E_{cm} , θ_{cm} - its energy and emission angle in the center-of-mass system, as well as a rough measure of the azimuthal emission angle ϕ , may be derived. It is an important property of this spectrometer design that the particle

energy measured at a specific longitudinal position, z , exactly reflects the energy dispersion in the center-of-mass system with the consequence that only the intrinsic detector resolution limits the spectral resolution; the kinematic effects that limit resolution for measurements done in inverse kinematics, are completely absent in this design.

Work is under way to assemble a limited device to demonstrate the spectrometer concept. It is planned to base it on a solenoid from a decommissioned MRI scanner (yet to be identified), which may have a lower than optimum field strength. The design of the beamline leading into the general purpose area of ATLAS, beam transport calculations, as well as simulations of the performance of the spectrometer using a measured field map for a similar solenoid are being carried out. Acquisition of the required electronics, Si detectors, and beamline vacuum components is ongoing.

*University of Manchester, United Kingdom, †Western Michigan University.

¹<http://www.phy.anl.gov/atlas/solenoid.html>.

²J. P. Schiffer and A. H. Wuosmaa, ORNL Workshop on RIA Instrumentation; J. P. Schiffer, Lawrence Berkeley National Laboratory, Report LBNL-43460 "Experimental Equipment for an Advanced ISOL Facility", Ed. I. Y. Lee, 1999, p. 22.

h.5. Commissioning of the APT Isobar Separator (J. Fallis,* G. Savard,† S. Caldwell,† J. A. Clark,* A. A. Hecht,¹§ D. Lascar,^{||} A. Levand, N. D. Scielzo, H. Sharma,* K. S. Sharma,* I. Tanihata, A. C. C. Villari,**7 Y. Wang,* F. Buchinger,‡ J. E. Crawford,‡ S. Gulick,‡ J. K. P. Lee,‡ and R. Segel¶)

One of the new components of the Advanced Penning Trap (APT) system is a gas filled Penning trap "Isobar

Separator". The Isobar Separator will be used to eliminate isobaric contaminants created in the fusion-

evaporation reactions that are used to create the isotopes of interest. The APT Isobar Separator is able to send the resulting extremely pure samples of radioactive ions to either the Beta Paul Trap (BPT) for decay studies or back to the CPT mass spectrometer for mass measurements. The increased purity of the ion samples being sent to the CPT will allow for measurements of even more weakly-produced and shorter-lived species, extending the range of attainable masses further away from stability.

The APT Isobar Separator Penning trap is located inside a 7 Tesla superconducting magnet. The high field will allow the mass resolution ($\Delta m/m$) to exceed 10^{-5} . An RF quadrupole electric field at the appropriate cyclotron frequency is used to recenter the ions of interest in the trap. It is applied for a specified finite duration and the ions are allowed to cool both before and after the excitation. To obtain the required resolution in a short time, an additional application of an RF dipole excitation at the magnetron motion frequency (ω_z) aids in exciting the undesirable isotopes out of the trap. The isotopes to be studied are also affected by this ω_z excitation but are more strongly re-centered by the applied cyclotron frequency.

Helium is used as a buffer gas inside the Isobar Separator due to its high ionization potential and low mass. Gas pressures maintained inside the trap during

operation are estimated to be between 1.2×10^{-4} and 3.0×10^{-4} Torr. A LN_2 cold trap similar to that installed in the helium line feeding the gas catcher has been added to the helium line feeding the APT Isobar Separator. This purifies the helium gas and has increased the lifetime of ions in the trap. Optimization of the mass resolution continues with a mass resolution of 4×10^{-5} having been achieved to date.

The electronics required for the rapid control of the quadrupole deflectors and ion optical elements during the bi-directional operation of the beamline (see Fig. I-52) have been completed, installed and tested. Ions from the gas catcher have been delivered to the APT Isobar Separator where they have been cooled, cleaned, ejected and then transferred backward in the same beamline to the CPT mass spectrometer for measurement. Optimization of this ion transport is ongoing.

During a recent run the APT Isobar Separator has been used to purify ion samples prior to their measurement in the CPT mass spectrometer. Even with a resolution ($\Delta m/m$) during the run of only 1.3×10^{-4} , a dramatic decrease in isobaric contamination was observed, leading to a corresponding decrease in the time required to achieve a given mass uncertainty. This improvement will be especially significant for the more weakly produced isotopes.

*Argonne National Laboratory and University of Manitoba, Winnipeg, Manitoba, †Argonne National Laboratory and The University of Chicago, ‡McGill University, Montreal, Quebec, §Argonne National Laboratory and University of Maryland, ¶Northwestern University, ||Argonne National Laboratory and Northwestern University, **Argonne National Laboratory and GANIL, Caen, France.

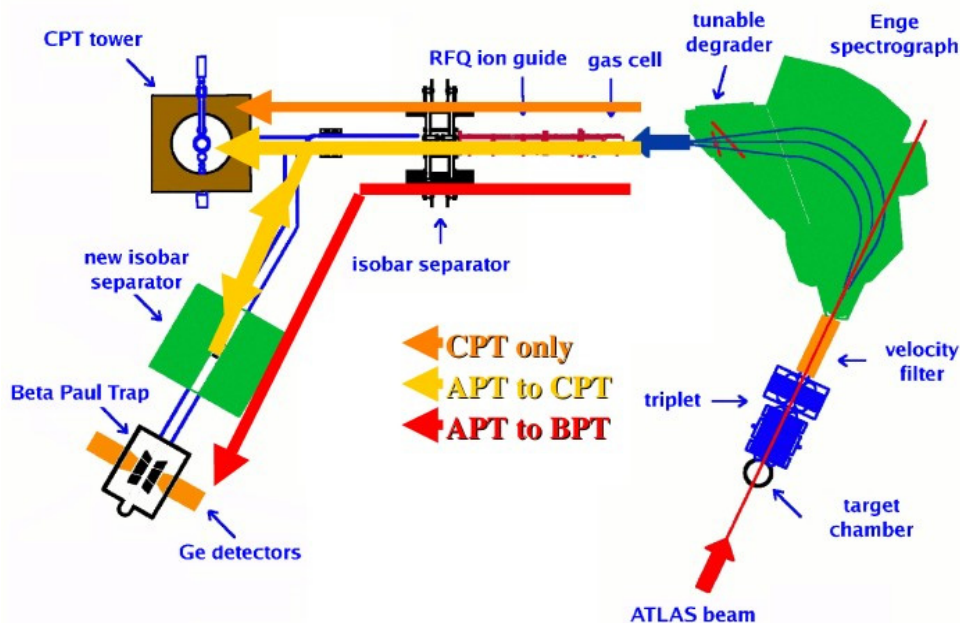


Fig. I-52. Diagram of three possible directions for ion travel in the CPT/APT system.

h.6. Gammasphere Operations (M. P. Carpenter, C. J. Lister, R. V. F. Janssens, T. L. Khoo, T. Lauritsen, J. Rohrer, E. F. Moore, D. Seweryniak, P. Wilt, S. Zhu, and F. G. Kondev*)

As reported last year, Gammasphere was moved in 2004 to a second beamline in area IV in order to operate separately from the FMA. In 2005, all Gammasphere experiments were performed on this beamline allowing for the device to run in conjunction with the ancillary detectors CHICO and Hercules. A move back to the FMA beamline will occur in early 2006. Twenty PAC approved experiments were performed with Gammasphere in 2005 which is similar in number to the 21 experiments performed in 2004.

By the end of 2005, Gammasphere had been operating at ATLAS for nearly three years, and it appears that the device will operate at our facility for the foreseeable future. In 1997, 2000 and 2002, Gammasphere was moved after approximately two years of operation at the host facility. In each instance, all Ge detectors were annealed and optimum energy resolution was restored to the array. Since Gammasphere is not scheduled to move from Argonne, we have undertaken a policy to anneal a detector once its resolution has degraded beyond 3 keV at 1.33 MeV.

As reported in the last annual report, due to failures of the resistors along the bias chain, we continue to see breakdowns on the BGO PMT bases. This results in a non-responsive channel. The PMT can be repaired by locating the failed resistor and replacing it, however, this is a very time consuming operation. While it is our plan to replace all of these bases with new components in the long run, we still are repairing the bases as they fail and as the schedule allows.

Several upgrade paths are being pursued. A replacement for the dual crate VME acquisition system has been developed and is in the final stages of debugging. It is our plan that this system will replace the dual crate system in 2006. A new Root based on-line histogramming program has been developed and is rapidly gaining acceptance by the Gammasphere Users as the default on-line monitoring system. VME readout capabilities should be available in 2006. Finally, a prototype board was tested which will allow the BGO energies to be readout when the trigger overlap is extended to 2 μ sec. It is planned to modify all VXI cards in 2006 so they have this capability.

*Nuclear Engineering Division, Argonne National Laboratory.

h.7. α -Calibration of the Twin-Ionization Chambers (X. D. Tang, M. Notani, N. Patel, J. Greene, D. Kahl, and K. E. Rehm)

For the extraction of the S-factor from measurements of the beta-delayed alpha decay of ^{16}N the energy calibration of the detector has to be known with an accuracy of better than 3×10^{-3} , which translates to less than 5 keV for energies in the vicinity of 1.5-2 MeV. In order to achieve this limit special emphasis has been put on measuring the α energy in the ^{16}N experiment with sufficient accuracy. A "sandwich" source of ^6Li -C- ^{10}B with a nominal thickness of $3 \times 10 \mu\text{g}/\text{cm}^2$ was mounted in the middle of the twin-ionization chamber and bombarded with neutrons from a PuBe source, which were thermalized in a 2.54 cm thick high-density polyethylene shield. With this geometry more than 95% are thermal neutrons, as tested by installing a 1 mm thick Cd layer outside the twin-ionization chambers. The thermal neutrons interacting with the ^{10}B and ^6Li foils produced α -particles via the (n, α) reaction with nominal energies of 2056, 1776 and 1472 keV, respectively. A two-dimensional plot of the Frisch-grid vs. anode signals is shown in Fig. I-53 for the upstream and downstream detectors, respectively. Particles emitted at small angles with respect to the

foils appear in the vicinity of the diagonal lines in these spectra, while alphas emitted perpendicular to the foil show up far away from the diagonals. The increased energy loss of particles emitted close to the foil results in a slight curvature in the grid vs anode signal. Because of the geometry of the 'sandwich' target, the curvature shows up in the ^{10}B -lines for the upstream detector and in the ^6Li -lines for the downstream detector. The thicknesses of the B, C and Li layers were determined by energy loss measurements with a ^{228}Th source using the Enge-split-pole spectrograph. The long term stability of the detectors was found to be better than 3×10^{-3} .

In order to investigate the sensitivity of the detectors to scattered neutrons, different counting gases (e.g. pure Ar and Ar-CO₂ mixtures) have been studied. They did not result in lower backgrounds and, since the energy resolution was found to be more dependent on the voltages used in the IC, we continued to use the P10 mixture in our experiments.

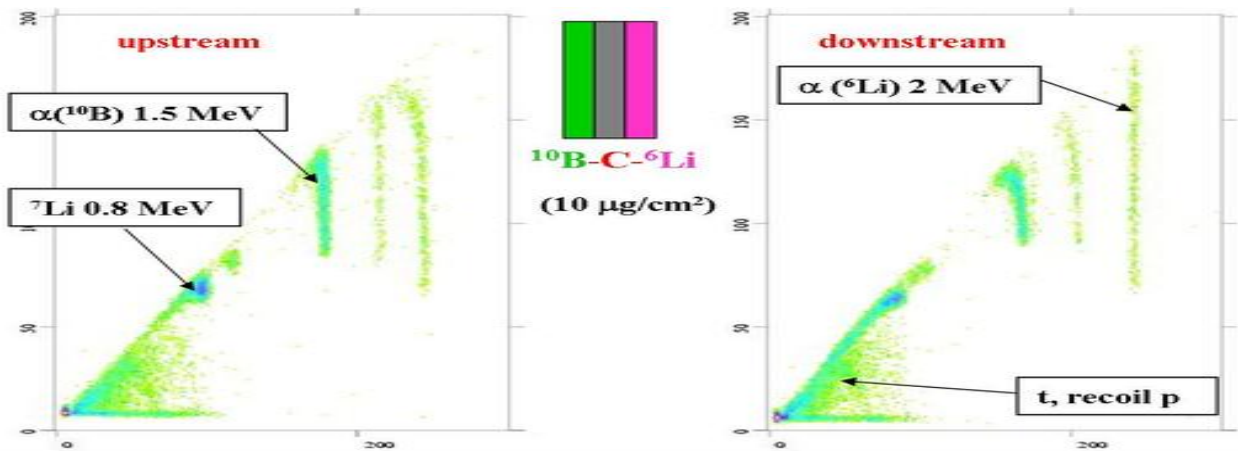


Fig. I-53. Two-dimensional spectra of Frisch grid signal vs. anode signal obtained from the twin-ionization detector with a mixed ^{10}B - ^6Li target. Bombarding this target with thermal neutrons from a PuBe source results in α - ^7Li and α -t coincidences, which are detected in the two ion chambers.

h.8. Nuclear Target Development (J. P. Greene)

The Physics Division operates a target development laboratory that produces targets and foils of various thicknesses and substrates, depending on the requirements, for experiments performed at the ATLAS and dynamitron accelerators. The targets are prepared

from both naturally occurring materials and stable isotopes that are supplied either in pure, elemental form or as stable compounds. In addition to ATLAS experiments, targets and foils are provided for all staff members whether working within the Physics Division

or undertaking experiments at other facilities. Whenever possible, support is provided to other ANL Divisions and, in particular, to requests from researchers at the University of Chicago as well as other universities (e.g. Yale and Notre Dame).

In the past year, numerous targets were fabricated either as self-supporting foils, on various substrates or as "sandwich" targets. Targets produced included Al, Au, $^{10,11}\text{B}$, Be, $^{12,13}\text{C}$, ^{48}CaO , ^{114}Cd , ^{50}Cr , Cu, $^{54,57}\text{Fe}$, ^{160}Gd , $^{74,76}\text{Ge}$, Grafoil, Havar, ^6LiF ^{26}Mg , MgH, ^{100}Mo , Mylar, ^{15}N , ^{58}Ni , $^{204,206,208}\text{Pb}$, polyethylene, polypropylene, phosphor, ^{198}Pt , Rh, ^{123}Sb , ^{28}Si , SiO, SiO₂, $^{144,154}\text{Sm}$, $^{120,124}\text{Sn}$, stainless steel, $^{128,130}\text{Te}$, Ti, TiC, U, UC₂, UF₄, W, $^{172,176}\text{Yb}$ and ^{96}Zr . Many of these target foils have been fabricated by mechanical rolling using our small rolling mill. A large fraction of these targets were prepared for experiments carried out at Gammasphere.

Beyond target development, thin plastic films and foils are produced for various detector systems used for experiments at ATLAS as well as energy degraders and windows for the Advanced Penning Trap. New materials and mounting technologies are being implemented with the gas cell needed for the CARIBU project and for astrophysics research using in-flight radioactive beams at SPS III and for gas targets at the FMA.

As part of ATLAS support, the target lab routinely produces carbon stripper foils of $2\ \mu\text{g}/\text{cm}^2$ for use in the Tandem as well as other thickness for additional stripping throughout the accelerator. For the production of enriched beams at ATLAS, there continues to be a need for the preparation of various dilutions of isotopic source material into suitable form for introduction into the ion sources, including ^{13}C , $^{136,138}\text{Ce}_2\text{O}_3$, ^{26}MgO , and ^{50}Ti .

The target development laboratory includes state-of-the-art equipment used for thin-film fabrication. The addition of a new, multi-purpose, computer-controlled vacuum evaporation system extends our capabilities and provides a stable platform for the continued production of accelerator targets. The available techniques consist of multiple resistive heating, focused ion beam sputtering, ion assisted deposition, electron beam and electron bombardment evaporation, carbon arc evaporation, electrodeposition and mechanical rolling. The evaporators are maintained under high vacuum and each vessel contains a quartz-crystal film-

thickness monitor with deposition rate indicators. Also included are movable shutters, quartz-lamp substrate heaters and thermocouple temperature sensors, allowing for complete process monitoring during target deposition.

Other auxiliary equipment used for target development includes electrodeposition apparatus, a small rolling mill, an alpha particle counting chamber, inert atmosphere glove box, laminar flow clean bench, pellet press, a reduction furnace, and a variety of precision balances. A turbo-pumped target storage facility is in operation for maintaining, under high vacuum, those targets that readily oxidize in air. This system utilizes computer-controlled circuitry to prevent targets from exposure to atmosphere during power interruptions. A second storage system employing a bank of vacuum desiccators and connected to a mechanically pumped manifold is available for use by individual experimenters. An additional set-up, consisting of two large plastic desiccator boxes, evacuated using a small turbo-pump system, is in operation for long-term material storage. This allows a separation of material storage from target storage, hence eliminating repeated exposure when transferring and retrieving targets.

A low-level radioactive source and target preparation laboratory exists at a separate location within the Division that is dedicated to the production of these sources and targets. Available preparation techniques include multiple resistive heating, employing a diffusion-pumped vacuum evaporator. A second, smaller evaporator system was constructed for close proximity evaporations of higher activity materials, to be used as targets as well as radioactive sources. Preparation and handling of actinide targets by electrodeposition as well as fission sources (mainly ^{252}Cf) has been done using this lab as well as high activity samples for a ^{18}F source experiment at Gammasphere and EDM studies using $^{225,226}\text{Ra}$.

An area of increased research effort has been toward development of ISOL targets for the RIA proposal involving a uranium compound production target. Toward this end, direct measurements of the thermal conductivity of uranium carbide have been made using a method developed at ANL. Sample material of small grain size uranium carbide is being prepared in collaboration with the ES Division in Building 212. This work is still in progress.

h.9. Completion of the SCARLET Data Acquisition System (K. Teh)

Deployment of the SCARLET data acquisition system was completed when the following were accomplished.

- Design, test, and construction of a trigger system.
- Construction of a supporting infrastructure.
- Development of a DAPHNE-like on-line sorter.

A custom trigger system which implements SCARLET's concurrent, multi-crate readout was designed and built by the Electronics group in the HEP division. It consists of a master trigger module that is connected to a slave trigger module in each crate. The purpose of the master trigger is to distribute event triggers to the slaves and to synchronize their BUSY states. Five trigger systems were procured, each system consisting a master and two slaves.

There are now three SCARLET systems outfitted with these new trigger systems. Two of them are on-line at the Spectrograph and ATSCAT experimental stations. One is located upstairs in the Strip Detector Lab and is used primarily for off-line detector development. There are two additional SCARLET systems in use; one at the BPT station, the other at the Advanced Photon Source (APS) Facility. These were not outfitted with the new trigger system and represent earlier single-crate versions of the SCARLET system.

The ATLAS data-room underwent a major renovation. The renovation efforts included the installation of new

network switches and a cabling infrastructure. These components were configured to create the data acquisition network ONENET. The ONENET network is a NAT network; its purpose is to allow access to the wider Internet while limiting access to it from the outside. In addition, a new computer cluster, the MUSIC cluster, was constructed. Its role is to support data acquisition and analysis of ATLAS experiments in the division. In addition to user workstations, the cluster includes:

- core servers such as a file and application server, database and web servers, etc.
- a large disk array where data collected with the SCARLET system are stored.
- an analysis farm; a collection of machines with high-speed access to the large disk array which can be used for off-line data analysis.

Finally, an on-line data sorting program was developed, prompted by complaints that the ROOT software package, while extremely powerful, was too unwieldy for the types of data analyses performed at ATLAS. This program functions as a SCARLET data consumer and uses the ROOT framework for data sorting and histogramming. Its interface is simplified by using the familiar command-line interface and recreating many of the original DAPHNE commands, such as, D1H, D2H, etc.

h.10. Evaluation of a Planar Germanium Detector with Amorphous Contacts (S. Gros, C. J. Lister, E. Hull,* and D. Pehl*)

Planar germanium counters have been used for some years to measure gamma ray polarization. Traditional counters, using ion-implanted Boron p-type contacts and Lithium drifted n-type contacts have been found to have shortcomings, especially for events occurring near the Li contact. The shortcomings include charge loss and mis-identified charge sharing which is not associated with cross-scattering. These shortcomings reveal the polarization measured by the Li-strips is attenuated by detector imperfection (see Fig. I-54).

To try to remedy this shortcoming, we have been working on a SBIR-funded project with PhDs Company of Oak Ridge Tennessee to develop amorphous-Ge

contacts on both faces of the counter. We have been evaluating a new technology counter to ascertain if it more appropriate for polarization work. We have collected data from Europium and Cesium sources, collected under identical conditions and with identical electronics to evaluate the electrode performance and try to separate detector shortcomings from other effects in the pulse processing path and in analysis. The new counter appears very promising in charge-sharing characteristics, though the current detector needs some refinement as it is prone to go into high-frequency oscillation when data is collected for all channels simultaneously.

*PhDs Company, Oak Ridge, TN.

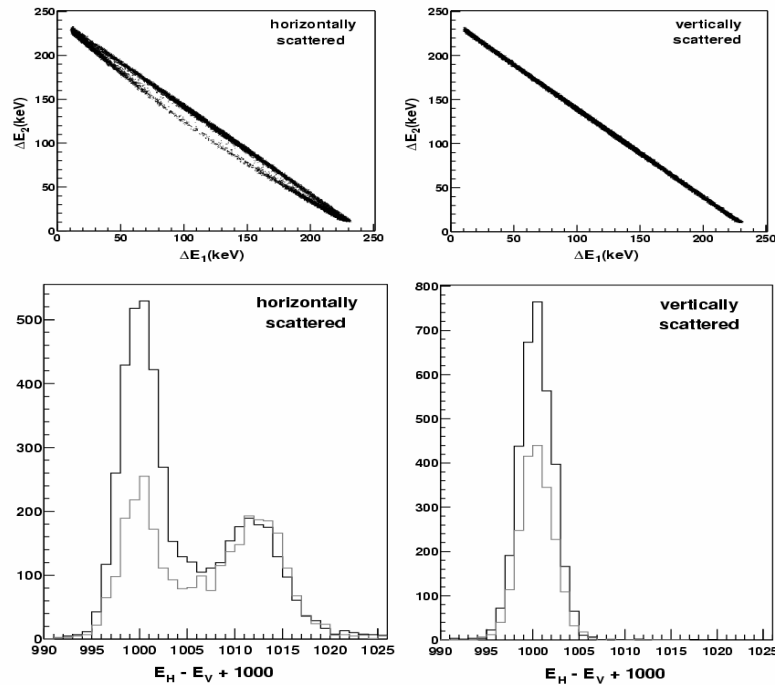


Fig. I-54. Imperfections in charge sharing in a planar germanium wafer. The events in the left panel, representing scattering between neighboring lithium strips, show distinct charge loss and have many false two-strip events.

h.11. Silicon Array Upgrade to MUSIC Detector (B. Shumard)

The MUSIC detector¹ was designed as a detector to study the (α, p) reaction in stable and radioactive beams. The detector was tested with success in 2005 and efforts to improve count efficiency as well as reaction product identification have been ongoing. In order to better detect the proton produced in either reaction channel (elastic scattering or $p+$ residual nucleus for (α, p) reactions).

The major improvement to the MUSIC chamber was the addition of a 15 strip silicon array at the rear end of the MUSIC detector to allow for the α -particle to be detected. The advantage of this detector system is twofold. First, it can be used to calculate a time-of-flight (TOF) from the silicon monitor detectors that exist outside of the MUSIC chamber. Second, it serves as a trigger to open the gating grid of the MUSIC chamber.

The silicon array is made up of 5 – 3 section trapezoidal Si detectors that are mounted to ceramic insulating plates. Ground, Si bias, and ring bias are carried into

the Si detectors via a pin connections on the ceramic insulator plate. The Si array is configured in such a way (see Fig. I-55) to allow for the maximum active area without interference from the bias and signal lines interfering. Due to this configuration the Si array covers nearly the entire $5\text{ cm} \times 5\text{ cm}$ window at the rear of the MUSIC chamber. This allows for increased efficiency in α detection due to the larger Si coverage of the back plane of the MUSIC chamber.

The development of the array also required the design of a new back plate for the MUSIC chamber. The silicon array required five individual high voltage supplies as well as a 16 pin ribbon cable output. These requirements led to a simple rear plate development that incorporated all of those elements in the most efficient way possible. The final design also incorporated a table mount for the silicon array. The table was separated from the back plate to increase the open angle coverage from the back of ion chamber section of the MUSIC chamber.

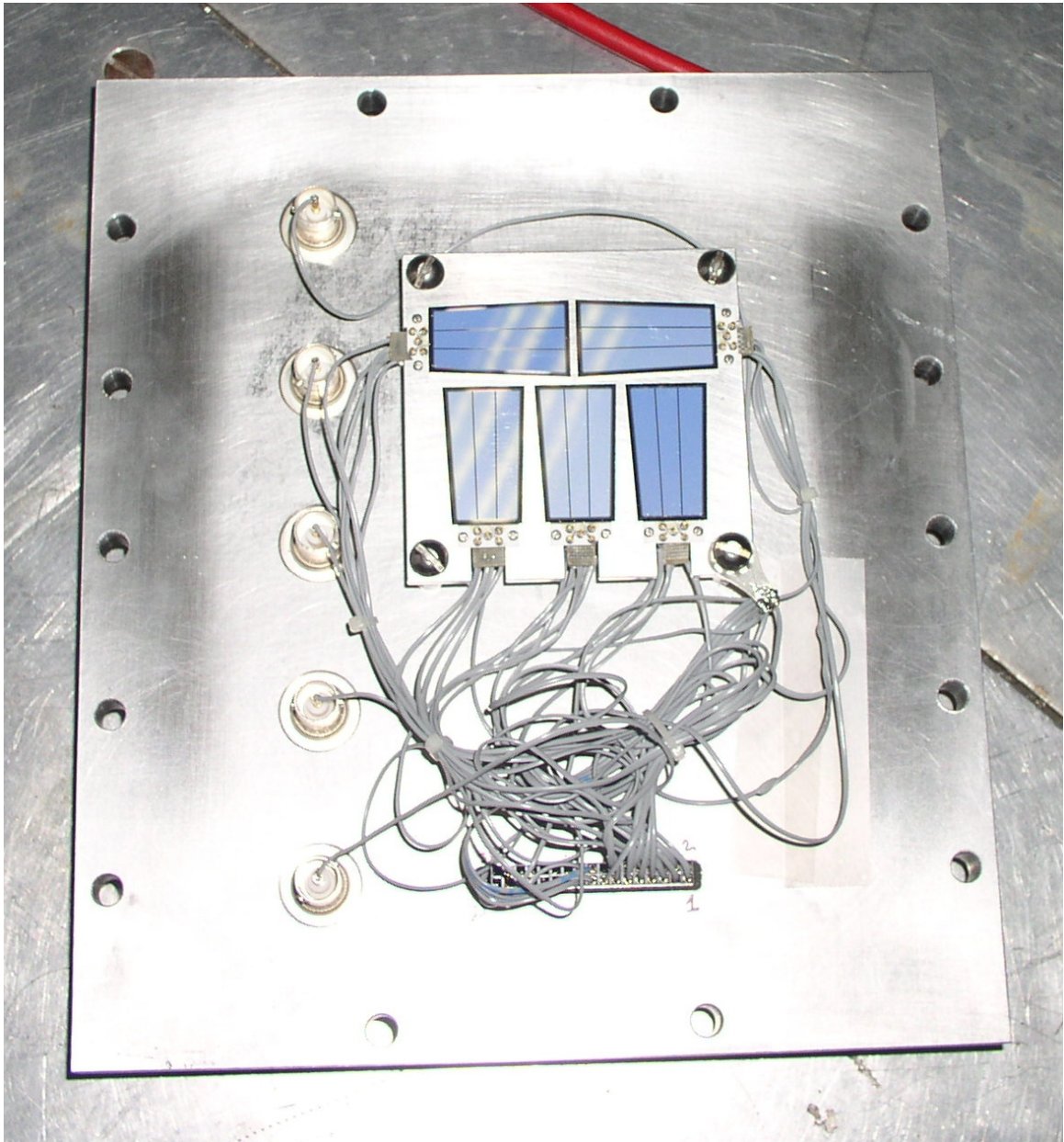


Fig. I-55. The silicon array mounted on the back flange of the MUSIC chamber. The $800\ \mu\text{m}$ trapezoidal detectors were originally used in the APEX project and cover a large solid angle.

I. HIGH-PRECISION AND HIGH-SENSITIVITY EXPERIMENTS

The powerful and sensitive techniques of nuclear physics can be turned to many fields. Frequently, important results can emerge. The ability to reliably perform such measurements remains at the heart of our program.

i.1. A Bragg Scattering Method to Search for the Neutron Electric Dipole Moment

(M. Peshkin, G. R. Ringo, M. Arif,[¶] T. W. Dombeck,^{*} D. Hussey,[¶] D. Jacobson,[¶] H. Kaiser,[†] D. Koetke,[‡] S. Shirvel,[‡] R. K. Smither,[§] and S. A. Werner[¶])

The goal of this project is to measure the neutron electric dipole moment (EDM) by observing the precession of the neutron spin in the crystalline electric field when the neutron undergoes several thousand Bragg reflections from a perfect silicon crystal. We expect to achieve a sensitivity around 5×10^{-27} e-cm, comparable with the sensitivity sought in the next round of ultra-cold neutron experiments but with significantly different systematic errors. In CY 2005 we carried out a crystal reflectivity measurement that also served as a shake-down experiment after moving our apparatus to the NIST reactor. A second reflectivity measurement is

planned for May or June 2006. Also, M. Arif of NIST joined the collaboration, and we submitted a proposal to NSF for support of a proof-of-principle experiment that will be needed for designing several details of the final EDM experiment. That proof-of-principle experiment will measure the interaction of the neutron's moving magnetic dipole moment in the same crystalline fields to calibrate those fields for the EDM experiment. It will also provide information about issues relating to the penetration of the neutrons into the crystal during Bragg reflection. A first experiment of that type is expected to commence around the end of CY 2006.

^{*}University of Hawaii, [†]University of Indiana, [‡]Valparaiso University, [§]APS User Program, Argonne National Laboratory, [¶]National Institute of Standards and Technology.

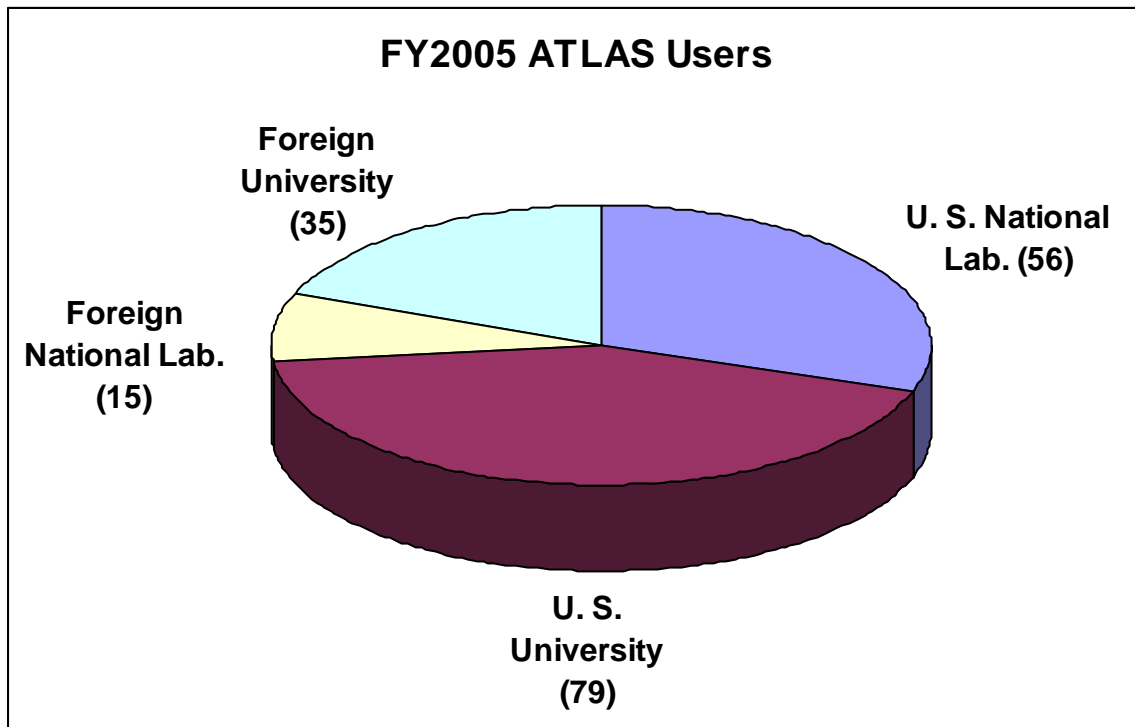
J. ATLAS USER PROGRAM (E. F. Moore)

During the fiscal year 2005, ATLAS hosted strong "campaigns" involving radioactive beams, the CPT, and, of course, Gammasphere. In May 2004, Gammasphere was moved over to the old APEX beamline. Through FY 2005, Gammasphere was operated in "stand alone" mode, allowing campaigns using CHICO and the Microball. It is anticipated that Gammasphere will return to the FMA in the spring of 2006.

Many of the experimental programs were driven by outside Users, and in all programs, there was considerable outside User involvement. Over 95% of all experiments performed in fiscal year 2005 included one or more outside Users and roughly 50% of the approved experiments had an outside User as the Principal Investigator. Frank Moore continued to be available in a user liaison capacity to handle the scheduling of ATLAS experiments, provide assistance in experiment proposal submission matters, and help facilitate the effective performance of research at ATLAS by outside scientists. In July 2005, Frank

moved over to the Argonne SCD Division to work full time for the U.S. Department of Energy, Radiological Assistance Program (RAP). He continues to provide limited assistance with scheduling and with the ATLAS web page. However, a large portion of the Heavy-Ion in-house scientific staff and members of the technical support staff spent substantial amounts of their time in experiment setup, preparation and assistance for the many different experiments performed at ATLAS.

A total of 185 Users from 48 different institutions were present at ATLAS for experiments in FY 2005. The pie chart below shows the distribution of the institutions represented by ATLAS Users and the number of Users of each type. Of the 56 Users from U.S. National Laboratories, 45 are from Argonne (including summer students and long-term visitors). There were 53 students at ATLAS for experiments this FY, of which 11 were based at Argonne long-term. The names and institutions of all outside Users who were present at ATLAS in FY 2005 are listed below in section (b).



The Program Advisory Committee met once during the 2005 fiscal year, on May 20-21, 2005 to recommend experiments for beam time allocation at ATLAS. In FY 2005 the Program Advisory Committee members were:

May 20-21, 2005

Ani Aprahamian	University of Notre Dame
Birger Back	Argonne National Laboratory
Art Champagne	University of North Carolina, Chapel Hill
Augusto Macchiavelli	Lawrence Berkeley National Laboratory
David Radford (<i>Chair</i>)	Oak Ridge National Laboratory
Gene Sprouse	State University of New York, Stony Brook
Piet Van Duppen	University of Leuven, Belgium

The PAC reviewed 59 proposals for 334 days of requested running time. Due to the large demand for Gammasphere beam time, the PAC was asked to prioritize experiments into two categories; those that must be run at any cost (*priority I*), and those that should be granted beam time if at all possible (*priority II*). Of the submitted proposals, the Program Advisory Committee recommended priority I acceptance of 28 proposals for a total of 119 days of running time, and priority II acceptance of 9 proposals for 46 additional days of beam time.

At the start of FY 2005, the ATLAS User Group Executive Committee consisted of Alan Wuosmaa (Chair, Western Michigan University), Jolie Cizewski (Rutgers University), Susan Fischer (De Paul University), and Walter Reviol (Washington University). An election for new membership was held in November 2004. The ATLAS User Community elected Ani Aprahamian (University of Notre Dame), Kris Starosta (Michigan State University), and Ingo Wiedenhöver (Florida State University) to fill the three vacant positions. Alan Wuosmaa remained on the Committee as the outgoing chair. The Committee then chose Ani Aprahamian as the new Chair.

a. Experiments Involving Outside Users

All experiments in which outside users directly participated during FY 2005 are listed below. The spokesperson for each experiment is given in square

brackets after the title, and the collaborators who were present for the experiment are given below each entry.

1. Preparations Towards a Search for Super-Heavy Elements at ATLAS: Production and Fine Structure in $Z = 108$ ^{265}Hs [Heinz]
N. Hoteling, A. Hecht, A. M. Heinz, W. B. Walters, B. Back, R. H. Scott, C-L. Jiang, D. Henderson, D. Seweryniak, D. A. Peterson, F. G. Kondev, E. F. Moore, G. Savard, J. Greene, J. P. Schiffer, C. J. Lister, M. P. Carpenter, P. Collon, R. C. Pardo, R. Vondrasek, R. V. F. Janssens, S. Zhu, T. L. Khoo, T. Lauritsen, X. Wang, R. R. Winkler, J. Qian, S. Gros, and A. B. Garnsworthy
2. High Energy Calibration of the Gammasphere Array [Jenkins]
D. Jenkins, C. J. Lister, N. S. Pattabiraman, R. Glover, and Krishichayan
3. Octupole Collectivity and Second Well Structures Around ^{220}Th [Reviol]
W. Reviol, D. G. Sarantites, C. J. Chiara, O. Pechenaya, S. A. Komarov, D. Seweryniak, M. P. Carpenter, R. V. F. Janssens, S. Zhu, T. L. Khoo, J. Greene, and M. Montero Diez
4. Properties of a High-K Isomer in ^{254}No [Khoo]
T. L. Khoo, D. Seweryniak, I. Ahmad, M. P. Carpenter, C. N. Davids, J. Greene, R. V. F. Janssens, F. G. Kondev, T. Lauritsen, C. J. Lister, E. F. Moore, S. Zhu, A. A. Hecht, B. Back, S. K. Tandel, U. S. Tandel, P. Chowdhury, A. M. Heinz, and D. G. Sarantites
5. Proton Decay of ^{121}Pr [Davids]
C. N. Davids, D. Seweryniak, W. B. Walters, P. J. Woods, A. P. Robinson, A. A. Hecht, R. V. F. Janssens, M. P. Carpenter, S. Sinha, and S. Zhu

6. Comprehensive Experiment Aimed at the Study of ^{252}Cf Binary and Ternary Fission [Hamilton]
J. H. Hamilton, A. V. Ramayya, D. J. Fong, J. C. Batchelder, A. Rodin, G. M. Ter-Akopian,
J. O. Rasmussen, G. S. Popeko, W. C. Ma, S. J. Kurtz, J. Kliman, K. Li, J-K. Hwang, A. S. Fomichev,
and A. V. Daniel
7. Internal Conversion Coefficients in ^{167}Lu : Confirmation of Wobbling Mode [Beausang]
C. W. Beausang, D. S. Brenner, G. Gurdal, E. T. Williams, H-C. Ai, D. J. Hartley, H. Amro, C. J. Lister,
D. Seweryniak, T. Lauritsen, B. P. Crider, and R. C. Raabe
8. Superdeformation in ^{132}Ce : Elucidation of the Decay-Out Path and Extension to Band Termination [Paul]
E. S. Paul, M. A. Riley, K. B. Lagergren, W. T. Cluff, P. Pipidis, R. Wadsworth, F. Johnston-Theasby,
P. Joshi, J. Simpson, D. T. Joss, L. Nelson, B. M. McGuirk, A. O. Evans, and A. J. Boston
9. Precise Doppler Reconstruction of γ -Rays Emitted From Fast-Moving Nuclei [Lister]
C. J. Lister, M. P. Carpenter, R. V. F. Janssens, T. L. Khoo, T. Lauritsen, D. Seweryniak, S. Gros,
A. P. Robinson, S. Zhu, and S. M. Fischer
10. Excitation of High-K States Associated with the 31-Year Isomer $^{178\text{m2}}\text{Hf}$ [Walker]
P. M. Walker, Z. F. Podolyak, S. J. Williams, Z. Liu, G. D. Jones, N. J. Thompson, A. B. Garnsworthy,
G. D. Dracoulis, G. J. Lane, G. Hackman, R. S. Chakrawarthy, J. J. Carroll, F. G. Kondev,
R. V. F. Janssens, T. L. Khoo, M. P. Carpenter, D. Seweryniak, S. Zhu, and P. Chowdhury
11. Study of Excited States in ^{13}O [Wuosmaa]
A. H. Wuosmaa, J. C. Lighthall, S. T. Marley, N. J. Goodman, K. E. Rehm, R. C. Pardo, C-L. Jiang,
R. V. F. Janssens, J. P. Schiffer, E. F. Moore, X. Tang, M. M. Notani, I. Tanihata, L. Jisonna, and
R. E. Segel
12. Structure of Threshold States in the $^{21}\text{Na}(p,\gamma)^{22}\text{Mg}$ Reaction [Woods]
P. M. Davidson, P. J. Woods, D. Seweryniak, C. N. Davids, J. M. Shergur, S. Sinha, M. P. Carpenter,
T. Lauritsen, R. V. F. Janssens, and D. G. Jenkins
13. High Spin States in the $T = 3/2$ Mirror Nuclei ^{37}Ca and ^{37}Cl , and the $T = 1/2$ Mirror Nuclei ^{37}K and ^{37}Ar
[Williams]
S. J. Williams, G. D. Jones, N. J. Thompson, A. B. Garnsworthy, M. A. Bentley, C. Chandler, Z. Liu,
and D. D. Warner
14. Studies of Excited States in ^{101}Sn . Phase I: Search for ^{101}Sn β -Delayed Protons [Seweryniak]
D. Seweryniak, S. Zhu, R. V. F. Janssens, C. J. Lister, M. P. Carpenter, N. Hammond, D. Henderson,
A. A. Hecht, W. B. Walters, D. A. Peterson, C. Vaman, G. Lotay, K. Starosta, P. J. Woods, S. Gros,
and N. Hoteling
15. $^{12}\text{N} + p$ Elastic Resonance Scattering [Tang]
X. Tang, D. Henderson, R. C. Pardo, B. Shumard, C-L. Jiang, E. F. Moore, M. M. Notani, J. P. Schiffer,
J. Greene, R. V. F. Janssens, L. Jisonna, and K. E. Rehm
16. Identification of Excited States in ^{107}Te with Recoil Decay Tagging Measurement [Starosta]
K. Starosta, C. Vaman, D. Seweryniak, A. P. Robinson, D. A. Peterson, K. B. Lagergren, P. J. Woods,
C. N. Davids, W. B. Walters, A. A. Hecht, S. Zhu, S. Gros, D. Henderson, G. Lotay, and N. Hoteling
17. High Seniority Configurations and Triaxial Strongly Deformed Structures in ^{174}W [Chowdhury]
P. Chowdhury, S. K. Tandel, U. S. Tandel, C. L. Parnell-Lampen, D. J. Hartley, C. J. Lister,
R. V. F. Janssens, T. L. Khoo, D. Seweryniak, M. P. Carpenter, T. Lauritsen, S. Zhu, and X. Wang
18. Improvement of Thick Film Coated Conductor by MILD Pinning Centers [Weinstein]
B. W. Mayes II, A. Gandini, R-P. Sawh, D. Parks, J. Tang, and R. Weinstein

19. Collective Enhancement of the Nuclear Level Density [Charity]
R. J. Charity, L. G. Sobotka, S. A. Komarov, A. L. Caraley, D. G. Sarantites, and C. J. Chiara
20. High Spin States in the $N = Z - 3$ Nucleus ^{49}Fe - Coulomb Effects at Large Proton Excess [Bentley]
M. A. Bentley, C. Chandler, D. D. Warner, S. J. Williams, G. D. Jones, Z. Liu, C. J. Lister, C. N. Davids, and D. Seweryniak
21. Multi-Nucleon Transfer and Spectroscopy of High-K States Near ^{177}Lu [Dracoulis]
G. D. Dracoulis, G. J. Lane, F. G. Kondev, I. Ahmad, A. P. Byrne, M. P. Carpenter, P. Chowdhury, R. V. F. Janssens, T. L. Khoo, T. Kibedi, T. Lauritsen, C. J. Lister, J. M. Nieminen, D. Seweryniak, H. Watanabe, and S. Zhu
22. Study of the Structure of the Lightest No Isotopes [Peterson]
D. A. Peterson, R. V. F. Janssens, T. L. Khoo, B. Back, C. J. Lister, C. N. Davids, D. Seweryniak, A. A. Hecht, M. P. Carpenter, T. Lauritsen, S. Zhu, X. Wang, C-L. Jiang, and A. M. Heinz
23. Towards a Measurement of the Charge Radius of ^8He [Lu]
P. Mueller, Z-T. Lu, K. E. Rehm, X. Tang, M. M. Notani, C-L. Jiang, R. C. Pardo, R. V. F. Janssens, D. Henderson, B. Shumard, J. Greene, J. P. Schiffer, K. Bailey, T. P. O'Connor, L-B. Wang, and R. J. Holt
24. Measurement of the β -Delayed α Spectrum of ^{16}N with a New Technique-3 [Rehm]
K. E. Rehm, C-L. Jiang, X. Tang, S. Sinha, D. Henderson, J. Greene, B. Shumard, J. P. Schiffer, R. V. F. Janssens, A. E. Champagne, G. Savard, R. C. Pardo, I. Ahmad, E. F. Moore, M. M. Notani, A. H. Wuosmaa, M. Paul, R. E. Segel, L. Jisonna, and A. A. Hecht
25. Study of Fusion Hindrance at Extreme Sub-Barrier Energies for a System with Small Negative Q-Value [Jiang]
C-L. Jiang, B. Back, K. E. Rehm, R. V. F. Janssens, D. Seweryniak, X. Tang, S. Zhu, I. Tanihata, M. M. Notani, D. Henderson, R. C. Pardo, M. Paul, and P. Collon
26. DSAM Lifetime Measurements for Fission Fragments Using Hercules [Reviol]
W. Reviol, D. G. Sarantites, C. J. Chiara, O. Pechenaya, S. A. Komarov, D. Seweryniak, M. P. Carpenter, R. V. F. Janssens, S. Zhu, T. L. Khoo, J. Greene, and M. Montero Diez
27. Sub-Barrier Fission in the $^{16}\text{O} + ^{238}\text{U}$ System [Back]
B. Back, C-L. Jiang, C. J. Lister, K. E. Rehm, I. Tanihata, X. Tang, D. A. Peterson, S. Zhu, and X. Wang
28. Identification of the Neutron $i_{13/2}$ State in ^{137}Xe by the $^{13}\text{C}(^{136}\text{Xe}, ^{12}\text{C})^{137}\text{Xe}$ Neutron-Transfer Reaction [Radford]
D. C. Radford, J. Pavan, E. Padilla-Rodal, C-H. Yu, D. G. Sarantites, W. Reviol, D. Seweryniak, S. Zhu, and X. Wang
29. Studying (α, p) Reactions using MUSIC and the Thick Target Technique [Tang]
K. E. Rehm, X. Tang, L. Jisonna, J. P. Schiffer, R. V. F. Janssens, S. Zhu, X. Wang, A. A. Hecht, and M. M. Notani
30. Production of ^{14}O for Future Measurements with the Advanced Penning Trap and Precision Measurement of the Q-Value of the Superaligned Branch [Scielzo]
N. D. Scielzo, G. Savard, J. Clark, A. Levand, S. L. Gulick, H. Sharma, K. S. Sharma, A. C. Villari, Y. Wang, I. Tanihata, and A. A. Hecht
31. A Search for Superaligned α Decays in $^{113,114}\text{Ba}$ [Hecht]
A. A. Hecht, C. J. Lister, D. Seweryniak, W. B. Walters, J. M. Shergur, N. Hoteling, C. Mazzocchi, and C. N. Davids
32. ^{138}Ce Beam Development [Pietralla]
C. J. Lister, M. P. Carpenter, S. Zhu, R. V. F. Janssens, T. Ahn, and G. I. Rainovski

33. Production of ^{14}O for Future Measurements with the Advanced Penning Trap and Precision Measurement of the Q-Value of the Superaligned Branch [Scielzo]
N. D. Scielzo, G. Savard, I. Tanihata, J. Clark, H. Sharma, Y. Wang, A. Levand, S. L. Gulick, A. A. Hecht, J. Fallis, and D. Lascar
34. Search for Triaxial Strongly Deformed Bands and Possible Wobbling Modes in ^{161}Tm [Lagergren]
K. B. Lagergren, M. A. Riley, C. Teal, Jr., A. L. Aguilar, D. T. Joss, D. J. Hartley, and X. Wang
35. Proton Decay Below the ^{100}Sn Double Shell Closure [Robinson]
A. P. Robinson, D. Seweryniak, P. J. Woods, C. N. Davids, S. Gros, S. Zhu, G. Lotay, A. A. Hecht, and B. Shumard
36. Measurement of the β -Delayed α Spectrum of ^{16}N with a New Technique-4 [Rehm]
X. Tang, M. M. Notani, N. Patel, C-L. Jiang, J. P. Schiffer, J. Greene, D. Henderson, B. Shumard, K. E. Rehm, R. V. F. Janssens, L. Jisonna, R. E. Segel, D. M. Kahl, C. Brune, A. H. Wuosmaa, M. Paul, A. E. Champagne, A. A. Hecht, and G. Savard
37. Measuring Radiation Damage from the Stopping of Uranium Beams in Material [Ahle]
L. E. Ahle, J. A. Nolen, R. M. Ronningen, I. Baek, G. Savard, and I. C. Gomes
38. Precision Measurement of the Q-Value of the Superaligned Decays of ^{42}Sc , ^{50}Mn , ^{54}Co , ^{34}Cl , and $^{26\text{m}}\text{Al}$ with the CPT Mass Spectrometer [Savard]
G. Savard, J. Clark, A. Levand, J. Fallis, H. Sharma, Y. Wang, N. D. Scielzo, A. C. Villari, P. J. Sloan, I. Tanihata, S. L. Gulick, R. E. Segel, A. A. Hecht, K. S. Sharma, J. C. Hardy, D. Lascar, M. Sternberg, C. L. Wrede, C. M. Deibel, D. Danaher, and C. Riviere
39. Quantifying the Level of Isospin Mixing in the $A = 31$ Mirror Nuclei [Pattabiraman]
N. S. Pattabiraman, R. Wadsworth, D. G. Jenkins, R. Glover, Krishichayan, C. J. Lister, S. Zhu, and M. P. Carpenter
40. K Conservation, Octupole Correlations, and Induced Depopulation of the 141 Year $K = 5^-$ Isomer in ^{242}Am [Cline]
D. Cline, A. Hayes, C-Y. Wu, I. Ahmad, M. P. Carpenter, J. Greene, R. V. F. Janssens, C. J. Lister, S. Zhu, T. Lauritsen, D. Seweryniak, X. Wang, J. J. Carroll, S. A. Karamyan, D. C. Gohlke, and R. J. Propri
41. Study of the $^{59}\text{Fe}(d,p)^{60}\text{Fe}$ Reaction as Surrogate to $^{59}\text{Fe}(n,\gamma)^{60}\text{Fe}$ [Paul]
M. Paul, X. Tang, K. E. Rehm, D. Henderson, A. H. Wuosmaa, P. Collon, I. Ahmad, J. Greene, N. Patel, R. C. Pardo, R. H. Scott, R. Vondrasek, Y. Kashiv, L. Jisonna, A. A. Hecht, D. Seweryniak, A. P. Robinson, C. N. Davids, and B. Shumard
42. Towards a Measurement of the ^8He Nuclear Charge Radius: Optimizing Production and Release [Mueller]
P. Mueller, M. M. Notani, X. Tang, K. Bailey, J. Greene, R. J. Holt, D. Henderson, R. V. F. Janssens, C-L. Jiang, Z-T. Lu, T. P. O'Connor, R. C. Pardo, K. E. Rehm, and J. P. Schiffer
43. Precise Mass Measurements of ^{65}As and ^{65}Ge with the Canadian Penning Trap Mass Spectrometer [Clark]
J. Clark, G. Savard, H. Sharma, N. D. Scielzo, A. A. Hecht, A. Levand, and F. M. Brodeur
44. High Spin Structure and Onset of Deformation in Neutron-Rich Ti and Cr Isotopes [Janssens]
S. Zhu, A. Gade, A. O. Macchiavelli, D. Cline, A. Hayes, C-Y. Wu, J. A. Becker, M. P. Carpenter, X. Wang, T. Lauritsen, D. Seweryniak, R. V. F. Janssens, R. A. Macri, and C. J. Lister

b. Outside Users of ATLAS During the Period October 1, 2004 - September 30, 2005

This list includes all outside Users who were an experiment spokesperson (a), alternate spokesperson (b), student (s), or collaborator actually present at ATLAS for an experiment. An additional 35 Users

listed as collaborators on the various experiment proposals were not at ATLAS in person, and thus are not represented in the list below.

1. Australian National University
 - A. P. Byrne
 - G. D. Dracoulis (a)
 - T. Kibedi
 - G. J. Lane
 - H. Watanabe
2. Beloit College
 - D. M. Kahl
3. Clark University
 - D. S. Brenner
 - G. Gurdal (s)
4. Daresbury Laboratory
 - J. Simpson
 - D. D. Warner (b)
5. De Paul University
 - S. M. Fischer
6. Florida State University
 - A. L. Aguilar (s)
 - W. T. Cluff (s)
 - K. B. Lagergren (a)
 - P. Pipidis (s)
 - M. A. Riley (b)
 - C. Teal, Jr. (s)
7. GANIL
 - C. Villari
8. Grenoble Nat'l. Engineering School for Physics
 - C. Riviere
9. Hebrew University of Jerusalem
 - Y. Kashiv
 - M. Paul (a)
10. Joint Institute for Nuclear Research
 - A. V. Daniel
 - A. S. Fomichev
 - S. A. Karamyan
 - J. Kliman
 - G. S. Popeko
 - A. Rodin
 - G. M. Ter-Akopian
11. Keele University
 - C. Chandler
12. Lawrence Berkeley National Laboratory
 - A. O. Macchiavelli
 - J. O. Rasmussen
13. Lawrence Livermore National Laboratory
 - S. Sinha
 - L. E. Ahle (a)
 - J. A. Becker
 - R. A. Macri
 - A. U. Schiller (b)
 - C-Y. Wu
14. McGill University
 - S. L. Gulick
 - P. J. Sloan
15. McMaster University
 - J. M. Nieminen
16. Michigan State University
 - I. Baek
 - A. Gade
 - R. M. Ronningen
 - K. Starosta (a)
 - C. Vaman (s)
17. Mississippi State University
 - W. C. Ma
18. Monmouth College
 - D. Danaher (s)
19. Northwestern University
 - L. Jisonna (s)
 - D. Lascar (s)
 - R. E. Segel
20. Oak Ridge National Laboratory
 - J. C. Batchelder
 - J. R. Beene (b)
 - J. Pavan
 - D. C. Radford (a)
 - C-H. Yu
21. Ohio University
 - C. Brune

22. SUNY at Oswego
A. L. Caraley
23. SUNY at Stony Brook
T. Ahn
G. Rainovski (b)
24. Saha Institute of Nuclear Physics
G. Mukherjee (b)
25. Texas A & M University
J. C. Hardy
26. TRIUMF
F. M. Brodeur
G. Hackman
27. UGC-DAE-CSR, Kolkata
Krishichayan (s)
28. United States Naval Academy
D. J. Hartley
29. University of Edinburgh
G. Lotay
P. J. Woods (a)
30. University of Houston
A. Gandini (b)
B. W. Mayes II
D. Parks
R-P. Sawh
J. Tang (s)
R. Weinstein (a)
31. University of Liverpool
A. J. Boston
A. O. Evans (s)
G. D. Jones
D. T. Joss
B. M. McGuirk (s)
L. Nelson (s)
E. S. Paul (a)
32. University of Manchester
R. S. Chakrawarthy
33. University of Manitoba
K. S. Sharma
34. University of Maryland
N. Hoteling
J. M. Shergur (s)
W. B. Walters
A. A. Hecht (s)
35. University of Massachusetts, Lowell
P. Chowdhury (a)
C. L. Parnell-Lampen
S. K. Tandel (b)
U. S. Tandel (s)
36. University of North Carolina, Chapel Hill
A. E. Champagne
37. University of Notre Dame
H. Amro (b)
P. Collon
S. J. Kurtz (s)
X. Wang (s)
S. Zhu (b)
38. University of Richmond
C. W. Beusang (a)
B. P. Crider
R. C. Raabe
39. University of Rochester
D. Cline (a)
A. Hayes (s)
40. University of Surrey
A. B. Garnsworthy (s)
Z. Liu
Z. F. Podolyak
P. H. Regan (b)
N. J. Thompson (s)
P. M. Walker (a)
S. J. Williams
41. University of Tennessee
C. Mazzocchi
42. University of York
M. A. Bentley (a)
R. Glover
D. G. Jenkins (a)
F. Johnston-Theasby (s)
P. Joshi
N. S. Pattabiraman (a)
R. Wadsworth
43. Vanderbilt University
D. J. Fong (s)
J. H. Hamilton (a)
J-K. Hwang
K. Li (s)
A. V. Ramayya (b)

44. Washington University

R. J. Charity (a)
C. J. Chiara
S. A. Komarov (s)
M. Montero Diez (s)
O. Pechenaya (s)
W. Reviol (a)
D. G. Sarantites (b)
L. G. Sobotka (b)

45. Western Michigan University

N. J. Goodman (s)
J. C. Lighthall (s)
S. T. Marley (s)
A. H. Wuosmaa (a)

46. Yale University

H-C. Ai (s)
C. M. Deibel
A. M. Heinz
J. Qian
E. Williams
R. R. Winkler
C. L. H. Wrede

47. Youngstown State University

J. J. Carroll
D. C. Gohlke
R. J. Propri

II. OPERATION AND DEVELOPMENT OF ATLAS

OVERVIEW

Highlights of the operation of the Argonne Tandem Linear Accelerator System (ATLAS), a DOE national user facility, and related accelerator physics R&D projects are described in this chapter. ATLAS is funded to provide heavy-ion beams for basic research in nuclear physics but also serves other areas of research and development, including material science. In addition, ATLAS has a rich program in developing the tools of accelerator mass spectroscopy (AMS) applied to wide ranging research programs such as oceanography, nuclear physics, astrophysics and geology. Over half of the beam time is allocated to experiments for which the spokesperson is an outside user. Recent ATLAS operating performance and related development projects are described in the next section. ATLAS personnel are also involved in developing technology in support of a future advanced facility, based on ATLAS technologies, for beams of short-lived nuclei.

ATLAS operated on a 5.3 day schedule through Fiscal Year 2005 and into Fiscal Year 2006 with some limited 7-day operation to accommodate runs approved for longer operation that would be disadvantaged by breaking into segments. Although not efficient use of the facility, this schedule has been brought about by budgetary constraints. For Fiscal Year 2005, ATLAS provided 30 beams of different isotopes to users. A total of 4686 hours of research beam time was provided for the research program, while the total scheduled operating hours for Fiscal Year 2005 was 5568 including startup time.

Since Fiscal Year 1995, ATLAS has made beams of short-lived rare isotopes (RIBs) available for nuclear physics research. A total of 15 different radioactive beams have been developed over those years and are generally available for use. Further development of RIBs is planned as required by the nuclear physics and nuclear astrophysics programs at ATLAS. In Fiscal Year 2005, beams of ^{12}N , ^{16}N , and ^{14}O were provided and constituted 9.7% of ATLAS running time.

Construction of a new cryostat and resonators for a major energy upgrade of the facility, which will increase the overall voltage of ATLAS by ~25%, nears completion. Initial cool down of the new cryostat occurred in December 2005. The final six resonators are now under construction. This project is made possible by AIP funds provided in Fiscal Years 2001 – 2005.

The proposal to create neutron-rich beams from fission fragments and accelerate those beams with the ATLAS accelerator, now known as CARIBU – Californium Rare Ion Beam Upgrade – was approved and the project began on January 1, 2006. The total project cost is estimated to be \$4.5 M and the first beam is planned for the second quarter of Fiscal Year 2009.




Table II-1. Summary of ATLAS experiments and user statistics.

	<u>FY2005*</u> (actual)	<u>FY2006</u> (extrap.)	<u>FY2007</u> (pred.)	<u>FY2008</u> (pred.)
<u>Beam Use for Research (hr)</u>				
Nuclear Physics	4570	4610	4580	4600
Accelerator R&D	92	70	70	150
Accelerator Mass Spectroscopy	0	150	150	100
Other	<u>24</u>	<u>50</u>	<u>100</u>	<u>50</u>
Total	4686	4880	4900	4900
Number of Experiments Receiving Beam	43	40	45	45
Number of Scientists Participating in Research	185	170	200	200
<u>Institutions Represented</u>				
Universities (USA)	25	25	26	26
DOE National Laboratories	4	5	5	5
Other	18	25	27	27
<u>Usage of Beam Time (%)</u>				
In-House Staff	50	45	35	35
Universities (USA)	22	35	35	35
Other DOE National Laboratories	6	5	15	15
Other Institutions	<u>22</u>	<u>15</u>	<u>15</u>	<u>15</u>
Total	100	100	100	100

A. OPERATION OF THE ACCELERATOR

a.1. Operations Summary (R. C. Pardo, D. Barnett, L. Carlquist, A. Deriy, G. Devane, R. Jenkins, A. Krupa, E. Lindert, S. McDonald, F. H. Munson, Jr., D. R. Phillips, M. Power, A. Ruthenberg, R. H. Scott, S. Sharamentov, P. Strickhorn, R. C. Vondrasek, and G. P. Zinkann)

ATLAS provided a total of 4686 hours of beam available to the research program in Fiscal Year 2005 and 5568 hours were scheduled for all operational activities during that period. The facility ran with a reliability factor of 95.2% for the fiscal year. A total of 30 different isotopes were provided during this period; the species distribution is shown in Fig. II-1. The focus of the research program continues to be on the lighter elements with $A \leq 58$ accounting for ~88% of all beam time. Nevertheless, the new beam in the ATLAS repertoire this year was ^{138}Ce .

The research program continues to push accelerator operations to higher beam currents. The programs

requiring the highest currents include RIB production, both the in-flight program (^{15}N @ 150 pA) and the ion-trap mass-measurement program; super-heavy element studies (^{50}Ti @ 200 pA); and a high K-Isomer search using ^{48}Ca @ 150 pA. These programmatic needs often push us to the limits of our previously set allowed maximum beam currents that have been reviewed and approved in a number of cases. A recent revision to the ATLAS SAD has improved our ability to provide the required currents, but additional changes in other areas, both administrative controls and hardware changes, are needed to allow the facility to meet the experimental program demands. Many of these changes will be pursued during the coming year.

The CARIBU project, a major new initiative for the facility, will provide a wide array of far-from-stability beams and is discussed in more detail in another section of this report. Although the project will draw on a large number of ATLAS operations personnel to implement

the project, we do expect normal ATLAS operations to continue, largely unaffected, until Fiscal Year 2008 when some time may be required for early tests. A larger amount of time will be required when commissioning activities begin in Fiscal Year 2009.

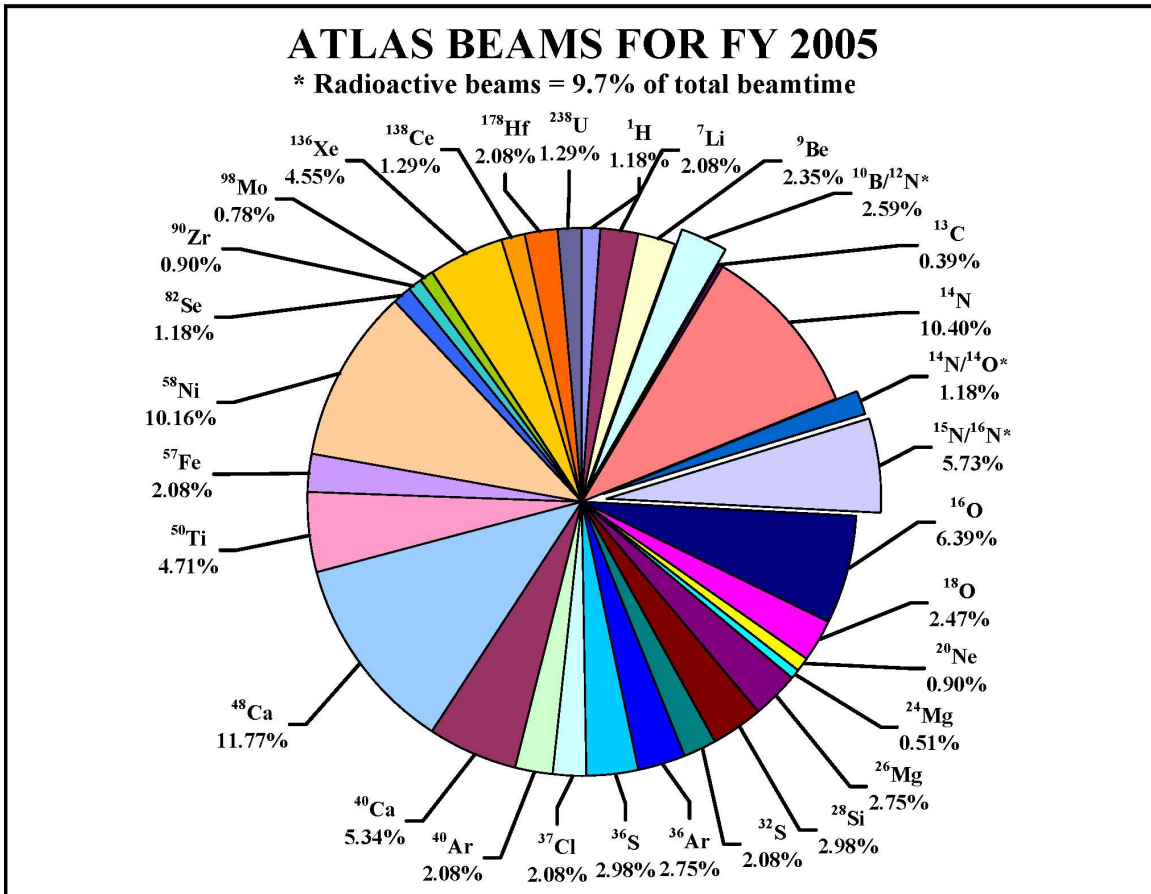


Fig. II-1. Distribution of beam time by isotope provided by ATLAS in Fiscal Year 2005. A total of 30 different isotopes were provided to the research program. Radioactive beams (indicated by an asterisk) comprised 9.7% (455 hours) of all beam time in Fiscal Year 2005.

B. DEVELOPMENTS RELATED TO ATLAS

b.1. Status of the ECR Ion Sources (R. C. Vondrasek and R. H. Scott)

b.1.1. Hexapole and Plasma Chamber Redesign Update

The cooling of the ECR2 permanent magnet hexapole was improved last year through a redesign of the chamber housing the magnets. The cooling water flow is now directed along the hexapole pole tips, where the majority of the heat from the plasma is deposited (Fig. II-2). After running in this new configuration for nine months, no degradation of the hexapole field has been detected.

The number of radial ports was increased from three ports for the old chamber to six for the new chamber. This has improved the pumping to the central region of the chamber thus lowering the base vacuum in the

region where the plasma is contained. At present, the source baseline vacuum without plasma is $<1.2 \times 10^{-8}$ Torr. This improved baseline vacuum appears to be responsible for an observed 20% improvement in beam current in the case of gases.

The increase in the number of radial ports also allows multiple solid material feeds to be mounted on the source simultaneously. For sputter samples, an air lock has been mounted on the source to allow for the rapid changing of samples without venting the source. This is especially useful for AMS runs where many samples need to be measured in a short period of time.

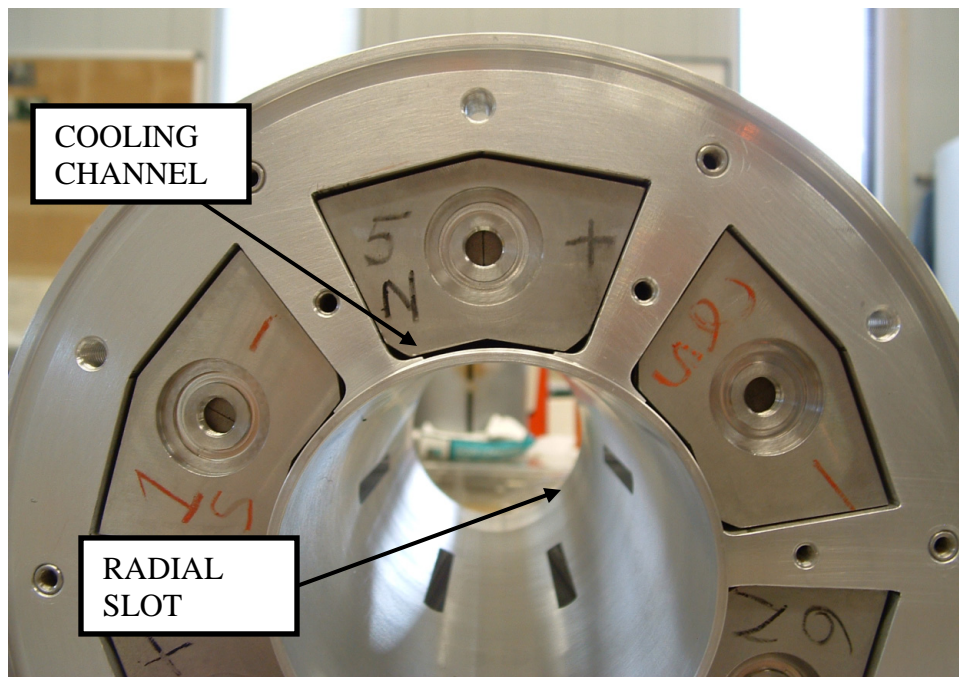


Fig. II-2. The ECR2 hexapole and chamber with the new canned hexapole bars loaded. The top position water channel is labeled and four of the six radial slots are visible.

b.1.2. Production of Ti-50 Using an Induction Oven

An induction oven was developed in the last year where the ultimate goal of the development work was the production of a high intensity Ti-50 beam. During off line tests the oven achieved a temperature of 1950°C.

However, several difficulties involving material interactions were encountered during the development activities.

The initial tests used a tungsten crucible to contain the titanium as well as act as the susceptor for the RF. At operating temperatures however (~1700°C) a reaction took place which enabled the titanium to “leak” through the tungsten crucible wall and eventually destroy the crucible (Fig. II-3). Conversations with members of the GSI ECR group confirmed that any contamination of the sample or crucible material with nickel (down to the 30 ppm level) would initiate a reaction between the

nickel and the tungsten crucible, leading to its destruction. A graphite crucible was then tested with natural titanium material. However, when the titanium melted it was fully absorbed into the graphite structure. To prevent the isotopic material from being absorbed into the crucible wall as well, the graphite crucible was first saturated with natural titanium. When the crucible could no longer absorb any more material, the enriched material was loaded.



Fig. II-3. The crucibles used for titanium production. The left crucible is graphite with natural titanium absorbed into the inner wall. The middle crucible is tungsten showing the effects of the reaction at high temperature due to the nickel contamination. The right crucible is the graphite crucible used for the Ti-50 run. The silvered appearance of the graphite is still not fully explained, but is probably due to the crucible’s extended exposure to very high temperatures.

The crucible also had to act as a susceptor for the induction RF which was provided from a commercial unit operating at a power of 800 W at 250 kHz. A nickel contaminant in the enriched sample, as well as titanium’s ability to attack refractory metals, ruled out using tantalum or tungsten as the crucible – both very good susceptors at elevated temperatures. While the graphite crucible was a good choice from a material interaction standpoint, it is not a good susceptor of RF at elevated temperatures. So a compromise configura-

tion was reached which incorporated an inner graphite crucible and an outer tantalum tube. This allowed the titanium to be contained within the graphite while the outer tantalum tube acted as the susceptor which then radiatively heated the graphite. This arrangement allowed us to reach the necessary operating temperature while protecting against destructive material interactions. Intensities of 200 pA on target were achieved with a run time of eight days.

b.1.3. Three-Frequency Heating on ECR1

Both ECR sources utilize two-frequency heating in order to better heat the plasma and produce higher charge states and higher beam intensities. The general behavior for a gas is a factor of 2-4 increase in the beam intensity when the second frequency is added and optimized. We wished to see if this effect could be

extended further through the addition of a third frequency.

A 14 GHz klystron was added to the ECR1 source configuration enabling the plasma to be simultaneously excited with three discrete frequencies. In studies with

three-frequency heating when compared to two-frequency heating, the beam intensity for O^{7+} increased from 70.4 to 84.2 μA , Kr^{23+} (mass 86, 99.9% enriched) increased from 3.5 to 7.2 μA , and Xe^{28+} (mass 136, 60% enriched) increased from 7.9 to 12.2 μA . This demonstrated that the multiple frequency effect could be extended to further improve source performance.

An additional test was performed where an RF power combiner was added to a TWTA which operates in the 10.5-13.0 GHz range at 500 W. The power combiner

allowed the TWTA to be driven simultaneously with two discrete frequencies. With the TWTA operating at 10.85 and 12.66 GHz, the intensities of O^{6+} increased 80% and O^{7+} doubled compared to single frequency operation, further demonstrating the multiple frequency heating effect except in this instance with a single transmitter. More importantly, the ability of the TWTA to provide beams at multiple frequency heating intensities while still using a single transmitter allows for greater operational flexibility.

b.2. New RF Amplifiers for ATLAS Superconducting Resonators (S. I. Sharamentov)

New RF amplifiers for ATLAS 48 MHz quarter-wave and 97 MHz split-ring superconducting resonators were designed. The goal was to replace existing RF amplifiers with more powerful and reliable model, allowing for decreasing the accelerator shut down time due to amplifier replacement and to minimize repair cost and time during routine operation.

The 97 MHz amplifier block diagram is shown in Fig. II-4. It has a newly designed 10 W preamplifier and a 300 W 72-109 MHz main RF module, mounted on a water cooled heatsink. A metering and protection board provides measurement and indication of the output RF power and forward/reflected waves, as well

as measurement of the RF amplifier module supply current. Circuits also protect the RF module against temperature overload, supply current overload, water flow trip and VSWR trip. All the trips can be reset by the reset button on the amplifier front panel.

The 48 MHz RF amplifier has a block diagram identical to the one shown in Fig. II-4. The difference is that the main 300 W 48 MHz RF module was slightly modified to accommodate the lower frequency. Eight 97 MHz and three 48 MHz amplifier were built in 2005. Six 97 MHz amplifiers were mounted in the first booster RF rack replacing the old amplifiers.

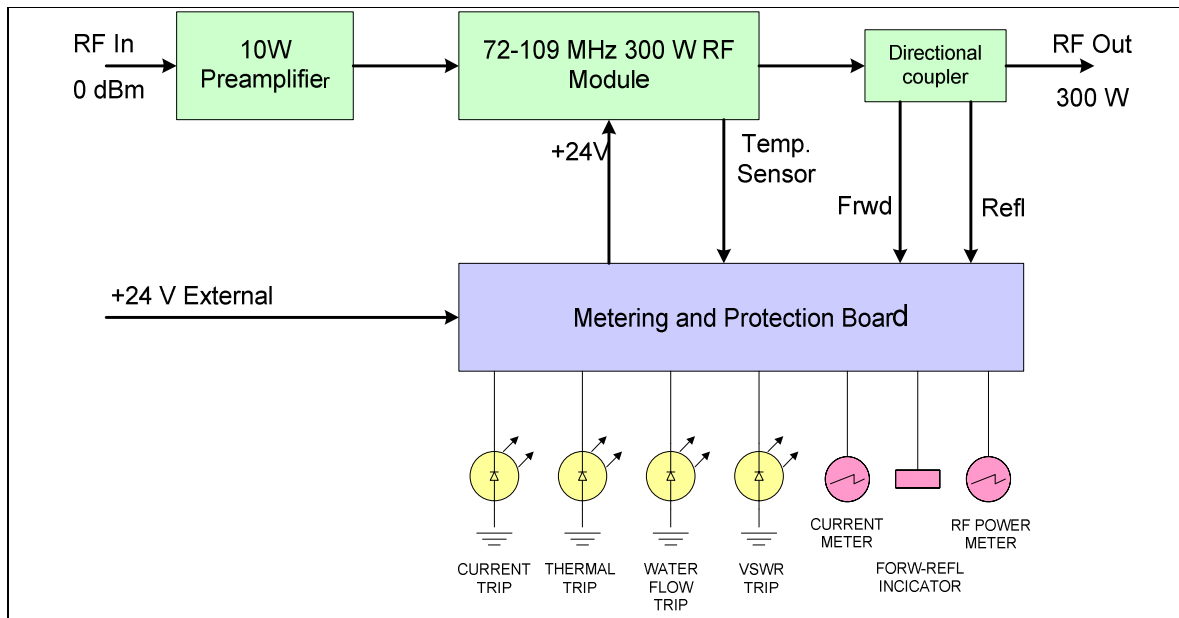


Fig. II-4. RF amplifier block diagram.

Figure II-5 shows rack front panel view with new amplifiers installed. Due to smaller size of the new amplifier it was possible to permanently install a TDS2022 digital oscilloscope in the rack for easier maintenance and troubleshooting of the RF equipment.

The plan is to replace all old amplifiers over the next two years. At least two more RF racks will be modified in 2006.



Fig. II-5. A view of the first modified booster rack.

b.3. ATLAS Control System (F. H. Munson, M. Power, and R. Carrier)

In the past, the primary operator interface to the ATLAS control system was a number of workstations running a variety of operating systems which supported the X Windows windowing system or an X Windows emulator. Since these systems were aging, all of these systems have either been replaced, or have been modified to extend their usefulness. The modification has been accomplished by utilizing a scheme that retrofits many of the existing systems, enabling them to run the Linux operating system that boots from CF (Compact Flash) memory. The result is an economical “diskless” system where the operating system and the X Windows process runs completely in RAM (Random Access Memory). The expected advantages of this

approach includes extending the lifetime and reliability of existing systems, reducing the number of proprietary operating system licenses (including OpenVMS and MS Windows), and providing some immediate and future cost savings.

ATLAS currently makes use of an in-house database management system called Hercules that provides an operator’s logbook, an equipment maintenance log, and a drawing index. Certain software components of this Novell DOS-based database management system did not support newer hardware components and peripherals, such as network interface cards and printers. Even though there are plans to create a

replacement for this DOS-based system, the entire Hercules system has been moved to a MS Windows platform to provide a short-term solution. The resulting benefits of this effort include the elimination of the Novell DOS operating system and the isolated Novell networking system previously used by Hercules. The system now utilizes the homogeneous ATLAS control system LAN, which enables the use of mainstream network interfaces, common network printers, and network file transfers used for database backups.

As mentioned previously the Hercules database management system is slated to be replaced in the future. Taking steps to achieve this goal, work is nearly completed and testing has begun on a WEB-based interface to a newly created database management system that will replace the "drawing index" portion of the older Hercules system. Unlike the Hercules system this new database will not be isolated, and controlled access will be made available to a much larger community outside of the confines of the ATLAS control system LAN. In addition, a feature not available in the older system will provide the user with the ability to view documents online in electronic format.

Device scaling features are used to assist the operator in reducing beam tuning time when restoring the accelerator to a previous tune configuration or changing accelerator energies. Up until now, during an accelerator energy change, only beam line devices such as quadrupoles, steering devices, and magnets were scaled to match the new energy. New prototype software has been written to apply similar scale factors to the accelerator's appropriate superconducting solenoids. This software is still in the testing stage, and is currently only functional for decreasing accelerator energies.

It would be desirable to use the current settings or the archived settings for one of ATLAS' ECR ion sources to set up a second ECR ion source to reproduce a given ion species and energy. However, the differences between the ECR 1 ion source and the ECR 2 ion source high voltage platform control and monitoring systems make it impractical for one to set the ion source

platform voltages to the same value, and expect the ion exit energy to be the same for each ion source. Part of the solution relies on being able to monitor the high voltage platform voltages of each ion source with high precision voltmeters. A prototype software utility and procedure have been developed to monitor the high precision voltmeters using a GPIB (General Purpose Interface Bus) connection, and to assist the operator in dealing with this problem. This procedure and accompanying software are still in the testing stages.

Power supply calibration is required for both existing power supplies whose calibration has changed over time and newly installed power supplies. This calibration is necessary to ensure that the remote control and monitoring of each power supply accurately represents the power supply's local front panel controls and metering. A prototype utility has been created to provide the user with the capability to calibrate a power supply's "control signal", "monitor signal", or both. This utility is implemented as a graphical display accessed through the main control system display options.

A new generation of software routines (implemented as "memory resident shareable images") have been added to communicate with those devices using the serial line (or RS-232) interface. This code, in the form of "device handlers", eliminates the need for stand-alone processes previously used for this type of application, and has significantly increased the rate at which these devices are read resulting in an increase in the rate that their values are displayed at the operators' consoles.

Finally, while remote login to the ATLAS control system has been available for some time using a VPN (Virtual Private Network) system, most recently the ability to have complete remote control and remote monitoring capability of the accelerator has been made available. This feature allows system experts for various subsystems of the accelerator to log on from locations outside of the laboratory, monitor the facility operation, and correct problems that arise. This has proven to be especially useful for monitoring and tuning ion sources at ATLAS.

b.4. ATLAS Cryogenic System (S. W. MacDonald, R. C. Jenkins, L. K. Carlquist, R. R. Mongado, and H. A. Nolan)

b.4.1. Gas Cell Solenoid Helium Recovery Project

A liquid helium cooled superconducting solenoid used for focusing radioactive beams produced in a gas cell was installed in 1998. This solenoid was originally intended to operate as a batch fill system separate from the ATLAS cryogenic system, with all helium boil off gas being vented to the atmosphere. The annual helium loss from this solenoid has come close to matching the normal annual loss of helium from the entire ATLAS cryogenic system. Recovering this helium then

presented an opportunity to provide a direct savings to operations. As a result, a helium recovery system was designed and installed to enable the recovery of boil off gas and is shown in Fig. II-6. Design considerations included; varying flow rates through the high current leads during normal operation and fill conditions, protection of the solenoid from loss of lead flow, and the effects of solenoid operation on the ATLAS cryogenic system.

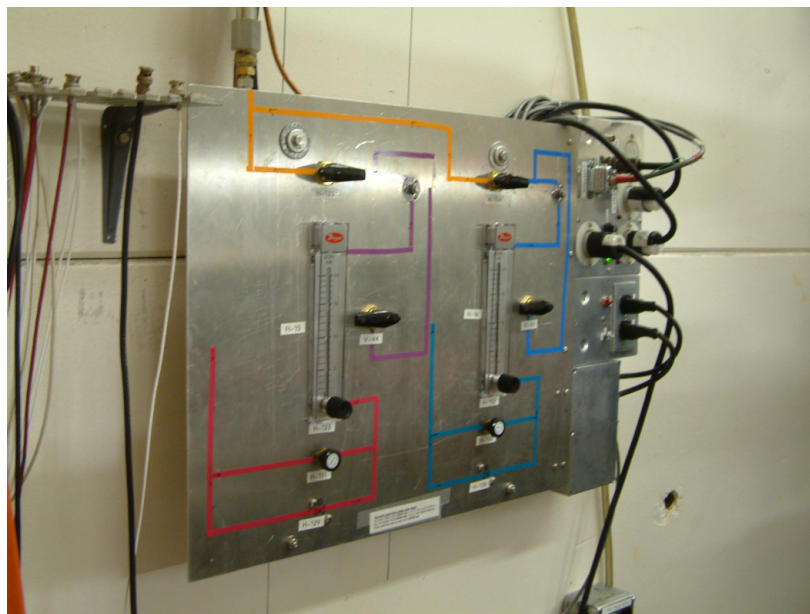


Fig. II-6. A manifold designed for controlling helium recovery from the gas cell solenoid high current leads.

b.4.2. Cryogenic Alarm System Project

A new cryogenic alarm system was developed using LabView and National Instruments, Inc. hardware. This system will eventually replace the existing PLC-based alarm system as well as provide for enough expandability to automate some critical cryogenic processes. The new alarm system is currently running

in parallel with the PLC system for reliability testing. The display interface is shown in Fig. II-7. In order to do this, a non-intrusive optical interface board was developed to enable monitoring the status of the existing signals without affecting the current PLC alarm system.



Fig. II-7. The new cryogenic alarm system control screen.

b.5. A 50-kV RF Chopper for In-Flight RIB Beams (J. Bogaty, R.C. Pardo, and S. I. Sharamentov)

The in-flight radioactive ion beam program at ATLAS uses charge-exchange or 1-2 nucleon transfer reactions to produce the ions of interest and then captures the recoiling ions using a superconducting solenoid, standard beam transport magnets and a superconducting resonator. The ions produced this way often have similar, but lower rigidity than the primary production beam. Therefore, primary beam ions in the straggling tail of the distribution may have the same magnetic rigidity as the RIB beam of interest and will be delivered to the experimental target along with the beam of interest. But these primary beam tails have significantly different velocity and so can be separated with an RF chopper or Wien velocity filter. For our situation, the RF chopper appears to be the best matched technology to eliminate these beam tails. Some example cases are shown below in Table II-2.

A high field-strength beam chopper has been built and tested for use in front of the spectrograph. Concerns

over radio frequency interference (RFI) problems were addressed by testing the chopper next to spectrograph electronics racks. While this is not equivalent to a beam line installation it was a severe test. Deflection voltages up to 50 kV were achieved with no evidence of RF contamination on spectrograph electronic signals. Less than 900 watts of RF drive was required to achieve 50 kV deflection potential. This is in excess of the 35 kV design requirement for the chopper. The chopper plates assembly and the cooper housing enclosing the plates are shown in Fig. II-8.

The chopper RF structure is equipped with tuning and RF matching mechanisms which will be driven by digital stepper motors. A vacuum vessel has been designed and formal drawings completed. Pending review, construction should proceed on the vessel and electronic control systems. Installation of the chopper in the spectrograph beamline is planned to occur in Fiscal Year 2007.

Table II-2. Example cases of interest for in-flight RIB program.

RIB Ion of Interest		Primary Beam Ion***		Δt (ns)*	Chopper Voltage (KV)**
ID	Energy(MeV)	ID	Energy(MeV)		
$^{16}\text{N}^{7+}$	60	$^{15}\text{N}^{7+}$	64	16	23
$^{17}\text{F}^{9+}$	63	$^{16}\text{O}^{8+}$	53	15	18
		$^{16}\text{O}^{7+}$	40	55	10
$^{21}\text{Na}^{11+}$	113	$^{20}\text{Ne}^{10+}$	98	10	36
		$^{20}\text{Ne}^{9+}$	79	36	13
$^{12}\text{N}^{7+}$	210	$^{12}\text{C}^{6+}$	154	20	51
		$^{12}\text{C}^{5+}$	107	48	31

* Drift distance assumed is 7 meters.

** 1 meter long plates, 10 cm gap.

*** The energy shown for the primary beam is that energy which provides the same magnetic rigidity as the RIB energy of interest.

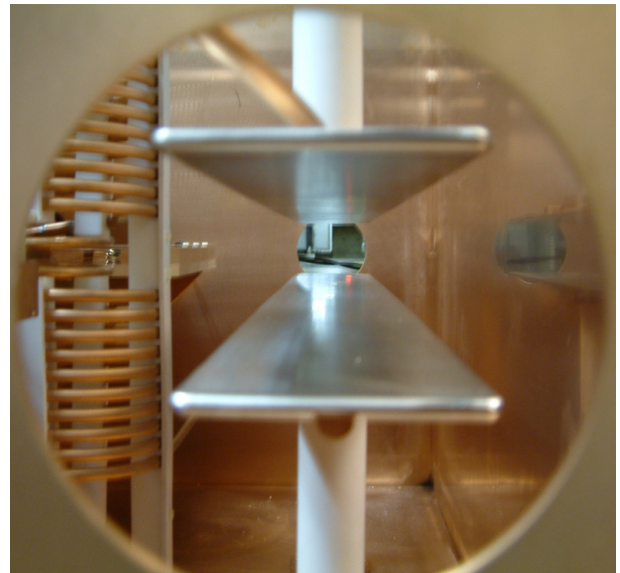
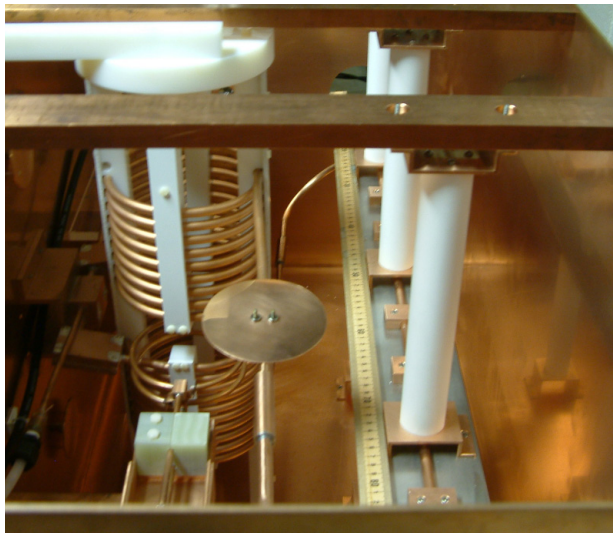


Fig. II-8. Views of RF chopper plates and resonant tank circuit for RIB in-flight chopper.

III. ACCELERATOR PHYSICS AND EXOTIC BEAM TECHNOLOGY

OVERVIEW

This chapter presents the results of R&D being carried out by the group at Argonne that was working on concepts for the U.S. Rare Isotope Accelerator Project (RIA). That work has now been generalized to projects related to advanced exotic beam facilities world-wide, and has also been extended to include work related to other accelerator projects such as the 8-GeV proton driver project at Fermi Lab and the International Linear Collider (ILC) Project.

The topics covered in this chapter are arranged in three main sub-sections: (A) Superconducting RF, (B) Beam Dynamics and Injectors, and (C) Rare Isotope Production and Separation.

Highlights of developments during 2005 include:

- Significant progress on the construction of a prototype RIA-type drift-tube cryomodule that will be used for an ATLAS Energy Upgrade Accelerator Improvement Project.
- Successful operation of a prototype triple-spoke $\beta = 0.63$ superconducting drift-tube resonator.
- Completion of a new clean room and surface processing facility in building 208 which was carried out as a joint FNAL/ANL project.
- Continued work on several aspects of the FNAL proton driver project including extensive studies of the beam dynamics of the full 8-GeV linac.
- Continued development of the beam dynamics for a high-power heavy-ion driver linac based on a 345-MHz triple-spoke resonator including studies to quantify the effects of misalignment and RF setting errors, and the development of algorithms for optimization and tuning of multiple-charge-state beams.

- Continuation of a failure modes and effects analysis (FMEA) to the RIA driver linac design.
- Update of the design of the low q/m injector for an exotic beam post accelerator.
- Significant progress towards to the construction of a full power prototype module of a cw RFQ for the high-power driver linac.
- Construction of a prototype system to demonstrate a thin film liquid lithium stripper for use with high intensity uranium beams in the driver linac.
- Characterization of a full-scale prototype fast gas catcher for high-energy heavy-ions at the GSI Fragment Separator.



A. SUPERCONDUCTING RF

a.1. Spoke Cavity Development for RIA (Z. Conway, J. Fuerst, M. Kedzie, M. Kelly, and K. W. Shepard)

A prototype 345 MHz, $\beta = 0.63$, triple-spoke-loaded superconducting niobium cavity, shown in Fig. III-1, has been completed and the results of cold tests are shown in Fig. III-2. Initially, (triangles in Fig. III-2) performance was limited by the presence of interstitial hydrogen in the niobium cavity. The hydrogen was removed by baking the cavity in a vacuum oven at 600 C for 24 hours. Subsequent testing yielded the performance shown by circles in Fig. III-2. In

operation at 1.9 K, the cavity could be operated cw at gradients above 10 MV/m with less than 9 watts of input RF power. At these gradients the 81 cm long cavity can provide more than 8 MV of accelerating potential for protons and ions at a velocity of 60% c. The cavity has been developed for the RIA driver linac, but could be used for cw or pulsed operation of a wide class of proton and/or ion linacs.



Fig. III-1. Niobium elements of the $\beta 0.63$, 345 MHz, triple-spoke cavity after electropolishing, just prior to the final, closure EB welds.

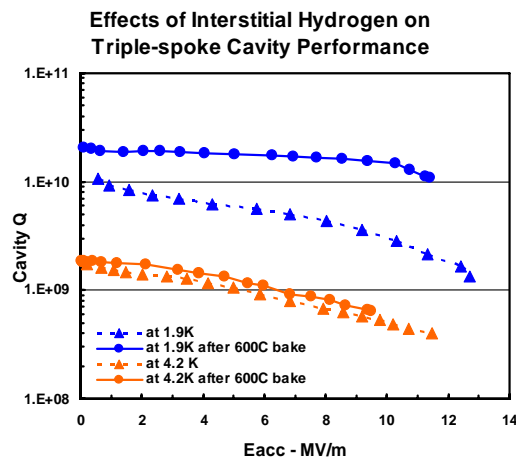


Fig. III-2. Cavity Q vs. accelerating field level before (triangles) and after (circles) baking the cavity at 600 C to remove interstitial hydrogen.

a.2. Joint ANL/FNAL Superconducting Cavity Surface Processing Facility (SCSPF)
(M. Kelly, M. Kedzie, and K. Shepard)

Major infrastructure on the joint ANL/FNAL SCSPF was completed in 2005. The facility includes a pair of separate large chemical processing rooms, one administered by each laboratory, a large clean anteroom, a pair of class 100 clean areas and a new

deionized water system. Hardware, under construction inside of the ANL portion of the chemistry facility, is shown in Fig. III-3. The shared anteroom is shown in Fig. III-4.



Fig. III-3. The ANL chemistry room portion of the joint ANL/FNAL SCSPF designed for electropolishing and buffered chemical polishing operations.



Fig. III-4. The common clean anteroom of the joint ANL/FNAL SCSPF. An additional pair of class-100 clean areas (not shown) lie through the doors to the left of the figure.

Facilities will be used to support of cavity upgrades for the ATLAS linacs and R&D for the International Linear Collider, a next-generation light source and proposed hadron linacs required for exotic beam and high-

intensity proton driver projects. Initial chemistry operations in the ANL chemistry room will begin in the summer of 2006.

a.3. Cavities and Prototype Cryomodule for RIA and the ATLAS Upgrade (Z. Conway, J. Fuerst, M. Kedzie, M. Kelly, S. MacDonald, and K. W. Shepard)

Construction of remaining quarter-wave cavities for the eight cavity ATLAS upgrade cryomodule continues. Fabrication of all six cavities proceeds in parallel to yield economies of scale. Figure III-5 (left) shows center conductors fixtured in preparation for electron beam welding the die-formed halves. Multiple setups reduce costs and are used as much as possible throughout production.



Cavities for the ATLAS upgrade and RIA are designed with integral stainless steel helium vessels surrounding the niobium cavity. A niobium to stainless steel braze transition based on an earlier CERN design has been successfully prototyped and mass produced for the upgrade. Figure III-5 (right) shows coupling port transitions (brazed in a single heat). This technique was developed in the ANL central shop.



Fig. III-5. Group of three center conductors set up in the electron beam welding chamber for seam welding halves together (left). Mass production of niobium to stainless steel braze transitions (right).

Both RIA and the ATLAS upgrade rely on clean handling and assembly techniques to achieve maximum cavity performance. A class 100 clean area has been established and assembly mock-ups have been performed using our prototype quarter-wave and half-wave cavities (Fig. III-6 right, center). Only those components integral to the clean assembly are involved in the clean room sequence, thereby minimizing the risk of particulate contamination.

Engineering tests have begun on the cryomodule without cavities installed. Preliminary cool down of the thermal shield has taken place and tests will continue into next year to verify subsystem performance.

Figure III-6 (left) shows the cryomodule being assembled for test. Future plans include complete cool down of the empty cryomodule with both helium and nitrogen, followed by cool down and operation of the module with prototype quarter-wave and half-wave cavities installed.

Plans for next year are to pursue completion of all six quarter-wave cavities, including helium vessels. The cryomodule will complete engineering tests and undergo disassembly in preparation for cavity installation. Final design work on subsystems already prototyped (including input couplers, slow tuners, and VCX fast tuners) will continue.

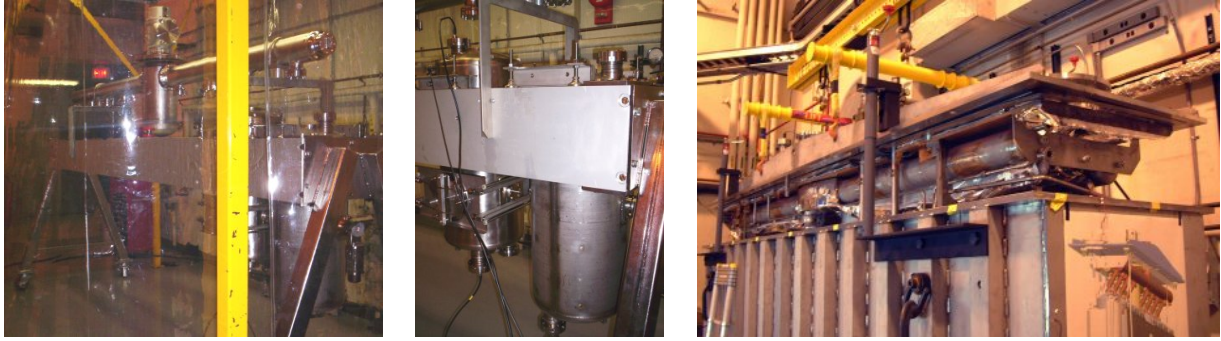


Fig. III-6. Assembly mock-up of prototype quarter-wave and half-wave cavities as seen through cleanroom curtain (right). Close-up of clean assembly during VCX fast tuner checkout (center). ATLAS upgrade cryomodule being assembled (without cavities) for engineering tests (left).

B. BEAM DYNAMICS AND INJECTORS

b.1. Injector System for High-Intensity Heavy-Ion Driver (P. N. Ostroumov, V. N. Aseev, T. V. Kulevoy,* R. Scott, M. Sengupta, and N. E. Vinogradov†)

The design goal of a 400 kW uranium beam in a Heavy-Ion Driver Linac (HIDL) for future exotic beam facilities can be achieved employing a concept of simultaneous acceleration of several charge states. We are developing a prototype of the injector system for the HIDL which includes a permanent magnet (PM) ECR ion source, a LEBT and one-segment of the prototype RFQ. Previously we re-commissioned a PM ECR source located at the ground potential. Detailed emittance measurements of various ion species produced by the PM ECR have been carried out prior to moving the source onto the HV platform. Careful analysis of the measured data was performed to verify that the ECR source forms a beam with similar phase space distributions of the neighboring charge states which is essentially important in the concept of simultaneous acceleration of two charge states developed for the RIA. Numerical studies of beam dynamics in the 2Q-LEBT have been performed using the multi-particle code TRACK developed especially for the RIA design purpose. The code TRACK

simulates a multiple-charge-state beam dynamics through preliminary calculated 3D-fields starting from the plasma surface and taking into account space-charge effects. The realistic geometry of the present 2Q-LEBT beam-line has been set up in the TRACK model. The stray magnetic field of the PM, the electrostatic fields in the initial part of the beam-line that consists of puller, Einzel lens and grounded electrodes have been calculated using the EMS code. 3D representation of the magnetic field including fringing fields was implemented using a genuine configuration of the 90° bending magnet. The phase space distribution parameters of the input beam were optimized to fit the measured output beam emittance. Figure III-7 illustrates the comparison between measured and calculated data for the case of Xenon beam. Typical simulations have been performed for 3×10^5 particles. The developed model provides a reasonable coincidence with experimental results and can be used for further design of the injector systems.

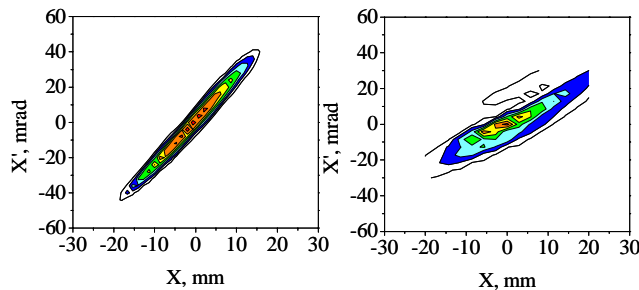


Fig. III-7. Calculated (left) and measured (right) emittance of $22 \text{ e}\mu\text{A } ^{128}\text{Xe}^{13+}$ beam.

Unlike in all other ECR ion sources being operated worldwide where the HV platform voltage is applied after analyzing of a specified q/m , in the proposed HIDL injector all ion species from the ECR source are accelerated by the platform voltage and the analyzing and selecting of appropriate ion charge states take place in the following achromatic bending system. We have developed and constructed HV platform using decommissioned 300 kV, 100 kW isolation transformer and Faraday cage available from previous accelerator projects. The PM ECR has been moved onto the HV platform. Significant effort has been undertaken for the commissioning of the PM ECR on HV platform. At present the injector system allows us to accelerate all

ion species up to the 100 keV total kinetic energy followed by charge analysis by the 90° magnet and emittance measurements. For the remote control of the PM ECR and other equipment located outside the HV platform, we have developed a control system based on Windows PC, LabView and NI control modules. The remote control of the PC located on the HV platform is provided by Ethernet fiber optics connection. Initial acceleration and ion beam analyzing by the existing 90° magnet have demonstrated increased intensities of 100 keV heavy ion species compared to the operation of the ECR at the ground potential. Currently the ECR source is being upgraded with an additional TWT rf amplifier operating at 14 GHz and an oven for

production of heavy metal ions. The design and construction of the achromatic bending system is in

progress. Figure III-8 shows general view on the injector system.

*Institute for Theoretical and Experimental Physics, Moscow, Russia, †Northern Illinois University.

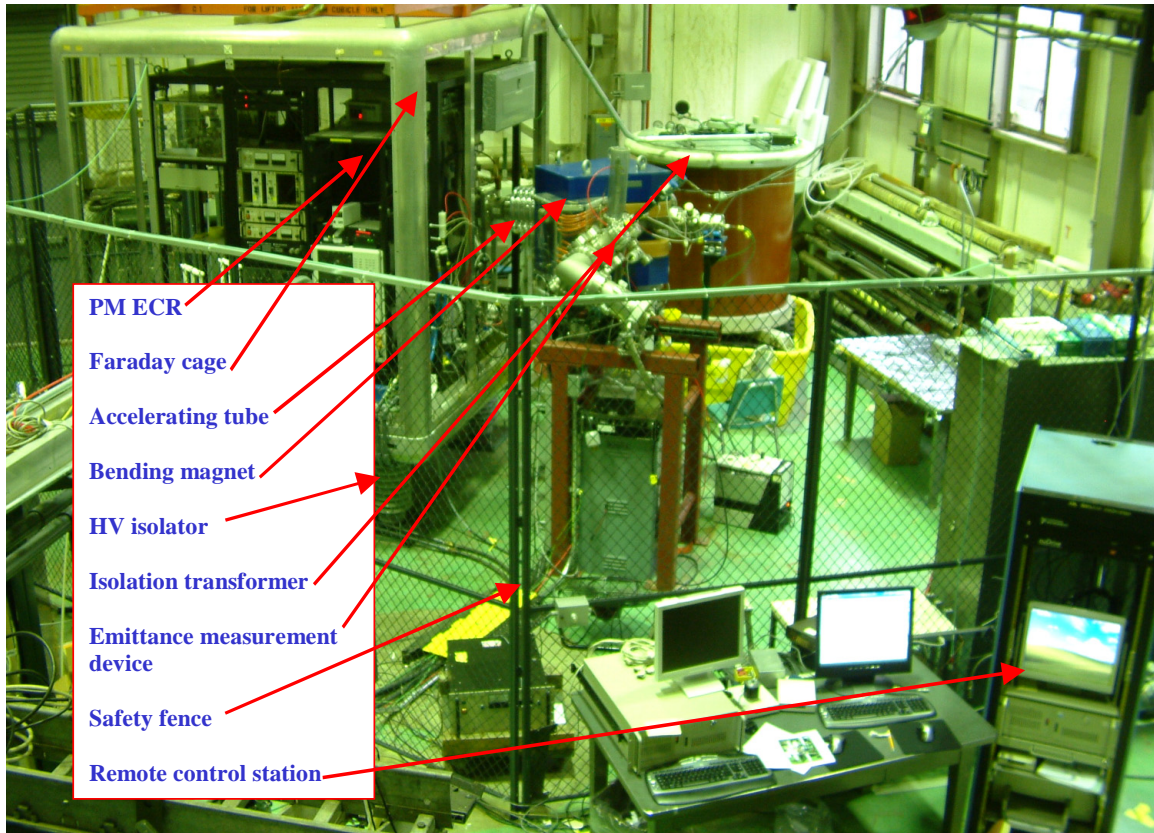


Fig. III-8. General view of the injector system.

b.2. Design, Construction and Test of a One-Segment Prototype of the RIA Driver RFQ (P. N. Ostroumov, A. Barcikowski, M. Bracken, B. Rusthoven, S. Sharma, W. F. Toter, and D. L. Schrage*)

High power heavy-ion drivers require a cw low-frequency RFQ for initial acceleration. We have already reported the design of the 57 MHz RFQ resonant structure which has moderate transverse dimensions and high quality accelerating-focusing fields required for simultaneous acceleration of multiple charge state ion beams in the RIA driver. We have decided to proceed with the technique of high-temperature furnace brazed OFE copper cavity which has proven to be very reliable for the production of high-quality cw accelerating structures.

The fabrication of the one-segment RFQ prototype cavity was successfully completed in 2005. The final pre-brazed machining and assembly was performed by Walco Tool & Engineering Corporation located near ANL. Walco provided good accuracy in the machining. CMM measurements confirmed that the pre-brazed assembly of the RFQ segment had $\sim 0.004''$ accuracy of the overall machining. Figure III-9 shows the pre-brazed assembled RFQ resonator body.

*TechSource, Santa Fe, NM.

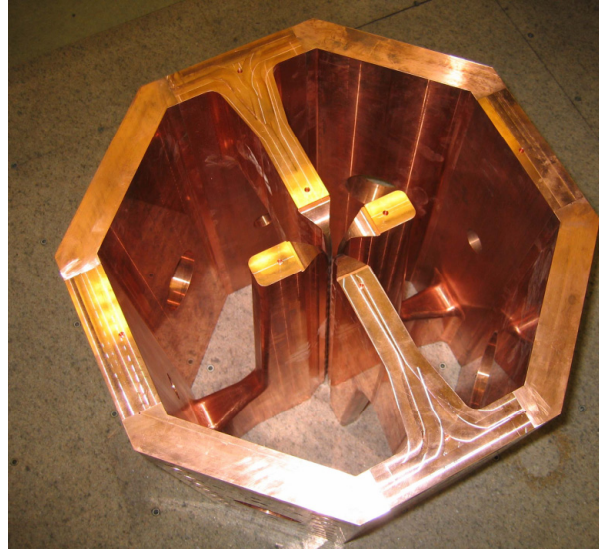


Fig. III-9. Top view of the pre-brazed assembly of the RFQ cavity.

Prior to shipping to the brazing vendor, California Brazing (Newark, CA), the cavity was disassembled, washed in Citronex bath, rinsed by distilled water, dried and packed in clean bags. ANL experts traveled to California Brazing to provide assembly of the cavity and final vacuum tests. The cavity is 29 inches in diameter at the flanges and is 25 inches in length. The total weight is 1300 #. As far as we know there are no resonators of this size that have been built using high-temperature furnace brazing. California Brazing's hydrogen furnaces are adequate for a furnace load of this size and weight. We were concerned that there was a nitrogen rather than a vacuum purge but the braze was successful. California Brazing was pre-qualified based on the experience of LANL and LBL. The RFQ cavity was tested for vacuum leaks and at a background level of $\sim 5 \times 10^{-10}$ Torr-liters/second, there were no detectable leaks. The cavity was thus determined to be leak tight. The cavity was shipped back to Walco on December 2nd, 2005 for the machining of the end flanges and other finishing mechanical work. Final CMM measurements after brazing show that the errors in the pin-to-pin distances V1-V5, V4-V5, etc. (see Fig. III-10) average less than 0.002" which is well within the tolerance.

The RF measurements show that the cavity's unloaded quality factor is 8860 which is 95% of the value obtained from numerical simulations by the codes MWS and HFSS assuming that the copper conductivity is $5.8 \cdot 10^7$ (Ohm·m)⁻¹. The cavity design was carried out using an earlier version of MWS with the 57.0 MHz target frequency. We have measured that the frequency of the resonator is 55.5 MHz without tuners inserted. The latest version of the MWS calculates 56.17 MHz while HFSS simulation shows 55.6 MHz. Currently, these calculations are being verified.

Final preparations of the RFQ cavity for the high power tests are being carried out. The water cooling system is being installed. A general view of the RFQ is shown in Fig. III-11. The coupling loop designed for 100 kW power is being fabricated and brazed in vacuum furnace. The ProEngineer rendering of the coupling loop is shown in Fig. III-12. The 20 kW 57.5 MHz amplifier was built by "Amplifier Systems", CA and delivered to ANL. The design field level in the RFQ resonator can be achieved at ~ 14 kW of cw power. The 20 kW amplifier will allow us to operate the resonator at slightly higher fields and approach the limiting surface fields. The amplifier has been installed and tested at 20 kW RF power dissipation on the dummy load.

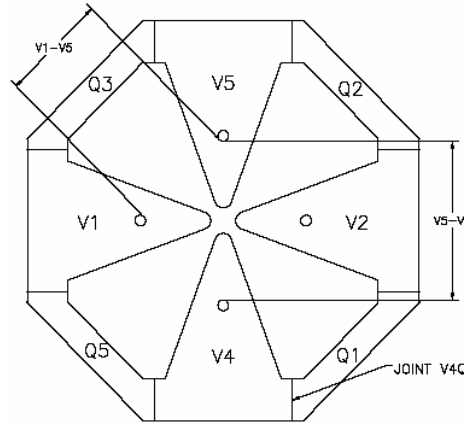


Fig. III-10. Top view of the resonator.

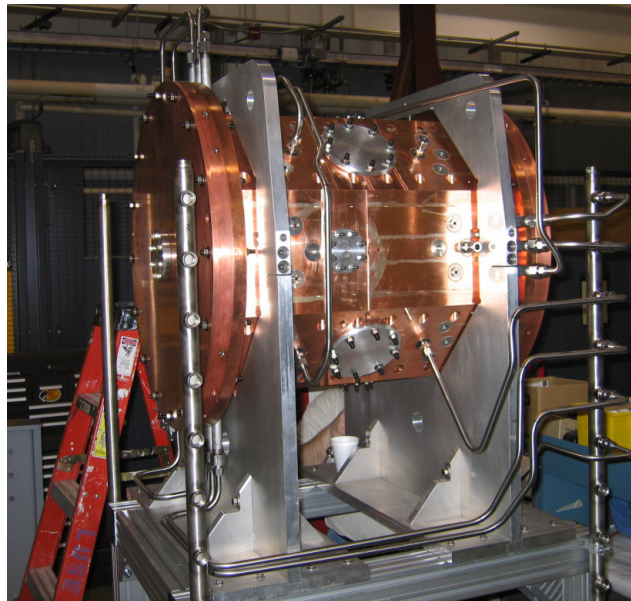


Fig. III-11. General view of the RFQ.

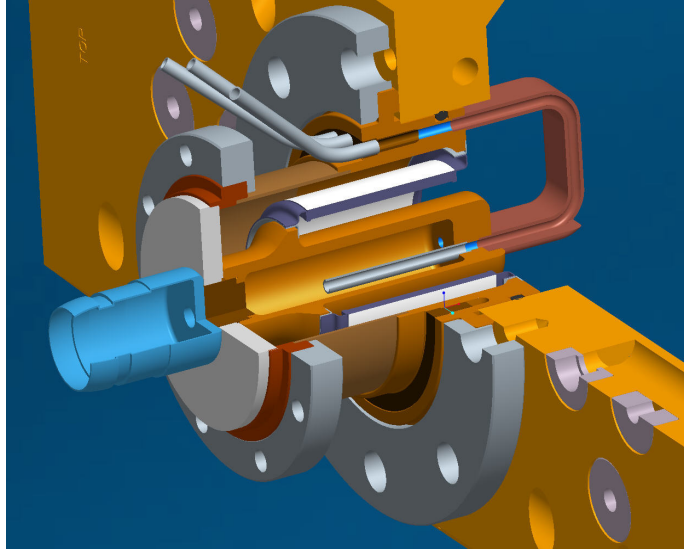


Fig. III-12. The cutaway view of the engineering model of the water-cooled coupling loop.

b.3. Study of Voltage Breakdown Limits in the 12 MHz RFQ (P. N. Ostroumov and M. Sengupta)

The purpose of the recent high power tests performed on the 12 MHz split-coaxial RFQ¹ was to determine the breakdown voltage in the cavity in both the cw and pulsed regimes and deduce the peak surface fields E_p . The value of E_p is a very important parameter for the design of new RFQs, particularly for the design of 12 MHz RFQ for acceleration of singly-charged Uranium for low charge-to-mass ratio radioactive beam injector to ATLAS.

Early high power tests performed in the absence of beam, report that the RFQ could be operated cw well above the design inter-vane voltage of 100 kV. At cw operation a vane voltage of 108 kV was obtained.¹ The vane tips of this structure however, are not directly water cooled and tend to get overheated under continuous operation. This factor may have contributed to the detuning and reduction of quality factor of the RFQ over a period of time. Following the last RFQ maintenance performed in May 2000, the RFQ was not operated until the year 2004. At that time it was observed that the RFQ cavity surface was unclean and had accumulated dirt and oil residue. A considerable amount of time and effort was expended to clean it up before trying to restore vacuum and resume experiments.

Several methods have been applied for the voltage calibration of the vanes of the 12 MHz RFQ. Early

calibrations have been performed by direct measurement of the vane potential at given rf power. We have introduced two additional methods such as a power loss measurements and the x-ray end point method. The latter provides a non-invasive and precise technique for measuring inter electrode voltage. In our experiments we have used a liquid nitrogen cooled Ge(Li) detector with a built-in pre-amplifier. The detector is biased to 1 kV, the preamplifier output is fed into an amplifier and then to the MCA. We used the gamma ray peaks of Am^{241} at 59.536, 26.345 and 20.18 keV to calibrate the Ge(Li) detector. For pulsed mode operation, in addition to gating the MCA around the pulses from the detector, one could also gate the MCA around the RF pulse, i.e. the MCA will be in the counting mode only in the presence of the RF pulse.

The RFQ was operated both in the pulsed and cw mode, at different values of RF power. X-ray spectra has been obtained corresponding to each value of the RF power. A typical x-ray spectrum is shown in Fig. III-13. From measurements we have found $\pm 1\%$ agreement between three methods of the voltage calibration. Experiments carried out to determine the maximum inter vane voltage show that the limiting value is 95 kV whereas earlier results report a higher value.

To measure the amount of misalignment, the Survey and Alignment Group from the APS Division performed a set of measurements on the 12 MHz RFQ. The transverse position of the vane tips were measured with respect to a known reference line. The rms deviation of the transverse (X,Y) positions of the vane tips in the upstream and downstream locations were measured to be equal 0.26 mm and 0.15 mm respectively. The accuracy of the above set of measurements is 0.08 mm. The measurements shown noticeable displacement of the vane tips. The effect of the misalignment on the peak surface fields has been approximated using Electro Magnetic Studio (EMS) simulation code. The EMS program extracts the peak surface field on each misaligned electrode. The extracted peak fields for the misaligned vanes are shown in the plots in Fig. III-14. The peak surface fields for the two cases at 100 kV inter-vane voltage are 12.8 MV/m and 15.8 MV/m respectively.

Based on our measurements and early experiments on 12 MHz RFQ, we can recommend peak surface field 14.5 MV/m and tolerances to the vane misalignments less than 2% of the RFQ average radius R_0 . For the perfectly aligned vanes and high-quality surface finish the design peak surface field can be accepted to be 16 MV/m.

The 12 MHz RFQ was originally designed for ions of q/m value 1/132 or higher. To be adapted for acceleration of ion beams such as Uranium ($q/m = 1/238$), the geometry of the vanes, i.e. the vane tip curvature radius and the average aperture have to be modified. Simulation studies suggest a vane tip curvature radius of 4.875 mm and an average aperture radius of 6.8 mm for Uranium ions. To implement this geometry, the existing electrode assembly has to be replaced by a new one. All the high power tests as discussed in this report have to be repeated for the new assembly as well.

¹K. W. Shepard and W. C. Sellyey, Proc. of the LINAC 96, p. 68.

²R. A. Kaye, K. W. Shepard, B. E. Clifft, and M. Kedzie, Proc. of the 1999 PAC, p. 524.

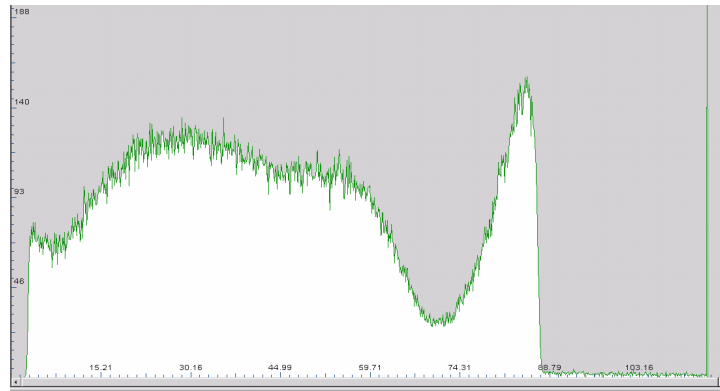


Fig. III-13. X-ray spectrum from the 12 MHz RFQ cavity operated at high power, corresponding to inter-vane voltages of 88 kV.

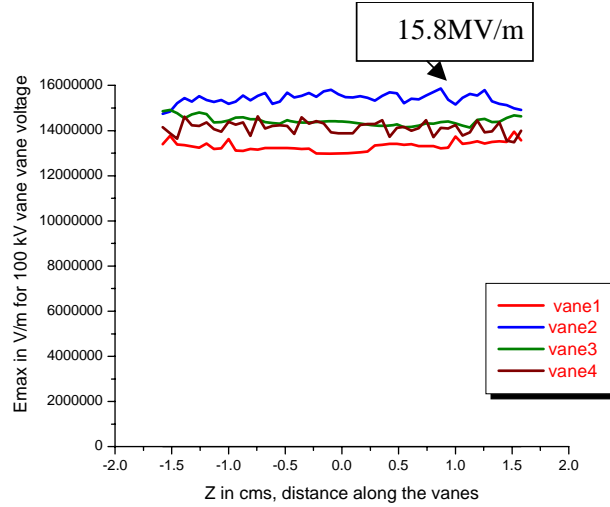


Fig. III-14. Peak surface field for the misaligned geometry of the RFQ vanes. The inter-vane voltage is equal to 100 kV.

b.4. Automatic Longitudinal Tuning of a Multiple-Charge-State Heavy-Ion Beam (B. Mustapha and P. N. Ostroumov)

We have successfully developed and tested an automatic longitudinal tuning procedure for multiple-charge-state heavy-ion beams.¹ As discussed in,² fine longitudinal tuning in the medium-energy section of the RIA driver linac (Baseline design) is essential to reduce beam loss in the subsequent high-energy section. The most important criteria for an optimum longitudinal tune is to minimize the overall emittance of the multiple charge state beam and to reach the stripper with an up-right beam ellipse in the longitudinal phase plane $\Delta\Phi$ - ΔW . Due to energy straggling in the stripper the beam emittance will blow-up along the energy axis. In addition, fluctuations in the stripper thickness tend to amplify this effect. Arriving with an up-right ellipse will minimize the effect of energy straggling and the beam emittance after the stripper. To realize these conditions the centroids of the individual charge state beams should coincide and their Twiss parameters matched at the stripper. Tracking the centroids (Φ_{qi} , W_{qi}) and Twiss parameters (α_{qi} , β_{qi}) of individual

charge state beams using the code TRACK,³ the following conditions should be met:

$$W_{q0} \rightarrow W_0$$

$$\Delta W_{qi} = W_{qi} - W_{q0} \rightarrow 0$$

$$\Delta\Phi_{qi} = \Phi_{qi} - \Phi_{q0} \rightarrow 0$$

$$\alpha_{qi} \rightarrow 0$$

$$\beta_{qi} \rightarrow \min$$

setting the slope α to 0 and minimizing the beam waist β should ensure that the beam ellipse is up-right. Using a minimization code such as MINUIT,⁴ we can define the function to minimize and the fit parameters then run the fit until it converges. In our case the fit function is:

$$F = \frac{(W_{q0} - W_0)^2}{\epsilon_w^2} + \sum_{qi} \frac{\Delta W_{qi}^2}{\epsilon_{\Delta W}^2} + \sum_{qi} \frac{\Delta\Phi_{qi}^2}{\epsilon_{\Delta\Phi}^2} + \sum_{qi} \frac{\alpha_{qi}^2}{\epsilon_{\alpha}^2} + \sum_{qi} \beta_{qi}$$

where ϵ_w is the allowed error on the beam energy, $\epsilon_{\Delta W}$ and $\epsilon_{\Delta\Phi}$ are the errors on the energy and phase deviations of the different charge states with respect to the reference charge state. ϵ_{α} is the allowed deviation of the slope α from 0.

The fit parameters are the synchronous phases Φ_s and the field levels F_{level} in the rf cavities. The field level F_{level} is used as a scaling factor in front of the effective voltage in the cavity.

Starting from a good manual tune, we performed the minimization described above by varying only the

synchronous phases of the 136 rf cavities used in the medium-energy section of the RIA driver linac. For stability of the longitudinal motion and to achieve the total energy gain Φ_s was constrained between -20° and -35° . The starting phases are not necessarily the same. In this particular case, all field levels are kept unchanged at their original values, $F_{\text{level}} = 1$, assuming the same field level in all cavities. The optimization could very well be performed for any field level profile. The optimization was performed for a five-charge state U-238 beam with $Q_0 = 74^+$ as the reference charge state and $Q_i = 72^+, 73^+, 75^+, 76^+$ the other charge states. The results for both the original manual tune and the automatically obtained tune are presented in Fig. III-15 for the beam centroids and Fig. III-16 for the final beam ellipses. We clearly see on Fig. III-15 that the automatic tuning made the centroids of the individual

charge state beams converge to the same points right before the stripper. On Fig. III-16 the originally arbitrarily oriented beam ellipses become almost perfectly aligned reducing the overall effective emittance by a factor of ~ 2 and the beam losses in the subsequent section by a factor of 3, see Fig. III-17.

In addition to producing optimum tunes from original rough tunes, this automatic procedure could also be used to retune the linac and restore the beam after one or more cavity failure.⁵ It is also very useful in developing longitudinal tunes for different ion species (with different charge-to-mass ratios).

We are actually developing an automatic transverse tuning procedure to have a fully automatic beam tuning tool that could be used for real machines.

¹B. Mustapha and P. N. Ostroumov, Phys. Rev. ST. Accel. Beams **8**, 090101 (2005).

²P. N. Ostroumov, V. N. Aseev, and B. Mustapha, Phys. Rev. ST. Accel. Beams **7**, 090101 (2004).

³“TRACK, The New Beam Dynamics Code”, V. N. Aseev *et al.*, in Proceedings of PAC-05.

⁴MINUIT–Function Minimization and Error Analysis, CERN Program Library Long Writeup D506.

⁵“Failure Mode and Recovery in the RIA Driver Linac”, B. Mustapha and P. Ostroumov, in Proceedings of the 34th ICFA Workshop on High Power Superconducting Linacs.

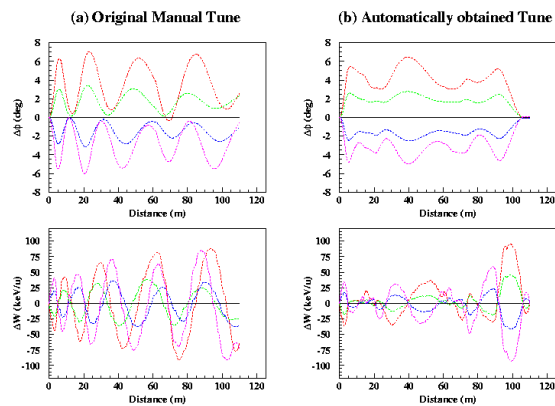


Fig. III-15. Beam centroids for five charge state beams before and after applying the automatic longitudinal tuning.

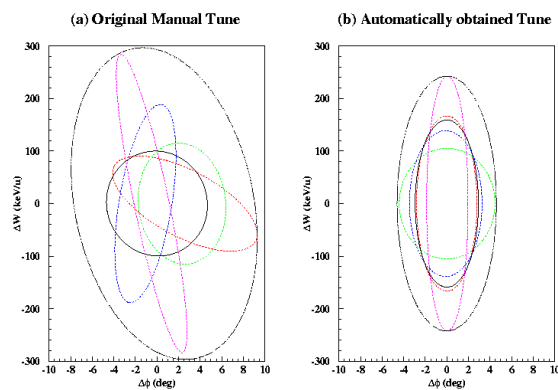


Fig. III-16. Beam ellipses right before the second stripper for five charge state beams before and after applying the automatic longitudinal tuning.

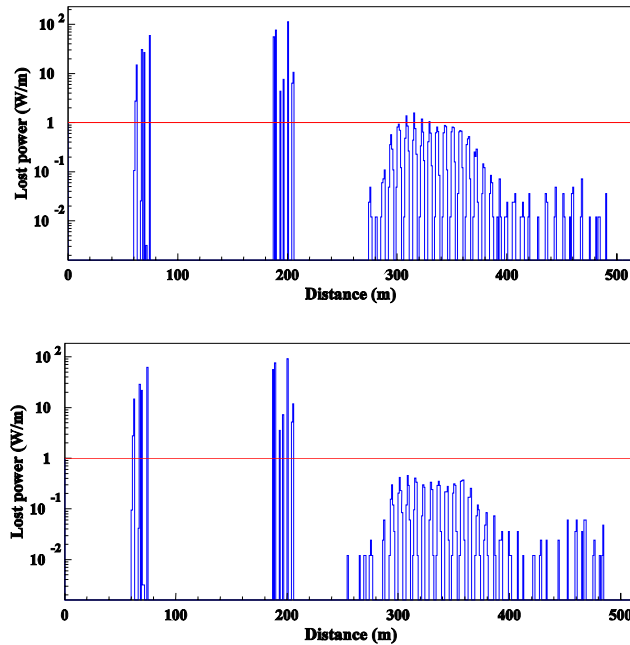


Fig. III-17. Beam loss in Watts/m along the RIA driver linac. We can clearly see that the losses are much reduced after applying the automatic longitudinal tuning - (top) before and (bottom) after automatic tuning.

b.5. Benchmarking the New Beam Dynamics Code TRACK (B. Mustapha, P. N. Ostroumov, V. N. Aseev, J. Qiang,* and R. D. Ryne*)

During the development of the code TRACK,¹ codes like TRANSPORT, COSY, GIOS and RAYTRACE were used to check TRACK's implementation of the different beam line elements. The benchmarking was essentially done for the end-to-end simulation of the RIA driver linac. The simulation of the low-energy part (from the ion source to the entrance of the SC linac) was compared with both DYNAMION² and PARMTEQ³ simulations and found to agree reasonably well. For the SC linac, we performed detailed comparisons with the code IMPACT.⁴ IMPACT has undergone many updates to meet the requirements of the RIA facility. Features such as multiple charge state acceleration and beam stripping have been added to the code. An excellent agreement was obtained between TRACK and IMPACT for the different linac sections.

Figure III-18 shows a detailed comparison between the codes TRACK and IMPACT for the medium-energy section of the RIA driver linac. More details and results are reported.⁵ In this case, space charge forces are negligible benchmarking only the tracking routines of the code. In order to check the space charge calculation for an intense beam we performed the same comparison for the proposed Fermilab proton driver linac.⁶ A 30 mA H- beam is accelerated from ~ 3 MeV to ~ 8 GeV including space charge. Figure III-19 shows the comparison between TRACK and IMPACT. An excellent agreement was obtained. The small difference in the beam's X emittance is believed to be associated with a minor mismatch in the transition from solenoid to quadrupole focusing which was treated differently by the two codes.

*Lawrence Berkeley National Laboratory.

¹"TRACK, The New Beam Dynamics Code", V. N. Aseev *et al.*, in Proceedings of PAC-05.

²A. A. Kolomiets *et al.*, Proceedings of the Sixth European Part. Accel. Conf., Stockholm, Sweden, June 22-26, 1998, edited by S. Myers *et al.*, p.1201.

³T. P. Wangler *et al.*, "Advanced Beam-Dynamics Simulation Tools for RIA", Proc. of LINAC 2004, Luebeck, Germany, 2004, p. 186.

⁴J. Qiang, R. D. Ryne, S. Habib, and V. Decyk, J. Comput. Phys. **163**, 434 (2000).

⁵"RIA Beam Dynamics: Comparing TRACK to IMPACT", B. Mustapha *et al.*, in Proceedings of PAC-05.

⁶"Lattice Design in a Multi-GeV H-Minus Linac", P. N. Ostroumov *et al.*, in Proceedings of the 34th ICFA Workshop on High Power Superconducting Linacs.

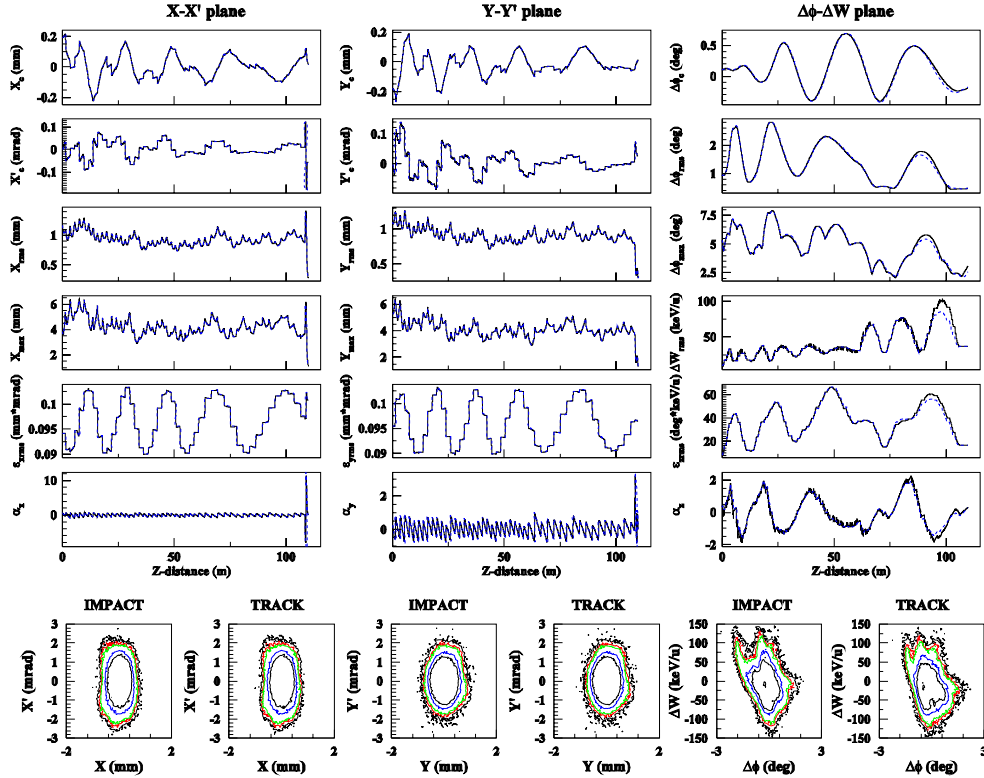


Fig. III-18. Comparison of IMPACT and TRACK simulations of the medium- β section of the RIA driver linac for a five charge state uranium beam ($Q = 72, 73, 74, 75, 76$). The black solid curves correspond to IMPACT and the blue dashed curves to TRACK. The top plots show the evolution of most important beam parameters as function of distance. The first column corresponds to the horizontal plane X-X' showing from top to bottom the beam centers X_c and X_c' the RMS value X_{rms} , the beam envelope X_{max} , the beam RMS emittance ϵ_{xrms} and the Twiss parameter α_x . The second column is similar to the first but for the vertical plane Y-Y'. The third column corresponds to the longitudinal plane $\Delta\Phi$ - ΔW , showing from top to bottom the beam central phase $\Delta\Phi_c$, the RMS value $\Delta\Phi_{rms}$, the phase envelope $\Delta\Phi_{max}$, the RMS value ΔW_{rms} , the beam RMS emittance ϵ_{xrms} and the Twiss parameter α_z . The unit of the phase $\Delta\Phi$ corresponds to the section's input frequency. The bottom plots compares particle coordinates in the three phase planes X-X', Y-Y' and $\Delta\Phi$ - ΔW at the end of the section. The colored contours represent different levels of particle density.

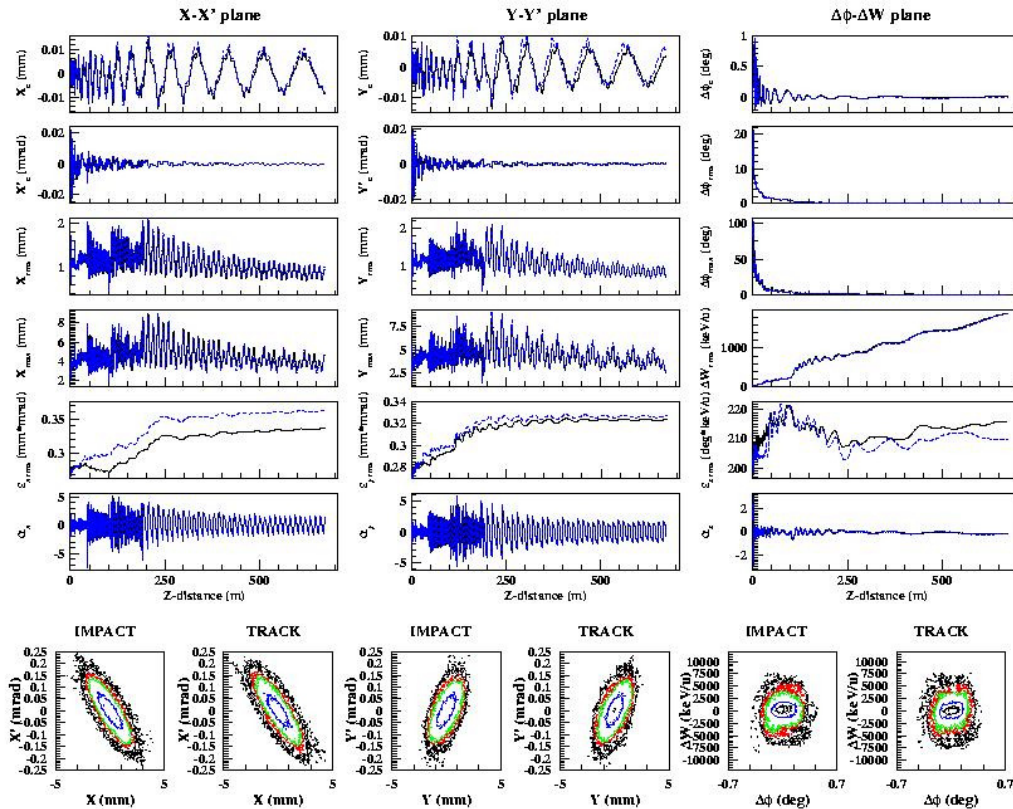


Fig. III-19. Same as Fig. III-18 but the Fermilab proton driver linac with a 30 mA H beam accelerated from the injector at ~ 3 MeV to the end of the linac at ~ 8 GeV. These results include space charge forces.

b.6. Proton Beam Dynamics in the RIA Driver Linac and Redesign of the Front-End (B. Mustapha, P. N. Ostroumov, A. A. Kolomiets, and V. N. Aseev)

Our recent simulations with the TRACK code revealed an important problem in the formation of proton and light ion bunches in the front end of the linac. To achieve 400 kW beam power the light ions must have higher electrical current than uranium ions. The space charge parameter of the bunched beam is defined as:

$$K = \frac{q}{A} \frac{I\lambda}{20\sqrt{5}\pi\epsilon_0 m_e c^3 \gamma^3 \beta^2},$$

where c is the speed of light, m_e is the atomic unit mass, γ is the relativistic factor, λ is the wavelength of rf field, ϵ_0 is the electric constant, q/A is the charge-to-mass ratio, β is the beam relative velocity, I is the beam current. As is seen the space charge parameter is proportional to both the beam current and the charge-to-mass ratio which makes it the largest for protons for fixed velocity regime. The latter is an inherent property of the front end of the RIA driver linac. We have

studied the bunching of 12 keV proton beam by the MHB. The dc proton beam current must be 1 mA to achieve the required power of the accelerated beam on the targets. The bunching of 1 mA beam by the same MHB that is used for uranium becomes ineffective due to the space charge effects. Figure III-20 shows the energy-phase plots at the entrance of the RFQ simulated for zero current and for 1 mA proton beam. As is seen, the space charge completely destroys the bunching effect. To mitigate space charge effects the buncher must be located closer to the RFQ. Also, we have found that only one-frequency buncher is effective for high current proton and light ion beams. To reduce space charge effects and increase capture efficiency the RFQ can operate at $\phi_s = -40^\circ$ which means that 18% higher inter-vane voltage with respect to the design voltage V_0 (the design phase is $\phi_{s0} = -25^\circ$) must be applied in the RFQ.

The buncher operating at the same frequency as RFQ 57.5 MHz is located 46 cm upstream of the RFQ. Figure III-21 shows the phase space plot before the RFQ after the redesign of the buncher section. 55% of injected particles are accelerated in the RFQ. The

longitudinal emittance of the proton beam is several times larger than the emittance of uranium beam. After several iterations an optimal linac tune was developed for protons in order to avoid excessive beam loss.

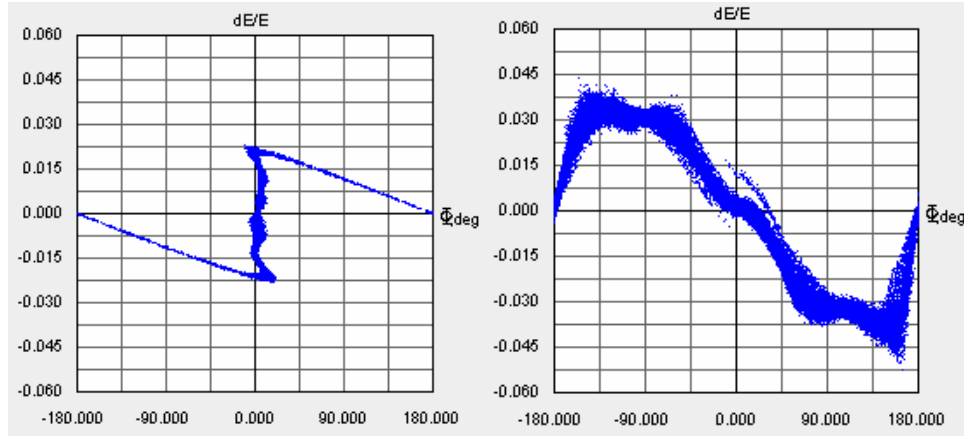


Fig. III-20. Phase space plots in the longitudinal phase space for zero current (left) and 1 mA proton beams entering the RFQ.

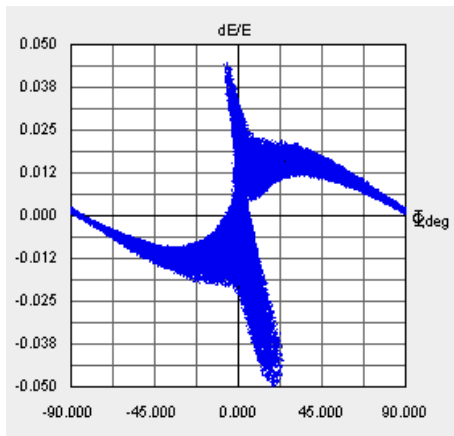


Fig. III-21. Phase space plot in the longitudinal phase space for 1 mA proton beam entering the RFQ after the redesign of the upstream buncher section.

After redesigning the front-end of the RIA driver to improve the transmission of protons and light ions in the presence of space charge forces, we were able to perform large-scale simulations of proton beam dynamics including all sources of error in order to study eventual beam losses and establish the tolerances of the design. Figure III-22 shows the beam power lost along the linac for different values of RF field amplitude and phase errors, which we identified as the most critical errors. We here distinguish between RF static and dynamic errors. Static errors are fixed and could be corrected for, whereas dynamic errors correspond to

fluctuations in time of the RF amplitude and phase. They cannot be corrected but they are usually smaller than static errors. Dynamic errors were kept unchanged at 0.5% for the amplitude and 0.5° for the phase while static errors were varied from (1%, 1°) to (4%, 4°). Correction of static errors was applied in these simulations. In Fig. III-22, the losses enclosed between two vertical dashed lines at ~ 50 m and ~ 170 m are controlled losses, they happen in the two chicane areas used for stripping beams of heavy ions. We notice that up to static errors of (2%, 2°) the uncontrolled losses are below the 1 W/m limit required

for hands-on maintenance. Therefore, the tolerances of the current design for RF errors are (2%, 2°) static and (0.5%, 0.5°) dynamic for a proton beam, which are reasonable values for accelerator operations. The

results of these simulations suggest that more design optimization may be needed to further reduce the uncontrolled beam losses.

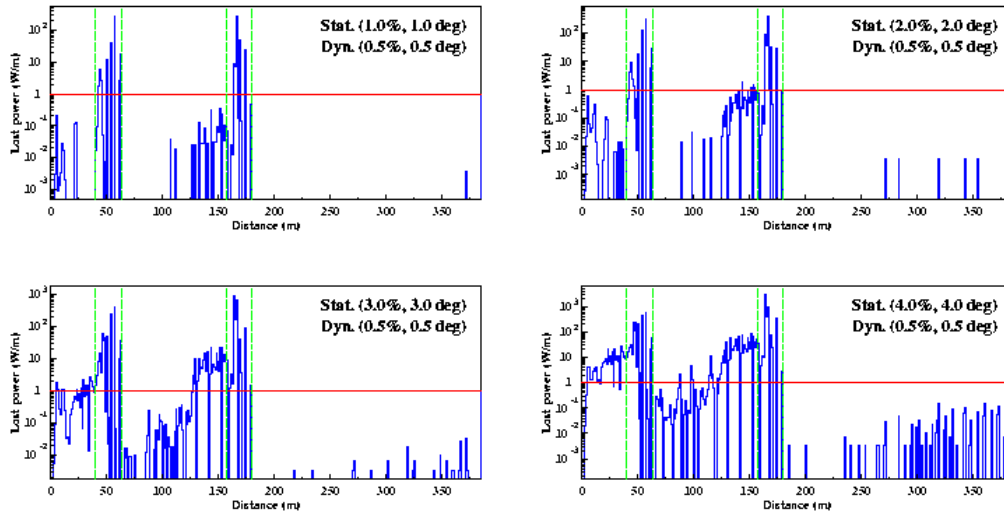


Fig. III-22. Proton beam power lost along the RIA driver linac for different values of RF errors (static and dynamic). The horizontal red line shows the 1 W/m limit required for hands-on maintenance. The losses at ~50 m and ~170 m are controlled losses in the chicane areas used for stripping heavy ions beams.

b.7. Parallel Beam Dynamic Simulation in Radio Frequency Quadrupole with Space Charge Effect (J. Xu, V. N. Aseev, B. Mustapha, and P. N. Ostroumov)

In beam dynamics simulations of linear accelerators, the space charge calculation is the most time consuming part. The potential associated with charged particle distribution is computed by solving the Poisson equation on the grid:

$$\frac{\partial^2 U}{\partial x^2} + \frac{\partial^2 U}{\partial y^2} + \frac{\partial^2 U}{\partial z^2} = -\frac{\rho}{\epsilon_0}, x, y, z \in [0, 2\pi]$$

The code TRACK has been developed during the past several years in the Physics division at ANL and has been successfully used for beam dynamic simulations. The code solves particle dynamic equations in 6 coordinates ($x, x', y, y', \varphi, \frac{dW}{W}$) as is detailed in Ref. 1. The shortcoming of the code TRACK is its computational speed. For example, the simulation of 1 million particles on a PC usually takes several days. We have developed the parallel model of the TRACK, and applied it for the 325 MHz RFQ simulation which comprises 269 accelerating periods.

We have designed and benchmarked several parallel models, and two of them have been compared in detail. The first model uses domain decomposition in the

longitudinal (z) direction as is shown on the left of Fig. III-23. The second model applies domain decomposition in the transverse (x, z) plane, as is shown on the right of Fig. III-23. We apply domain decomposition for the field computation, and also distribution of beam macro-particles into different processors. The overall diagram of the proposed procedure is shown in Fig. III-24 (the left diagram). The right diagram of Fig. III-24 shows the procedure to compute space charge forces. Since both the space charge grid domain and particle coordinates have been divided into different processors, each processor calculates the space charge deposition on a global mesh for the particles located in its processor which is followed by a global summation needed to calculate the space charge deposition on global mesh. After space charge calculation, global data exchange is also needed for particle integration on each processor.

We have used the parallel TRACK code to simulate beam dynamics in the 325 MHz Radio Frequency Quadrupole (RFQ) which accelerates H^+ ions from 50 keV to 2.5 MeV. The results of single- and parallel-

processor simulations have been compared. As expected, the results are practically identical as can be seen in Fig. III-25. On the left, we compared the particle distribution in longitudinal phase plane, the upper plot is the parallel computation result, and the lower plot is the PC computation. On the upper right corner, we compared the beam profiles along x, y and t; the lower right corner compared the quantity of log

$(1 - N/N_0)$ in transverse and longitudinal planes.

With parallel computation, the speed of code TRACK has been significantly improved. Using 64 processors simulation of one million particles takes only 2.2 hours. The capability of the code TRACK has been greatly extended allowing us to simulate 100 million particles on 1024 processors.

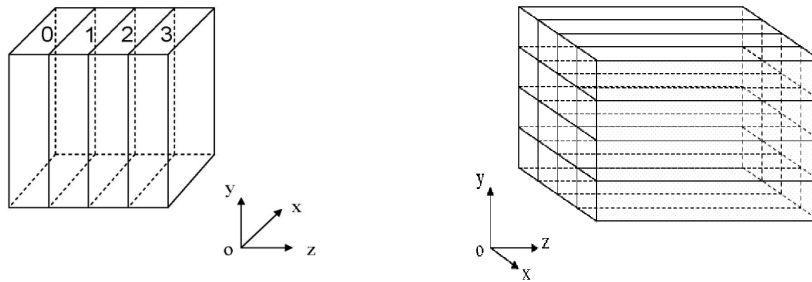


Fig. III-23. Parallel Models.

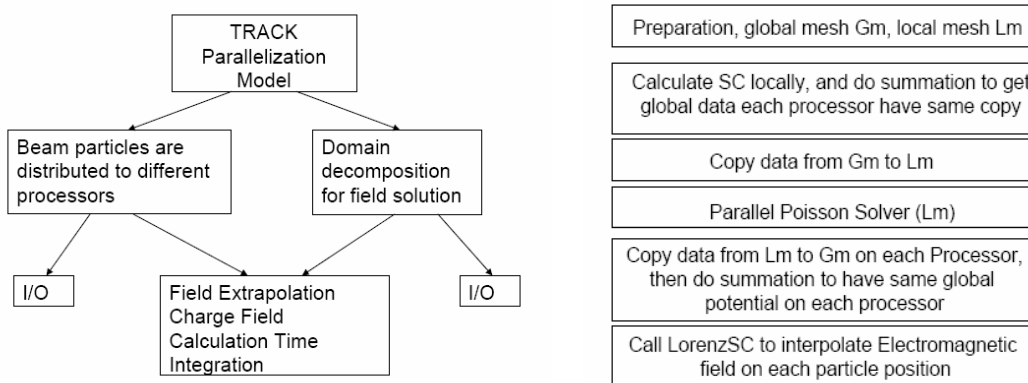


Fig. III-24. Parallel model for code TRACK.

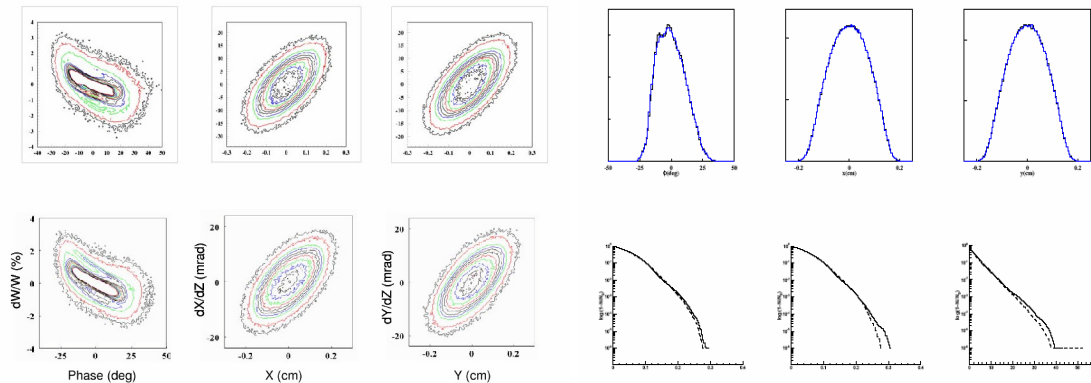


Fig. III-25. Comparison of serial and parallel computation.

¹P. N. Ostroumov and V. N. Aseev, "TRACK - A Code for Beam Dynamics Simulations in SC Linac with 3D Electric and Magnetic Fields", ANL Technical Report (2003).

b.8. Beam Dynamics of the 8-GeV H-Minus Linac (P. N. Ostroumov, V. N. Aseev, and A. A. Kolomiets*)

Significant effort in FY-05 has been devoted to the lattice development of the Proton Driver (PD) which is considered as a major part of the High Intensity Neutrino Source (HINS) at FNAL. The two-frequency option of the FNAL PD¹ has been accepted as a baseline design. Most of the voltage gain from ~420 MeV to 8 GeV is provided by superconducting (SC) cavities operating at 1300 MHz originally developed for the International Linear Collider (ILC) project. Significant cost savings are expected from the use of an rf power fan out from high-power klystrons to multiple cavities. The front end of the linac operates at 325 MHz and will be based on multiple-spoke cavities. A room temperature (RT) section comprised of a conventional RFQ and short RT H-type resonators is proposed for the initial acceleration of an H-minus or proton beam up to 10 MeV. The SC section of the front end consists of two types of single spoke resonators (SSR-1, SSR-2) and triple-spoke resonators (TSR) and accelerates H⁻ ion beam up to 420 MeV.

The physics design of the PD lattice was a primary focus of our studies. Particularly, a procedure has been developed for the physics design of high-intensity RFQs. The procedure is a modification of previously known RFQ design concepts unified with new entirely three-dimensional codes for the design and simulation of the RFQ beam dynamics. For a moderate beam current of ~40 mA, there is no transverse emittance growth, the longitudinal emittance is low and there is no non-Gaussian beam halo. For the FNAL PD application one of the main design criteria was to keep the RFQ length short to avoid complicated geometry of the resonator. A simple two-dimensional vane cut provides a high degree of linearity to the particle motion in the RFQ. A comprehensive report on the RFQ design has been published elsewhere.²

The cost-effective design of SC linac has the following properties: A) The acceleration is provided with several types of cavities designed for fixed beam velocity. At the same voltage performance of the SC cavities there is a significant variation of real-estate accelerating gradient as a function of beam velocity. B) The length of the focusing period for given type of cavity is fixed.

C) There is a sharp change of the focusing period length in the transitions between the linac sections with different types of cavities. D) The cavities and focusing elements are combined into relatively long cryostats with inevitable drift space between them. There are several focusing periods within a cryostat.

The lattice design of a SC linac includes the following main steps:

1. Select geometrical beta of the cavities using simplified formula for the cavity Transit Time Factor (TTF).
2. Select a type of cavities that is suitable for the given velocity range. Optimize electrostatics and mechanical design of the cavities. By numerical simulation, design the cavities with the reduced ratio of peak surface field to the accelerating field, reduce peak magnetic field.
3. Assume experimentally proven peak surface fields in SC cavities. Use the ratio of the peak surface field to the accelerating field obtained from optimized cavity geometry.
4. Select the focusing lattice taking into account the above mentioned requirements. Select the cryostat length, inter-cryostat spaces working with cryogenic and mechanical engineers.
5. Develop lattice tuning for the beam without space charge. Avoid zero-current resonances.
6. Using rms envelope equations check the lattice tune to verify and avoid strong space charge resonances.
7. Provide matching of the beam with the design peak current in all lattice transitions.
8. Simulate beam dynamics using multi-particle codes. Study beam losses using large number ~10⁶ of multi-particles.
9. Iterate the procedure to obtain linac design which satisfies engineers and provides high quality accelerated beams.

We have applied this procedure for the lattice design of the FNAL PD. Table III-1 shows the final basic parameters of the focusing and accelerating elements in the PD. Figure III-26 shows evolution of wave

numbers of transverse and longitudinal oscillations along the linac calculated for zero-current beam. In a high-current linac (above ~100 mA) the curves of this type should be adiabatic to avoid emittance growth of the beam and provide “current-independent” lattice tune. The smooth change of the wave-number of the betatron oscillations is provided by selecting appropriate length of the focusing periods as is shown in Table III-1 and focusing field strength. Smooth change of the wave-number of longitudinal oscillations is provided mainly by adjusting synchronous phase. However, in Fig. III-26 one can notice irregular jumps of the wave numbers which are necessary for the

purpose of beam matching in the inter-cryostat spaces and in the lattice transitions. The linac has a four-fold frequency transition which complicates adiabatic matching of synchrotron motion. In principle, such a matching can be provided by long adiabatic section which would be an expensive piece of the linac. In the design of the PD, the matching is provided by 90° “bunch rotation” in the longitudinal phase space which requires -60° phase setting in the last five TSRs. Correspondingly, there is a jump in wave number of synchrotron oscillations in the period number 73 as is seen in Fig. III-26.

Table III-1. Main parameters of the FNAL PD lattice. S-solenoid; R-resonator; F, D –quadrupoles.

Section	CH	SSR-1	SSR-2	TSR	S-ILC	ILC-1	ILC-2
β_G	-	0.2	0.4	0.6	0.83	1.0	
Peak surface field (MV/m)	-	30	28	30	52	52	
Number of resonators	16	18	33	42	56	63	224
Number of cryostats	-	2	3	7	7	9	28
Focusing lattice	SR	SR	SRR	FRDR	FR ² DR ^{2*}	FR ⁴ DR ³	FR ⁸ DR ⁸
Length of the focusing period L _p , m	0.515-0.75	0.75	1.60	3.81	6.1	12.2	24.4

*R² = RR

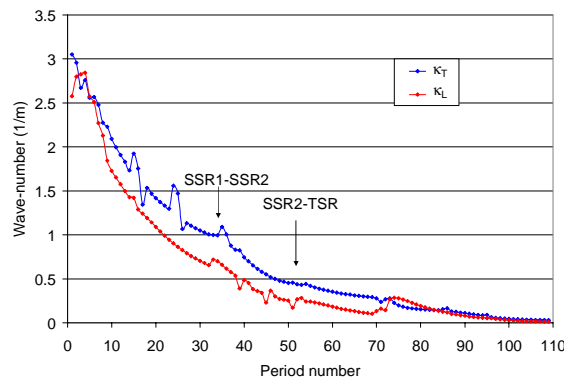


Fig. III-26. Wave numbers of transverse and longitudinal oscillations along the linac.

Prior to the beam dynamics simulations a careful matching of the 43.25-mA beam Twiss parameters in the lattice and inter-cryostat transitions has been provided. Figure III-27 shows rms, total envelopes and rms emittances of the beam along the linac. There is an acceptable level of emittance growth caused mainly by imperfections of beam matching in the lattice

transitions. Finally, the phase space plots at the end of the linac are shown in Fig. III-28. One can observe some halo development in all phase planes. The proposed design of the 8-GeV proton driver shows that the linac can provide high-quality beams both for the injection into the main ring and experiments.

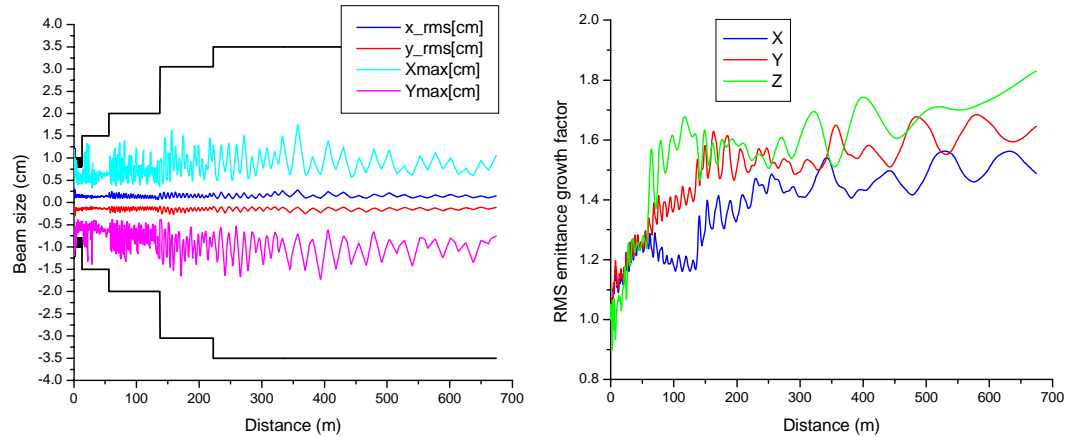


Fig. III-27. Transverse envelopes of 43.25 mA beam along the linac (the left plots) and the rms emittance growth factor along the linac. The black solid line shows the aperture.

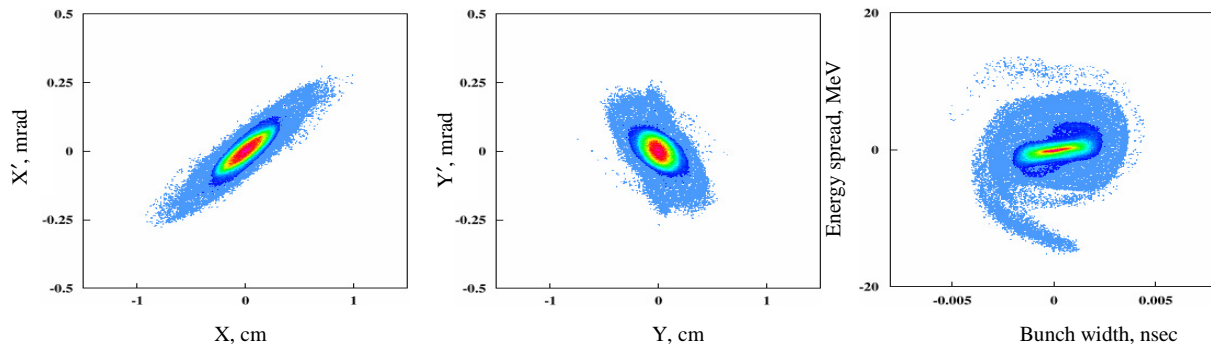


Fig. III-28. Phase space plots of 43.25 mA beam at the end of PD.

*Institute for Theoretical and Experimental Physics (ITEP), Moscow, Russia.

¹P. N. Ostroumov, K. W. Shepard, and W. G. Foster, "Superconducting Linacs for Production of Multi-GeV H-Minus or Proton Beams", 2003 Argonne Physics Division Annual Report, p. 143.

²P. N. Ostroumov, V. N. Aseev, and A. A. Kolomiets, "Application of a New Procedure for Design of 325 MHz RFQ", Journal of Instrumentation, JINST 1 P04002,

http://ej.iop.org/links/q34/dbzp2Q6dWZfbx19f65AYLg/jinst6_04_p04002.pdf.

b.9. Optimization of Steering Elements in the RIA Driver Linac (E. S. Lessner, V. S. Aseev, and P. N. Ostroumov)

The driver linac of the projected RIA facility is a versatile accelerator, a 1.4-GV, cw superconducting (SC) linac designed to simultaneously accelerate several heavy-ion charge states, providing beams from proton to uranium at 400 MeV/u at power levels at a minimum of 100 kW and up to 400 kW for most beams. Acceleration of multiple-charge-state uranium beams places stringent requirements on the linac design. A steering algorithm was derived that fulfilled the driver's

real estate requirements, such as placement of steering dipole coils on SC solenoids and of beam position monitors outside cryostats, and beam-dynamics requirements, such as coupling effects induced by the focusing solenoids. The algorithm has been fully integrated into the tracking code TRACK and it is used to study and optimize the number and position of steering elements that minimize the multiple-beam centroid oscillations and preserve the beam emittance

under misalignments of accelerating and transverse focusing elements in the driver linac.

A correction algorithm applied to the driver must comply with real-estate limitations of very tight drift spaces and coupling introduced by solenoidal focusing elements was derived previously. In this paper, we present the algorithm as fully implemented in the code TRACK, a multi-purpose tracking simulation code specially suited to simulations of acceleration of heavy-ions in SC linacs. The algorithm has been rewritten for computational efficiency, and has additional features such as the assignment of accuracy and precision errors to each monitor. We present the algorithm in its new implementation and preliminary studies to optimize the number and location of steering elements in the SC driver linac.

The algorithm can be implemented in “correction sections”, whereby N correctors and M monitors are related by:

$$(R + \Delta R) F = - (X + \Delta X), \tag{1}$$

where R and X represent the transport matrix and monitor vector coordinates for the ideal lattice, respectively. ΔR denotes the matrix deviations due to lattice errors (misalignments and field errors), and ΔX are errors in the monitor-coordinates vector introduced by monitor inaccuracies. The corrector strengths are then determined by minimizing the function Ω given in Eq. 2. Ω includes statistical weights, w_i , useful in evaluating the correction scheme effectiveness. Figure III-29 displays a possible scheme for a correction section. The minimization must obey constraints imposed by realistic limits, C, on the corrector strengths:

$$\Omega(F) = \sum_{i=1}^{2M} \left(\frac{\sum_{k=1}^{N_x+N_y} (R_{ik} + \Delta R_{ik}) F_k + X_i + \Delta X_i}{w_i} \right)^2, |F_k| \leq C_k. \tag{2}$$

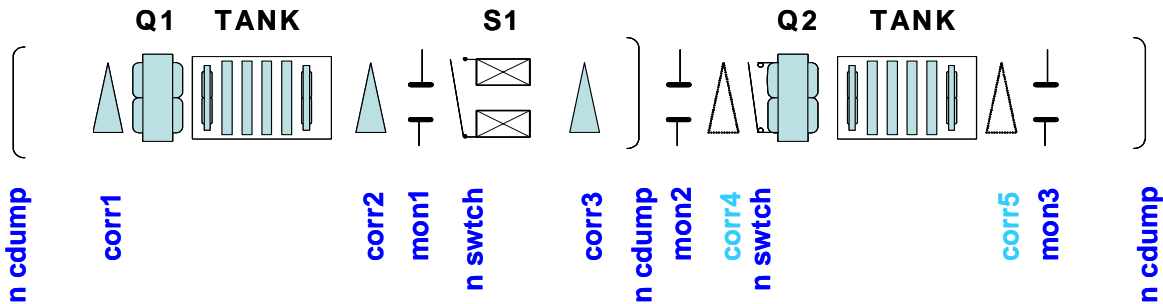


Fig. III-29. A possible correction section showing focusing, steering elements, and tanks, or cryostats, containing accelerating elements. The correctors in light blue correspond to correctors not used in the depicted correction section.

Simulations were carried for random-uniform resonator misalignments of 0.05-cm, solenoid misalignments varying from 0.015 for the shortest solenoids up to 0.05-cm for the longest solenoids, and quadrupole

misalignments of 0.02 cm. Monitor precision errors were set at 100 μ m. The number of focusing and steering elements used in the simulations is given in Table III-2.

Table III-2. Steering elements distribution in the three SC driver sections. Accelerating and focusing components are also shown.

Element	Low Energy	Med. Energy	High Energy
Resonator	83	184	172
Solenoid	40	45	0
Quadrupole	0	0	84
Corrector	13	19	22
Monitor	7	18	41

Figures III-30 and III-31 show the corrected horizontal vertical (top) and horizontal (bottom) corrector strength distributions, respectively.

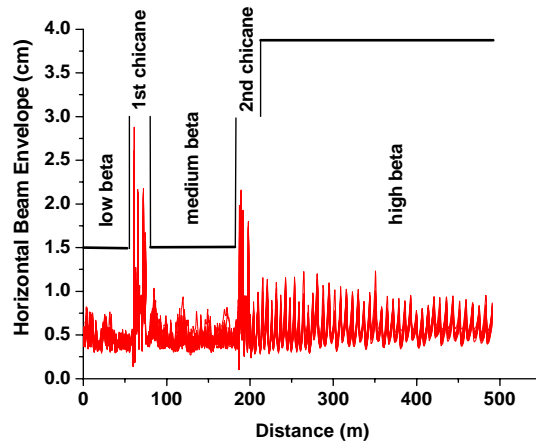


Fig. III-30. Corrected horizontal envelope, where the aperture radius is indicated for 60 seeds.

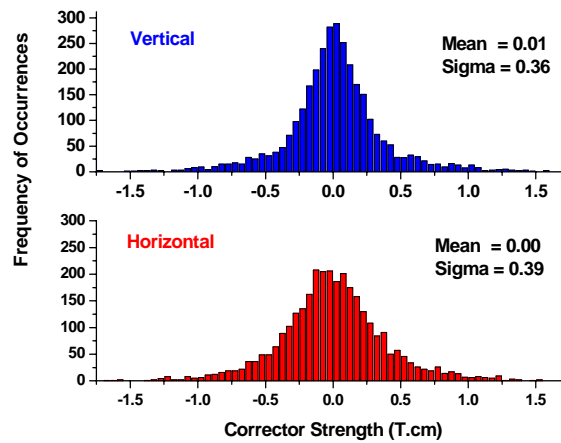


Fig. III-31. Vertical (top) and horizontal (bottom), corrector strength distributions over 60 seeds.

A 4D minimization algorithm tailored to multiple-beam steering can correct position and angle and account for solenoid-induced couplings. It is a beam-based algorithm and amenable to be implemented

experimentally. It has been optimized for computational efficiency in its full integration in TRACK. It is being used to optimize the number and position of correcting elements in the RIA driver linac.

Additional features will include a realization of correction by dipole coils mounted on solenoids and

automatic evaluation of correction scheme effectiveness.

b.10. Reliability and Availability Studies in the RIA Driver Linac (E. S. Lessner and P. N. Ostroumov)

The Rare Isotope Accelerator (RIA) facility will include various complex systems and must provide radioactive beams to many users simultaneously. The availability of radioactive beams for most experiments at the fully-commissioned facility should be as high as possible within design cost limitations. To make a realistic estimate of the achievable reliability a detailed analysis is required. The RIA driver linac is a complex machine containing a large number of superconducting (SC) resonators and capable of accelerating multiple-charge-state beams. At the pre-CDR stage of the design it is essential to identify critical facility subsystem failures that can prevent the driver linac from operating. The reliability and availability of the driver linac were studied using expert information and data from operating machines such as ATLAS, APS, JLab, and LANL. Availability studies are performed with a Monte-Carlo simulation code previously applied to availability assessments of the NLC facility and the results used to identify subsystem failures that most affect the availability and reliability of the RIA driver, and guide design iterations and component specifications to address identified problems.

Analysis of the RIA SC linac driver availability is based on simulations using a code developed at SLAC to assess the impact of various technologies or configuration choices in the Next Linear Collider (NLC) performance. The code emulates failures in a Monte-Carlo process that uses real-time as the independent variable. It calculates the machine average availability based on:

- i. given Mean Time Between Failures (MTBF) and Mean Time To Repair (MTTR) values for each component,
- ii. degradation of parameter affected by component failure,
- iii. redundancy of components,
- iv. number of repair people available for tunnel access,
- v. recovery and tuning time, and
- vi. total number of people available for repairs.

A detailed list of machine components, and, for each component, its number, MTBF and MTTR are required.

Availability data for individual components were based on data from different accelerator facilities, namely ATLAS, APS, JLab, LANL, and from reports of planned machines such as NLC and APT. Also required is an estimate of the degradation in the appropriate machine parameter caused by a component failure. For instance, we can tune around a failed resonator and degrade the beam energy by the resonator's accelerating field integrated over its length. Access requirements are divided in three categories: a) component failure brings the accelerator down but does not require access to repair, b) repair/replacement of the component requires access to the accelerator tunnel, or c) the component can be repaired while the accelerator is running ("hot repair"). Included in the category of "broken but no access needed" are failures of single resonators that require rephasing of neighboring resonators (retuning) and may degrade the beam energy, but repair can wait until a long access is required. The calculations take into account the constraints imposed by the number of people available for repair during an access.

For the availability analysis of the SC driver linac we imposed that a minimum beam power at the target be maintained, while, at this stage of the machine design, making assumptions about component failure effects. These assumptions were based on the performance of existing accelerators and experienced operators, and need to be validated with detailed Failure Modes and Effects Analysis (FMEA) studies. Listed below are some of the requirements and assumptions made.

- Some parameters have a minimum value that, when reached, cause the accelerator to be declared broken. The meaningful parameter for RIA is the beam power on the target, which will be specified as a percentage of the user requested beam power. As an initial assumption, the minimum acceptable beam power is set to 60% of the user requested power. Since beam power is proportional to its energy and intensity, both energy and current are used as "budget" parameters according to the criteria given below.

- Some component failures cause the machine to go down, such as failure of the Machine Protection System, and require immediate tunnel access to repair; others cause the machine to go down, but the machine can be retuned without tunnel access.
- Each time a component breaks the intensity is decreased by the specified amount, and the component is scheduled for repair, immediately if it can be fixed hot, or at the next downtime. When the minimum allowed operational energy or intensity is reached the accelerator is declared broken, and many accumulated repairs are done.
- Downtime planning: after a budget parameter reaches its allowable limit, the code computes the time necessary to fix the components affecting the parameter. An additional time can be added to the downtime to repair other components.
- Except for the first cryostat in the low-energy section, where failures cause the beam to be lost, failure of a whole cryostat can be recovered by retuning.
- Amplifiers and other RF power equipment are situated in a separate utility building and can be replaced quickly, if there is sufficient redundancy.

- Solenoid failure increases beam losses by 10%. Beam can be retuned, with a MTTR of 4 hours. The driver is declared broken if losses are higher than twice the initial nominal setting.
- Quadrupoles are warm. Failure increases beam losses by 10%.
- Power supplies, water pumps, etc, are located in the support building and can be repaired hot.

Figure III-32 shows on the left the downtime distribution per region of the linac driver, including the front end, cryo plant, site power, and the low-, medium-, and high-energy sections of the SC linac. A more detailed distribution per systems in the SC linac is shown on the right of Fig. III-32. For the current design, with values based on the historical data and engineering expertise from many accelerator groups the SC linac availability is 96%. The high availability comes from assuming an “universal spare” cold cryostat that can be used to replace a broken unit in eight hours, SC magnets run in persistent mode, high redundancy of power supply elements for the warm magnets and redundant amplifiers and klystrons. By assuming a support building, where power supply and controllers, and RF power sources are located, the number of tunnel accesses is reduced significantly.

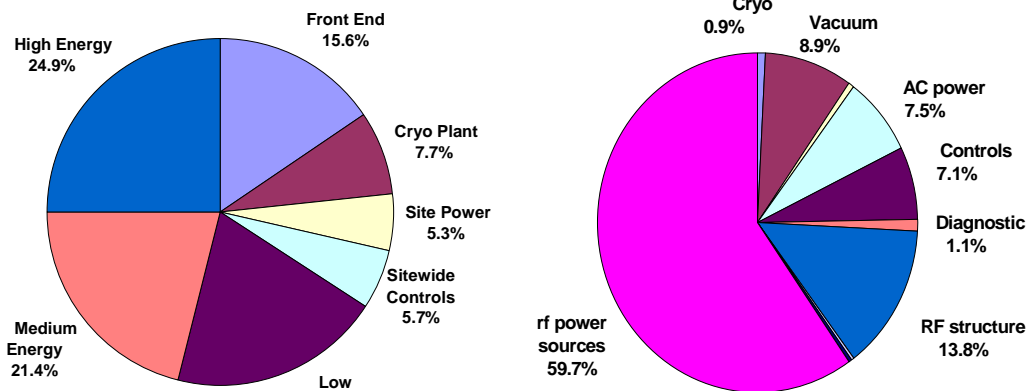


Fig. III-32. The distribution of downtime per region is shown on the left. Distribution due to systems contributing more than 0.4% of the SC linac downtime is shown on the right.

C. RARE ISOTOPE PRODUCTION AND SEPARATION

c.1. Development of Windowless Liquid Lithium Stripper for RIA (J. A. Nolen, C. B. Reed,* V. J. Novick,* J. R. Specht, and Y. Momozaki*)

Introduction

This section summarizes the on-going development of windowless liquid lithium stripper for the RIA project. Variety of preliminary experiments using simulants was performed and a Li loop was designed based on these results. For the film production, the indirect method using a stationary deflector was the scheme of choice. Other critical design parameters determined were; (1) the nozzle diameter of ~0.5 mm, (2) Li jet velocity

≥ 100 -150 m/s (corresponding maximum drive pressure of 9-18 MPa that includes additional pressure for initial blow off), (3) the angle of incident being between 30-45 degree, and (4) the relative position of the nozzle to the deflector needs to be adjustable in an accuracy of ~ 0.1 m¹. The objective of the current phase of this project is to experimentally demonstrate a formation of a thin liquid lithium film.

Liquid Lithium Thin Film Loop

The whole system consisted of a lithium system (see Fig. III-33), a vacuum system, a high-pressure gas system, and a low pressure gas system. The inventory of Li in the system was 11.5 kg (~22.3 liters) of which the maximum usable quantity was ~16.7 liters. The major components of the system were fabricated from stainless steel for compatibility with liquid lithium. Connections that were in contact with liquid lithium were welded as much as possible; however, several metal-to-metal connections were also used. The nozzle assembly consisted of a A.M. Gatti's Hi-cohesive nozzle adaptor (P/N 3210) and specially ordered all stainless steel, high-performance waterjet orifice assembly [P/N 3024 with a 0.5 mm (20 mil) round opening]. An air cooled diffusion pump using Santovac

5 diffusion oil maintained the system under vacuum of low 10^{-7} Torr range at room temperature and low 10^{-6} Torr range during operation. The high-pressure gas system provided high purity (99.998%), high pressure Ar gas up to 13.9 MPa (2000 psig) to the pressure vessel for driving liquid lithium out from the nozzle. The low-pressure gas system provided an ultra high purity (>99.999%) and low pressure (<3 psig) Ar gas as a cover gas and driving pressure to transfer liquid lithium from the collection chamber to the pressure vessel after each run. This system could drive liquid lithium at up to 13.9 MPa (2000 psia) through a nozzle with an opening as large as 1 mm (40 mil) in diameter into a vacuum chamber.

*Nuclear Engineering Division, Argonne National Laboratory.

¹J. A. Nolen, C. B. Reed, V. J. Novick, J. R. Specht, and Y. Momozaki, "Development of Windowless Liquid Lithium Stripper for RIA," Physics Division Annual Report 2004, ANL-05/61, pp. 174-189.

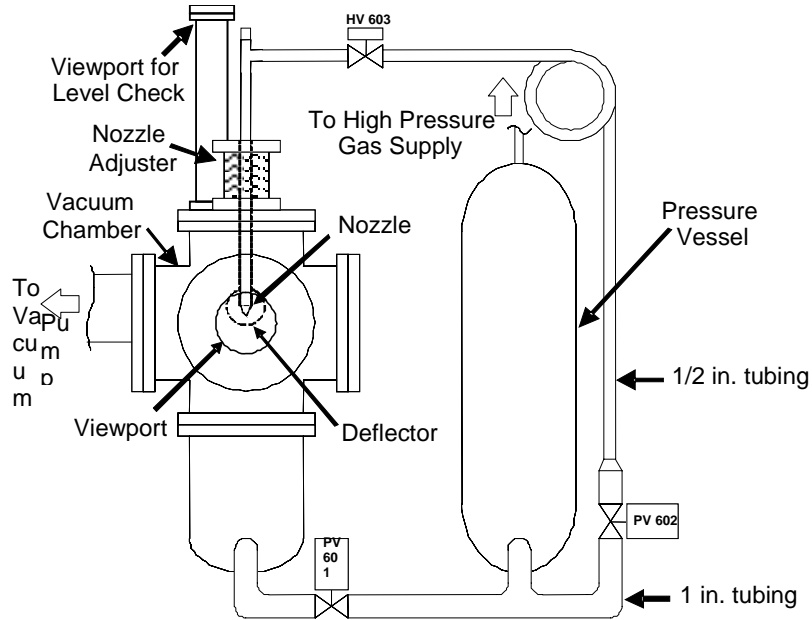


Fig. III-33. Schematic of Li loop.

A typical experiment started by heating the system to $\sim 220^\circ\text{C}$. After all temperatures along the system were stabilized and the nozzle and deflector temperatures exceeded the melting point of Li, the pressure vessel was pressurized with Ar gas to a desired value. Then the valve was opened to initiate a Li jet. The drive pressure was usually set above $\sim 700\text{ kPa}$ ($\sim 100\text{ psia}$).

Results

A few experiments for demonstrating formation of a thin liquid lithium film were performed at various driving pressures up to $\sim 4\text{ MPa}$ ($\sim 600\text{ psia}$). This system employed the once-through concept to achieve very high Li jet velocity, limiting continuous operation. However, due to relatively small flow rate of Li, the duration of a run at $\sim 700\text{ kPa}$ ($\sim 100\text{ psia}$) was as long as ~ 40 minutes.

The formation of the jet was confirmed through the viewport. After establishing the jet flow, the position of the nozzle was adjusted to optimize the location of the impaction point for the best looking film. The temperatures and pressures were recorded at a set interval. A digital camcorder recorded visual images of the Li film from the viewport during experiments.

Figure III-34 shows a photograph of a liquid Li thin film obtained on 12/02/2005. The drive pressure was $\sim 860\text{ kPa}$ ($\sim 125\text{ psia}$). The chamber pressure was in the 10^{-6} Torr range during the test, suggesting Li vapor was not a major contributor to the chamber pressure. During this run, observed Li temperature was $\sim 250^\circ\text{C}$, at which Li saturated vapor pressure is $4.5 \times 10^{-6}\text{ Pa}$ ($3.4 \times 10^{-8}\text{ Torr}$). An estimated upper bound for the film thickness was $13\ \mu\text{m}$.

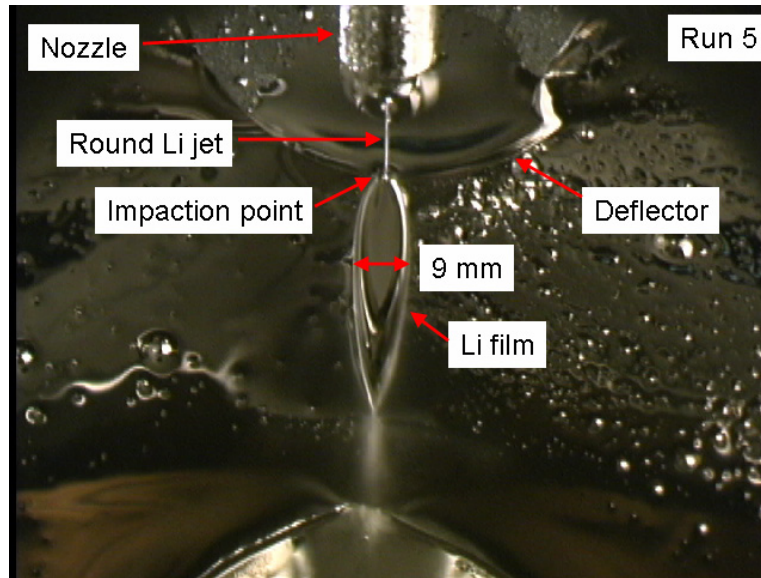


Fig. III-34. Photograph of a thin Li film.

c.2. Fragment Separator Design and Simulations (B. Erdelyi and J. Nolen)

The next generation fragment separators for high intensity beams present challenges in terms of the ion optical design due to large acceptances and large magnet apertures. Also, the computational framework that combines charged particle optics with nuclear processes that the beams undergo needs to be programmed.

Our group embarked on a code development program that had the purpose to provide a framework for end-to-end fragment separator simulations, including high order aberrations, accurate treatment of beam-material interactions, and the processes of energy loss, and angular and energy straggling. Also, fragmentation and fission cross-sections and charge state evolution needed to be taken into account. Our choice was to take a state-of-the-art charged particle dynamics simulation code and implement and extend it to contain the new features needed for the above mentioned simulations. To this end, the functionalities of a suite of nuclear physics codes have been made an integral part of COSY Infinity.

COSY is a general purpose nonlinear dynamics code with a Differential Algebra (DA) based computation engine at its heart. It has a flexible object oriented input language that allows relatively straightforward addition of a new element to its already existing extensive list of dipoles, multipoles, cavities, both

electric and magnetic, as well as elements for glass optics. A very important feature of the code is the existence of fitting procedures at the language level. With a choice of different optimizers the optimization problem can be cast in terms of the usual loops (FIT-ENDFIT).

We chose to include ATIMA (the spline-based version) for calculation of energy loss functions, and the various stragglings. We used EPAX 2.1 for calculation of fragmentation cross-sections. We implemented GLOBAL for calculation of charge state evolutions. All these stand-alone codes are now available as intrinsic function calls in COSY. The implementation of a limited fission model (both cross-sections and kinematics) is underway.

Another element of the simulation framework implemented is the circumvention of the non-existence of a global coordinate system in COSY. If one needs to track all particles, including background, the large range of rigidities makes it necessary to implement secondary maps, in which the range of rigidities is split into n pieces, and a transfer map is computed for each piece, glued together smoothly by coordinate transformations.

We envision two running modes for the code: map mode and Monte-Carlo mode. In the map mode all

deterministic effects are included in the map, and optimization can be done on the map quite rapidly. For the details and evaluating the performance of the whole system the MC mode will be used.

The other main thrust of this program is to find innovative layouts for fragment separators that intrinsically have low aberration content and a theory of aberration correction using minimal number of magnets with low strengths.

The whole system consists of two achromats with different separation cut angles in the mass-charge plane. Our approach to the problem is by “dividing and

conquering” each subsystem. The main ingredient of this approach relies on utilizing symmetries, namely mirror and symplectic symmetries. A theory was developed that shows that a minimal system should be designed in such a way that linearly the system is point-to-point imaging and parallel-to-parallel in both planes, and has energy independent angles at the dispersive image. Also, these conditions reduce the number of second order aberrations to be minimized to 10 and the third order ones to 21. Moreover, it completely decouples aberrations of different orders. More work is underway to work out explicitly the minimum number of sextupoles and octupoles needed for a perfect third order achromat.

c.3. Development of Uranium Carbide Material for High Power ISOL Applications (J. P. Greene, J. A. Nolen, A. Davila, T. Burtseva,* and A. C. C. Villari†)

One option for a high power isotope separator on-line (ISOL) production target for facilities based on high energy light ions is a two-step, neutron-generator concept.¹ Neutrons, first generated via spallation reactions in a cooled, refractory, primary target, induce fission in a surrounding assembly of uranium carbide.

A prototype target to demonstrate this concept at ISAC was designed by TechSource, Inc.² It will use fine-grained, high thermal conductivity UC₂ target material to be supplied by our group at Argonne. The primary target will be a liquid cooled rhenium cylinder, irradiated by the ISAC driver beam, 500-MeV protons. Thermal conductivities on the order of 2 W/m-K (or greater) over the operating temperature range are required to minimize the temperature differences in the uranium carbide secondary target which is primarily heated by the fission power.

As the uranium carbide used for this research is no longer commercially available, an in-house manufacturing method was developed using the method of arc melting.³ As grain size may prove to play an important role in ultimate densities, thermal conductivities and release properties achieved, this prepared material is characterized using sieves for selecting the fine-grain material. The initial runs produced 20 g of powder (-325 mesh), grain size 44 μm. Investigations are now underway employing samples prepared with this material.

Disks for thermal conductivity measurement were prepared in a laboratory hood by first weighing out UC₂ powder together with carbon (ratio of 8:1) in the form

of high-purity synthetic graphite powder which is necessary to hold the refractory material in the form of a pellet. In the first samples the mixture, with albumin are added as a binder, was poured into a 13 mm compaction die and pressed to 5 tons using a laboratory press. Recently, sample disks of TiC, WC, and UC₂ have been prepared using a type of exfoliated graphite obtained through Superior Graphite avoiding the need for using albumin as a binder. Densities of 5 g/cc and greater have been achieved, meeting design specifications. These thin sample pellets then have their thermal conductivity measured using an electron bombardment technique.⁴ The sample is heated on the bottom face by a vertical electron beam source installed within a vacuum evaporator. After achieving thermal equilibrium, the temperature of both faces of the sample was measured with the aid of a two-color pyrometer. Recently modifications to the original design were performed including adding ceramic rods which replaced the previous glass cylindrical support in order to avoid charging of the glass which caused a deviation of the electron beam. An intermediate tungsten collimator was also installed beneath the pellet support to prevent a halo from the electron beam from hitting the Ta sample holder. Sample data and results from these measurements are presented in the section below.

The desired release of the fission products produced under sample irradiation is being explored as a function of density/grain size. The target/ion source (UNIRIB) facility is being used for characterization of the secondary target material release properties. We are working closely with Dan Stracener and Ken Carter at ORNL who are doing the release measurements and

analysis. Uranium carbide samples manufactured from fine grain size material has been shipped there for these measurements.

Next steps involve the development of fabrication methods for the actual secondary target disks using custom designed dies for much larger diameter disks. To make these larger diameter disks we are also

Sample Thermal Conductivity Measurements

Thermal conductivity measurements of new samples of uranium carbide prepared as described above were done during the summer of 2005 at the ANL target laboratory using the electron-beam method.³ A grafoil sample with known thermal properties was used to determine the characteristics of the electron beam. Grafoil runs were done before and after the uranium carbide runs to verify that the beam properties did not change during the period of measurements. The measurements took place from June 2nd to June 13th. The uranium carbide sample was measured several times, each of which involved heating it from room temperature to ~2000 K, to verify the stability of the thermal properties. The sample data are shown below.

Samples

- Uranium carbide sample characteristics: (sample #UC2-ALB-C).
- ANL-W uranium carbide 325 mesh + Alb + C 200 mesh. Sample series number #5.
- Before heating: 13.03 mm diameter, 0.93 mm thickness, 0.6518 g weight. (density 5.26 g/cm³).
- After heating: 12.45 mm diameter, 0.97 mm thickness, 0.6291 g weight. (density 5.33 g/cm³).
- Grafoil characteristics: 0.030" thickness and ½" diameter.

Data

The grafoil runs were used in conjunction with the FlexPDE program⁵ to calibrate the method, determining the effective electron beam diameter and the effective field of view of the two-color pyrometer. An electron beam Gaussian distribution with 6.4-mm FWHM was

investigating the use of a new electro-consolidation process that was recently demonstrated under a separate ANL/Superior Graphite collaboration. It is believed that the densities and thermal conductivity achieved for these UC₂ samples are sufficient for a prototype high-power two-step target to be built and tested under experimental conditions.

used to fit the grafoil data, and the parameters were the same before and after the uranium carbide runs.

The uranium carbide sample was irradiated four times on different days and after opening and closing the vacuum system. Also, the pyrometer was re-positioned for each measurement. We believe that, with this procedure, a good estimation of errors related with the positioning of the pyrometer of the results can be made. This is the main factor which affects the reproducibility of our results. Another factor to be considered is the positioning of the sample in the holder, with respect to the electron beam center. This was verified in all measurements. A clear hottest zone appears in the center of the sample, if it is correctly positioned. Data were taken during heating and cooling of the sample. Also, we waited for the equilibrium to be established before reading the pyrometer. Figure III-35 shows the temperatures of the lower surface (hotter, red) and the upper surface (cooler, blue) as a function of the incident electron beam power hitting the lower surface. The black dots were obtained from the FlexPDE program adjusting the thermal conductivity and emissivity of the sample to get a best fit. This fit was obtained with a constant emissivity of 1. Figure III-36 shows the extracted values of the thermal conductivity vs. the average temperature of the sample. There is very little temperature variation of the conductivity and the average value is approximately 11.5 W/m-K. The density of the sample was 5.33 g/cm³ after the runs and increased by only 1% from the initial value. The thermal conductivity is much higher, by about a factor of 10, than our earlier measurements of low-density (~2.5 g/cm³) uranium carbide made by the oxide reduction method.

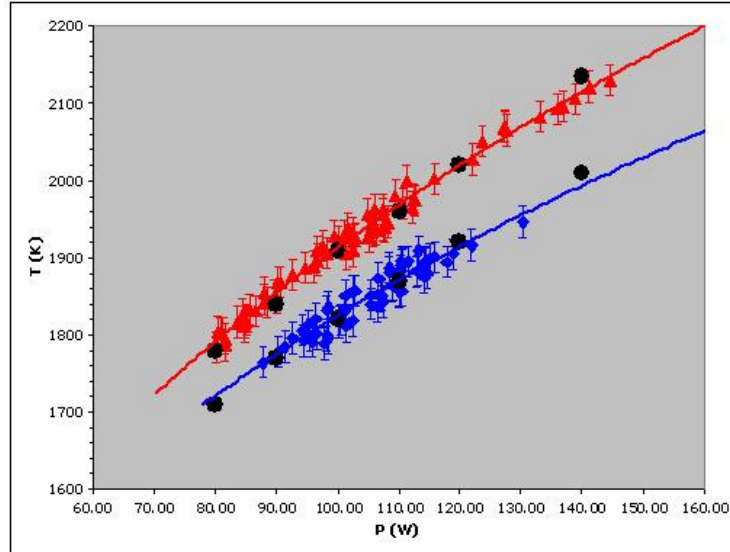


Fig. III-35. Lower surface (red) and upper surface (blue) temperatures of the uranium carbide sample as a function of the beam power. The black dots correspond to the FlexPDE fit.

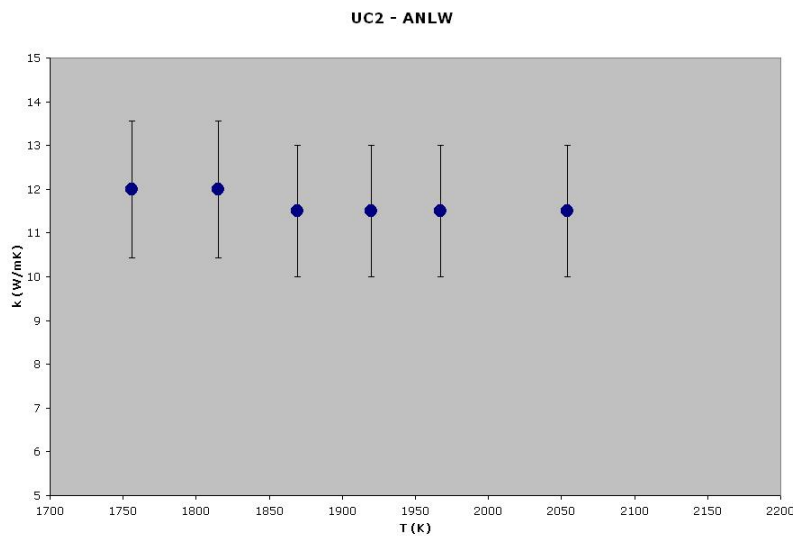


Fig. III-36. Thermal conductivity of the uranium carbide sample as a function of its average temperature.

*Energy Technology Division, Argonne National Laboratory, †Argonne National Laboratory and GANIL, Caen, France.

¹Report to ATLAS Users Facility, **ANL-ATLAS-99-1**, March (1999).

²W. Talbert *et al.*, TechSource, Inc. (SBIR Grant).

³J. Crane, F. B. Litton, and H. S. Kalish, *Arc Skull Melting and Casting of Uranium Carbide*, ASM Trans. Quarterly **56**, 176 (1963).

⁴J. P. Greene, A. Levand, J. Nolen, and T. Burtseva, Nucl. Phys. **A746**, 425c-428c (2004).

⁵FlexPDE 4.2.7s (student version) www.pdesolutions.com.

c.4. Conductance Measurement of Permeable Samples (A. C. C. Villari,* J. Greene, T. Burtseva, and J. A. Nolen)

Definition of the Method

A method for measuring the conductance of permeable samples was developed in the Physics Division target laboratory. This technique allows measuring the conductance of permeable samples being traversed by any gas. The size of the samples can vary from some millimeters to a maximum of 3 cm diameter. This

limitation is presently given by the size of the vacuum chambers used in the set-up, but it can easily be changed. The value of the conductance is obtained by comparing the difference of pressure between the two sides of the sample with the one obtained with a calibrated orifice. The set-up is shown in Fig. III-37.

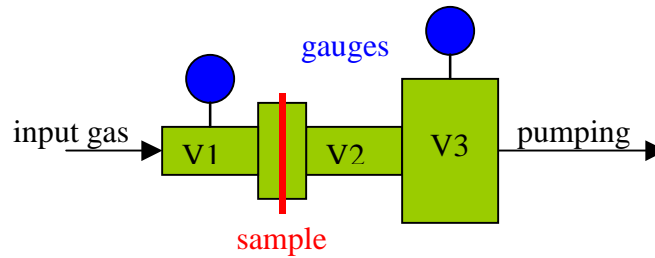


Fig. III-37. Set-up for measuring the conductance of permeable samples.

When a vacuum steady-state is established in the system, the quantity of gas circulating in the volumes V1, V2 and V3 are the same and equal to Q. Therefore, one can write the following relationship between the conductance C_s of the sample or orifice, the conductance C_2 of the pipe V2 and the pressures in V1, V2 and V3:

$$Q = (P_1 - P_2)C_s = (P_2 - P_3)C_2 = (P_1 - P_3)C_{2s} \quad (1)$$

where P_1 , P_2 and P_3 are the pressures in volumes V1, V2 and V3 and

$$C_{2s} = (1/C_s + 1/C_2)^{-1} \quad (2)$$

Moreover, the pumping speed (S_3) in the volume V3 is constant, therefore, one can write:

$$Q = S_3 \cdot P_3 \quad (3)$$

Substituting (3) in (1), one obtains the following relation between the pressures P_1 and P_3 :

$$P_1 = (S_3/C_{2s} + 1)P_3 \quad (4)$$

Knowing the conductance of the pipe in V2 (by construction) and measuring the pressures P_1 and P_3 for a calibrated orifice allows one to obtain the pumping speed S_3 , which in turn, can be used for calculating the conductance of the sample given the pressures P_1 and P_3 measured with the sample. The procedure adopted for obtaining the conductance of a sample is:

1. Deduce the value of S_3 using a calibrated orifice via the measurement of pressures P_1 and P_3 .
2. Measure the pressures P_1 and P_3 with the sample, deduce the value of $(S_3/C_{2s} + 1)$ from equation (4) and extract the conductance from the relationship (2).

Fig. III-38 shows a picture of the experimental set-up.

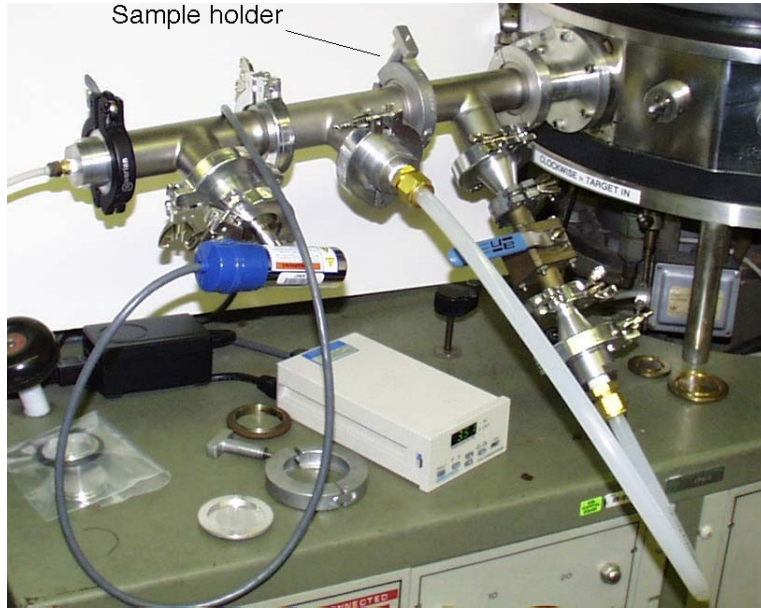


Fig. III-38. Picture of the experimental set-up. The blue valve is a by-pass between volumes V1 and V2.

Calibration of the Pumping Speed

The calibration of the pumping speed of the system was made using an orifice of 1 cm². Air was injected in the

system and the following values of pressures were measured (Table III-3).

Table III-3. Pressure P₁ and P₃ measured with a calibrated orifice of 1 cm² area.

	P ₁ (torr)	P ₃ (torr)
1	3 · 10 ⁻³	2 · 10 ⁻⁵
2	6.2 · 10 ⁻³	4 · 10 ⁻⁵
3	9.3 · 10 ⁻³	6 · 10 ⁻⁵

From this data, and using the plot given in Fig. III-39, one could deduce the value of (S₃/C_{2s} +1) for the calibration orifice as being equal to 157.5. Given that the conductance of an orifice of 1 cm² area for air at 20° C is 11.6 l/s and the conductance of the pipe V2

is 30 l/s, the pumping speed at V3 is equal to: S₃ = 1321.4 l/s. This value is compatible with the speed of the diffusion pump (v = 2400 l/s) used in the test bench, if one considers that the pump is not placed directly on the volume V3.

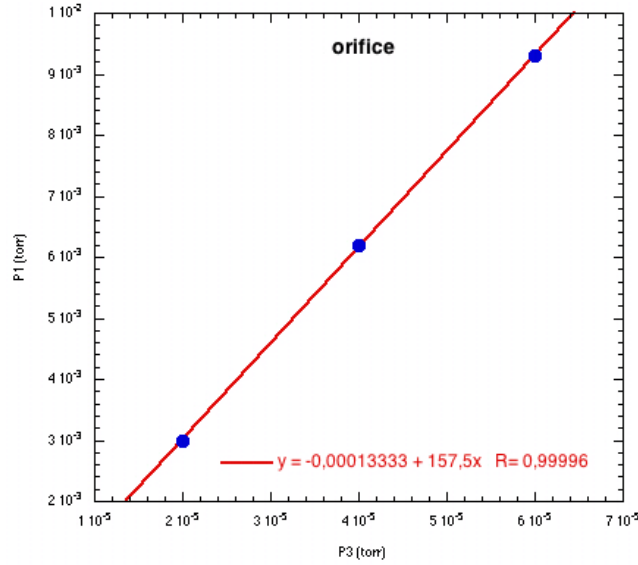


Fig. III-39. Pressures in the volumes V1 and V3 using a calibrated orifice of 1 cm² area.

Measurement of Carbon Aerogel Conductance

The Southern Institute provided the carbon aerogel used in the measurement. Samples were cut from this material with dimensions corresponding to approximately 2 cm × 2 cm with thickness of 2 mm. No treatment was performed after the cut process. The

sample was glued onto a circular orifice of 1 cm² area between volumes V1 and V2 (see Fig. III-40). The data obtained (P₁ and P₃) is shown in Table III-4 and Fig. III-41.

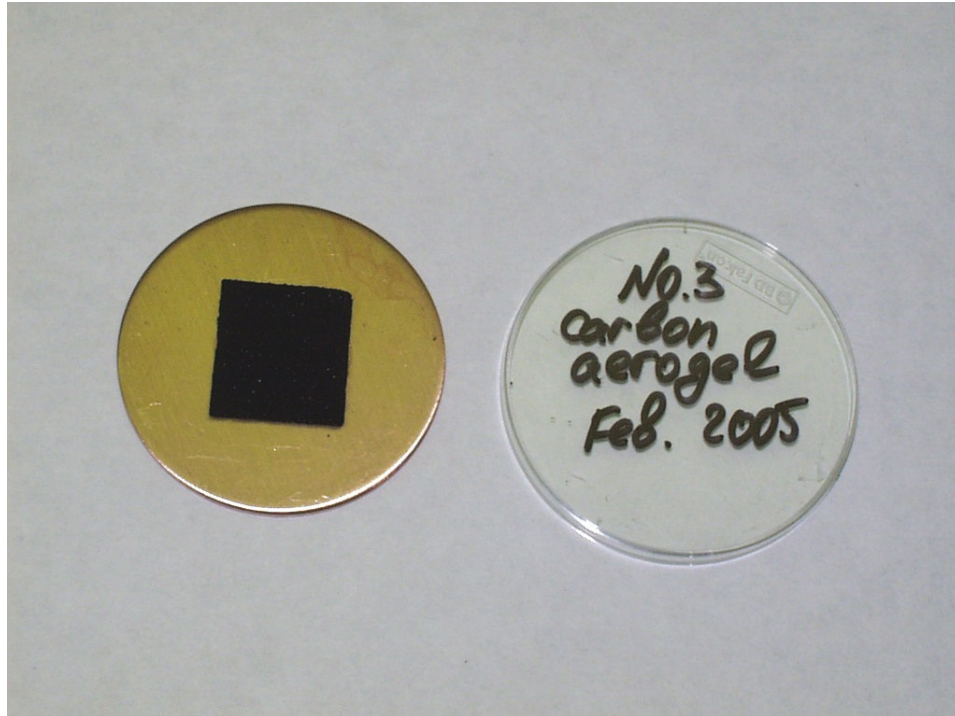


Fig. III-40. Carbon aerogel glued onto a copper disk.

Table III-4. Pressures in volumes V1 and V3 with carbon aerogel sample.

	P ₁ (torr)	P ₂ (torr)
1	252 10 ⁻³	3 10 ⁻⁶
2	400 10 ⁻³	5 10 ⁻⁶
3	556 10 ⁻³	7 10 ⁻⁶
4	1250 10 ⁻³	1.7 10 ⁻⁶
5	2530 10 ⁻³	3.3 10 ⁻⁶
6	3700 10 ⁻³	5.8 10 ⁻⁵

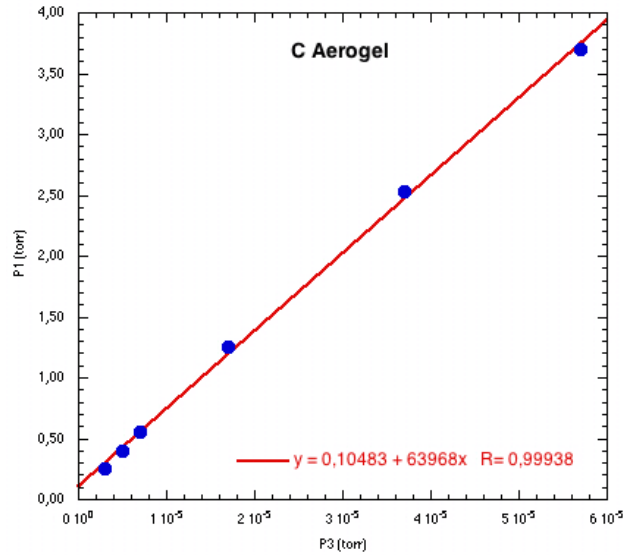


Fig. III-41. Pressures in volumes V1 and V3 with carbon aerogel sample.

Using equation (4), one can obtain from the fit in Fig. III-41: $S_3/C_{2S} + 1 = 63968$. Using the value of S_3 deduced in the preceding section and using equation (2), one can deduce that for the carbon aerogel sample of 2 mm thickness and 1 cm² diameter:

$$C_s = 0.0206 \text{ l/s}$$

The conductance can be expressed for any diameter size as a conductance density (for 2 mm thickness) as: $c = 0.0206 \text{ l cm}^{-2} \text{ s}^{-1}$. For this particular aerogel sample, this corresponds to a reduction in conductance of approximately a factor of 563, when compared with an

open orifice of the same area. The equivalent orifice would have a diameter of 0.42 mm.

The error of the measured conductance can originate from the relative calibration of the vacuum gauges, small leaks or degassing of the system, and parasitic conductance between V1, V3 and the vacuum gauges. In Fig. III-39 and Fig. III-41 we observed that the two straight lines do not cross “zero” as they should, probably due to calibration offset. Each of these errors contributes approximately 10% of error to the final value. Therefore, a crude estimate would give an overall error of 20% for the measured conductance.

*Argonne National Laboratory and GANIL, Caen, France.

c.5. Testing of the Full-Scale RIA Gas Catcher Prototype at High Energy at GSI

(G. Savard, J. P. Greene, A. Levand, N. Scielzo, W. Trimble, B. J. Zabransky, K.-H. Behr,* A. Bruenle,* G. Chubarian,† J. Clark,‡ Z. Di,§ A. Fettouhi,* H. Geissel,* W. Hueller,* C. Karagiannis,* B. Kindler,* Y. Kudryavtsev,¶ B. Lommel,* M. Maier,‡ D. Morrissey,¶ M. Petrick,§ W. Plass,§ M. Portillo,¶ C. Scheidenberger,* K. S. Sharma,‡ H. Weick,* M. Winkler,* and the S258 Collaboration)

The principal difficulty in radioactive beam facilities has to do with the production and rapid extraction of short-lived radioactive isotopes. One key approach to overcome this difficulty at RIA is the gas catcher system that will provide access to low-energy beams of short-lived isotopes not amenable to the standard ISOL technique. The gas catcher concept for RIA is a new approach to the extraction of radioactive ions that was proposed in 1998 based on developments at lower energy at the CPT spectrometer at Argonne. The gas catcher stops fast recoils in high purity helium and uses a combination of DC and RF electric fields together with gas flow to obtain high efficiency and short delay times in the extraction of the radioactive ions. Since then significant R&D efforts at Argonne have demonstrated the feasibility of this approach with numerous physics results obtained from the gas catcher injection system in use at the CPT and the construction of a RIA scale prototype that was characterized off-line and on-line at ATLAS where high efficiency (typically 30-50%), fast extraction times (~40 ms) and confirmation by mass identification that the activity was extracted as radioactive ions, were obtained (see Argonne Physics Division 2003 annual report). The efficient operation of a gas catcher having been demonstrated, the remaining questions for the application of the gas catcher concept to RIA were the

operation at high energy and the maximum intensity the device can handle (the radioactive ion production technique used for the on-line tests at ATLAS limited the intensities available to 5×10^5 ions per second entering the gas catcher). Preparation for a high intensity test of the gas catcher is ongoing and is discussed in section c.6., the first test at RIA energy is discussed here.

The RIA gas catcher prototype constructed and tested at Argonne was moved to GSI for operation at the FRS, installed and tested there in an off-line area (see Fig. III-42) with sources and the pumping system available on location while waiting for first beamtime at the FRS fragment separator that came in February 2005. The gas catcher and extraction RFQ were mounted on a rigid platform that allowed moving the complete structure as a whole without dismantling it. The device was moved to the confined space behind the FRS focal plane and aligned in the 2 days preceding the run (see Fig. III-43). The pumping system was also moved to the area behind the FRS focal plane and the whole system restarted in location. A small vacuum leak was found in the system after reinstallation but, due to time constraints and the time required after an opening for the system to recover, it was decided to run under these conditions.

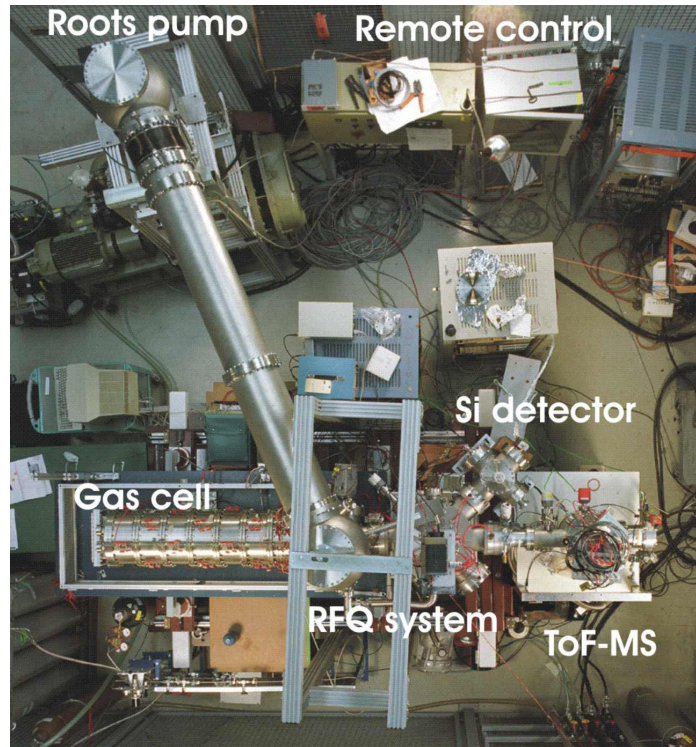


Fig. III-42. Bird's eye view of the off-line area where the gas catcher was first installed and commissioned with the local pumping system at GSI.

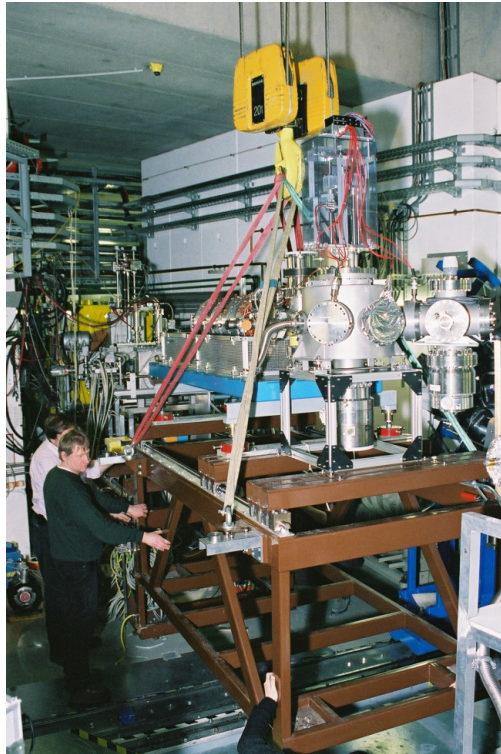


Fig. III-43. Installation of the gas catcher platform behind the focal plane of the FRS fragment separator at GSI.

The primary beam used for the experiment was ^{58}Ni at 375 MeV/u with the fragment separator tuned to transmit the produced $N = Z$ nuclei so that ^{56}Ni , ^{54}Co , ^{52}Fe were transported to the gas catcher. The range of the reaction products was tuned using a tunable homogeneous degrader made of two optical quality (surface roughness below 10 nm) SiO_2 opposing wedges on linear drives while the recoil energy spread was minimized using two wedge degraders of similar quality on rotating stages so that the effective wedge angle could be changed. The recoils were detected and uniquely identified by the MUSIC transmission detectors before entering the gas catcher so that the incoming ion flux could be measured precisely. The recoils go through air before entering the gas catcher (and the MUSIC detector internal pressure varies with atmospheric pressure) so that the degrader thickness had to be adjusted to correct for atmospheric pressure variations.

Available diagnostics besides the FRS detectors were a silicon detector and a time-of-flight mass spectrometer located on two beamlines after the gas catcher's RFQ extraction and switchyard sections. The gas catcher itself could also be used as an ionization chamber by

either rewiring the electrodes or looking at the ion flux through the time-of-flight detector so that the ionization created by the radioactive ions inside the device could be determined. This proved particularly useful for the initial determination of the correct thickness of degrader required.

In Fig. III-44 below is plotted the ionization created by the recoils in the gas catcher as a function of the thickness of the tunable degrader. The first peak in ionization is the Bragg peak of the ^{56}Ni ions stopping inside the gas catcher. As the degrader thickness is increased, the Bragg peak of the stopping ^{54}Co ions is visible. A third weaker peak at even higher thickness corresponds to stopping ^{52}Fe isotopes. The corresponding Fig. III-45 shows the measured beta activity extracted from the gas catcher and transported to the silicon detector also as a function of degrader thickness. The first Bragg peak does not show an increase in activity since the lifetime of ^{56}Ni is long, but the activity of the short-lived ^{54}Co and ^{52}Fe isotopes is clearly visible at the range corresponding to the Bragg peaks (stopping inside the gas catcher) for these species.

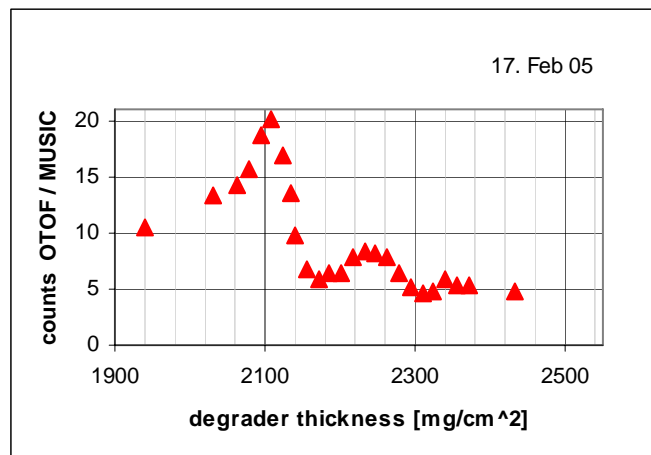


Fig. III-44. Ionization in the gas catcher (normalized to the number of radioactive ions entering the gas catcher) as a function of the degrader thickness. The peak at 2.1 g/cm^2 corresponds to the Bragg peak of ^{56}Ni while the second peak at 2.27 g/cm^2 corresponds to ^{54}Co .

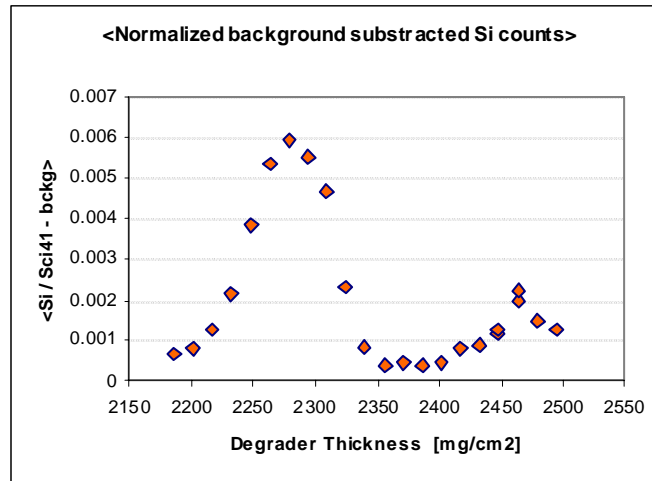


Fig. III-45. Beta activity extracted from the gas catcher and transported to the silicon detector, measured as a function of the degrader thickness. The first peak at 2.27 g/cm² corresponds to ⁵⁴Co isotopes while the second peak corresponds to ⁵²Fe.

The measured activity extracted from the gas catcher can be compared to the initial number of radioactive ions of the same species stopped inside the gas catcher. Taking into account the stopping fraction determined from the Bragg curve and the known RFQ transport and silicon detector efficiencies, we obtain a preliminary efficiency of $(40 \pm 10) \%$ for the gas catcher (ratio of ions extracted as beam to those stopped in the gas catcher). The mean extraction time for the radioactive ions could not be measured directly in this first experiment at GSI but decay curves of the activity extracted when ⁵⁴Co was stopped in the cell were obtained as shown in Fig. III-46. These decay curves clearly confirm the extraction and transfer of the short-lived isomer of ⁵⁴Co from the gas catcher in a ratio with

respect to the longer-lived ground state consistent with the relative production rates. This indicates a mean extraction time much shorter than the 200 ms lifetime, consistent with the 40 ms extraction time measured on-line with pulsed beams at ATLAS using the same gas catcher.

This first run at RIA type energy demonstrated that the device works under these conditions just as well as it did at lower energies. A second run at the FRS, with the gas catcher small vacuum leak fixed, the device baked to higher temperature, and more complete diagnostics such as a time-gated transfer to correlate directly activity with mass such as was done at ATLAS, would be desirable and is planned.

*GSI, Darmstadt, Germany, †Texas A&M University, ‡University of Manitoba, Winnipeg, Manitoba, §Justus-Liebig University, Giessen, Germany, ¶Katholieke Universiteit Leuven, Belgium, |Michigan State University.

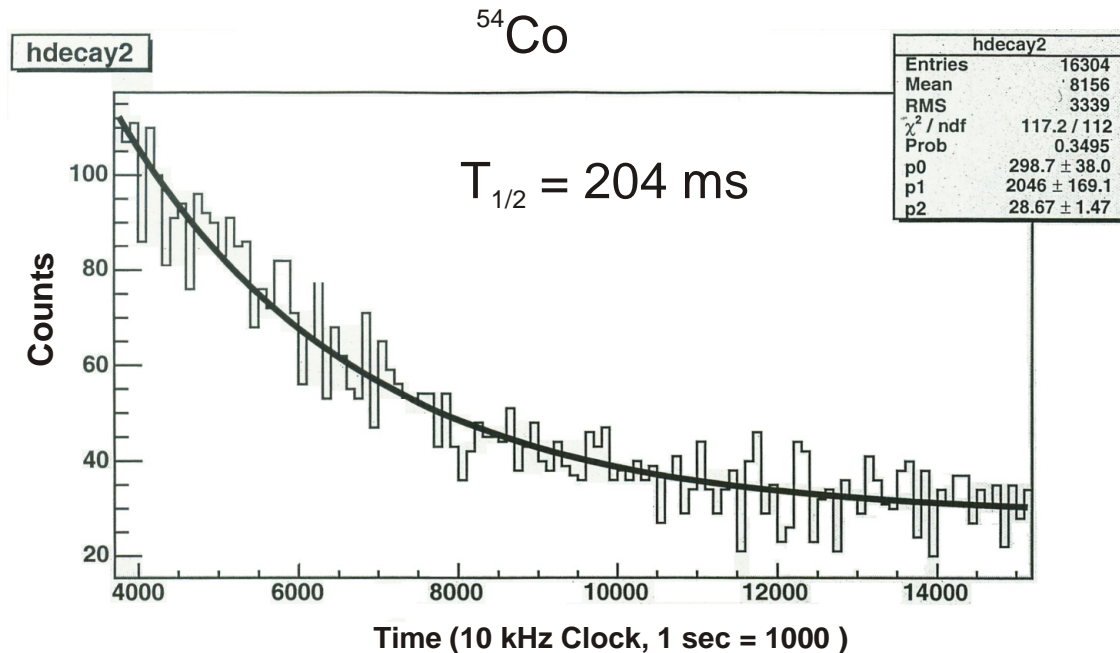


Fig. III-46. Histogram of the decay of the activity extracted from the gas catcher and transported to the detector when the degrader thickness is tuned to the Bragg peak of ^{54}Co isotopes (stopping ^{54}Co into the gas catcher).

c.6. Preparation for the High Intensity RIA Gas Catcher Test at ATLAS (G. Savard, S. Gerbick, J. P. Greene, A. Levand, N. Scielzo, M. Sternberg, B. J. Zabransky, J. Clark,* and K. S. Sharma*)

The remaining technical question that can have the maximum impact on the estimated RIA yields is the uncertainty in the maximum ion beam intensity the gas catcher can tolerate. The RIA yields were calculated assuming the gas catcher could operate at 20% efficiency with up to 10^9 ions per second entering it. In the tests of the RIA gas catcher prototype, we have operated it at about twice that efficiency with up to 5×10^5 ions per second, the maximum we could obtain under controllable conditions in the initial tests at ATLAS and subsequently in the first high-energy test at GSI. While this is already sufficient for the most exotic isotopes at RIA, the over 3 orders of magnitude higher ionization rate expected in the more abundant production region is an enormous uncertainty if operation in these conditions cannot be demonstrated. Testing operation in this regime requires a beam with properties similar to those expected behind the fragment separator at RIA and some modifications to the gas catcher to obtain stable operation in that regime. Both have been undertaken in preparation for a RIA like ionization density test at ATLAS at the end of FY2006.

The preparation has involved three main components: development of realistic simulations of space-charge build up in the gas catcher, development of a suitable source of ionization and diagnostics, and completion of the second gas catcher prototype that will be used for these tests.

The first task was the development of proper simulations of the space-charge effect. Over the years we have developed simulations of the gas catcher incorporating gas flow, static and RF fields and a realistic modeling of the ion/gas atom collisions. These state-of-the-art calculations reproduce the main features observed so far in the low-energy tests of the gas catcher at low intensity. They however do not take into account the interaction between ions in the gas. This task is actually enormously complicated since each ion stopping in the gas creates 10^5 to 10^6 helium ion-electron pairs which also interact with the stopped incoming ions and with each other and must all be transported by the program in a fashion similar to the initial ions. Treating this problem exactly is actually computationally intractable since dealing with even a single incoming ion, which would generate close to a million helium ions, would require accounting for close

to 10^{12} pairwise interactions at each of the typically 10^7 steps of the Runge-Kutta program. It is however possible to obtain a realistic rendition of the effect using the fact that the ion density is high enough that a bulk representation of the field distribution generated by this ion cloud would be sufficient. We therefore developed a Monte-Carlo program to create the initial ion stopping distribution and generate a representative helium ion cloud along each initial ion path to simulate the ionization created by the stopping. These ions are then transported by our standard gas catcher simulation program. By keeping track of the ions along their paths we can construct a time-averaged ion distribution inside the gas catcher. This ion distribution is then inserted into the proper boundary conditions and the Poisson

equation solved to obtain the electrostatic field distortion created by the ion distribution. This field distortion is then added to the DC and RF fields of the non-perturbed simulations and the initial ion clouds transported under these new conditions. Repeating the procedure a number of times leads to a self-consistent solution that properly accounts for the field distortion created by the ion stopping distribution. The validity of this approach was tested in simplified cases that can be treated exactly and with simulations of the $1/4$ scale RIA gas catcher prototype (see Fig. III-47). These calculations agree with the exact solutions in the simplified cases and yield general agreement with our experience with the $1/4$ scale prototype.

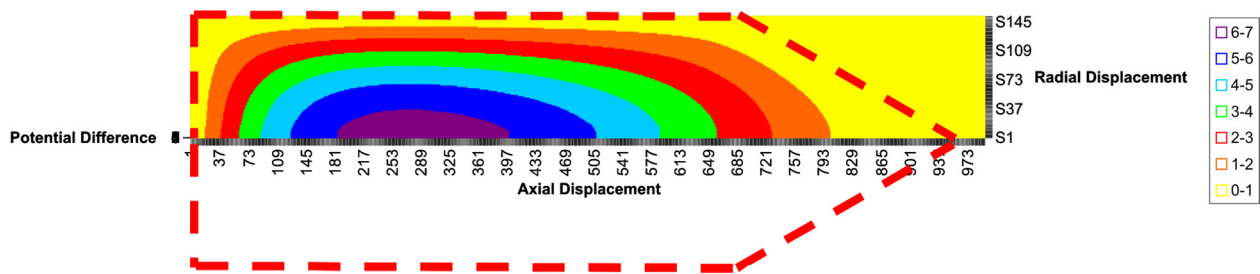


Fig. III-47. Potential perturbation created by 2.5×10^5 Cs ions stopping homogeneously in the $1/4$ scale RIA gas catcher prototype. The resulting ion density creates a potential distortion of almost 7 volts close to the center of the gas catcher. This distortion slows down the extraction of ions stopped close to the window and exerts a diverging radial force that must be compensated to ensure that ions created off axis get to the RF cone and the extraction nozzle.

These calculations are used to guide our setting up of the high-intensity test and will be crucial in our analysis of the results. Simulations of the large gas catcher system indicate that the initial distribution of ionization can strongly influence the transmission at a given ion implantation rate. That might make the gas catcher system much more difficult to tune in cases of high intensity operation. At low intensity, we essentially have one common mode of operation for all radioactive ions implanted above mass 50 or so. For lighter species the RF focusing force decreases slowly and operating parameters are readjusted accordingly. For high intensity operation, the results of our simulations indicate a much more complex interplay between the different forces present. They also indicate that an additional complication sets in since depending on the

purity of the gas, part of the ionized helium will transfer charge to impurities in the gas and that these impurities have different transport properties in the gas catcher and will change the averaged charge distribution and hence the distortion of the field by the space charge. The simulations are extremely time consuming, one iteration of one configuration takes over a day for a representative sample of ionization, convergence on one configuration at one ionization rate takes over a week, and any change means restarting anew. We have been running the code extensively to define operating conditions that must be obeyed and get an estimate of how much more sensitive to contamination the device will be in high intensity mode. These results have consequences that are being implemented in the two following tasks.

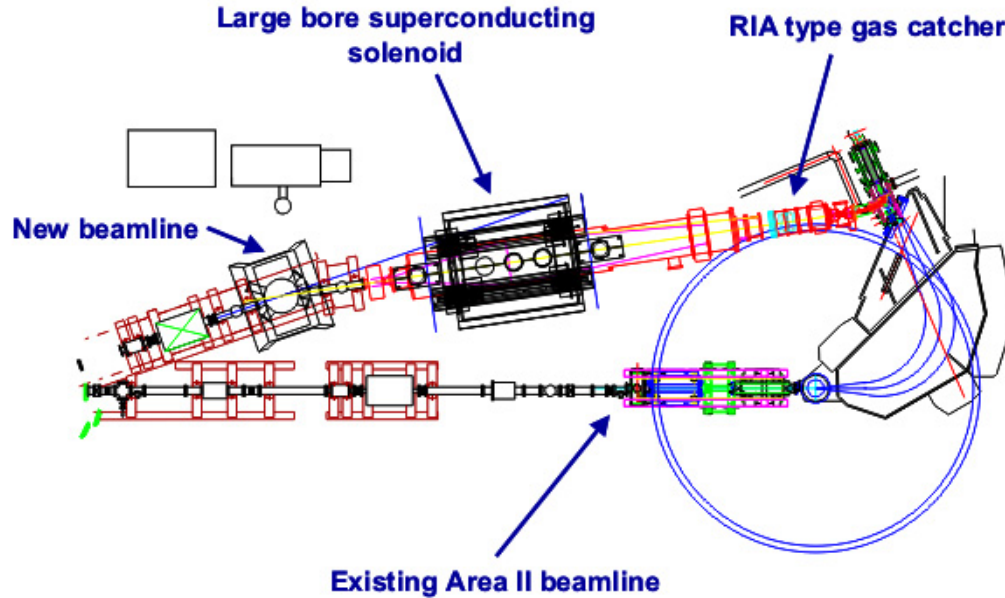


Fig. III-48. Proposed layout of the high intensity gas catcher setup to be located in experimental area II of the ATLAS superconducting linac.

The second task deals with the creation of the ionization density in the gas catcher and of specific activities to diagnose transport efficiency and delay time in the high intensity tests. The simulations indicate that an ionization pattern similar to that expected at RIA is required and that delay time measurements provide important diagnostics at the onset of saturation. Creating the ionization required in a roughly uniform manner over a 20 cm diameter spot and a meter or so length cannot be easily accomplished with existing beam transport systems at ATLAS. A solution requiring a large solenoid was however identified. Such a solenoid was being surplused at the University of Manitoba and was given to us free of charge. In addition, various large aperture elements were obtained from previous experiments at the Dynamitron at Argonne. Optical calculations were performed to find conditions under which the required quasi-homogeneous illumination of the gas catcher from secondary products at the required intensity levels could be obtained. The primary beam intensity that can be delivered by ATLAS to area II is sufficient and the

high-intensity rotating target developed for the CPT will be used for these tests. The scheme requires a total distance of 4 to 5 meters between the target and gas catcher and a beam stop after the target to remove the concentrated primary beam below 3 degrees scattering angle. This can be accommodated in area II. The large momentum acceptance of this transport system yields a range profile similar to that of the monochromatized fragmentation products but with an aerial distribution, mass distribution and overall intensity that no fragmentation facility can provide at present. The transport system (shown schematically in Fig. III-48) will provide the required ionization density and yield overall efficiency versus ionization information for various mass ranges. Status of this second task is that the ion optics calculations are completed, the support structure for the beamline was constructed and installed, and the superconducting solenoid and related equipment have now been installed on the support structure in area II (see Fig. III-49). The beamline is under construction.



Fig. III-49. The large 65 cm bore 1.5 T superconducting solenoid inside its passive iron shield installed in location on its support structure in experimental area II.

The third and remaining task in preparation for the high intensity gas catcher test has to do with the actual gas catcher. We have been assembling the second gas catcher prototype with the spare components remaining after the first prototype left for GSI. New electronic circuits feeding the DC and RF voltages have been put together and connected to the system. We also worked on improving the RF distribution on the system which was not ideal in the initial gas catcher. A new balanced circuit reduces RF noise from the cone region. Also, detailed amplitude matching of the 278 electrodes on the cone is difficult since standard measurement devices were affected by RF pickup and amplitudes measured depended at the 20% level or so on the inductance created by the path of the probe wires. We developed a new probe that takes its ground essentially at the measurement point and rectifies the RF signal at that point so that a DC signal proportional to the RF amplitude (but insensitive to RF pickup) is measured. With this we were able to achieve a more homogeneous RF amplitude distribution (variations now below 10%) on the new cone but we are still trying to improve this figure and plan to implement the same tuning on the gas catcher currently at GSI). A new movable platform and high voltage cage were constructed and the new catcher was installed in area II. A new bent RFQ was designed so that the system can be connected to the CPT diagnostics system which will allow much better identification of the extracted activities than was possible in the earlier tests of the large gas catcher. Machining of the components of this transfer line and

assembly is completed. Installation will take place in the remainder of FY2006. The simulations indicate that we will be more sensitive to contamination at higher intensity and we decided that not only diagnostics needed to be improved but also active steps needed to be taken to reach optimum conditions. The pumping system was improved with the addition of a dry screw-type backing pump that replaces a large roots blower. The pumping speed is not affected and the system will be much cleaner. Further cleanliness improvements are being investigated in particular with the possible use of a different approach to seal the large insulating rings in the gas catcher using techniques developed for the AGS at BNL. This modification could be retrofitted to the system and would remove the present 80 C limitation on heating temperature and make the system more sturdy overall. The existing gas purification system available in area II will feed gas to the high-intensity gas catcher. The required modifications to this system are in the design stage. In addition, the simulations indicate that the weak RF focusing along the body of the gas catcher needs to be strengthened for high intensity operation to defeat the space charge repulsion. This is being implemented by modifying the electrode structure on the gas catcher body (the cone will not be affected by this change).

The overall preparation for this full RIA-intensity gas catcher test is moving on schedule and we expect first on-line tests by the end of FY2006.

IV. MEDIUM-ENERGY NUCLEAR PHYSICS RESEARCH

OVERVIEW

The overall goals of the Medium-Energy Physics research program in the Argonne Physics Division are to test our understanding of the structure of hadrons and provide tests of the Standard Model. In addition, we develop and exploit new technologies for high-impact applications in nuclear physics as well as other national priorities. In order to test our understanding of the structure of hadrons and the structure of nuclei within the framework of quantum chromodynamics, the medium-energy research program emphasizes the study of nucleons and nuclei on a relatively short distance scale. Because the electromagnetic interaction provides an accurate, well-understood probe of these phenomena, primary emphasis is placed on experiments involving electron scattering, real photons and Drell-Yan processes. The electron beams of the Thomas Jefferson National Accelerator Facility (JLab) are ideally suited for studies of nuclei at hadronic scales and represent one center of the experimental program. Staff members led in the construction of experimental facilities, served as spokespersons or co-spokespersons for 19 experiments and were actively involved in others. The group constructed the general-purpose Short Orbit Spectrometer (SOS) which forms half of the coincidence spectrometer pair that is the base experimental equipment in Hall C. Argonne led the first experiment to be carried out at JLab in Fiscal Year 1996 and has completed 15 other experiments. We have continued to develop the optical trap program and have applied this new technique to the study of neutron-rich light nuclei and began the search for a non-zero electric dipole momentum in a nucleus.

Recently, staff members have focused increasingly on studies of the nucleon and the search for exotic phenomena. A study of the constraints on two-photon exchange effects from the world's data on electron and positron scattering was performed. In the past year, preliminary analyses were completed for the search for pentaquark partners, for polarization in deuteron photodisintegration, for the EMC effect in light nuclei, and for transparency in ρ electroproduction in nuclei.

The HERMES experiment in the HERA electron ring at DESY-Hamburg has two novel features: (1) polarized electron scattering from internal polarized or

unpolarized atomic gas targets, and (2) a dual-radiator ring imaging Cerenkov counter (RICH). Deep inelastic scattering has been measured with polarized electrons on polarized hydrogen, deuterium and ^3He . Argonne has concentrated on the hadron particle identification of HERMES, a unique capability compared to other spin structure experiments. In 1999 and under Argonne leadership, the RICH was brought into operation at the design specifications to provide complete hadron identification in the experiment. The RICH has been operating routinely since its installation. This has allowed HERMES to make decisive measurements of the flavor dependence of the spin distributions. Last year, HERMES met one of its principal objectives by providing a direct measurement of the strange quark helicity distribution. HERMES has also provided the first information for the Sivers and Collins effects. During the past year, HERMES installed a proton recoil detector and plans a year-long run on unpolarized targets. These results are expected to provide new and significant data for deeply virtual Compton scattering as well as accurate d/u ratios in the valence region.


Measurements of high mass virtual photon production in high-energy proton-induced reactions have determined the flavor dependence of the sea of antiquarks in the nucleon. These measurements gave insight into the origin of the nucleon sea. In the same experiment, the high-x absolute Drell-Yan cross sections were measured. Work is underway to extract the angular distribution of the Drell-Yan process in free proton-proton scattering. In Fiscal Year 2001, a new initiative was approved by the FNAL PAC to continue these measurements with much higher luminosity at the FNAL Main Injector. These Drell-Yan experiments not only provide the best means to measure anti-quark distributions in the nucleon and nuclei, but represent an outstanding opportunity to perform these measurements at an ideal proton beam energy of 120 GeV. Plans are underway to prepare this experiment at FNAL.

The technology of laser atom traps provides a unique environment for the study of nuclear and atomic systems and represents a powerful new method that is opening up exciting new opportunities in a variety of fields, including nuclear physics. In particular, the group has developed a high-efficiency, high-sensitivity magneto-optical trap for rare, unstable isotopes of krypton. In 2004, a highlight was the optical trapping of single atoms of ^6He and performing precision laser spectroscopy on the individual atoms to determine the nuclear charge radius of ^6He nuclei. Our proposal to measure the charge radius for ^8He was approved at GANIL. During the past year, we have improved the helium atom trap for the ^8He experiment.

A new initiative to search for an electric dipole moment (EDM) of ^{225}Ra is in progress. The ultimate goal is to search for a non-zero EDM for ^{225}Ra and improve the sensitivity for nuclear EDM searches by approximately two orders of magnitude. This test of time-reversal symmetry represents an outstanding opportunity to search for new physics beyond the Standard Model. During the

past year, radium atoms were optically trapped for the first time. In addition, several key atomic properties of radium isotopes were also measured.

A new experiment to measure parity violation in deep inelastic scattering from the deuteron was approved by the JLab PAC. The ultimate goal of this experiment is to provide the best possible measurement for the neutral current axial vector coupling to the quarks.



A. HADRON PROPERTIES

a.1. The Charged Pion Form Factor (J. Arrington, R. J. Holt, P. E. Reimer, E. C. Schulte, X. Zheng, and the JLab E01-004 Collaboration)

A complete understanding of the structure of the nucleon is the defining problem in QCD. However, while experiments on the proton are relatively easy, the complicated structure of a three light-quark system makes modeling of the proton in realistic, QCD-based models, difficult. The pion structure is simpler, and can in some cases provide a better meeting ground between theory and experiment in the study of QCD. Experiment E01-004 is an extension to the previous JLab measurement¹ of the pion form factor, and will improve measurements of the form factor at 1.6 GeV²,

the highest value at which the form factor has been measured, as well as extend measurements to 2.5 GeV². Preliminary results are shown in Fig. IV-1. These measurements can be used to test models of hadron structure in a simpler system than the nucleon, where more advanced calculations can be performed. The form factor provides information on spatial distribution of the pion constituents, complementary to the information on the quark momentum distributions from the pion structure function measurements.

¹J. Volmer *et al.*, Phys. Rev. Lett. **86**, 1713 (2001).

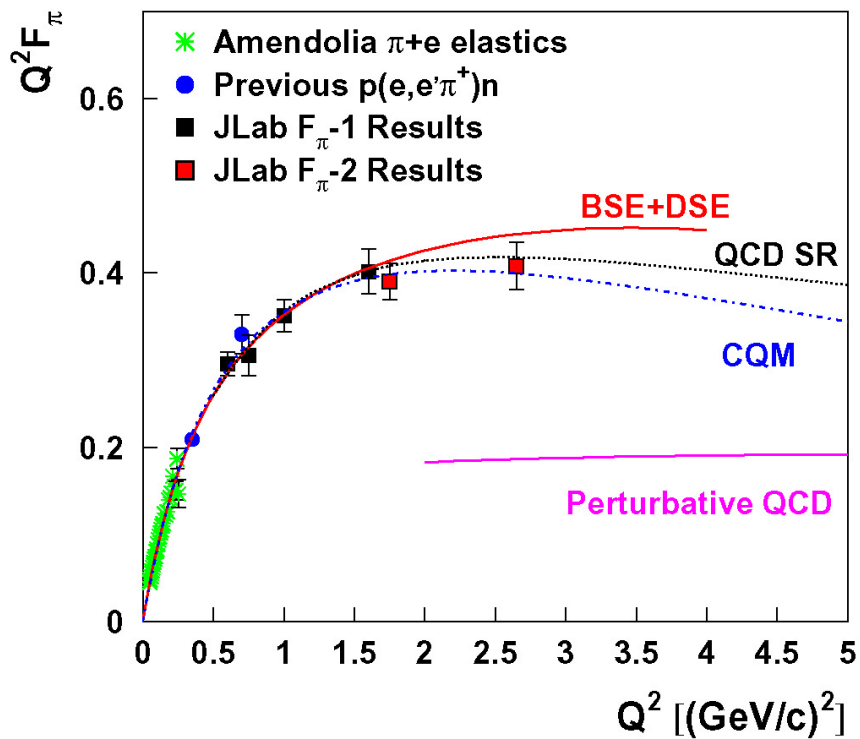


Fig. IV-1. Preliminary results for the pion form factor from E01-004 (red), along with previous world's data.

a.2. Precision Measurements the Proton Electromagnetic Form Factors and Two-Photon Exchange Effects (J. Arrington, R. Beams, K. Hafidi, R. J. Holt, I. A. Qattan, E. C. Schulte, K. Wijesooriya, X. Zheng, B. Zeidman, and the JLab E01-001 Collaboration)

Jefferson Lab Experiment E01-001 used a modified experimental technique to perform an extremely high precision Rosenbluth extraction of the proton electromagnetic form factor ratio, G_{Ep}/G_{Mp} . By detecting the struck proton rather than the scattered electron, the experiment dramatically improved the uncertainties compared to previous measurements.¹ These results convinced the community that there was a real discrepancy between Rosenbluth and polarization transfer measurements that is now attributed to two-photon exchange corrections.

E01-001 has provided significant information on the nature of the two-photon exchange corrections necessary to explain the discrepancy. While two-photon exchange corrections can introduce non-linearities in the ϵ -dependence of the Rosenbluth plot, these data show that any such nonlinearities are very small.² In addition, the data allow us to test the range of Q^2 over which calculations of two-photon exchange explain the discrepancy in a hadronic model. Recent calculations,³ including only the unexcited intermediate state, are nearly sufficient to resolve the discrepancy at the lowest Q^2 value of the measurement (2.6 GeV^2), but can explain only half of the discrepancy at 4.1 GeV^2 . A careful evaluation of this calculation and extraction of the proton form factors applying the calculated TPE corrections is underway.⁴

These results also led to a careful re-examination of previous searches for two-photon exchange effects in comparisons of positron-proton and electron-proton scattering. These data provide evidence for two-photon exchange corrections,⁵ and we have two new experiments that will make improved comparisons of positron-proton and electron-proton scattering.⁶

By combining the existing constraints from positron measurements with the observed discrepancy between Rosenbluth and polarization transfer measurements, we have extracted two-photon exchange amplitudes that can explain all of the data,⁷ under the assumption that these amplitudes are independent of scattering angle. Figure IV-2 shows the size of the correction to G_{Mp} based on this analysis. The correction is three to four times larger than the experimental uncertainties over a large portion of the Q^2 range, meaning that the TPE corrections to G_{Mp} cannot be neglected. The cyan band indicates the uncertainty, which for G_{Mp} is dominated by the large uncertainties in the Rosenbluth data, which make it difficult to extract the size of the TPE correction necessary to simultaneously describe the Rosenbluth and polarization data. There is an additional model dependence related to the assumption that the amplitude is independent of scattering angle. This is less important for G_{Mp} , but yields the largest uncertainty on the correction to the polarization transfer measurements of G_{Ep} and G_{Mp} . We have proposed additional measurements that will reduce both of these uncertainties.

The demonstration of the improved technique in E01-001 has led to a follow-up experiment to extend the Q^2 and ϵ range of these high precision Rosenbluth measurements.⁸ These measurements, combined with the new positron-proton scattering measurements, will provide constraints on the two-photon exchange corrections, allowing a reliable extraction of the proton form factors. Precise knowledge of the proton electromagnetic form factors, especially at low Q^2 , is needed as input in the analysis of quasielastic neutrino-nucleons scattering and high-precision $A(e,e'p)$ measurements of nuclear structure.⁹

¹I. A. Qattan *et al.*, Phys. Rev. Lett. **94**, 142301 (2005).

²V. Tvaskis, J. Arrington, M. E. Christy, R. Ent, C. E. Keppel, Y. Liang, and G. Vittorini, Phys. Rev. C **73**, 025206 (2006).

³P. G. Blunden, W. Melnitchouk, and J. A. Tjon, Phys. Rev. Lett. **91**, 142304 (2003).

⁴J. Arrington and W. Melnitchouk, in progress.

⁵J. Arrington, Phys. Rev. C **69**, 032201(R) (2004).

⁶J. Arrington, D. M. Nikolenko *et al.*, nucl-ex/0408020; JLab experiment E06-116, "Beyond the Born Approximation: A Precise Comparison of Positron-Proton and Electron-Proton Elastic Scattering in CLAS," A. Afanasev, J. Arrington, W. K. Brooks, K. Joo, B. A. Raue, and L. B. Weinstein, spokespersons.

⁷J. Arrington, Phys. Rev. C **71**, 015202 (2005).

⁸JLab experiment E05-017, "A Measurement of Two-Photon Exchange in Unpolarized Elastic Electron-Proton Scattering," J. Arrington, spokesperson.

⁹J. Arrington, Phys. Rev. C **69**, 022201(R) (2004); H. Budd, A. Bodek, and J. Arrington, hep-ex/0308005; D. Dutta *et al.*, Phys. Rev. C **68**, 064603 (2003).

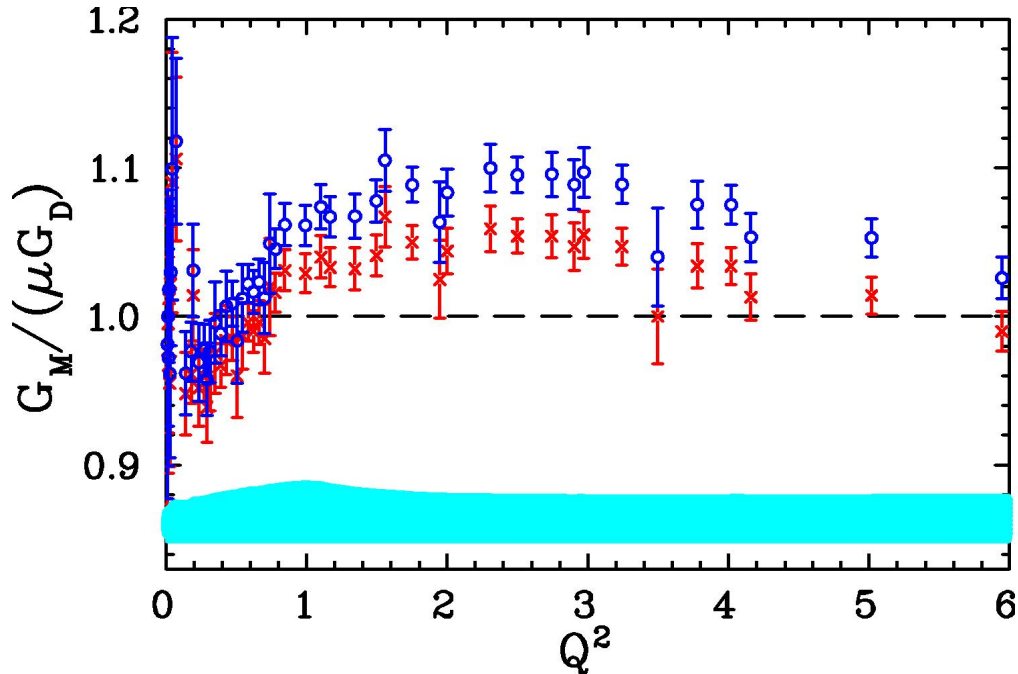


Fig. IV-2. The proton magnetic form factor as extracted in the Born approximation (red crosses) and after applying a correction for two-photon exchange based on a global analysis of electron, positron, and polarization transfer data (blue circles). The cyan band shows the estimated uncertainty in the two-photon exchange correction.

a.3. Parity Violating Electron-Proton Scattering and the Strangeness Content of the Nucleon (J. Arrington, K. Hafidi, P. E. Reimer, X. Zheng, and the JLab E99-115, E00-114, and E05-109 Collaborations)

Measurements of the electromagnetic proton and neutron form factors can be combined to separate the up and down quark contributions. Parity violating elastic scattering provides additional sensitivity to the strange quarks, allowing an extraction of the strange quark contributions to the electric and magnetic form factors.¹

In 2004, the HAPPEX collaboration made a high precision measurement of parity violating e - p scattering at $Q^2 = 0.1 \text{ GeV}^2$, as a measure of the strangeness contribution to the magnetic moment of the proton. In addition, elastic scattering from ^4He was measured, which provides a clean measure of the strangeness radius of the proton.¹ Preliminary results indicate that G_{Es} and G_{Ms} are smaller than previously believed at $Q^2 = 0.1 \text{ GeV}^2$. A proposal to extend these

measurements to higher precision at $Q^2 = 0.5 \text{ GeV}^2$ (E05-109) was approved.

Parity violating scattering is expected to be relatively insensitive to the effects of two-photon exchange.² However, the extraction of the strangeness form factors does rely on having precise knowledge of the proton and neutron electromagnetic form factors. An analysis of low- Q^2 nucleon form factors, including two-photon exchange effects from the calculation of Blunden *et al.*³ is currently underway.⁴ This will provide the input needed to make precise extractions of both neutron form factors and the strangeness contributions to the nucleon form factors. This will provide the foundation for a full flavor decomposition of the nucleon form factors into their contributions from up, down, and strange quarks.

¹D. H. Beck, Phys. Rev. D **39**, 3248 (1989); R. D. McKeown, Phys. Lett. **B219**, 140 (1989).

²A. Afanasev and C. E. Carlson, Phys. Rev. Lett. **94**, 212301 (2005).

³P. G. Blunden, W. Melnitchouk, and J. A. Tjon, Phys. Rev. Lett. **91**, 142304 (2003).

⁴J. Arrington and I. Sick, in progress.

a.4. $N \rightarrow \Delta$ Transition Form Factors (J. Arrington, K. Hafidi, R. J. Holt, P. E. Reimer, E. C. Schulte, X. Zheng, and the JLab E01-002 Collaboration)

Measurements of the nucleon transition form factors provide additional information on the structure of the nucleon and nucleon excitations, which complement the measurements of the nucleon elastic form factors. Experiment E01-002 was performed in the spring of 2003 and measured electroproduction of the $\Delta(1232)$ and $S_{11}(1535)$ baryon resonances. The experiment is an extension of previous, lower energy electroproduction experiments¹ at JLab, and at the higher momentum transfers achieved in this experiment we can probe the transition to the high-energy region where perturbative QCD is expected to describe the reaction. Data were taken to separate out the magnetic dipole (M1), electric dipole (E2), and Coulomb (C2) contributions to the $N \rightarrow \Delta$ transition. The data are currently under analysis, and preliminary cross sections and angular

distributions have been extracted for pion electroproduction in the Δ region, but without the final radiative corrections. In addition, preliminary cross sections for η production are nearly available.

These measurements will provide a stringent test of recent calculations, several of which have come from the Argonne theory group. T.-S. H. Lee has done extensive work on a dynamical model for pion electroproduction in the Δ region,² A. Krassnigg and C. D. Roberts are exploring the effects of axial-vector diquark and pion cloud contributions to the nucleon elastic and $N \rightarrow \Delta$ transition form factors,³ while F. Coester has performed similar explorations of relativistic effects in the elastic and transition form factors.⁴

¹V. Frolov *et al.*, Phys. Rev. Lett **82**, 45 (1999); C. S. Armstrong *et al.*, Phys. Rev. D **60**, 052004 (1999).

²T. Sato and T.-S. H. Lee, Phys. Rev. C **63**, 055201 (2001); T. Sato, T.-S. H. Lee, and T. Nakamura, Int. J. Mod. Phys. A **20**, 1668 (2005).

³R. Alkofer *et al.*, nucl-th/0412045 (2004).

⁴B. Julia-Diaz *et al.*, Phys. Rev. C **69**, 035212 (2004).

a.5. Separated and Unseparated Structure Functions in the Nucleon Resonance Region (J. Arrington, D. Gaskell, D. F. Geesaman, K. Hafidi, R. J. Holt, D. H. Potterveld, P. E. Reimer, E. C. Schulte, X. Zheng, and the E94-110, E00-002, E00-108, and E00-116 Collaborations)

High-energy inclusive electron scattering provides a clean and direct probe of the quark distributions in nucleons. At low energy, this simple picture of electron-quark scattering is not valid and the scattering is better understood in terms of resonance excitations and pion production. Measurements of the unpolarized F_2 structure function show a smooth transition between the deep inelastic regime of quasifree quark scattering to the resonance excitation regions, and on average, the resonance region structure function reproduces the deep inelastic limit^{1,2} when taken as a function of ξ . At large momentum transfer, ξ is equivalent to Bjorken- x and represents the momentum fraction of the struck quark. At lower momentum transfers, ξ takes into account

scaling violations due to the finite target mass. In addition the resonance region structure function shows a valence-like behavior² at very low ξ values, approaching zero as $\xi \rightarrow 0$.

A more recent experiment, E94-110, performed a Rosenbluth separation of both F_1 and F_2 in the resonance region. These data provided the first observation of duality in both the longitudinal and transverse channels for the proton. They also provided the first indication of significant longitudinal contributions to resonance electroproduction. Final results have been obtained for the L-T separation of both the resonance region structure function³ and the

elastic electron-proton cross sections.⁴ In 2003, three additional measurements were performed in Hall C to further investigate the nature of duality: E00-116, E02-002, and E00-108. Measurements of F_2 for both the proton and deuteron were extended to higher Q^2 values than in the initial investigations. Preliminary results are available from this analysis, and the results are expected to be final in the fall of 2006. Measurements of the separated structure functions, F_1 and F_2 , were performed at very low x and Q^2 , to

investigate in more detail the valence-like nature of the resonance region structure functions. These data are still under analysis. Finally, these measurements were extended beyond inclusive scattering, to determine if a similar duality is observed in semi-inclusive scattering, where a single high-momentum pion is tagged in the final state. The analysis of the semi-inclusive duality is completed (see Fig. IV-3), and the results should be submitted for publication in 2006.

¹E. D. Bloom and F. J. Gilman, Phys. Rev. Lett. **25**, 1140 (1970).

²I. Niculescu *et al.*, Phys. Rev. Lett. **85**, 1182 (2000); *ibid.*, **85**, 1186 (2000).

³M. E. Christy *et al.*, Phys. Rev. C **70**, 015206 (2004).

⁴Y. Liang *et al.*, nucl-ex/0410027 (2004).

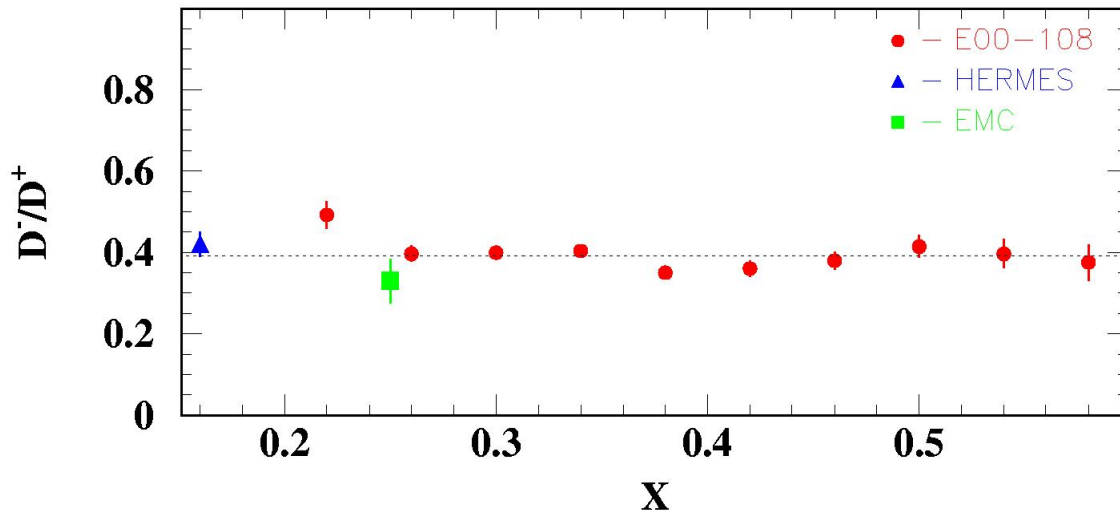


Fig. IV-3. Ratio of unfavored to favored fragmentation functions (extracted in leading order) as a function of x for $z = 0.55$. The JLab data, mostly in the resonance region, are independent of x , as expected if factorization holds.

a.6. Search for Additional Pentaquark States at JLab (P. E. Reimer, J. Arrington, K. Hafidi, E. C. Schulte, X. Zheng, and the E04-012 Collaboration)

All observed hadrons can be placed into two categories: mesons with valence quark-antiquark pair mesons ($\bar{q}q$) and baryons composed of three valence quarks (qqq). These are, however, not the only configurations of quarks and antiquarks allowed by the underlying theory, Quantum Chromodynamics and other configurations not fitting into the meson and baryon framework are known as “exotics”. One possible exotic configuration is the pentaquark state with four quarks and an antiquark ($qqqq\bar{q}$). Recently, experimental evidence and theoretical work have suggested the existence of a pentaquark state, known as

the Θ^+ with a mass near 1540 MeV. Within the Chiral Soliton model, the Θ^+ is a member of a set of 10 pentaquark states known as an antidecuplet. Using Hall A at JLab, E04-012¹ was able to search for evidence of an exotic isospin partner state, the Θ^{++} , in the $H(e,e'K^+)X$ reaction, as well as the Σ^0 member of the antidecuplet in the reaction $H(e,e'K^+)X$ and the N^0 member in the reaction $H(e,e'\pi^+)X$, by reconstructing the missing mass of the system. Although the Σ^0 and N^0 states are not explicitly exotic, the discovery of a narrow state would be a valuable confirmation of the existence of an antidecuplet of states. The experiment

used collected data in May and June 2004, using the HRS spectrometers to detect the scattered electron and the K^- , and K^+ and π^+ respectively. Preliminary results show no evidence for any narrow resonances within the candidate regions. The cross section upper limits, σ_{\max} ,

depend on the exact mass and width of the resonance. In the relevant mass regions and a maximum width of $\Gamma = 8$ MeV, preliminary results show $\sigma_{\max}(\Theta^{++}) < 5.5$ nb/sr, $\sigma_{\max}(\Sigma^0) < 18$ nb/sr and $\sigma_{\max}(N^0) < 10$ nb/sr.

¹J. P. Chen *et al.*, "High Resolution Study of the 1540 Exotic State," Proposal 04012 to the JLab PAC," P. E. Reimer and B. Wojtsekhowski, spokespersons, December 2, 2003.

B. HADRONS IN THE NUCLEAR MEDIUM

b.1. Measurement of the EMC Effect in Very Light Nuclei (J. Arrington, D. F. Geesaman, K. Hafidi, R. J. Holt, H. E. Jackson, D. H. Potterveld, P. E. Reimer, E. C. Schulte, X. Zheng, B. Zeidman, and the E03-103 Collaboration)

For more than twenty years, it has been known that the quark momentum distribution of nuclei is not simply the sum of the quark distributions of its constituent protons and neutrons. The structure function is suppressed in heavy nuclei at large values of x (corresponding to large quark momenta), and enhanced at lower x values. Measurements to date indicate that the overall form of this modification is the same for all nuclei, but the magnitude of the enhancement and suppression is larger for heavier nuclei. Many attempts have been made to explain the EMC effect, but none of the proposed models can fully reproduce the observed modifications, and there is still no consensus on which effect or combination explain the data.

Experiment E03-103¹ ran in Hall C in late 2004 and measured the EMC effect for ^3He , ^4He , and a series of heavier nuclei. Because ^4He has an anomalously large density for a light nucleus, it is the most sensitive test to determine if the EMC effect scales with A or with nuclear density. More importantly, these measurements of the EMC effect can be compared to exact few body calculations. If the EMC effect is caused by few

nucleon interactions, the universal shape observed in heavy nuclei may be a result of a saturation of the effect, and the shape may be different in few-body nuclei. While most existing data on heavy nuclei show the same x -dependence, there are hints of an A -dependence at large x values,² and calculations³ predict significantly different dependences for very light nuclei. By making precise measurements in light nuclei, we will be able to distinguish between different models of the EMC effect based on their predictions for few-body nuclei. Preliminary results for ^4He are shown in Fig. IV-4.

Finally, a measurement of $A \leq 4$ nuclei will help constrain models of the EMC effect in deuterium. Models of nuclear effects in deuterium and ^3He must be used to extract information on neutron structure, and a high precision measurement including ^1H , ^2H , ^3He , and ^4He will give a single set of data that can be used to evaluate these models in several light nuclei. This will help to quantify the model dependence of the neutron structure functions inferred from measurements on ^2H and ^3He .

¹JLab experiment E03-103, "A Precise Measurement of the Nuclear Dependence of the EMC Effect in Light Nuclei," J. Arrington and D. Gaskell, spokespersons.

²J. Arrington, R. Ent, C. E. Keppel, J. Mammei, and I. Niculescu, Phys. Rev. C **73**, 035205 (2006).

³G. I. Smirnov *et al.*, Eur. Phys. J. C **10**, 239 (1999); V. V. Burov *et al.*, Phys. Lett. **B466**, 1 (1999); I. R. Afnan *et al.*, Phys. Rev. C **68**, 035201 (2003); O. Benhar, private communication.

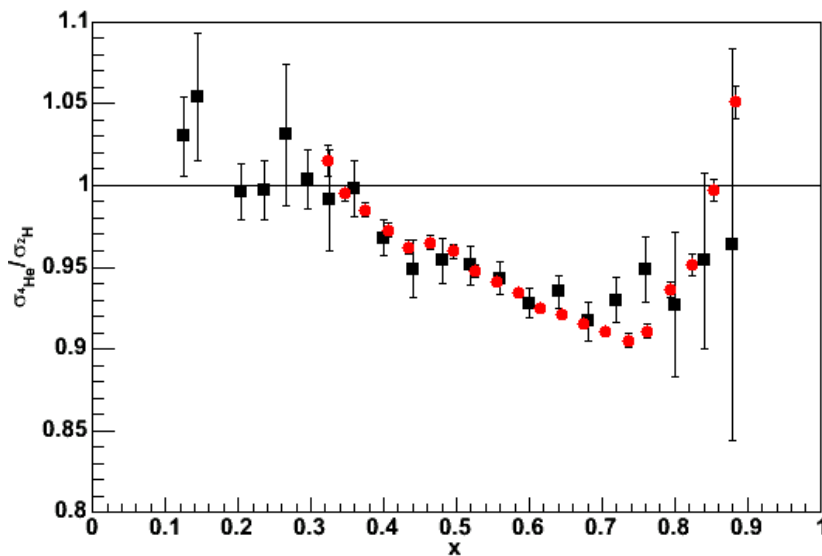


Fig. IV-4. Preliminary EMC ratio for ${}^4\text{He}$. Black points are previous data, red points are the E03-103 preliminary results showing only the statistical uncertainties.

b.2. Search for the Onset of Color Transparency: JLab E02-110 Experiment (K. Hafidi, B. Mustapha, J. Arrington, L. El Fassi, D. F. Geesaman, R. J. Holt, D. H. Potterveld, P. E. Reimer and Hall-B Collaboration)

According to QCD, point colorless systems, such as those produced in exclusive processes at high Q^2 have quite small transverse sizes. Therefore, they are expected to travel through nuclear matter experiencing very little attenuation. This phenomenon is known as Color Transparency (CT). An analogous mechanism is well known in QED: the interaction cross section of an electric dipole is proportional to its square size. As a result the cross section vanishes for objects with very small electric dipole moments. Since color in QCD is equivalent to the charge in QED, the cross section of a color-neutral dipole, as formed by a pair of oppositely colored quarks for instance, is also predicted to vanish for small sized hadrons. Color transparency cannot be explained by Glauber theory and calls upon quark degrees of freedom. Earlier measurements were mainly focused on quasi-elastic hadronic $(p, 2p)^1$ and leptonic $(e, e'p)^2$ scattering from nuclear targets. None of these experiments were able to produce evidence for CT up to $Q^2 \sim 8 \text{ GeV}^2$. The strongest evidence for CT so far comes from Fermilab experiment E791 on the A-dependence of coherent diffractive dissociation of 500 GeV/c pions into dijets.³ A recent measurement performed by the HERMES collaboration using exclusive ρ^0 electroproduction from nitrogen adds further evidence for the existence of CT.⁴

The main goal of E02-110 experiment⁵ is to search for the onset of CT in the incoherent diffractive ρ^0 electro and photoproduction on deuterium, carbon and copper. In this process (see Fig. IV-5), the virtual photon fluctuates into $q\bar{q}$ pair which travels through the nuclear medium evolving from its small initial state with a transverse size proportional to $1/Q$, to a "normal size" vector meson detected in the final state. Therefore, by increasing the value of Q^2 one can squeeze the size of the produced $q\bar{q}$ wave packet. The photon fluctuation can propagate over a distance which is known as the coherence length l_c . The coherence length can be estimated relying on the uncertainty principle and Lorentz time dilatation as $l_c = 2v/(Q^2 + M_{q\bar{q}}^2)$, where v is the energy of the virtual photon and $M_{q\bar{q}}$ is the mass of $q\bar{q}$ pair dominated by the ρ^0 mass in the case of the exclusive ρ^0 electroproduction. What is measured in the reaction is how transparent the nucleus appears to "small size" ρ^0 by taking the ratio of the nuclear per-nucleon (σ_A/A) to the free nucleon (σ_N) cross-sections, which is called nuclear transparency $T_A = \sigma_A/A\sigma_N$. Consequently, the signature of CT is an increase in the nuclear transparency T_A with increasing hardness (Q^2) of the reaction. Recent theoretical calculations by Kopeliovich *et al.*⁶ predicted an increase of more than

40% at $Q^2 \sim 4 \text{ GeV}^2$. However, one should be careful about other effects that can imitate this signal. Indeed, measurements by HERMES have shown that T_A increases when l_c varies from long to short compared to the size of the nucleus. This so-called coherence length effect can mock the signal of CT and should be under control to avoid confusing it with the CT effect. Therefore, experiment E02-110 intends to measure the Q^2 dependence of the transparency T_A at fixed coherence length l_c .

The experiment was performed using the CEBAF Large Acceptance Spectrometer (CLAS)⁷ in Hall B at Jefferson Lab. The data were taken with both 4 and 5 GeV electron beams incident on 2 cm liquid deuterium target and a solid target (0.4 mm thick ^{56}Fe and 1.72 mm thick ^{12}C) simultaneously to reduce systematic uncertainties. The run period was from December 2003 to March 2004. The data were recorded at an instantaneous luminosity of

$2 \times 10^{34} \text{ cm}^{-2} \text{ s}^{-1}$. The detectors calibration is completed and a new set of data (pass 1) is generated taking into account the new calibration constants. Much effort went into checking the data quality and determining the best requirements for good particle identification. Figure IV-6 shows $\Delta\beta = \beta_{\text{Meas}} - \beta_{\text{Cal}}$ as a function of particle momentum. β_{Meas} is measured using time of flight while β_{Cal} is calculated assuming the particle is a pion. In these measurements we are interested in the scattered electron and the two pions from the ρ^0 decay in the low t region below 0.5 GeV^2 . Figure IV-7 shows the normalized invariant mass of the two charged pions for hydrogen, deuterium and iron. A clean ρ^0 peak is obtained for the three targets. The Q^2 dependence of the pion absorption is found to be of the order of 7%. We are currently studying and modeling the background contributing to the ρ^0 peak which is mainly coming from Δ^{++} , Δ^0 and the non-resonant background. Preliminary results are expected soon.

¹A. S. Carroll *et al.*, Phys. Rev. Lett. **61**, 1698 (1988); Y. Mardor *et al.*, Phys. Rev. Lett. **81**, 5085 (1998);

A. Leksanov *et al.*, Phys. Rev. Lett. **87**, 212301 (2001).

²N. C. R. Makins *et al.*, Phys. Rev. Lett. **72**, 1986 (1994); T. G. O'Neill *et al.*, Phys. Lett. **B351**, 87 (1995);

D. Abbott *et al.*, Phys. Rev. Lett. **80**, 5072 (1998); K. Garrow *et al.*, Phys. Rev. C **66**, 044613 (2002).

³E. M. Aitala *et al.*, Phys. Rev. Lett. **86**, 4773 (2001).

⁴A. Airapetian *et al.*, Phys. Rev. Lett. **90**, 052501 (2003).

⁵JLab experiment E02-110, " Q^2 Dependence of Nuclear Transparency for Incoherent ρ^0 Electroproduction," K. Hafidi, B. Mustapha, and M. Holtrop, spokespersons.

⁶B. Kopeliovich *et al.*, Phys. Rev. C **65**, 035201 (2002).

⁷B. Mecking *et al.*, Nucl. Instrum. Methods **A503**, 513 (2003).

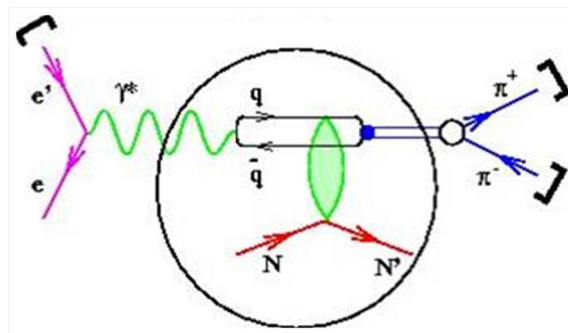


Fig. IV-5. Exclusive lepton production of the ρ^0 meson.

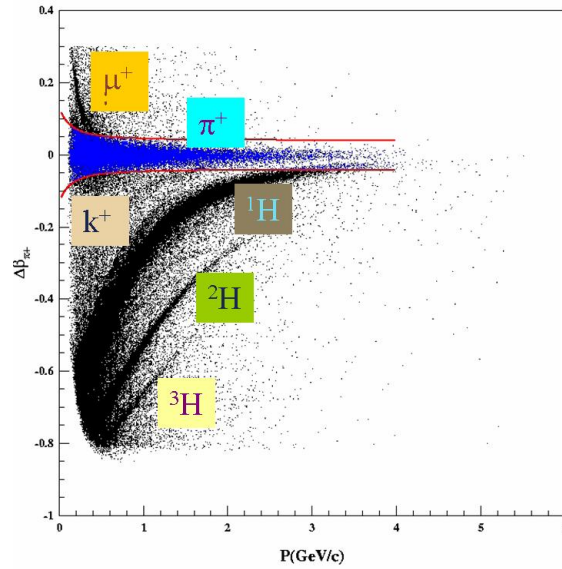


Fig. IV-6. $\Delta\beta$ for π^+ as a function of the particle momentum.

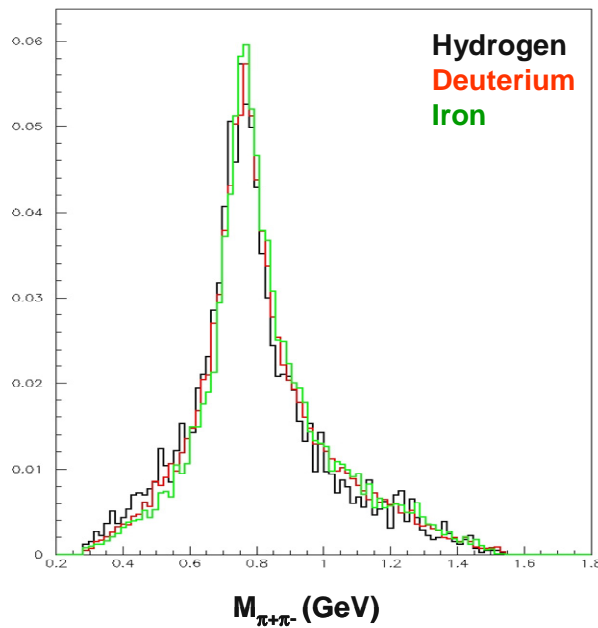


Fig. IV-7. Normalized $\pi^+\pi^-$ invariant mass for ^1H , ^2H and ^{56}Fe targets.

b.3. Search for Color Transparency in Pion Electroproduction (J. Arrington, L. El Fassi, X. Zheng, and the E01-107 Collaboration)

Argonne also participated in an experiment to search for color transparency in pion electroproduction. Measurements were made for the $A(e,e'\pi)$ reaction from ^2H , ^{12}C , ^{63}Cu , and ^{197}Au over a range in Q^2 . As

with production of vector mesons, color transparency is expected to set in at lower Q^2 than in the case of $A(e,e'p)$ measurements, and there is some hint of color transparency in pion photoproduction.¹

Experiment E01-107 was performed at Jefferson Lab Hall C in late 2004. The experiment measured the exclusive electroproduction of pions from nuclei by detecting the scattered electron and the knocked out pions in coincidence. The nuclear transparency is extracted by comparing the pion production from heavy nuclei to that from deuterium. The analysis of the data

is underway and preliminary results look promising. Figure IV-8 shows the ratio of the pion electroproduction from carbon, normalized by a PWIA calculation, relative to the production from deuterium, also normalized to the PWIA expectation. The final results are expected to be available by the end of the calendar year.

¹D. Dutta *et al.*, Phys. Rev. C **68**, 021001 (2003).

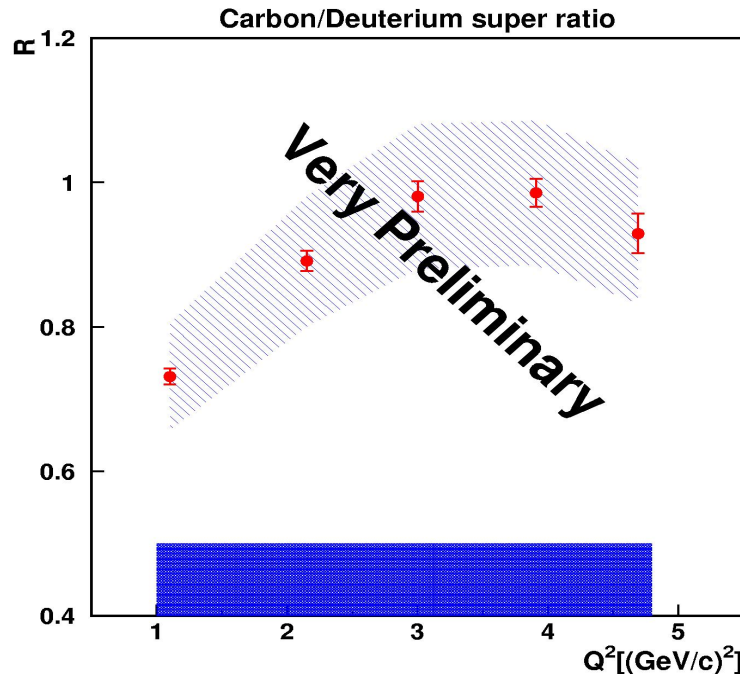


Fig. IV-8. The super-ratio of data to simulation for carbon vs deuterium as a function of momentum transfer squared. The blue band corresponds to the present estimate of the systematic uncertainty.

b.4. Measurement of High Momentum Nucleons in Nuclei and Short Range Correlations

(J. Arrington, D. F. Geesaman, K. Hafidi, R. J. Holt, H. E. Jackson, P. E. Reimer, E. C. Schulte, X. Zheng, and the E02-019 Collaboration)

Inclusive scattering from nuclei at low energy transfer (corresponding to $x > 1$) is dominated by quasielastic scattering from nucleons in the nucleus. As the energy transfer decreases, the scattering probes nucleons of increasing momentum allowing us to map out the distribution of high momentum nucleons. These data can be used to constrain the high momentum components of nuclear spectral functions,¹ probing nucleons in excess of 1000 MeV/c even for deuterium. Because the high momentum nucleons are dominantly generated by short-range correlations (SRCs), these

data allow us to examine the strength of two-nucleon and multi-nucleon correlations in heavy nuclei.

Experiment² E02-019 ran in late 2004 and measured inclusive scattering at large Q^2 over a broad range in x (up to $x = 3$). The high Q^2 values in this experiment should simplify the extraction of the high momentum components, because effects such as final state interactions are reduced at large Q^2 . The measurement focused on ²H, ³He, and ⁴He, but data were also taken on several heavier nuclei. Measurements with few-body nuclei allow contact with theoretical calculations

via essentially "exact" calculations for few-body systems (see Fig. IV-9). This can be used to study in detail contributions to the interaction beyond the impulse approximation (*e.g.*, final state interactions for scattering from correlated nucleons). Data on heavy nuclei can then be used to constrain the high momentum components of their spectral functions, as well as allowing an extrapolation to infinite nuclear matter.

Direct comparisons of heavy nuclei to deuterium at large x will allow us to map out the strength of two-nucleon correlations in both light and heavy nuclei. These data are expected to be significantly more sensitive to the presence of multi-nucleon correlations.

Just as the ratio of heavy nuclei to deuterium at $x \geq 1.5$ shows that the distribution in heavy nuclei is dominated by two-nucleon correlations, similar ratios of heavy nuclei to ${}^3\text{He}$ at $x \geq 2.5$ provide a measure of the strength of three-nucleon correlations.

In addition to probing nucleon distributions and short-range correlations, these data fill in a significant void in our knowledge of nuclear structure functions. Data at large x are important in the study of scaling and duality in nuclei,³ higher twist effects,⁴ and nuclear dependence of the structure function.^{3,5} In addition, the structure function at $x > 1$ must be included in studies of the energy-momentum sum rule and analysis of the QCD moments.⁵

¹J. Arrington *et al.*, Phys. Rev. Lett. **82**, 2056 (1999).

²JLab experiment E02-019, "Inclusive Scattering from Nuclei at $x > 1$ and High Q^2 with a 6 GeV Beam," J. Arrington, D. B. Day, A. F. Lung, and B. W. Filippone, spokespersons.

³J. Arrington, R. Ent, C. E. Keppel, J. Mammei, and I. Niculescu, Phys. Rev. C **73**, 035205 (2006).

⁴I. Niculescu, C. Keppel, S. Liuti, and G. Niculescu, Phys. Rev. D **60**, 094001 (1999).

⁵I. Niculescu, J. Arrington, R. Ent, and C. E. Keppel, Phys. Rev. C **73**, 045206 (2006).

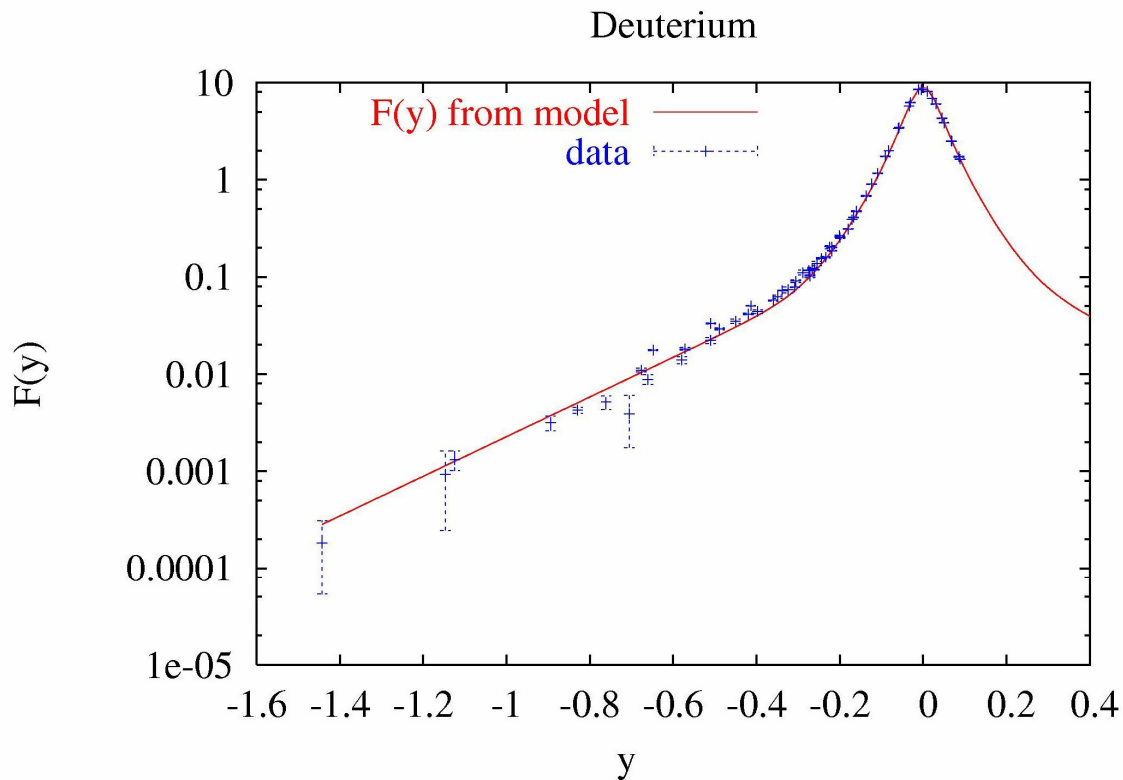


Fig. IV-9. Preliminary scaling function, $F(y)$, for deuterium, after subtracting the inelastic contributions which dominate for $y > 0$. In the Impulse Approximation, y represents the longitudinal momentum of the struck nucleon, and $F(y)$ is related to the nucleon momentum distribution. The solid line shows the model being used for the data analysis, where the exponential falloff is related to the momentum distribution of short-range correlations.

b.5. Proton Polarization Angular Distribution in Deuteron Photo Disintegration

(R. J. Holt, J. Arrington, K. Hafidi, P. E. Reimer, E. C. Schulte, K. Wijesooriya, and JLab E00-007 Collaboration)

The overall goal of experiment¹ E00-007 is to determine the mechanism that governs photoreactions in the GeV energy region. Our previous measurements² of induced polarization in deuteron photodisintegration produced surprising results at photon energies between 1 and 2 GeV. First these results disagreed markedly with previous experiments and secondly there was a remarkable disagreement with the meson-exchange model. The induced polarizations above 1 GeV and at $\theta_{\text{cm}} = 90^\circ$ were near zero, consistent with hadron helicity conservation. The goal of this experiment was to determine the angular dependence of the polarization. Data were taken for a photon energy of 2 GeV and at five center-of-mass angles: 37° , 53° , 70° , 90° and 110° . The induced polarizations as well as polarization transfers were measured. A new polarimeter that contains both a C and a CH₂ scatterer was used for this experiment.

The results are shown in Fig. IV-10 for the polarization transfers, C_x' and C_z' , and the induced polarization p_y . First, the results taken with the C and CH₂ analyzer are in good agreement with one another. The results for p_y and C_z' are also in good agreement with the previous values.² It appears that the induced polarization results are consistent with a $\sin(2\theta)$ dependence and not uniformly zero. This behavior is indicative of partial wave interference in the final state and not consistent with hadron helicity conservation. The quark gluon string model is in good agreement with the C_z' , but the HRM appears to give the wrong sign for C_x' . Theoretical calculations that simultaneously describe these three observables and the differential cross section will be necessary to fully understand photodisintegration of the deuteron in the GeV region.

¹JLab proposal E00-007, "Proton Polarization Angular Distribution in Deuteron Photodisintegration," R. Gilman, R. J. Holt, and Z.-E. Meziani, spokespersons.

²K. Wijesooriya *et al.*, Phys. Rev. Lett. **86**, 2975 (2001).

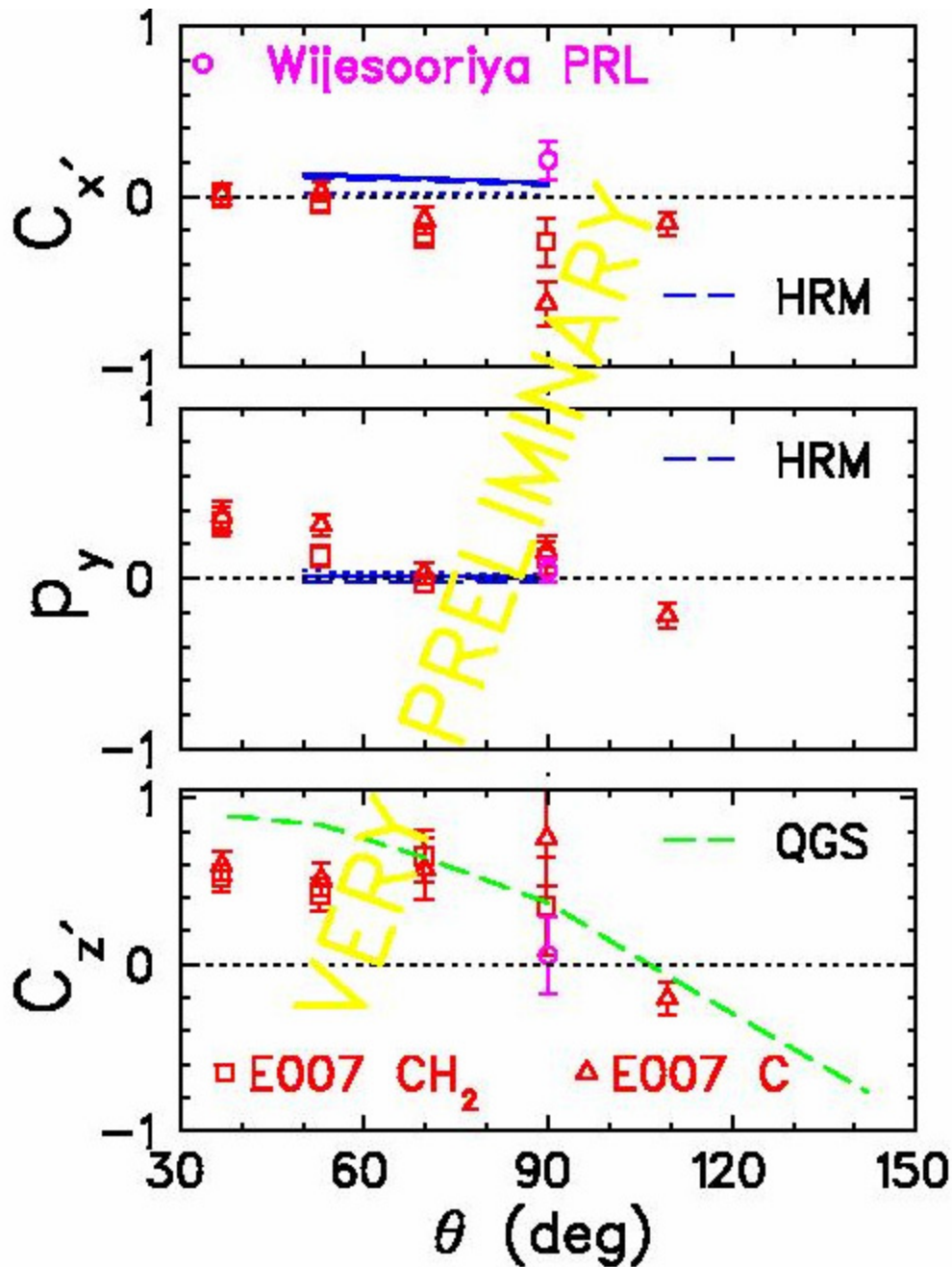


Fig. IV-10. The induced polarization, p_y , and polarization transfers, C_x' and C_z' , as a function of the c.m. reaction angle. The open squares refer to data recorded with a CH₂ polarimeter, while the open triangles refer to those data with a C polarimeter. The curves refer to the Hard Re-scattering (HRM) and Quark Gluon String (QGS) models.

b.6. Measurements of the Nuclear Dependence of $R = \sigma_L/\sigma_T$ at Low Q^2 (J. Arrington, D. F. Geesaman, T. G. O'Neill, D. Potterveld, and the E99-118 Collaboration)

Inclusive electron scattering is a well-understood probe of the partonic structure of nucleons and nuclei. Deep inelastic scattering has been used to make precise measurements of nuclear structure functions over a

wide range in x and Q^2 . The ratio $R = \sigma_L/\sigma_T$ has been measured reasonably well in deep inelastic scattering at moderate and high Q^2 using hydrogen and deuterium targets. However, R is still one of the most poorly

understood quantities measured in deep inelastic scattering and few measurements exist at low Q^2 or for nuclear targets. Existing data rule out significant nuclear effects in R only at moderate to large values of Q^2 .

JLab experiment E99-119 is a direct measurement of R at low x and low Q^2 . The experiment was performed in July of 2000 and data were taken for hydrogen, deuterium, and heavier nuclei. The cross section extraction at extremely small values of x and Q^2

involves very large radiative corrections. While these corrections will limit the region for which R can be extracted precisely, these data are ideal for testing the radiative correction procedures in such extreme kinematics, and in particular will help constrain the corrections coming from the nuclear elastic contributions. Final results for hydrogen and deuterium (Fig. IV-11) are available and will be submitted for publication in 2006. The analysis of the nuclear targets, with the larger radiative corrections, will be available shortly thereafter.

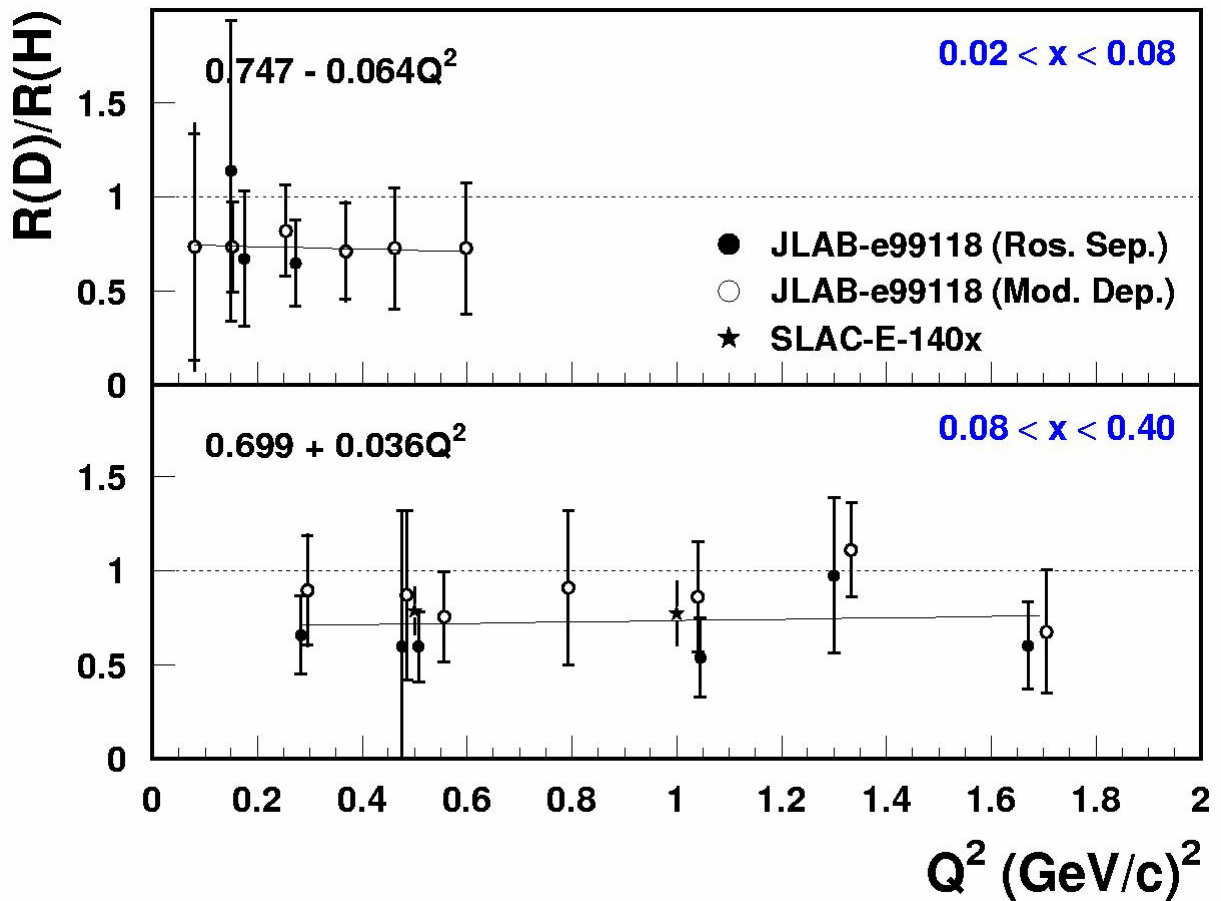


Fig. IV-11. Preliminary results for the comparison of $R = \sigma_L/\sigma_R$ for deuterium compared to hydrogen. These data suggest a different longitudinal contribution in deuterium.

C. QUARK STRUCTURE OF MATTER

c.1. Studies of Nucleon Spin Structure and Related Measurements of Deep-Inelastic Scattering at HERA (H. E. Jackson, A. El Alaoui, K. G. Bailey, T. P. O'Connor, K. Hafidi, D. H. Potterveld, P. E. Reimer, Y. Sanjiev, and the HERMES Collaboration)

HERMES, HERA measurement of spin, is an international collaboration of 30 institutions formed to address a basic question of hadron structure. How do the spins of its constituent quarks combine with the spin of the glue and the angular momentum of the partons to give the proton its spin of $1/2$? The HERMES experiment uses polarized internal targets in the HERA 30 GeV e^+/e^- storage ring at the DESY Laboratory. By emphasizing semi-inclusive deep-inelastic scattering (DIS) in which an identified hadron is observed in coincidence with the scattered lepton, HERMES has brought a new dimension to studies of nucleon spin structure. In recent years, HERMES reached a major milestone with the completion of a quark-flavor decomposition of the spin of the proton based on measurements of semi-inclusive double spin asymmetries¹ which avoids the need for use of data from hyperon decay and the assumption of SU(3) symmetry. The data have provided the first separate determinations of the polarizations of the up, down, and strange quarks. They show that the largest contribution to the nucleon spin comes from the valence region, while the polarizations of the sea quarks are all consistent with zero. To increase the sensitivity and precision of the flavor decomposition, HERMES is expanding the database in this analysis to include neutral pions and kaons. In addition, a novel technique has been developed to measure directly the polarization of the strange quark sea using inclusive and semi-inclusive charged kaons asymmetries for a deuteron target. A final full flavor decomposition of expanded scope including all HERMES measurements is planned. HERMES has also reported the first evidence that the gluon polarization is positively polarized, and during the final running period in 2006-2007 HERMES is exploring the possibilities of probing the parton angular momenta by measuring spin asymmetries in hard exclusive reactions that leave the target nucleon intact.

Activities during HERA Run II that ended in late 2005 were focused on measurements with a transversely polarized target which probes the effects of transverse motion of the quarks. The single-spin asymmetries generated with transverse polarization probe the third structure function, transversity, required to describe nucleon spin structure in leading order. Because it is

odd under chirality transformations, it can only be probed by processes involving additional chiral-odd structure, such as chiral-odd fragmentation in semi-inclusive DIS. Data from the first phase of this study² include a striking result that a large signal is observed for negative pions, larger than that for positive pions. With additional data already accumulated, HERMES will clarify this surprising result, and with measurements of the Collins fragmentation functions from the BELLE Collaboration will extract a first measurement of transversity.

The same data probe a second class of distribution function that depends not only on the longitudinal momentum fractions carried by the quarks, but also upon their transverse momentum fraction inside the nucleon. Current efforts are directed at measurement of the Sivers distribution function that describes distribution of unpolarized quarks as a function of their transverse momentum distribution. This function must vanish in the absence of quark orbital angular momentum. The observation of a large positive Sivers moment for positive pions provides first evidence for this non-vanishing T-odd distribution function. Current data analysis is devoted to extraction of this quantity for up and down quarks.

HERMES already has studied several exclusive reactions, including exclusive production of charged and neutral pions, and of ρ mesons. Recent measurements of deeply virtual Compton scattering (DVCS) include the first measurements of a beam-charge asymmetry. The intense interest in these processes stems from their description in terms of Generalized Parton Distributions (GPDs) which are expected to provide access to the quark total angular momentum content of the nucleon. Because of their complex structure, it is necessary to study their behavior for several processes over an extended kinematic domain. In particular, measurements with transversely polarized targets at HERMES are sensitive to the GPD's that play a dominant role in determining the total angular momentum carried by the quarks in the nucleon. A measurement of the target spin asymmetry for DCVS using an unpolarized beam and transversely polarized target has been used to make the first model-

dependent extraction of the total angular momentum carried by the up quarks.

The final phase of this program from 2006 to 2007 will continue these exclusive studies with the installation of a large acceptance recoil detector that will enhance the solid angle acceptance and missing mass resolution in measurements of hard exclusive processes such as electroproduction of mesons and DVCS. With the new detector, the exclusivity of events will be established by positive identification of the recoil proton and measurement of its recoil momentum. The enhanced selectivity of these measurements will provide a unique opportunity to assess the promise of GPDs as the next step in understanding the spin structure of the nucleon.

A very productive program of measurements of unpolarized DIS continues with the use of high-

¹A. Airapetian *et al.*, Phys. Rev. D **71**, 012003 (2005).

²A. Airapetian *et al.*, Phys. Rev. Lett. **94**, 012002 (2005).

c.1.1. Polarization of the Strange Quark Sea in the Proton from Semi-Inclusive Deep-Inelastic Scattering on the Deuteron (H. E. Jackson, A. El Alaoui, K. G. Bailey, T. P. O'Connor, K. Hafidi, D. H. Potterveld, P. E. Reimer, Y. Sanjiev, and the HERMES Collaboration)

The helicity distribution of the strange quark sea is of great interest as a probe of the spin properties of the quark sea in the nucleon. Because strange quarks carry no isospin, the total strange quark helicity density $\Delta S(x) = \Delta s(x) + \Delta \bar{s}(x)$ can be extracted from measurements of scattering of the deuteron alone which is isoscalar. In effect, measurements of the inclusive spin asymmetries provide an estimate of the helicity density $\Delta Q(x) = \Delta u(x) + \Delta \bar{u}(x) + \Delta d(x) + \Delta \bar{d}(x)$ of the non-strange sea. Using the spin asymmetries measured for the charged kaons as the second experimental data set, it is possible to extract $\Delta S(x)$. By measuring the charged kaon multiplicities with the same data set, the fragmentation functions relevant to the extraction process can be obtained without resort to other experiments. Aside from the assumption of isospin symmetry between the proton and the neutron, the only assumption required in the analysis is charge-conjugation invariance in the fragmentation process. A precise "isoscalar" extraction of $\Delta S(x)$ using semi-inclusive DIS on a polarized deuteron target has been carried out at HERMES.

Scattered beam leptons and coincident hadrons are detected by the HERMES spectrometer. Leptons are

luminosity dedicated running exclusively for HERMES during the last hour of each fill of the HERA e^+/e^- storage ring. Searches for exotic 5-quark states have continued. Studies of quark propagation in nuclear matter include measurements of the ratio of hadron multiplicities in heavy targets to those in deuterium. Data on the kinematic dependences of these ratios as measured for different hadron types provide new insights into the propagation process. Data on the multiplicities measured for proton and deuteron targets currently under analysis have provided accurate measurements of quark fragmentation functions specifically at HERMES kinematics, and a rigorous test of factorization. The HERA accelerator will continue operations through the summer of 2007. Every effort is being made to maximize the impact of the beam time that remains. Highlights of recent results are presented below.

identified with an efficiency exceeding 98% and a hadron contamination of less than 1% using an electromagnetic calorimeter, a transition-radiation detector, a pre-shower scintillation counter and a Cerenkov detector. Charged kaons are identified using a dual-radiator ring-imaging Cerenkov detector. Events were selected subject to the kinematic requirements $Q^2 > 1 \text{ GeV}^2$, $W^2 > 10 \text{ GeV}^2$ and $y < 0.85$, where W is the invariant mass of the photon-nucleon system, and $y = v/E$. Coincident hadrons were accepted if $0.2 < z < 0.8$ and $x_F \approx 2p_L/W > 0.1$, where p_L is the longitudinal momentum of the hadron with respect to the virtual photon direction in the photon-nucleon center of mass frame.

The helicity distributions $\Delta Q(x)$ and $\Delta S(x)$ have been extracted directly from the measured values of $A_{1,d}(x)$ and $A_{1,d}^{K^\pm}(x)$ using the fragmentation functions defined above as measured with the same data set and the parton distributions $Q(x)$ and $S(x)$ taken from the latest compilations. The resulting strange and non-strange helicity distributions weighted by Bjorken x are presented in Fig. IV-12. The non-strange helicity distribution is in excellent agreement with that derived from the published five-component flavor

decomposition¹ of the proton helicities. While of much improved precision and free of the systematic uncertainties in the fragmentation functions, the strange helicity distribution also agrees well with the results reported therein, and is consistent with zero over the measured range. The first moment of $\Delta S(x)$ in the measured region is $0.006 \pm 0.029(\text{stat.}) \pm 0.007(\text{sys.})$. The result for the first moment of $\Delta Q(x)$ is $0.0286 \pm 0.026(\text{stat.}) \pm 0.011(\text{sys.})$ which is in excellent agreement with values previously measured at HERMES.¹ The first moment of $\Delta S(x)$ is consistent with zero in the measured region. Because the very small density of strange quarks above $x = 0.3$, the contribution of any non-zero helicity density in this region is negligible compared to the systematic error of

the measurement. Consequently, the value for $S(x)$ can be safely taken as the moment over the Bjorken x range 0.02-1.0. The vanishing values recently reported for $g_{1,d}(x)$ at lower values of x , suggest that any contribution to the first moment of $\Delta Q(x)$ below $x = 0.02$ will be very small. While an anomalously large contribution to the strange moment at $x < 0.02$ can not be ruled out, the data reported here strongly suggest that the first moment vanishes. If true, the violation of the Ellis-Jaffe sum rule observed in inclusive scattering is not due to a significant negative polarization of the strange sea. The result for the first moment of the octet axial charge $\Delta a_8 = \int (\Delta Q(x) - 2\Delta S(x)) dx$ is $0.0286 \pm 0.026(\text{stat.}) \pm 0.011(\text{sys.})$, substantially less than the value inferred from hyperon decay.

¹A. Airapetian *et al.*, Phys. Rev. D **71**, 012003 (2005).

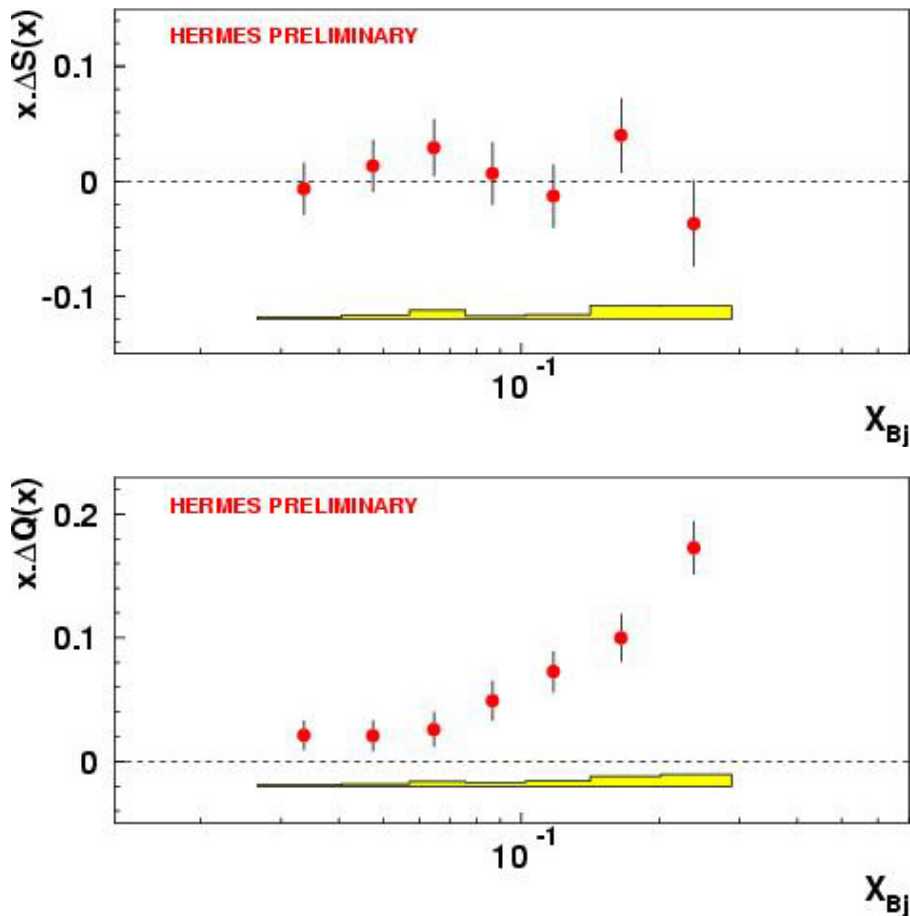


Fig. IV-12. Strange and non-strange quark helicity and polarization distributions from the isoscalar extraction method at $\langle Q^2 \rangle = 2.5 \text{ GeV}^2$ as a function of Bjorken x . The error bars are statistical, and the bands at the bottom represent the systematic uncertainties.

c.1.2. Collins and Sivers Asymmetries for Charged Kaons with a Transversely Polarized Target (H. E. Jackson, A. El Alaoui, K. G. Bailey, T. P. O'Connor, K. Hafidi, D. H. Potterveld, P. E. Reimer, Y. Sanjiev, and the HERMES Collaboration)

At leading twist, the quark structure of the nucleon is described by three parton distribution functions: the momentum distribution $q(x, Q^2)$, the known helicity distribution $\Delta(x, Q^2)$, and the unknown transversity distribution $\delta(x, Q^2)$. In the helicity basis, transversity is related to a quark-nucleon forward scattering amplitude involving helicity flip of both nucleon and quark. Because it is chiral-odd it cannot be probed in inclusive measurements. At HERMES transversity in conjunction with the chiral-odd Collins fragmentation function is accessible in azimuthal single-spin asymmetries (SSA) in semi-inclusive DIS in a transversely polarized target. The Collins fragmentation function describes the correlation between the transverse polarization of the struck quark and the transverse momentum of the hadron produced. The Sivers mechanism can also produce a SSA. The T-odd Sivers distribution function describes the correlation between the transverse polarization of the nucleon and the transverse momentum of the quarks within. A non-zero Sivers effect signals a nucleon spin flip without quark helicity flip, which must therefore involve orbital angular momentum inside the nucleon.

HERMES has already published data¹ on a transversely polarized target which allowed extraction of Collins

and Sivers moments for charged pions. Positive moments have been observed for π^+ in both the Collins and Sivers cases, while only the Collins moment is non-zero and negative for π^- . Because of the dual-radiator RICH, HERMES can also extract Collins and Sivers moments for other hadrons. Kaons are of particular interest because their production in DIS suffers less from contamination by exclusive vector-meson production than in the case of pions. The smaller contribution from exclusive vector-meson production simplifies the interpretation of the results. The different quark-flavor structure of the kaon also provides a contrasting sensitivity to the quark structure of the target nucleon, as compared to that of the pion. The Collins and Sivers moments obtained by HERMES for charged kaons are presented in Figs. IV-13 and IV-14. The results for the Sivers moments are unexpected. Due to u-quark dominance for a hydrogen target, the Sivers moments for positive pions and kaons are expected to be similar. However, the kaon moments are twice as large as the pion moments (apart from the high bins). Hopefully, explanations of this unexpected behavior will provide insights into the Sivers mechanism.

¹A. Airapetian *et al.*, Phys. Rev. Lett. **94**, 012002 (2005).

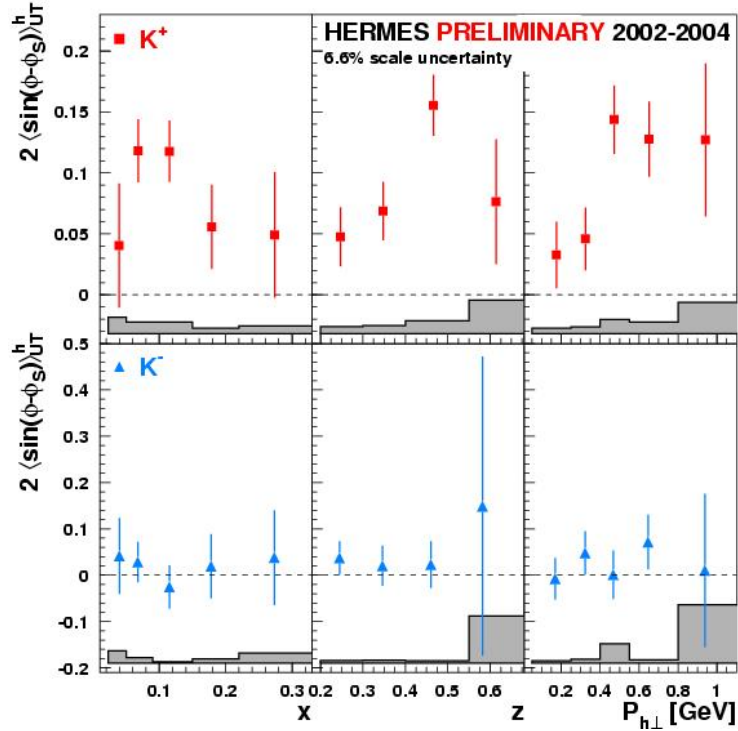


Fig. IV-13. Measured Siverts moments for charged kaons as a function of x , z , and $P_{h\perp}$, multiplied by two to have the possible range ± 1 . The error bands represent the maximal systematic uncertainties in the measurement.

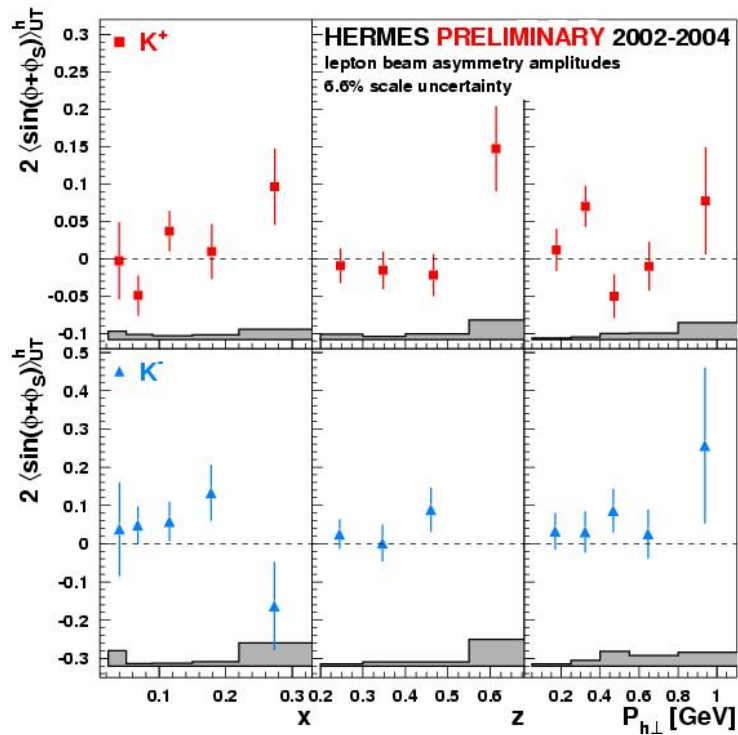


Fig. IV-14. Measured Collins moments for charged kaons as a function of x , z , and $P_{h\perp}$, multiplied by two to have the possible range ± 1 .

c.1.3. Transverse Single-Spin Asymmetries in Leptoproduction of Charged Pion Pairs

(H. E. Jackson, A. El Alaoui, K. G. Bailey, T. P. O'Connor, D. H. Potterveld, P. Reimer, Y. Sanjiev, and the HERMES Collaboration)

To date, HERMES measurements of single-spin asymmetries for single hadrons in semi-inclusive DIS have been the only measurements used to probe transversity. However, already in 1993 it was pointed out that single-spin asymmetries in semi-inclusive dihadron production could also be sensitive to transversity,¹ hence providing an independent way of accessing transversity. When the production of hadron pairs is considered, even after integration over the transverse momentum of the hadron pair relative to the virtual photon direction, the relative momentum of the pair can have a transverse component. The transverse polarization of the struck quark can influence the relative orbital angular momentum of the pair, so that the quark polarization can be revealed through the distribution of these pairs in the azimuthal angle of the hadron plane relative to the virtual photon direction. To zeroth order in α_s and up to subleading twist the

azimuthal single-spin asymmetry is related to the product of the twist-two chiral-odd transversity δq times a twist-two chiral-odd dihadron fragmentation function. A single-spin asymmetry has been measured in the azimuthal distribution of $\pi^+\pi^-$ pairs produced in semi-inclusive deep-inelastic scattering on a transversely polarized target. The data are presented in Fig. IV-15 where they are plotted against the sum of the hadron azimuthal angle and the target azimuthal angle. These data provide evidence for a correlation between the transverse target polarization and the azimuthal orientation of the plane containing the two pions. This asymmetry is expected to allow extraction of the product of transversity and the dihadron fragmentation function. With the independent measurement of the fragmentation function in collider experiments, it will be possible to extract δq from these data.

¹J. C. Collins, S. F. Hepplemann, and G. A. Ladinsky, Nucl. Phys. **B420**, 565 (1994).

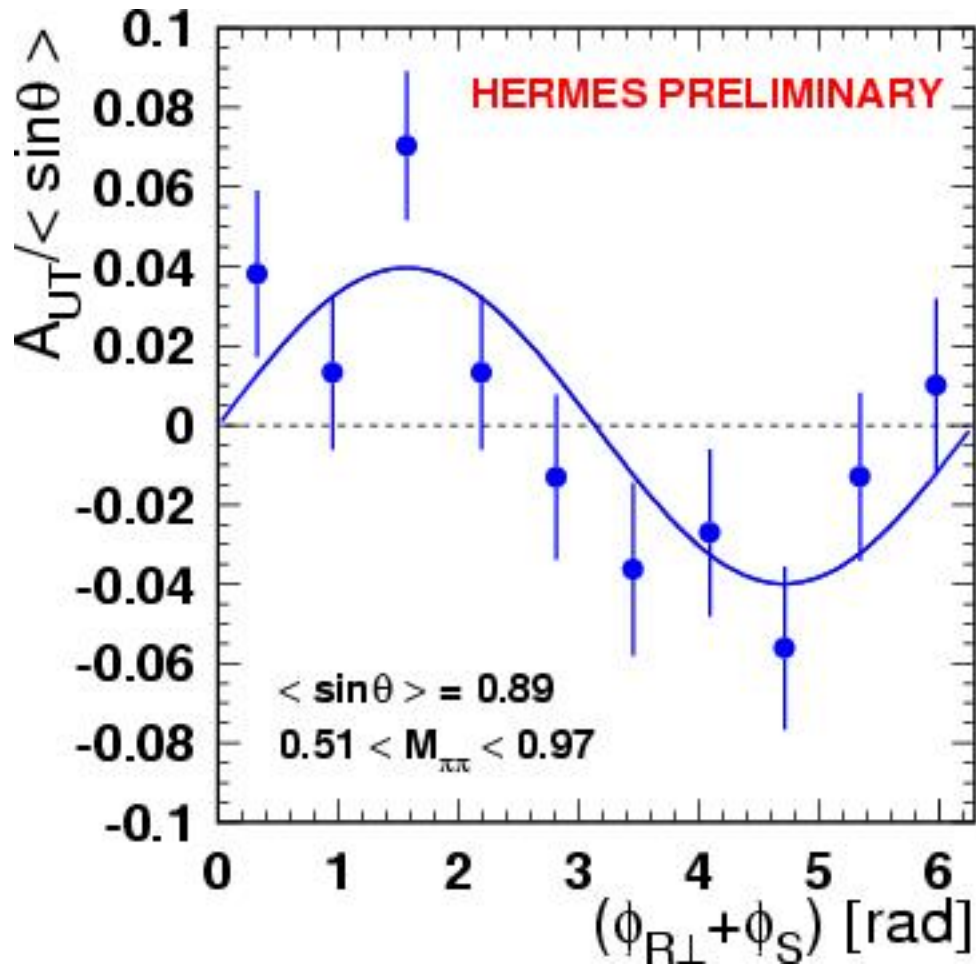


Fig. IV-15. Target single-spin asymmetry $A_{UT}/\langle \sin\theta \rangle$ of the pion pair as a function of sum of the azimuthal angle of the pion pair production plane and the azimuthal angle of the target polarization relative to the virtual photon direction. The invariant mass of the pion pair is $0.51 < M_{\pi\pi} < 0.97$ GeV. The curve corresponds to a $\sin\theta$ moment of $2\sin(\varphi_{R\perp} + \varphi_S)\sin(\theta) = 0.040 \pm 0.009$.

c.1.4. A Model-Dependent Constraint on $J_u + J_d$ from Deeply-Virtual Compton Scattering at HERMES (H. E. Jackson, A. El Alaoui, K. G. Bailey, T. P. O'Connor, K. Hafidi, D. H. Potterveld, P. Reimer, Y. Sanjiev, and the HERMES Collaboration)

At the present time the only known strategy for extracting generalized parton distributions (GPDs) from measurements is to assume a functional form of the GPDs with a number of adjustable parameters, and to fit these parameters by comparing the resulting observables with experimental data. A general parameterization of GPDs has been given by Goeke, Polyakov, and Vanderhaegen.¹ The parameters entering this parameterization of the GPD E include the total angular momentum carried by the quarks in the nucleon, J_q ($q = u, d$). For this GPD model it has been found that in Deeply-virtual Compton scattering,

specific azimuthal amplitudes in the transverse target-spin asymmetry are sensitive to J_u (and J_d) and much less sensitive to other parameters. In particular, the amplitude corresponding to the angular dependence $\sin(\varphi - \varphi_S)\cos\varphi$ displays such a sensitivity. Therefore, reasonable constraints on a linear combination of J_u and J_d may be expected from transverse target spin asymmetries within such a GPD model. Such model dependent constraints have been extracted from the transverse target spin asymmetry amplitudes measured with HERMES data 2002-04 data for a polarized proton target. The resulting constraint on J_u and J_d can be

parameterized as $J_u + J_d/2.9 = 0.42 \pm 0.21 \pm 0.06$. The first uncertainty represents the experimental uncertainty in the measured amplitude and the second is the model uncertainty originating from unknown b-profile

parameters in the GPD parameterization. The resulting constraints are presented in Fig. IV-16. Also shown in the plot is a lattice result from the QCDSF collaboration.²

¹K. Goeke, M. V. Polyakov, and M. Vanderhaegen, Prog. Part. Nucl. Phys. **47**, 401 (2001).

²M. Goekeler *et al.*, (QCDSF Collaboration), Phys. Rev. Lett. **92**, 042002 (2004).

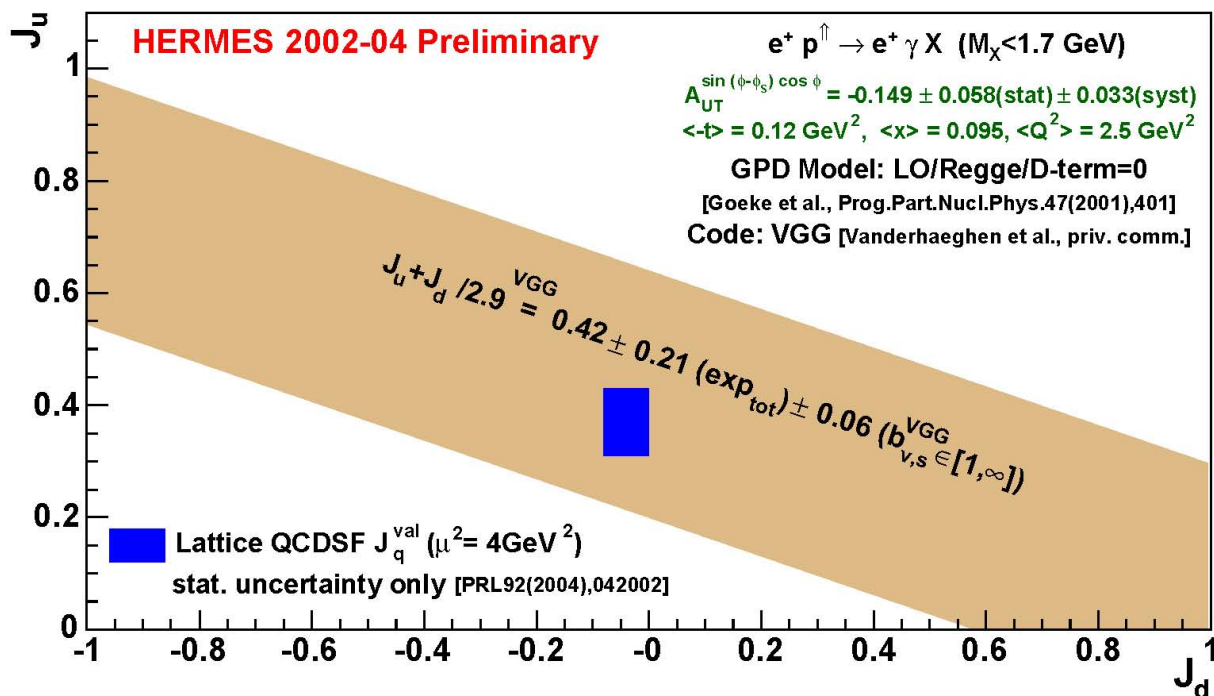


Fig. IV-16. A model-dependent constraint on J_u and J_d obtained by comparing the transverse target spin amplitude extracted from HERMES 2002-04 data with theoretical calculations based on the GPD model proposed in Ref. 2. The red shaded area corresponds to $J_u + J_d/2.9 = 0.42 \pm 0.21 \pm 0.06$. Also shown is the result from a recent lattice calculation.²

c.1.5. Double-Hadron Leptoproduction in the Nuclear Medium (H. E. Jackson, A. El Alaoui, K. G. Bailey, T. P. O'Connor, K. Hafidi, D. H. Potterveld, P. Reimer, Y. Sanjiev, and the HERMES Collaboration)

Hadron production from a free nucleon in deep-inelastic scattering is generally described by fragmentation functions that contain nonperturbative information about parton hadronization. These functions are expected to be different for nuclear targets because of several effects: energy loss of the propagating quarks, rescattering during the prehadronic formation process, or interactions of the final state hadrons within the nucleus. Double-hadron production offers a unique way of studying hadronization. If partonic energy loss of the struck quark were the only mechanism involved, it would be naively expected that the attenuation effect does not depend strongly on the

number of hadrons involved, and the double-hadron to single-hadron ratio for a nuclear target should only be slightly dependent on the mass number A . On the contrary, if the final hadron absorption were the dominant process, the requirement of an additional slower sub-leading hadron that is more strongly absorbed would suppress the two-hadron yield from heavier nuclei, so that this ratio should decrease with A .

The first measurements of double-hadron production in deep-inelastic scattering within the nuclear medium have been made with the HERMES spectrometer at DESY HERA using a 27.6 GeV positron beam. By

comparing data for deuterium, nitrogen, krypton, and xenon nuclei, the influence of the nuclear medium on the ratio of double-hadron to single-hadron yields was investigated. Nuclear effects on the additional hadron are clearly observed, but with little or no difference among nitrogen, krypton, or xenon, and with smaller magnitude than effects seen on previously measured single-hadron multiplicities. Data are presented in Fig. IV-17 where they are compared with two models

of hadronization. Comparisons have been made with models based on partonic energy loss or prehadronic scattering and with a model based on a purely absorptive treatment of final state interactions. While the ratios vary only slightly with A , they do not support models that interpret modifications to fragmentation as being due to prehadronic scattering or partonic energy loss.

¹T. Falter *et al.*, Phys. Lett. **B594**, 61 (2004), Phys. Rev. C **70**, 054609 (2004); K. Gallmeister and W. Cassing, Nucl. Phys. **A748**, 241 (2005).

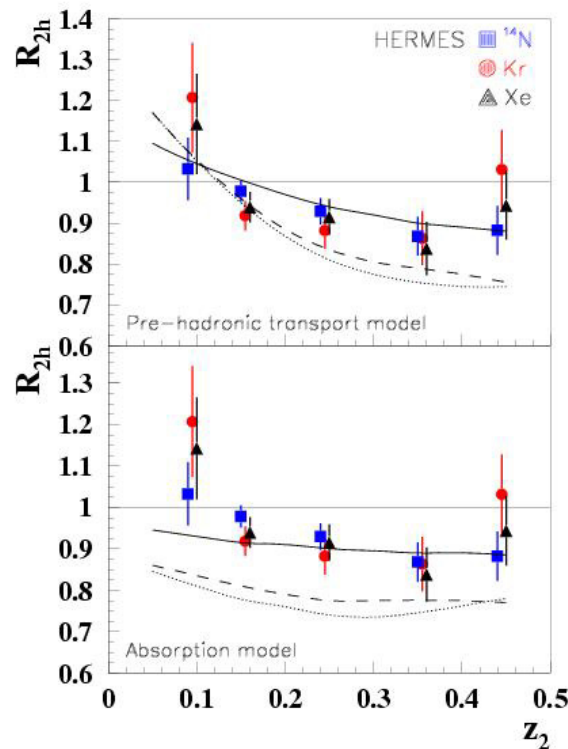


Fig. IV-17. The ratio R_{2h} as a function of $z_2 = E_2/hv$ for N (squares), Kr (circles), and Xe (triangles) with $z_1 > 0.5$. The systematic uncertainty is 2% for all targets and is independent of z_2 . In the upper panel, the curves (solid for N, dashed for Kr, dotted for Xe) are calculated within a transport model.¹ In the bottom panel, the same data are shown with calculations that assume only absorption for the three nuclei (same line types as in the upper plot).

c.1.6. HERMES Dual Radiator RICH – Performance and Impact (H. E. Jackson, A. El Alaoui, K. G. Bailey, T. P. O'Connor, D. H. Potterveld, P. E. Reimer, and the HERMES Collaboration)

The HERMES ring-imaging Cerenkov detector (RICH) is a novel device which provides clean particle identification of pions, kaons, and protons over the traditionally difficult momentum region of 2-15 GeV/c.

Particle identification with this instrument has proven to be essential to almost all recent HERMES physics studies. The device is shown in Fig. IV-18. The Cerenkov radiators are a wall of aerogel at the entrance

to the detector and C_4F_{10} gas which occupies the full volume of the radiator box. Cerenkov rings from the radiators are reconstructed in a 1932 pmt matrix which serves as the photon detector. The system has performed with no detectable deterioration since its installation in the HERMES spectrometer in 1998. Particle identification is accomplished by reconstructing for each particle hypothesis the distribution of angles for pmt hits in an appropriate angular range. The likelihoods of the hit patterns for the two radiators are combined in an overall likelihood and identification is based on the highest likelihood. The performance of the system is summarized by a P-matrix which gives the probabilities for correct

identification as well as the probabilities for cross contamination through misidentification. The P-matrices used to unfold the detector effects to obtain the true particle populations are generated by Monte Carlo simulations. Recent efforts has been devoted to refining the analysis procedures through a more comprehensive tabulation of the P-matrices which includes the dependence of the matrices on the event topologies, identified particle types, and physical reaction process under study. For example, because of substantial variations in event topologies there are significant differences in the P-matrix families for deep-inelastic scattering and quasi-real photon production.



Fig. IV-18. Front view during installation of the upper section of the HERMES RICH detector with the aerogel wall removed. The image of the photon detector matrix is visible in its reflection in the mirror array. The inset shows a cover of the CERN courier which contains a picture of the pmt matrix.

c.2. Measurement of the Absolute Drell-Yan Cross Section on Hydrogen and Deuterium (P. E. Reimer, D. F. Geesaman, S. B. Kaufman, N. C. R. Makins, B. A. Mueller, and the FNAL E866/NuSea Collaboration)

Very little is known about the regime in which only one parton carries much of proton's momentum – there is very little data available to serve as a guide. In addition, different theoretical treatments prescribe different behaviors as $x \rightarrow 1$, where x represents the fraction of the proton's momentum carried by the interacting parton. In the fixed target environment, the Drell-Yan process is sensitive to the high- x behavior of the *beam's* quarks and the low- and intermediate- x behavior of the target antiquarks. E866 has measured the absolute cross sections for *proton-proton* and *proton-deuteron* Drell-Yan.¹ As $x \rightarrow 1$, these data are

dominated by the beam proton's quark distribution of $4u(x) + d(x)$. The measured absolute cross sections, relative to a next-to-leading order (NLO) calculation are shown in Fig. IV-19. The quark distributions used in the calculation *over-predict* the measured cross sections at large- x by a significant amount. This effect could be mimicked by radiative corrections, however, these effects can only account for 3-5% of the observed difference at intermediate and large- x . This difference will be further investigated by a new Drell-Yan experiment, Fermilab E906, which is scheduled to run in 2009.

¹J. C. Webb *et al.*, (Fermilab E866/NuSea Collaboration), "Absolute Drell-Yan Dimuon Cross Sections in 800 GeV/c pp and pd Collisions," hep-ex/0302019.

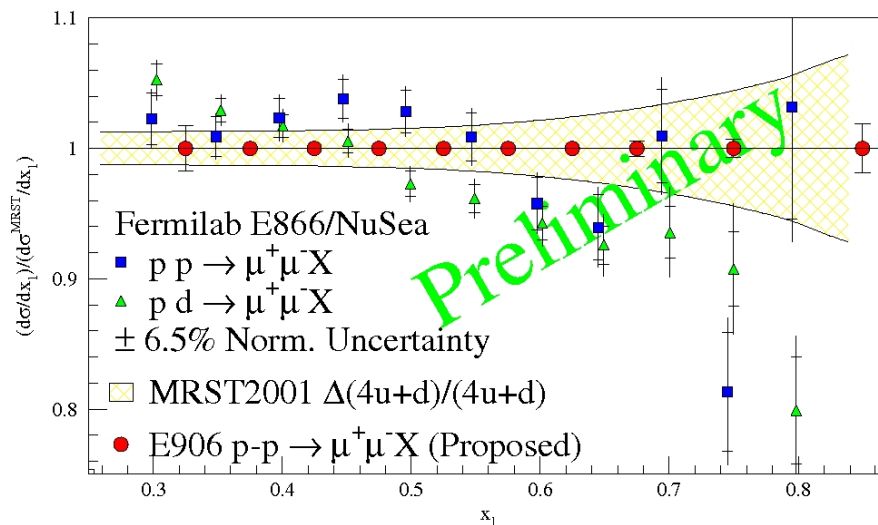


Fig. IV-19. The ratio of Drell-Yan cross section, including radiative corrections, measured by Fermilab E866/NuSea for proton-deuteron (triangles) and proton-proton (squares) to calculated NLO cross section based on the MRST2001 parton distributions. The error bars on the red circles indicate the expected statistical uncertainty which will be achieved in the new Fermilab E906 experiment. The yellow band represents the uncertainty given by MRST2001 on $4u(x) + d(x)$.

c.3. Measurement of the Drell-Yan Angular Distributions (P. E. Reimer, D. F. Geesaman, S. B. Kaufman, N. C. R. Makins, B. A. Mueller, and the FNAL E866/NuSea Collaboration)

In leading order QCD, the Drell-Yan process is the annihilation of a quark-antiquark pair into a virtual photon. The virtual photon then decays into a lepton-

antilepton pair that is detected. The general expression for the angular distribution for Drell-Yan scattering is given by

$$d\sigma = 1 + \lambda \cos^2\theta + \mu \sin 2\theta \cos 2\phi + \nu/2 \sin^2\theta \cos 2\phi.$$

Theoretically, for massless quarks or a transversely polarized virtual photon in a reference frame with θ defined relative to the quark-antiquark annihilation axis, $\lambda = 1$ and $\mu = \nu = 0$. More generally, in any reference frame, the Lam-Tung rule, $1 - \lambda = 2\nu$, is expected to hold. Experimentally, these angular distributions have only been studied in pion-induced Drell-Yan scattering experiments using nuclear targets at CERN and at Fermilab. In both cases, the data indicate the Lam-Tung rule is violated and sizeable $\cos 2\phi$ contributions to the angular distributions were

observed. These results were more pronounced at large transverse momentum (p_T). To verify these effects, we are studying the angular distributions from Fermilab E866 proton induced Drell-Yan scattering on hydrogen and deuterium targets. Preliminary results show that, for proton induced Drell-Yan, the Lam-Tung rule holds, and the $\cos 2\phi$ contributions to the angular distributions are small. We are also studying the possibilities of more precise measurements of the angular distributions with future Drell-Yan experiments such as Fermilab E906.

c.4. Drell-Yan Measurements with 120 GeV Protons, FNAL E906 (P. E. Reimer, D. F. Geesaman, J. Arrington, K. Hafidi, R. J. Holt, D. H. Potterveld, and the FNAL E906 Collaboration)

The proton and the neutron are composite objects, made of quarks, antiquarks and gluons, collectively known as partons. While many of the properties of the proton may be attributed to its three valence quarks, it is, in fact, much more complicated, with over 50% of its momentum being carried by the its non-valence (sea) quarks and gluons. To understand the structure of the proton, it is necessary to understand the sea quarks, their origins and their interactions with the gluons that bind the proton together. E906 is specifically designed to use Drell-Yan scattering to probe the sea quarks of the proton.¹

The Drell-Yan mechanism provides a powerful tool to study the structure of the proton at the quark level. In Drell-Yan scattering a quark (or antiquark) in the proton beam annihilates with an antiquark (or quark) in the target. The resulting annihilation produces a virtual photon that decays into a pair of leptons, which are seen in the detector. The kinematics of the detected leptons can be used to select interactions between beam valence quarks and target antiquarks. This was successfully exploited by Fermilab E866/NuSea using an 800 GeV/c proton beam provided new insight into the antiquark sea in the proton^{2,3} and nuclear dependence phenomena.⁴ FNAL E906 has been approved by Fermilab to extend Drell-Yan measurements to larger values of x (the fraction of the proton's momentum carried by the struck quark) using the new 120 GeV Main Injector at Fermilab. The new data obtained by this experiment will address several outstanding questions.

Vacuum polarization accounts for the creation of a flavor symmetric sea. Previous E866 Drell-Yan data, however, exhibit a large asymmetry between \bar{d} and \bar{u} for $x < 0.25$ (where x represents the fraction of the protons momentum carried by the interacting quark) clearly indicating a non-perturbative origin to the sea. Above $x > 0.28$ these data, albeit with poor statistical uncertainty, indicate the ratio \bar{d}/\bar{u} returns to unity. This result dramatically changed the sea quark parton distribution fits and was completely unpredicted by meson cloud and other non-perturbative models. The return of \bar{d}/\bar{u} to unity clearly signals a change in the mechanism by which the sea is generated.^{2,3,5} Fermilab E906 will determine \bar{d}/\bar{u} and $\bar{d} - \bar{u}$ for $0.1 \leq x \leq 0.45$, encompassing the non-perturbative region and extending well into the region where the sea appears to return to symmetry, allowing for the study of the relative importance of the perturbative and non-perturbative sea. The current parton distributions now reproduce the previous Drell-Yan data for $0.28 < x < 0.3$, but allow $\bar{d}/\bar{u} < 1$ as x increases above 0.3. This is not expected by *any* models of the proton, either meson or perturbative, and is simply indicative of the complete lack of data. E906 will provide this data, as shown in Fig. IV-20.

Very little is known about the regime in which only one parton carries much of proton's momentum – different theoretical treatments prescribe different behaviors as $x \rightarrow 1$ and very little data is available to serve as a guide. Through the partons in the beam proton, Fermilab E906 will access these distributions. The Drell-Yan cross section is dominated by the distribution of $4u(x) + d(x)$ as $x \rightarrow 1$. E906 will extend the data

provided by Fermilab E866 to higher x and provide much more precise *proton* data than is currently available.

Models based on the hypothesis that nuclear binding is governed by the exchange of mesons have been used to quite successfully describe the nuclear force. Given the success of these models, it is natural to look for direct experimental evidence for the presence of these mesons in nuclei. Thus far, however, no direct evidence has been found.⁶ If present, these mesons will lead to an enhancement of antiquarks in the nucleus, and Drell-Yan is ideally suited to measure this enhancement. Fermilab E906 will collect data using nuclear targets, in addition to hydrogen and deuterium to look for these effects.

From deep inelastic scattering (DIS) experiments, we know that the quark level structure of a nucleon within a nucleus is different from that of a free nucleon. In the range $0.10 < x < 0.25$, a surplus of quarks (approximately 2-4%) in nuclei, known as antishadowing, is clearly observed in DIS data. To understand these phenomena, it is important to determine if it is a general property of the quark and antiquark distributions, or just a property of the valence or sea quarks. Drell-Yan, with its ability to measure sea-only quark effects, is the ideal reaction in which to measure this. Early Drell-Yan data indicate that this surplus might not be present,⁶ but with poor statistical uncertainty (3-5%). The Fermilab E906 measurements will clearly determine if there is antishadowing in the sea, with statistical uncertainties of less than 1% throughout this region (see Fig. IV-20).

Using the same nuclear target data, Fermilab E906 will also study the propagation of colored partons in

strongly interacting, cold nuclear matter. By comparing the Drell-Yan yields from different nuclear targets and looking for apparent shifts in the beam parton's momentum distributions between nuclei, E906 will be able to measure the beam parton's energy loss. Previous Drell-Yan studies have placed upper limits on parton energy loss.⁷ With increased sensitivity from the 120 GeV beam and better statistical accuracy, Fermilab E906 will turn these upper limits into measurements. These measurements will aid in the understanding of jet suppression data from RHIC.

FNAL E906 is able to make these improvements over previous measurements because of the lower beam energy available at the Fermilab Main Injector. For fixed x_{beam} and x_{target} the cross section scales as the inverse of the beam energy. Thus a factor of seven more events for the same integrated luminosity can be achieved. At the same time, the primary background to the measurement, muons from J/ψ decays, decreases with decreasing beam energy, allowing for an increase in instantaneous luminosity by another factor of seven. These two factors combine to provide roughly 50 times more events for the same beam time.

FNAL E906 has been approved by the Fermilab PAC and will begin collecting data in 2009. Much of the new spectrometer will come from detector elements recycled from the E866 Drell-Yan spectrometer. To increase the rate and triggering capabilities of the spectrometer, some new detectors will be fabricated. In addition, because of the significantly different kinematics of the 120 GeV experiment, the new spectrometer will require a new, large dipole magnet to focus the Drell-Yan muons.

¹L. D. Isenhower *et al.*, (Fermilab E906 Collaboration), "Proposal for Drell-Yan Measurements of Nucleon and Nuclear Structure with the FNAL Main Injector," April 1, 2001.

²E. A. Hawker *et al.*, (Fermilab E866/NuSea Collaboration), *Phys. Rev. Lett.* **80**, 3715 (1998).

³R. S. Towell *et al.*, (Fermilab E866/NuSea Collaboration), *Phys. Rev. D* **64**, 05202 (2001).

⁴M. J. Leitch *et al.*, (Fermilab E866/NuSea Collaboration), *Phys. Rev. Lett.* **84**, 3256 (2000).

⁵J. C. Peng *et al.*, (Fermilab E866/NuSea Collaboration), *Phys. Rev. D* **58**, 092004 (1998).

⁶D. M. Alde *et al.*, *Phys. Rev. Lett.* **64**, 2479 (1990).

⁷M. A. Vasiliev *et al.*, (Fermilab E866/NuSea Collaboration), *Phys. Rev. Lett.* **83**, 2304 (1999).

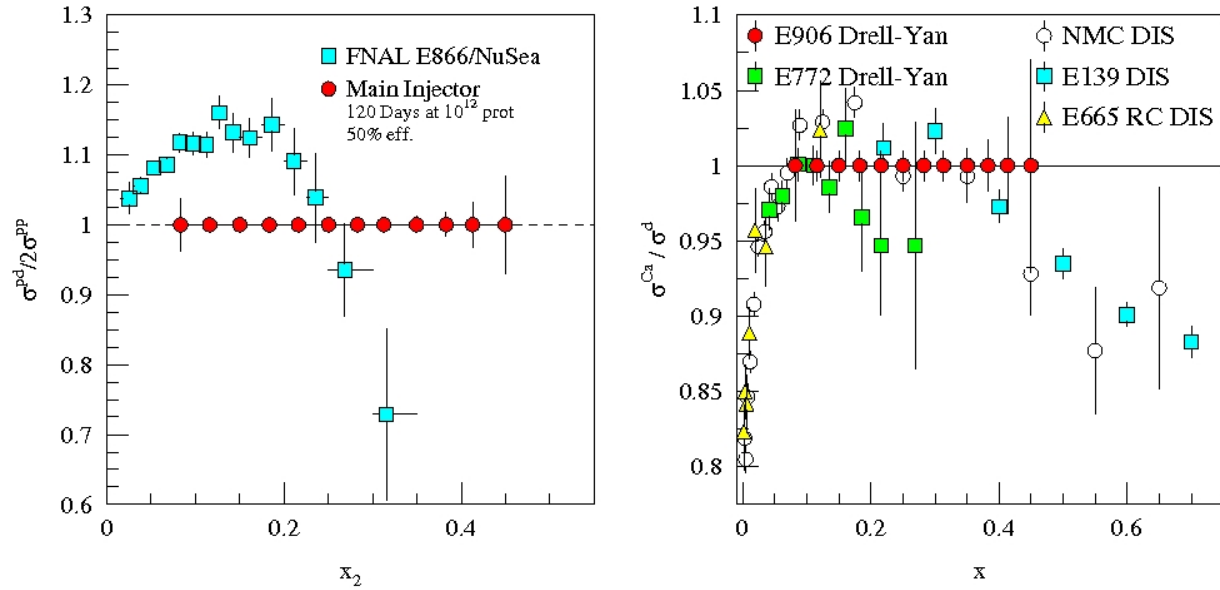


Fig. IV-20. The statistical uncertainty of the proposed E906 measurement of the ratio of hydrogen to deuterium cross sections (arbitrarily plotted at 1) compared with the E866 measurements of the same quantity (left). The statistical uncertainty of E906's measurement of the ratio of deuterium to Calcium cross sections (arbitrarily plotted at 1) compared with previous Drell-Yan and deep inelastic scattering (DIS) measurements (right).

D. FUNDAMENTAL SYMMETRIES IN NUCLEI

d.1. Laser Trapping of ^{226}Ra Atoms and Progress Towards an EDM Measurement

(J. R. Guest, N. D. Scielzo, I. Ahmad, K. Bailey, J. P. Greene, R. J. Holt, Z.-T. Lu, T. P. O'Connor, and D. H. Potterveld)

Permanent electric dipole moments (EDMs) in atoms or molecules are a signature of Time (T)-and Parity (P)-violation and represent an important window onto physics beyond the Standard Model. We are developing a next-generation EDM search around laser-cooled and -trapped ^{225}Ra ($t_{1/2} = 15$ d) atoms. Due to octupole deformation of the nucleus, ^{225}Ra is predicted to be two to three orders of magnitude more sensitive to T-violating interactions than ^{199}Hg (stable), which currently sets the most stringent limits in the nuclear sector. The scheme is to collect ^{225}Ra atoms in a magneto-optical trap (MOT) and transfer the sample to an optical dipole trap. In this second trap, the atoms will be polarized by optical pumping and the EDM measurement will be performed.

Figure IV-21 shows the atomic energy levels, lifetimes, and relative transition rates of radium.^{1,2} In order to achieve a MOT, beams of laser light must excite the atoms repeatedly on a cycling or a quasi-cycling transition. A Ra atom excited by the allowed singlet-to-singlet transition, $7s^2\ ^1S_0 - 7p\ ^1P_1$, only cycles for an average of 500 times before it leaks to either the $6d\ ^1D_2$ or $6d\ ^3D_2$ level. On the other hand, an atom excited by the singlet-to-triplet transition, $7s^2\ ^1S_0 - 7p\ ^3P_1$, cycles for an average of 2×10^4 times before leaking to the $6d\ ^3D_1$ level, from which the atom can be pumped back to the ground-level via the $6d\ ^3D_1 - 7p\ ^1P_1$ transition followed by a spontaneous decay from $7p\ ^1P_1$. This

repump transition at 1428 nm can be excited for an average of 500 times before the atom leaks to other metastable levels. Therefore, with the repump in place, an atom can cycle for an average of 8×10^6 times and stay in the MOT for at least 7 s in an ideal vacuum.

We have recently realized the world's first laser trap of radium atoms; the apparatus is shown in Fig. IV-22. We use a Ti:Sapphire ring laser system to generate the 714 nm light to excite the $7s^2\ ^1S_0 - 7p\ ^3P_1$ transition for laser-cooling. We have demonstrated transverse cooling, Zeeman slowing, and trapping of ^{226}Ra ($t_{1/2} = 1599$ a) atoms. By applying repumping with a diode laser at 1428 nm, we have extended the trap lifetime of the atoms from milliseconds to seconds. The total trap capture efficiency is approximately 3×10^{-7} . Figure IV-23 shows the fluorescence of these trapped atoms and compares it to the fluorescence signal from the atomic beam (scaled by 100 x). As seen in the loading and trap lifetime curves in the inset of Fig. IV-23, the atoms stay in the trap for an average time of 1 s. This is presently still limited by collisions with background gas in a vacuum of 2×10^{-8} Torr. The trap allows us to perform measurements on the lifetimes and frequencies associated with the repump transition. We are preparing to laser-cool and trap ^{225}Ra , and the development of the optical dipole trap and the EDM measurement apparatus are underway.

¹V. A. Dzuba, V. V. Flambaum, and J. S. M. Ginges, Phys. Rev. A **61**, 062509 (2000).

²N. D. Scielzo, J. R. Guest, E. C. Schulte, I. Ahmad, K. Bailey, D. L. Bowers, R. J. Holt, Z.-T. Lu, T. P. O'Connor, and D. H. Potterveld, Phys. Rev. A **73**, 010501(R) (2006).

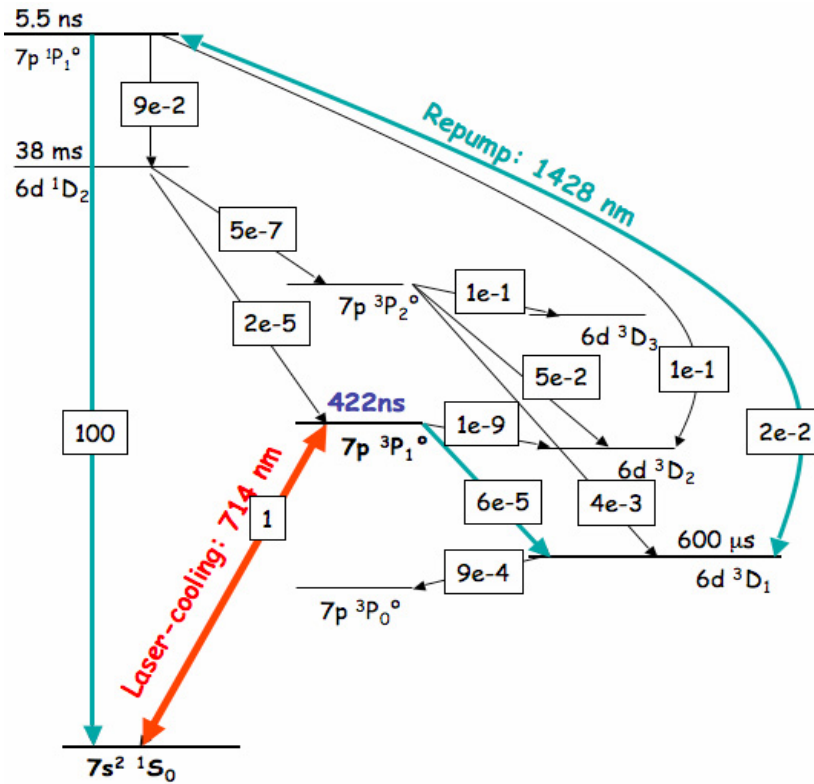


Fig. IV-21. Atomic energy diagram of radium. In this scheme, spontaneous scattering force is generated by repeatedly exciting the $7s^2 \ ^1S_0 - 7p \ ^3P_1$ transition, with the help of repumping on the $6d \ ^3D_1 - 7p \ ^1P_1$ transition. The numbers in the rectangle frames are relative transition rates derived from the line strengths calculated by V. A. Dzuba et al.¹

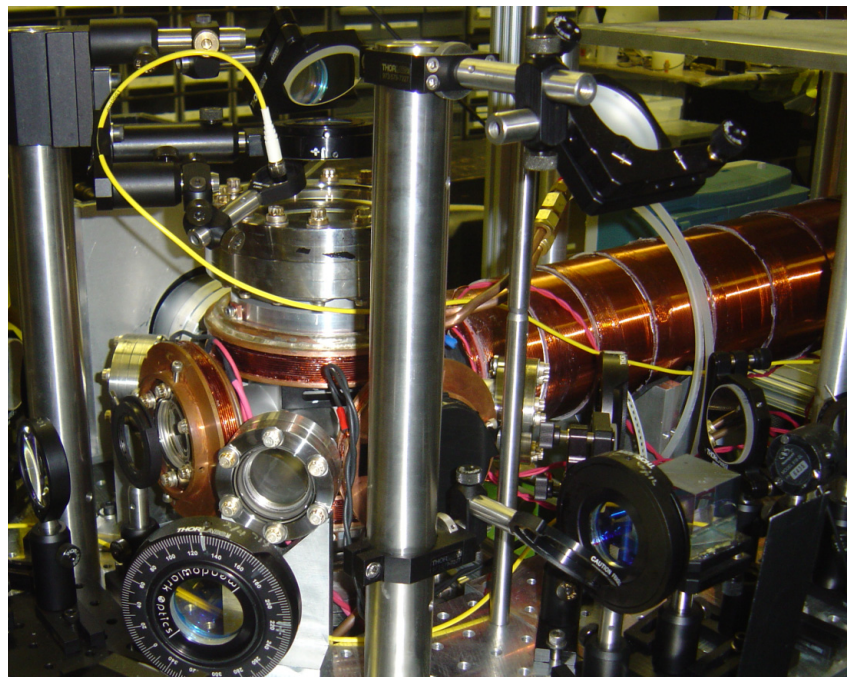


Fig. IV-22. Photograph of the radium Zeeman slower and magneto-optical trap.

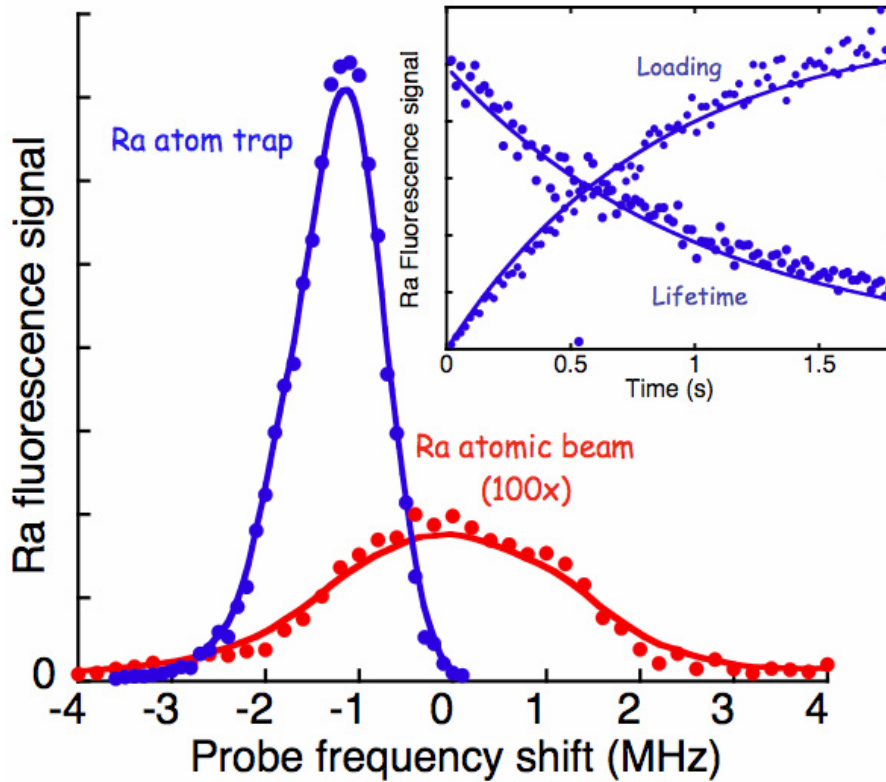


Fig. IV-23. Fluorescence signal of ^{226}Ra atoms in the MOT is compared to the signal from the atomic beam (scaled by 100 x). The frequency of the transverse-cooling, slowing, and trapping beams at 714 nm are fixed to 800 kHz, 4.4 MHz and 2.4 MHz below the resonance of $7s^2\ ^1S_0 - 7p\ ^3P_1$ transition, respectively. The repump laser at 1428 nm is on resonance with the $6d\ ^3D_1 - 7p\ ^1P_1$ transition. The inset shows loading and lifetime curves from the trap which are obtained by unshuttering and shuttering the slowing laser at $t = 0$, respectively.

d.2. Measurement of $\sin^2\theta_W$ Through Parity Violation in Deep Inelastic Scattering (PV DIS) on Deuterium (P. E. Reimer, X. Zheng, J. Arrington, K. Hafidi, R. J. Holt, H. E. Jackson, and D. H. Potterveld)

A basic parameter of the Standard Model is $\sin^2\theta_W$ representing the relative coupling strength of the weak and electromagnetic forces. The Standard Model predicts the observed value $\sin^2\theta_W$ will vary (or run) as a function of Q^2 , the energy squared at which it is probed, due to radiative corrections. At an energy equivalent to the mass of the Z-boson ($Q^2 = M_z^2$), $\sin^2\theta_W$ is well measured; for $Q^2 < M_z^2$, however, only a few measurements exist. One way to probe $\sin^2\theta_W$ is through the asymmetry in parity violation (PV) in polarized deep inelastic scattering (DIS). The asymmetry (A_d) is relatively large ($A_d \approx 10^{-4} Q^2$), making it experimentally quite accessible. The sensitivity to $\sin^2\theta_W$ is through the product of the axial Z-electron and vector Z-quark couplings (C_{1q}) and the

product of the vector Z-electron and axial Z-quark couplings (C_{2q}). A program of DIS parity violation measurement at Jefferson Lab with both 6 and 11 GeV electron beams is being developed.

A preliminary measurement at JLab with a 6 GeV beam has been approved (E05-007).¹ These data will provide a measurement of $(2C_{2u} - C_{2d})$. Current experimental knowledge of this quantity has an uncertainty of 180% and is subject to model dependence in their interpretation. The complete measurement at 6 GeV will reduce this uncertainty by a factor of five. In addition, the 6 GeV experiment will explore the contribution of higher-twist effects to the asymmetry, providing crucial guidance to interpreting this data and

future PV-DIS measurement with the 12 GeV upgrade to JLab.

Once the JLab 12 GeV upgrade is completed, a measurement of both $\sin^2\theta_W$ and $(2C_{2u} - C_{2d})$ will be completed using the baseline equipment.² Because of the large parity violating asymmetry, this measurement can be completed with only two to three weeks of beam time and will provide a measurement of

$$\delta\sin^2\theta_W/\sin^2\theta_W = \pm 0.26\% \text{ (stat)} \pm 0.36\% \text{ (sys)},$$

competitive with other measurements below M_z^2 .

Finally, investigations are underway to construct a large-acceptance solenoid-based spectrometer to use DIS-Parity to not only measure $\sin^2\theta_W$ but also probe parton distributions at large- x . This spectrometer would also take advantage of the 11 GeV polarized electron beam at JLab.

¹J. Arrington *et al.*, " \bar{e} -²H Parity Violating Deep Inelastic Scattering at CEBAF 6 GeV," proposal 05007 to the JLab PAC, P. E. Reimer and X. Zheng, spokespersons, December 6, 2004.

²*Conceptual Design Report for the 12 GeV Upgrade of CEBAF*, J. Arrington *et al.*, eds., JLab, February 2005.

E. ATOM TRAP TRACE ANALYSIS

e.1. Measuring the Nuclear Charge Radius of ${}^8\text{He}$ ¹ (P. Mueller, K. Bailey, R. J. Holt, R. V. F. Janssens, Z.-T. Lu, T. P. O'Connor, J. P. Schiffer, I. Sulai, L.-B. Wang,* M.-G. Saint Laurent,† J.-Ch. Thomas,† A. C. C. Villari,† O. Naviliat-Cuncic,‡ X. Flechard,‡ and M. Paul§)

The two short-lived isotopes of helium, ${}^6\text{He}$ and ${}^8\text{He}$, exhibit an interesting nuclear structure with a loosely bound neutron halo around a ${}^4\text{He}$ -like core. Precision measurements of these isotopes provide insight into the fundamental interactions among the nucleons in very neutron rich systems and constitute important benchmarks for nuclear structure theories of light nuclei.

We have recently determined the nuclear charge radius of ${}^6\text{He}$ with a relative uncertainty of 0.7%.² The experiment was based on a measurement of the atomic isotope shift between ${}^6\text{He}$ and ${}^4\text{He}$ using high resolution laser spectroscopy of single helium atoms cooled and confined in a magneto-optical trap. The resulting rms charge radius value of 2.054(14) fm corroborated the neutron halo structure of ${}^6\text{He}$ and verified the strong correlation between the halo neutrons predicted by most theoretical calculations. We now are working towards extending our technique to also measure the nuclear charge radius of ${}^8\text{He}$, which has the highest neutron-to-proton ratio of all known nuclei.

The main experimental challenge of this new effort is the sufficient production of ${}^8\text{He}$ and its efficient transfer into the laser spectroscopic setup. A minimum production rate of $5 \times 10^4 \text{ s}^{-1}$ is needed for an isotope shift measurement. In 2005 we conducted two exploratory experiments at ATLAS (1058X and 1122X) to investigate achievable production rates of ${}^8\text{He}$. The results clearly indicated that the required ${}^8\text{He}$ production rate could not be met. Subsequently, the

GANIL facility (Grand Accelérateur National d'Ion Lourds) in Caen, France was identified as an ideal alternative place to conduct this experiment in terms of production rate and accessibility of the ${}^8\text{He}$ for laser spectroscopy.

At GANIL, ${}^8\text{He}$ is produced by impinging a $\sim 70 \text{ MeV/u}$ ${}^{13}\text{C}$ beam of up to 2.2 μA current on a carbon target that is optimized for helium isotope production. The helium is subsequently ionized, mass separated and delivered into the experimental area as a low energy ($\sim 20 \text{ keV}$) ion beam. In previous experiments the low energy ${}^8\text{He}$ flux was as high as $6 \times 10^5 \text{ s}^{-1}$. In addition, the available experimental area is suitable to accommodate the atomic beam line and the laser system. Based on these favorable conditions a proposal for the ${}^8\text{He}$ nuclear charge radius measurement was submitted to the GANIL PAC. In December 2005, the proposal received full approval for a total of seven days of on-line beam time.

Currently, preparations for moving the experimental setup to GANIL are fully underway. In parallel, the overall trapping efficiency of the MOT setup has been improved through upgrades of the trapping laser system. Further improvements are expected from refinements of the spectroscopic setup. Pending final safety approvals at GANIL, a ${}^8\text{He}$ measurement is expected to take place in 2007 with a goal of reaching the 1% level of relative uncertainty for the nuclear charge radius.

*Los Alamos National Laboratory, †Grand Accelérateur National D'Ion Lourds (GANIL), Caen, France,

‡Laboratoire de Physique Corpusculaire (LPC), Caen, France, §Hebrew University, Jerusalem, Israel.

¹Project homepage: <http://www-mep.phy.anl.gov/atta/>.

²L.-B. Wang *et al.*, Phys. Rev Lett. **93**, 142501 (2004).

e.2. ATTA-3: The Next-Generation Instrument for ^{81}Kr -Dating (Z.-T. Lu, Y. Ding, K. Bailey, A. M. Davis,* R. W. Dunford,† S.-M. Hu,‡ P. Mueller, T. P. O'Connor, N. C. Sturchio,§ and L. Young†)

Atom Trap Trace Analysis (ATTA) has been used to analyze two rare isotopes: ^{81}Kr (isotopic abundance $\sim 10^{-12}$) and ^{85}Kr ($\sim 10^{-11}$), in environmental samples. Radiokrypton dating enabled by the ATTA method can now be used to determine the ages of old groundwater in the range of 50,000-1,000,000 years. The present apparatus (ATTA-2) has an overall counting efficiency of 0.01% and, for ^{81}Kr dating, requires a water sample of at least 1,000 liters. We are developing a new apparatus (ATTA-3) to trap and count ^{81}Kr atoms with the goal of reaching a counting efficiency of 1%. If successful, the required sample size would be reduced down to 10 liters of water or ice, and a wider range of applications in the earth sciences can be realized.

The total counting efficiency of ATTA is directly proportional to the efficiency of producing Kr^* atoms in the atomic beam source. So far, this has been

achieved by an RF driven discharge. We have recently tested a microwave-driven discharge, and found that it can increase the Kr^* flux by a factor of 2-3 over the RF source. Moreover, instead of the discharge source, direct optical production of Kr^* atoms is also under investigation. We have developed a setup to investigate the efficiency of transferring Kr atoms from the ground level to the metastable $5s[3/2]_2^0$ level via a 3-photon process: excitation with a vacuum ultraviolet photon at 124 nm and an infrared photon at 819 nm, followed by a spontaneous decay at 760 nm. All three transitions are of the allowed E1 type. This optical production scheme is a clean and potentially very efficient way of producing a well-collimated beam of Kr^* atoms. If successfully implemented, this scheme will enable the analysis of small samples required by many cosmochemistry and geochemistry applications.

*Enrico Fermi Institute and University of Chicago, †Chemistry Division, Argonne National Laboratory, ‡Hefei National Laboratory, University of Science and Technology of China, Hefei, China §University of Illinois at Chicago.

V. THEORETICAL PHYSICS

OVERVIEW

Our research addresses the five key questions that comprise the Nation's nuclear physics agenda. We place heavy emphasis on the prediction of phenomena accessible at Argonne's ATLAS facility, at JLab, and at other laboratories around the world; and on anticipating and planning for RIA. Our program in theoretical and computational nuclear astrophysics addresses such issues as the origin of the heaviest elements through the actinide region and the basic mechanisms of supernova explosions, and serves to identify critical nuclear parameters and systematic properties to be explored with RIA. We employ quantum chromodynamics to explore the structure of light- and heavy-hadrons: in vacuum, as relevant to programs such as those pursued at JLab; and in-medium, as appropriate to the early universe, compact astrophysical objects, and the RHIC program. Interactions between light hadrons are studied via the development of reaction theories that exploit modern ideas of hadron structure, which are then used to predict the outcomes of experiments at; e.g., JLab, MIT-Bates and Mainz. The structure of atomic nuclei is explored in *ab-initio* many-body calculations based on the realistic two- and three-nucleon potentials we have constructed. These potentials give excellent fits to nucleon-nucleon elastic scattering data and the properties of light nuclei. In addition, we use quantum Monte-Carlo methods to, e.g., compute nucleon-nucleus scattering phase shifts, transition amplitudes, and a variety of electroweak reactions important to astrophysics. Our nuclear structure and reaction program includes: coupled-channels calculations of heavy-ion reactions near the Coulomb barrier; calculations of observables in breakup reactions of nuclei far from stability, the determination of radiative capture rates from Coulomb dissociation experiments, and studies of high-spin deformation and the structure of the heaviest elements. Our programs provide much of the scientific basis for the drive to physics with rare isotopes. Additional research in the Group focuses on: atomic and neutron physics; fundamental quantum mechanics; quantum computing; and tests of fundamental symmetries and theories unifying all the forces of nature, and the search for a spatial or temporal variation in Nature's basic parameters. The pioneering development and use of massively parallel numerical simulations using hardware at Argonne and elsewhere is a major component of the Group's research.

A. NUCLEAR DYNAMICS WITH SUBNUCLEONIC DEGREES OF FREEDOM

The objective of this research program is: to investigate the role of quark-gluon degrees of freedom in hadron structure and interactions, and in nuclear dynamics; to explore the properties and phase structure of hot, dense Quantum Chromodynamics (QCD) and its possible consequences for the structure of compact astrophysical objects; to develop theoretical methods and tools to place reliable constraints on the variation of Nature's fundamental parameters and physics beyond the Standard Model; the development and application of reaction theories for use in exploring hadron structure using the data from meson and nucleon-resonance production experiments at modern experimental facilities; and to investigate relations of Poincaré covariant dynamics specified by mass operators to complementary dynamics specified by Green functions.

At the level of quark-gluon degrees of freedom, the Dyson-Schwinger equations (DSEs) provide a Poincaré covariant, nonperturbative method for studying QCD in the continuum. A hallmark of present-day DSE applications in hadron physics is the existence of a symmetry preserving truncation that enables the simultaneous exploration of phenomena such as: confinement, dynamical chiral symmetry breaking, and bound state structure and interactions. In addition the DSEs provide a generating tool for perturbation theory and hence yield model-independent results for the ultraviolet behavior of strong interaction observables. This means that model studies facilitate the use of physical processes to constrain the long-range behavior of the interaction between light-quarks in QCD, which is poorly understood and whose elucidation is a key goal of modern experimental programs. The last year saw numerous successful applications. For example, we studied σ -terms for hadrons and constituent-quarks. For a given object, this quantity describes its current-quark mass dependence, and that information is important when attempting to use observational data to place constraints on the variation of nature's fundamental parameters. In addition, we used the techniques of non-equilibrium quantum mean-field theory to study electron-positron pair production in fields that can be produced by modern optical lasers. Significant polarization of the QED vacuum is achievable. These dynamical effects may be signaled by the appearance of coincident photon pairs, from e^+e^- annihilation, with a mean energy of ~ 1 MeV and an intensity of 5-10 events per laser pulse. This represents a nonlinear transformation of soft laser photons to γ -quanta with a frequency ratio of $>10^6$.

At the level of meson and baryon degrees of freedom, we are continuing our effort to develop a dynamical coupled-channels model for use in analyzing the very extensive set of data for electromagnetic meson production reactions. A key objective is the development of an interpretation for this data in terms of the quark-gluon substructure of nucleon resonances (N^*). We aim to draw the connection between this data and the predictions made by QCD-based hadron models and numerical simulations of lattice-regularized QCD. In the past year we demonstrated the importance of the three-body $\pi\pi N$ unitarity condition in determining the two-pion production cross sections. We also made material progress in quantifying coupled-channel effects on the KY and ωN photoproduction reactions. Our results indicate clearly that previous analyses, based on tree-diagrams or K -matrix models are invalid. In addition, we have taken a lead role in an ambitious project at JLab; namely, the newly-formed Excited Baryon Analysis Center (EBAC), for which our experience with dynamical coupled-channels model is essential. The goal is a comprehensive and accurate analysis of JLab's meson production data by 2009.

Moreover, we predicted the neutrino-nucleus reaction cross sections on a range extending to a few GeV, in order to facilitate analyses of experiments that are aimed at measuring the fundamental properties of neutrinos, and completed a review article on the search for a Θ^+ (pentaquark) state.

Relativistic quantum dynamics requires a unitary representation of space-time symmetries (Poincaré group) and localization of states, such that states localized in relatively space-like regions are causally independent. We have recently focused on the application and elucidation of complementary mathematical representations of hadron phenomena.

a.1. Possible Evidence for “Dark Radiation” from Big Bang Nucleosynthesis Data (V. V. Flambaum* and E. V. Shuryak†)

We explored¹ a possible discrepancy between Big-Bang Nucleosynthesis (BBN) calculations and measurements based, for example, on recent inferences from BBN of the “effective number of extra neutrinos,” which tends to be negative: $\Delta N_\nu = -0.65 \pm 0.35$. Including other forms of matter, e.g., right-handed neutrinos, the discrepancy increases. At present, the effect is only two standard-deviations. Hence, it may not be serious.

Nevertheless, it is of interest to explore the ramifications of such a discrepancy.

We restricted our discussion to the simplest version of brane cosmology, with a single brane in a multi-dimensional space. New terms owing to second-order effects in density and a bulk gravity field appear in the effective evolution equation on the brane:

$$\begin{aligned} dp/d\tau + 3(1 + \omega) (\rho/a) da/d\tau = -T^{\text{leak}} = - (d\chi/d\tau + 4(\chi/a)da/d\tau), \\ [(1/a) da/d\tau]^2 = a \rho^2 + [8\pi/(3M_p^2)][\rho + \chi], \end{aligned}$$

where a is associated with the cosmological *Ansatz* for the metric, ρ is the energy-density on the brane, M_p is the Planck mass and $\omega = p/\rho$ is the usual equation of state for brane matter. The “dark radiation” term χ is the leading correction to standard cosmology. It has the same evolution as radiation-dominated matter, for which $\omega = 1/3$. The term T^{leak} describes “leakage” of energy from the brane to the bulk, which happens during the early (nonlinear) stage of evolution. N.B. The sum $(\rho + \chi)$ is conserved.

brane universe, it is quite natural to obtain negative χ .

One may express the BBN discrepancy as $\chi/\rho \approx 0.15 \Delta N_\nu \approx -0.10 \pm 0.05$.

In addition, as both BBN and Cosmic Microwave Background (CMB) coincide with the radiation-dominated era, the ratio χ/ρ should be fixed. N.B. The last change in the effective number of degrees-of-freedom occurred after e^+e^- annihilation. The most recent results for the effective number of neutrinos (Table 10, Ref. 2) may be interpreted as $\chi/\rho = 0.39^{+0.03}_{-0.47}$ for the WMAP+SDSS combination of data, $\chi/\rho = -0.05^{+0.04}_{-0.23}$ for WMAP+2dFGRC, and $\chi/\rho = 0.04^{+0.06}_{-0.29}$ for WMAP+LSS+SN. Better data on both BBN and CMB might test whether one value of χ/ρ is consistent with both. If that is not the case, the brane cosmology model becomes questionable.

The coefficient 0.15 is based on the effective number of degrees of freedom during BBN. For an expanding

*Argonne Fellow, Physics Division, and University of New South Wales, Sydney, Australia, †State University of New York at Stony Brook.

¹V. V. Flambaum and E. V. Shuryak, to appear in *Europhys. Lett.* **74** (2006).

²D. N. Spergel *et al.*, *astro-ph/0603449*.

a.2. Space-Time Variation of Strong Interactions and Fine Structure Constant (V. V. Flambaum*)

Grand Unification Models suggest that the fundamental masses ($m_{electron}$, m_{quark}) and the strong interaction scale Λ_{QCD} may vary much faster than the QED fine structure constant α . A number of theoretical and experimental papers devoted to temporal variation of m/Λ_{QCD} were recently published. There is some evidence for this parameter variation in Big Bang nucleosynthesis, quasar absorption spectra and Oklo natural nuclear reactor data. The need for an interpretation of these measurements and the search for new, enhanced effects have created a topical field of research: strong interaction calculations of the dependence of nuclear parameters on quark masses. We have been active in this area.

As described more fully below, we calculated the current-quark-mass dependence of nucleon and meson masses. This information is needed as input for a determination of the m/Λ_{QCD} dependence of: the nuclear interactions between nucleons; nuclear energy levels; and nuclear magnetic moments.

We showed¹ that the relative effects of a variation in α and m_{quark}/Λ_{QCD} are enhanced by 5-6 orders-of-magnitude in a very narrow ultraviolet transition between the ground and first excited state in ^{229}Th (energy ~ 5 eV). An experiment capitalizing on this can potentially improve sensitivity to a variation in Nature's fundamental parameters by 7-10 orders-of-magnitude (exposing a variation of up to 10^{23} /year).

We demonstrated² that atomic scattering lengths, which can be measured in Bose-Einstein condensate and Feshbach molecule experiments, are extremely sensitive to the variation of Nature's fundamental constants, in particular, to the electron-to-proton mass ratio (m_e/m_p). Based on a single- and two-channel scattering model, we showed how this variation in the mass ratio is communicated to the scattering length. Our results suggest that a variation in m_e/m_p on the level of $10^{-11} \sim 10^{-13}$ can be detected near a narrow magnetic or an optical Feshbach resonance by monitoring the scattering length on the 1% level. The formulae we have derived may also be used to estimate the isotopic shift in the scattering length.

We calculated³ the dependence of nuclear magnetic moments on the current-quark masses, including an

estimate of the effect of spin-spin interactions, and obtained limits on the variation of α and (m_{quark}/Λ_{QCD}) by using recent atomic clock experiments that examine the hyperfine transitions in H, Rb, Cs, Yb^+ and Hg^+ and the optical transition in H, Hg^+ and Yb^+ .

To expose a possible variation of α in laboratory experiments, we proposed using narrow lines that correspond to atomic transitions between close-lying, long-lived atomic states with different configurations.⁴ The small transition frequency, coupled with differences in electron structure ensure a strong enhancement of the relative frequency change compared to a possible change in α . The small linewidth makes it possible to perform very accurate measurements. When combined, these two features make the measurements very sensitive to any variation of α .

We demonstrated⁵ that the configuration interaction in many-electron atoms may cause anomalies in the atom's fine structure, which makes the intervals very small and very sensitive to a variation in α . For example, in ^{52}Te the enhancement factor is approximately 100.

An accurate *ab-initio* method for calculating both isotope and relativistic shifts in atomic spectra was presented.⁶ Numerical results for neutral carbon and three carbon ions were obtained. The relativistic shifts are needed to search for α variation using cosmic spectra. The isotope shifts can be used to measure isotope abundances in gas clouds, study nuclear reactions in stars and supernova, and test models of the chemical evolution of the Universe. The variation of isotope abundances is also needed in order to exclude an important systematic error in the α -variation studies.

We found⁷ that the relative effect of a variation in α on microwave transitions between very close and narrow rotational-hyperfine levels may be enhanced by 2-3 orders-of-magnitude in diatomic molecules with unpaired electrons, such as LaS, LaO, LuS, LuO, YbF, and similar molecular ions. The enhancement results from cancellation between the hyperfine and rotational intervals.

*Argonne Fellow, Physics Division, and University of New South Wales, Sydney, Australia.

¹V. V. Flambaum, physics/0604188.

²Cheng Chin and V. V. Flambaum, cond-mat/0603607.

³V. V. Flambaum and A. F. Tedesco, to appear in Phys. Rev. C, nucl-th/0601050.

⁴E. J. Angstromann, V. A. Dzuba, V. V. Flambaum, S. G. Karshenboim, and A. Yu. Nevsky, J. Phys. B **39**, 1937 (2006).

⁵V. A. Dzuba and V. V. Flambaum, Phys. Rev. A **72**, 052514 (2005).

⁶J. C. Berengut, V. V. Flambaum, and M. G. Kozlov, Phys. Rev. A **73**, 012504 (2006).

⁷V. V. Flambaum, Phys. Rev. A **73**, 034101 (2006).

a.3. Coulomb Problem for Vector Bosons (V. V. Flambaum* and M. Yu. Kuchiev†)

There is a difficulty with the Coulomb problem for vector bosons. Indeed, soon after Proca formulated a theory for vector particles it became clear that it produces inadequate results for the Coulomb problem. This inspired Corben and Schwinger to modify Proca's theory, tuning the Lagrangian and the equations of motion so as to force the vector boson's gyromagnetic ratio to acquire the value $g = 2$. (N.B. $g = 2$ is the Standard Model value for W_{\pm}). They obtained a simple Sommerfeld-type formula for the spectrum valid up to $Z\alpha = 1/2$.

However, the problem has not completely disappeared: for $j = 0$ states the charge of the boson localized in the vicinity of the attractive Coulomb center remains infinite. We re-derived¹ these results for the spectrum and wave function starting from the Standard Model and then displayed a clear way to properly formulate the Coulomb problem for vector particles. Our main

observation is that the polarization of the QED vacuum has a profound impact on the problem, forcing the density of charge of a vector boson to decrease exponentially at the origin thus making the Coulomb problem stable and well defined.

At first glance this result may be surprising because the vacuum polarization increases the strength of the attractive field at the origin. Moreover, the vacuum polarization for spinor and scalar particles in the Coulomb field is known to produce only small, perturbative effects. In contrast, we find for the vector particle a *strong reduction* in its charge density near the origin. To grasp the physical mechanism involved it is necessary to notice that the equation of motion for vector particles contains a particular term, which has no counterparts for scalars and spinors; namely, the last term in the following equation:

$$(\partial^2 + m^2) W^\mu + 2ie F^{\mu\nu} W_\nu + (ie/m^2) \partial^\mu (j_\nu W^\nu) = 0.$$

This additional term is responsible for a strong repulsion arising from the vacuum polarization and makes the Coulomb problem stable. The effective potential becomes large and positive when $r \rightarrow 0$; viz., $U(r) \approx Z^2 \alpha^3 \beta / (m^2 r^4)$.

Here the factor β is the lowest coefficient of the Gell-Mann–Low function. Both the Standard Model and experimental data indicate that $\beta > 0$, presumably, up to the Grand Unification limit. Hence the vacuum polarization results in an intense repulsion near the origin for even arbitrarily small values of $Z^2 \alpha^3$.

The wave function decreases exponentially at small distances: $\varphi(r) \sim \exp(-Z\alpha (\alpha\beta)^{1/2} / [m r])$, so that the charge density of the W-boson also decreases exponentially at the origin. Thus, accounting for the QED vacuum polarization eliminates the difficulty related to the infinite charge of a vector boson located at the Coulomb center.

For small Z the energy shift of discrete energy levels owing to the vacuum polarization is found to be small, which makes the Sommerfeld formula applicable for the spectrum of vector bosons.

*Argonne Fellow, Physics Division, and University of New South Wales, Sydney, Australia, †University of New South Wales, Sydney, Australia.

¹M. Yu. Kuchiev and V. V. Flambaum, Mod. Phys. Lett. A **21**, 781 (2006).

a.4. Pair Production and Optical Lasers (C. D. Roberts, D. B. Blaschke,*
A. V. Prozorkevich,† S. M. Schmidt,‡ and S. A. Smolyansky†)

In the presence of a strong external electric field the vacuum of QED “breaks down” via the emission of electron-positron pairs. A theoretical understanding of this phenomenon is well established, but hitherto an experimental verification is lacking. A key obstacle is the very high value of the electric field required to achieve it; namely, for electrons,

$$E_{cr} = m^2/e = 1.3 \times 10^{16} \text{ V/cm.}$$

According to Schwinger's formula, the pair creation rate in a constant electric field is exponentially damped for $E \ll E_{cr}$. However, a very different situation exists when the electric field is strongly time-dependent. In this case vacuum decay is a far-from-equilibrium, time-dependent process and hence kinetic theory provides an appropriate descriptive framework.

We studied electron-positron pair creation in a standing wave using a parameter-free quantum kinetic equation introduced in Ref. 1, which allows one to consider pair production as a dynamical process while accounting properly for the initial conditions. This method is essentially nonperturbative and possesses novel features. For example, it incorporates the essentially non-Markovian character of pair production in quantum

field theory and its dependence on particle statistics, and provides for a description of the complete momentum-dependence of the single-particle distribution function. A characteristic feature of the kinetic approach is an ability to describe quasiparticle excitations during all stages in the evolution of an external field.

We found that field strengths and frequencies corresponding to modern optical lasers induce a material polarization of the QED vacuum, which may be characterized as a plasma of e^+e^- quasiparticle pairs with a density of approximately 10^{20} cm^{-3} . The plasma vanishes almost completely when the laser field is zero, leaving a very small residual pair density, n_r , which is the true manifestation of vacuum decay. The average pair density per period is proportional to the laser intensity but independent of the frequency, ν . The density of residual pairs also grows with laser intensity but n_r is proportional to ν^2 . Our calculations revealed that with optical lasers at the forefront of the current generation, these dynamical QED vacuum effects can plausibly generate 5-10 observable two-photon annihilation events per laser pulse.

An article describing this work was published.²

*Gesellschaft für Schwerionenforschung (GSI), Darmstadt, Germany, and Joint Institute for Nuclear Research, Dubna, Russia, †Saratov State University, Russia, ‡Helmholtz-Gemeinschaft, Jülich, Germany.

¹S. M. Schmidt *et al.*, Int. J. Mod. Phys. E **7**, 709 (1998).

²D. B. Blaschke, A.V. Prozorkevich, C. D. Roberts, S. M. Schmidt, and S. A. Smolyansky, Phys. Rev. Lett. **96**, 140402 (2006).

a.5. The Strange Star Surface: A Crust with Nuggets (P. Jaikumar, S. Reddy* and
A. W. Steiner*)

Strange quark stars, made entirely of quark matter in a deconfined state, can exist if dense quark matter at sufficiently high density is absolutely stable at zero pressure. Based upon a picture of homogeneous quark matter satisfying local charge neutrality, it was widely accepted that the surface of quark stars was characterized by an enormous density gradient (10^{26} g/cm^4) and large electric fields (10^{16} V/cm). We re-examined the surface composition of strange stars and found that, provided the surface tension of quark matter is small enough, the homogeneous phase is unstable against the formation of a heterogenous one

consisting of quark nuggets immersed in a uniform background of electrons.

We analyzed the phase stability and structure of quark matter in a model-independent way by identifying two quantities, the charge density and the charge susceptibility, that determine the criterion for phase separation into quarks and electrons. We evaluated this criterion in the framework of the Bag model of dense quark matter, and found that the Gibbs free energy would be lower in a mixed phase in which quark matter lumps together to form positively charged nuggets of size $\sim 10 \text{ fm}$. The mixed phase satisfies global charge

neutrality and its structure is particularly sensitive to finite size effects.

If strange quark stars possess a heterogeneous crust, the thermal conductivity and neutrino opacity is very similar to that in the crust of neutron stars, making a distinction between the two classes of stars quite

difficult. The presence of a solid crust at low temperatures can also help explain the observed glitches in the spin-period of neutron stars.

An article describing this work was published¹ and a précis appeared in Physical Review Focus.²

*Los Alamos National Laboratory.

¹P. Jaikumar, S. Reddy, and A. W. Steiner, Phys. Rev. Lett. **96**, 041101 (2006).

²P. Jaikumar *et al.*, Phys. Rev. Focus, February 3, 2006.

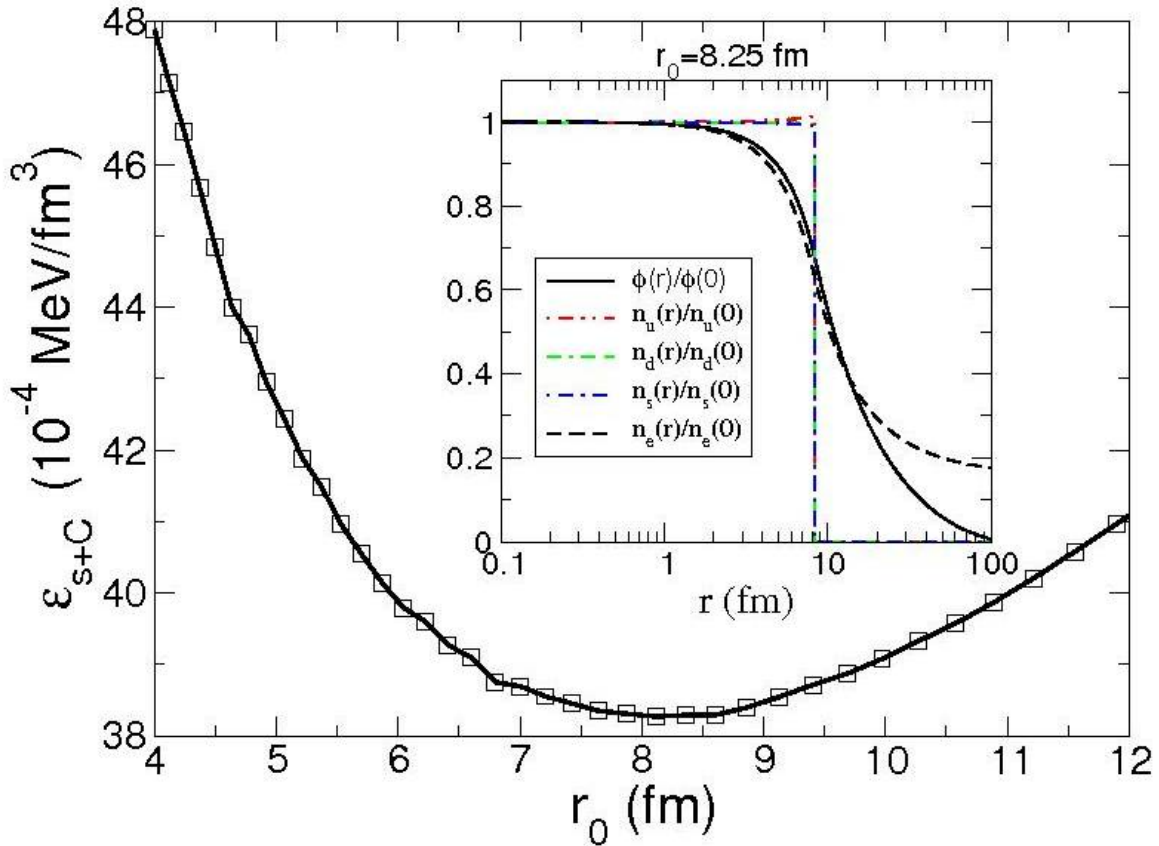


Fig. V-1. The sum of surface and Coulomb energies associated to the formation of a quark nugget of size r_0 (fm). The optimal size, for our choice of surface tension and bag constant, is given by the minimum of the curve at $r_0 = 8.25 \text{ fm}$. The inset shows the electrostatic potential as well as the quark and electron number densities inside and outside the quark nugget.

a.6. Bremsstrahlung Neutrinos from Electron-Electron Scattering in a Relativistic Degenerate Electron Plasma (P. Jaikumar, C. Gale,* and D. Page†)

Energy loss through neutrino emission is the driving force in the evolution of supernovae and neutron stars. We studied neutrino pair bremsstrahlung emission in

collisions of relativistic particles (electrons) including medium modifications of photons exchanged in the collision and other many-body effects. Soft photon

exchange in the magnetic sector is Landau damped, and we provided the first estimate of this effect on the neutrino emission rate. Our results revealed that bremsstrahlung pair emission can dominate over other sources of neutrino emission, particularly in the superfluid crust of neutron stars just above nuclear saturation density and in the core, if it is in a superfluid state.

The photon exchange in electron-electron scattering was described by the one-loop resummed photon propagator in the hard dense loop limit, and corrections to the emissivity from multiple photon exchange, vertex dressing, as well as non-Fermi liquid effects were shown to be small. The neutrino emissivity was found

to be enhanced by several orders of magnitude at low temperatures ($T \leq 10^8$ K) in comparison with previous works that neglected Landau damping effects.

Based upon a comparison with other neutrino emission mechanisms, we also established the relevance of neutrino bremsstrahlung rates for cooling of black-hole accretion tori. Neutrino pair bremsstrahlung becomes the dominant cooling process in the low density ($\rho \leq 10^{10}$ g/cm³) and low temperature ($T \leq 10^{10}$ K) regions of the black-hole accretion torus. It also provides the most copious source for antineutrinos which are believed to play an important role in triggering Gamma ray bursts in the collapsar scenario. An article describing this work was published.¹

*McGill University, Montreal, Quebec, †National Autonomous University of Mexico, Mexico City, Mexico.

¹P. Jaikumar, C. Gale, and D. Page, Phys. Rev. D **72**, 123004 (2005).

a.7. Direct Urca Neutrino Rate in Color Superconducting Quark Matter (P. Jaikumar, C. D. Roberts, and A. Sedrakian*)

The direct urca process of neutrino emission in quark matter ($d \rightarrow u + e + \nu_e$ and $u + e \rightarrow d + \nu_e$) is the most efficient cooling mechanism for neutron stars containing unpaired quark matter in their core. If the quark matter is in a superconducting phase, neutrino emission is modified by the presence of the pairing gap. We evaluated the impact of pairing on the neutrino emission rate in fully and partially gapped regimes. Our results showed that the pairing-induced suppression of the rate below the critical temperature T_c was not as severe as previously believed, and that Cooper pair-breaking and recombination makes an important contribution to the total neutrino emissivity.

We explored a minimal realistic scenario of two-flavor (u, d) quark matter, with spin-singlet pairing, constrained by charge neutrality and β -equilibrium. In this case, we found that the quark dispersion relation could be either fully or partially gapped. Including interaction corrections linear in the strong coupling parameter α_s , pairing-induced phase space corrections and Cooper pair-breaking and recombination effects, we found the neutrino rate was: (1) suppressed only linearly on a material domain of temperatures below the critical temperature T_c for the fully gapped phase; and (2) moderately enhanced above that of unpaired quark matter at low temperatures in the partially gapped phase. These results are illustrated in Fig. V-2.

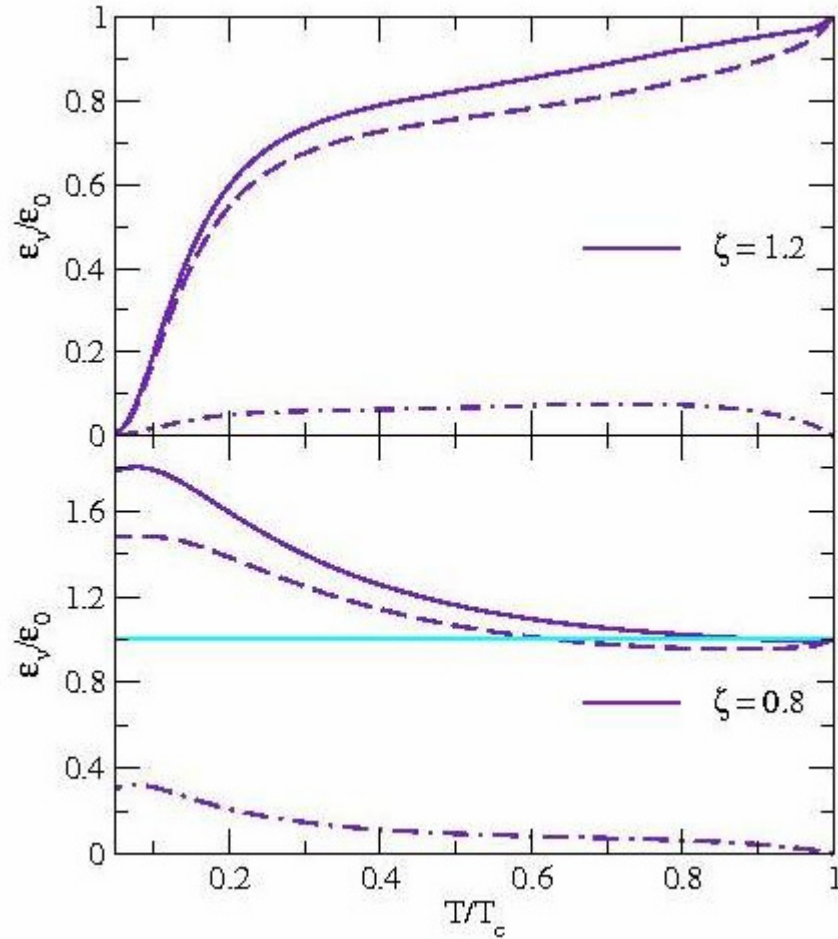


Fig. V-2. Temperature dependence of the emissivity normalized to its value at the critical temperature. Upper panel - fully gapped regime; and lower panel - partially gapped regime. In both panels, the dashed and dash-dotted curves are, respectively, normal and pair-breaking contributions; and the solid line is their sum. In the lower panel, the horizontal line $\varepsilon_{\nu}/\varepsilon_0 = 1$ is the result for unpaired matter. The quark chemical potentials are typical of two-flavor superconducting matter.

Our calculation in the two-flavor regime is indicative of similar results for the neutrino rate in phases of gapped quark matter with three flavors. Considered together with neutrino opacities, which are large at $T \sim T_c$, our results are pertinent to any detailed computation of the

cooling history of a star that undergoes a phase transition from nuclear matter to superconducting quark matter.

An article describing this work was published.¹

*University of Tübingen, Germany.

¹P. Jaikumar, C. D. Roberts, and A. Sedrakian, Phys. Rev. C **73**, 042801 (2006).

a.8. Quark Deconfinement in Neutron Star Cores: The Effects of Spin-Down (P. Jaikumar, J. Staff,* and R. Ouyed*)

We studied the role of spin-down of isolated neutron stars in driving quark deconfinement in its high-density core. We concluded that light neutron stars (≤ 1.6 solar

masses) are the most likely to currently support a quark phase if their central densities are large enough to permit the transition to occur. We also found that more

massive neutron stars (≥ 1.8 solar masses) can enter a quark phase only if they are spinning faster than about 3 milliseconds as observed now.

We created sequences of neutron star models using numerical methods developed specifically to treat rapidly rotating neutron stars. We obtained typical timescales to reach quark deconfinement in the core of neutron stars that are born with Keplerian frequencies.

We found this time to be least for equations of state that support the largest minimum mass at zero spin, unless the moment of inertia is very high. For each equation of state, we also determined the minimum and maximum neutron star masses, as well as the current minimum spin periods that will allow for deconfinement in a Hubble time via spin-down only. These results are presented in Tables V-1 and V-2.

Table V-1. Column-I: equation of state, see Ref. 1; Column-II: minimum gravitational mass at zero spin; Column-III: maximum gravitational mass at Kepler rotation; and Column-IV: minimum density at Kepler rotation that can reach the fiducial critical density ($\rho_c = 5 \rho_0$) due to spindown.

EOS	$M_{\min} (M_{\odot})$	$M_{\max} (M_{\odot})$	$\rho_{\min} (\rho_0)$
BBB2	1.46	1.79	3.92
APR	1.78	2.16	4.12
C	1.53	1.83	3.88
OBJ	2.8	3.36	2.52

Table V-2. Time taken for a minimum mass star to spin down from Kepler frequency to within 1% of ρ_c for different magnetic field strengths (B).

EOS	$M_{\min} (M_{\odot})$	B = 10^{15} G	Time		
			10^{14} G	10^{13} G	10^{12} G
BBB2	1.46	96 min	6.7 days	667 days	183 years
APR	1.78	73 min	5.1 days	505 days	152 years
C	1.53	89 min	6.2 days	619 days	170 years
OBJ	2.80	348 min	24 days	2418 days	663 years

Our results directly address the issue of forming a quark star in the spin-down epoch of a neutron star, and present a window in mass and spin-periods in which observers are likely to discover quark stars. They also suggest that the existence of quark stars is predicated

upon having a low deconfinement threshold of less than five-times the saturation density of nuclear matter.

An article describing this work was submitted.¹

*University of Calgary, Alberta, Canada.

¹J. Staff, R. Ouyed, and P. Jaikumar, submitted to *Astrophys. J. Lett.*, astro-ph/0603743.

a.9. Pseudoscalar Meson Radial Excitations (A. Höll, A. Krassnigg, and C. D. Roberts)

The known meson spectrum contains three pseudoscalars [$I^G (J^{PC}) = 1^- (0^{++})$], all with masses below 2 GeV: $\pi(140)$; $\pi(1300)$; and $\pi(1800)$. The lightest of these, the pion [$\pi(140)$], is much studied and well understood as QCD's Goldstone mode. It is the key

degree of freedom in chiral effective theories, and a veracious explanation of its properties requires an approach to possess a valid realization of chiral symmetry and its dynamical breaking. The $\pi(1300)$ is likely the first radial excitation of $\pi(140)$ and while the

$\pi(1800)$ may be the second radial excitation, it could also be a hybrid; i.e., a state with nontrivial constituent-gluon-like content. A hallmark in the contemporary use of Dyson-Schwinger equations is the existence of a nonperturbative, symmetry preserving truncation scheme. We used this scheme to prove that of all pseudoscalar mesons supported by QCD, only the Goldstone modes possess a nonzero leptonic decay constant in the chiral limit when chiral symmetry is dynamically broken. The decay constants of all other pseudoscalar mesons vanish, whether they are radial excitations or hybrids; viz., $f(\pi_n) = 0$ for all $n \geq 1$. ($n = 0$ denotes the ground state while $n \geq 1$ denotes higher mass states.) This means that in the chiral limit every pseudoscalar meson is blind to the weak interaction except the $\pi(140)$. This exact result places a very tight constraint on all models and nonperturbative methods in their application to hadron spectroscopy and interactions, particularly in connection with the search for exotic and hybrid states in the 1-2 GeV range.

We illustrated these features and aspects of their impact on the meson spectrum using a model of the kernels in the gap and Bethe-Salpeter equations. This work

provides the first Poincaré covariant and symmetry preserving analysis of meson excited states. Moreover, it shows that at realistic current-quark masses the leptonic decay constant of the first radial excitation is two orders of magnitude smaller than that of the $\pi(140)$; and gives the first direct indication that when the current-quark mass is nonzero the leptonic decay constants of mesons on the pseudoscalar trajectory alternate in sign; viz., the decay constants of the ground state and the 2nd, 4th, etc. heaviest states are positive, while those of the 1st, 3rd, etc. are negative. *A posteriori* it is apparent that this outcome is necessary to ensure that the spectral density in the I^{++} channel is non-negative. Nevertheless, the result was not anticipated nor reported previously.

The model was also used to predict: $f(\eta_c) = 0.233$ GeV and $m(\eta_c) = 3.42$ GeV. In addition, studies were made within this framework that provide support for an interpretation of $\eta(1295)$ and $\eta(1470)$ as radial excitations of $\eta(1295)$ and $\eta(1470)$, respectively; and $K(1460)$ as the first radial excitation of the kaon.

Articles describing this work were published.^{1,2}

¹A. Höll, A. Krassnigg, and C. D. Roberts, Phys. Rev. C **70**, 042203(R) (2004).

²A. Höll, A. Krassnigg, C. D. Roberts, and S. V. Wright, Int. J. Mod. Phys. A **20**, 1778 (2005).

a.10. Electromagnetic Properties of Ground and Excited State Pseudoscalar Mesons

(A. Höll, A. Krassnigg, C. D. Roberts, S. V. Wright, and P. Maris*)

The strong interaction spectrum exhibits trajectories of mesons with the same spin+parity, J^P . One may distinguish between the states on these trajectories by introducing an integer label n , with $n = 0$ denoting the lowest-mass state, $n = 1$ the next-lightest state, etc. The Bethe-Salpeter equation (BSE) yields the mass and amplitude of every bound state in a given channel specified by J^P . Hence it provides a practical tool for the Poincaré covariant study of mesons on these trajectories. A significant feature of such applications is the fact that at least one nonperturbative and symmetry preserving Dyson-Schwinger equation (DSE) truncation scheme exists. This supports the proof of exact results such as, e.g., in the chiral limit excited state 0^- mesons do not couple to the axial-vector current; viz., $f(\pi_n) \equiv 0$ for all $n \geq 1$.

We demonstrated that the leading-order (rainbow-ladder) term in the DSE truncation scheme, when consistently implemented, is necessary and sufficient to express the Abelian anomaly. It can therefore be used

to illustrate the anomaly's observable consequences. We capitalized on this to show that even though excited state pseudoscalar mesons decouple from the axial-vector current in the chiral limit, they nevertheless couple to two photons. It follows that the Primakov process, as employed for example in *PrimEx* at JLab may be used as a tool for their production and study. We established in addition that the strength of the two-photon coupling is materially affected by the continuum contribution to the Abelian anomaly.

A renormalization-group-improved rainbow-ladder truncation is guaranteed to express the one-loop renormalization group properties of QCD. We exploited this and thereby determined the leading power-law behavior of the $\gamma^* \pi_n \gamma^*$ transition form factor. When the current-quark mass is nonzero then this form factor behaves as $(4\pi^2/3) (f(\pi_n)/Q^2)$ at deep spacelike momenta. For all but the Goldstone mode this leading order contribution vanishes in the chiral limit. In that case, however, the form factor remains

nonzero and the ultraviolet behaviour is $\approx (4\pi^2/3) (-\langle \bar{q} q \rangle / Q^4)$. Although only exposed starkly in the chiral limit for excited states, this subleading power-law contribution to the transition form factor is always present and in general its coefficient is not simply related to $f(\pi_n)$.

As one might rationally expect, the properties of excited ($n \geq 1$) states are sensitive to the pointwise behavior of what might be called the confinement potential between light-quarks. We illustrated this by laying out the evolution of the charge radii of the $n = 0, 1$ pseudoscalar mesons. As it is shielded by Goldstone's theorem, the ground state's radius can be insensitive to details of the long-range part of the interaction. However, that is not true of $r(\pi_1)$, the radius of the first excited state. This state is orthogonal to the vacuum. An increase in the length-scale that characterizes the range of the confining potential

reduces $r(\pi_1)$. This result states that increasing the confinement force compresses the excited state: indeed, it is possible to obtain $r(\pi_1) < r(\pi_0)$. However, our current best estimate is $r(\pi_1) \approx 1.4 r(\pi_0)$.

A detailed exploration of the properties of collections of mesons on particular J^P trajectories offers the hope of exposing features of the long-range part of the interaction between light-quarks. In principle, this interaction can be quite different to that between heavy-quarks. The pseudoscalar trajectory is of particular interest because its lowest mass entry is QCD's Goldstone mode. Chiral current conservation places constraints on some properties of every member of this trajectory, whose study may therefore provide information about the interplay between confinement and dynamical chiral symmetry breaking.

An article describing this work was published.¹

*University of Pittsburgh.

¹A. Höll, A. Krassnigg, P. Maris, C. D. Roberts, and S. V. Wright, Phys. Rev. C **71**, 065204 (2005).

a.11. Nucleon Electromagnetic Form Factors (A. Höll, A. Krassnigg, C. D. Roberts, S. V. Wright, R. Alkofer,* and M. Kloker*)

Modern, high-luminosity experimental facilities that employ large momentum transfer reactions are providing remarkable and intriguing new information on nucleon structure. At values of momentum transfer, $Q^2 > M^2$, where M is the nucleon's mass, a veracious understanding of these data requires a Poincaré covariant description of the nucleon. We employed a Poincaré covariant Faddeev equation that describes baryons as composites of confined-quarks and confined-diquarks, and solved this equation to obtain masses and amplitudes for the nucleon and Delta. Two parameters appear in the model Faddeev equation: masses of the scalar and axial-vector diquark correlations. They were fixed by fitting stipulated masses of the baryons. We interpreted the masses and Faddeev amplitudes thus obtained as representing properties of the baryons' *quark core* and argued that this should be augmented in a consistent fashion by chiral-loop corrections.

We described the formulation of a nucleon-photon vertex, which automatically ensures the vector Ward-Takahashi identity is fulfilled for on-shell nucleons described by the calculated Faddeev amplitudes. This guarantees current conservation. The vertex *Ansatz* involves three parameters. Two of these specify

electromagnetic properties of axial-vector diquarks and a third measures the strength of electromagnetically induced axial-vector-diquark \leftrightarrow scalar-diquark transitions. These quantities are also properties of the nucleons' quark core.

These elements are sufficient for a calculation of the quark contribution to the nucleons' electromagnetic form factors. We explored a reasonable range of nucleon-photon-vertex parameter values and found that an accurate description of the nucleons' static properties was not possible with the core components alone. However, this mismatch with experiment was greatly reduced by the inclusion of chiral-loop corrections. Since true pseudoscalar mesons are not pointlike their contribution to baryon form factors diminishes with increasing momentum transfer. Hence, experiments on nucleons involving $Q^2 > 2\text{GeV}^2$ probe properties of the Poincaré covariant quark core.

We calculated ratios of the proton's form factors. On the whole domain of nucleon-photon-vertex parameter values explored, the calculated behavior of $G_{Ep}(Q^2)/G_{Mp}(Q^2)$ for $Q^2 > 2\text{GeV}^2$ agrees with that inferred from contemporary polarization transfer data, and this ratio exhibits a zero at $Q^2 \approx 6.5\text{GeV}^2$.

Since the parameters in the nucleon-photon vertex do not influence these outcomes, we judge they are manifestations of features intrinsic to the nucleon's Faddeev amplitude. In the nucleon's rest frame, this amplitude corresponds to a relativistic wave function with s -, p - and even d -wave quark orbital angular momentum components.

Our study supports a view that baryons can realistically be seen as a dominant Poincaré covariant quark core,

*University of Tübingen, Germany.

¹R. Alkofer, A. Höll, M. Kloker, A. Krassnigg, and C. D. Roberts, *Few-Body Systems* **37**, 1 (2005).

²A. Höll, R. Alkofer, M. Kloker, A. Krassnigg, C. D. Roberts, and S. V. Wright, *Nucl. Phys.* **A755**, 298 (2005).

a.12. Sigma Terms of Light-Quark Hadrons (V. V. Flambaum,* A. Höll, P. Jaikumar, C. D. Roberts, and S. V. Wright)

A calculation of the current-quark mass dependence of hadron masses can help in using observational data to place constraints on the variation of nature's fundamental parameters. A hadron's sigma-term, σ_H , which is obtained from the matrix element

$$\langle H(x) | m J_\sigma(z) | H(y) \rangle,$$

is a measure of this dependence.

We illustrated the connection between a hadron's sigma-term and the Feynman-Hellmann theorem via an explicit calculation for the pion using a rainbow-ladder truncation of the DSEs: in the vicinity of the chiral limit $\sigma_\pi = 1/2 m_\pi$.

This truncation also provides a decent estimate of σ_ρ because the two dominant self-energy corrections to the ρ -meson's mass largely cancel in their contribution to σ_ρ . The truncation is less accurate for the ω , however, because there is little to compete with an $\omega \rightarrow \rho\pi$ self-energy contribution that magnifies the value of σ_ω by approximately 25%.

augmented by pseudoscalar meson cloud contributions that, e.g., make a noticeable contribution to form factors for $Q^2 < 2\text{GeV}^2$. Since meson compositeness ensures that such contributions diminish with increasing Q^2 , experiments at larger Q^2 serve as an instructive probe of correlations in baryon wave functions; i.e., their Faddeev amplitudes. A good understanding of QCD's long-range dynamics is required in order to obtain a reliable quark-core wave function.

Articles describing this work were published.^{1,2}

The analysis was extended to a scalar meson composed of u, d quarks, and yielded a description compatible with a picture of the lightest O^{++} as a bound state of a dressed-quark and anti-quark supplemented by a material pion cloud.

We also employed the Poincaré covariant Faddeev equation described above, which represents baryons as composites of confined-quarks and confined-nonpointlike-diquarks, to obtain the current-quark mass dependence of the masses of the nucleon and Δ , and thereby σ_N and σ_Δ . This “quark-core” piece was augmented in a consistent fashion by the “pion cloud” contribution, which is positive. Together, the contributions yield $\sigma_N \approx 60$ MeV and $\sigma_\Delta \approx 50$ MeV.

The insight we gained into the current-quark mass dependence of hadron masses can be summarized in terms of the ratio

$$\delta m_H / m_H = (\sigma_H / m_H) (\delta m_q / m_q)$$

where m_q is the current-quark mass, and our results are presented in Table V-3.

Table V-3. Meson, baryon and constituent-quark σ -terms calculated as described in Refs. 1,2. All results are renormalization-point-independent and were obtained with current-quark masses: $m_{u,d}(\zeta) = 3.7$ MeV, $m_s(\zeta) = 82$ MeV, $m_c(\zeta) = 0.97$ GeV and $m_b(\zeta) = 4.1$ GeV, where the renormalization point $\zeta = 19$ GeV. Perturbative evolution can be used to determine the associated renormalization-point-independent current-quark-masses.

H	π	π_l	σ	
σ_H/m_H	0.498	0.017	0.013	
H	ρ	ω	N	Δ
σ_H/m_H	0.021	0.034	0.064	0.041
Q	u,d	s	c	b
σ_Q/M_Q^E	0.023	0.230	0.637	0.851

The last two rows are novel. One measure of the importance of dynamical chiral symmetry breaking to the dressed-quark mass function is the magnitude, relative to the current-quark mass, of the Euclidean constituent-quark mass; viz.,

$$(M^E)^2 := s | s = [M(s)]^2.$$

A constituent-quark σ -term can subsequently be defined. For light-quarks the ratio σ_Q/M_Q^E must vanish because the magnitude of their constituent-mass owes primarily to dynamical chiral symmetry breaking, while for heavy-quarks the ratio approaches one.

An article describing this research was published¹ and another was submitted.²

*Argonne Fellow, Physics Division, and University of New South Wales, Sydney, Australia.

¹V. V. Flambaum, A. Höll, P. Jaikumar, C. D. Roberts, and S. V. Wright, *Few Body Systems* **38**, 31 (2006).

²A. Höll, P. Maris, C. D. Roberts, and S. V. Wright, *Schwinger Functions and Light-Quark Bound States, and Sigma Terms*; contribution to the proceedings of the “Workshop on Light-Cone QCD and Nonperturbative Hadron Physics 2005 (LC 2005),” Cairns, Queensland, Australia, July 7-15, 2005.

a.13. Nucleon Weak and Strong Form Factors (A. Höll, C. D. Roberts, and S. V. Wright)

The framework used in the Poincaré covariant study of nucleon electromagnetic form factors, which is described above, can naturally also be employed to calculate weak and strong form factors of the nucleon. These form factors are sensitive to different aspects of quark-nuclear physics and should prove useful, *e.g.*, in constraining coupled-channel models for medium-energy production reactions on the nucleon, such as those described below.

We have obtained preliminary results in the chiral limit for three such form factors: the axial-vector, $G_A(Q^2)$, and pseudoscalar, $G_P(Q^2)$, nucleon form factors, which appear in the axial-vector--nucleon current, and the pion-nucleon coupling, $g_{\pi NN}(Q^2)$. These first calcu-

lations were based on an axial-vector nucleon vertex constructed from components that are necessary but not sufficient to ensure fulfillment of the axial-vector Ward-Takahashi identity for on-shell nucleons. Work on improvement is underway.

In Fig. V-3, we depict our result for $G_P(Q^2)$. This pseudoscalar form factor is dominated by the pion pole in the neighborhood of $Q^2 = -m_\pi^2$, which for our chiral-limit calculation is $Q^2 = 0$. The comparison with data is favorable, particularly once one allows for a shift of the pion pole to $Q^2 = 0$, as appropriate for our chiral-limit calculation. We attribute this to an accurate realization of dynamical chiral symmetry breaking in the quark and pion sectors.

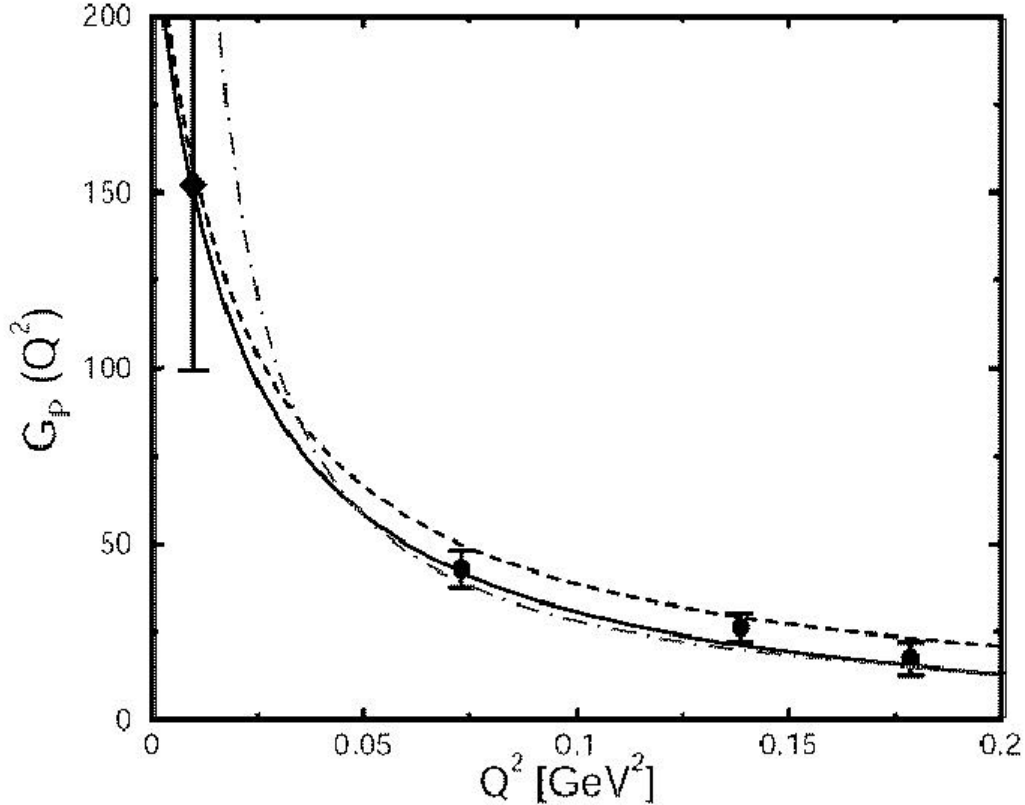


Fig. V-3. Chiral-limit result for $G_p(Q^2)$, dash-dot curve. Data obtained via pion electroproduction [filled circles, S. Choi *et al.*, *Phys. Rev. Lett.* **71**, 3927 (1993)] and world average for muon capture at $Q^2 = 0.88m_\mu^2$ (filled diamond). Dashed curve – current-algebra result; and solid curve – next-to-leading order chiral perturbation theory result [V. Bernard, L. Elouadrhiri, and U.-G. Meissner, *J. Phys. G* **28**, R1 (2002)].

That view is supported by our result for $g_{\pi NN}(Q^2)$, which is depicted in Fig. V-4. Within reasonable variation of the parameters that characterize our model pion-nucleon vertex, the calculated value of $g_{\pi NN}(Q^2 = 0)$ is consistent with standard phenomenology. We obtain a chiral-limit value $r_{\pi NN}^0 \approx 0.51 \pm 0.02$ fm. For

comparison, a massive-quark value of $r_{\pi NN}^0 \approx 0.51$ fm appears in Ref. 1, while $r_{\pi NN}^0 \approx 0.93\text{--}1.06$ fm is employed in Ref. 2.

An article outlining these results was submitted for publication.³

¹R. Machleidt, *Adv. Nucl. Phys.* **19**, 189 (1989).

²T. Sato and T.-S. H. Lee, *Phys. Rev. C* **54**, 2660 (1996).

³A. Höll, C. D. Roberts, and S. V. Wright, *A Perspective on Hadron Physics*, contribution to the proceedings of the “10th Mexican Workshop on Particles and Fields,” Morelia, Mexico, November 6-12, 2005.

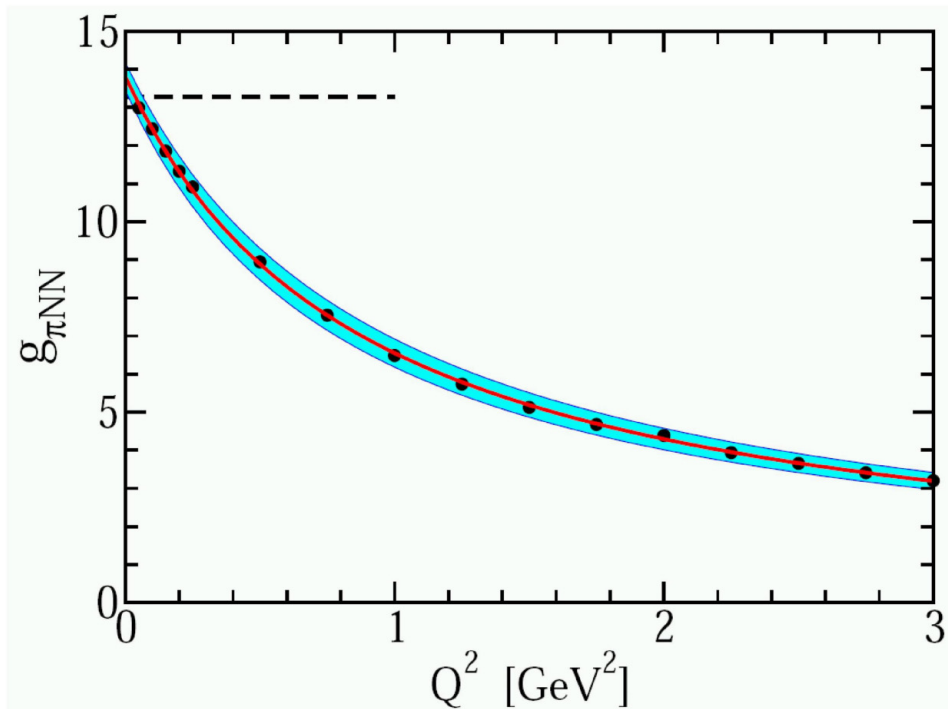


Fig. V-4. Filled circles – calculated chiral limit result for $g_{\pi NN}(Q^2)$. Solid line – monopole fit to the calculation, with mass-scale $m_M^\pi = 0.95$ GeV. The shaded band delimits our result's variation subject to 10% changes in model parameter values. The inferred experimental value of the πNN coupling ($g_{\pi NN} = 13.4$) is marked by a dashed line.

a.14. Hadron Masses from Schwinger Functions (M. Bhagwat, A. Höll, C. D. Roberts, and S. V. Wright)

We explored the viability of using solely spacelike information about a Schwinger function to extract properties of bound states. In a concrete example it was not possible to determine properties of states with masses more than approximately 1.2 GeV. This has direct relevance, for example, to DSE and lattice-QCD studies; and moreover to building bridges between

these two approaches and between lattice and continuum methods in general.

An article reporting these preliminary results was submitted.¹ The work plainly needs more development. That is ongoing because the insight to be gained is potentially very important.

¹A. Höll, P. Maris, C. D. Roberts, and S. V. Wright, *Schwinger Functions and Light-Quark Bound States, and Sigma Terms*; contribution to the proceedings of the “Workshop on Light-Cone QCD and Nonperturbative Hadron Physics 2005 (LC 2005),” Cairns, Queensland, Australia, July 7-15, 2005.

a.15. Dynamical Coupled-Channel Model of Meson Production Reactions in the Nucleon Resonance Region (T.-S. H. Lee, A. Matsuyama,* and T. Sato†)

A dynamical coupled-channel model has been developed for studying nucleon resonances (N^*) in meson production reactions induced by pions and photons. The model is based on an energy-independent

Hamiltonian that is derived from effective Lagrangians by using a unitary transformation method.

The constructed model Hamiltonian consists of (a) Γ_V for describing the transitions $N^* \leftrightarrow MB$, $\pi\pi N$ with

$MB = \gamma N, \pi N, \eta N, \pi\Delta, \rho N, \sigma N$, and $\rho \leftrightarrow \pi\pi$ and $\sigma \leftrightarrow \pi\pi$, (b) v_{22} for non-resonant $MB \rightarrow M'B'$ and $\pi\pi \rightarrow \pi\pi$ interactions, (3) $v_{MB,\pi\pi N}$ for non-resonant $MB \rightarrow \pi\pi N$ transitions, and (4) $v_{\pi\pi N,\pi\pi N}$ for non-resonant $\pi\pi N \rightarrow \pi\pi N$ interactions.

The model satisfies the unitarity conditions within the channel space spanned by the considered two-particle meson-baryon states and the three-particle $\pi\pi N$. The resulting coupled-channel equations are cast into a form such that the meson cloud effects on the N^* excitations can be explicitly calculated. A numerical method based on the spline-function expansion has been developed for solving these coupled-channel equations which are complicated by the singularities due to the $\pi\pi N$ unitarity cut. The required computation code was developed and checked in FY 2005. We have started to investigate the most dominant and least understood two pion production channels. In Fig.V-5, we show that our model can give a good account of the $\pi^+\pi^-$

photoproduction data from JLab. In Fig.V-6, we show that when the $\pi\pi N$ unitarity cut effects are neglected, the predicted differential cross sections are changed drastically. Our results indicate strongly that the nucleon resonance parameters can reliably be extracted from the meson production data only when a rigorous dynamical coupled-channel calculation with the $\pi\pi N$ unitarity cut is performed.

This model is currently being developed further for performing a comprehensive dynamical coupled-channel analysis of all of the meson production data from JLab. This ambitious project is the main component of the Excited Baryon Resonance Center (EBAC) at the Theory Center of JLab. It is aimed at reaching one of the DOE milestones by the year of 2009. We are playing a leading role in conducting this research project involving about 10 investigators from around the world.

*Shizuoka University, Japan, †Osaka University, Japan.

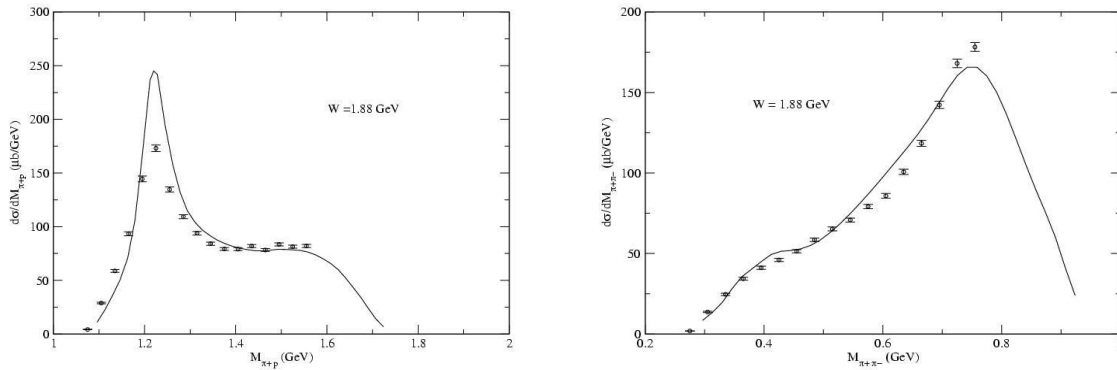


Fig. V-5. Differential cross sections for the $\gamma p \rightarrow \pi^+ \pi^- p$ reaction with respect to the invariant mass $M_{\pi^+ p}$ (left), $M_{\pi^+ \pi^-}$ (right) at $W = 1.880 \text{ GeV}$.

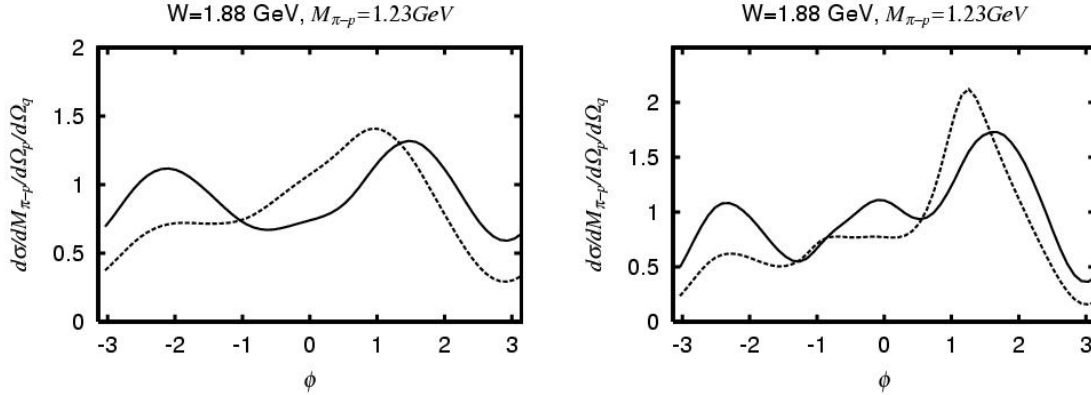


Fig. V-6. Differential cross sections for $\gamma p \rightarrow \pi^+ \pi^- p$ at $W=1.880$ GeV. The outgoing π^+ momentum is \vec{p} and the relative momentum between π^- and p is \vec{q} . ϕ is the azimuthal angle of \vec{q} . The results are for $M_{\pi^- p}=1.23$ GeV, $\cos\theta_p = 0.183$, $\phi_p = -3.1$ rad. The left (right) panel is for $\cos\theta_p = -0.96$ (-0.525). The dashed curves are obtained when $\pi\pi N$ cut effects are neglected.

a.16. Effects of Nucleon Resonances on Hyperon Production Reactions (T.-S. H. Lee, B. Julia-Diaz,*† B. Saghai,* and F. Tabakin†)

As a step toward applying the dynamical coupled-channel model described in section a.15., we carried out a comprehensive investigation of recent data on the $\gamma p \rightarrow K^+ \Lambda$ reaction. The channels included in our dynamical coupled-channel calculations are γN , πN , and $K\Lambda$. The non-resonant interactions are derived from effective Lagrangians using a unitary transformation method. All three and four star N^* listed by the Particle Data Group are included in the calculations.

The calculation of photoproduction amplitudes are simplified by casting the coupled-channel equations into a form such that the empirical $\gamma N \rightarrow \pi N$ amplitudes are input and only the parameters associated with the KY channel are determined by performing χ^2 -fits to all

available data for $\pi p \rightarrow K^0 \Lambda$, $K^0 \Sigma^0$ and $\gamma p \rightarrow K^+ \Lambda$. Good agreement between our models and those data are obtained.

In the fits to $\pi N \rightarrow KY$ channels, most of the parameters are constrained within $\pm 20\%$ of the values given by the Particle Data Group and/or quark model predictions, while for $\gamma p \rightarrow K^+ \Lambda$ parameters, ranges compatible with broken $SU(6) \otimes O(3)$ symmetry are imposed. The main reaction mechanisms in $K^+ \Lambda$ photoproduction are singled out and issues related to newly suggested resonances S_{11} , P_{13} , and D_{13} are studied. The effects of these three resonances on differential cross sections are shown in Fig.V-7. In Fig.V-8, we show the importance of the initial and final state interaction effects.

*CEA, Saclay, France, †University of Pittsburgh.

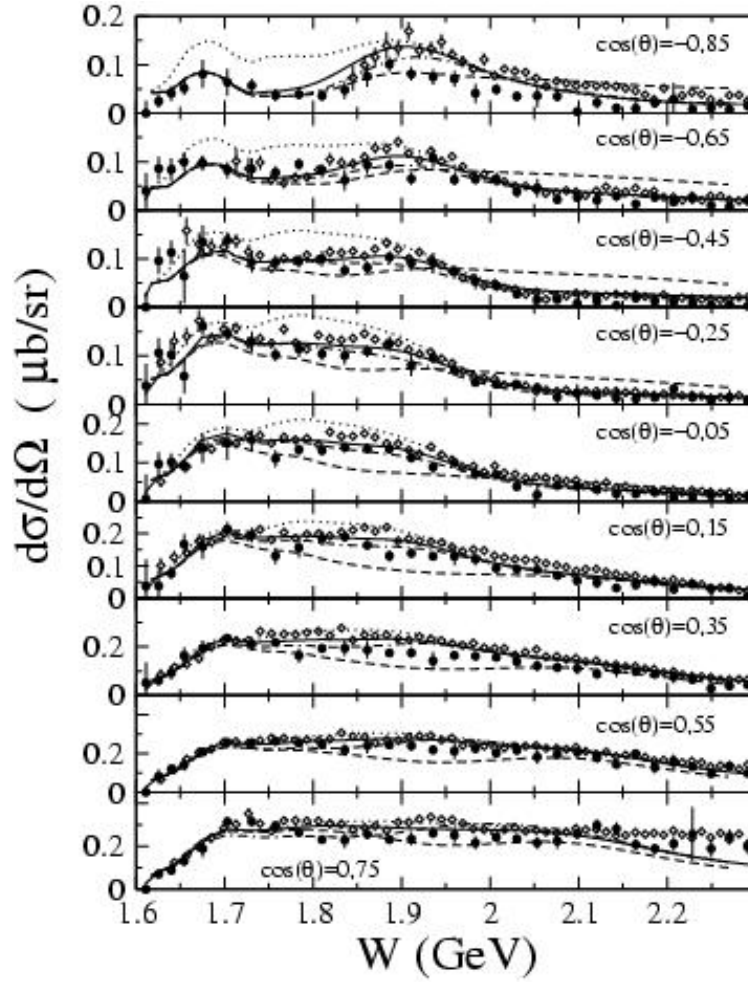


Fig. V-7. Differential cross section for the reaction $\gamma p \rightarrow K^+ \Lambda$ as a function of the total center-of-mass energy. Solid curves correspond to the full model. Dotted, dot-dashed, and dashed curves correspond to the full model without the $3^{rd}S_{11}$, $3^{rd}P_{13}$, and $3^{rd}D_{13}$, respectively.

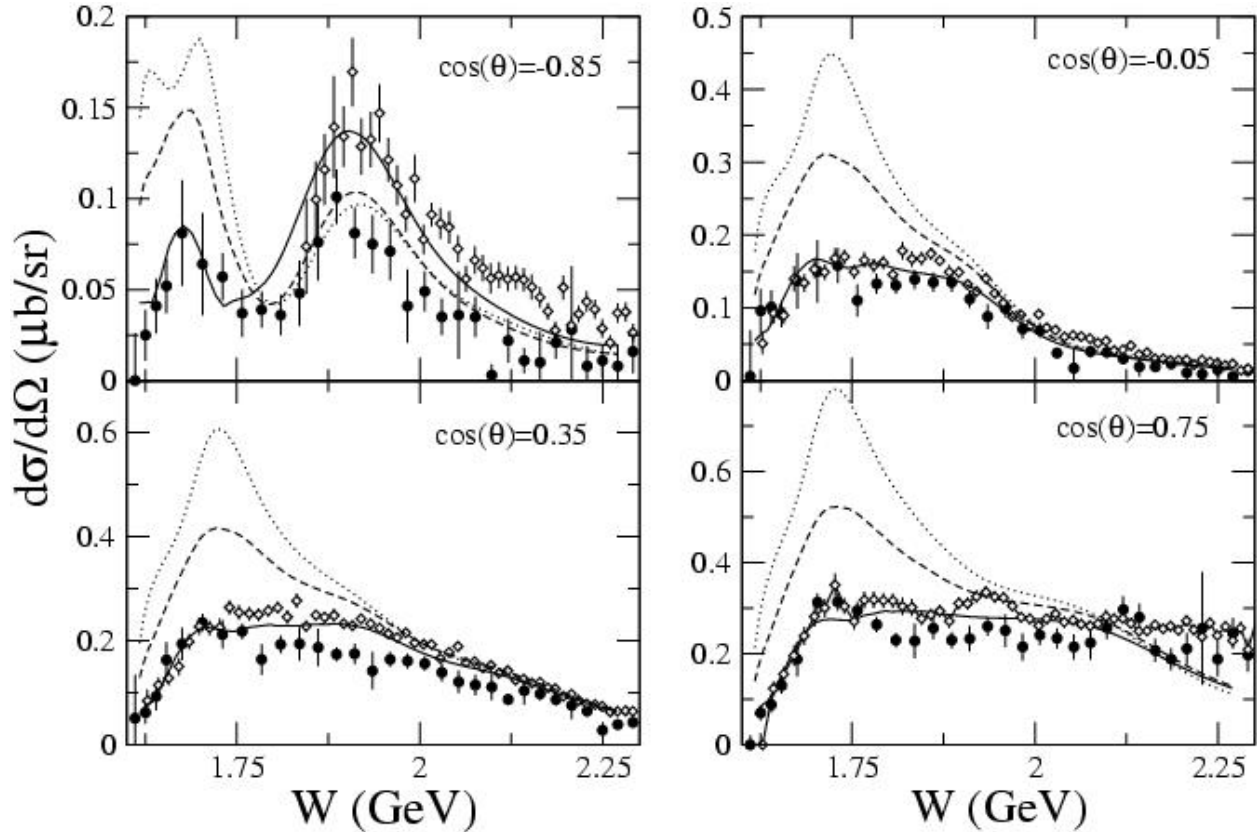


Fig. V-8. Differential cross section at four angles for $\gamma p \rightarrow K^+ \Lambda$. The curves are: full calculations (full curves), direct-channel results obtained by turning-off multi-step processes in the full calculations, (dotted curves), off-shell effects switched-off in the full calculations.

a.17. Effects of Nucleon Resonances on ω Production Reactions (T.-S. H. Lee, Y. Oh,* and K. Nakayama*)

As a step toward applying the dynamical coupled-channel model described in section a.15. to analyze the JLab data on ω photoproduction, we investigated nucleon resonance effects in $\pi p \rightarrow \omega N$ reactions. The calculation was performed using the distorted-wave approximation.

The initial πN interactions are calculated from the empirical πN amplitudes. The non-resonant $\pi N \rightarrow \omega N$ and $\omega N \rightarrow \omega N$ interactions are calculated from effective Lagrangians using a unitary transformation method. All three and four stars N^* listed by the Particle Data Group are included with the resonance

parameters taken from the available data or quark models.

We are able to fit the available differential cross section data on $\pi p \rightarrow \omega N$ with a parametrization of the final ωN interactions in terms of scattering lengths and effective ranges. We have found that the nucleon resonances play a dominant role in the ω production reactions.

Our results are shown in Fig. V-9. The initial and final state interactions are found to be crucial, as seen in Fig. V-10.

*University of Georgia.

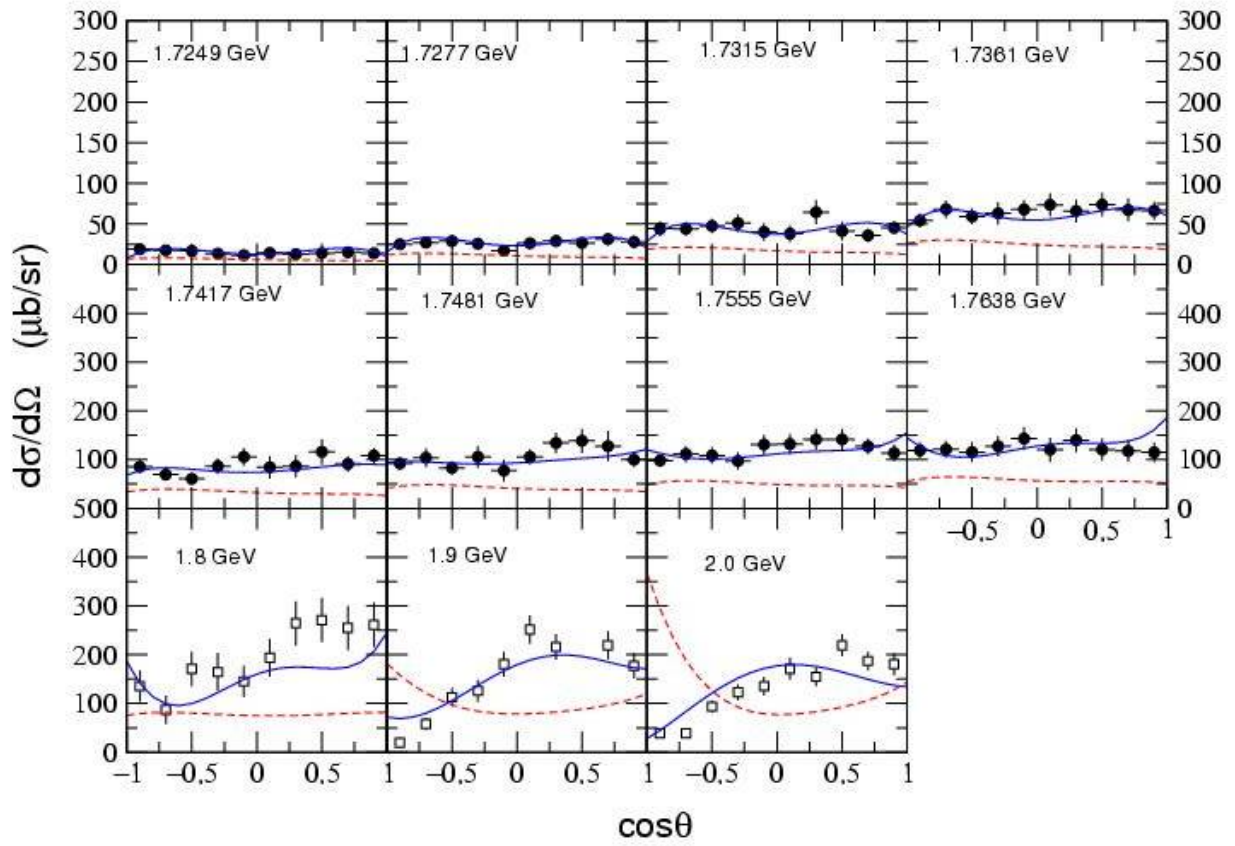


Fig. V-9. The differential cross sections for $\pi p \rightarrow \alpha n$. The dotted curves are obtained by setting N^* contributions to zero.

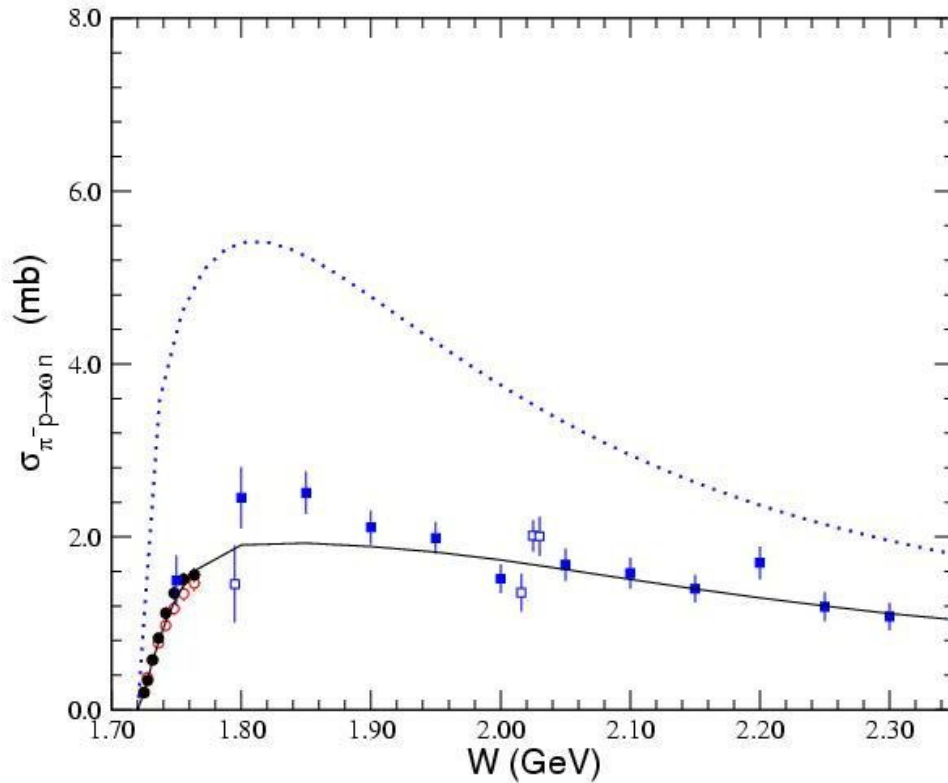


Fig. V-10. The total cross sections for $\pi^- p \rightarrow \omega n$. The dotted curve is obtained by setting the initial πN and final ωN interactions to zero.

a.18. Electroweak Meson Production on Nuclei (T.-S. H. Lee, B. Szczerbinka,*
K. Kubodera,* and T. Sato†)

We have applied the dynamical pion production model developed by Sato and Lee to predict electroweak reactions on nuclei. Our objective is to provide information for analyzing the new-generation neutrino experiments for determining various fundamental properties of neutrinos, in particular the oscillation to electron neutrinos.

The calculations have been performed by taking into account effects due to Fermi motion, Pauli blocking, and nucleon-nucleon correlations. It has been found

that the predicted cross sections are strongly influenced by all of these effects. The calculated cross sections for inclusive $^{12}\text{C}(e,e')$ reaction reproduce the main features of the data with discrepancies restricted mainly to the dip region.

Our sample results are shown in Fig.V-11. The predicted neutrino-induced cross sections are shown in Fig.V-12. They are the input to the analyses of the data from various new neutrino experiments.

*University of South Carolina, †Osaka University, Japan.

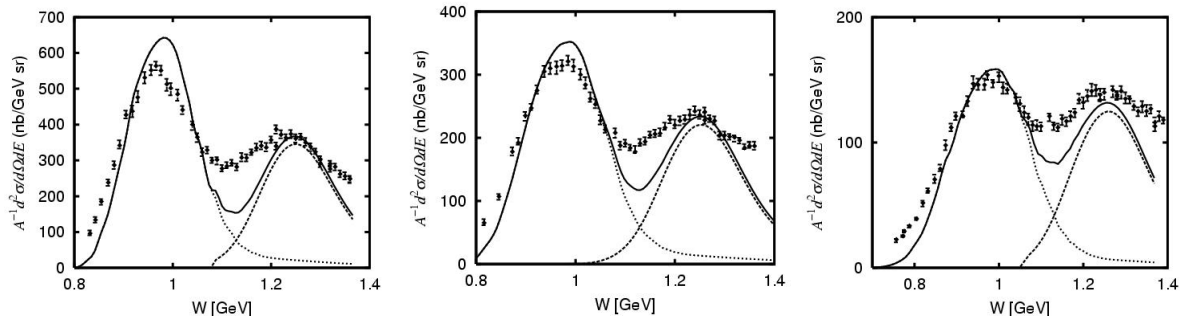


Fig. V-11. Inclusive cross sections for $^{12}\text{C}(e, e')$ at $E_e = 0.96$ GeV (left), 1.1 GeV (middle) and 1.3 GeV (right). The dotted (dashed) curves are from quasi-free nucleon knockout (pion production) processes. The solid curves are the sum of the two contributions.

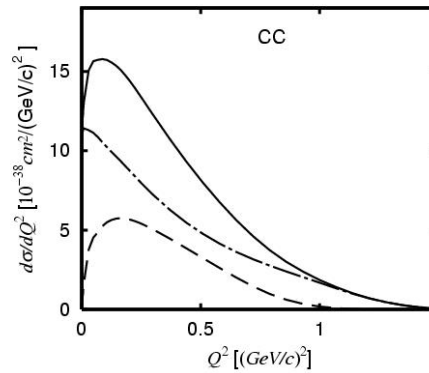


Fig. V-12. $d\sigma/dQ^2$ for $\nu_\mu + ^{12}\text{C} \rightarrow \mu^- + X$ at $E_\nu = 1$ GeV. The dash-dotted (dashed) curve is for the quasi-free nucleon knockout (pion production) process. The solid curve is the sum of the two contributions.

a.19. Pentaquark $\Theta^+(1540)$ Production in $\gamma N \rightarrow K\bar{K}N$ Reactions (T.-S. H. Lee, Y. Oh,* and K. Nakayama*)

Recent developments in the search for exotic pentaquark hadrons are reviewed.

We then investigate how the exotic pentaquark $\Theta(1540)$ baryon production can be identified in $\gamma N \rightarrow K\bar{K}N$ reactions, focusing on the influence of the background (non- Θ production) mechanisms. By imposing SU(3) symmetry and using various quark model predictions, we are able to fix the coupling constants for evaluating the so-called Drell diagrams; namely, $K\bar{K}$ production through intermediate vector meson and tensor meson photoproduction, and the mechanisms involving intermediate $\Lambda(1116)$, $\Lambda(1405)$, $\Lambda(1520)$, $\Sigma(1193)$, $\Sigma(1385)$, and $\Delta(1232)$ states. The vector meson photoproduction part is calculated from a

phenomenological model which describes well the experimental data at low energies.

We point out that the neutral tensor meson production cannot be due to π^0 -exchange as employed by A. R. Dzierba *et al.*¹ because of C parity. The neutral tensor meson production is estimated by considering the vector meson exchange and found to be too weak to generate any peak at the position near $\Theta(1540)$.

For $\Theta(1540)$ production, we assume that it is an isoscalar and hence can only be produced in $\gamma n \rightarrow K^+ K^- n$ and $\gamma p \rightarrow K^0 \bar{K}^0 p$ reactions, but not in $\gamma p \rightarrow K^+ K^- p$ and $\gamma n \rightarrow K^0 \bar{K}^0 n$. The total cross section data of $\gamma p \rightarrow K^+ K^- p$ is thus used to fix the form factors which regularize the background amplitudes so that the signal

of $\Theta(1540)$ in $\gamma n \rightarrow K^+ K^- n$ and $\gamma p \rightarrow K^0 \bar{K}^0 p$ cross sections can be predicted.

We find that the predicted $K^+ K^-$ and $K^+ n$ invariant mass distributions of the $\gamma n \rightarrow K^+ K^- n$ reaction can qualitatively reproduce the shapes of the JLab data.

High statistics experiments are needed to resolve the problem. We have also identified the kinematic region where the differential cross sections of $\gamma n \rightarrow K^+ K^- n$ can be sensitive to the parity of $\Theta(1540)$. Our results are shown in Fig. V-13.

*University of Georgia.

¹A. R. Dzierba *et al.*, Phys. Rev. D **69**, 051901(R) (2004).

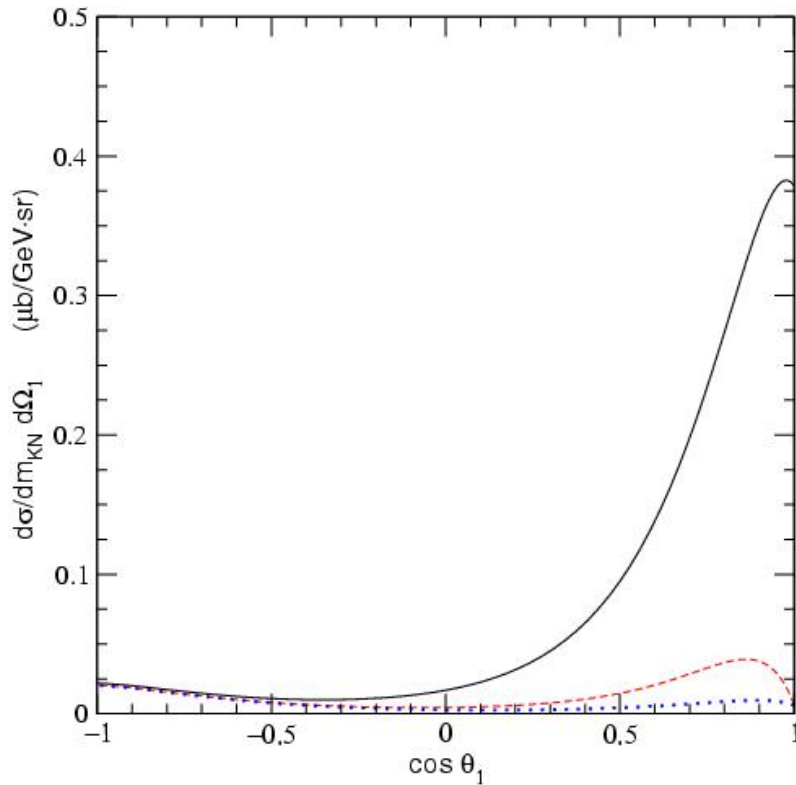


Fig. V-13. Double differential cross section $d\sigma/dm_{KN}d\Omega_1$ as a function of $\cos\theta_1$, where θ_1 is the polar angle of K in the center of mass frame, for $\gamma n \rightarrow K^+ K^- n$ with $E_\gamma = 2.3$ GeV and $m_{KN} = 1.54$ GeV. The dotted line is obtained without $\Theta(1540)$, while the solid (dashed) line is with even (odd) parity for Θ .

B. NUCLEAR FORCES AND NUCLEAR SYSTEMS

The goal of this program is to achieve a description of nuclear systems ranging in size from deuterium and tritium to nuclear matter and neutron stars using a single parametrization of the nuclear forces. Aspects of our program include both the construction of two- and three-nucleon potentials and the development of many-body techniques for computing nuclear structure and reactions with these interactions. Detailed quantitative, computationally-intensive studies are essential parts of this program.

Quantum Monte Carlo (QMC) calculations of light ($A \leq 12$) nuclei with realistic interactions have been the main focus of our recent efforts. Our nonrelativistic Hamiltonian contains the accurate Argonne v_{18} two-nucleon (NN) potential, which includes charge-independence breaking terms, and either the Urbana IX three-nucleon (NNN) potential, or one of several Illinois NNN models. The QMC calculations include both variational (VMC) and Green's function (GFMC) methods. We begin with the construction of variational trial functions based on sums of single-particle determinants with the correct total quantum numbers, and then act on them with products of two- and three-body correlation operators. Energy expectation values are evaluated with Metropolis Monte Carlo integration and parameters in the trial functions are varied to minimize the energy. These optimized variational wave functions can then be used to study other nuclear properties. They also serve as a starting point for the GFMC calculations, which systematically remove higher excited-state components from the trial wave functions by propagation in imaginary time.

We are currently studying all $A \leq 10$ nuclei, including more than 100 ground or excited states, as well as ^{12}C . These are the first calculations to treat $A \geq 6$ nuclei directly with realistic NN and NNN interactions. In GFMC calculations, with our best Hamiltonian, we can reproduce most of the experimental ground- and excited-state energies to within 0.6 MeV.

This year we extended a study of higher excited states, *i.e.*, second or higher states of given spin and parity, to $A = 9-10$ nuclei. We also made GFMC calculations for a wide range of unnatural-parity states in $A = 9$ nuclei, including two very high-lying but narrow states in ^9Be . The first VMC calculations for unnatural-parity states in $A = 10$ nuclei were made, and successfully reproduced the observed ordering of levels in ^{10}Be and ^{10}B . Two new calculations of ^{12}C with significantly better starting wave functions demonstrated the convergence of our results for the largest nucleus attempted with GFMC.

Many excited states in the light nuclei are not particle stable and should be treated as scattering states, though our efforts prior to this year treated all of them as bound. A major effort was made this year to extend our GFMC program to nucleon-nucleus scattering, and substantial progress was made on ^5He , or $n\alpha$ scattering. The results indicate we can make *ab-initio* calculations of the low-energy scattering cross section, and extract resonance energies and widths. A major long term goal of this effort is to use GFMC wave functions to predict reaction cross sections for astrophysics as part of the Theory Group's nuclear astrophysics effort.

We also continued a systematic survey of cluster form factors and spectroscopic factors in the light p-shell nuclei using VMC wave functions. The correlations in these wave functions can

provide significant quenching of spectroscopic factors compared to traditional shell-model calculations. Specific applications were made for two (d,p) experiments performed at ATLAS using rare-isotope beams in inverse kinematics and preliminary calculations were made for a new $(d,^3\text{He})$ experiment. The calculated cluster form factors are used as input to the distorted-wave Born approximation (DWBA) program PTOLEMY, developed here many years ago, to provide the theoretical analysis of the experiments.

Calculations with order 1% accuracy of the rms radii of helium isotopes are needed for comparison to experiment but had proven impossible to achieve. This year we made considerable progress in solving this problem.

A simple but useful guide for understanding the structure of light nuclei was formulated, based on counting the number of interacting pairs in different spin-isospin states for a given spatial symmetry and estimating the overall binding according to the spin-isospin operator expectation value taken from one-pion exchange. The overall binding of light nuclei, various aspects of their excitation structure, and clustering characteristics are all given a simple physical interpretation. This model correlates many of the results from our detailed QMC calculations of the last several years.

b.1. Quantum Monte Carlo Calculations of Light Nuclei Energies (S. C. Pieper, R. B. Wiringa, K. M. Nollett, and J. Carlson*)

We have been studying the ground states and excitation spectra of light nuclei as A -body problems with realistic nucleon-nucleon (NN) and three-nucleon (NNN) interactions using advanced quantum Monte Carlo (QMC) many-body methods. Our preferred Hamiltonian contains the Argonne v_{18} NN potential (AV18), which gives an excellent fit to elastic NN scattering data and deuteron properties, and the Illinois-2 NNN potential (IL2), which we have fit to binding energies of $A \leq 8$ nuclei. The QMC methods include both variational Monte Carlo (VMC), which gives an initial approximate solution to the many-body Schrodinger equation, and Green's function Monte Carlo (GFMC), which systematically improves on the VMC starting solution. The GFMC method produces absolute binding energies that are accurate at the 1-2% level.

The VMC calculations begin with the construction of an antisymmetric Jastrow trial wave function that includes single-particle orbits coupled to the desired JM values of the state of interest as well as pair and triplet correlations. A symmetrized product of two- and three-body spin, isospin, and tensor correlation operators (induced by the NN and NNN potentials) is applied to the Jastrow product to produce the full trial function. The wave function is diagonalized in the small basis of

different spatial symmetry components to project out multiple states with the same quantum numbers.

In GFMC calculations an imaginary-time propagator, $\exp[-(H-E_0)\tau]$, where H is the Hamiltonian, E_0 is an estimate of the eigenvalue, and τ is the imaginary time, is applied to the VMC trial function. The excited-state components of the trial function are damped out for large τ , leaving the exact lowest eigenfunction with the quantum numbers of the input VMC trial function. The expectation value of H is computed for a sequence of increasing values of τ to determine the convergence.

In 2004 we demonstrated that GFMC can be used to compute higher excited states with the same quantum numbers as lower states if the propagation is started with a trial function that is orthogonal to the starting wave functions for the lower states. We systematically computed all the p -shell states in the $A = 6,7,8$ nuclei, doubling the number of states we had been able to study previously. This past year we calculated many additional excited states in the $A = 9,10$ nuclei.

In November 2005, NERSC made the new Bassi computer available in friendly user mode. We were able to complete two calculations of the ground state of ^{12}C using a new form of the starting wave function

developed by V. R. Pandharipande. This form has $^1S[444]$ symmetry but differs from our previous $^1S[444]$ wave function in allowing three clusters of 4 nucleons each to be tightly confined with weaker confinement of nucleons in different clusters. For the AV18+IL2 Hamiltonian the starting energy was 31 MeV better than previously and the final energy was only 2.6 +/- 1.4 MeV less bound than previously.

We are also working on unnatural-parity states caused by the excitation of one p -shell nucleon to the sd -shell. These states can appear fairly low in the excitation spectrum of $A \geq 7$ nuclei, and particle-stable states occur in ^{10}Be and ^{10}B . We studied ^7He positive-parity states for the first time in support of an ATLAS experiment, discussed below in connection with spectroscopic factors. Our latest GFMC calculations of

the low-lying positive-parity states in ^9Be are in good agreement with experimental data. Recently, we studied two experimentally narrow resonances at the large excitation energies of 16.7 and 17.5 MeV which have tentative spin assignments of $5/2^+$ and $7/2^+$. There are many lower states in ^9Be with the same J^π but these are presumably the first to be dominantly $[4311]$ symmetry rather than $[441]$. We found that GFMC propagation of $[4311]$ symmetry starting wave functions gives stable excitation energies of 17.5 and 18.2 MeV, respectively, in very good agreement with the data. We made first VMC calculations of the positive-parity states in $A = 10$ nuclei, and obtained excitation energies in the 4-9 MeV range in agreement with data. The experimentally observed ordering of levels, $1^-, 2^-, 3^-, 4^-$ in ^{10}Be , and $2^-, 3^-, 4^-, 1^-$ in ^{10}B was also reproduced.

*Los Alamos National Laboratory.

b.2. Scattering Methods for Quantum Monte Carlo Calculations (K. M. Nollett, S. C. Pieper, R. B. Wiringa, and J. Carlson*)

Our calculations of properties of light nuclei have concentrated on energies of discrete levels, because the quantum Monte Carlo methods have until recently required that unbound states be treated as bound states. We have therefore been restricted to bound or narrow states and unable to compute the widths of resonances. A smaller amount of effort has gone into computing transition probabilities and radiative-capture cross sections using VMC wave functions, along with calculations of a few static nuclear properties like RMS radii.

It is desirable to expand the range of the QMC methods to include unbound states treated as such and the computation of phase shifts and reaction cross sections. This will greatly expand the number of observables against which the computational methods and potentials can be tested. It will also open the door to accurate quantitative predictions of reaction cross sections for astrophysics, at least in the light systems important for solar neutrinos, big-bang nucleosynthesis, and seeding the r -process in alpha-rich freezeout.

We are developing methods to compute unbound states, using an R-matrix-like boundary condition to specify the state being computed. As a first application, we have computed low-energy phase shifts in the first three

partial waves in ^4He -neutron scattering. In VMC, the boundary condition is set as a condition on the correlation between the ^4He nucleus and the last neutron. In GFMC, the boundary condition is enforced through a method of images that enforces a specified logarithmic derivative in the wave function normal to a specified surface of fixed ^4He - n separation (9 fm in most of our calculations). Useful calculations require an accuracy of about 50 keV or better. This in turn requires careful work to eliminate dependence of the result on the GFMC path constraint, the starting wave function, and the radius at which the boundary condition is imposed.

Results after carefully controlling these sources of error are shown in Fig. V-14 for the Argonne v_{18} + Illinois-2 potential. This potential reproduces the experimental energies for the given boundary conditions with remarkable precision, particularly when contrasted to the ~700 keV RMS deviation of the potential from the experimental energies of the 59 narrow or bound states computed previously.

This work opens the door to several additional calculations in light nuclei, particularly neutron resonances, states in ^4H , and the $^7\text{Be}(p,\gamma)^8\text{B}$ radiative capture reaction.

*Los Alamos National Laboratory.

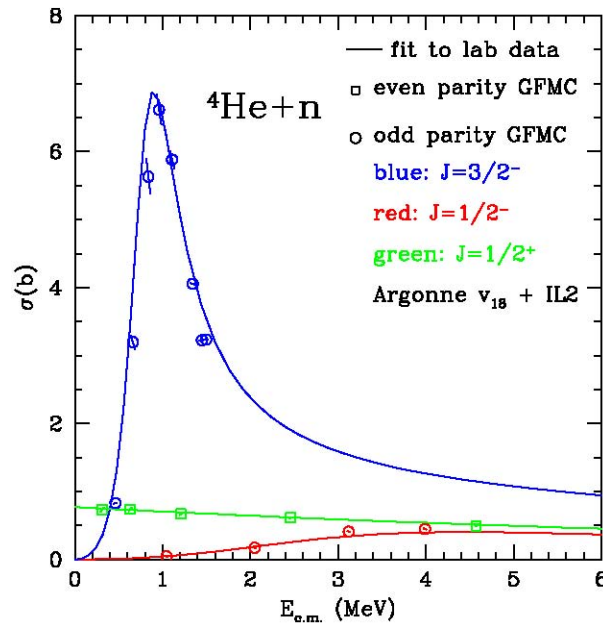


Fig. V-14. Cross sections for ${}^4\text{He}$ -neutron scattering, broken down by partial wave. Solid curves are an R-matrix fit to the measured cross sections. Points with Monte Carlo error bars are results of GFMC calculations.

b.3. Spectroscopic Factors and Cluster Form Factors of Light Nuclei (R. B. Wiringa, S. C. Pieper, D. Kurath, and D. J. Millener*)

The cluster form factor is defined as the overlap between A -body and $(A-1)$ -body nuclear states, either in configuration or momentum space, $\langle (A-1)_J/a_j/A_J' \rangle$, where a_j is a nucleon annihilation operator. It is a very useful quantity in analyzing pickup reactions such as (p,d) , where A_J' is a ground state, or stripping reactions such as (d,p) , where $(A-1)_J$ is a ground state, or nucleon-knockout reactions such as $(e,e'p)$. The cluster form factor can be folded into a DWBA calculation to help extract experimental information. The spectroscopic factor S is just the normalization of this wave function overlap, and provides a simple characterization of nuclear structure aspects of such reactions.

We have been calculating the cluster form factors and spectroscopic factors for all $A \leq 10$ nuclei using VMC wave functions from the AV18+UIX Hamiltonian. The spectroscopic factors are being compared to predictions from the Cohen-Kurath (CK) shell model. The CK spectroscopic factors for transitions between stable nuclei were first published in 1967, but many additional transitions are now experimentally accessible with the advent of rare-isotope beams at Argonne, MSU, and other facilities.

The main difference between the CK and VMC spectroscopic factors is that the latter can show significant reductions due to the correlations in the VMC wave functions. An example is the ${}^7\text{Li}(e,e'p){}^6\text{He}(J)$ reaction where $J = 0, 2$ for the ground state or first excited state of the residual ${}^6\text{He}$ nucleus. The CK values for these two states are 0.59 and 0.40, while the VMC calculation gives 0.36 and 0.25, respectively, or just 2/3 the strength. This kind of reduction in strength is consistent with electron-scattering experiments. However, the VMC spectroscopic factors are not always significantly reduced compared to CK, indicating considerable dependence on details of the nuclear structure.

Two specific applications were made in 2004-2005 in conjunction with experiments carried out at ATLAS with rare-isotope beams. These were studies of the experimental spectrum of ${}^9\text{Li}$ using the ${}^8\text{Li}(d,p){}^9\text{Li}$ reaction, and a search for excited states in ${}^7\text{He}$ using the ${}^6\text{He}(d,p){}^7\text{He}$ reaction, both in inverse kinematics. We computed excited state spectra for ${}^9\text{Li}$ and ${}^7\text{He}$, including positive-parity states in the latter case. We then evaluated the cluster form factors for transitions to the different states and fed them into the DWBA program PTOLEMY to compare theoretical predictions

with experimental differential cross sections. For ${}^9\text{Li}$ the DWBA results are generally in good agreement with experiment, both for the magnitude and shape of the angular distributions. For ${}^7\text{He}$ the ground-state distribution is well described, but a large, broad, peak around 2.5 MeV excitation energy can only be partially

accounted for.¹ A new experiment, ${}^8\text{Li}(d,{}^3\text{He}){}^7\text{He}$ in inverse kinematics, has begun and we have calculated VMC cluster form factors $\langle {}^7\text{He}_j/a_j/{}^8\text{Li}_j \rangle$ to estimate the spectroscopic factors. We also have calculations of $\langle d/a_j/{}^3\text{He} \rangle$ overlaps to fold into the PTOLEMY calculation for differential cross sections.

*Brookhaven National Laboratory.

¹A. H. Wuosmaa *et al.*, Phys. Rev. C **72**, 061301(R) (2005).

b.4. Calculations of RMS Radii of Helium Isotopes (S. C. Pieper, R. B. Wiringa, and J. Carlson*)

In October 2004, a group led by the Physics Division's Zheng-Tian Lu published a measurement, with better than 1% accuracy, of the rms charge radius of ${}^6\text{He}$. The measurement prompted us to attempt a correspondingly accurate calculation of the ${}^6\text{He}$ point proton and neutron rms radii. Our initial calculations, completed in June 2004, failed because the rms radius had large fluctuations as a function of GFMC propagation imaginary time (τ). Usually we obtain stable energies for $\tau > 0.1 \text{ MeV}^{-1}$. For the ${}^6\text{He}$ calculations we went 70 times further, to $\tau = 7 \text{ MeV}^{-1}$. The energy indeed showed just the expected random statistical fluctuations. However the rms radii showed large long-term fluctuations which made the extraction of a meaningful average impossible.

In early 2005, Argonne's Mathematics and Computer Science Division brought an IBM Blue Gene/L computer on line and we could obtain a large amount of time on it. This enabled extensive studies of the fluctuations. We realized that one input to the GFMC had been poorly calculated and we managed to improve

it significantly. We have proceeded since to make many calculations of the ${}^6\text{He}$ rms radii using different starting wave functions and different GFMC propagator Hamiltonians. We find reasonably stable results for most cases but for a given case the rms radius depends on the precise (to the level of $\sim 50 \text{ keV}$) separation energy (relative to ${}^4\text{He}$) that is computed. (One should note that ${}^6\text{He}$ is bound by only 0.97 MeV relative to ${}^4\text{He}$ -- this is the smallest separation energy of any bound ground state that we have attempted.) Because our GFMC energies are generally assumed to be good to only 1%, this still makes it difficult to assign precise rms radii to a given nuclear Hamiltonian. However the proton radius that is obtained for energies corresponding to the experimental ${}^6\text{He}$ energy agrees well with the experiment. We also obtain a smaller rms proton radius for ${}^8\text{He}$; Lu's group hopes to measure the ${}^8\text{He}$ radius in 2006. We are still trying to improve these calculations and expect to publish results, along with results for lithium isotopes (which seem much easier to compute) soon.

*Los Alamos National Laboratory.

b.5. Pair Counting, Pion-Exchange Forces, and the Structure of Light Nuclei (R. B. Wiringa)

A simple but useful guide for understanding the structure of light nuclei has been formulated. It is based on counting the number of interacting pairs in different spin-isospin (ST) states for a given spatial symmetry and estimating the overall binding according to the sum of $\sigma_i \cdot \sigma_j \tau_i \cdot \tau_j$ expectation values. This choice is motivated by long-range one-pion exchange (OPE), which in the microscopic quantum Monte Carlo (QMC) calculations gives about 75% of the net potential energy, although most of the contribution comes from

the tensor component of the OPE potential rather than the spin-isospin part. This operator conveys a key feature of NN forces, namely that they are moderately attractive in $(ST)=(10)$ and (01) pairs, slightly repulsive in (11) pairs, and very repulsive in (00) pairs.

The number of pairs of different (ST) combinations, $P_A(ST)$ for a given nuclear state can be obtained knowing the total spin, isospin, and spatial symmetry. The energy estimate is

$$E_{OPE} = C[9P_A(00)-3P_A(01)-3P_A(10)+P_A(11)]$$

where C is a scale factor in units of energy. With this estimate, the binding energy of the deuteron, triton, and alpha are $-3C$, $-9C$, and $-18C$, respectively. This is actually a good estimate of the relative potential energies obtained in our QMC calculations, but not of the total binding because the positive kinetic energy contribution grows less rapidly. However, in the p -shell something like a virial theorem is established, with the ratio of kinetic to potential energy having a fairly constant value $0.76-0.80$, so E_{OPE} does become a binding energy estimator.

As nucleons are added in the p -shell, they essentially decouple from the s -shell, in that the contribution to E_{OPE} from pairs where one nucleon is in the s -shell and one in the p -shell vanishes. Thus the energy prediction for ${}^5\text{He}$ is $-18C$, the same as for ${}^4\text{He}$, indicating that the relative stability will be determined by finer details of the force and requirements of Fermi statistics. In general, the energies of p -shell nuclei are predicted to

be basically the energy of their sub-cluster components, which helps explain why light nuclei show considerable clustering. This feature is also seen in the QMC calculations with the full AV18 NN potential; much of the cluster-cluster binding is provided by adding an NNN potential. The overall trend in binding energies is shown in Fig.V-15 where the experimental ground state energies are compared to E_{OPE} with the scale factor C set to 1.5 MeV. The simple prediction is fairly good up to $A \sim 10$ and then gradually underbinds more and more for larger A .

This model also gives a simple explanation for various aspects of the excitation spectra. When various spatial symmetry states can combine to give a specific total spin, those combinations that have the least amount of very repulsive (00) pairs will lie lowest. For example, in ${}^7\text{Li}$ the states that are predominantly $4P[421]$ symmetry are below those with $2P[421]$ symmetry, because they have more (11) pairs and fewer (00) pairs. It can also be used to predict orderings of some sd -shell intruder states.

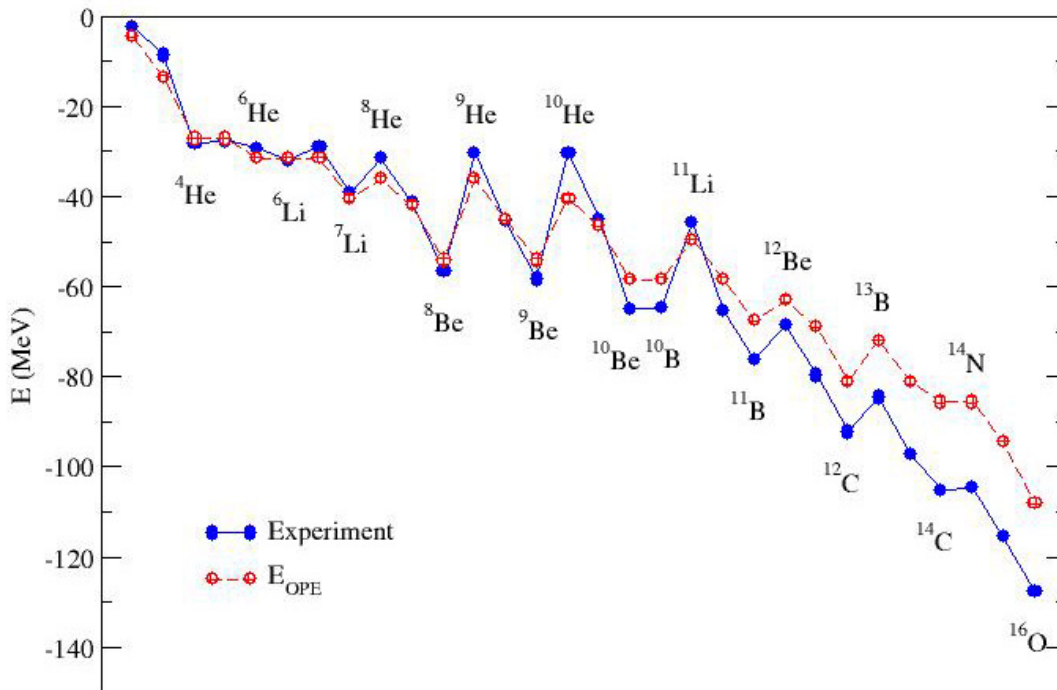


Fig. V-15. Ground-state binding energies for $A \leq 16$ s - and p -shell nuclei.

C. NUCLEAR ASTROPHYSICS

The objective of this research program is to investigate nuclear processes that take place in stars, in the big bang, and in interstellar and intergalactic space. Nuclear phenomena are ubiquitous in the universe. The stars shine by nuclear energy, and the chemical compositions observed in the solar system and elsewhere are the results of nuclear processes that occurred in the big bang and inside the several generations of stars that have formed since then. Many astrophysical phenomena may only be understood by a combination of nuclear physics with methods more familiar to astrophysicists.

A particularly important problem is to determine rates for the nuclear reactions that occur in astrophysical environments. There are many applications (for example, the rapid neutron capture process) where large contributions from theoretical nuclear physics – particularly masses and cross sections - will always be necessary as input, and we maintain research interests in these areas. We have applied advances in the theoretical descriptions of light nuclei to compute cross sections important for big-bang nucleosynthesis, the solar neutrino flux, and seeding of the *r*-process. This work continues in close connection with our other work on light nuclei, and the main goals at present are to improve the wave functions and computational methods as described in section b.2. In the last year, we have participated in work to improve the computational methods used to compute weak-interaction rates important for the collapse and subsequent supernova explosions of massive stars. In addition, studies are underway of electroweak reaction rates relevant to astrophysical processes in dense nuclear matter. These are a part of our attempt to predict observable features of quark matter in compact astrophysical objects.

Understanding nucleosynthesis and energy generation in a particular astrophysical environment requires calculations of nuclear reaction networks. Even for cases in which the detailed astrophysical phenomena can only be understood from difficult calculations coupling a reaction network and hydrodynamics, simpler network calculations can identify the crucial reactions and other nuclear properties to be determined by more detailed theoretical and experimental work. Ongoing work in this area involves big-bang nucleosynthesis, nuclear burning in low-mass stars, and photon-nucleus reactions in high-energy cosmic rays.

A major goal of nucleosynthesis studies is to determine the specific physical conditions that gave rise to abundance patterns seen in nature: what mix of different kinds of stellar environments gave rise to observed chemical compositions? Large amounts of important new data on abundance patterns are now being collected, with important evidence arising from low-metallicity stars in our own galaxy, absorption-line systems backlit by distant quasars, and primitive inclusions and pre-solar grains embedded in meteorites. These data contain important clues about the nucleosynthetic history of the universe, both locally and globally, and the effort to disentangle the clues into information on stellar sources and galactic chemical evolution is necessarily coupled to our work on nucleosynthesis. Close connections between these observational studies and researchers in the theory group have been fostered by participation in the Joint Institute of Nuclear Astrophysics (JINA).

Nucleosynthesis and chemical evolution are increasingly important probes of the overall star formation history of the universe. The first stars had a very simple composition produced by the

cosmological big bang: only hydrogen, deuterium, ^3He , ^4He , and ^7Li . Stars and supernovae synthesize essentially all other nuclei, from carbon through uranium, and eject them into the interstellar gas from which subsequent generations of stars form. The heavy-element inventory (metallicity) builds up over time, and the history of this process is written in the compositions of the stars and gas in our Galaxy and other galaxies as functions of their age. Contributions both from massive stars ($M > 10 M_{\odot}$) with their associated Type II supernovae and from thermonuclear (Type Ia) supernovae are particularly important in this process. Our studies of the nuclear physics of nucleosynthesis, of the natures of the sites of nucleosynthesis, and of the compositions of the stars as a function of age all contribute to efforts to understand the overall star formation history of the universe.

c.l. Moments Methods for Response Functions with Momentum Transfer Dependence (K. Nollett, W. Haxton,* and K. Zurek*)

Models of the supernova explosions of massive stars are very sensitive to the neutrino transport properties of the stellar core, which in turn have large contributions from inelastic neutrino scattering on nuclei in the mass range near iron. The scattering response of these nuclei is dominated by the Gamow-Teller resonance. In a shell-model approach, this contribution to the cross section can be separated into an energy-dependent factor and a separate response function that is independent of momentum transfer q . The response function is found by the Lanczos algorithm, an iterative procedure that casts the Hamiltonian into a tridiagonal form. To find a response function, one applies the operator of interest (in this case, the Gamow-Teller operator) to the initial state, and uses the resulting state as the first basis vector in a Lanczos tridiagonalization. The eigenvectors of the tridiagonal matrix are then easily related to the response function of the operator.

To determine Gamow-Teller rates averaged over a neutrino energy distribution, one need only apply this procedure once. However, there may be significant contributions from forbidden transitions, introducing more complicated q dependence into the operator, so that the response function has to be re-computed completely for each q . In the usual shell model approach for nuclei of mass comparable to iron, this is computationally prohibitive, so that groups who found Gamow-Teller strengths from the Lanczos procedure have switched to the random-phase approximation to incorporate forbidden transitions in their calculations.

We have taken a different approach and sought ways to break up the Lanczos algorithm into two parts:¹ first a computationally-expensive setup phase that is performed only once, and then a much smaller procedure that takes information computed in the first phase and produces the response function at a given value of q . We have produced four such algorithms, one of which – the piecewise moments method – is stable, converges to the true answer as the number of Lanczos iterations increases, and produces squared matrix elements that are non-negative. The approximate response functions produced are necessarily smoothed by convolution with some smoothing function (*e.g.*, Gaussian or Lorentzian), but this is desirable for many applications of the method. We tested our new algorithms by application to inelastic electron scattering on ^{28}Si – a problem that contains many of the same kinds of operators as the calculation of weak responses. Convergence of both the ordinary Lanczos procedure and the piecewise moments method with increasing number of Lanczos iterations is shown in Fig. V-16.

The piecewise moments method (as well as our other algorithms) is faster than the ordinary Lanczos algorithm by a factor of the ratio of the dimension of the Hamiltonian to the number of values of q at which the response is to be computed. This will always be a large number (several orders of magnitude) for the astrophysical applications that we have in mind.

*University of Washington.

¹W. C. Haxton, K. M. Nollett, and K. M. Zurek, Phys. Rev. C **72**, 06551 (2005).

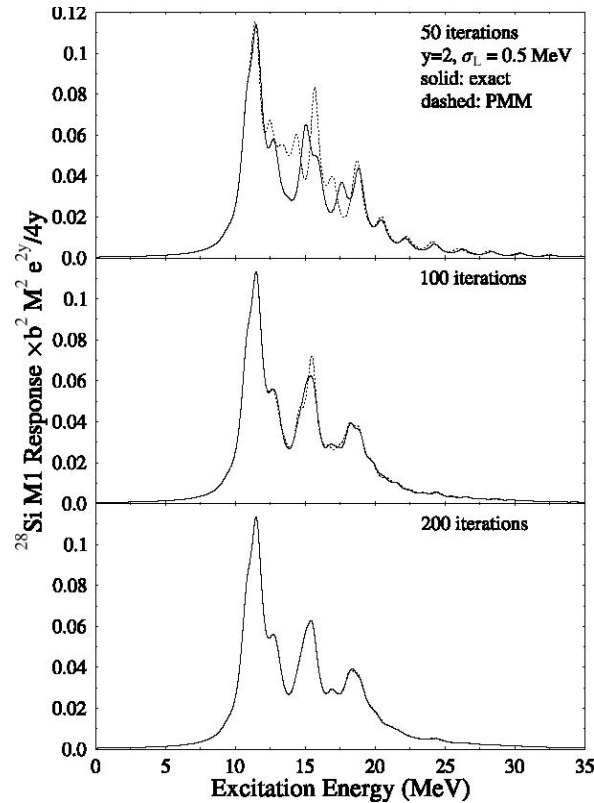


Fig. V-16. M1 response of ^{28}Si at a particular value of $y = (qb/2)^2$, where q is the momentum transfer and b the shell-model oscillator parameter. The results include a Lorentzian smoothing profile of width 0.5 MeV and include the same number of Lanczos iterations for both the ordinary Lanczos algorithm (solid) and the piecewise moments method (dotted).

c.2. Sedimentation and Type I X-Ray Bursts at Low Accretion Rates (F. Peng,* E. F. Brown,† and J. W. Truran‡)

An ionized plasma in a gravitational field develops an electric field sufficient to levitate the ions and ensure overall charge neutrality. When there is more than one species of ion present, the ions will experience a differential force: lighter ions float upward (defined by the local gravitational field) and heavier ions sink downward. The high surface gravity of compact objects makes the timescale for isotopes to stratify often comparable to or faster than other timescales of interest. In particular, sedimentation of heavier isotopes is important in understanding the surface compositions of white dwarf stars (Vauclair *et al.* 1979) and isolated neutron stars (Chang & Bildsten 2003). For accreting white dwarfs, diffusion between the accreted envelope and underlying white dwarf was proposed as a means to enrich the ejecta of classical novae in CNO isotopes (Priyalnik & Kovetz 1984; Iben, Fujimoto, & MacDonald 1992).

Accreting neutron stars, with their strong surface gravity $\approx 2 \times 10^{14} \text{ cm s}^{-2}$, are an ideal place to look for the effects of sedimentation. The sedimentation of heavy elements and resulting nucleosynthesis in the envelope of isolated neutron stars cooling from birth was first described by Rosen (1969) and has more recently been studied in detail by Chang & Bildsten (2003, 2004). For accreting neutron stars, the rapid stratification removes heavy nuclei from the photosphere for accretion rates $dM/dt \leq 10^{-12} M_{\odot} \text{ yr}^{-1}$ (Bildsten, Salpeter, & Wasserman 1992). Deeper in the neutron star envelope, the differentiation of the isotopes can alter the nuclear burning, namely unstable H/He burning and the rapid proton-capture process (rp -process), that powers Type I X-ray bursts. Some estimates of the relative importance of sedimentation and diffusion were made by Wallace, Woosley, & Weaver (1982), who studied accretion at rates

$dM/dt = 2 \times 10^{-11} M_{\odot} \text{ yr}^{-1}$ and argued that the partial separation of the H and He layers might play a role in setting the ignition conditions and subsequent burst nucleosynthesis.

Neutron stars, with their strong surface gravity, have interestingly short timescales for the sedimentation of heavy elements. Motivated by observations of Type I x-ray bursts from sources with extremely low persistent accretion luminosities, $L_X < 10^{36} \text{ ergs s}^{-1}$ ($0.01 L_{\text{Edd}}$), we study how sedimentation effects the distribution of isotopes and the ignition of H and He in the envelope of an accreting neutron star. For local mass accretion rates $dm/dt < 10^{-2} dm_{\text{Edd}}/dt$ (for which the ignition of H is unstable), where $dm_{\text{Edd}}/dt = 8.8 \times 10^4 \text{ g cm}^{-2} \text{ s}^{-1}$, the helium and CNO elements settle out of the accreted fuel layer before the temperature is reached at which H would ignite. Using one-zone calculations of the thermonuclear burning, we identify a range of accretion rates for which the unstable ignition of hydrogen does

not trigger unstable helium burning. This range depends on the emergent flux from reactions in the deep neutron star crust; for $F = 0.1 \text{ MeV} [(dm/dt)/m_u]$, the range is

$$3 \times 10^{-3} dm_{\text{Edd}}/dt \leq dm/dt \leq 10^{-2} dm_{\text{Edd}}/dt.$$

We speculate that sources accreting in this range will build up a massive He layer that later produces an energetic and long X-ray burst. At mass accretion rates lower than this range, we find that the hydrogen flash leads to a strong mixed H/He flash. Surprisingly, even at accretion rates $dm/dt \geq 0.1 dm_{\text{Edd}}/dt$, although the H and He do not completely segregate, the H abundance at the base of the accumulated layer is still reduced. While following the evolution of the x-ray burst is beyond the scope of this introductory paper, we note that the reduced proton-to-seed ratio favors the production of ^{12}C , an important ingredient for subsequent superbursts.

*University of Chicago, †Michigan State University, ‡Argonne National Laboratory and University of Chicago.

c.3. Capturing the Fire: Flame Energetics and Neutronization for Type Ia Supernova Simulations (J. W. Truran,* A. C. Calder,† D. M. Townsley,† O. E. B. Messer,‡ I. R. Seitenzahl,† F. Peng,† N. Vladimirova,† E. F. Brown,§ and D. Q. Lamb†)

Type Ia supernovae (SNe) are bright explosions characterized by a lack of hydrogen spectral features and strong silicon *P Cygni* features near maximum light. The currently favored interpretation is the disruption of a near-Chandrasekhar-mass C/O white dwarf by a thermonuclear runaway. These events are fascinating in and of themselves and are important both for their contribution to the cosmic abundance of iron-peak elements and for their role as standard candles.

Models of Type Ia SNe necessarily involve a mechanism for incinerating the star by a thermonuclear runaway, and the nature of this mechanism is the subject of contemporary research. In the explosion, a thermonuclear flame propagates through the C/O fuel of the white dwarf as either a subsonic deflagration front or a supersonic detonation wave and releases sufficient energy to unbind the star. However, models involving either a pure deflagration or a pure detonation have traditionally been unable to provide an explanation for both the observed expansion velocities and the spectra produced by ejecta that are rich in both intermediate-mass and iron-peak elements. Recent

work, however, suggests that a fast deflagration alone may provide sufficient energy to unbind the star.

There has been considerable progress recently in hydrodynamic simulations of deflagrations of C/O white dwarfs that model the entire star. This is a complicated endeavor, predominantly due to the vast range of length scales: the laminar flame width is $\sim 10^{-3} - 10 \text{ cm}$, some 8 to 12 orders of magnitude smaller than the stellar radius. Because the computational requirements for simulations with these disparate scales demand resources well beyond current capabilities, multidimensional Type Ia models must make use of an appropriate sub-grid-scale model for the evolution of the thermonuclear burning front. Moreover, large-scale simulations are very demanding of computational resources, and it is not feasible at present to include enough isotopes to allow for directly computing the reaction kinetics. A realistic model must nevertheless accurately describe the nuclear energy that is released, the timescale on which it is released, and the compositional changes that occur in the flame. In addition, the burned material continues to evolve after the passage of the flame due to both weak interactions

and hydrodynamic evolution, and realistic simulations must describe this "post-flame" evolution.

This paper presents a study of the nuclear burning that occurs during C/O deflagrations, with the goal of providing a realistic flame model for simulations of Type Ia supernovae. Our flame model builds on the advection-diffusion-reaction model of Khokhlov and includes electron screening and Coulomb corrections to the equation of state in a self-consistent way. We calibrate this model flame—its energetics and timescales for energy release and neutronization—with self-heating reaction network calculations that include both these Coulomb effects and up-to-date weak interactions. The burned material evolves post-flame due to both weak interactions and hydrodynamic changes in density and temperature. We develop a scheme to follow the evolution, including neutronization, of the nuclear statistical equilibrium (NSE) state subsequent to the passage of the flame front. As a result, our model flame is suitable for deflagration simulations over a

wide range of initial central densities and can track the temperature and electron fraction of the burned material through the explosion and into the expansion of the ejecta.

The importance of such a detailed consideration of the consequences of nuclear burning and neutronization via electron captures is to provide an accurate determination of the ^{56}Ni abundance in the ejecta of a Type Ia supernova. For a value of $Y_e \approx 0.5$, the matter in nuclear statistical equilibrium following expansion and cooling is dominated by the self-conjugate nucleus ^{56}Ni . At high densities, however, electron captures on both protons and heavy nuclei effect neutronization of the matter and Y_e falls below 0.5 . Such neutron enrichment favors neutron-rich isotopes at the expense of ^{56}Ni . Since the brightness of SNe Ia at maximum is a direct function of the mass of ^{56}Ni ejected, an accurate determination of the composition of the ejecta is critical to the use of SNe Ia as distance indicators.

*University of Chicago and Argonne National Laboratory, †University of Chicago, ‡University of Chicago and Oak Ridge National Laboratory, §Michigan State University.

D. NUCLEAR STRUCTURE AND HEAVY-ION REACTIONS

This research focuses on nuclear structure in unusual regimes: nuclei near the proton and neutron driplines, and superdeformed nuclei at high spin. We also study heavy-ion reactions near the Coulomb barrier. Much of this work is closely tied to experiments performed at ATLAS and at radioactive beam facilities.

Our studies of heavy-ion reactions include coupled-channels calculations of fusion reactions, elastic and inelastic scattering. The calculated fusion cross sections are usually quite sensitive to the structure and the radii of the reacting nuclei, and it is often possible to reproduce the measurements quite well. However, the calculations can be challenging for very heavy systems because the couplings are strong and the calculations become sensitive to higher-lying states. Another difficulty occurs at energies far below the Coulomb barrier, where the measured cross sections start to fall off steeply compared to calculations.

The hindrance of heavy-ion fusion at low energy is a general phenomenon which has now been observed in many systems, ranging from medium-heavy to heavy systems. The hindrance can be seen clearly by plotting the S factor for fusion. The S factor develops a maximum at low energy, and the energy where that occurs is a good way to characterize the phenomenon. The fusion hindrance is expected to be an entrance channel effect because it occurs at a rather high value of the excitation energy of the compound nucleus, but it has so far not been possible to explain it by conventional coupled-channels calculations.

As part of our continued interest in extracting the rate of radiative capture reactions from experiments, we have focused on proton capture on ${}^7\text{Be}$, which is relevant to the production of ${}^8\text{B}$ in the sun. We have completed a study of the constraints one can obtain on the capture rate from charge symmetry and from the experimental information about the ${}^7\text{Li}(n,\gamma){}^8\text{Li}$ reaction. The result of the study is not unreasonable in comparison to most measurements but it is smaller than the most accurate direct capture measurements.

Many measurements of the ${}^7\text{Be}+p$ capture rate have been performed in recent years, using both direct and indirect methods. One indirect method is to measure the Coulomb dissociation of ${}^8\text{B}$ on a high- Z target and from the data analysis to extract the ${}^7\text{Be}+p$ capture rate. The results obtained are often smaller than the results of direct capture measurements, and it is of interest to understand what causes the discrepancy. We have therefore tested the validity of the first-order approximation that is commonly used in the analysis of Coulomb dissociation experiments by comparing it to more complete dynamical calculations, which include the excitation of ${}^8\text{B}$ to all orders in the Coulomb and nuclear fields from the target. We find that it is necessary to go beyond the conventional first-order analysis if accuracies of 10% or better are required in the extracted capture rate.

We are continuing the development of a program for calculating many-body variational wave functions. This approach puts pairing and particle-hole interactions on an equal footing. These wave functions strictly conserve particle-number and parity. Particle number and parity are projected before variation. In studies of nuclides near the $N = Z$ line, we also project states of good Q , the number parity of $T = 0$ pairs, before variation. This treatment explains many of the

unusual features of nuclei having almost equal numbers of protons and neutrons, such as the Wigner energy anomaly in a simple way.

We have developed a code for configuration mixing of the wave functions used to describe n - p pairing. We have applied these wave functions to explore n - p pair transfer probabilities in $N = Z$ nuclides. We find that this quantity is very sensitive to $T = 0$ and $T = 1$ correlations in the many-body wave function. Experimental studies of the pair transfer probability in ^{44}Ti will establish the magnitude of $T = 0$ pairing interaction correlations in nuclei near the $N = Z$ line.

We are developing a method that goes beyond the usual configuration mixing approach. We utilize the power of the variational method in combination with the configuration interaction method. The method determines an optimal improvement to a wavefunction with a given number of configurations. We have applied the method to the pairing force interaction and to the n - p pairing interaction problem. In both cases, the results are extremely good. In the pairing case, which we studied in detail, this new approach gave well over 99.9% of the total correlation energy. We are now extending this approach to more general interactions.

The low-lying states of odd mass nuclei provide a good test of the parametrizations of single particle potentials. Study of the spectroscopy of the heavy elements is particularly valuable, as it gives insights into the structure of super-heavy elements. In a collaborative effort with the experimental spectroscopy group at Argonne, we have analyzed low-lying neutron and proton single particle states in the mass 250 region. We have studied neutron single-particle states in ^{247}Cm and ^{251}Cf , as well as proton single particle states in ^{249}Bk , and determined single-particle potentials that are consistent with these analyses. The study of ^{251}Cf is particularly important as it has 153 neutrons, giving information on the neutron single particle states above the deformed gap at 152 neutrons. Nine single particle states have been identified in this nuclide. These studies constrain potentials that are used to describe superheavy elements

d.1. Sensitivity to Multi-Phonon Excitations in Heavy-Ion Fusion Reactions

(H. Esbensen)

Measurements of heavy-ion fusion cross sections can often be reproduced fairly accurately by coupled-channels calculations at energies close to the Coulomb barrier. For a medium heavy system, like $^{64}\text{Ni} + ^{64}\text{Ni}$, it is necessary to include couplings to the one- and two-phonon as well as mutual excitations of the low-lying 2^+ and 3^- states in projectile and target, and nuclear couplings up to second order in the deformation amplitudes, in order to achieve a good fit to the data.¹ This is the standard two-phonon (2PH) coupling scheme. When the reacting nuclei are heavy and soft the calculated fusion cross sections become sensitive to multi-phonon excitations and higher-order couplings. This leads to two serious complications. First of all, the calculations will be sensitive to the nuclear structure properties of multi-phonon states, which are often poorly known empirically. Secondly, it is difficult to

make the calculations converge because of the large number of channels one would have to include in the calculations.

In order to study the transition from medium heavy to heavy and soft systems, where the coupled-channels calculations become more challenging, the fusion data for the following systems was analyzed: $^{64}\text{Ni} + ^{64}\text{Ni}$,¹ $^{64}\text{Ni} + ^{74}\text{Ge}$,² $^{74}\text{Ge} + ^{74}\text{Ge}$,³ and $^{64}\text{Ni} + ^{100}\text{Mo}$.⁴ These systems were chosen because the projectiles and targets are both fairly neutron rich and couplings to transfer channels are expected to have a minor impact on fusion. The results of the standard two-phonon calculations (2PH) are compared to the data in Fig. V-17. The no-coupling limit (NO-C) is also shown. At low energies the 2PH calculation is shifted with respect to the no-coupling limit and the energy shift is seen to increase as

the system becomes heavier and soft, reflecting a larger effect of the couplings.

The calculations were based on the Akyüz-Winther heavy-ion potential. A small adjustment was made in the radius parameter in order to optimize the fit to the $^{64}\text{Ni} + ^{64}\text{Ni}$ data. The fit is excellent for this system, with a χ^2 per point less than one, but the fits deteriorate for the heavier systems. It is possible to improve the fit to the $^{64}\text{Ni} + ^{74}\text{Ge}$ data by including up to four-phonon excitations (reducing the χ^2 per point from 6.4 to 2.6). Similar calculations for $^{74}\text{Ge} + ^{74}\text{Ge}$ and $^{64}\text{Ni} + ^{100}\text{Mo}$ do not improve dramatically the fits to the data.

Another way to improve the calculations is to go beyond the quadratic term in the expansion of the

nuclear interaction in terms of the deformation amplitudes. One complication is, however, that the empirical knowledge of the matrix elements of such higher-order couplings is poor, so it will be necessary to rely on structure models in order to proceed. This work was published.⁵

The fusion cross sections for $^{64}\text{Ni} + ^{64}\text{Ni}$ ¹ and $^{64}\text{Ni} + ^{100}\text{Mo}$ ⁴ were actually measured down to about 10 nb but they were only analyzed and shown down to 10 μb in Fig. V-17 because the calculations discussed here are not able to reproduce the smaller cross sections. The data are suppressed or hindered with respect to the calculations. This is the subject of the next section.

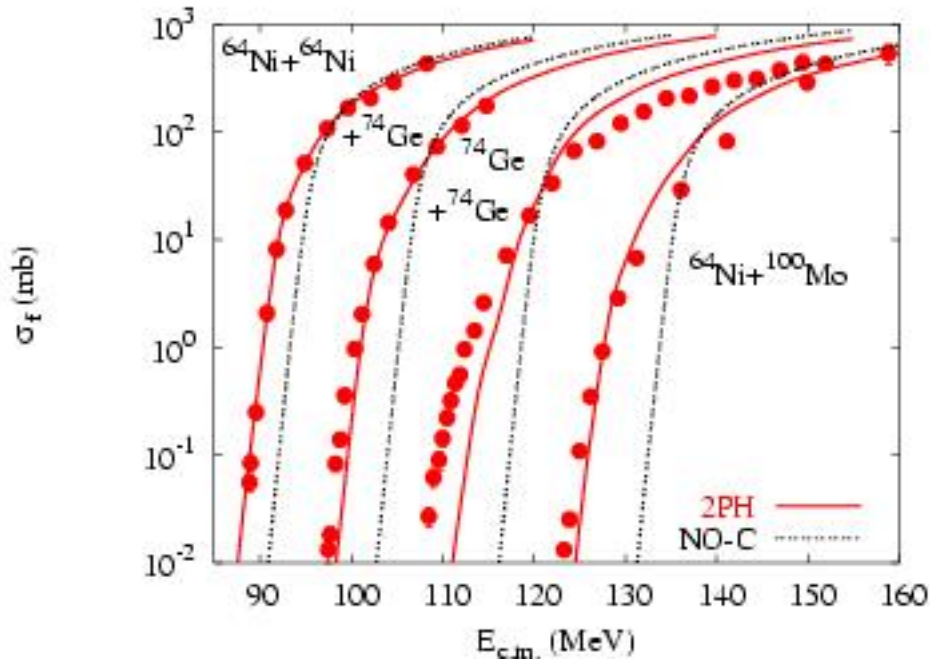


Fig. V-17. Measured cross sections for the fusion of $^{64}\text{Ni} + ^{64}\text{Ni}$,¹ $^{64}\text{Ni} + ^{74}\text{Ge}$,² $^{74}\text{Ge} + ^{74}\text{Ge}$,³ and $^{64}\text{Ni} + ^{100}\text{Mo}$ ⁴ are compared to the standard two-phonon (2PH) coupled-channels calculations. The dashed curves show the no-coupling limit (NO-C) of the calculations.

¹C. L. Jiang *et al.*, Phys. Rev. Lett. **93**, 012701 (2004).

²M. Beckerman *et al.*, Phys. Rev. C **25**, 837 (1982).

³M. Beckerman *et al.*, Phys. Rev. C **28**, 1963 (1983).

⁴C. L. Jiang *et al.*, Phys. Rev. C **71**, 044613 (2005).

⁵H. Esbensen, Phys. Rev. C **72**, 054607 (2005).

d.2. Hindrance of Heavy-Ion Fusion Due to Nuclear Incompressibility (H. Esbensen and Ş. Mişicu*)

The hindrance of heavy-ion fusion cross sections at energies far below the Coulomb barrier is now a well established phenomenon.¹ The best signature of the hindrance is the development of a maximum in the S factor for fusion, and the energy E_s where that occurs is used to characterize the phenomenon.¹ The low-energy fusion data are also hindered with respect to model calculations, including the coupled-channels calculations that are based on the Akyüz-Winther (AW) potential. In fact, that is how the phenomenon was first identified² and it has been a challenge to theory to explain what causes it.

The fusion hindrance was expected from the beginning² to be an entrance channel phenomenon because it occurs at high excitation energies of the compound nucleus, of the order of 20-40 MeV. What governs the entrance channel is the Coulomb and the nuclear potential but the latter is only well established at large distances between the reacting nuclei, where it has been obtained by the double-folding technique. The nuclear potential, as for example the AW potential, is usually parametrized in terms of a simple Woods-Saxon well at shorter distances. This parametrization has been quite successful, not because it is realistic but because the observables that have been calculated have not been sensitive to the short distance behavior of the potential.

We have recently proposed a mechanism that explains what causes the fusion hindrance and why coupled-channels calculations have not been able to reproduce the fusion data at low energies. We believe that the saturation properties of nuclear matter are causing a hindrance to a large overlap of the reacting nuclei and

this should be taken into account when constructing the nuclear ion-ion potential at short distances. Thus we find that supplementing the conventional double-folding potential (based on the M3Y+exchange NN interactions) with a repulsive potential derived from the nuclear incompressibility, we produce an entrance channel potential that has a rather shallow pocket inside the Coulomb barrier. This is the M3Y+repulsion potential, which is illustrated in the left panel of Fig. V-18 for the heavy-ion system $^{64}\text{Ni} + ^{64}\text{Ni}$. The M3Y double-folding potential (including exchange) is also shown. It produces an extremely deep pocket, which is even deeper than the energy of the ground state of the compound nucleus. The AW potential, which is also shown in Fig. V-18, is more reasonable, but it is still too deep to explain the low-energy fusion data.

Applying the M3Y+repulsion potential in the coupled-channels calculations that were discussed in section d.1., instead of the AW potential, we obtain an excellent fit to the $^{64}\text{Ni} + ^{64}\text{Ni}$ fusion data³ as can be seen in the right panel of Fig. V-18. The best χ^2 per point is about 1, whereas the calculations based on the AW potential give a best χ^2 per point of 10. The largest improvement occurs at cross sections smaller than 0.1 mb. Thus there is nothing wrong with the coupled-channels technique *per se*. Coupled-channels calculations have merely failed in the past to reproduce the low-energy fusion data because the ion-ion potentials that were used were unrealistic at shorter distances between the reacting nuclei. This work was published.⁴

*Fulbright Fellow, Argonne National Laboratory, and National Institute of Nuclear Physics, Bucharest-Magurele, Romania.

¹C. L. Jiang *et al.*, Phys. Rev. C **73**, 014613 (2006).

²C. L. Jiang *et al.*, Phys. Rev. Lett. **89**, 052701 (2002).

³C. L. Jiang *et al.*, Phys. Rev. Lett. **93**, 012701 (2004).

⁴Ş. Mişicu and H. Esbensen, Phys. Rev. Lett. **96**, 112701 (2006).

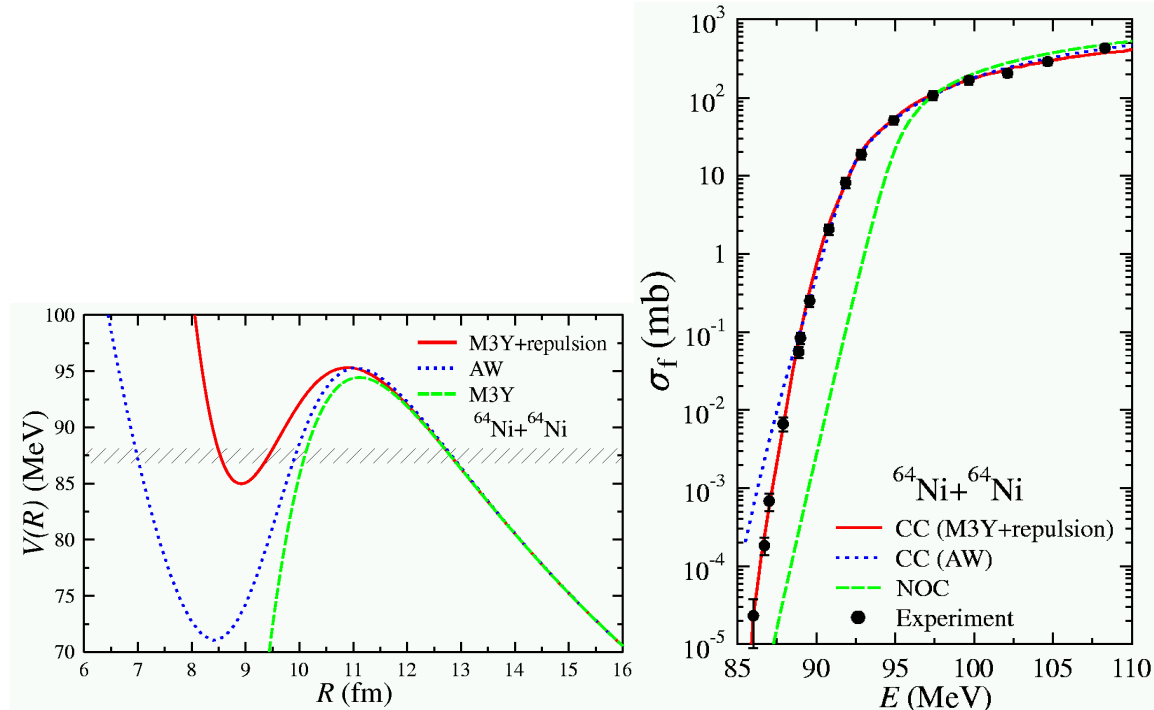


Fig. V-18. Entrance channel potentials for $^{64}\text{Ni} + ^{64}\text{Ni}$, obtained from the M3Y and the M3Y+repulsion double-folding potentials, are compared to the Akyüz-Winther (AW) potential. The dashed strip shows the energy E_s where the experimental S -factor² reaches a maximum.

d.3. Signature of Shallow Quasi-Molecular Potentials in Sub-Barrier Fusion (H. Esbensen and Ş. Mişicu*)

We have extended our calculations of the nuclear potential for $^{64}\text{Ni} + ^{64}\text{Ni}$ discussed in the previous section to other heavy-ion systems.¹ The calculations are based on the M3Y double-folding potential, including corrections for exchange and a repulsive term, which is calibrated to be consistent with the nuclear incompressibility. We refer to that as the M3Y+repulsion potential. We find that the repulsive correction is an essential ingredient in producing a shallow pocket and a thicker barrier in the potential between two heavy ions (see the left panel of Fig. V-18), and that this potential explains the observed hindrance of fusion at low energies (see the right panel of Fig. V-18).

We have applied the M3Y+repulsion potential, instead of the Akyüz-Winther (AW) potential, in the same coupled-channels calculations that were discussed in section d.1. We have performed calculations for heavy-ion systems that clearly exhibit the fusion hindrance phenomenon by developing a maximum in the S factor for fusion at low energies. Some results are shown in

Fig. V-19. The calculations reproduce the data fairly well, and much better than the calculations that are based on the AW potential. Thus the calculated S factors develop a maximum essentially at the same energy where the data show a maximum.

There are some minor oscillations in the calculated S factor for $^{64}\text{Ni} + ^{100}\text{Mo}$ but they should not be taken seriously because the calculations have not fully converged with respect to multi-phonon excitations, as mentioned in section d.1. The oscillations in the calculated S factor for $^{58}\text{Ni} + ^{58}\text{Ni}$ with two well-developed maxima, on the other hand, is a much more robust prediction which can be tested experimentally.

The fusion hindrance, which has now been observed for many systems, is explained in a natural way by a shallow pocket in the entrance channel potential. Thus we have observed a close correlation between the energy E_s where the S factor develops a maximum and the energy of the pocket. The two energies are separated by roughly 3-5 MeV.¹ Fusion should in

principle still be possible at energies below the pocket because the compound nucleus exists at even much lower energies, at least in the three cases discussed here. However, the fusion is expected to be strongly hindered at such low energies and it would require a much more complicated dynamics to describe it.

A clear signature of the shallow pocket in the entrance channel potential we predict is a narrowing of the spin

distribution for fusion when the center-of-mass energy is below the critical energy E_s and approaches the pocket energy. A narrower spin distribution results in a reduction in the multiplicity of γ -rays emitted from the compound nucleus, a feature that has not been observed before but it is a signature that can be tested experimentally.

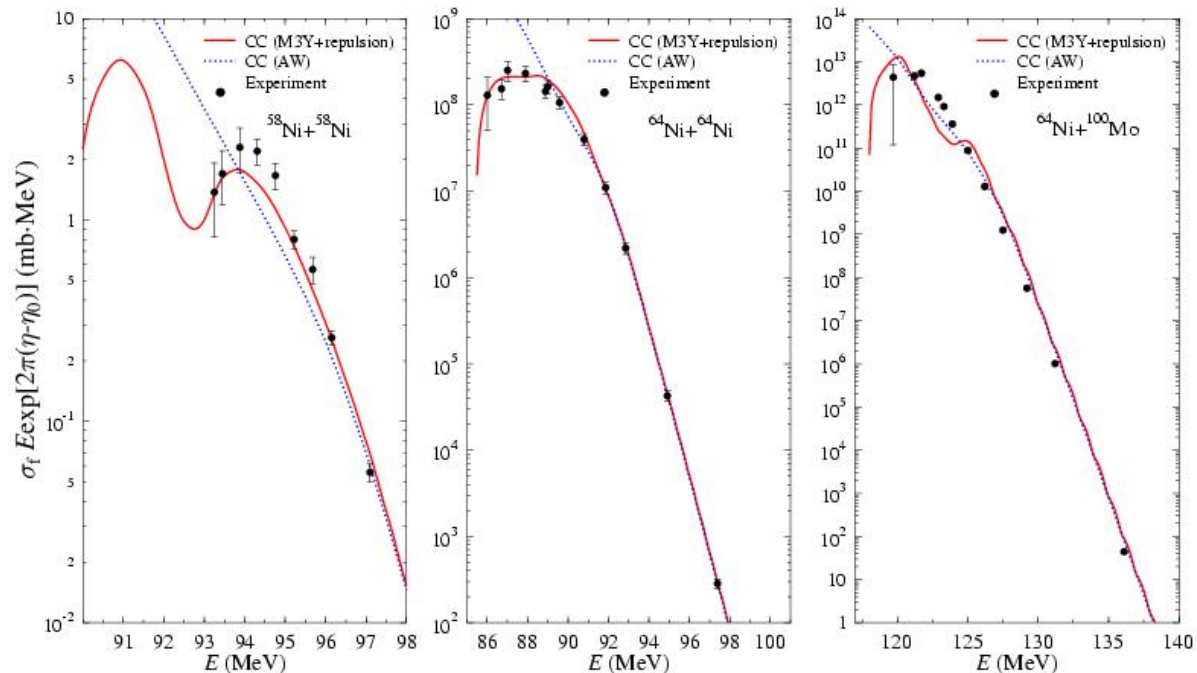


Fig. V-19. S factors for the fusion of $^{58}\text{Ni} + ^{58}\text{Ni}$,² $^{64}\text{Ni} + ^{64}\text{Ni}$,³ and $^{64}\text{Ni} + ^{100}\text{Mo}$.⁴ The dotted curves are based on the Akyüz-Winter, and the solid curves on the M3Y+repulsion potential.

Finally we note that a similar sensitivity to the nuclear potential at shorter distances has also been recognized in calculations of the quasi-molecular states that explain

the resonance structures observed in light-ion scattering and in calculations of cluster radioactivity in very heavy nuclear systems.

*Fulbright Fellow, Argonne National Laboratory, and National Institute of Nuclear Physics, Bucharest-Magurele, Romania.

¹Ş. Mişicu and H. Esbensen (work in progress).

²M. Beckerman *et al.*, Phys. Rev. **25**, 837 (1982).

³C. L. Jiang *et al.*, Phys. Rev. Lett. **93**, 012701 (2004).

⁴C. L. Jiang *et al.*, Phys. Rev. C **71**, 044613 (2005).

d.4. Reconciling Coulomb Dissociation and Radiative Capture Measurements

(H. Esbensen, G. F. Bertsch,* and K. A. Snover*)

There has been a significant discrepancy between the results of recent measurements of the radiative capture (RC) of protons on ^7Be and measurements of the

Coulomb dissociation (CD) of ^8B . The status reported in 2003 by the Seattle group¹ is summarized in Fig. V-20 where the solid points show the extrapolation

to zero relative energy of the S factor, $S_{17}(0)$, obtained from different RC and CD experiments. It is seen that S factors extracted from the CD experiments are on average about 10% smaller than obtained in the direct RC measurements. We have tried to reconcile this discrepancy by examining the assumptions that are commonly made in the analysis of the CD experiments.²

Our model calculations show that the first-order perturbation theory, which is normally used in the analysis of CD experiments, can be inaccurate by up to 20%, depending on the conditions of the experiments. One reason that the first-order theory fails is the dynamic polarization of ${}^8\text{B}$, which is particularly strong at low beam energies. Another reason is that the far-field approximation, which is used in the multipole expansion of the Coulomb field from the target nucleus, becomes invalid when there is an overlap between projectile and target during the collision. It is difficult to avoid such an overlap because of the weak binding and the extended density distribution of the valence proton in ${}^8\text{B}$. For the same reason one should also consider the nuclear induced breakup as well. We have included all of these effects in semi-classical calculations of the ${}^8\text{B} \rightarrow {}^7\text{Be} + p$ breakup by solving the time-dependent Schrödinger equation for the ${}^7\text{Be} + p$

two-body system to all orders in the Coulomb and nuclear fields from a high- Z target.

We find that all of the effects mentioned above lead to a suppression of the calculated decay energy spectrum when compared to the conventional first-order calculation at low relative energies. This implies that the low-energy S factors, which have been extracted from CD experiments using the first-order theory, have been underestimated and should be revised. Examples of revised values are shown by triangles in Fig. V-20. The value extracted from the NSCL experiment has been increased by about 5% as we suggested in Ref. 2. A recent analysis of the RIKEN data performed by Ogata *et al.*³ included all the corrections we have suggested and gave an 11% higher S factor than obtained in the original analysis.

The GSI2 experiment⁴ was recently reanalyzed⁵ and an 8% higher value of the extrapolated S factor was obtained. The new result was actually obtained with the conventional first-order perturbation theory. This is justified because the dynamic polarization should not play any role at the high beam energy of 254 MeV/u, but a better first-order theory (beyond the far-field approximation) might give a slightly larger S factor.

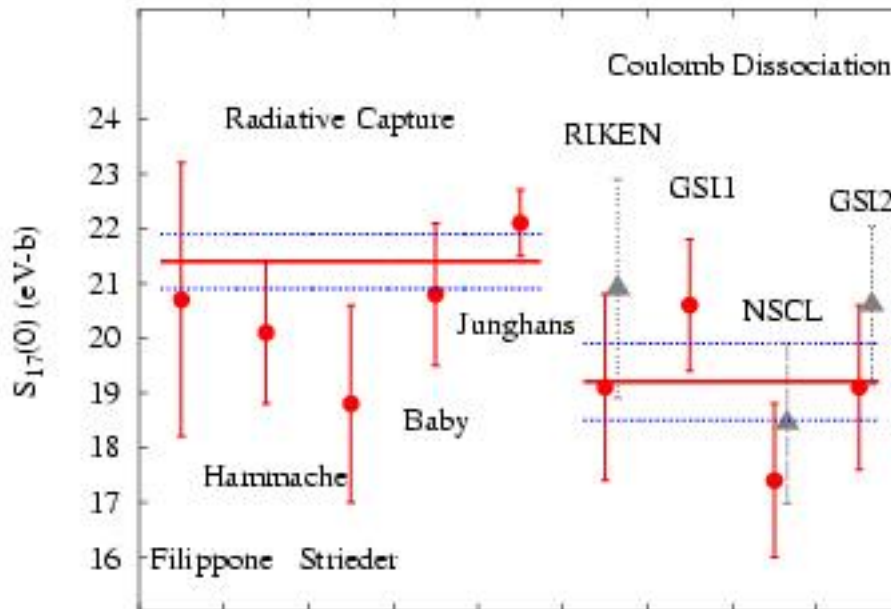


Fig. V-20. S factors extrapolated to zero relative energy from direct capture (left) and Coulomb dissociation (right) experiments.² The triangles are the revised values discussed in the text.

The comparison in Ref. 1 of the RC and CD experiments showed that the slope parameter b , which appears in the expansion $S(E) = a(1 + bE)$ of the

relative energy dependence of the S factor, is usually larger when extracted from CD experiments. This feature is also explained by our model calculations.² In

a recent Comment, Moshe Gai⁶ has challenged the value of the slope parameter determined in Ref. 1 for the RIKEN experiment. However, the significance of the Comment is not clear because it was not possible to reach a consensus about the uncertainty on the extracted

value of b .⁷ Anyway, the discrepancy between the RC and CD experiments has been reduced significantly in recent years, partly by making the corrections we suggested. Our work was published.^{2,7}

*University of Washington.

¹A. R. Junghans *et al.*, Phys. Rev. C **68**, 065803 (2003).

²H. Esbensen, G. F. Bertsch, and K. A. Snover, Phys. Rev. Lett. **94**, 042502 (2005); H. Esbensen, AIP Conf. Proc. **819**, 518 (2006).

³K. Ogata *et al.*, Phys. Rev. C **73**, 024605 (2006).

⁴F. Schümann *et al.*, Phys. Rev. Lett. **90**, 232501 (2003).

⁵F. Schümann *et al.*, Phys. Rev. C **73**, 015806 (2006).

⁶Comment by Moshe Gai, Phys. Rev. Lett. **96**, 159201 (2006).

⁷H. Esbensen, G. F. Bertsch, and K. A. Snover, Phys. Rev. Lett. **96**, 159202 (2006).

d.5. Dipole Response and Charge Radius of Two-Neutron Halo Nuclei (H. Esbensen and T. Nakamura*)

The study of two-neutron halo nuclei, such as ${}^6\text{He}$ and ${}^{11}\text{Li}$, is still rather incomplete. Recently the charge radii of these two nuclei were measured,^{1,2} and this provides a valuable constraint on theory and other measurements. The dipole strength distribution, for example, which has been measured for both nuclei in Coulomb dissociation experiments, is still uncertain and it is inconsistent with the predictions of three-body models (3BM). It is therefore of interest to study the relation between the dipole response and the charge radius in order to test the consistency of the two observables.

The dipole strength distribution we obtain in our 3BM of ${}^{11}\text{Li}$ ³ is shown in Fig. V-21. The strong peak at low energy (solid curve) is the result of the final state interaction between the two neutrons. Without this final state interaction, the strong low-energy peak disappears, as shown by the dashed curve. The calculated distribution obtained in Ref. 4 has a similar low-energy peak but the strength is weaker because it only includes the three-body resonance contribution. The peaks of the measured distributions are generally broader and located at higher energies than predicted by the two theories (see, for example, Fig. 5 of Ref. 4).

The situation is also poor for ${}^6\text{He}$. The measured dipole strength⁵ is uncertain and it does not reproduce the low-energy peak predicted by theory⁶ (see Fig. 4 of Ref. 5).

This is very unfortunate because it should be possible to construct a realistic 3BM of ${}^6\text{He}$. The measured charge radius, for example, is described quite well by several such models.¹

In order to test and put constraints on the measured or calculated dipole response of a two-neutron halo nucleus, we have studied the relation to the charge radius. Thus the total dipole strength associated with dipole excitations of the halo with respect to the core is closely related to the mean-square distance between the core and the center-of-mass of the halo.³ This distance, in turn, relates the charge radii of the halo nucleus and the core nucleus.¹ Thus one can test whether a given dipole strength is consistent with the measured charge radius.

We have applied this method to test the dipole response of ${}^{11}\text{Li}$, which was recently measured at RIKEN.⁷ The measured strength distribution has essentially the same shape as the calculated distribution shown in Fig. V-21, with a strong peak at low energy. The calculation can be scaled to fit the data up to 3 MeV, and one can then use the calibrated 3BM to estimate the total experimental dipole strength and the associated charge radius. The estimate gives a charge radius of ${}^{11}\text{Li}$ which is slightly below the value 2.467 ± 0.037 fm obtained in the recent high precision laser spectroscopy measurement.² This work is in progress.

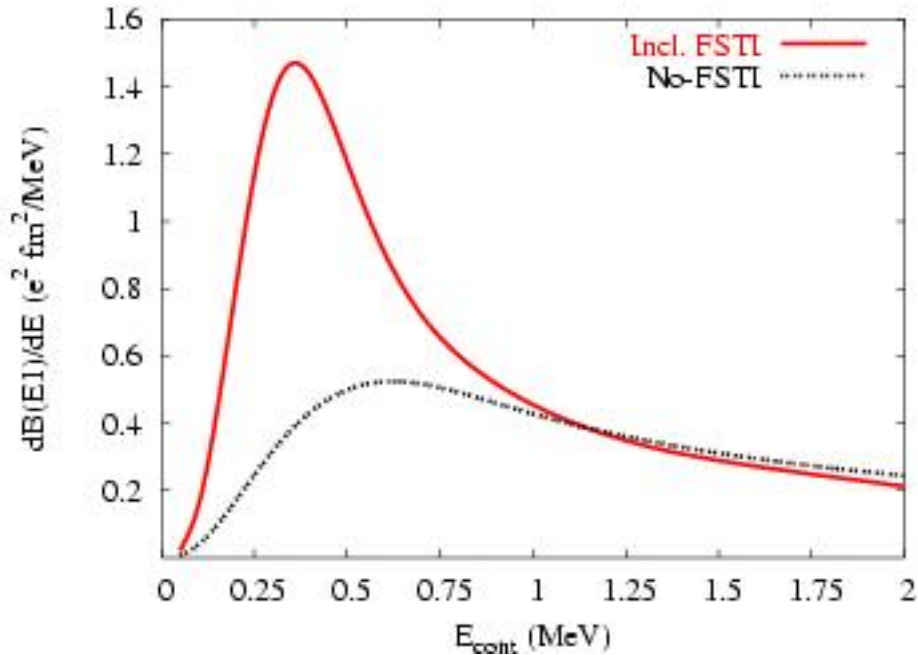


Fig V-21. The dipole response of ^{11}Li obtained in Ref. 3 with (solid) and without (dashed curve) the final state neutron-neutron interaction, as function of the three-body continuum energy E_{cont} .

*Tokyo Institute of Technology, Japan.

¹L.-B. Wang *et al.*, Phys. Rev. Lett. **93**, 142501 (2004).

²R. Sanchez *et al.*, Phys. Rev. Lett. **96**, 033002 (2006).

³H. Esbensen and G. F. Bertsch, Nucl. Phys. **A542**, 310 (1992).

⁴E. Garrido, D. V. Fedorov, and A. S. Jensen, Nucl. Phys. **A708**, 277 (2002).

⁵T. Aumann *et al.*, Phys. Rev. C **59**, 1252 (1999).

⁶A. Cobis, D. V. Fedorov, and A. S. Jensen, Phys. Rev. Lett. **79**, 2411 (1997).

⁷T. Nakamura *et al.* (unpublished).

d.6. Mean Field and Many Body Wave Functions (R. R. Chasman)

We are continuing our long-term effort to develop programs for calculating many-body variational wave functions. In our approach, pairing and particle-hole two-body interactions are treated on an equal footing. The complexity of the wave functions depends only on the number of levels included in the valence space. In these wave functions, we strictly conserve particle number and parity; projecting states of good particle number and parity before carrying out the variational calculations. We have extended our approach to improve the treatment of neutron-proton pairing and we can now explain several of the unusual features of nuclides near the $N = Z$ line in a very simple way. An essential feature of our approach is the direct inclusion of independent amplitudes for the four particle

configuration consisting of two neutrons and two protons in the same J_z sub-state.

Many of the techniques that we have developed to treat n - p (neutron-proton) pairing can be profitably applied to Hamiltonians that contain particle-hole interactions in addition to pairing interactions. We are developing a code to explore that possibility.

The major limitation of shell model calculations is that the number of configurations becomes unmanageable as the valence space is increased. The wave functions that we are developing contain large numbers of configurations – *e.g.*, 10^{22} configurations in the wave functions that we use for Hamiltonians that include n - p

pairing interactions. However, these wave functions are product wave functions and the number of independent amplitudes is quite small, *e.g.*, 150 independent amplitudes in a wave function that has 10^{22} configurations. To fully utilize this simple wave

function structure, a systematic approach to configuration interaction is needed. We have recently developed such an approach by extending the variational method for use in the context of configuration interaction calculations.

d.7. Variational Approach to Configuration Interaction (R. R. Chasman)

Methods for the systematic improvement of solutions to quantum-mechanical problems play an essential role in the accurate theoretical description of physical phenomena. We are developing a class of many-body wave functions that are a product of terms. Each of the terms in the product is, in turn, a sum of terms. In such a case, the number of independent variational amplitudes is orders of magnitude smaller than the number of configurations in the wave function. In a simple pairing interaction, in a system with 32 doubly degenerate levels and 16 pairs of nucleons, there are approximately 10^9 configurations, but the BCS solution for this problem has only 32 independent amplitudes. For the n - p pairing Hamiltonian that we have studied, there are roughly 10^{22} configurations for a half-filled system with 30 quadruply degenerate levels, each capable of holding two neutrons and two protons. In our product wave function, there are just 150 independent amplitudes.

We have found that such solutions can be systematically improved by using the variational method. The basic idea is to take linear combinations of wave functions, all with the same general structure, to construct more accurate solutions. We start with a variational solution of the product form. We then calculate amplitudes for a second wave function having the same form. The amplitudes of the second wave function are determined variationally as the optimal improvement to the original wave function for a wave function of that form. A third wave function is then calculated as the optimal improvement on the first two wave functions. The method can be continued indefinitely.

There are exact solutions available for a pairing Hamiltonian with constant matrix elements. We tested our approach by comparing our results with the exact energy for the model pairing Hamiltonian. We got agreement to 1 keV, by taking 80 basis states. Using only 40 basis states, the error is just 3 keV. In the case of the n - p pairing Hamiltonian, there are no exact solutions available. We found that the wave function with 80 basis states improves the binding energy by 1 MeV relative to the wave function consisting of a single optimized state. In Fig. V-22, we show the improvement in binding energy as a function of the number of basis states for both interactions.

The usual stumbling block to adding more and more wave functions in configuration interaction calculations is that, at some point, the overlap between the added wave function and those already in place approaches 1 and there is no improvement in the energy. Our variational approach avoids the problem of overlap pileup. In Fig. V-23, we show the number of overlaps as a function of the magnitude of the overlap for wave functions that have 80 basis states. We also plot this overlap function for a wave function with basis states calculated using the generator coordinate method. In the latter case, there is a substantial pileup of overlaps near 1.0.

We have published¹ the study of this approach for the pairing interactions discussed above. We are extending the method to handle Hamiltonians with both pairing and particle-hole interactions.

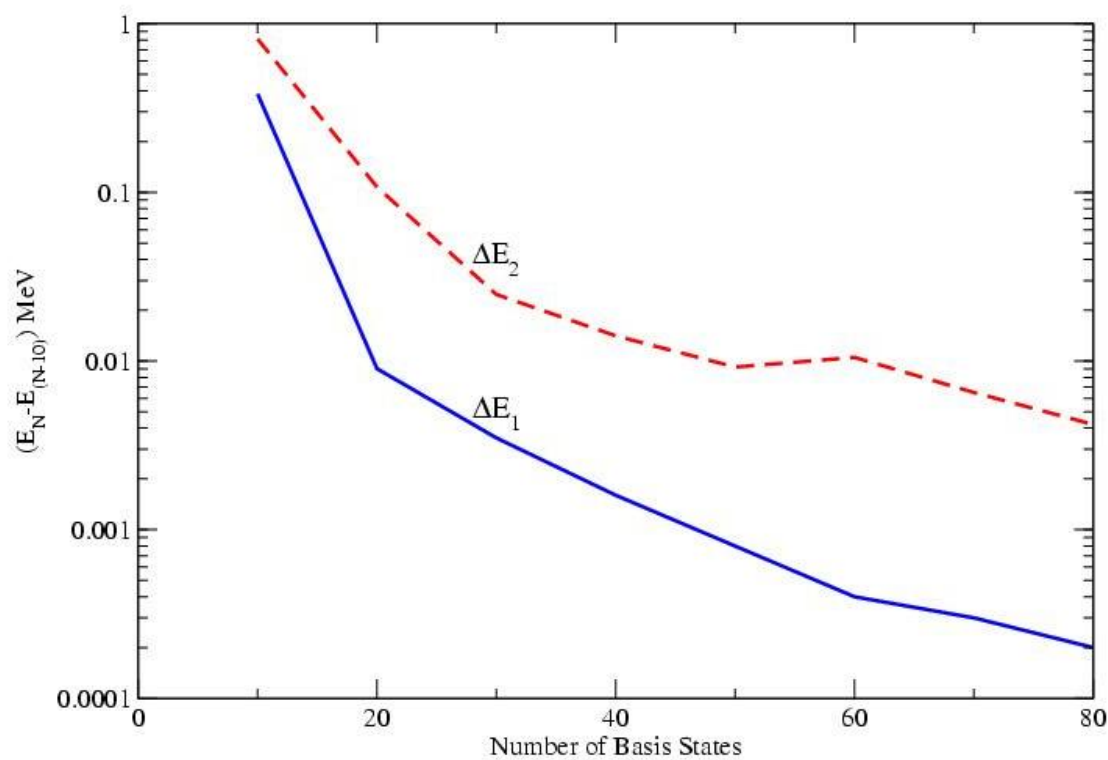


Fig. V-22. Improvement in correlation energy as a function of the number of variational wave functions. The increase in correlation energy per 10 basis functions is plotted for the simple pairing interaction (ΔE_1) and for the n - p pairing interaction (ΔE_2).

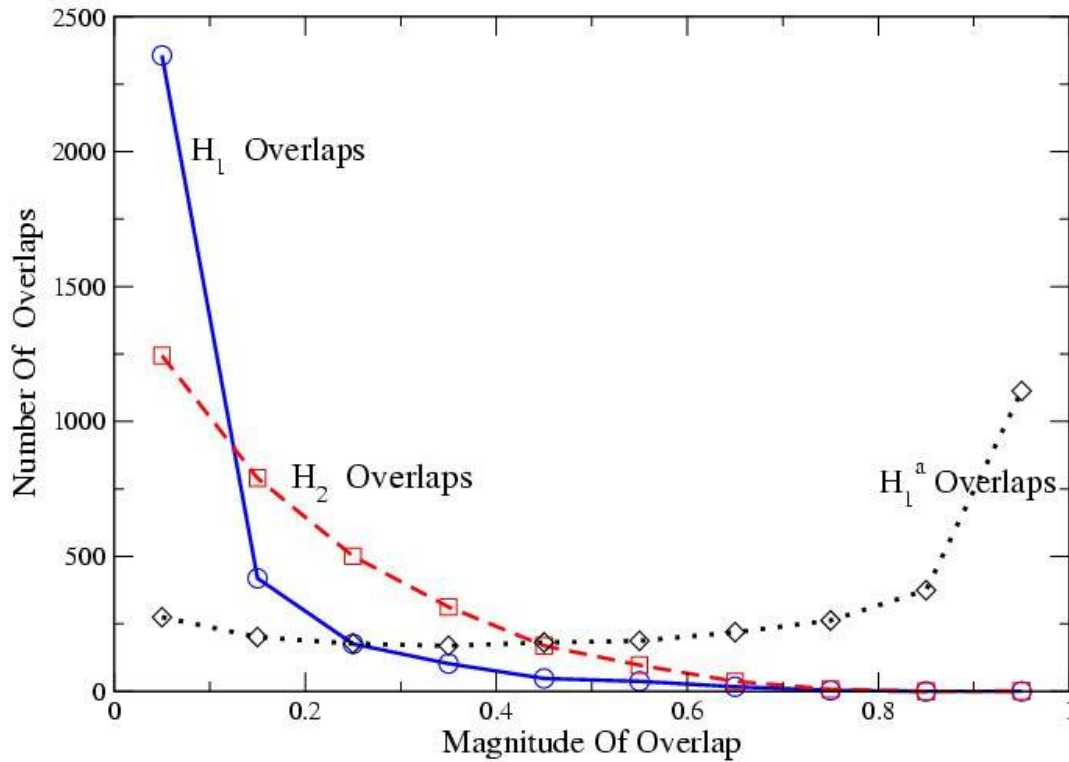


Fig.V-23. Number of off-diagonal basis state overlaps as a function of the absolute value of the overlap. The curve labeled H_1 applies to simple pairing wave functions. The curve labeled H_2 applies to n - p pairing wave functions. The curve labeled H_1^a applies to the simple pairing interaction when the generator coordinate method is used to construct the configuration interaction set of basis states.

¹R. R. Chasman, Phys. Rev. Lett. **95**, 262501 (2005).

d.8. Neutron-Proton Pairing (R. R. Chasman)

We have developed¹⁻³ a treatment of neutron-proton pairing that explains many features of nuclear structure seen near the $N = Z$ line. Our many-body treatment includes n - p pairing, as well as like particle pairing. We do a full projection of neutron and proton particle number before the variational calculation. We also found that there is a new quantum number that holds exactly for collective states; *i.e.*, those states in which no levels are blocked. This new quantum number (Q) is the number parity of the $T = 0$ and $T = 1$ n - p pairs. Fixing the number parity of one n - p mode fixes the other, because we conserve proton number and neutron

number exactly. This number parity is closely related to the isospin quantum number. These collective states are the ground states for $N = Z$ nuclides. We project Q before doing a variational calculation. The form of our variational wave function includes an explicit amplitude for “alpha like” correlations in each level as well as the usual amplitudes for n - n , p - p and n - p pairs. We have added terms to the n - p pairing interaction, which allow pairs of particles in the same orbitals, giving states with maximum angular momentum. Because of the exclusion principle, these must be n - p pairs and $T = 0$.

In odd-odd $N = Z$ nuclei, the ground state is a degenerate doublet, consisting of a $Q = 0$ and $Q = 1$ state, when the $T = 0$ and $T = 1$ pairing strengths are equal. The splitting of this ground state doublet affords some information about the relative strengths of the $T = 0$ and $T = 1$ pairing strengths. In even-even nuclei, there is a large splitting between the $0^+ T = 1$ ground state and the $1^+ T = 0$ excited state. Our model explains this feature in a transparent way. Most of the excitation energy owes to the breaking of a quartet and the single particle excitation energy involved in making a $T = 0$ pair. In the odd-odd $N = Z$ nuclei case, neither of these effects applies for the $T = 0$ state.

Our detailed calculations of the dependence of the binding energies on the relative strengths of the $T = 0$ and $T = 1$ pairing strengths shows that the differences are small as a function of the variation of the relative strengths. Other observables are needed to establish the

magnitude of $T = 0$ correlations in nuclei. To that end, we have carried out a calculation of the n - p pair transfer spectroscopic factor. In our calculation, the initial state is an even-even $N = Z$ nuclide and the final states are the lowest $T = 1$ and $T = 0$ states in the neighboring odd-odd ($Z + 1, N + 1$) nucleus. The relative spectroscopic factors show a considerable sensitivity to the relative strengths of the $T = 0$ and $T = 1$ pairing strengths. A 20% reduction of the $T = 0$ pairing strength gives a 40% reduction in the ratios of $T = 0/T = 1$ pair transfer probabilities. The interaction is semi-realistic in this calculation, as we use constant matrix elements for each of the pairing modes.

We are extending the pair transfer calculations to study pair transfer reactions in ^{44}Ti . Experimental studies of this nucleus are being planned.

¹R. R. Chasman, Phys. Lett. **B524**, 81 (2002).

²R. R. Chasman, Phys. Lett. **B553**, 204 (2003).

³R. R. Chasman, Phys. Lett. **B577**, 47 (2003).

d.9. Energy Levels of the Heavy Elements (I. Ahmad and R. R. Chasman)

The study of single-particle states in the heavy elements is a long-term collaborative project. The low-lying states in odd-mass nuclides provide a good test of the parametrizations of single particle models. Vibrational admixtures are usually small for these states. The single-particle energy level spacings in the heavy elements provide useful guidance for single-particle potentials that are appropriate for super-heavy elements. Seven single-particle states have been identified¹ in ^{247}Cm , so this nuclide provides a good test of neutron single particle potentials. The study² of ^{251}Cf is particularly important as it has 153 neutrons, giving information on the neutron single particle states

above the deformed gap at 152 neutrons. Nine single particle states have been identified in this nuclide. Eight single-particle levels have been identified³ in ^{249}Bk . This provides a very good test of proton single-particle potentials in the very heavy elements. When pairing effects are extracted⁴ from the observed levels in ^{247}Cm , ^{251}Cf and ^{249}Bk , the orderings and spacings of levels are in good agreement with the levels obtained from our parametrization of a deformed Woods-Saxon potential. These analyses will provide useful constraints on other parametrizations of superheavy potentials.

¹I. Ahmad *et al.*, Phys. Rev. C **68**, 044306 (2003).

²I. Ahmad *et al.*, Phys. Rev. C **72**, 054308 (2005).

³I. Ahmad *et al.*, Phys. Rev. C **71**, 054305 (2005).

⁴R. R. Chasman, Phys. Rev. C **14**, 1935 (1976).

E. ATOMIC THEORY AND FUNDAMENTAL QUANTUM MECHANICS

In addition to research on hadron and nuclear physics, and nuclear astrophysics, we also conduct research in atomic physics, neutron physics, and quantum computing.

Work in atomic physics includes the studies of interactions of electrons or high-energy photons with matter, in support of experiments performed at Argonne's Advanced Photon Source (APS). Theoretical studies are being conducted on the physics of the photoeffect and Compton scattering by bound electrons, focusing on topics selected in view of basic importance, timeliness, and potential in applications. Comprehensive surveys of photo-interaction data for silicon and graphite are underway. Some of the results are useful for underpinning cross sections and stopping power for charged-particle interactions, namely, basic data for radiation physics.

Ongoing theoretical work in support of a new experiment to measure the neutron electric-dipole moment (EDM) is currently focusing mostly on issues relating to the penetration of neutrons into a perfect silicon crystal in the Bragg reflection process. Preliminary reflectivity measurements at the NIST reactor have been performed and the main instrumental issues appear to have been identified. An experiment to measure the interaction of the neutron's known magnetic dipole moment with the crystalline electric field, intended both to test the principle of the EDM experiment and to calibrate the electric field, is planned for late in CY 2006.

Work was completed on representations of complex rational numbers as states of finite strings of two types of qubits, one for real and one for imaginary numbers. These rational string states representations were extended to a representation of real and complex numbers by defining Cauchy sequences of the rational string states. The definition of the Cauchy condition, which mirrored that used in mathematical analysis, was given for sequences of states of the form $|s_n\rangle$, where $s_n: \{1, \dots, n\} \rightarrow \{0, 1\}$ is a 0-1 valued function, and extended to linear superpositions of sequences of these states. Much of the work to show that (equivalence classes) of these state sequences represent real and complex numbers consists in verifying that definitions of addition and multiplication and their inverses have the requisite properties and that the set is complete (the set is closed under taking of limits).

e.1. Interactions of Photons with Matter (M. Inokuti and D. Y. Smith*)

In support of experiments in atomic and condensed-matter physics with the use of synchrotron radiation, theoretical studies are being conducted on the physics of photo-absorption and Compton scattering, focusing on topics selected in view of basic importance, timeliness, and potential applications.

One theme of long-term studies has been the use of dispersion relations and sum rules for indices of response of matter over the entire range of photon energies. A comprehensive analysis of optical data on crystalline silicon is nearly complete. Work on graphite is also in progress.

*University of Vermont.

e.2. Interactions of Charged Particles with Matter (M. Inokuti)

Stopping power, the total yield of ionization, and its statistical fluctuations are examples of quantities describing the penetration of charged particles through matter and are important to applications such as the detection of particles and the analysis of their charges and kinetic energies. The understanding of those quantities in terms of individual collisions and associated cross sections remains a major challenge and is the goal of our continuing effort. Current work is the evaluation of the mean excitation energies, namely, the I values, in the Bethe stopping-power formula from the oscillator-strength spectra for 9 atoms and 23 molecules that are treated by Berkowitz.¹ Results are reported in a full paper.²

Extensive work for the International Commission on Radiation Units and Measurements (ICRU) continues

¹J. Berkowitz, *Atomic and Molecular Photoabsorption. Absolute Total Cross Sections* (Academic Press 2002).

²S. Kamakura, N. Sakamoto, H. Ogawa, H. Tsuchida, and M. Inokuti, in Program and Abstracts, submitted to J. Appl. Phys.

on the editing of its reports and on physical data such as stopping powers and various interaction cross sections.

The main line of Inokuti's life-long study concerns interactions of energetic charged particles with matter and consequent changes in the structure and properties of matter. This topic forms a basis for particle detection and analysis in experimental nuclear and particle physics, as well as for mechanistic considerations in radiation chemistry and biology, and in materials science. He has begun to write a manuscript for a monograph entitled "Principles of Radiation Physics". The book will be a comprehensive presentation of his major observations and findings in about 600 printed pages.

e.3 Representation of Real and Complex Numbers in Quantum Theory (P. Benioff)

Work was completed on a representation of complex rational numbers as finite strings of two types of qubits, one for real and the other for imaginary rational numbers.¹ The states were defined in a Fock space for both bosons and fermions as products of creation operators, $a_{\alpha j}^\dagger$, $b_{\beta j}^\dagger$ acting on the vacuum state $|0\rangle$. Here $\alpha, \beta = +, -$ and j is any integer. The states $a_{\alpha j}^\dagger |0\rangle$, $b_{\beta j}^\dagger |0\rangle$ correspond to the numbers $\alpha 2^j$ and $i\beta 2^j$. Complex rational number states have the form $(a_{\alpha}^\dagger)^s (b_{\beta}^\dagger)^t |0\rangle$ where s, t are finite subsets of integers. This representation of rational numbers is based on the observation that the 0s in a binary representation do not contribute to the value of the number. They just serve as placeholders.

Basic arithmetic relations ($=, \leq$) and operations ($+, \times, -, \div$) were defined on these states and were shown to have the required properties. (\div denotes division to any accuracy $a_{+, -\ell}^\dagger |0\rangle$.) The proofs of this were based on properties of the states only and did not use the usual numerical values of these states as sums of powers of 2.

This work on complex rational numbers as states of strings of qubits was extended to a representation of real and complex numbers in quantum theory by defining the Cauchy condition for sequences of

complex rational string states.² The definition mirrored the usual, except that arithmetic closeness of states in the sequence was defined relative to the state $a_{+, -\ell}^\dagger |0\rangle$ instead of 2^ℓ . The definition was given for sequences of states of the form $\psi_n = (a_{\alpha_n}^\dagger)^{s_n} (b_{\beta_n}^\dagger)^{t_n} |0\rangle$, where s_n and t_n are n dependent finite sets of integers, and α_n, β_n indicate a possible n dependence of the signs. The definition was extended to apply to more general states that were linear superpositions of complex rational string states.

Real and complex numbers were defined as equivalence classes of Cauchy sequences of these states. Two sequences were equivalent if they became arbitrarily close arithmetically as n increased without bound. The definitions of arithmetic relations and operations on complex rational string states were "lifted" to definitions of $=, \leq$, and $+, \times, -, \div$ on Cauchy sequences. Much of the work was devoted to showing that (equivalence classes of) the Cauchy sequences of real rational string states satisfied the required properties of real numbers, *i.e.*, that they were an ordered field that was complete. Complex number properties are included as they are ordered pairs of real numbers with appropriate definitions of multiplication and other arithmetic operations and relations.

¹P. Benioff, Phys. Rev. A **72**, 032314 (2005).

²P. Benioff, A Representation of Real and Complex Numbers in Quantum Theory, ArXiv preprint quant-ph/0508219.

F. OTHER ACTIVITIES

f.1. New Theoretical Tools for Nucleon Resonance Analysis (A. Höll, T.-S. H. Lee, C. D. Roberts, and S. V. Wright)

It has long been recognized that a veracious description of nucleon resonances (N^*) is one of the most important requirements in the development of a fundamental understanding of strong interactions. Indeed, the 2004 Office of Science Strategic Plan for Nuclear Science states that connecting the observed properties of baryons with the underlying theoretical framework provided by quantum chromodynamics (QCD) is one of the central challenges of modern science. It is necessary to determine the manner in which the structure of N^* can emerge from QCD, the fundamental theory of strong interactions. A key step along the way is the development of an understanding of the models of hadron physics and the fidelity of their predictions.

Two puzzles in particular stand out: the so-called *missing resonance problem*, which refers to the fact that numerous N^* states predicted by the $SU(6) \times O(3)$ constituent-quark model are not seen in π - N scattering; and the problem of the *interpretation of nucleon*

resonance parameters, which addresses the issue of just how can one relate QCD calculations of hadron properties to the parameters extracted in amplitude analyses?

Motivated by these considerations, we secured funding from the Argonne Theory Institute (<http://www.anl.gov/ati/>) to host two one-week workshops, which focused on the development of reaction theory for the electromagnetic production of mesons with a particular emphasis on bridging the gap between observation and QCD. They were very timely because an enormous amount of data on the photo- and electro-production of mesons (π , η , K , ω , ϕ and $\pi\pi$) has been accumulated at Thomas Jefferson National Accelerator Facility (JLab), and several other facilities around the world, and the understanding of this data needs new theoretical tools. Our program was a natural complement and precursor to the creation of an Excited Baryon Analysis Center at JLab.

f.2. 18th Annual Midwest Theory Get-Together (C. D. Roberts)

The Theory Group hosted the seventeenth Annual Midwest Theory Get-Together on October 7-8, 2005. Nuclear theorists from thirteen Midwest universities and ANL met to learn about the research goals and foci of different individuals and groups throughout the region. While the organizational duties rotate amongst the participants, Argonne is the regular host site because of its meeting facilities and central location. The organizers for 2005 were George Fai and Peter Tandy from the Kent State University. The meeting provides a good chance for students to broaden their outlook and get some practical speaking experience in a

friendly atmosphere. The format is informal, with an agenda of talks being volunteered at the beginning of the meeting. In 2005 we had forty-eight registered participants: faculty, postdocs and students. Over the Friday afternoon and Saturday morning twenty-eight presentations were made, covering topics such as: effective field theories; hadron physics and QCD; QCD-AdS/CFT correspondence; the nuclear shell model, nuclear pairing and nucleon matter; quantum Monte-Carlo methods; relativistic heavy ion collisions; and relativistic quantum mechanics for few body systems. It was a successful event.

VI. OTHER EDUCATIONAL AND COMMUNITY OUTREACH ACTIVITIES

OVERVIEW

Education remains a key part of our mission, especially training young nuclear physicists for the next generation of research, stewardship and homeland security. We are involved in many programs, including education at undergraduate, graduate, and post-doctoral level. We are also involved in using our expertise and capabilities to support programs in local Universities and in our community.

a. **Minority Program** (B. Zeidman)

The primary aim of the minority program is increasing the number and quality of minority participants in physics and other sciences. This involves ongoing interactions with minority students and faculty during visits to colleges and universities with substantial minority populations and a number of other activities. Among these efforts is inclusion of qualified scientists and students from minority institutions in research being performed by ANL scientists; e.g., collaborations on experiments, short-term appointments, and internships, such as SRP and SULI. In addition, attendance at meetings of minority organizations and visits to educational institutions provide chances for individual interactions and discussion of a wide variety of topics, e.g., research opportunities at ANL and other DOE laboratories, graduate education, internships, employment possibilities, etc., that influence choices of major field and career development.

The strongest interactions with minority students result from visits to minority institutions where it is possible to have discussions in depth with individual students. During the academic year, the program involves recruiting trips to minority schools, many having been visited in prior years. Included in these visits are seminars that discuss research performed by the Physics Division, particularly in the Medium Energy and Heavy

Ion programs. Since ANL experiments at JLab include collaborators (both faculty and student) from some of these universities, (e.g., Florida International University, Hampton University, North Carolina A&T University, Southern University, New Orleans, UTEP) some members of the audience are often active participants in the research being discussed. Inasmuch as many students from these colleges may also have been at ANL as participants in the SRP and SULI (ERULF) programs, it is possible to make direct connections between the research being discussed and persons present or known to the audience. SRP and SULI students recruited under the programs performed research in several ANL divisions other than PHY during the past year. Institutions recently visited include: Clark-Atlanta University; Morehouse; Spelman; North Carolina A&T; North Carolina Central; Hampton; Norfolk State; University of Texas-El Paso; New Mexico State; Lincoln; Howard University; Morgan State; Fisk; and Vanderbilt. Southern University, Xavier University, and Dillard University, all in Louisiana are normally visited annually, but the effects of hurricane Katrina delayed visits until next year. A FAST (Faculty And Student Team) team from Southern-Baton Rouge has worked with the RIA group during the past two summers.

b. Recruitment Efforts at the 2006 Joint Annual Conference of the National Society of Black Physicists and the National Society of Hispanic Physicists (S. M. Fischer, J. Arrington, B. Zeidman, U. Kriplani,* and T. Rodriguez†)

As part of a continuing effort to recruit minority scientists to the laboratory (from undergraduates to those seeking permanent positions), several members of the Physics Division attended the 2006 Joint Annual Conference of the National Society of Black Physicists and the National Society of Hispanic Physicists. The conference was held from February 15-19 in San Jose, California. Argonne has, for many years, been an exhibitor at this conference providing information about internships, post-doctoral appointments, and other research opportunities at the laboratory for minority

students and faculty members. This year, as part of Argonne's diversity outreach effort, several laboratory scientists had the opportunity to work with Human Resources as members of the exhibitor team. This allowed conference attendees to obtain information about laboratory programs both in terms of eligibility and deadlines, and also to discuss some of the specific research done at Argonne and within the Physics Division. John Arrington also presented a talk on "Physics with High Energy Positron Beams."

*Biology Division, Argonne National Laboratory.

†Division of Human Resources, Argonne National Laboratory.

STAFF MEMBERS OF THE PHYSICS DIVISION

Listed below is the staff of the Physics Division for the year ending December 31, 2005.
The program headings indicate only the individual's current primary activity.

SCIENTIFIC STAFF EXPERIMENTAL NUCLEAR PHYSICS STAFF

Regular Staff

- John R. Arrington, Ph.D., California Institute of Technology, 1998
 Birger B. Back, Ph.D., University of Copenhagen, Denmark, 1974
 Michael P. Carpenter, Ph.D., University of Tennessee, 1987
 ‡ Cary N. Davids, Ph.D., California Institute of Technology, 1967
 § Bela Erdelyi, Ph.D., Michigan State University, 2001
 * Susan M. Fischer, Ph.D., University of Notre Dame, 1994
 ¶¶ Donald F. Geesaman, Ph.D., State University of New York-Stony Brook, 1976
 Kawtar Hafidi, Ph.D., University of Paris XI, France, 1999
 †† Walter F. Henning, Ph.D., Technical University of Munich, Germany, 1968
 §§ Roy J. Holt, Ph.D., Yale University, 1972
 ** Robert V. F. Janssens, Ph.D., University Catholique de Louvain, Belgium, 1978
 ¶ Cheng-lie Jiang, Ph.D., China Institute of Atomic Energy, 1960
 Michael P. Kelly, Ph.D., University of Washington, 1999
 Teng Lek Khoo, Ph.D., McMaster University, Canada, 1972
 Torben Lauritsen, Ph.D., State University of New York-Stony Brook, 1990
 ∞ Eliane S. Lessner, Ph.D., Syracuse University, 1975
 Christopher J. Lister, Ph.D., University of Liverpool, United Kingdom, 1977
 ⊕ Zheng-tian Lu, Ph.D., University of California, Berkeley, 1994
 ∞∞ Eugene F. Moore, Ph.D., Florida State University, 1988
 ⌘ Brahim Mustapha, Ph.D., University of Paris XI, France, 1999
 ● Jerry A. Nolen, Jr., Ph.D., Princeton University, 1965
 Petr N. Ostroumov, Ph.D. Moscow Engineering and Physical Institute, Russia, 1982
 Richard C. Pardo, Ph.D., University of Texas, 1976
 David H. Potterveld, Ph.D., California Institute of Technology, 1988
 K. Ernst Rehm, Ph.D., Technical University of Munich, Germany, 1973
 Paul E. Reimer, Ph.D., University of Illinois at Urbana-Champaign, 1996
 ⊕⊕ Guy Savard, Ph.D., McGill University, Canada, 1988
 ⌘ John P. Schiffer, Ph.D., Yale University, 1954
-
- ‡ Adjunct Professor, Vanderbilt University
 § Joint appointment with Northern Illinois University
 * Joint appointment with DePaul University
 ¶¶ Director of the Physics Division
 †† On leave of absence at GSI, Darmstadt
 §§ Adjunct Professor, University of Illinois at Urbana-Champaign
 ** Associate Director of the Physics Division. Adjunct Professor at Michigan State University, Vanderbilt University, and the University of Notre Dame
 ¶ Retired February 2005
 ∞ Terminated September 2005
 ⊕ Professor Coterminous, University of Chicago
 ∞∞ Transferred out of PHY July 2005
 ⌘ Term Appointment
 ● Director of the ATLAS Facility. Adjunct Professor, Michigan State University
 ⊕⊕ Professor Coterminous, University of Chicago and Adjunct Professor, University of Manitoba
 ⌘ Professor Emeritus, University of Chicago

Dariusz Seweryniak, Ph.D., Uppsala University, Sweden, 1994
Kenneth W. Shepard, Ph.D., Stanford University, 1970
Kenneth M. Teh, Ph.D., Vanderbilt University, 1988

Special Appointments

Irshad Ahmad, Ph.D., University of California, 1966
Lowell M. Bollinger, Ph.D., Cornell University, 1951
William J. Childs, Ph.D., University of Michigan, 1956
Donald S. Gemmell, Ph.D., Australian National University, Australia, 1960
Harold E. Jackson, Jr., Ph.D., Cornell University, 1959
* Michael Paul, Ph.D., Hebrew University of Jerusalem, Israel, 1973
† Ben Zeidman, Ph.D., Washington University, 1957

THEORETICAL NUCLEAR PHYSICS STAFF

Regular Staff

Henning Esbensen, Ph.D., University of Århus, Denmark, 1977
Tsung-Shung Harry Lee, Ph.D., University of Pittsburgh, 1973
Kenneth Nollett, Ph.D., University of Chicago, 2000
Steven C. Pieper, Ph.D., University of Illinois at Urbana-Champaign, 1970
Craig D. Roberts, Ph.D., Flinders University of South Australia, Australia, 1989
‡ James W. Truran, Ph.D., Yale University, 1965
Robert B. Wiringa, Ph.D., University of Illinois at Urbana-Champaign, 1978

Special Appointments

Paul Benioff, Ph.D., University of California-Berkeley, 1959
Richard R. Chasman, Ph.D., University of California-Berkeley, 1959
Fritz Coester, Ph.D., University of Zurich, Switzerland, 1944
Mitio Inokuti, Ph.D., University of Tokyo, Japan, 1962
Dieter Kurath, Ph.D., University of Chicago, 1951
Malcolm H. Macfarlane, Ph.D., University of Rochester, 1955
§ Vijay Pandharipande, Ph.D., University of Bombay, India, 1969
Murray Peshkin, Ph.D., Cornell University, 1951

* Special Term Appointee, Hebrew University of Jerusalem, India
† Special Term Appointee, Adjunct Professor, Hampton University
‡ Joint appointment with the University of Chicago
§ Special Term Appointee, University of Illinois at Urbana-Champaign

TEMPORARY APPOINTMENTS

Sebastian Gros (from the University of Liverpool, United Kingdom)

Research at ATLAS
(May 2005 -)

* Jeffrey R. Guest (from the University of Michigan)

Medium-energy physics studies
(August 2004 -)

Arne Hoell (from the University of Rostock, Germany)

Theoretical studies
(October 2003 - September 2005)

Prashanth Jaikumar (from McGill University, Canada)

Theoretical physics studies
(September 2004 -)

§ Peter Mueller (from the Johannes Gutenberg-University, Germany)

Medium-energy physics studies
(July 2004 -)

Donald A. Peterson (from Oregon St. University)

Research at ATLAS
(January 2004 -)

Andrew Robinson (from the University of Edinburgh, United Kingdom)

Research at ATLAS
(May 2005 -)

Elaine C. Schulte (from the University of Illinois at Urbana-Champaign)

Medium-energy physics studies
(February 2002 - January 2005)

Nicholas D. Scielzo (from the University of California-Berkeley)

Medium-energy physics
(July 2003 -)

Nikolai Vinogradov (from the Moscow Engineering Physical Institute, Russia)

ATLAS operation and development
(November 2001 - November 2005)

Hariprakash Sharma (from the University of Manitoba, Canada)

Research at ATLAS
(July 2004 -)

Xiaodong Tang (from Texas A&M University)

Research at ATLAS
(May 2003 -)

* Argonne Scholar – AHCPF (Arthur Holly Compton Postdoctoral Fellowship)

§ Argonne Scholar – WFLPF (Willard Frank Libby Postdoctoral Fellowship)

Stewart V. Wright (from the University of Liverpool, United Kingdom)
Theoretical physics studies
(September 2004 -)

Xiaochao Zheng (from the Massachusetts Institute of Technology)
Medium-energy physics
(January 2003 - December 2005)

Jin Xu (from Brown University)
Research at ATLAS
(August 2005 -)

Shaofei Zhu (from the University of Notre Dame)
Research at ATLAS
(January 2004 -)

TECHNICAL AND ENGINEERING STAFF

(and areas of activity)

Kevin G. Bailey (B.S., University of Nebraska, 1989)
Technical assistance, medium-energy physics

Donald Barnett
ATLAS operations

* John M. Bogaty (A.A.S., DeVry University, 1961)
Electrical systems, ATLAS operation and development

L. Kevin Carlquist (A.S., College of DuPage, 1986)
ATLAS operations

* Benny E. Clift (A.S.E.E., DeVry University, 1959)
Electrical systems, ATLAS operation and development

* Donald Cyborski
Computer operations

Alex Deriy (B.S., University of Illinois-Chicago, 1988)
ATLAS operations

Gregory Devane
ATLAS operations

* Joseph Falout (B.S.M.E., University of Illinois, 1970)
Experimental equipment design

Joel Fuerst (M.S.M.E., Northwestern University, 1990)
Cryogenic development at ATLAS

Scott M. Gerbick (B.S., Purdue University, 2003)
ATLAS experimental equipment maintenance, technical assistance, heavy-ion physics

* Special Term Appointee

John P. Greene (M.S., DePaul University, 1982)
Target preparation

Gerald Gribbon (A.A., DeVry University, 1992)
ATLAS operations

* Ray E. Harden (A.A.S., Milwaukee School of Engineering, 1957)
ATLAS operations

* Dale J. Henderson (B.S., Elmhurst College, 1951)
Detector development, technical assistance, heavy-ion physics

Robert Jenkins
ATLAS operations

Mark Kedzie
ATLAS experimental equipment development

* Raymond B. Kickert
ATLAS experimental equipment maintenance, technical assistance, heavy-ion physics

* David Kurth
Graphic specialist

Anthony Krupa (A.A.S.-E.E.T., Purdue University, 1987)
ATLAS operations

Anthony Levand (B.S.M.E., University of Illinois at Urbana-Champaign, 1986)
Experimental equipment design at ATLAS

Eric Lindert (B.S., University of Wisconsin-Milwaukee, 1992)
ATLAS operations

* Paul Markovich (B.S., Purdue University, 1972)
Surface chemistry, ATLAS development and operation

Thomas P. Mullen (B.S., Marquette University, 1966)
Division ESH/QA engineer

Floyd Munson, Jr. (A.A.S., DeVry University, 1966, B.S. Lewis University, 1993)
Control system for ATLAS

Bruce G. Nardi (A.A.S., Morton Jr. College, 1967; A.A.S. DeVry University, 1969)
Electronics design and maintenance

** Janelle Neubauer (B.S., University of Illinois-Chicago, 2004)
Target preparation

Ilana Percher (B.A., Oberlin College, 2005)
Heavy-ion research at ATLAS

Tom O'Connor (M.S., DePaul University, 1995)
Technical assistance, medium-energy physics

* Special Term Appointee

** Special Term Appointee (terminated July 2005)

Donald Phillips (A.S., DeVry University, 1974)
ATLAS operations

- * John Phillips (M.S., University of Illinois-Chicago, 1986)
Consulting ESH/QA engineer

Maria Power (M.S., Illinois Institute of Technology, 1993)
Technical assistance, ATLAS control system

John Rohrer
Experimental equipment support, heavy-ion physics

Robert Scott (B.S., University of Illinois-Chicago, 1995)
ATLAS operations

Sergey Sharamentov (M.S., Moscow Engineering Physical Institute, Russia, 1976)
Electrical systems, ATLAS operation and development

Brent R. Shumard (B.S., University of Valparaiso, 2002)
Detector development, technical assistance, heavy-ion physics

- * James R. Specht (A.A.S., DeVry University, 1964)
Cryogenics engineer. ATLAS development and operation

Philip Strickhorn (B.S., DeVry University, 1990)
Electrical and technical assistance with ATLAS operations

- ** Cory Stuart (B.S., Lewis University, 2002)
Computer operations

Richard Vondrasek (B.S., University of Chicago, 1990)
ATLAS ECR source

- * Loren Weber (M.S., Northern Illinois University, 1974)
ATLAS operations

Philip R. Wilt (Johnstown Technical School, 1973)
Electronics design and maintenance

Bruce J. Zabransky (M.S., University of Illinois-Chicago, 1973)
Mechanical engineer

Gary P. Zinkann (B.S., DeVry University, 1975)
ATLAS operations supervisor

* Special Term Appointee

** Transferred out of PHY September 1, 2005

ADMINISTRATIVE STAFF

- § Allan Bernstein, M.B.A., Rosary College, 1986
 § James E. Nelson, B.A., University of Illinois-Chicago, 1975
 ** Karen J. Thayer
 † Barbara Fletcher (B.A., DePaul University, 1998)
 Janet Bergman (Administrative Secretary)
 Jeannie Glover (Administrative Secretary)
 †† Jessica Herrera (Secretary)
 Debra Morrison (Administrative Secretary)
 ††† Katherine Peters (Administrative Secretary)
 Elizabeth Rizzo (Administrative Assistant)
 Colleen Tobolic (Administrative Secretary)
 Barbara Weller (Administrative Secretary)

-
- § Assistant Director of the Physics Division
 ** Special Term Appointee (Terminated July 2005)
 † Executive Secretary
 †† Terminated January 2005
 ††† Terminated September 2005

VISITORS AND STUDENTS**Long-Term Visitors** (at Argonne more than 4 months)

Vladislav Asseev (from the Institute for Nuclear Research of the Russian Academy of Sciences, Russia)
 Accelerator development
 (October 2003 -)

* Van D. Bistrow (from the University of Chicago)
 Medium-energy physics
 (July 2005 -)

† Victor Flambaum (from the University of South Wales, Australia)
 Theoretical physics studies
 (August 2005 -)

William Karstens (from Saint Michaels College-Burlington)
 Theoretical physics studies
 (July 2003 -)

Andrei Kolomiets (from the Institute of Theoretical and Experimental Physics, Russia)
 Research at ATLAS
 (April 2004 -)

Andreas Krassnigg (from the University of Graz, Austria)
 Theoretical physics studies
 (January 2003 - January 2005)

-
- * Guest Faculty Research Participant
 † Argonne Fellow

‡ Serban Misicu (from Horia Hulubei National Institute of Physics & Nuclear Engineering, Romania)
Theoretical physics studies
(October 2005 -)

Masahiro Notani (from Michigan State University)
Heavy-ion research at ATLAS
(January 2004 - May 2005)

Iouri Sanjiev (from St. Petersburg Nuclear Physics Institute, Russia)
Medium energy studies
(November 2000 -)

Hariprakash Sharma (from the University of Manitoba, Canada)
Heavy-ion research at ATLAS
(July 2004 -)

Kumar Sharma (from the University of Manitoba, Canada)
Heavy-ion research at ATLAS
(July 2004 - July 2005)

* Eugene Shiles (from the University of Vermont-Burlington)
Theoretical physics studies
(August 2002 -)

* David Smith (from the University of Vermont-Burlington)
Theoretical physics studies
(February 2002 -)

Isao Tanihata (from the Institute of Physical and Chemical Research (RIKEN), Japan)
Heavy-ion research at ATLAS
(March 2004 - September 2005)

Antonio Villari (from GANIL, France)
Heavy-ion research at ATLAS
(August 2004 - August 2005)

Short-Term Visitors (at ANL for less than 4 months at a time)

* Christopher Fasano (from Monmouth College)
Theoretical studies
(February 1999 -)

Shuiming Hu (from the University of Science and Technology, China)
Medium-energy physics
(October 2005 - December 2005)

Leonard Kalinine (from the Russian Institute of High Power Radio Equipment, Russia)
Research at ATLAS
(October 2005 - November 2005)

‡ Fulbright Fellow

* Guest Faculty Research Participant

Rachid Nouicer (from the University of Chicago)
Heavy-ion research at ATLAS
(April 1998 -)

Guillaume Olry (from the Institut de Physique Nucleaire, France)
Research at ATLAS
(July 2005 - September 2005)

* Terrence Resse (from Southern University A&M College)
Research at ATLAS
(May 2005 - August 2005)

* Alan Wuosmaa (from Western Michigan University)
Research at ATLAS
(June 2005 -)

Resident Graduate Students

Jason Clark (from University of Manitoba, Canada)
Heavy-ion research at ATLAS
(May 1999 – June 2005)

Zachary Conway (from University of Illinois at Urbana-Champaign)
Research at ATLAS
(June 2003 -)

Moulay Ahmed El Alaoui (from Mohammed V University, Morocco)
Medium-energy physics
(February 2001 – December 2005)

Mahuya Sengupta (from Michigan State University)
Research at ATLAS
(November 2005 -)

Nidhi Patel (from Colorado School of Mines)
Research at ATLAS
(May 2005 -)

Jason Shergur (from University of Maryland)
Research at ATLAS
(January 2002 – April 2005)

Peter Simko (from Illinois Institute of Technology)
Computer operations
(October 2003 – August 2005)

* Guest Faculty Research Participant

Guest Graduate Students

Hui Dai (from the University of Chicago)
Medium-energy physics
(June 2005 - September 2005)

Lamiaa El Fassi (from Mohammed V University, Morocco)
Medium-energy physics
(September 2003 -)

Jennifer Fallis (from the University of Manitoba, Canada)
Heavy-ion research at ATLAS
(May 2005 - August 2005)

Nathan Hoteling (from the University of Maryland)
Research at ATLAS
(February 2003 -)

Louis Jisonna (from Northwestern University)
Heavy-ion research at ATLAS
(June 2000 -)

Daniel Lascar (from Northwestern University)
Heavy-ion research at ATLAS
(June 2005 - October 2005)

Issam Qattan (from Northwestern University)
Medium-energy physics studies
(September 2001 – November 2005)

Ibrahim Sulai (from the University of Chicago)
Medium-energy physics studies
(June 2005 - September 2005)

Li-Bang Wang (from the University of Illinois at Urbana-Champaign)
Medium-energy studies
(September 2001 - July 2005)

Xiaofeng Wang (from the University of Notre Dame)
Research at ATLAS
(March 2005 - December 2005)

Yuyan Wang (from the University of Manitoba, Canada)
Research at ATLAS
(September 2003 - August 2005)

Undergraduate Students

Michael Bertolli (Colorado School of Mines)
Robyn Brewer (DeVry University)
Joshua Brady (Northern Illinois University)
Andrew Bump (DeVry University)
Maxime Brodeur (University of Montreal, Canada)
Shane Caldwell (DePaul University)
Robert Carrier (St. Xavier University)
Mark Chantell (the University of Chicago)

Jeremy Chapman (Syracuse University)
David Danaher (Monmouth College)
Alan Davila (University of Texas-El Paso)
Mark Durante (North Central College)
Mark Gieras (DeVry University)
Ian Guerassio (Colorado School of Mines)
Chad Huibregtse (Beloit College)
David Kahl (Beloit College)
Michael Kern (DeVry University)
Roman Mongado (DeVry University)
Jared Nance (Beloit College)
Holly Nolan (North Central College)
Peter Probst (University of Illinois-Chicago)
Gregory Puckett (Southern University)
Colas Riviere (Grenoble National Engineering School for Physics, France)
Christopher Rosenthal (Illinois Institute of Technology-Chicago)
Peter Sloan (McGill University, Canada)
Matthew Sternberg (University of Oregon)
Cacey Stevens (Southern University-Baton Rouge)
Gregory Waligorski (DeVry University)

LOW-ENERGY NUCLEAR PHYSICS RESEARCH

Level Structure of ^{22}Mg : Implications for the $^{21}\text{Na}(p,\gamma)^{22}\text{Mg}$ Astrophysical Reaction Rate and for the ^{22}Mg Mass
 D. Seweryniak, P. J. Woods, M. P. Carpenter, T. Davinson, R. V. F. Janssens, D. G. Jenkins, T. Lauritsen, C. J. Lister, C. Ruiz, J. Shergur, S. Sinha, and A. Woehr
 Phys. Rev. Lett. **94**, 032501/1-4 (2005)

Centrality Dependence of Charged Hadron Transverse Momentum Spectra in Au + Au Collisions from $\sqrt{s_{NN}} = 62.4$ to 200 GeV
 B. B. Back *et al.* (PHOBOS Collaboration)
 Phys. Rev. Lett. **94**, 082304/1-4 (2005)

Neutron Spectroscopic Factors in ^9Li from $^2\text{H}(^8\text{Li},p)^9\text{Li}$
 A. H. Wuosmaa, K. E. Rehm, J. P. Greene, D. J. Henderson, R. V. F. Janssens, C. L. Jiang, L. Jisonna, E. F. Moore, R. C. Pardo, M. Paul, D. Peterson, Steven C. Pieper, G. Savard, J. P. Schiffer, R. E. Segel, S. Sinha, X. Tang, and R. B. Wiringa
 Phys. Rev. Lett. **94**, 082502/1-4 (2005)

Stellar (n, γ) Cross Section of ^{62}Ni
 H. Nassar, M. Paul, I. Ahmad, D. Berkovits, M. Bettan, P. Collon, S. Dababneh, S. Ghelberg, J. P. Greene, A. Heger, M. Heil, D. J. Henderson, C. L. Jiang, F. Kappeler, H. Koivisto, S. O'Brien, R. C. Pardo, N. Patronis, T. Pennington, R. Plag, K. E. Rehm, R. Reifarh, R. Scott, S. Sinha, X. Tang, and R. Vondrasek
 Phys. Rev. Lett. **94**, 092504/1-4 (2005)

Publisher's Note: Neutron Spectroscopic Factors in ^9Li from $^2\text{H}(^8\text{Li},p)^9\text{Li}$ [Phys. Rev. Lett. **94**, 082502 (2005)]
 A. H. Wuosmaa, K. E. Rehm, J. P. Greene, D. J. Henderson, R. V. F. Janssens, C. L. Jiang, L. Jisonna, E. F. Moore, R. C. Pardo, M. Paul, D. Peterson, Steven C. Pieper, G. Savard, J. P. Schiffer, R. E. Segel, S. Sinha, X. Tang, and R. B. Wiringa
 Phys. Rev. Lett. **94**, 109904 (2005)

Energy Dependence of Elliptic Flow Over a Large Pseudorapidity Range in Au + Au Collisions at the BNL Relativistic Heavy Ion Collider
 B. B. Back *et al.* (PHOBOS Collaboration)
 Phys. Rev. Lett. **94**, 122303/1-4 (2005)

Structure of the Odd-A, Shell-Stabilized Nucleus $^{253}_{102}\text{No}$
 P. Reiter, T. L. Khoo, I. Ahmad, A. V. Afanasjev, A. Heinz, T. Lauritsen, C. J. Lister, D. Seweryniak, P. Bhattacharyya, P. A. Butler, M. P. Carpenter, A. J. Chewter, J. A. Cizewski, C. N. Davids, J. P. Greene, P. T. Greenlees, K. Helariutta, R.-D. Herzberg, R. V. F. Janssens, G. D. Jones, R. Julin, H. Kankaanpää, H. Kettunen, F. G. Kondev, P. Kuusiniemi, M. Leino, S. Siem, A. A. Sonzogni, J. Uusitalo, and I. Wiedenhöver
 Phys. Rev. Lett. **95**, 032501/1-4 (2005)

Ground State Proton Radioactivity from ^{121}Pr : When Was This Exotic Nuclear Decay Mode First Discovered?
 A. P. Robinson, P. J. Woods, D. Seweryniak, C. N. Davids, M. P. Carpenter, A. A. Hecht, D. Peterson, S. Sinha, W. B. Walters, and S. Zhu
 Phys. Rev. Lett. **95**, 032502/1-4 (2005)

Q Value of the Superallowed Decay of ^{46}V and Its Influence on V_{ud} and the Unitarity of the Cabibbo-Kobayashi-Maskawa Matrix
 G. Savard, F. Buchinger, J. A. Clark, J. E. Crawford, S. Gulick, J. C. Hardy, A. A. Hecht, J. K. P. Lee, A. F. Levand, N. D. Scielzo, H. Sharma, K. S. Sharma, I. Tanihata, A. C. C. Villari, and Y. Wang
 Phys. Rev. Lett. **95**, 102501/1-4 (2005)

High-Spin Isomers and Three-Neutron Valence Configurations in ^{211}Pb

G. J. Lane, K. H. Maier, A. P. Byrne, G. D. Dracoulis, R. Broda, B. Fornal, M. P. Carpenter, R. M. Clark, M. Cromaz, R. V. F. Janssens, A. O. Macchiavelli, I. Wiedenhöver, and K. Vetter
Phys. Lett. **B606**, 34-42 (2005)

Wobbling Excitations in Strongly Deformed Hf Nuclei?

D. J. Hartley, M. K. Djongolov, L. L. Riedinger, G. B. Hagemann, R. V. F. Janssens, F. G. Kondev, E. F. Moore, M. A. Riley, A. Aguilar, C. R. Bingham, D. B. Campbell, M. P. Carpenter, P. Chowdhury, M. Cromaz, D. M. Cullen, M. Danchev, G. D. Dracoulis, P. Fallon, J. Goon, R. A. Kaye, T. L. Khoo, R. W. Laird, T. Lauritsen, A. O. Macchiavelli, B. McClain, G. Mukherjee, E. Ngijoi-Yogo, H. I. Park, G. Sletten, S. K. Tandel, P. M. Walker, and Jing-Ye Zhang
Phys. Lett. **B608**, 31-38 (2005)

Strength of Octupole Correlations in the Actinides: Contrasting Behavior in the Isotones ^{237}U and ^{239}Pu

S. Zhu, R. V. F. Janssens, G. J. Lanes, I. Wiedenhöver, M. P. Carpenter, I. Ahmad, A. P. Byrne, P. Chowdhury, D. Cline, A. N. Deacon, G. D. Dracoulis, S. J. Freeman, N. J. Hammond, G. D. Jones, T. L. Khoo, F. G. Kondev, T. Lauritsen, C. J. Lister, A. O. Macchiavelli, E. F. Moore, D. Seweryniak, J. F. Smith, and C. Y. Wu
Phys. Lett. **B618**, 51-59 (2005)

Changes in $\nu g_{9/2}$ Shape Polarisation Across the Odd Neutron-Rich Cr Isotopes

A. N. Deacon, S. J. Freeman, R. V. F. Janssens, F. R. Xu, M. P. Carpenter, I. R. Calderin, P. Chowdhury, N. J. Hammond, T. Lauritsen, C. J. Lister, D. Seweryniak, J. F. Smith, S. L. Tabor, B. J. Varley, and S. Zhu
Phys. Lett. **B622**, 151-158 (2005)

First Observation of Very Neutron-Deficient ^{122}Ce

J. F. Smith, C. J. Chiara, M. P. Carpenter, H. J. Chantler, P. T. W. Choy, C. N. Davids, M. Devlin, J. L. Durell, D. B. Fossan, S. J. Freeman, R. V. F. Janssens, N. S. Kelsall, T. Koike, D. R. LaFosse, E. S. Paul, P. Reiter, D. G. Sarantites, D. Seweryniak, K. Starosta, R. Wadsworth, A. N. Wilson, and P.-H. Heenen
Phys. Lett. **B625**, 203-211 (2005)

Erratum to: "Changes in $\nu g_{9/2}$ Shape Polarisation Across the Odd-Neutron-Rich Cr Isotopes" [Phys. Lett. B **622** (2005) 151]

A. N. Deacon, S. J. Freeman, R. V. F. Janssens, F. R. Xu, M. P. Carpenter, I. R. Calderin, P. Chowdhury, N. J. Hammond, T. Lauritsen, C. J. Lister, D. Seweryniak, J. F. Smith, S. L. Tabor, B. J. Varley, and S. Zhu
Phys. Lett. **B625**, 375 (2005)

Doorway States as a Principal Decay Pathway in $^{12}\text{C}(^{12}\text{C},\gamma)$ Radiative Capture

D. G. Jenkins, B. R. Fulton, J. Pearson, C. J. Lister, M. P. Carpenter, S. J. Freeman, N. J. Hammond, R. V. F. Janssens, T. L. Khoo, T. Lauritsen, A. H. Wuosmaa, P. Fallon, A. Gørgen, A. O. Macchiavelli, M. McMahan, M. Freer, and F. Haas
Phys. Rev. C **71**, 041301(R)/1-5 (2005)

Reduced Transition Probabilities to the First 2^+ State in $^{52,54,56}\text{Ti}$ and Development of Shell Closures at $N = 32, 34$

D.-C. Dinca, R. V. F. Janssens, A. Gade, D. Bazin, R. Broda, B. A. Brown, C. M. Campbell, M. P. Carpenter, P. Chowdhury, J. M. Cook, A. N. Deacon, B. Fornal, S. J. Freeman, T. Glasmacher, M. Honma, F. G. Kondev, J.-L. Lecouey, S. N. Liddick, P. F. Mantica, W. F. Mueller, H. Olliver, T. Otsuka, J. R. Terry, B. A. Tomlin, and K. Yoneda
Phys. Rev. C **71**, 041302(R)/1-4 (2005)

Search for X-Ray Induced Decay of the 31-Yr Isomer of ^{178}Hf Using Synchrotron Radiation

I. Ahmad, J. C. Banar, J. A. Becker, T. A. Bredeweg, J. R. Cooper, D. S. Gemmell, A. Kraemer, A. Mashayekhi, D. P. McNabb, G. G. Miller, E. F. Moore, P. Palmer, L. N. Pangault, R. S. Rundberg, J. P. Schiffer, S. D. Shastri, T.-F. Wang, and J. B. Wilhelmy
Phys. Rev. C **71**, 024311/1-16 (2005)

Structure of Two-, Four-, and Six-Quasiparticle Isomers in ^{174}Yb and K -Forbidden Decays

G. D. Dracoulis, G. J. Lane, F. G. Kondev, A. P. Byrne, T. Kibédi, H. Watanabe, I. Ahmad, M. P. Carpenter, S. J. Freeman, R. V. F. Janssens, N. J. Hammond, T. Lauritsen, C. J. Lister, G. Mukherjee, D. Seweryniak, P. Chowdhury, and S. K. Tandel
 Phys. Rev. C **71**, 044326/1-15 (2005)

Hindrance of Heavy-Ion Fusion at Extreme Sub-Barrier Energies in Open-Shell Colliding Systems

C. L. Jiang, K. E. Rehm, H. Esbensen, R. V. F. Janssens, B. B. Back, C. N. Davids, J. P. Greene, D. J. Henderson, C. J. Lister, R. C. Pardo, T. Pennington, D. Peterson, D. Seweryniak, B. Shumard, S. Sinha, X. D. Tang, I. Tanihata, S. Zhu, P. Collon, S. Kurtz, and M. Paul
 Phys. Rev. C **71**, 044613/1-9 (2005)

Spherical and Deformed Structures in ^{189}Pb

A. M. Baxter, A. P. Byrne, G. D. Dracoulis, P. M. Davidson, T. Kibédi, R. V. F. Janssens, M. P. Carpenter, C. N. Davids, T. L. Khoo, and T. Lauritsen
 Phys. Rev. C **71**, 054302/1-11 (2005)

Energy Levels of ^{249}Bk Populated in the α Decay of $^{253}_{99}\text{Es}$ and β^- Decay of $^{249}_{96}\text{Cm}$

I. Ahmad, F. G. Kondev, E. F. Moore, M. P. Carpenter, R. R. Chasman, J. P. Greene, R. V. F. Janssens, T. Lauritsen, C. J. Lister, D. Seweryniak, R. W. Hoff, J. E. Evans, R. W. Lougheed, C. E. Porter, and L. K. Felker
 Phys. Rev. C **71**, 054305/1-16 (2005)

Multiparticle Configurations in $N = 84$ Isotones Located at the Proton Drip Line

D. Seweryniak, J. Uusitalo, P. Bhattacharyya, M. P. Carpenter, J. A. Cizewski, K. Y. Ding, C. N. Davids, N. Fotiadis, R. V. F. Janssens, T. Lauritsen, C. J. Lister, A. O. Macchiavelli, D. Nisius, P. Reiter, W. B. Walters, and P. J. Woods
 Phys. Rev. C **71**, 054319/1-9 (2005)

Level Structure of Odd-Odd ^{134}Sb Populated in the β^- Decays of $^{134,135}\text{Sn}$

J. Shergur, A. Wöhr, W. B. Walters, K.-L. Kratz, O. Arndt, B. A. Brown, J. Cederkall, I. Dillmann, L. M. Fraile, P. Hoff, A. Joinet, U. Köster, and B. Pfeiffer
 Phys. Rev. C **71**, 064321/1-9 (2005)

Identification of Low-Spin States in ^{111}Sb : Test of Spin-Orbit Coupling in Light Nuclei

J. Shergur, D. J. Dean, D. Seweryniak, W. B. Walters, A. Wöhr, P. Boutachkov, C. N. Davids, I. Dillmann, A. Juodagalvis, G. Mukherjee, S. Sinha, A. Teymurazyan, and I. Zartova
 Phys. Rev. C **71**, 064323/1-8 (2005)

Mirror Energy Differences in the $A = 31$ Mirror Nuclei, ^{31}S and ^{31}P , and Their Significance in Electromagnetic Spin-Orbit Splitting

D. G. Jenkins, C. J. Lister, M. P. Carpenter, P. Chowdhury, N. J. Hammond, R. V. F. Janssens, T. L. Khoo, T. Lauritsen, D. Seweryniak, T. Davinson, P. J. Woods, A. Jokinen, and H. Penttila
 Phys. Rev. C **72**, 031303(R)/1-5 (2005)

Scaling of Charged Particle Production in $d + \text{Au}$ Collisions at $\sqrt{s_{NN}} = 200$ GeV

B. B. Back *et al.* (PHOBOS Collaboration)
 Phys. Rev. C **72**, 031901(R)/1-5 (2005)

Centrality and Pseudorapidity Dependence of Elliptic Flow for Charged Hadrons in Au + Au Collisions at $\sqrt{s_{NN}} = 200$ GeV

B. B. Back *et al.* (PHOBOS Collaboration)
 Phys. Rev. C **72**, 051901 (R)/1-5 (2005)

Search for Excited States in ^7He with the (d,p) Reaction

A. H. Wuosmaa, K. E. Rehm, J. P. Greene, D. J. Henderson, R. V. F. Janssens, C. L. Jiang, L. Jisonna, E. F. Moore, R. C. Pardo, M. Paul, D. Peterson, Steven C. Pieper, G. Savard, J. P. Schiffer, R. E. Segel, S. Sinha, X. Tang, and R. B. Wiringa
Phys. Rev. C **72**, 061301(R)/1-5 (2005)

Investigation of High-Spin States in ^{53}Fe

R. du Rietz, S. J. Williams, D. Rudolph, J. Ekman, C. Fahlander, C. Andreoiu, M. Axiotis, M. A. Bentley, M. P. Carpenter, C. Chandler, R. J. Charity, R. M. Clark, M. Cromaz, A. Dewald, G. de Angelis, F. Della Vedova, P. Fallon, A. Gadea, G. Hammond, E. Ideguchi, S. M. Lenzi, A. O. Macchiavelli, N. Märginean, M. N. Mineva, O. Möller, D. R. Napoli, W. Reviol, C. Rusu, B. Saha, D. G. Sarantites, D. Seweryniak, D. Tonev, and C. A. Ur
Phys. Rev. C **72**, 014307/1-10 (2005)

Attempt to Confirm Superheavy Element Production in the $^{48}\text{Ca} + ^{238}\text{U}$ Reaction

K. E. Gregorich, W. Loveland, D. Peterson, P. M. Zielinski, S. L. Nelson, Y. H. Chung, Ch. E. Düllmann, C. M. Folden III, K. Aleklett, R. Eichler, D. C. Hoffman, J. P. Omtvedt, G. K. Pang, J. M. Schwantes, S. Sovarna, P. Sprunger, R. Sudowe, R. E. Wilson, and H. Nitsche
Phys. Rev. C **72**, 014605/1-7 (2005)

Identification of Shell-Model States in ^{135}Sb Populated via β^- Decay of ^{135}Sn

J. Shergur, A. Wöhr, W. B. Walters, K.-L. Kratz, O. Arndt, B. A. Brown, J. Cederkall, I. Dillmann, L. M. Fraile, P. Hoff, A. Joinet, U. Köster, and B. Pfeiffer
Phys. Rev. C **72**, 024305/1-9 (2005)

Shape Coexistence in ^{71}Br and the Question of the Ground-State Spin of ^{71}Kr

S. M. Fischer, T. Anderson, P. Kerns, G. Mesoloras, D. Svelnys, C. J. Lister, D. P. Balamuth, P. A. Hausladen, and D. G. Sarantites
Phys. Rev. C **72**, 024321/1-16 (2005)

Near-Yrast, Medium-Spin Structure of the ^{107}Mo Nucleus

W. Urban, T. Rzaca-Urban, J. A. Pinston, J. L. Durell, W. R. Phillips, A. G. Smith, B. J. Varley, I. Ahmad, and N. Schulz
Phys. Rev. C **72**, 027302/1-4 (2005)

Yrast Structure of Neutron-Rich ^{53}Ti

B. Fornal, S. Zhu, R. V. F. Janssens, M. Honma, R. Broda, B. A. Brown, M. P. Carpenter, S. J. Freeman, N. Hammond, F. G. Kondev, W. Królas, T. Lauritsen, S. N. Liddick, C. J. Lister, S. Lunardi, P. F. Mantica, N. Marginean, T. Mizusaki, E. F. Moore, T. Otsuka, T. Pawlat, D. Seweryniak, B. E. Tomlin, C. A. Ur, I. Wiedenhöver, and J. Wrzesiński
Phys. Rev. C **72**, 044315/1-8 (2005)

Energy Levels of ^{251}Cf Populated in the α Decay of $^{255}_{100}\text{Fm}$ and EC Decay of $^{251}_{99}\text{Es}$

I. Ahmad, J. P. Greene, E. F. Moore, F. G. Kondev, R. R. Chasman, C. E. Porter, and L. K. Felker
Phys. Rev. C **72**, 054308/1-11 (2005)

Measurement of $E2$ Transition Strengths in $^{32,34}\text{Mg}$

J. A. Church, C. M. Campbell, D.-C. Dinca, J. Enders, A. Gade, T. Glasmacher, Z. Hu, R. V. F. Janssens, W. F. Mueller, H. Olliver, B. C. Perry, L. A. Riley, and K. L. Yurkewicz
Phys. Rev. C **72**, 054320/1-6 (2005)

β -Decay of Odd-A ^{57}Ti and ^{59}V

S. N. Liddick, P. F. Mantica, R. Broda, B. A. Brown, M. P. Carpenter, A. D. Davies, B. Fornal, M. Horoi, R. V. F. Janssens, A. C. Morton, W. F. Mueller, J. Pavan, H. Schatz, A. Stolz, S. L. Tabor, B. E. Tomlin, and M. Wiedeking
Phys. Rev. C **72**, 054321/1-9 (2005)

Structural Behavior of $^{157,158,159}\text{Dy}$ in the $I = 30\text{-}50 \hbar$ Spin Regime

A. Pipidis, M. A. Riley, J. Simpson, R. V. F. Janssens, F. G. Kondev, D. E. Appelbe, A. P. Bagshaw, M. A. Bentley, T. B. Brown, M. P. Carpenter, D. M. Cullen, D. B. Campbell, P. J. Dagnall, P. Fallon, S. M. Fischer, G. B. Hagemann, D. J. Hartley, K. Lagergren, R. W. Laird, T. Lauritsen, J. C. Lisle, D. Nisius, S. L. Shepard, A. G. Smith, S. Törmänen, and I. Ragnarsson
Phys. Rev. C **72**, 064307/1-11 (2005)

Detailed High-Spin Spectroscopy and the Search for the Wobbling Mode in ^{171}Ta

D. J. Hartley, W. H. Mohr, J. R. Vanhoy, M. A. Riley, A. Aguilar, C. Teal, R. V. F. Janssens, M. P. Carpenter, A. A. Hecht, T. Lauritsen, E. F. Moore, S. Zhu, F. G. Kondev, M. K. Djongolov, M. Danchev, L. L. Riedinger, G. B. Hagemann, G. Sletten, P. Chowdhury, S. K. Tandel, W. C. Ma, and S. W. Ødegård
Phys. Rev. C **72**, 064325/1-16 (2005)

Consequences of Energy Conservation in Relativistic Heavy-Ion Collisions

B. B. Back
Phys. Rev. C **72**, 064906/1-8 (2005)

Temperature and Spin Dependence of the Giant Dipole Resonance Width

P. Heckman, B. B. Back, T. Baumann, M. P. Carpenter, I. Diószegi, D. J. Hofman, T. L. Khoo, S. Mitsuoka, V. Nanal, T. Pennington, J. P. Seitz, M. Thoennessen, E. Tryggestad, and R. L. Varner
Nucl. Phys. **A750**, 175-184 (2005)

Observation of the Hot GDR in Neutron-Deficient Thorium Evaporation Residues

J. P. Seitz, B. B. Back, M. P. Carpenter, I. Diószegi, K. Eisenman, P. Heckman, D. J. Hofman, M. P. Kelly, T. L. Khoo, S. Mitsuoka, V. Nanal, T. Pennington, R. H. Siemssen, M. Thoennessen, and R. L. Varner
Nucl. Phys. **A750**, 245-255 (2005)

The PHOBOS Perspective on Discoveries at RHIC

B. B. Back *et al.* (PHOBOS Collaboration)
Nucl. Phys. **A757**, 28-101 (2005)

EMMA: A Recoil Mass Spectrometer for ISAC-II at TRIUMF

Barry Davids and Cary N. Davids
Nucl. Instrum. Methods **A544**, 565-576 (2005)

Ambiguity of Gamma-Ray Tracking of "Two-Interaction" Events

N. J. Hammond, T. Duguet, and C. J. Lister
Nucl. Instrum. Methods **A547**, 535-540 (2005)

A New Focal-Plane Detector System for Low Fusion-Evaporation Cross Section Measurements

C. L. Jiang, D. J. Henderson, D. Seweryniak, I. Tanihata, K. E. Rehm, C. N. Davids, D. Peterson, B. B. Back, P. Collon, J. P. Greene, R. V. F. Janssens, S. Kurtz, C. J. Lister, R. C. Pardo, M. Paul, T. O. Pennington, B. Shumard, S. Sinha, X. D. Tang, and S. Zhu
Nucl. Instrum. Methods **A554**, 500-513 (2005)

First Observation of Excited States in the ^{111}Tc Nucleus - A New Region of Deformation at $40 \leq Z \leq 46$, $N \geq 68$?

W. Urban, T. Rzaca-Urban, J. L. Durell, A. G. Smith, and I. Ahmad
Eur. Phys. J. A **24**, 161-165 (2005)

Nuclear Physics: Elusive Magic Numbers

Robert V. F. Janssens

Nature **435**, 897-898 (2005)

Alpha Decay

I. Ahmad

Chapter in *Encyclopedia of Physics*, 3rd Edition, eds. Rita G. Lerner and George L. Trigg (Wiley-VCH Verlag GmbH & Co. KGaA, Weinheim 2005) pp. 67-70

Gamma-Ray Spectrometers

M. P. Carpenter and R. V. F. Janssens

Chapter in *Encyclopedia of Physics*, 3rd Edition, eds. Rita G. Lerner and George L. Trigg (Wiley-VCH Verlag GmbH & Co. KGaA, Weinheim 2005) pp. 875-877

Nuclear Structure at the Limits: Continued Exploration with Gammasphere

R. V. F. Janssens

Proceedings of the 22nd International Nuclear Conference (INPC2004), Göteborg, Sweden, June 27-July 2, 2004; Nucl. Phys. **A751**, 244c-247c (2005)

Study of Stellar Reactions in Explosive Hydrogen Burning with CRIB

S. Kubono *et al.*Proceedings of the 8th International Symposium on Nuclei in the Cosmos (NIC8), Vancouver, BC, July 19-23, 2004; Nucl. Phys. **A758**, 733c-736c (2005)Reevaluation of the $^{22}\text{Na}(p,\gamma)$ Reaction Rate

D. G. Jenkins, B. R. Fulton, C. J. Lister, R. V. F. Janssens, T. L. Khoo, E. F. Moore, K. E. Rehm, B. Truett, A. H. Wuosmaa, M. Freer, and J. José

Proceedings of the 8th International Symposium on Nuclei in the Cosmos (NIC8), Vancouver, BC, July 19-23, 2004; Nucl. Phys. **A758**, 749c-752c (2005)Atomic Mass Ratios for Some Stable Isotopes of Platinum Relative to ^{197}Au

K. S. Sharma, J. Vaz, R. C. Barber, F. Buchinger, J. A. Clark, J. E. Crawford, H. Fukutani, J. P. Greene, S. Gulick, A. Heinz, J. K. P. Lee, G. Savard, Z. Zhou, and J. C. Wang

Proceedings of the 4th International Conference on Exotic Nuclei and Atomic Masses (ENAM'04), Pine Mountain, GA, September 12-16, 2004; Eur. Phys. J. A **25**, 45-46 (2005)Behavior of Intruder Based States in Light Bi and Tl Isotopes: the Study of ^{187}Bi α Decay

J. C. Batchelder, K. S. Toth, C. R. Bingham, L. T. Brown, L. F. Conticchio, C. N. Davids, R. J. Irvine, D. Seweryniak, W. B. Walters, J. Wauters, E. F. Zganjar, J. L. Wood, C. DeCoster, B. Decroix, and K. Heyde

Proceedings of the 4th International Conference on Exotic Nuclei and Atomic Masses (ENAM'04), Pine Mountain, GA, September 12-16, 2004; Eur. Phys. J. A **25**, 49-52 (2005)New Level Information on $Z = 51$ Isotopes, $^{111}\text{Sb}_{60}$ and $^{134,135}\text{Sb}_{83,34}$

J. Shergur, N. Hoteling, A. Wöhr, W. B. Walters, O. Arndt, B. A. Brown, C. N. Davids, D. J. Dean, K.-L. Kratz, B. Pfeiffer, D. Seweryniak, and the ISOLDE Collaboration

Proceedings of the 4th International Conference on Exotic Nuclei and Atomic Masses (ENAM'04), Pine Mountain, GA, September 12-16, 2004; Eur. Phys. J. A **25**, 121-122 (2005)Recoil Decay Tagging Study of ^{146}Tm

A. P. Robinson, C. N. Davids, D. Seweryniak, P. J. Woods, B. Blank, M. P. Carpenter, T. Davinson, S. J. Freeman, N. Hammond, N. Hoteling, R. V. F. Janssens, T. L. Khoo, Z. Liu, G. Mukherjee, C. Scholey, J. Shergur, S. Sinha, A. A. Sonzogni, W. B. Walters, and A. Woehr

Proceedings of the 4th International Conference on Exotic Nuclei and Atomic Masses (ENAM'04), Pine Mountain, GA, September 12-16, 2004; Eur. Phys. J. A **25**, 155-157 (2005)

Particle-Core Coupling in the Transitional Proton Emitters ^{145,146,147}Tm

D. Seweryniak, C. N. Davids, A. Robinson, P. J. Woods, B. Blank, M. P. Carpenter, T. Davinson, S. J. Freeman, N. Hammond, N. Hoteling, R. V. F. Janssens, T. L. Khoo, Z. Liu, G. Mukherjee, J. Shergur, S. Sinha, A. A. Sonzogni, W. B. Walters, and A. Woehr

Proceedings of the 4th International Conference on Exotic Nuclei and Atomic Masses (ENAM'04), Pine Mountain, GA, September 12-16, 2004; *Eur. Phys. J. A* **25**, 159-160 (2005)

Nuclear Pairing and Coriolis Effects in Proton Emitters

Alexander Volya and Cary Davids

Proceedings of the 4th International Conference on Exotic Nuclei and Atomic Masses (ENAM'04), Pine Mountain, CA, September 12-16, 2004; *Eur. Phys. J. A* **25**, 161-163 (2005)

Investigating the rp-Process with the Canadian Penning Trap Mass Spectrometer

J. A. Clark, R. C. Barber, B. Blank, C. Boudreau, F. Buchinger, J. E. Crawford, J. P. Greene, S. Gulick, J. C. Hardy, A. A. Hecht, A. Heinz, J. K. P. Lee, A. F. Levand, B. F. Lundgren, R. B. Moore, G. Savard, N. D. Scielzo, D. Seweryniak, K. S. Sharma, G. D. Sprouse, W. Trimble, J. Vaz, J. C. Wang, Y. Wang, B. J. Zabransky, and Z. Zhou

Proceedings of the 4th International Conference on Exotic Nuclei and Atomic Masses (ENAM'04), Pine Mountain, GA, September 12-16, 2004; *Eur. Phys. J. A* **25**, 629-632 (2005)

Ion Manipulation with Cooled and Bunched Beams

G. Savard

Proceedings of the 4th International Conference on Exotic Nuclei and Atomic Masses (ENAM'04), Pine Mountain, GA, September 12-16, 2004; *Eur. Phys. J. A* **25**, 713-718 (2005)

Ultra-Relativistic Au + Au and d + Au Collisions: Experimental Studies by PHOBOS

B. B. Back for the PHOBOS Collaboration

Proceedings of the 8th Workshop on Non-Perturbative Chromodynamics, Paris, France, June 7-11, 2004; *Int. J. Mod. Phys. A* **20**, 4405-4411 (2005)

Elliptic Flow in Au + Au Collisions at RHIC

Carla M. Vale (for the PHOBOS Collaboration)

Proceedings of the Workshop for Young Scientists on the Physics of Ultra-Relativistic Nucleus-Nucleus Collisions (Hot Quarks 2004), Taos Valley, NM, July 18-24, 2004; *J. Phys. G* **31**, S41-S47 (2005)

The Magnetic Properties of Collective States in $A \sim 100$ Fission Fragments

A. G. Smith, R. Orlandi, D. Patel, G. S. Simpson, R. M. Wall, J. F. Smith, O. J. Onakanmi, I. Ahmad, J. P. Greene, M. P. Carpenter, T. Lauritsen, C. J. Lister, R. V. F. Janssens, F. G. Kondev, D. Seweryniak, B. J. P. Gall, O. Dorvaux, and B. Roux

Proceedings of the International Conference on the Interface Between Nuclear Structure, Astrophysics and Reactions (NUSTAR'05), Guildford, England, January 5-8, 2005; *J. Phys. G* **31**, S1433-S1438 (2005)

Structure of the Neutron-Rich Cr Isotopes

S. J. Freeman, R. V. F. Janssens, A. N. Deacon, F. Xu, I. V. Calderin, M. P. Carpenter, P. Chowdhury, S. M. Fischer, N. J. Hammond, M. Honma, T. Lauritsen, C. J. Lister, T. L. Khoo, G. Mukherjee, D. Seweryniak, J. F. Smith, S. L. Tabor, B. J. Varley, and S. Zhu

Proceedings of the International Conference on the Interface Between Nuclear Structure, Astrophysics and Reactions (NUSTAR'05), Guildford, England, January 5-8, 2005; *J. Phys. G* **31**, S1465-S1470 (2005)

Proton Decay: Spectroscopic Probe Beyond the Proton Drip Line

D. Seweryniak, C. N. Davids, A. Robinson, P. J. Woods, B. Blank, M. P. Carpenter, T. Davinson, S. J. Freeman, N. Hammond, N. Hoteling, R. V. F. Janssens, T. L. Khoo, Z. Liu, G. Mukherjee, J. Shergur, S. Sinha, A. A. Sonzogni, W. B. Walters, and A. Woehr

Proceedings of the International Conference on the Interface Between Nuclear Structure, Astrophysics and Reactions (NUSTAR'05), Guildford, England, January 5-8, 2005; *J. Phys. G* **31**, S1503-S1508 (2005)

Studies of Neutron-Deficient Nuclei Near the $Z = 82$ Shell Closure via Cold Fusion Reactions

Michael P. Carpenter, Filip G. Kondev, and Robert V. F. Janssens

Proceedings of the International Conference on the Interface Between Nuclear Structure, Astrophysics and Reactions (NUSTAR'05), Guildford, England, January 5-8, 2005; *J. Phys. G* **31**, S1599-S1604 (2005)

Beyond Band Termination in ^{157}Er and the Search for Wobbling Excitations in Strongly Deformed ^{174}Hf

M. A. Riley, M. K. Djongolov, A. O. Evans, D. J. Hartley, R. V. F. Janssens, E. S. Paul, J. Simpson, A. A. Aguilar, D. E. Appelbe, C. R. Bingham, D. B. Campbell, M. P. Carpenter, P. Chowdhury, P. T. W. Choy, R. M. Clark, M. Cromaz, D. M. Cullen, M. Danchev, G. D. Dracoulis, P. Fallon, A. Görgen, G. B. Hagemann, D. T. Joss, J. Goon, R. A. Kaye, T. L. Khoo, F. G. Kondev, R. W. Laird, K. Lagergren, T. Lauritsen, A. O. Macchiavelli, B. McClain, E. F. Moore, G. Mukherjee, E. Ngijoi-Yogo, P. J. Nolan, H. I. Park, A. Pipidis, L. L. Riedinger, G. Sletten, S. K. Tandel, P. M. Walker, D. Ward, I. Ragnarsson, F. Sarić, and Jing-ye Zhang
Proceedings of the International Conference on the Interface Between Nuclear Structure, Astrophysics and Reactions (NUSTAR'05), Guildford, England, January 5-8, 2005; *J. Phys. G* **31**, S1735-S1740 (2005)

Quadrupole Moment Measurements of TSD1 and TSD2 Bands in ^{167}Lu

G. Gürdal, H. Amro, C. W. Beausang, D. S. Brenner, M. P. Carpenter, R. F. Casten, C. Engelhardt, G. B. Hagemann, C. R. Hansen, D. J. Hartley, B. Herskind, H. Hübel, T. L. Khoo, T. Lauritsen, W. C. Ma, D. A. Meyer, E. F. Moore, A. Neusser, P. Bringel, D. G. Roux, G. Sletten, R. B. Yadav, and Y. Zhang
Proceedings of the International Conference on the Interface Between Nuclear Structure, Astrophysics and Reactions (NUSTAR'05), Guildford, England, January 5-8, 2005; *J. Phys. G* **31**, S1873-S1876 (2005)

Structure of Multi-Quasiparticle Isomers in the Region of ^{177}Lu

G. D. Dracoulis, F. G. Kondev, G. J. Lane, A. P. Byrne, T. Kibédi, I. Ahmad, M. P. Carpenter, S. J. Freeman, R. V. F. Janssens, N. J. Hammond, T. Lauritsen, C. J. Lister, D. Seweryniak, G. Mukherjee, P. Chowdhury, and S. K. Tandel
Proceedings of the Conference on "Nuclei at the Limits", Argonne, IL, July 26-30, 2004, eds. Dariusz Seweryniak and Teng Lek Khoo, AIP Conference Proceedings **764**, 3-8 (2005)

Search for Wobbling Excitations in Hf Nuclei: Are the SD Bands Triaxial?

D. J. Hartley, M. K. Djongolov, L. L. Riedinger, G. B. Hagemann, R. V. F. Janssens, F. G. Kondev, E. F. Moore, M. A. Riley, A. A. Aguilar, C. R. Bingham, D. B. Campbell, M. P. Carpenter, P. Chowdhury, M. Cromaz, D. M. Cullen, M. Danchev, G. D. Dracoulis, P. Fallon, J. Goon, R. A. Kaye, T. L. Khoo, R. W. Laird, T. Lauritsen, A. O. Macchiavelli, B. McClain, G. Mukherjee, E. Ngijoi-Yogo, H. I. Park, G. Sletten, S. K. Tandel, P. M. Walker, and Jing-ye Zhang
Proceedings of the Conference on "Nuclei at the Limits", Argonne, IL, July 26-30, 2004, eds. Dariusz Seweryniak and Teng Lek Khoo, AIP Conference Proceedings **764**, 15-20 (2005)

Decay-Out of Superdeformed Bands by Coupling to Ordered or Chaotic Spectra

T. Døssing, A. P. Lopez-Martens, T. L. Khoo, T. Lauritsen, and S. Åberg
Proceedings of the Conference on "Nuclei at the Limits", Argonne, IL, July 26-30, 2004, eds. Dariusz Seweryniak and Teng Lek Khoo, AIP Conference Proceedings **764**, 27-33 (2005)

Rotational Damping, Ridges and the Quasi-Continuum of γ Rays in ^{152}Dy

T. Lauritsen, R. V. F. Janssens, T. L. Khoo, I. Ahmad, M. P. Carpenter, A. M. Heinz, D. G. Jenkins, F. G. Kondev, C. J. Lister, E. F. Moore, D. Seweryniak, S. Zhu, T. Døssing, B. Herskind, R. M. Clark, M. Cromaz, P. Fallon, G. Lane, A. O. Macchiavelli, D. Ward, A. Korichi, A. Lopez-Martens, and A. J. Larabee
Proceedings of the Conference on "Nuclei at the Limits", Argonne, IL, July 26-30, 2004, eds. Dariusz Seweryniak and Teng Lek Khoo, AIP Conference Proceedings **764**, 34-39 (2005)

Search for Hyperdeformation in Xe Nuclei

C. Rønn Hansen, G. B. Hagemann, B. Herskind, D. R. Jensen, G. Sletten, J. N. Wilson, S. Ødegård, P. Bringel, C. Engelhardt, H. Hübel, A. Neusser, A. K. Singh, G. Benzoni, A. Bracco, F. Camera, S. Leoni, A. Maj, Th. Byrski, D. Curien, P. Bednarczyk, A. Korichi, J. Roccoz, J. C. Lisle, T. Steinhardt, O. Thelen, M. P. Carpenter, R. V. F. Janssens, T. L. Khoo, T. Lauritsen, R. M. Clark, and P. Fallon
Proceedings of the Conference on “Nuclei at the Limits”, Argonne, IL, July 26-30, 2004, eds. Dariusz Seweryniak and Teng Lek Khoo, AIP Conference Proceedings **764**, 46-51 (2005)

Spherical and Deformed Structures in ^{189}Pb

A. M. Baxter, G. D. Dracoulis, A. P. Byrne, T. Kibédi, P. M. Davidson, R. V. F. Janssens, M. P. Carpenter, C. N. Davids, T. L. Khoo, and T. Lauritsen
Proceedings of the Conference on “Nuclei at the Limits”, Argonne, IL, July 26-30, 2004, eds. Dariusz Seweryniak and Teng Lek Khoo, AIP Conference Proceedings **764**, 62-67 (2005)

Neutron-Rich Ti Isotopes and Possible $N = 32$ and $N = 34$ Shell Gaps

D.-C. Dinca, R. V. F. Janssens, A. Gade, B. Fornal, S. Zhu, D. Bazin, R. Broda, C. M. Campbell, M. P. Carpenter, P. Chowdhury, J. M. Cook, P. J. Daly, A. N. Deacon, S. J. Freeman, T. Glasmacher, Z. W. Grabowski, N. J. Hammond, F. G. Kondev, W. Krolas, T. Lauritsen, J.-L. Lecouey, S. N. Liddick, C. J. Lister, P. F. Mantica, E. F. Moore, W. F. Mueller, H. Olliver, T. Pawlat, D. Seweryniak, K. Starosta, J. R. Terry, B. E. Tomlin, J. Wrzesinski, and K. Yoneda
Proceedings of the Conference on “Nuclei at the Limits”, Argonne, IL, July 26-30, 2004, eds. Dariusz Seweryniak and Teng Lek Khoo, AIP Conference Proceedings **764**, 131-135 (2005)

Structure of the Neutron-Rich Cr Isotopes: Inadequacy of the fp Model Space and Onset of Deformation

S. J. Freeman, R. V. F. Janssens, B. A. Brown, I. V. Calderin, M. P. Carpenter, P. Chowdhury, A. N. Deacon, S. M. Fischer, N. J. Hammond, M. Honma, T. Lauritsen, C. J. Lister, T. L. Khoo, G. Mukherjee, D. Seweryniak, J. F. Smith, S. L. Tabor, B. J. Varley, M. Whitehead, and S. Zhu
Proceedings of the Conference on “Nuclei at the Limits”, Argonne, IL, July 26-30, 2004, eds. Dariusz Seweryniak and Teng Lek Khoo, AIP Conference Proceedings **764**, 142-147 (2005)

First Observation of Excited States in the $T = -1$, Odd-Odd Nucleus ^{48}Mn

C. Chandler, M. A. Bentley, M. P. Carpenter, C. N. Davids, R. Du Rietz, J. Ekman, S. J. Freeman, G. Hammond, R. V. F. Janssens, S. M. Lenzi, and D. Seweryniak
Proceedings of the Conference on “Nuclei at the Limits”, Argonne, IL, July 26-30, 2004, eds. Dariusz Seweryniak and Teng Lek Khoo, AIP Conference Proceedings **764**, 199-204 (2005)

Decay Rate of Triaxially Deformed Proton Emitters

Cary N. Davids and Henning Esbensen
Proceedings of the Conference on “Nuclei at the Limits”, Argonne, IL, July 26-30, 2004, eds. Dariusz Seweryniak and Teng Lek Khoo, AIP Conference Proceedings **764**, 213-216 (2005)

Recoil Decay Tagging Study of Transitional Proton Emitters $^{145,146,147}\text{Tm}$

A. P. Robinson, C. N. Davids, D. Seweryniak, P. J. Woods, B. Blank, M. P. Carpenter, T. Davinson, S. J. Freeman, N. Hammond, N. Hoteling, R. V. F. Janssens, Z. Liu, G. Mukherjee, C. Scholey, J. Shergur, S. Sinha, A. A. Sonzogni, W. B. Walters, and A. Woehr
Proceedings of the Conference on “Nuclei at the Limits”, Argonne, IL, July 26-30, 2004, eds. Dariusz Seweryniak and Teng Lek Khoo, AIP Conference Proceedings **764**, 217-222 (2005)

Electrons from a 0.3s Isomer in ^{254}No

G. Mukherjee, T. L. Khoo, R. Blinstrup, D. Seweryniak, I. Ahmad, P. A. Butler, M. P. Carpenter, P. Chowdhury, J. A. Cizewski, C. N. Davids, S. J. Freeman, J. Greene, N. J. Hammond, A. Heinz, R. D. Herzberg, P. J. C. Ikin, R. V. F. Janssens, M. S. Johnson, G. D. Jones, F. G. Kondev, T. Lauritsen, C. J. Lister, E. F. Moore, E. Ngijoi-Yogo, P. Reiter, and S. Sinha
Proceedings of the Conference on “Nuclei at the Limits”, Argonne, IL, July 26-30, 2004, eds. Dariusz Seweryniak and Teng Lek Khoo, AIP Conference Proceedings **764**, 243-248 (2005)

Proton Single-Particle States in the Heaviest Actinide Nuclei

I. Ahmad, F. G. Kondev, E. F. Moore, R. R. Chasman, M. P. Carpenter, J. P. Greene, R. V. F. Janssens, T. Lauritsen, C. J. Lister, D. Seweryniak, R. W. Hoff, J. E. Evans, R. W. Lougheed, C. E. Porter, and L. K. Felker

Proceedings of the Conference on "Nuclei at the Limits", Argonne, IL, July 26-30, 2004, eds. Dariusz Seweryniak and Teng Lek Khoo, AIP Conference Proceedings **764**, 251-256 (2005)

A New $^{13}\text{N}(p,\gamma)^{14}\text{O}$ Reaction Rate and Its Influence in Novae Nucleosynthesis

X. Tang, A. Azhari, Changbo Fu, C. A. Gagliardi, A. M. Mukhamedzhanov, F. Pirlepesov, L. Trache, R. E. Tribble, V. Burjan, V. Kroha, F. Carstoiu, and B. F. Irgaziev

Proceedings of the Conference on "Nuclei at the Limits", Argonne, IL, July 26-30, 2004, eds. Dariusz Seweryniak and Teng Lek Khoo, AIP Conference Proceedings **764**, 329-334 (2005)

Structure and Decay of Neutron-Rich Nuclides in the $115 \leq A \leq 138$ Mass Range and r-Process Nucleosynthesis

W. B. Walters, M. A. Stoyer, J. Shergur, N. Hoteling, J. J. Ressler, J. Rikovska, K.-L. Kratz, A. Wöhr, B. Pfeiffer, O. Arndt, P. F. Mantica, B. Tomlin, H. Schatz, F. Montes, B. A. Brown, D. Seweryniak, H. Ravn, V. Fedoseyev, U. Köster, and the ISOLDE Collaboration, C. Y. Wu, D. Cline, H. Hua, A. B. Hayes, and R. Teng

Proceedings of the Conference on "Nuclei at the Limits", Argonne, IL, July 26-30, 2004, eds. Dariusz Seweryniak and Teng Lek Khoo, AIP Conference Proceedings **764**, 335-339 (2005)

Linear Polarization Measurements of Gamma Rays Following Alpha Decay

G. D. Jones, N. J. Hammond, C. J. Lister, K. Teh, and E. F. Moore

Proceedings of the Conference on "Nuclei at the Limits", Argonne, IL, July 26-30, 2004, eds. Dariusz Seweryniak and Teng Lek Khoo, AIP Conference Proceedings **764**, 349-353 (2005)

Doorway States as Principal Decay Pathway in $^{12}\text{C}(^{12}\text{C},\gamma)$ Radiative Capture

D. G. Jenkins, B. R. Fulton, J. Pearson, C. J. Lister, M. P. Carpenter, S. J. Freeman, N. J. Hammond, R. V. F. Janssens, T. L. Khoo, T. Lauritsen, A. H. Wuosmaa, P. Fallon, A. Görgen, A. O. Macchiavelli, M. McMahan, F. Haas, and the DRAGON E947 Collaboration

Proceedings of the Conference on "Nuclei at the Limits", Argonne, IL, July 26-30, 2004, eds. Dariusz Seweryniak and Teng Lek Khoo, AIP Conference Proceedings **764**, 367-372 (2005)

Excited States in ^7He from $d(^6\text{He},p)^7\text{He}$

A. H. Wuosmaa, K. E. Rehm, J. P. Greene, D. J. Henderson, R. V. F. Janssens, C. L. Jiang, E. F. Moore, R. C. Pardo, D. Peterson, S. C. Pieper, G. Savard, J. P. Schiffer, S. Sinha, X. Tang, R. B. Wiringa, L. Jisonna, and R. E. Segel

Proceedings of the Conference on "Nuclei at the Limits", Argonne, IL, July 26-30, 2004, eds. Dariusz Seweryniak and Teng Lek Khoo, AIP Conference Proceedings **764**, 393-398 (2005)

Measurement of Residual Nucleus Cross Sections and Recoil Energies in $p + \text{Fe}$ Collisions at 300, 500, 750, 1000 and 1500 MeV

C. Villagrasa *et al.*

Proceedings of the International Conference on Nuclear Data for Science and Technology (ND2004), Santa Fe, NM, September 26-October 1, 2004, eds. Robert C. Haight, Mark B. Chadwick, Toshihiko Kawano, and Patric Talou, AIP Conference Proceedings **769**, 842-845 (2005)

Shape Coexistence at the Outer Edges of Stability

M. P. Carpenter, F. G. Kondev, and R. V. F. Janssens

Proceedings of the International Conference on Nuclear Data for Science and Technology (ND2004), Santa Fe, NM, September 26-October 1, 2004, eds. Robert C. Haight, Mark B. Chadwick, Toshihiko Kawano, and Patric Talou, AIP Conference Proceedings **769**, 894-897 (2005)

Studies of Multiplicity in Relativistic Heavy-Ion Collisions

B. B. Back

Proceedings of "Focus on Multiplicity: International Workshop on Particle Multiplicity in Relativistic Heavy Ion Collisions", Bari, Italy, June 17-19, 2004; J. Phys. Conf. Ser. **5**, 1-16 (2005)

Using Multiplicity as a Fractional Cross-Section Estimation for Centrality in PHOBOS

Richard S. Hollis for the PHOBOS Collaboration

Proceedings of "Focus on Multiplicity: International Workshop on Particle Multiplicity in Relativistic Heavy Ion Collisions", Bari, Italy, June 17-19, 2004; J. Phys. Conf. Ser. **5**, 46-54 (2005)

Measuring Mid-Rapidity Multiplicity in PHOBOS

Aneta Iordanova for the PHOBOS Collaboration

Proceedings of "Focus on Multiplicity: International Workshop on Particle Multiplicity in Relativistic Heavy Ion Collisions", Bari, Italy, June 17-19, 2004; J. Phys. Conf. Ser. **5**, 97-104 (2005)

Simulations of Cold, Confined, One-Component Plasmas

John Schiffer

Proceedings of the RIKEN BNL Research Center Workshop on Strongly Coupled Plasmas: Electromagnetic, Nuclear and Atomic, Upton, NY, December 16-17, 2004, Report BNL-73867-2005, pp. 33-37 (2005)

Perspective on Recent Developments in Nuclear Physics

John P. Schiffer

Proceedings of the DAE-BRNS 50th Symposium on Nuclear Physics, Mumbai, India, December 12-16, 2005, eds. S. Kailas, Suresh, and Kumar L. M. Pant (Prime Time Education 2005) Vol. 50, p. 1

Search for Hyperdeformation in Nuclei at High Spin

A. K. Singh *et al.*

Proceedings of the DAE-BRNS 50th Symposium on Nuclear Physics, Mumbai, India, December 12-16, 2005, eds. S. Kailas, Suresh Kumar, and L. M. Pant (Prime Time Education 2005) Vol. 50, pp. 183-189

High Spin Spectroscopy of ^{103}Cd

A. Chakraborty, Krishichayan, S. Mukhopadhyay, S. Ray, N. S. Pattabiraman, S. S. Ghugre, A. K. Sinha, S. Sarkar, S. K. Basu, M. Saha Sarkar, P. V. Madhusudhna Rao, U. Garg, B. Kharraja, S. Zhu, R. V. F. Janssens, M. P. Carpenter, F. G. Kondev, and T. Lauritsen

Proceedings of the DAE-BRNS 50th Symposium on Nuclear Physics, Mumbai, India, December 12-16, 2005, eds. S. Kailas, Suresh Kumar, and L. M. Pant (Prime Time Education 2005) Vol. 50, p. 248

Electromagnetic Properties of Rotational States in Fission Fragments

A. G. Smith, R. Orlandi, D. Patel, G. S. Simpson, R. M. Wall, J. F. Smith, I. Ahmad, J. P. Greene, M. P. Carpenter, T. Lauritsen, C. J. Lister, R. V. F. Janssens, F. G. Kondev, D. Seweryniak, B. J. P. Gall, and O. Dorvaux

International Conference on the Interface Between Nuclear Structure, Astrophysics and Reactions (NUSTAR'05), Guildford, England, January 5-8, 2005, Book of Abstracts, p. C3 (2005)

Structure of Neutron-Rich Cr Isotopes: Inadequacy of the fp Model Space and the Onset of Deformation

S. J. Freeman, R. V. F. Janssens, B. A. Brown, I. V. Calderin, M. P. Carpenter, P. Chowdhury, A. N. Deacon, S. M. Fischer, N. J. Hammond, M. Honma, T. Lauritsen, C. J. Lister, T. L. Khoo, G. Mukherjee, D. Seweryniak, J. F. Smith, S. L. Tabor, B. J. Varley, M. Whitehead, and S. Zhu

International Conference on the Interface Between Nuclear Structure, Astrophysics and Reactions (NUSTAR'05), Guildford, England, January 5-8, 2005, Book of Abstracts, p. D6 (2005)

Proton Decay: Spectroscopic Probe Beyond the Proton Drip Line

D. Seweryniak, C. N. Davids, A. Robinson, P. J. Woods, B. Blank, M. P. Carpenter, T. Davinson, S. J. Freeman, N. Hammond, N. Hoteling, R. V. F. Janssens, Z. Liu, G. Mukherjee, J. Shergur, S. Sinha, A. A. Sonzogni, W. B. Walters, and A. Woehr

International Conference on the Interface Between Nuclear Structure, Astrophysics and Reactions (NUSTAR'05), Guildford, England, January 5-8, 2005, Book of Abstracts, p. F1 (2005)

"Cold" Fusion Reactions to Reach Neutron-Deficient Nuclei Near the $Z = 82$ Shell Closure

Michael P. Carpenter, Filip G. Kondev, and Robert V. F. Janssens

International Conference on the Interface Between Nuclear Structure, Astrophysics and Reactions (NUSTAR'05), Guildford, England, January 5-8, 2005, Book of Abstracts, p. I3 (2005)

Beyond Band Termination in $N \sim 90$ Er Isotopes and the Search for Wobbling Excitations in Strongly Deformed ^{174}Hf

M. A. Riley *et al.*

International Conference on the Interface Between Nuclear Structure, Astrophysics and Reactions (NUSTAR'05), Guildford, England, January 5-8, 2005, Book of Abstracts, p. N1 (2005)

Quadrupole Moment Measurements of TSD1 and TSD2 Bands in ^{167}Lu

G. Gürdal, H. Amro, C. W. Beausang, D. S. Brenner, M. P. Carpenter, R. F. Casten, C. Engelhardt, G. B. Hagemann, C. R. Hansen, D. J. Hartley, H. Herskind, H. Hübel, T. L. Khoo, T. Lauritsen, W. C. Ma, D. A. Meyer, E. F. Moore, A. Neusser, P. Pringle, D. G. Roux, G. Sletten, R. B. Yadav, and Y. Zhang

International Conference on the Interface Between Nuclear Structure, Astrophysics and Reactions (NUSTAR'05), Guildford, England, January 5-8, 2005, Book of Abstracts, p. 22 (2005)

In-Beam γ Spectroscopy of the Proton Emitter ^{117}La

Z. Liu, D. Seweryniak, P. J. Woods, M. P. Carpenter, C. N. Davids, T. Davinson, R. V. F. Janssens, A. Robinson, J. Shergur, W. B. Walters, and F. R. Xu

International Conference on the Interface Between Nuclear Structure, Astrophysics and Reactions (NUSTAR'05), Guildford, England, January 5-8, 2005, Book of Abstracts, p. 34 (2005)

In-Beam γ -Spectroscopy of Low-Spin Mixed-Symmetry States of ^{138}Ce with Gammasphere in Singles-Mode

N. Pietralla, G. Rainovski, T. Ahn, M. P. Carpenter, R. V. F. Janssens, C. Lister, and S. Zhu

12th International Conference on Capture Gamma-Ray Spectroscopy and Related Topics, Notre Dame, IN, September 4-9, 2005, Book of Abstracts, p. 15 (2005)

Search for Enhanced Alpha Performance in the $N = Z + 1$ Nuclei ^{113}Ba , ^{109}Xe , ^{105}Te

A. A. Hecht, C. J. Lister, C. N. Davids, A. Heinz, N. Hoteling, C. Mazzocchi, J. Palombo, D. Seweryniak, J. Shergur, M. Stoyer, W. B. Walters, P. J. Woods, and S. Zhu

12th International Conference on Capture Gamma-Ray Spectroscopy and Related Topics, Notre Dame, IN, September 4-9, 2005, Book of Abstracts, p. 83 (2005)

Doorway States in the $^{12}\text{C}(^{12}\text{C},\gamma)^{24}\text{Mg}$ Radiative Capture Process

C. J. Lister, M. P. Carpenter, S. J. Freeman, N. J. Hammond, P. Chowdhury, A. H. Wuosmaa, R. V. F. Janssens, T. L. Khoo, T. Lauritsen, D. G. Jenkins, B. R. Fulton, J. Pearson, P. Fallon, A. Gorgen, A. O. Macchiavelli, M. McMahan, M. Freer, and F. Haas

12th International Conference on Capture Gamma-Ray Spectroscopy and Related Topics, Notre Dame, IN, September 4-9, 2005, Book of Abstracts, p. 89 (2005)

Rotational Damping, Ridges and the Quasicontinuum of γ Rays in ^{152}Dy

T. Lauritsen, I. Ahmad, M. P. Carpenter, A. M. Heinz, R. V. F. Janssens, D. G. Jenkins, T. L. Khoo, F. G. Kondev, C. J. Lister, D. Seweryniak, P. Fallon, A. O. Macchiavelli, D. Ward, R. M. Clark, M. Cromaz, G. Lane, A. Lopez-Martens, A. Korichi, S. Siem, B. Herskind, T. Dossing, A. J. Larabee, and P. Chowdhury

12th International Conference on Capture Gamma-Ray Spectroscopy and Related Topics, Notre Dame, IN, September 4-9, 2005, Book of Abstracts, p. 105 (2005)

Single Particle Gaps and the Structure of Neutron-Rich Nuclei Above ^{48}Ca

C. J. (Kim) Lister

2nd Joint Meeting of the Nuclear Physics Divisions of the American Physical Society and the Japanese Physical Society, Kapalua, Maui, HI, September 18-22, 2005; Bull. Am. Phys. Soc. **50**, 21 (2005)Magnetic Moment of the Extremely Proton Rich Nucleus ^{23}Al Takashi Nagatomo *et al.*2nd Joint Meeting of the Nuclear Physics Divisions of the American Physical Society and the Japanese Physical Society, Kapalua, Maui, HI, September 18-22, 2005; Bull. Am. Phys. Soc. **50**, 51 (2005)Precision β -Decay Studies in a RFQ Ion Trap

N. D. Scielzo, A. Levand, G. Savard, I. Tanihata, B. J. Zabransky, J. A. Clark, H. Sharma, K. S. Sharma, Y. Wang, and A. A. Hecht

2nd Joint Meeting of the Nuclear Physics Divisions of the American Physical Society and the Japanese Physical Society, Kapalua, Maui, HI, September 18-22, 2005; Bull. Am. Phys. Soc. **50**, 76 (2005)Measurement of Proton Transfer Reaction for Single-Particle States in ^{23}F S. Michimasa *et al.*2nd Joint Meeting of the Nuclear Physics Divisions of the American Physical Society and the Japanese Physical Society, Kapalua, Maui, HI, September 18-22, 2005; Bull. Am. Phys. Soc. **50**, 85 (2005)Study of Neutron-Rich $A \sim 30$ Nuclei in Multi-Nucleon Transfer Reactions

Mathis Wiedeking, P. Fallon, E. Rodriguez-Vieitez, R. M. Clark, M. Cromaz, M. Descovich, I-Y. Lee, M-A. Deleplanque, A. O. Macchiavelli, F. S. Stephens, D. Ward, M. P. Carpenter, D. Cline, R. Teng, and C. Y. Wu

2nd Joint Meeting of the Nuclear Physics Divisions of the American Physical Society and the Japanese Physical Society, Kapalua, Maui, HI, September 18-22, 2005; Bull. Am. Phys. Soc. **50**, 86 (2005)Strongly Deformed Structures in $^{172,171}\text{Hf}$

W. C. Ma, Y. Zhang, E. Ngijoi-Yogo, D. G. Roux, J. A. Winger, R. B. Yadav, M. P. Carpenter, R. V. F. Janssens, T. L. Khoo, F. G. Kondev, T. Lauritsen, E. F. Moore, S. Zhu, D. J. Hartley, D. Cullen, S. V. Rigby, D. T. Scholes, P. Chowdhury, S. Odegard, and M. K. Djongolov

2nd Joint Meeting of the Nuclear Physics Divisions of the American Physical Society and the Japanese Physical Society, Kapalua, Maui, HI, September 18-22, 2005; Bull. Am. Phys. Soc. **50**, 93 (2005)Delayed Nucleon Alignment and Search for Prolate-To-Oblate Shape Transition in ^{180}Hf at High Spins

U. S. Tandel, P. Chowdhury, S. K. Tandel, S. Sheppard, D. Cline, C. Y. Wu, M. P. Carpenter, R. V. F. Janssens, T. L. Khoo, T. Lauritsen, C. J. Lister, D. Seweryniak, and S. Zhu

2nd Joint Meeting of the Nuclear Physics Divisions of the American Physical Society and the Japanese Physical Society, Kapalua, Maui, HI, September 18-22, 2005; Bull. Am. Phys. Soc. **50**, 94 (2005) γ -Rays from the Decay of the 0.26 s Isomer in ^{254}No

S. K. Tandel, T. L. Khoo, D. Seweryniak, P. Chowdhury, U. S. Tandel, I. Ahmad, B. Back, M. P. Carpenter, C. N. Davids, A. Hecht, R. V. F. Janssens, F. G. Kondev, T. Lauritsen, C. J. Lister, E. F. Moore, D. Peterson, X. F. Wang, S. F. Zhu, G. Mukherjee, A. Heinz, P. Reiter, P. A. Butler, R. Herzberg, and G. Jones

2nd Joint Meeting of the Nuclear Physics Divisions of the American Physical Society and the Japanese Physical Society, Kapalua, Maui, HI, September 18-22, 2005; Bull. Am. Phys. Soc. **50**, 95 (2005)

Production and Decay of Light Thorium Isotopes

J. Qian, A. Heinz, R. Winkler, R. V. F. Janssens, D. Peterson, D. Seweryniak, B. Back, M. P. Carpenter, A. Hecht, C.-L. Jiang, F. G. Kondev, T. Lauritsen, C. J. Lister, S. Zhu, P. Collon, X. Wang, and N. Hoteling

2nd Joint Meeting of the Nuclear Physics Divisions of the American Physical Society and the Japanese Physical Society, Kapalua, Maui, HI, September 18-22, 2005; Bull. Am. Phys. Soc. **50**, 95 (2005)

Study of High-Spin States in Neutron-Rich Ti Isotopes

M. Niikura *et al.*2nd Joint Meeting of the Nuclear Physics Divisions of the American Physical Society and the Japanese Physical Society, Kapalua, Maui, HI, September 18-22, 2005; Bull. Am. Phys. Soc. **50**, 108 (2005)Electron Capture Branch of ^{100}Tc and the Efficiency of a Proposed Mo Neutrino DetectorSky Sjue *et al.*2nd Joint Meeting of the Nuclear Physics Divisions of the American Physical Society and the Japanese Physical Society, Kapalua, Maui, HI, September 18-22, 2005; Bull. Am. Phys. Soc. **50**, 115 (2005)

Test of Nuclear Wavefunctions for Neutrinoless Double Beta Decay

J. P. Schiffer, S. J. Freeman, K. E. Rehm, and A. C. C. Villari

2nd Joint Meeting of the Nuclear Physics Divisions of the American Physical Society and the Japanese Physical Society, Kapalua, Maui, HI, September 18-22, 2005; Bull. Am. Phys. Soc. **50**, 115 (2005)New Measurement of the El Component of the $^{12}\text{C}(\alpha,\gamma)^{16}\text{O}$ Reaction

X. D. Tang, M. Notani, K. E. Rehm, I. Ahmad, J. Greene, A. A. Hecht, D. Henderson, R. V. F. Janssens, C. L. Jiang, E. F. Moore, R. C. Pardo, G. Savard, J. P. Schiffer, S. Sinha, M. Paul, L. Jisonna, R. E. Segel, C. Brune, A. Champagne, and A. Wuosmaa

2nd Joint Meeting of the Nuclear Physics Divisions of the American Physical Society and the Japanese Physical Society, Kapalua, Maui, HI, September 18-22, 2005; Bull. Am. Phys. Soc. **50**, 119 (2005)Excited States in the Nucleus ^{73}Br

Rafael Yah, Susan Fischer, and Kim Lister

2nd Joint Meeting of the Nuclear Physics Divisions of the American Physical Society and the Japanese Physical Society, Kapalua, Maui, HI, September 18-22, 2005; Bull. Am. Phys. Soc. **50**, 141 (2005)A New Measurement of the Strength of the Superallowed Fermi Branch in the Beta Decay of ^{10}C with Gammasphere

B. K. Fujikawa, T. I. Banks, S. J. Freedman, P. A. Vetter, W. T. Winter, S. J. Asztalos, J. T. Burke, J. P. Greene, and N. D. Scielzo

2nd Joint Meeting of the Nuclear Physics Divisions of the American Physical Society and the Japanese Physical Society, Kapalua, Maui, HI, September 18-22, 2005; Bull. Am. Phys. Soc. **50**, 168 (2005)

Progress and Physics with Planar Germanium Strip Detectors (HpGeDSSDs)

C. J. (Kim) Lister

2nd Joint Meeting of the Nuclear Physics Divisions of the American Physical Society and the Japanese Physical Society, Kapalua, Maui, HI, September 18-22, 2005; Bull. Am. Phys. Soc. **50**, 172 (2005)

OPERATION AND DEVELOPMENT OF ATLAS and ACCELERATOR PHYSICS AND EXOTIC BEAM TECHNOLOGY

Automatic Longitudinal Tuning of a Multiple-Charge-State Heavy-Ion Beam

B. Mustapha and P. N. Ostroumov

Phys. Rev. ST Accel. Beams **8**, 090101/1-8 (2005)

An Innovative Concept for Acceleration of Low-Energy Low-Charge-State Heavy-Ion Beams

P. N. Ostroumov, A. A. Kolomiets, S. Sharma, N. E. Vinogradov, and G. P. Zinkann

Nucl. Instrum. Methods **A547**, 259-269 (2005)

Summary of the 34th ICFA Advanced Beam Dynamics Workshop on High Power Superconducting Ion, Proton, and Multi-Species Linacs (HPSL2005)

Petr Ostroumov

ICFA Beam Dynamics Newsletter **37**, 148-152 (2005)

Conductance Measurements of Permeable Samples

A. C. C. Villari, J. Greene, T. Burtseva, and J. A. Nolen

Int. Nucl. Target Dev. Society Newsletter **32**, 10-13 (2005)

ECRIS Operation with Multiple Frequencies

R. Vondrasek, R. Scott, R. Pardo, H. Koivisto, O. Tarvainen, P. Suominen, and D. H. Edgell

Proceedings of the 16th International Workshop on ECR Ion Sources (ECRIS'04), Berkeley, CA, September 26-30, 2004, ed. M. Leitner, AIP Conference Proceedings **749**, 31-34 (2005)

Plasma Potential Measurements with a New Instrument

O. Tarvainen, P. Souminen, T. Ropponen, H. Koivisto, R. C. Vondrasek, and R. H. Scott

Proceedings of the 16th International Workshop on ECR Ion Sources (ECRIS'04), Berkeley, CA, September 26-30, 2004, ed. M. Leitner, AIP Conference Proceedings **749**, 61-66 (2005)

Radioactive Beams from ^{252}Cf Fission Using a Gas Catcher and an ECR Charge Breeder at ATLAS

Guy Savard, Richard C. Pardo, E. Frank Moore, Adam A. Hecht, and Sam Baker

Proceedings of the 16th International Workshop on ECR Ion Sources (ECRIS'04), Berkeley, CA, September 26-30, 2004, ed. M. Leitner, AIP Conference Proceedings **749**, 75-78 (2005)

2Q-Lebt Prototype for the RIA Facility

N. E. Vinogradov, V. N. Aseev, P. N. Ostroumov, R. C. Pardo, and R. Scott

Proceedings of the 16th International Workshop on ECR Ion Sources (ECRIS'04), Berkeley, CA, September 26-30, 2004, ed. M. Leitner, AIP Conference Proceedings **749**, 215-218 (2005)

Heavy-Ion Driver Linac for the RIA Facility and the Feasibility of Producing Multi-Megawatt Beams

P. N. Ostroumov, J. A. Nolen, and K. W. Shepard

Proceedings of the 33rd ICFA Advanced Beam Dynamics Workshop on High Intensity and High Brightness Hadron Beams, Bensheim, Germany, October 18-22, 2004, eds. I. Hofmann, J.-M. Lagniel, and R. W. Hasse, AIP Conference Proceedings **773**, 89-93 (2005)

Beam Intensity Adjustment in the RIA Driver Linac

P. N. Ostroumov, J. A. Nolen, S. I. Sharamentov, and A. V. Novikov-Borodin

Proceedings of the XXII International Linear Accelerator Conference (LINAC2004), Lübeck, Germany, August 16-20, 2004, pp. 49-51 (2005)

Advanced Beam-Dynamics Simulation Tools for RIA

T. P. Wangler, R. W. Garnett, K. R. Crandall, J. Qiang, R. Ryne, N. Aseev, P. Ostroumov, D. Gorelov, and R. York
Proceedings of the XXII International Linear Accelerator Conference (LINAC2004), Lübeck, Germany, August 16-20, 2004, pp. 202-204 (2005)

Alternating Phase Focusing in Low-Velocity Heavy-Ion Superconducting Linac

P. N. Ostroumov, A. A. Kolomiets, K. W. Shepard, and E. S. Masunov
Proceedings of the XXII International Linear Accelerator Conference (LINAC2004), Lübeck, Germany, August 16-20, 2004, pp. 374-376 (2005)

Superconducting $\beta = 0.15$ Quarter-Wave Cavity for RIA

M. P. Kelly, Z. A. Conway, J. D. Fuerst, M. Kedzie, and K. W. Shepard
Proceedings of the XXII International Linear Accelerator Conference (LINAC2004), Lübeck, Germany, August 16-20, 2004, pp. 605-607 (2005)

Cold Tests of a Superconducting Co-Axial Half-Wave Cavity for RIA

M. Kelly, J. D. Fuerst, M. Kedzie, and K. W. Shepard
Proceedings of the XXII International Linear Accelerator Conference (LINAC2004), Lübeck, Germany, August 16-20, 2004, pp. 608-610 (2005)

End-To-End Beam Dynamics Simulations for the ANL RIA Driver Linac

P. N. Ostroumov
Proceedings of the XXII International Linear Accelerator Conference (LINAC2004), Lübeck, Germany, August 16-20, 2004, pp. 628-632 (2005)

Progress with the 2Q-LEBT Facility for the RIA Project

N. E. Vinogradov, V. N. Aseev, M. R. L. Kern, P. N. Ostroumov, R. C. Pardo, and R. Scott
Proceedings of the Particle Accelerator Conference (PAC05), Knoxville, TN, May 16-20, 2005, IEEE 0-7803-88593, 253-255 (2005)

Reliability and Availability Studies in the RIA Driver Linac

E. S. Lessner and P. N. Ostroumov
Proceedings of the Particle Accelerator Conference (PAC05), Knoxville, TN, May 16-20, 2005, IEEE 0-7803-88593, 443-445 (2005)

Radioactive Beams from ^{252}Cf Fission Using a Gas Catcher and an ECR Charge Breeder at ATLAS

Richard C. Pardo, Guy Savard, E. Frank Moore, Adam A. Hecht, and Sam Baker
Proceedings of the Particle Accelerator Conference (PAC05), Knoxville, TN, May 16-20, 2005, IEEE 0-7803-88593, 1000-1002 (2005)

A Fast Chopper for Intensity Adjustment of Heavy-Ion Beams

A. V. Novikov-Borodin, V. A. Kutuzov, and P. N. Ostroumov
Proceedings of the Particle Accelerator Conference (PAC05), Knoxville, TN, May 16-20, 2005, IEEE 0-7803-88593, 1692-1694 (2005)

RF-Based Accelerators for HEDP Research

John W. Staples, Andrew Sessler, Roderich Keller, Petr Ostroumov, and Weiren Chou
Proceedings of the Particle Accelerator Conference (PAC05), Knoxville, TN, May 16-20, 2005, IEEE 0-7803-88593, 1829-1831 (2005)

TRACK: The New Beam Dynamics Code

V. N. Aseev, P. N. Ostroumov, E. S. Lessner, and B. Mustapha
Proceedings of the Particle Accelerator Conference (PAC05), Knoxville, TN, May 16-20, 2005, IEEE 0-7803-88593, 2053-2055 (2005)

RIA Beam Dynamics: Comparing Track to Impact

B. Mustapha, V. N. Aseev, P. N. Ostroumov, J. Qiang, and R. D. Ryne

Proceedings of the Particle Accelerator Conference (PAC05), Knoxville, TN, May 16-20, 2005, IEEE 0-7803-88593, 2095-2097 (2005)

Upgrade of the ATLAS Positive Ion Injector Bunching System

S. Sharamentov, J. Bogaty, B. E. Clift, and R. Pardo

Proceedings of the Particle Accelerator Conference (PAC05), Knoxville, TN, May 16-20, 2005, IEEE 0-7803-88593, 2161-2163 (2005)

Front End Design of a Multi-GeV H-Minus Linac

P. N. Ostroumov, K. W. Shepard, G. W. Foster, I. V. Gonin, and G. V. Romanov

Proceedings of the Particle Accelerator Conference (PAC05), Knoxville, TN, May 16-20, 2005, IEEE 0-7803-88593, 3286-3288 (2005)

Heavy-Ion Beam Dynamics in the RIA Post-Accelerator

P. N. Ostroumov, A. A. Kolomiets, and V. N. Aseev

Proceedings of the Particle Accelerator Conference (PAC05), Knoxville, TN, May 16-20, 2005, IEEE 0-7803-88593, 3301-3303 (2005)

Review of a Spoke-Cavity Design Option for the RIA Driver Linac

P. N. Ostroumov, K. W. Shepard, and J. R. Delayen

Proceedings of the Particle Accelerator Conference (PAC05), Knoxville, TN, May 16-20, 2005, IEEE 0-7803-88593, 3360-3362 (2005)

Optimization of Steering Elements in the RIA Driver Linac

E. S. Lessner, V. S. Aseev, and P. N. Ostroumov

Proceedings of the Particle Accelerator Conference (PAC05), Knoxville, TN, May 16-20, 2005, IEEE 0-7803-88593, 3600-3602 (2005)

A Magnetostrictive Tuning System for Particle Accelerators

Chiu-Ying Tai, Jordan Cormier, William Espinola, Zhixiu Han, Chad Joshi, Anil Mavanur, Livia Racz, Kenneth Shepard, Edward Daly, and Kirk Davis

Proceedings of the Particle Accelerator Conference (PAC05), Knoxville, TN, May 16-20, 2005, IEEE 0-7803-88593, 3762-3764 (2005)

An Improved Pneumatic Frequency Control for Superconducting Cavities

G. P. Zinkann, S. Sharamentov, and B. Clift

Proceedings of the Particle Accelerator Conference (PAC05), Knoxville, TN, May 16-20, 2005, IEEE 0-7803-88593, 4090-4092 (2005)

Advanced Beam-Dynamics Simulation Tools for RIA

R. W. Garnett, T. P. Wangler, J. H. Billen, J. Qiang, R. Ryne, K. R. Crandall, P. Ostroumov, R. York, and Q. Zhao

Proceedings of the Particle Accelerator Conference (PAC05), Knoxville, TN, May 16-20, 2005, IEEE 0-7803-88593, 4218-4220 (2005)

Prototype Superconducting Triple-Spoke Cavity for $\beta = 0.63$

K. W. Shepard, M. P. Kelly, J. D. Fuerst, M. Kedzie, and Z. A. Conway

Proceedings of the Particle Accelerator Conference (PAC05), Knoxville, TN, May 16-20, 2005, IEEE 0-7803-88593, 4338-4340 (2005)

Superconducting Triple-Spoke Cavity for $\beta = 0.5$ Ions

K. W. Shepard, M. P. Kelly, J. D. Fuerst, M. Kedzie, and Z. A. Conway

Proceedings of the Particle Accelerator Conference (PAC05), Knoxville, TN, May 16-20, 2005, IEEE 0-7803-88593, 4344-4346 (2005)

Two-Charge-State Injector Prototype for the RIA Project

N. E. Vinogradov, V. N. Aseev, M. R. L. Kern, P. N. Ostroumov, R. C. Pardo, and R. Scott
Particle Accelerator Conference (PAC05), Knoxville, TN, May 16-20, 2005, Book of Abstracts, p. 18
(2005)

Optimization of Steering Elements in the RIA Driver Linac

V. N. Aseev, E. S. Lessner, and P. N. Ostroumov
Particle Accelerator Conference (PAC05), Knoxville, TN, May 16-20, 2005, Book of Abstracts, p. 30
(2005)

RIA Beam Dynamics: Comparing TRACK to IMPACT

B. Mustapha, P. N. Ostroumov, V. N. Aseev, J. Qiang, and R. D. Ryne
Particle Accelerator Conference (PAC05), Knoxville, TN, May 16-20, 2005, Book of Abstracts, p. 86
(2005)

TRACK: The New Beam Dynamics Code

V. N. Aseev, P. N. Ostroumov, E. S. Lessner, and B. Mustapha
Particle Accelerator Conference (PAC05), Knoxville, TN, May 16-20, 2005, Book of Abstracts, p. 86
(2005)

Radioactive Beams from ²⁵²Cf Fission Using a Gas Catcher and an ECR Charge Breeder at ATLAS

G. Savard, R. C. Pardo, E. F. Moore, A. A. Hecht, and S. Baker
Particle Accelerator Conference (PAC05), Knoxville, TN, May 16-20, 2005, Book of Abstracts, p. 103
(2005)

Prototype Superconducting Triple-Spoke Cavity for Beta = 0.62

K. Shepard, Z. A. Conway, J. Fuerst, M. Kedzie, and M. Kelly
Particle Accelerator Conference (PAC05), Knoxville, TN, May 16-20, 2005, Book of Abstracts, p. 137
(2005)

Superconducting Triple-Spoke Cavity for Beta = 0.5 Ions

K. Shepard, Z. A. Conway, J. Fuerst, M. Kedzie, and M. Kelly
Particle Accelerator Conference (PAC05), Knoxville, TN, May 16-20, 2005, Book of Abstracts, p. 137
(2005)

Upgrade of the ATLAS Positive Ion Injector Bunching System

S. I. Sharamentov, J. Bogaty, B. Clifft, and R. C. Pardo
Particle Accelerator Conference (PAC05), Knoxville, TN, May 16-20, 2005, Book of Abstracts, p. 169
(2005)

An Improved Pneumatic Frequency Control for Superconducting Cavities

G. Zinkann and S. I. Sharamentov
Particle Accelerator Conference (PAC05), Knoxville, TN, May 16-20, 2005, Book of Abstracts, p. 177
(2005)

RF-Based Accelerators for HEDP Research

J. W. Staples, A. Sessler, P. Ostroumov, W. Chou, and R. Keller
Particle Accelerator Conference (PAC05), Knoxville, TN, May 16-20, 2005, Book of Abstracts, p. 205
(2005)

A Magnetostrictive Tuning System for Particle Accelerators

C-Y. Tai, J. Cormier, W. Espinola, Z. Han, C. Joshi, A. Mavanur, L. Racz, K. Shepard, E. Daly, and K. Davis
Particle Accelerator Conference (PAC05), Knoxville, TN, May 16-20, 2005, Book of Abstracts, p. 240
(2005)

Reliability and Availability Studies in the RIA Linac Driver

E. S. Lessner and P. N. Ostroumov

Particle Accelerator Conference (PAC05), Knoxville, TN, May 16-20, 2005, Book of Abstracts, p. 264 (2005)

Front End Design of a Multi-GeV H-Minus Linac

P. N. Ostroumov, A. A. Kolomiets, K. W. Shepard, G. W. Foster, I. V. Gonin, and G. V. Romanov

Particle Accelerator Conference (PAC05), Knoxville, TN, May 16-20, 2005, Book of Abstracts, p. 275 (2005)

Heavy-Ion Beam Dynamics in the RIA Post-Accelerator

P. N. Ostroumov, V. N. Aseev, and A. A. Kolomiets

Particle Accelerator Conference (PAC05), Knoxville, TN, May 16-20, 2005, Book of Abstracts, p. 275 (2005)

Review of a Spoke-Cavity Design Option for the RIA Driver LINAC

P. N. Ostroumov, K. W. Shepard, and J. R. Dealyen

Particle Accelerator Conference (PAC05), Knoxville, TN, May 16-20, 2005, Book of Abstracts, p. 275 (2005)

A Fast Chopper for Intensity Adjustment of Heavy-Ion Beams

A. Valerievich Novikov-Borodin, Valeriy Alexandrovich Kutuzov, and P. Ostroumov

Particle Accelerator Conference (PAC05), Knoxville, TN, May 16-20, 2005, Book of Abstracts, p. 287 (2005)

Update of Advanced Beam-Dynamics Simulation Tools for RIA

R. Garnett, J. Billen, T. Wangler, P. Ostroumov, J. Qiang, R. Ryne, R. York, and K. Crandall

Particle Accelerator Conference (PAC05), Knoxville, TN, May 16-20, 2005, Book of Abstracts, p. 298 (2005)

Production of Neutron-Rich Isotopes from UC Targets for RIB Development

E. H. Spejewski, H. K. Carter, A. Kronenberg, D. W. Stracener, J.-C. Bilheux, A. L. Gaddis, W. H. Brantley, J. A. Nolen, Jr., A. C. C. Villari, J. P. Greene, T. A. Burtseva, and W. L. Talbert

2nd Joint Meeting of the Nuclear Physics Divisions of the American Physical Society and the Japanese Physical Society, Kapalua, Maui, HI, September 18-22, 2005; Bull. Am. Phys. Soc. **50**, 98 (2005)

MEDIUM-ENERGY NUCLEAR PHYSICS RESEARCH

Single-Spin Asymmetries in Semi-Inclusive Deep-Inelastic Scattering on a Transversely Polarized Hydrogen Target

A. Airapetian *et al.* (The HERMES Collaboration)

Phys. Rev. Lett. **94**, 012002/1-6 (2005)

Fine Structure of the $1s3p\ ^3P_J$ Level in Atomic ^4He : Theory and Experiment

P. Mueller, L.-B. Wang, G. W. F. Drake, K. Bailey, Z.-T. Lu, and T. P. O'Connor

Phys. Rev. Lett. **94**, 133001/1-4 (2005)

Precision Rosenbluth Measurement of the Proton Elastic Form Factors

I. A. Qattan, J. Arrington, R. E. Segel, X. Zheng, K. Anoil, O. K. Baker, R. Beams, E. J. Brash, J. Calarco, A. Camsonne, J.-P. Chen, M. E. Christy, D. Dutta, R. Ent, S. Frullani, D. Gaskell, O. Gayou, R. Gilman, C. Glashauser, K. Hafidi, J.-O. Hansen, D. W. Higinbotham, W. Hinton, R. J. Holt, G. Huber, H. Ibrahim, L. Jisonna, M. K. Jones, C. E. Keppel, E. Kinney, G. J. Kumbartzki, A. Lung, D. J. Margaziotis, K. McCormick, D. Meekins, R. Michaels, P. Monaghan, P. Moussiegt, L. Pentchev, C. Perdrisat, V. Punjabi, R. Ransome, J. Reinhold, B. Reitz, A. Saha, A. Sarty, E. C. Schulte, K. Slifer, P. Solvignon, V. Sulkosky, K. Wijesooriya, and B. Zeidman

Phys. Rev. Lett. **94**, 142301/1-5 (2005)

Measurement of the Tensor Structure Function b_1 of the Deuteron

A. Airapetian *et al.* (The HERMES Collaboration)

Phys. Rev. Lett. **95**, 242001/1-6 (2005)

Subleading-Twist Effects in Single-Spin Asymmetries in Semi-Inclusive Deep-Inelastic Scattering on a Longitudinally Polarized Hydrogen Target

A. Airapetian *et al.* (HERMES Collaboration)

Phys. Lett. **B622**, 14-22 (2005)

Extraction of Two-Photon Contributions to the Proton Form Factors

J. Arrington

Phys. Rev. C **71**, 015202/1-8 (2005)

Cross Section Measurements of Charged Pion Photoproduction in Hydrogen and Deuterium from 1.1 to 5.5 GeV

L. Y. Zhu, J. Arrington, T. Averett, E. Beise, J. Calarco, T. Chang, J. P. Chen, E. Chudakov, M. Coman, B. Clasie, C. Crawford, S. Dieterich, F. Dohrmann, D. Dutta, K. Fissum, S. Frullani, H. Gao, R. Gilman, C. Glashauser, J. Gomez, K. Hafidi, O. Hansen, D. W. Higinbotham, R. J. Holt, C. W. de Jager, X. Jiang, E. Kinney, K. Kramer, G. Kumbartzki, J. LeRose, N. Liyanage, D. Mack, P. Markowitz, K. McCormick, D. Meekins, Z.-E. Meziani, R. Michaels, J. Mitchell, S. Nanda, D. Potterveld, R. Ransome, P. E. Reimer, B. Reitz, A. Saha, E. C. Schulte, J. Seely, S. Širca, S. Strauch, V. Sulkosky, B. Vlahovic, L. B. Weinstein, K. Wijesooriya, C. Williamson, B. Wojtsekhowski, H. Xiang, F. Xiong, W. Xu, J. Zeng, and X. Zheng

Phys. Rev. C **71**, 044603/1-17 (2005)

Pion Parton Distribution Function in the Valence Region

K. Wijesooriya, P. E. Reimer, and R. J. Holt

Phys. Rev. C **72**, 065203/1-5 (2005)

Quark Helicity Distributions in the Nucleon for Up, Down, and Strange Quarks from Semi-Inclusive Deep-Inelastic Scattering

A. Airapetian *et al.* (The HERMES Collaboration)

Phys. Rev. D **71**, 012003/1-36 (2005)

Search for an Exotic $S = -2$, $Q = -2$ Baryon Resonance at a Mass Near 1862 MeV in Quasireal Production

A. Airapetian *et al.* (The HERMES Collaboration)

Phys. Rev. D **71**, 032004/1-5 (2005)

The HERMES Polarized Hydrogen and Deuterium Gas Target in the HERA Electron Storage Ring

A. Airapetian *et al.*

Nucl. Instrum. Methods **A540**, 68-101 (2005)

Atom Trap, Kr-81, and Saharan Water

X. Du and Z.-T. Lu

Chinese Physics **34**, 6 (2005)

Searches for Stable Strangelets in Ordinary Matter: Overview and a Recent Example

Z.-T. Lu, R. J. Holt, P. Mueller, T. P. O'Connor, J. P. Schiffer, and L.-B. Wang

Proceedings of the 8th International Conference on Hypernuclear and Strange Particle Physics, Newport News, VA, October 14-18, 2003; Nucl. Phys. **A754**, 361c-368c (2005)

Measurement of Transverse Target-Spin Asymmetries at HERMES

W.-D. Nowak (on behalf of the HERMES Collaboration)

Proceedings of the 10th International Conference on the Structure of Baryons (BARYONS'04), Palaiseau, France, October 25-29, 2004; Nucl. Phys. **A755**, 325c-328c (2005)

Pentaquark Search at HERMES

Avetik Airapetian (on behalf of the HERMES Collaboration)

Proceedings of the 10th International Conference on the Structure of Baryons (BARYONS'04), Palaiseau, France, October 25-29, 2004; Nucl. Phys. **A755**, 379c-382c (2005)

Current Status and Future Measurements of DVCS at HERMES

Michael Düren (on behalf of the HERMES Collaboration)

Proceedings of the 10th International Conference on the Structure of Baryons (BARYONS'04), Palaiseau, France, October 25-29, 2004; Nucl. Phys. **A755**, 533c-536c (2005)

Exclusive Pion Production at HERMES

Cynthia Hadjidakis (on behalf of the HERMES Collaboration)

Proceedings of the 10th International Conference on the Structure of Baryons (BARYONS'04), Palaiseau, France, October 25-29, 2004; Nucl. Phys. **A755**, 557c-560c (2005)

Exclusive Electroproduction of Vector Mesons at HERMES

A. Borissov (on behalf of the HERMES Collaboration)

Proceedings of the 10th International Conference on the Structure of Baryons (BARYONS'04), Palaiseau, France, October 25-29, 2004; Nucl. Phys. **A755**, 634c-637c (2005)

The HERMES Dual Radiator RICH - Performance and Impact

H. E. Jackson

Proceedings of the 5th International Workshop on Ring Imaging Cherenkov Counters (RICH2004), Playa del Carmen, Mexico, November 30-December 5, 2004; Nucl. Instrum. Methods **A553**, 205-209 (2005)

What Have We Learned from the Nucleon Spin Structure?

X. Zheng

2005 April Meeting of the American Physical Society, Tampa, FL, April 16-19, 2005; Bull. Am. Phys. Soc. **50**, 27 (2005)

Two Facets of the Deuteron

R. Holt

2005 April Meeting of the American Physical Society, Tampa, FL, April 16-19, 2005; Bull. Am. Phys. Soc. **50**, 160 (2005)

Search for Exotic Baryons at HERMES

H. E. Jackson

2nd Joint Meeting of the Nuclear Physics Divisions of the American Physical Society and the Japanese Physical Society, Kapalua, Maui, HI, September 18-22, 2005; Bull. Am. Phys. Soc. **50**, 19 (2005)

What Do We Know and What Do We Need to Know in Nuclear Science

Donald F. Geesaman

2nd Joint Meeting of the Nuclear Physics Divisions of the American Physical Society and the Japanese Physical Society, Kapalua, Maui, HI, September 18-22, 2005; Bull. Am. Phys. Soc. **50**, 19 (2005)

Laser Spectroscopic Determination of the Nuclear Charge Radius of ${}^6\text{He}$ and ${}^8\text{He}$

P. Mueller, L.-B. Wang, K. Bailey, J. P. Greene, D. Henderson, R. J. Holt, R. V. F. Janssens, C. L. Jiang, Z.-T. Lu, T. P. O'Connor, R. C. Pardo, K. E. Rehm, J. P. Schiffer, X. D. Tang, and G. W. F. Drake

2nd Joint Meeting of the Nuclear Physics Divisions of the American Physical Society and the Japanese Physical Society, Kapalua, Maui, HI, September 18-22, 2005; Bull. Am. Phys. Soc. **50**, 56 (2005)

Azimuthal Dependence in Unpolarized Proton-Induced Drell-Yan Process

Lingyan Zhu, Jen-Chieh Peng, Paul Reimer, and Fermilab E866 Collaboration

2nd Joint Meeting of the Nuclear Physics Divisions of the American Physical Society and the Japanese Physical Society, Kapalua, Maui, HI, September 18-22, 2005; Bull. Am. Phys. Soc. **50**, 110 (2005)

Progress Towards the Measurement of the Electric Dipole Moment of ${}^{225}\text{Ra}$

J. R. Guest, N. D. Scielzo, E. C. Schulte, I. Ahmad, K. Bailey, J. P. Greene, R. J. Holt, Z.-T. Lu,

T. P. O'Connor, D. H. Potterveld, and H. Gould

2nd Joint Meeting of the Nuclear Physics Divisions of the American Physical Society and the Japanese Physical Society, Kapalua, Maui, HI, September 18-22, 2005; Bull. Am. Phys. Soc. **50**, 169 (2005)

THEORETICAL PHYSICS

Reconciling Coulomb Dissociation and Radiative Capture Measurements

H. Esbensen, G. F. Bertsch, and K. A. Snover
Phys. Rev. Lett. **94**, 042502/1-4 (2005)

A Variational Approach to Configuration Interaction

R. R. Chasman
Phys. Rev. Lett. **95**, 262501/1-4 (2005)

Charge Form Factors of Quark-Model Pions

F. Coester and W. N. Polyzou
Phys. Rev. C **71**, 028202/1-4 (2005)

Self-Consistent Description of Multipole Strength in Exotic Nuclei: Method

J. Terasaki, J. Engel, M. Bender, J. Dobaczewski, W. Nazarewicz, and M. Stoitsov
Phys. Rev. C **71**, 034310/1-15 (2005)

Electromagnetic Properties of Ground and Excited State Pseudoscalar Mesons

A. Höll, A. Krassnigg, P. Maris, C. D. Roberts, and S. V. Wright
Phys. Rev. C **71**, 065204/1-12 (2005)

Quark-Hadron Duality and Parity Violating Asymmetry of Electroweak Reactions in the Δ Region

K. Matsui, T. Sato, and T.-S. H. Lee
Phys. Rev. C **72**, 025204/1-14 (2005)

Axial-Vector Mesons in a Relativistic Point-Form Approach

A. Krassnigg
Phys. Rev. C **72**, 028201/1-4 (2005)

Sensitivity to Multi-Phonon Excitations in Heavy-Ion Fusion Reactions

H. Esbensen
Phys. Rev. C **72**, 054607/1-10 (2005)

Piecewise Moments Method: Generalized Lanczos Technique for Nuclear Response Surfaces

Wick C. Haxton, Kenneth M. Nollett, and Kathryn M. Zurek
Phys. Rev. C **72**, 065501/1-16 (2005)

A Representation of Complex Rational Numbers in Quantum Mechanics

P. Benioff
Phys. Rev. A **72**, 032314 (2005)

Fine-Structure Anomalies and Search for Variation of the Fine-Structure Constant in Laboratory Experiments

V. A. Dzuba and V. V. Flambaum
Phys. Rev. A **72**, 052514/1-4 (2005)

On Nucleon Electromagnetic Form Factors

R. Alkofer, A. Höll, M. Kloker, A. Krassnigg, and C. D. Roberts
Few-Body Systems **37**, 1-31 (2005)

Towards a Coherent Theory of Physics and Mathematics: The Theory-Experiment Connection

Paul Benioff
Foundations of Physics **35**, 1825-1856 (2005)

Excited States of the Mean Field

M. Bender and P.-H. Heenen
J. Phys. G **31**, S1367-S1375 (2005)

Martin Jacob Berger Obituary

Stephen M. Seltzer and Mitio Inokuti
Physics Today **58**, 67-68 (2005)

Quantum Monte Carlo Calculations of Light Nuclei

Steven C. Pieper
Proceedings of the 22nd International Nuclear Physics Conference (INPC2004), Göteborg, Sweden, June 27-July 2, 2004; Nucl. Phys. **A751**, 516c-532c (2005)

On Nucleon Electromagnetic Form Factors: A Précis

A. Höll, R. Alkofer, M. Kloker, A. Krassnigg, C. D. Roberts, and S. V. Wright
Proceedings of the 10th International Conference on the Structure of Baryons (BARYONS'04), Palaiseau, France, October 25-29, 2004; Nucl. Phys. **A755**, 298c-302c (2005)

Dynamical Coupled-Channel Study of $K^+\Lambda$ Photoproduction

B. Juliá-Díaz, B. Saghai, F. Tabakin, W.-T. Chiang, T.-S. H. Lee, and Z. Li
Proceedings of the 10th International Conference on the Structure of Baryons (BARYONS'04), Palaiseau, France, October 25-29, 2004; Nucl. Phys. **A755**, 463c-466c (2005)

Confinement, DCSB, Bound States, and the Quark-Gluon Vertex

A. Hoell, A. Krassnigg, and C. D. Roberts
Proceedings of the Workshop on QCD Down Under, Adelaide, Australia, March 10-19, 2004; Nucl. Phys. **B141**, 47-52 (2005)

Microscopic Models for Exotic Nuclei

M. Bender and P.-H. Heenen
Proceedings of the 4th International Conference on Exotic Nuclei and Atomic Masses (ENAM'04), Pine Mountain, CA, September 12-16, 2004; Eur. Phys. J. A **25**, 519-524 (2005)

Skyrme-QRPA Calculations of Multipole Strength in Exotic Nuclei

J. Terasaki, J. Engel, M. Bender, J. Dobaczewski, W. Nazarewicz, and M. Stoitsov
Proceedings of the 4th International Conference on Exotic Nuclei and Atomic Masses (ENAM'04), Pine Mountain, CA, September 12-16, 2004; Eur. Phys. J. A **25**, 539-540 (2005)

Dynamical Model of Electroweak Pion Production Reaction

T. Sato and T.-S. H. Lee
Proceedings of the 10th International Symposium on Meson-Nucleon Physics and the Structure of the Nucleon (MENU2004), Beijing, China, August 29-September 4, 2004; Int. J. Mod. Phys. A **20**, 1668-1673 (2005)

On the Complexion of Pseudoscalar Mesons

A. Höll, A. Krassnigg, C. D. Roberts, and S. V. Wright
Proceedings of the 10th International Symposium on Meson-Nucleon Physics and the Structure of the Nucleon (MENU2004), Beijing, China, August 29-September 4, 2004; Int. J. Mod. Phys. A **20**, 1778-1784 (2005)

Tightening the Theory-Experiment Connection in Physics: R_n Based Space and Time

P. Benioff
Proceedings of the International Meeting on Quantum Information Science "Foundations of Quantum Information", Camerino, Italy, April 16-19, 2004; Int. J. Quantum Inform. **3**, 1-8 (2005)

Ultraviolet Color Centers and Refraction in Silicate Glasses

D. Y. Smith, E. Shiles, and Mitio Inokuti

Proceedings of the 15th International Conference on Defects in Insulating Materials (ICDIM2004), Riga, Latvia, July 11-16, 2004; Phys. Stat. Sol. (c) **2**, 310-313 (2005)

Mean-Field Methods: Where Are We and Where Do We Go?

P.-H. Heenen and M. Bender

Proceedings of the Conference on "Nuclei at the Limits", Argonne, IL, July 26-30, 2004, eds. Dariusz Seweryniak and Teng Lek Khoo, AIP Conference Proceedings **764**, 118-124 (2005)

Correlation Energies by the Projected Generator Coordinate Method

M. Bender, G. F. Bertsch, and P.-H. Heenen

Proceedings of the Conference on "Nuclei at the Limits", Argonne, IL, July 26-30, 2004, eds. Dariusz Seweryniak and Teng Lek Khoo, AIP Conference Proceedings **764**, 268-273 (2005)

Dyson-Schwinger Equation Study of the First Excited State of the Pion

A. Höll, A. Krassnigg, and C. D. Roberts

Proceedings of the 19th European Conference on Few-Body Problems in Physics, Groningen, The Netherlands, August 23-27, 2004, AIP Conference Proceedings **768**, 378 (2005)Pseudoscalar and Vector Mesons as $q\bar{q}$ Bound States

A. Krassnigg and P. Maris

Proceedings of the First Meeting of the American Physical Society "Topical Group on Hadronic Physics," Fermilab, Batavia, IL, October 24-26, 2004; J. Phys. Conf. Ser. **9**, 153-160 (2005)The Theory Experiment Connection: R_n Space and Inflationary Cosmology

P. Benioff

Proceedings of the International Symposium on Quantum Infomatics 2004, Moscow, Russia, October 5-7, 2004, ed. Yuri I. Ozhigov (SPIE, Bellingham, WA 2005) Vol. 5833, pp. 1-14

Radiative Capture Versus Coulomb Dissociation Experiments

Henning Esbensen

12th International Conference on Capture Gamma-Ray Spectroscopy and Related Topics, Notre Dame, IN, September 4-9, 2005, Book of Abstracts, p. 115 (2005)

Dynamical Models of Electromagnetic Production of Hyperons and Hypernuclei

Tsung-Shung H. Lee

2nd Joint Meeting of the Nuclear Physics Divisions of the American Physical Society and the Japanese Physical Society, Kapalua, Maui, HI, September 18-22, 2005; Bull. Am. Phys. Soc. **50**, 14 (2005)

